foods

Food Contaminant Components

Source, Detection, Toxicity and Removal

Edited by
Dapeng Peng and Yongzhong Qian

MDPI

Food Contaminant Components: Source, Detection, Toxicity and Removal

Food Contaminant Components: Source, Detection, Toxicity and Removal

Editors

Dapeng Peng
Yongzhong Qian

Editors

Dapeng Peng
Huazhong Agricultural
University
Wuhan, China

Yongzhong Qian
Chinese Academy of
Agricultural Sciences
Beijing, China

This is a reprint of articles from the Special Issue published online in the open access journal *Foods* (ISSN 2304-8158) (available at: https://www.mdpi.com/journal/foods/special_issues/food_contamination).

For citation purposes, cite each article independently as indicated on the article page online and as indicated below:

Lastname, A.A.; Lastname, B.B. Article Title. *Journal Name* **Year**, *Volume Number*, Page Range.

Contents

About the Editors

Dapeng Peng

Dapeng Peng is a Professor and Doctoral Supervisor at Huazhong Agricultural University. He is on the front line of scientific research and teaching, carrying out research on the basic theories and key technologies of veterinary drug residues and food safety, as well as the training of particularly talented students. He has solved the problem of the difficult preparation of broad-spectrum monoclonal antibodies for small molecule compounds, and invented a series of small molecule haptens, immunogens and coating antigens with completely independent intellectual property rights. He has created a variety of sensitive, high-yield and high-quality monoclonal antibodies, and developed reagent kits and test strips based on these antibodies. He has been presented with more than ten national and provincial scientific and technological awards, including the second prize in the National Technology Invention Award, and has published more than a hundred scientific research papers.

Yongzhong Qian

Dr. Qian is currently the Director General of IQSTAP, at which he is also a Professor. He has been focusing his research interests on the theories and technologies of risk monitoring and assessment, as well as theoretical policy research of management for the quality and safety of agro-products. He has been the Principal Investigator of a series of national research projects funded by the Ministry of Science and Technology and the Ministry of Agriculture relevant to agro-product quality and safety, technical barriers to trade (TBT), quality standards, risk assessment and testing technologies. He is the author of 15 books and more than 120 articles. He has been awarded several times at both the provincial level and ministerial level for his excellence in scientific research. He holds positions in several professional societies and organizations, namely as Vice Chairman of Agro-product Quality and Safety Sub-society of China Society of Agronomy, and Member and Chief of Administration Office of National Expert Committee of Risk Assessment on Quality and Safety for Agro-products. He has served as standing Vice Editor-in-Chief and Editorial Director for the journal of Quality and Safety of Agro-Products. He also has some publications in international journals, including Food Chemistry, Journal of Agricultural and Food Chemistry, Environmental Pollution, Journal of Hazardous Materials, and more.

Article

Development and Validation of a High-Performance Liquid Chromatography–Tandem Mass Spectrometry Method to Determine Promethazine and Its Metabolites in Edible Tissues of Swine

Dehui Wen [1], Rong Shi [1], Haiming He [1], Rundong Chen [1], Yingzi Zhang [1], Rong Liu [2] and Hong Chen [1,*]

[1] National Reference Laboratory of Veterinary Drug Residues, Guangdong Provincial Key Laboratory of Veterinary Pharmaceutics Development and Safety Evaluation, College of Veterinary Medicine, South China Agricultural University, Guangzhou 510642, China; 20203073135@stu.scau.edu.cn (D.W.)

[2] Quality Supervision, Inspection and Testing Center for Domestic Animal Products (Guangzhou), Ministry of Agriculture and Rural Affairs, College of Veterinary Medicine, South China Agricultural University, Guangzhou 510642, China

* Correspondence: shuyi@scau.edu.cn

Abstract: This study aimed to determine promethazine (PMZ) and its metabolites, promethazine sulfoxide (PMZSO) and monodesmethyl-promethazine (Nor$_1$PMZ), in swine muscle, liver, kidney, and fat. A sample preparation method and high-performance liquid chromatography–tandem mass spectrometry (LC–MS/MS) analysis were established and validated. The samples were extracted using 0.1% formic acid–acetonitrile and purified with acetonitrile-saturated n-hexane. After concentration by rotary evaporation, the extract was re-dissolved in a mixture of 0.1% formic acid-water and acetonitrile (80:20, *v/v*). Analysis was performed using a Waters Symmetry C$_{18}$ column (100 mm × 2.1 mm i.d., 3.5 μm) with 0.1% formic acid–water and acetonitrile as the mobile phase. The target compounds were determined using positive ion scan and multiple reaction monitoring. PMZ and Nor$_1$PMZ were quantified with deuterated promethazine (PMZ-d6) as the internal standard, while PMZSO was quantified using the external standard method. In spiked muscle, liver, and kidney samples, the limits of detection (LOD) and limits of quantification (LOQ) for PMZ and PMZSO were 0.05 μg/kg and 0.1 μg/kg, respectively, while for Nor$_1$PMZ, these values were 0.1 μg/kg and 0.5 μg/kg, respectively. For spiked fat samples, the LOD and LOQ for all three analytes were found to be 0.05 μg/kg and 0.1 μg/kg, respectively. The sensitivity of this proposed method reaches or exceeds that presented in previous reports. The analytes PMZ and PMZSO exhibited good linearity within the range of 0.1 μg/kg to 50 μg/kg, while Nor$_1$PMZ showed good linearity within the range of 0.5 μg/kg to 50 μg/kg, with correlation coefficients (r) greater than 0.99. The average recoveries of the target analytes in the samples varied from 77% to 111%, with the precision fluctuating between 1.8% and 11%. This study developed, for the first time, an HPLC–MS/MS method for the determination of PMZ, PMZSO, and Nor$_1$PMZ in four swine edible tissues, comprehensively covering the target tissues of monitoring object. The method is applicable for monitoring veterinary drug residues in animal-derived foods, ensuring food safety.

Keywords: promethazine; promethazine sulfoxide; monodesmethyl-promethazine; swine edible tissues; high-performance liquid chromatography–tandem mass spectrometry

1. Introduction

Promethazine (PMZ) is a first-generation antihistamine drug known for its anti-allergic properties. It exhibits additional central inhibitory effects on the subcortical regions of the brain, resulting in significant central sedation, hypnotic, antiemetic, and antipyretic effects, making it commonly used for sedation and sleep [1–3]. In China, PMZ is approved for treating allergic reactions in animals such as sheep and pigs, including urticaria and serum

sickness. Occasionally, a small number of farmers illegally use it in the breeding process of food animals in order to reduce animal movement, speed up weight gain, or reduce stress reactions during transportation [4].

There have been reports of adverse reactions due to PMZ abuse in humans, including drug-induced mental disorders and cardiovascular diseases in certain individuals [5–7]. However, the illegal use of PMZ in animal feed and breeding can also pose health hazards to consumers through drug residues in animal-derived foods and result in environmental pollution and other risks [8,9]. Chinese Ministry of Agriculture Announcements No. 176 and No. 2583 prohibit the use of promethazine hydrochloride in animal feed and drinking water. In March 2010, the Chinese Ministry of Health published the fourth batch of "non-food substances that may be illegally added to food and food additives that are easily abused" list, which included promethazine. Regulations in Japan, the United States, and the European Union also prohibit the residuals of thiazine tranquilizers and their metabolites in animal-derived foods. Furthermore, the use of PMZ formulations in food animals has not been approved in the European Union, the United States, and other countries and regions. The Ministry of Agriculture and Rural Affairs of China, in order to ensure the safety of animal-derived food and regulate the use of veterinary drugs, has arranged research projects which include PMZ residue studies. We were fortunate to participate in these research projects, to establish a detection method for PMZ and its metabolites in accordance with the Ministry of Agriculture and Rural Affairs of China's No. 326 Announcement "Guiding Principles for Veterinary Drug Residue Elimination Tests" and the "Technical Guiding Principles for Quantitative Analysis Method Validation of Biological Samples", released on 20 June 2022. In these technical guiding principles, experimental approaches, standards, parameters, and reference threshold values for detection method comply with the current international norms, such as COMMISSION IMPLEMENTING REGULATION (EU) 2021/808 of 22 March 2021.

According to previous reports, PMZ is primarily metabolized by CYP450 enzymes in animals [10–12]. Studies on PMZ metabolism in pig tissues seem to be scarce; no literature on PMZ metabolism in pigs was found. However, from the existing literature (see Table S1), PMZ metabolizes into five to eight metabolites, including PMZSO and Nor_1PMZ in humans, rats, and mice. PMZSO and Nor_1PMZ appear to be stable when present and account for a high proportion of metabolites which can be found in humans, rats, and mice. If drugs metabolize in mammals through CYP450 enzymes, there is a certain similarity in the metabolic pathways. Hence, we initially attempted to establish an LC–MS/MS analytical method for PMZ, PMZSO, and Nor_1PMZ in pig plasma and tissues, then carried out a dosing trial in three experimental pigs. After a single intramuscular injection of PMZ, PMZ and its metabolites PMZSO and Nor_1PMZ were found in the plasma of all three pigs. Ten days after the injection, PMZ, PMZSO, and Nor_1PMZ were still present in plasma and tissue above the limit of quantification. Therefore, we eventually chose PMZ and its metabolites PMZSO and Nor_1PMZ as the target analytes. Nor_1PMZ was chosen as a target compound of analysis on drug residues in edible tissues for the first time in this study.

Various methods have been employed to detect PMZ, including enzyme-linked immunosorbent assay [13,14], spectroscopy [15–17], capillary electrophoresis [18,19], high performance liquid chromatography [20,21], gas chromatography–mass spectrometry [22–29], and liquid chromatography–tandem mass spectrometry (LC–MS/MS) [30–43]. However, most of the reported detection methods are used for PMZ formulations or detecting illegally added PMZ in animal feed [32,35,44,45]. Only a handful of methods have been developed to detect PMZ residues, or PMZ along with one of its metabolites, PMZSO, in animal-derived foods [14,21,33,37,41,43,44]. These methods are applicable to only certain edible tissues such as muscle, liver, and kidney. Notably, previous studies have not included fat tissue, which is an important animal source food. Therefore, in this study, fat tissue was included as a research object for the first time, considering its significance as an animal source food and as one of the target tissues for monitoring drug residues in food. The objective of this study was to establish a sample preparation and LC–MS/MS method for

detecting PMZ and two of its metabolites in all edible tissues of swine, in order to provide technical support for monitoring PMZ and its metabolites in swine edible tissues, ensuring food safety.

2. Materials and Methods

2.1. Standards and Reagents

A 99.5% pure Promethazine Hydrochloride standard was procured from the China National Institute for Food and Drug Control, China. A Promethazine-d6 Hydrochloride standard with 98% chemical purity and 99.5% isotopic purity, a Promethazine Sulfoxide (PMZSO) standard with 96% purity, and a Monodesmethyl-Promethazine Hydrochloride standard with 97% purity were all sourced from Toronto Research Chemicals, Canada.

HPLC-grade acetonitrile (ACN) and methanol (MeOH) were obtained from Thermo Fisher Scientific, Waltham, MA, USA. HPLC-grade formic acid was bought from Shanghai Macklin Biochemical Co., Ltd., Shanghai, China. Analytical grade n-hexane was purchased from Tianjin Damao Chemical Reagent Factory, Tianjin, China. Ultrapure water was acquired from a Milli-Q water purification system (Millipore, Billerica, MA, USA).

2.2. Instruments and Equipment

Experiments utilized a high-performance liquid chromatography–tandem mass spectrometer (LC-30AD 220V liquid chromatograph, Shimadzu Corporation, Kyoto, Japan), equipped with an ESI5500 tandem quadrupole mass spectrometer and a Turbo Ionspray electrospray interface, as well as an Analyst 1.6.3 software workstation (Applied Biosystems, ABI, Corporation, MA, USA).

The chromatographic column employed was a Symmetry C_{18} (100 mm × 2.1 mm i.d., 3.5 μm) from Waters Corporation, Milford, MA, USA. A rotary evaporator (N-1300V-W, Tokyo Rikakikai Co., Ltd., Tokyo, Japan), a high-speed desktop centrifuge (LEGEND MACH 1.6R, Thermo Corporation, Waltham, MA, USA), and a vortex mixer (Vortex 3000, WIGGENS Co., Ltd., Straubenhardt, Germany) were also utilized. Nylon syringe filters, 13 mm, 0.22 μm, disposable, were sourced from Shanghai Ampu Company, Shanghai, China.

2.3. Preparation of Solution

Standard stock solution: Promethazine hydrochloride standard (calculated as PMZ, $C_{17}H_{20}N_2S$), PMZSO standard (PMZSO, $C_{17}H_{20}N_2OS$), and Monodesmethyl-Promethazine hydrochloride standard (calculated as Nor_1PMZ, $C_{16}H_{18}N_2S$) were accurately weighed and separately dissolved in HPLC-grade ACN in 50 mL volumetric flasks to achieve a concentration of 1000 μg/mL. These solutions were stored at −22 °C.

PMZ-d6 standard stock solution: A mass of 10 mg of promethazine-d6 hydrochloride standard ($C_{17}H_{15}D_6ClN_2S$) was transferred to a 10 mL volumetric flask, dissolved in HPLC-grade MeOH to achieve a concentration of 1000 μg/mL, sealed, and stored at −22 °C.

Mixed standard working solution: A volume of 1 mL of each of PMZ, PMZSO, and Nor_1PMZ standard stock solutions were combined and diluted with HPLC-grade ACN to obtain series working solutions at concentrations of 2.5 μg/mL, 1.0 μg/mL, 0.5 μg/mL, 0.25 μg/mL, 0.05 μg/mL, 0.025 μg/mL, 0.005 μg/mL, and 0.0025 μg/mL. These solutions were stored at 4 °C.

PMZ-d6 working solution: An appropriate amount of PMZ-d6 standard stock solution was diluted with HPLC-grade ACN to obtain an internal standard solution to a final concentration of 1.0 μg/mL, sealed, and kept at 4 °C.

Acetonitrile saturated n-hexane: An appropriate amount of analytical grade n-hexane was added to an appropriate amount of ACN, mixed well, and allowed to stand until layered.

Formic Acid Solution (0.1%) in Water: A volume of 1.00 mL of HPLC-grade formic acid was transferred, diluted to 1 L volume with ultrapure water, and mixed well.

Formic Acid (0.1%) in Acetonitrile: A volume of 1.00 mL of HPLC-grade formic acid was transferred, and ACN was added to form a volume of 1 L.

Formic Acid Solution (0.1%) in Water–Acetonitrile (80:20, *v/v*): A volume of 200 mL of HPLC-grade ACN was transferred to a 1 L volumetric cylinder, approximately 800 mL of 0.1% formic acid solution in water was added, and the combination was mixed well.

2.4. Chromatography and Mass Spectrometry Parameters

A Symmetry C_{18} (100 mm × 2.1 mm i.d., 3.5 μm) was used. The mobile phases were composed of phase A (0.1% formic acid solution in water) and phase B (acetonitrile, ACN). A flow rate of 0.3 mL/min was maintained with a gradient elution procedure, as presented in Table 1.

Table 1. Gradient program.

Time (min)	Phase B (%)	Phase A (%)	Flow Rate (μL/min)
1.5	10	90	300
6.7	50	50	300
7.0	10	90	300
8	10	90	300

The mass spectrometer was operated in positive ion mode (ESI+), utilizing a multiple reaction monitoring (MRM) scan mode. The primary operating parameters are presented in Table 2.

Table 2. Operating parameters for mass spectrometer.

Parameter	Condition
The source temperature, TEM	550 °C
Collision Gas, CAD	8 psi
Curtain gas, CUR	40 psi
Nebulizer gas1, GS1	55 psi
Ionspray, IS	5500 V
Sheath gas (N_2) flow	25 arbitrary units
Entrance Potential, EP	10 V
Collision Cell Exit Potertial, CXP	18 V
Ion source gas2, GS2	55 psi
Dwell time, DT	50 ms

The standard stock solution from Section 2.3 was diluted to 1 μg/mL with ACN and injected directly into the spectrometer for mass spectrometric optimization. Molecular ion peaks of the target analytes and the internal standard were identified by full-scan mass spectrometry in positive ion mode: m/z was 285.2 for PMZ, 301.3 for PMZSO, 271.3 for Nor_1PMZ, and 291.3 for PMZ-d6. Each precursor ion underwent MS/MS scanning to determine and evaluate monitored ions for each analyte as a quantitative ion and a qualitative ion. The operation parameters for each ion were optimized using the mass spectrometric scan mode of multiple reaction monitoring (MRM). Consequently, the m/z of 86.2 and 198.1 were established as the quantitative and qualitative ions for PMZ, 198.2 and 239.1 for PMZSO, 197.9 and 240.3 for Nor_1PMZ, and 92 and 240.3 for PMZ-d6. The quantitative and qualitative ion pairs, declustering potential, and collision energy for each target compound are listed in Table 3. For quantification, PMZ and Nor_1PMZ utilized PMZ-d6 as the internal standard, while PMZSO employed an external standard method.

2.5. Sample Preparation

The blank matrix used in this study came from the muscles, liver, kidneys, and fat of several different pigs and was not mixed during the processing.

Approximately 500 g of muscle, liver, and kidney samples had connective tissue, blood vessels, and fat removed before being chopped into a uniform slurry using a homogenizer. About 5.0 g ± 0.1 g of this slurry was weighed into a 50 mL centrifuge tube, mixed with

100 µL of PMZ-d6 internal standard working solution (1 µg/mL), vortexed for 30 s, and left to stand for 30 min. After adding 10 mL of 0.1% formic acid in acetonitrile, the mixture was vortexed for 1 min and shaken for 10 min at 100% speed on a platform shaker before being centrifuged at 10,000 rpm for 10 min. The supernatant was transferred to a pear-shaped bottle. Another 10 mL of 0.1% formic acid acetonitrile was added to the residue in the centrifuge tube, and the above steps were repeated for a second extraction. Both extraction liquids were collected in a pear-shaped bottle for purification and concentration.

Table 3. Qualitative and quantitative ion pairs, declustering voltage, collision energy, and retention time for analytes and internal standard.

Analyte	Precursor Ion (*m/z*)	Product Ions (*m/z*)	Declustering Voltage (v)	Collision Energies (Ev)	Retention Time (min)
PMZ	285.2	86.2 */198.1	60	25/33	5.99
PMZSO	301.3	198.2 */239.1	60	51/31	4.30
Nor$_1$PMZ	271.3	197.9 */240.3	60	35/20	5.91
PMZ-d6	291.3	92 */240.1	60	27/20	5.99

Note: The sub ions marked with "*" are the quantification ions.

Around 500 g of subcutaneous fat from pig, free from muscle and connective tissue, was homogenized to produce a uniform slurry. About 5.0 ± 0.1 g of this fat slurry was weighed into a 50 mL centrifuge tube, into which 100 µL of PMZ-d6 internal standard working solution (1 µg/mL) were added, before being vortexed for 30 s and left to stand for 30 min. Then, 10 mL of acetonitrile saturated n-hexane was added, vortexed until the fat was completely dissolved, and left to stand for 30 min. After adding 10 mL of 0.1% formic acid in acetonitrile, the fat mixture was vortexed for 1 min and shaken for 10 min at 100% speed on a platform shaker, before being centrifuged at 10,000 rpm for 10 min. The upper hexane layer was discarded, and the lower extraction liquid was transferred to a new 50 mL centrifuge tube for purification.

The extraction liquids of muscle, liver, kidney, and fat were added to 10 mL of acetonitrile-saturated n-hexane and vortexed for about 30 s to mix. After settling, the upper hexane layer was discarded and the lower extraction liquid was added to 10 mL of anhydrous ethanol. This was then reduced in volume by using a rotary evaporator at 45 °C, then 5 mL of 0.1% formic acid water–acetonitrile was added and vortexed for 30 s to dissolve the residue completely. After this, 5 mL of n-hexane-saturated acetonitrile was added to the solution and vortexed to mix, then left to stand for layering. Approximately 1 mL of the lower solution was transferred to a 1.5 mL centrifuge tube and centrifuged at 14,000 r/min, 0 °C, for 10 min. The clarified middle liquid was filtered using 0.22 µm nylon syringe filters, sealed in an autosampler vial, and stored at 4 °C for analysis.

2.6. Limit of Detection and Limit of Quantification

To establish the limit of detection (LOD) and limit of quantification (LOQ), a blank tissue sample homogenate (5 ± 0.1 g) was spiked with 100 µL of PMZ-d6 internal standard working solution (1 µg/mL) and 100 µL of mixed standard working solution. Thus, spiked samples at varying concentrations of 0.05 µg/kg, 0.1 µg/kg, 0.5 µg/kg, and 1 µg/kg were prepared. These samples were processed and analyzed by the method described in Sections 2.4 and 2.5. The concentration of the sample with a signal-to-noise ratio (S/N) ≥ 3 was considered the LOD, and the concentration with an S/N ≥ 10 was regarded as the LOQ.

2.7. Calibration Curve and Linearity

Blank tissue sample slurries (5 ± 0.1 g) were spiked with a 1 µg/mL PMZ-d6 internal standard working solution (100 µL) and a mixed standard working solution (100 µL) to achieve varying concentrations—for PMZ and PMZSO, ranging from 0.1 µg/kg to 50 µg/kg; for Nor$_1$PMZ, ranging from 0.5 µg/kg to 50 µg/kg. These samples were processed and analyzed by the method described in Sections 2.4 and 2.5. The calibration curve and

correlation coefficient (r) were determined using a weighted least-squares method with the ratio of the concentration of PMZ, Nor_1PMZ, and PMZ-d6 as the abscissa and the peak area ratio of the quantitative ion pairs of PMZ, Nor_1PMZ, and PMZ-d6 as the ordinate, with the weight chosen as $1/X^2$. The calibration curve and correlation coefficient of PMZSO were obtained using a weighted least-squares method with the concentration of PMZSO as the abscissa and the peak area of the PMZSO quantitative ion pair as the ordinate, with the weight chosen as $1/X^2$. The experiment was repeated in triplicate.

2.8. Recovery and Precision

To assess recovery and precision, blank tissue samples slurry (5 ± 0.1 g) were spiked with mixed standard working solutions of low, medium, and high concentration. These spiked samples at concentrations of 0.5 μg/kg, 5 μg/kg, and 50 μg/kg were processed and analyzed. The recovery and relative standard deviation (RSD) of the sample determination values were calculated, with RSD serving as an indicator of precision. The experiment was repeated for three batches to test inter-day precision.

2.9. Investigation of Matrix Effects

A homogenized blank tissue sample of 5 g $\pm$ 0.1 g, processed as delineated in Section 2.5, was utilized to generate a sample matrix solution. The mixed standard working solution from Section 2.3, amounting to 100 μL, was separately integrated into the sample matrix solution, thus forming matrix-matched samples at concentrations of 0.1 μg/kg, 0.5 μg/kg, 1 μg/kg, 5 μg/kg, 10 μg/kg, 20 μg/kg, and 50 μg/kg. These samples were analyzed by the method described in Section 2.4, and the matrix-matched sample curve was subsequently plotted. This experiment was conducted thrice.

The mixed standard working solution, described in Section 2.3, was diluted with methanol, resulting in concentrations of 0.1 μg/L, 0.5 μg/L, 1 μg/L, 5 μg/L, 10 μg/L, 20 μg/L, and 50 μg/L. The analysis was conducted as per the conditions specified in Section 2.4, enabling the derivation of the standard working solution curve.

The matrix effect, which refers to the extent of the sample matrix's influence on target compound determination, was evaluated by comparing the slope of the matrix-matched sample curve with the standard working solution of equivalent concentration. Matrix enhancement is indicated by ME > 0, while ME < 0 signifies matrix suppression. Low signal interference from the matrix, which can be overlooked, occurs when $0 \leq |ME| \leq 20\%$. Moderate matrix interference is signaled by $20\% < |ME| < 50\%$, and strong matrix interference is inferred when $|ME| \geq 50\%$.

Matrix effect is calculated using the following formula:

$$ME = \left(\frac{S_m}{S_s} - 1 \right) \times 100\% \tag{1}$$

ME: Matrix Effect;
S_m: Slope of the curve of matrix-matched samples;
S_s: Slope of the curve of standard working solution.

2.10. Stability Test

A homogenized blank tissue sample (5 ± 0.1 g), combined with a low or high concentration of the mixed standard working solution, was used to yield a quality control (QC) sample. QC samples, boasting target drug concentrations of 0.5 μg/kg and 50 μg/kg, were processed in accordance with the method delineated in Section 2.5. The stability of these samples was assessed at different situations: after 30 days of storage at $-22\,°C$, after a week's storage at 4 °C, after three freeze–thaw cycles, and after exposure to room temperature and light for 24 h. Each concentration was replicated thrice. The actual measured concentration was compared with the theoretical added concentration. The deviation

between each concentration's mean value and the theoretical concentration was calculated, with the relative standard deviation (RSD) aimed to be within 15%.

3. Results

3.1. Optimization of HPLC–MS/MS Conditions

The Symmetry C_{18} column (100 mm $\times$ 2.1 mm i.d., 3.5 μm), supplied by Waters, USA, was chosen for separation in this study. Several mobile phase combinations were tested, including 0.1% formic acid water–acetonitrile, 0.1% acetic acid water–acetonitrile, 0.2% formic acid water–acetonitrile, and a blend of 0.1% formic acid and 0.1% acetonitrile. The results indicated that the 0.1% formic acid water–acetonitrile mobile phase system provided the optimum response value and retention time. Figure 1 depicts the characteristic ion mass spectrometry of a mixed standard working solution of 0.005 μg/mL, with mobile phase of 0.1% formic acid in water and acetonitrile.
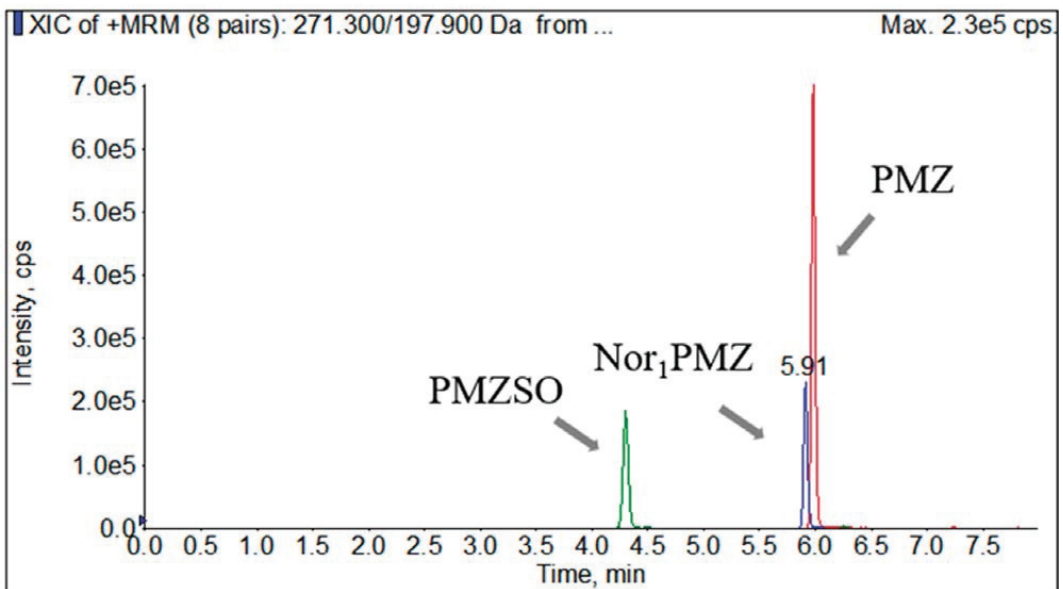
Figure 1. The characteristic ion mass spectrometry of the mixed standard working solution of 0.005 μg/mL.

After the optimization of operational parameters, the molecular ions and the product ions of PMZ, PMZSO, Nor_1PMZ, and PMZ-d6 in standard working solutions were scanned under suitable conditions, as illustrated in Figure 2.

3.2. Selection of Extraction Reagents

The actual absolute recoveries of four analytes in muscle, liver, kidney, and fat tissue were compared using four extraction reagents: acetonitrile, 0.1% formic acid in acetonitrile, a blend of ethyl acetate and acetonitrile (20/80, v/v), and 1% ammoniated acetonitrile, as depicted in Figure 3. In Figure 3, the bar represents the average absolute recovery rate of each analyte in four types of tissues, extracted using different extraction reagents, and the error bar represents the standard deviation. The extraction efficiency of 0.1% formic acid in acetonitrile was superior to the others. Consequently, it was chosen as the extraction reagent for the four analytes.
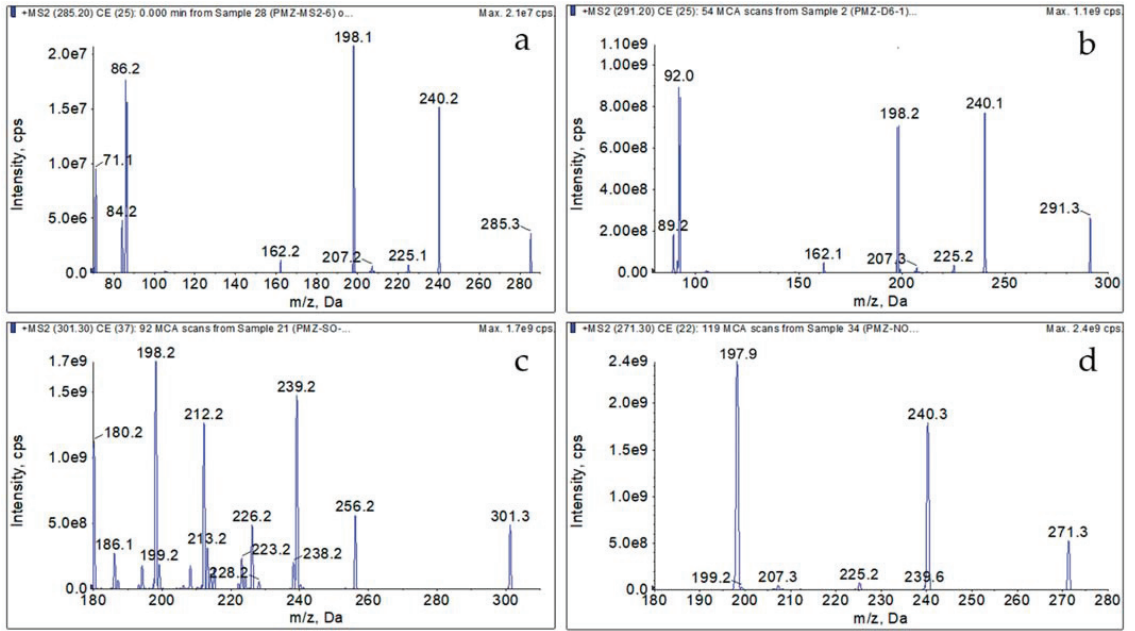
Figure 2. Representative MRM chromatograms of the precursor ions and primary product ions of the analytes and internal standard in the standard working solution: (**a**) PMZ, (**b**) PMZ-d6, (**c**) PMZSO, and (**d**) Nor_1PMZ.
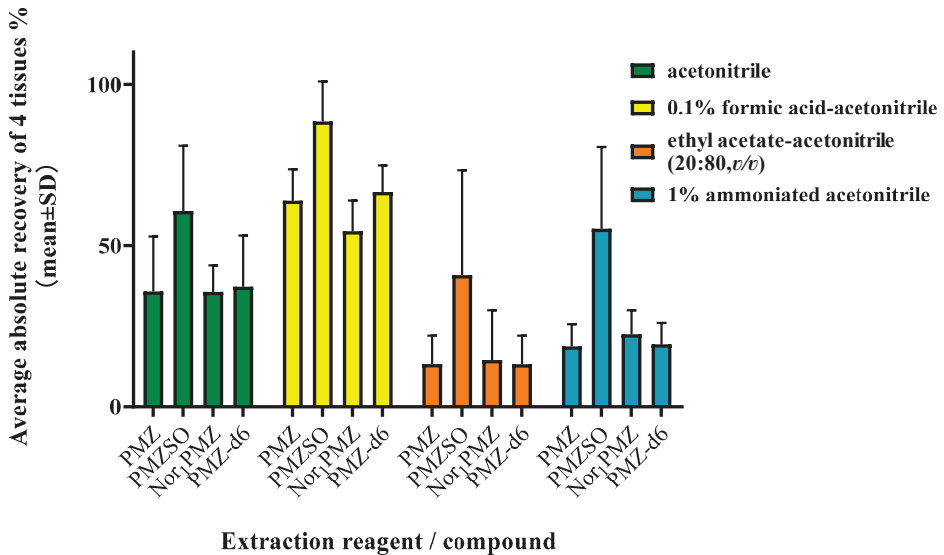
Figure 3. Average absolute recoveries of four analytes in four types of tissues in different extraction reagents.

3.3. Methodological Validation

Selectivity was evaluated by comparing the chromatograms derived from spiked tissue samples and blank tissue samples, processed and detected following the method outlined in Sections 2.4 and 2.5. It was demonstrated that no endogenous peaks from blank

samples were present, and no interfering signals were observed at the retention times of each monitored ion of the analytes. As such, the method developed in this study allowed for accurate qualitative and quantitative analysis of PMZ and its metabolites, PMZSO and Nor$_1$PMZ.

The limit of detection (LOD), limit of quantification (LOQ), linear range, and linearity were assessed using spiked samples. After processing and detecting the samples in accordance with Section 2.6, the LOD and LOQ for PMZ and PMZSO were determined to be 0.05 μg/kg and 0.1 μg/kg, respectively, in muscle, liver, and kidney samples; for Nor$_1$PMZ, the LOD and LOQ were 0.1 μg/kg and 0.5 μg/kg, respectively. For spiked fat samples, the LOD and LOQ for all three analytes were found to be 0.05 μg/kg and 0.1 μg/kg, respectively. Employing the method described in Section 2.7, PMZ and PMZSO displayed good linear relationships in the range of 0.1 μg/kg to 50 μg/kg across the four tissue types. Nor$_1$PMZ also exhibited a strong linear relationship in the range of 0.5 μg/kg to 50 μg/kg, with correlation coefficients (r) exceeding 0.99. Refer to Table 4 for additional details.

Table 4. Linear equations, correlation coefficient (r), limit of detection (LOD), and limit of quantification (LOQ) of PMZ and its two metabolites.

Tissues	Analyte	Linear Range	Regression Equation *	r	LOD (μg/kg)	LOQ (μg/kg)
Muscle	PMZ	0.1–50 μg/kg	Y = 2.43x − 0.0116	0.9993	0.05	0.1
	PMZSO		Y = 1.49x + 0.00797	0.9977		
	Nor$_1$PMZ	0.5–50 μg/kg	Y = 1.19x − 0.00557	0.9993	0.1	0.5
Liver	PMZ	0.1–50 μg/kg	Y = 2.82x − 0.062	0.9992	0.05	0.1
	PMZSO		Y = 2.79x + 0.0583	0.9992		
	Nor$_1$PMZ	0.5–50 μg/kg	Y = 1.19x − 0.0316	0.9996	0.1	0.5
Kidney	PMZ	0.1–50 μg/kg	Y = 2.22x + 0.0125	0.9997	0.05	0.1
	PMZSO		Y = 1.53x + 0.022	0.9972		
	Nor$_1$PMZ	0.5–50 μg/kg	Y = 0.812x + 0.00942	0.9988	0.1	0.5
Fat	PMZ	0.1–50 μg/kg	Y = 1.38x + 0.0595	0.9990	0.05	0.1
	PMZSO		Y = 0.583x + 0.0102	0.9996		
	Nor$_1$PMZ		Y = 0.926x + 0000146	0.9985		

* Y: peak area of analyte, x: concentration of analyte.

Recovery and precision were evaluated using spiked samples, following the methodology presented in Section 2.8. As can be seen in Table 5 (original data are shown in Table S2), average recoveries for PMZ, PMZSO, and Nor$_1$PMZ in muscle, liver, kidney and fat ranged from 77% to 111%. The intra-day and inter-day precision for all tissues remained less than 15%, thereby meeting the Ministry of Agriculture and Rural Affairs of China's technical guiding principles for residue analysis methods.

After processing and analyzing the samples as described in Section 2.9, the matrix effects were determined, as presented in Table 6. The matrix effects for the four types of tissue were predominantly negative, signifying a suppression effect on the signal of the compounds. The matrix effect on the three target compounds in pig fat tissue suggested weak matrix interference. In contrast, the matrix effect on the three target compounds in pig muscle and kidney tissues indicated moderate matrix interference. In pig liver tissue, the matrix effect on the three target compounds signified strong matrix interference. These findings underscore the necessity for thoughtful consideration of tissue matrix types when analyzing analytes, as varying matrices can influence the accuracy of the results.

<p style="text-align:center">Table 5. Recovery and precision of spiked blank samples.</p>

Tissues	Analyte	Concentration (µg/kg)		Recovery (%, $\overline{X}$, n = 6)	Intra-Day RSD (%, n = 6)			Inter-Day RSD (%)
		Spiked	Found ($\overline{X}$, n = 6)		Batch I	Batch II	Batch III	
Muscle	PMZ	0.1	0.077~0.082	77~82	7.1	11	11	9.9
		5	4.72~5.00	92~100	2.8	3.2	4.8	5.1
		50	47.15~52.33	94~105	5.7	3.8	3.8	6.1
	PMZSO	0.1	0.099~0.10	99~103	7.0	8.1	10	8.3
		5	4.64~5.31	93~106	2.1	3.0	7.7	7.6
		50	43.12~45.23	86~90	2.4	3.3	3.2	3.5
	Nor$_1$PMZ	0.5	0.45~0.52	90~104	7.6	8.4	9.4	10
		5	4.75~5.04	95~101	6.5	3.6	4.9	5.5
		50	45.92~55.58	92~111	3.2	3.3	6.0	9.3
Liver	PMZ	0.1	0.097~0.1	97~104	11	7.1	6.3	8.4
		5	4.35~5.37	87~107	2.3	8.0	5.2	10
		50	44.37~45.42	89~91	5.0	5.6	4.4	4.8
	PMZSO	0.1	0.098~0.1	98~101	8.1	5.1	9.8	7.6
		5	4.54~5.01	91~100	6.6	3.9	5.5	6.9
		50	48.23~52.20	96~104	4.4	5.3	1.8	5.1
	Nor$_1$PMZ	0.5	0.47~0.49	94~97	8.6	6.9	6.4	7.5
		5	4.57~4.93	91~98	5.5	9.4	7.0	7.8
		50	47.32~50.40	95~101	4.1	4.4	3.6	4.6
Kidney	PMZ	0.1	0.086~0.094	86~94	5.0	2.9	7.8	6.7
		5	4.22~4.48	84~90	5.9	4.8	4.3	5.4
		50	44.78~45.88	90~92	3.0	6.3	1.8	4.0
	PMZSO	0.1	0.095~0.10	95~100	10	11	6.8	9.1
		5	5.02~5.23	101~105	4.3	5.6	3.1	4.6
		50	45.47~49.58	91~99	1.8	4.0	2.0	4.6
	Nor$_1$PMZ	0.5	0.47~0.50	94~99	6.8	12	5.4	8.6
		5	4.93~5.22	97~104	7.1	11	5.9	7.9
		50	47.95~52.18	96~104	5.6	7.2	2.7	6.3
Fat	PMZ	0.1	0.096~0.10	96~100	7.6	7.6	9.5	7.6
		5	4.88~5.20	98~105	3. 7	3.1	3.2	4.1
		50	48.83~52.35	98~101	6.6	5.6	5.6	6.4
	PMZSO	0.1	0.094~0.10	95~101	7.2	10	9.0	9.1
		5	4.23~4.89	85~98	4.6	4.2	5.3	7.7
		50	45.48~46.40	91~93	3.6	5.1	3.2	4.8
	Nor$_1$PMZ	0.1	0.096~0.10	96~101	9.9	9.0	11	9.7
		5	5.00~5.26	100~105	6.5	7.4	5.2	6.4
		50	43.43~49.38	87~99	5.0	7.7	7.9	7.5

The stability of the samples was assessed following the methodology outlined in Section 2.10. As detailed in Table 7, the relative standard deviations (RSDs) for each analyte concentration within tissue samples, subjected to conditions such as ambient temperature and light exposure for 24 h, refrigeration at 4 °C for 48 h, a three-cycle freeze–thaw process,

and prolonged storage for a month, typically hovered around ±15%. Hence, the structural and compositional stability of PMZ, PMZSO, and Nor_1PMZ in tissue samples proved to be fairly robust under a range of conditions.

Table 6. Matrix effects (%) of PMZ and its metabolites in four tissue types (n = 3).

Matrix	PMZ	SD (%)	PMZSO	SD (%)	Nor$_1$PMZ	SD (%)
Muscle	−34.15	1.52	−24.94	2.05	−36.05	1.05
Liver	−56.68	0.86	−50.77	2.27	−49.15	1.01
Kidney	−19.75	1.91	−27.55	2.76	−22.96	2.71
Fat	−9.14	1.63	5.14	1.65	−0.14	1.86

Table 7. Stability investigation of target compounds in various tissues, RSDs (%, n = 3).

Analyte	Tissues	Liver		Kidney		Fat		Muscle	
	Spiked (µg/kg)	0.5	50	0.5	50	0.5	50	0.5	50
Content detected of PMZ after treated	Room temperature and light for 24 h	9.06	9.54	5.71	9.54	4.21	5.44	8.68	4.68
	Stored at 4 °C for 48 h	5.96	6.68	8.70	6.81	7.27	7.32	8.23	4.92
	Stored at −22 °C for 30 days	11.80	13.47	15.06	13.47	5.15	6.72	11.98	8.11
	Repeated freeze–thawing 3 times	5.75	8.34	7.73	8.34	7.79	5.69	7.72	9.87
Content detected of PMZSO after treated	Room temperature and light for 24 h	9.66	9.69	6.43	5.86	5.92	7.63	10.42	6.05
	Stored at 4 °C for 48 h	10.68	8.23	6.12	3.59	7.84	6.67	7.28	3.96
	Stored at −22 °C for 30 days	11.71	9.64	11.89	10.56	8.85	8.95	12.86	13.62
	Repeated freeze–thawing 3 times	9.58	11.88	6.66	14.79	5.52	8.44	8.48	13.99
Content detected of Nor$_1$PMZ after treated	Room temperature and light for 24 h	9.12	8.09	8.76	4.50	3.78	6.38	8.17	7.25
	Stored at 4 °C for 48 h	11.06	9.14	7.77	7.44	6.12	2.30	7.34	2.06
	Stored at −22 °C for 30 days	10.19	12.55	13.48	11.21	14.19	10.44	12.16	13.83
	Repeated freeze–thawing 3 times	13.48	6.70	7.45	10.04	6.64	7.24	7.20	11.85

4. Discussion

Thiophene compounds encompass amino groups, which, when dissociated in water, exhibit alkalinity. These compounds may be adsorbed by residual silicon hydroxyl groups present on the surface of the stationary phase of a chromatographic column. To address this issue, the selection of fully end-capped C_{18}, phenyl, and C_8 chromatographic columns is recommended. The Symmetry C_{18} column (100 mm × 2.1 mm i.d., 3.5 µm, Waters, Milford, MA, USA) was utilized for separation in this investigation. In LC–MS/MS analysis, the ESI+ mode is favorable for alkaline PMZ and its metabolites, while acidic mobile phase systems tend to form $[M + H]^+$ ions. Acetonitrile and water, which are frequently used as mobile phases, can be proportioned according to specific requirements. Formic acid or acetic acid serve as typical protonation reagents in the LC–MS mobile phase. This study examined the effects of introducing different ratios of formic acid or acetic acid into the mobile phase. It was discovered that acetic acid increased the baseline of the Nor_1PMZ representative ion chromatogram, rendering it unsuitable. The most optimal retention time and representative ion chromatograms for the analytes were achieved by adding 0.1% (by volume) formic acid to the aqueous phase.

Matrix effects from animal tissue samples can interfere with the accuracy of drug content analysis in tissues. The internal standard method is routinely employed to mitigate matrix effects and significantly enhance the accuracy and precision of the analysis. Numerous studies have reported the use of the internal standard method in determining PMZ and its metabolite content. Metronidazole served as the internal standard for estimating PMZ and PMZSO in rat plasma and various tissues [36]. PMZ-d6 and PMZSO-d6 were utilized as internal standards to detect the content of PMZ and PMZSO in pig muscle, liver, and kidney [43]. Donepezil was used to detect drugs, include PMZ, in human plasma and urine [31]. Haloperidol was reported to be used as internal standard to quantify chlorpromazine and PMZ in pig kidneys [21], and loratadine was used as internal standard when

studying PMZ and ephedrine mixture [38]. The PMZ-d6, a deuterated isotope of PMZ, was employed as the internal standard for quantification in this study.

In the research work, it was found that PMZ, PMZSO, Nor$_1$-PMZ, and PMZ-d6 stock solutions and working solutions were stable long-term at $-20\ °C$ and $4\ °C$, and were stable at room temperature and during the sample preparation process. However, after evaporating the solvent of PMZ-d6 working solution, the response value of PMZ-d6 detected by LC–MS/MS significantly decreased after one week at room temperature and exposed to the air. Therefore, we sealed and stored the solution containing PMZ-d6 in the refrigerator. After the solvent of the sample solution containing PMZ-d6 is evaporated by a rotary evaporator, it should be immediately re-dissolved, sealed, and stored at $4\ °C$.

It was found that the recovery of PMZSO was generally significantly high (>120%) while quantified by PMZ-d6 with internal standard method, though the recovery of PMZ and Nor$_1$PMZ was in the range of 80–120%. After investigations, it was found that, in spiked samples, the actual extraction recovery of PMZ, PMZ-d6, and Nor$_1$PMZ were all between 60% and 70%, which were very close. However, the actual extraction recovery of PMZSO was above 85%, which was significantly different from the internal standard and other analytes, as shown in Figure 3. As such, PMZ-d6 is unsuitable for quantification analysis of PMZSO. As a metabolite, PMZSO shows stronger polarity than PMZ, with its chemical properties differing from those of PMZ, PMZ-d6, and Nor$_1$PMZ. Finally, the internal standard method was used for quantifying PMZ and Nor$_1$PMZ, and the external standard method was used for quantifying PMZSO.

Based on the physicochemical characteristics of the target analytes in this study, along with evidence from previous studies [33,41,46], several extraction solvents, including ACN, 0.1% formic acid in ACN, ethyl acetate—ACN (20:80, *v/v*), and 1% ammoniated ACN, were investigated for their extraction recovery efficacy in pig tissues. Results indicated that formic acid–acetonitrile combination exhibited the most efficient extraction recovery across all analytes, as depicted in Figure 3. Considering the efficiency of extraction for PMZ, PMZSO, Nor$_1$PMZ, and PMZ-d6 across four tissue samples, 0.1% formic acid in ACN was utilized as the extraction solvent for this study. It was observed that the extraction efficiency could be boosted by adding a slight amount of acid. However, with an increasing increment in formic acid volume, the extraction liquid for liver and kidney became darker, harboring more impurities, and, thus, posing interference in instrument detection. Consequently, an optimal extractant ratio of 0.1% formic acid in ACN was established.

Fat tissue is a significant animal source food and one of the target tissues for monitoring drug residues. However, fat samples pose challenges in sample preparation and detection procedures due to their high lipophilic impurity content. The extraction recovery of analytes in fat is generally low. In this study, various procedures were explored to enhance extraction and purification efficacy in fat samples. It was determined that complete dissolution of the fat sample slurry in n-hexane prior to analyte extraction improved extraction recovery. During the sample concentration and purification process, the lipid-rich impurity content in the sample solvent could be discarded through extraction with n-hexane, both before and after the extraction solvent was removed using a rotary evaporator. Centrifuging the sample solution at $0\ °C$ or lower facilitated the upward migration of lipid-interfering substances. Finally, the parameters of the fat tissue detection method complied with the requirements of technical guiding principles.

5. Conclusions

We have, for the first time, developed and validated an LC–MS/MS method for the determination of promethazine and its two metabolites across all edible tissues of swine, in accordance with the Ministry of Agriculture and Rural Affairs of China's technical guiding principles. In this method, 0.1% formic acid in acetonitrile served as the extraction solvent, and LC–MS/MS was used for analyte detection. The limit of quantification ranged between 0.1 μg/kg and 0.5 μg/kg, demonstrating a sensitivity equal to or surpassing previous reports. This study included swine fat as a research subject for the first time and Nor$_1$-PMZ

as one of the target analytes, thereby presenting an accurate and reliable detection method for monitoring PMZ residues and its metabolites in swine edible tissues.

References

1. Liu, Y. *Solution Structure of Chlorpromazine Hydrochloride and Promethazine Hydrochloride and Electrochemical Performance of Their Interaction with DNA*; Nanjing University of Science and Technology: Nanjing, China, 2007.
2. Alyami, H.S.; Ibrahim, M.A.; Alyami, M.H.; Dahmash, E.Z.; Almeanazel, O.T.; Alghatani, T.S.; Alanazi, F.; Alshora, D.H. Formulation of sublingual promethazine hydrochloride tablets for rapid relief of motion sickness. *Saudi Pharm. J.* **2021**, *29*, 478–486. [CrossRef]
3. Wang, J.; Lu, C.; Liu, X.; Zhang, G.; Zhang, J.; Gao, M.; Liu, D.; Zhang, X.; Liu, Y. Histamine H1 receptor antagonist attenuates catecholamine surge and organ injury after severe burns. *Front. Endocrinol.* **2023**, *14*, 1068925. [CrossRef] [PubMed]
4. Gao, Q. *Determination of Phenothiazine Sedatives, Neonicotinic Insecticides, and Amide Herbicides in Food by LC-MS/MS*; Hebei Normal University: Heibei, China, 2016.
5. Abeysundera, H.; Craig, B.; Pullich, Z. Promethazine-induced delirium with perceptual abnormalities: Are we thinking broadly when assessing patients? *BMJ Case Rep.* **2021**, *14*, e241784. [CrossRef] [PubMed]
6. Chiappini, S.; Schifano, F.; Corkery, J.M.; Guirguis, A. Beyond the 'purple drank': Study of promethazine abuse according to the European Medicines Agency adverse drug reaction reports. *J. Psychopharmacol.* **2021**, *35*, 681–692. [CrossRef]
7. Adie, S.; Ingebrigtson, M.; Hamilton, D.; Tam, M. A Case Of Promethazine-Induced Polymorphic Ventricular Tachycardia: Conduction Down The Tankfrom Consuming "Purple Drank". *J. Am. Coll. Cardiol.* **2021**, *77*, 1870. [CrossRef]
8. Ignoto, S.; Pecoraro, R.; Scalisi, E.M.; Buttigè, S.E.; Contino, M.; Ferruggia, G.; Salvaggio, A.; Brundo, M.V. Acute Toxicity of a Marine Emerging Pollutant (Promethazine Hydrochloride) on *Artemia* sp. *ACS Omega* **2022**, *7*, 39619–39623. [CrossRef]
9. Zhou, Y.; Hua, X. The hazard and status quo of veterinary drug residues in animal derived food in China. *Grain Oil* **2021**, *34*, 18–20.
10. Bornschein, I.; Pfeifer, S. Biotransformation of promethazine (Prothazin). *Die Pharm.* **1979**, *34*, 750.
11. Bornschein, I.; Pfeifer, S. Further sulfone metabolites of promethazine (Prothazin). *Die Pharm.* **1980**, *35*, 648–649.
12. Ramanathan, R.; Geary, R.S.; Bourne, D.W.; Putcha, L. Bioavailability of intranasal promethazine dosage forms in dogs. *Pharmacol. Res.* **1998**, *38*, 35–39. [CrossRef]
13. Gao, B.L.; Liu, J.; Dong, L.X.; Zhang, L.; Qin, J.H.; Wang, J.P. Broad specific enzyme-linked immunosorbent assay for determination of residual phenothiazine drugs in swine tissues. *Anal. Biochem.* **2014**, *454*, 7–13. [CrossRef]
14. Shi, F.S.; Liu, J.; Zhang, L.; Liu, J.X.; Wang, J.P. Development of an enzyme linked immunosorbent assay for the determination of phenothiazine drugs in meat and animal feeds. *J. Environ. Sci. Heal. Part B* **2016**, *51*, 715–721. [CrossRef]
15. WU, Y.; Xing, L.; XU, Y. Determination of promethazine and its metabolite in Urine by solid-phase extraction with celite and UV derivative spectrophotometry. *Chin. J. Forensic Med.* **2008**, *23*, 89–91.
16. Zhang, S.R.; Yang, J.D. Simultaneous Determination of Chlorpromazine Hydrochloride and Promethazine Hydrochloride by Resonance Rayleigh Scattering Spectra. *J. Instrum. Anal.* **2009**, *12*, 1362–1367.
17. Yang, J.; Yang, Q.; Zou, S.; Wu, L.; Zhu, Q. Simultaneous determination of chlorpromazine hydrochloride and promethazine hydrochloride using near-infrared spectroscopy. *J. Anal. Sci.* **2013**, *29*, 61–64.
18. Wang, L.; Yang, X.; Mo, J. Determination of Epinephrine, Chlorpromazine and Promethazine by Capillary Electrophoresis with Scanning Voltammetric Detector. *Chin. J. Chromatogr.* **1999**, *5*, 435–437.
19. Li, X.; Yang, Y.; Zhou, K. Simultaneous determination of chlorpromazine, promethazine, and their main metabolites by capillary electrophoresis electrophoresis with electrochemiluminescence. *Chin. J. Chromatogr.* **2012**, *9*, 938–942.

20. Vanapalli, S.R.; Kambhampati, S.P.; Putcha, L.; Bourne, D.W. A liquid chromatographic method for the simultaneous determination of promethazine and three of its metabolites in plasma using electrochemical and UV detectors. *J. Chromatogr. Sci.* **2001**, *39*, 70–72. [CrossRef]

21. Chen, P.; Fan, S.; Huang, L.; Yuan, Z. Establishment of detection method for chlorpromazine and promethazine residues in swine kidney. *Chin. J. Vet. Med.* **2005**, *4*, 412–413, 416.

22. Hui-Qin, W.; Yong-Chun, J.; Ming-Zha, C.; Xiao-Lao, H.; Zhi-Xin, Z. Simultaneous determination of 10 mental drugs by gas chromatography-mass spectrometry. *Chin. J. Anal. Chem.* **2007**, *35*, 500–504.

23. Huang, K.; Zhu, D.; Li, H.; Ling, C.; Li, L.; Liu, X. Analysis of promethazine and its metabolites in rat urine by GC-MS. *J. Instrum. Anal.* **2010**, *3*, 220–225.

24. Cheng, L.; Zhang, Y.; Shen, J.; Wu, C.; Zhang, S. GC–MS Method for Simultaneous Determination of Four Sedative Hypnotic Residues in Swine Tissues. *Chromatographia* **2009**, *71*, 155–158. [CrossRef]

25. Tapadia, K.; Shrivas, K.; Upadhyay, L.S.B. GC–MS Coupled with Hollow-Fiber Drop-to-Drop Solvent Microextraction for Determination of Antidepressants Drugs in Human Blood Sample. *Chromatographia* **2011**, *74*, 437–442. [CrossRef]

26. Li, W.; Lin, D.; Sun, H.; Mutailifu, M.; Wang, L. ASE-GC /MS analysis of common sedative hypnotic drugs in blood. *Chin. J. Forensic Med.* **2014**, *5*, 451–454.

27. Li, W.; Li, X.; Lin, D.; Sun, H.; Shao, K. Analysis of Five Hypnotic Sedative Drugs in Blood by Gas Chromatography—Mass Spectrometry with Supported Liquid Extraction. *Anal. Test. Technol. Instrum.* **2018**, *24*, 34–38.

28. Zhao, S.R.D. Determination of Four Sedative-hypnotic Drugs with GC/MS for a Case of Abnormal Death. *Forensic Sci. Technol.* **2020**, *45*, 545–547.

29. Rosenberger, W.; Teske, J.; Klintschar, M.; Dziadosz, M. Detection of pharmaceuticals in "dirty sprite" using gas chromatography and mass spectrometry. *Drug Test. Anal.* **2022**, *14*, 539–544. [CrossRef] [PubMed]

30. Liang, Q.; Qu, J.; Luo, G.; Wang, Y. Rapid and reliable determination of illegal adulterant in herbal medicines and dietary supplements by LC/MS/MS. *J. Pharm. Biomed. Anal.* **2006**, *40*, 305–311. [CrossRef]

31. Liu, P.; Liang, S.; Wang, B.-J.; Guo, R.-C. Development and validation of a sensitive LC-MS method for the determination of Promethazine hydrochloride in human plasma and urine. *Eur. J. Drug Metab. Pharmacokinet.* **2009**, *34*, 177–184. [CrossRef]

32. Suo, D.-C.; Zhao, G.-L.; Li, L.; Su, X.-O. Simultaneous Determination of Seven Mental Drugs in Feeds by Liquid Chromatography-Tandem Mass Spectrometry. *Chin. J. Anal. Chem.* **2010**, *38*, 1023–1026.

33. Li, C.; Yue, Z.; Zhao, F.; Hua, H.; Han, R.; Li, L. Study on the Determination of Phenothiazide Residues in Aquatic Products by Liquid Chromatography Tandem Mass Spectrometry. *Chin. J. Vet. Med.* **2010**, *3*, 384–387, 392.

34. He, L.; Wang, J.; Zhang, G.; Liu, R.; Fang, B. Simultaneous Determination of Tranquilizers and Carazolol Residues in Swine Tissues by Liquid Chromatography-Tandem Mass Spectrometry. *Anal. Lett.* **2012**, *45*, 1377–1389. [CrossRef]

35. Suo, D.C.; Zhao, G.L.; Wang, P.L.; Su, X.O. Simultaneous Determination of beta-Agonists and Psychiatric Drugs in Feeds by LC-MS-MS. *J. Chromatogr. Sci.* **2014**, *52*, 604–608. [CrossRef] [PubMed]

36. Liang, L. *Application of Physiologically Based Pharmacokinetic Models for Assessing the Disposition of Promethazine in Simulated Weightless Rats*; The Fourth Military Medical University: Xi'an, China, 2015.

37. Cheng, L.; Shen, J.; Zhang, Q.; Zhang, Y.; Zhang, S. Simultaneous Determination of Three Tranquillizers in Lamb Liver by Ultra-Performance Liquid Chromatography–Tandem Mass Spectrometry. *Food Anal. Methods* **2014**, *8*, 1876–1882. [CrossRef]

38. Lin, G. Pharmacokinetic study of promethazine ephedrine combination in rats under the simulated microgravity condition. *J. Beijing Univ. Technol.* **2018**, *38*, 216–220.

39. Gao, S.; Zhou, X.; Lang, L.; Liu, H.; Li, J.; Li, H.; Wei, S.; Wang, D.; Xu, Z.; Cai, H.; et al. Simultaneous Determination of Schisandrin and Promethazine with Its Metabolite in Rat Plasma by HPLC-MS/MS and Its Application to a Pharmacokinetic Study. *Int. J. Anal. Chem.* **2019**, *2019*, 1–13. [CrossRef]

40. Proença, P.; Monteiro, C.; Mustra, C.; Claro, A.; Franco, J.; Corte-Real, F. Identification and Quantification of Antipsychotics in Blood Samples by LC–MS-MS: Case Reports and Data from Three Years of Routine Analysis. *J. Anal. Toxicol.* **2020**, *44*, 915–922. [CrossRef]

41. Wang, J.; Ye, J.; Wang, X.; Zhong, S.; Chen, Q. Determination of 15 sedative drug residues in livestock and poultry meat by ultra-high performance liquid chromatography tandem mass spectrometry. *Farm Prod. Process.* **2020**, *7*, 45–49.

42. Fan, L.; An, J.; Cui, Y.; Dong, Z. Development, validation, and application of a simple UPLC-MS/MS method for simultaneous quantification of five traditional antipsychotics in human plasma. *Biomed. Chromatogr.* **2021**, *35*, e5143. [CrossRef]

43. Chen, X.; Zhou, J.; Jin, M. Determination of 4 chlorpromazine and promethazine and their metabolites in swine tissues by liquid chromatography-tandem mass spectrometry with isotope internal standard dilution technique. *J. Hyg. Res.* **2022**, *51*, 476–482.

44. Qi, L.; Duan, L.-M.; Sun, X.-H.; Zhang, J.; Zhang, Z.-Q. Simultaneous determination of three banned psychiatric drugs in pig feed and tissue using solid-phase reactor on-line oxidizing and HPLC-fluorescence detection. *Biomed. Chromatogr.* **2015**, *29*, 1535–1540. [CrossRef]

45. Cunha, R.R.; Ribeiro, M.M.; Muñoz, R.A.; Richter, E.M. Fast determination of codeine, orphenadrine, promethazine, scopolamine, tramadol, and paracetamol in pharmaceutical formulations by capillary electrophoresis. *J. Sep. Sci.* **2021**, *44*, 1815–1823. [CrossRef] [PubMed]

46. Huang, M.; Gao, J.-Y.; Zhai, Z.-G.; Liang, Q.-L.; Wang, Y.-M.; Bai, Y.-Q.; Luo, G.-A. An HPLC–ESI-MS method for simultaneous determination of fourteen metabolites of promethazine and caffeine and its application to pharmacokinetic study of the combination therapy against motion sickness. *J. Pharm. Biomed. Anal.* **2012**, *62*, 119–128. [CrossRef] [PubMed]

47. Li, R.; Yang, L.; Zhang, P.; Luo, Y.; Zhang, P.; Gao, Y. Rapid screening of 24 tranquillizer drugs in fish and fishery products by ultra-high performance liquid hromatographyquadrupole /electrostatic field orbitrap high resolution mass spectroscopy. *Chin. J. Chromatogr.* **2018**, *36*, 125–135. [CrossRef] [PubMed]

48. Wang, K.; Cao, Q.; Zhao, L.; Chen, L.; Gao, Q.; Yang, L. Determination of Promethazine and Chlorpromazine in Poultry Eggs by High Performance Liquid Chromatography Tandem Mass Spectrometry. *Food Ind.* **2020**, *41*, 299–302.

49. Sun, L.; Zhang, L.; Xu, Q.; Wang, S.; Wang, X. Determination of ten sedative residues in pork and kidney by ultra performance liquid chromatography- tandem mass spectrometry. *Chin. J. Chromatogr.* **2010**, *28*, 38–42. [CrossRef]

50. Li, Z.; Li, H.; Ma, Y.; Wang, S.; Ren, N.; Guo, W.; Guo, C.; Li, Y. High Performance Liquid Chromatography-Tandem Mass Spectrometry Detection of Promethazine in Animal-Derived Foods. *Food Sci.* **2019**, *40*, 320–324.

51. Wang, J.; Ye, J.; Zhong, S.; Wang, X.; Chen, Q. Determination of Antihistamine Residues in Livestock and Poultry Products by Ultra Performance Liquid Chromatography–Quadrupole–Time of Flight Mass Spectrometry. *Sci. Technol. Food Ind.* **2021**, *42*, 250–256, 264.

52. Liang, Y.; Li, Y.; Guo, X.; Li, R.; Gao, L.; Wang, J.; Fu, G.; Wan, Y. Determination of chlorpromazine, promethazine, and vancomycin in pork product by liquid chromatography-mass spectrometry. *Cereal Feed Ind.* **2016**, *346*, 69–73.

MDPI

Article

Development and Validation of a High-Performance Liquid Chromatography–Tandem Mass Spectrometry Method to Determine Promethazine and Its Metabolites in Edible Tissues of Swine

Myung-Sub Yun [1,2] and Hoon Choi [1,*]

[1] Department of Life and Environmental Sciences, College of Agriculture and Food Sciences, Wonkwang University, Iksan 54538, Republic of Korea

[2] Hanearl Science Ltd., Sungnam 13207, Republic of Korea

* Correspondence: hchoi0314@wku.ac.kr; Tel.: +82-63-850-6678; Fax: +82-63-850-7308

Abstract: Unintentional pesticide contamination in rotational crops, often caused by soil contamination from pesticide use in the preceding crops, is a major concern in a positive list system. The residue and dissipation pattern of fluopyram in soil and scallions were investigated to evaluate the uptake of fluopyram from the soil by scallions. In addition, the management concentration in soil (MC_{soil}) was calculated based on bioconcentration factors (BCFs) and the maximum residue limit (0.2 mg/kg) in leaf-and-stem vegetables. In a field experiment, plots in two different trials, A and B, were treated with 0.06 g fluopyram/m^2 and maintained for 30 days according to OECD guidelines. Scallion seedlings were cultivated for 48 days. Soil samples were taken at three different time points: DAP (Days after planting) 0, 34, and 48. Scallion samples were collected at five different time points: DAP 20, 27, 34, 41, and 48. The initial amounts of fluopyram in soil at DAP 0 were 0.94 ± 0.03 and 0.96 ± 0.04 mg/kg in trials A and B, respectively. The half-life of fluopyram in the soil was 87–231 days. Fluopyram uptake by the roots increased over time, but fluopyram residue in the scallions decreased due to the dilution effect caused by an increase in plant weight. The residues in the scallions at DAP 48 were 0.22 ± 0.01 and 0.15 ± 0.01 mg/kg in trials A and B, respectively. The BCFs of scallions for fluopyram were 0.21–0.24 (trial A) and 0.14–0.18 (trial B). The MC_{soil} was proposed as 0.8 mg/kg, and may be utilized as a safe management guideline for precautionary practices to cultivate safe rotational crops.

Keywords: fluopyram; bioconcentration factor; scallion; rotational crop; uptake

1. Introduction

Pesticides sprayed on crops attach to their surfaces, fall to the soil, and either remain in the soil or transported to water systems [1,2]. Pesticides decompose and dissipate over time through various physico-chemical and biological processes, but in some cases a significant amount of the pesticide can be introduced into the soil, resulting in soil contamination. When plants are grown in contaminated soil, trace amounts of pesticides can be taken up by the plant roots and transferred to other parts of the plant [3,4], leading to pesticide contamination of the plants. Leafy vegetables and leaf-and-stem vegetables are more prone to this type of contamination compared to fruits, as they have a higher chance of accumulating pesticides due to their edible parts [5–7]. This accumulation can result in unintentional contamination of agricultural products and pose health risks to consumers.

Fluopyram is a benzamide-based fungicide that inhibits the function of succinate dehydrogenase (SDH) inside the mitochondrial membrane, thereby controlling pathogenic fungi in plants [8]. Fluopyram is widely used in Korea to control fungal growth, such as grey mold (*Botrytis*) and powdery mildew in fruits and vegetables. The organic carbon adsorption coefficient for fluopyram (K_{oc}), which is a representative indicator of the mobility

of pesticides in soil, is 233–400 mL/g, indicating a moderate level of mobility [9]. Additionally, fluopyram is heat-stable and very stable during hydrolysis and photolysis in acidic, neutral, and alkaline conditions, and the half-life in soil was reported as 119 days [10]. Therefore, owing to high soil persistence and moderate mobility of fluopyram, there is a strong possibility that it would remain in the soil and be absorbed into crops. Furthermore, the Korean cropping system has the characteristics of a short uncultivated period and frequent continuous/mixed cultivation, which has increased the possibility of pesticide uptake and contamination of rotational crop plants. In a survey on pesticide residues conducted by the Korean Ministry of Agriculture, Food and Rural Affairs in 2019, the residual amount of fluopyram was the highest among 13 unregistered pesticides detected in scallions, a leaf-and-stem vegetable [11]. A positive list system (PLS) has been implemented to strengthen domestic pesticide safety management. In this system, the maximum residue limit (MRL) applies a standard legal limit of 0.01 mg/kg to all non-registered pesticides. As a result, unintentional contamination of agricultural products due to pesticides remaining in the soil has become a more considerable problem than before the implementation of PLS. Therefore, it is necessary to establish safety management standards for residual pesticides in the soil by evaluating the uptake and translocation of soil residual pesticides into crops.
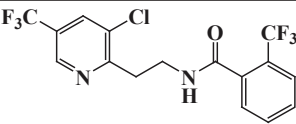
Scallion (*Allium fistulosum*) belongs to the genus *Allium* of the Liliaceae family and is a major leaf-and-stem vegetable in Korea with a cultivation area of 17,170 ha and an annual production of 463,721 tons [12]. In addition, unintentional persistence of fluopyram has been reported for scallions, raising safety concerns [11]. To the best of my knowledge, there are no previous reports on the potential for fluopyram residues to be present in scallions as a result of uptake from soil. Therefore, this study assesses the uptake of the fungicide fluopyram from the soil by scallions and proposed a management concentration for fluopyram in the soil to ensure the safety of agricultural products. The residual patterns of fluopyram in soil and scallion were analyzed, and the bioconcentration factor (BCF) was calculated as the absorption rate of fluopyram into scallions.

2. Materials and Methods

2.1. Reagents and Materials

Fluopyram (purity: 98%) was purchased from Sigma-Aldrich (St. Louis, MO, USA). The structure and physico-chemical properties of fluopyram are shown in Table 1 [10].

Table 1. Physico-chemical properties of fluopyram.

Pesticide	Fluopyram
Structure	
Chemical name	N-{2-[3-chloro-5-(trifluoromethyl)-2-pyridyl]ethyl}-α,α,α-trifluoro-o-toluamide
Molecular weight	396.72
Solubility	In water 16.0 mg/L (20–25 °C), soluble in acetone and methanol (>250 g/L)
Log K_{ow}	3.3 (pH 6.5)

As a crop protection product, 40% suspension concentrate (SC) of fluopyram (Mercury, Bayer Crop Science Co., Ltd., Daejeon, Republic of Korea) was selected and purchased from a commercial agrochemical vendor. The analytical solvents, including acetonitrile and methanol, were purchased from J.T. Baker (Center Valley, PA, USA). High-performance liquid chromatography (HPLC) grade formic acid (purity: 99%) was purchased from Wako (Osaka, Japan) and ammonium formate (purity: ≥97%) was obtained from DAEJUNG (Siheung, Republic of Korea). Reagents used in the quick, easy, cheap, effective, rugged, and safe (QuEChERS) pretreatment method were purchased from Agilent Technology (Santa Clara, CA, USA). QuEChERS extract pouches (EN 15,662 method extraction kit; 4 g MgSO$_4$, 1 g NaCl, 1 g sodium citrate dehydrate, and 0.5 g sodium hydrogencitrate

sesquihydrate) were used for partitioning, and dispersive solid phase extraction (d-SPE, 2 mL, 150 mg $MgSO_4$ and 25 mg primary secondary amine (PSA)) was used for purification. A 100 mg/L stock solution was prepared by dissolving 10.20 mg of standard fluopyram (purity: 98%) in 100 mL of acetonitrile, and serially diluted using blank sample extracts to construct the matrix-matched working solutions at 1, 2, 5, 10, 20, 50, and 100 μg/L, which were used to correct for any matrix effects during the instrumental analysis. The stock and working solutions were stored at −20 °C in a freezer.

2.2. Field Experiment

The field experiment was carried out at a cultivation facility located in Jeonju, Jeollabuk-do, Republic of Korea (35°52′09″ N 127°06′30″ E). For a test crop, a Heukgang cultivar (*Allium fistulosum*, Farm Hannong Co., Ltd., Seoul, Republic of Korea) was cultivated in a greenhouse and scallion seedlings were used for field experiments 63 days after germination. For the field experiments, two different trials, A and B, were used, each with an area of 30 m^2 (2 m × 15 m), and each equally divided into three repeating plots. Each trial was separated with a 6 m^2 (2 m × 3 m) buffer zone. The physico-chemical properties of the soil were analyzed according to the official soil analysis methods outlined by the rural development administration (RDA) [13] and are indicated in Table 2.

Table 2. Physico-chemical properties of soil.

pH (1:5)	EC [1] (dS/m)	OM [2] (g/kg)	Exchangeable Cations (cmol/kg)			CEC [3] (cmol/kg)	Particle Distribution (%)			Soil Texture
			K	Ca	Mg		Sand	Silt	Clay	
4.3	4.6	74.8	1.1	6.5	1.7	21.2	32.2	50.8	17.1	Silt loam

[1] Electrical conductivity; [2] Organic matter; [3] Cation exchange capacity.

The spray suspension was prepared by mixing 5 mL of 40% Mercury SC (suspenstion concentrate) with 20 L of water and sprayed on the trials using a power sprayer (MSB1500Li, Maruyama, Japan). The application rate of fluopyram was 0.06 g a.i. (active ingredient)/m^2, which was the maximum seasonal rate determined from the maximum label rate and the maximum number of applications according to OECD (organization for economic co-operation and development) guidelines [14]. After application, the soil was homogenized to a depth of 10 cm. The plots were irrigated by spraying 100 L of water on each trial once a week to maintain 20% soil moisture content and maintained for 30 days (PBI-30; Plant back intervals) in a greenhouse. The seedlings were planted at a density of 15 × 15 cm after tillage to a depth of 15 cm and cultivated for 48 days. In each trial, 100 L of water was drip-irrigated every two days during cultivation. During the cultivation period, CAS data loggers (EL-21CFR-2-LCD, Lascar electronics, PA, USA) were used to monitor temperature (16.2–31.0 °C) and humidity (48.3–86.7%) in the facility.

2.3. Sample Collection and Preparation

At least 1 kg of topsoil (a depth 0–10 cm) was collected on the day after planting (DAP 0—days after planting), 34 days after planting (DAP 34), and 48 days after planting (DAP 48) using a soil sampling auger (diameter, 2.3 cm; and height, 10 cm). The soil samples were sieved using a <2 mm diameter sieve, and then stored at −20 °C until analysis. The moisture content of soil samples was determined by calculating the difference in soil weight before and after drying at 105 °C for 24 h. Scallion samples were collected on the 20, 27, 34, 41, and 48 days (100% mature) after planting (DAP 20, 27, 34, 41, and 48). The individual weight and height of each sample were measured to compare the growth status at the time of sample collection. After removing the root of the scallion and adding dry ice, samples were homogenized using a blender (Blixer® 2, Lobot Coupe, Montceau-les-Mines, France), and then stored at −20 °C until analysis.

2.4. Extraction and Purification of Fluopyram

The residual analysis of fluopyram in soil and scallion samples was carried out based on the QuEChERS EN method for rapid analysis. Soil (5 g) or scallion samples were weighted and placed into 50 mL conical tubes. Thereafter, 20 mL of acetonitrile was added for extraction and samples were shaken at 1300 rpm for 3 min using a high-speed shaker (2010/Grinder, SPEX® Sample Prep, Metuchen, NJ, USA). Subsequently, QuEChERS extract pouches (4 g of MgSO$_4$, 1 g of NaCl, 1 g of sodium citrate dehydrate, and 0.5 g of sodium hydrogencitrate sesquihydrate) were added, followed by shaking at 1300 rpm for 90 s. After centrifugation at 4000 rpm for 5 min (Combo-408, Hanil Science Inc., Gimpo, Republic of Korea), a 1 mL aliquot of the supernatant was transferred into a d-SPE tube containing 150 mg of MgSO$_4$ and 25 mg of PSA for purification. After shaking at 1300 rpm for 90 s and centrifugation at 13,000 rpm for 3 min, the supernatant was filtered through a 0.2 μm syringe filter. Thereafter, the filtrate (800 μL) was mixed with acetonitrile (200 μL). A 5 μL aliquot of the mixture was injected into a high-performance liquid chromatography-tandem mass spectrometer (HPLC-MS/MS).

2.5. Instrumental Conditions for HPLC-MS/MS Analysis

A Shimadzu Nexera HPLC coupled to a Shimadzu LCMS-8045 triple quadrupole mass spectrometer (Shimadzu Corp., Kyoto, Japan) was used for the analysis of fluopyram in soil and scallion samples. The chromatographic separation was achieved using a Cadenza C18 column (150 mm × 2.0 mm, 3 μm, Imtakt, Portland, OR, USA) at 40 °C with a 0.3 mL/min flow rate. The mobile phase was composed of water (Solvent A) and methanol (Solvent B), containing 0.1% formic acid and 10 mM ammonium formate, respectively. The gradient system of the mobile phase was programmed at a 0.3 mL/min flow rate as follows: 0–2 min, 20% B; 2–5 min, 20–80% B; 5–10 min, 80% B; 10–13 min, 80–20% B; 13–17 min, 20% B. The injection volume was 5 μL. MS/MS detection was achieved in positive ion mode with electrospray ionization (ESI). The source parameters were optimized as follows: desolvation line temperature, 250 °C; interface temperature, 300 °C; heat block temperature, 400 °C; nebulizing gas, 3 L/min; heating gas (air), 10 L/min; drying gas (N$_2$), 10 L/min. In positive ion mode, *m/z* 396.8 was detected as the precursor ion, and *m/z* 173.0 and 144.9 were selected as the quantifier and qualifier at 30 and 50 V of collision energies, respectively. Instrument control, data acquisition, and processing were performed by the Shimadzu LabSolutions software package (ver. 5.97, Shimadzu Corp., Kyoto, Japan).

2.6. Method Validation for Quality Assurance

The analytical method was validated using the following parameters: matrix-dependent limits of quantitation (MLOQs), linearity of matrix-matched calibration curve, and recovery efficiencies, as recommended by the European SANTE/12682/2019 guideline [15]. The instrumental limit of quantitation (ILOQ) was the concentration level with signal-to-noise (S/N) ratio of 10. ILOQ of fluopyram was computed by analyzing matrix-matched working solutions at 0.01–10 μg/L. The MLOQs were determined from the ILOQ, injection volume, dilution factor, sample amount, and extract solvent volume [16]. The linearity was evaluated using the linear regression and coefficient of determination (R^2) at 1–100 μg/L of the matrix-matched working solutions. A calibration curve using matrix-matched working solutions was utilized to quantify the amount of fluopyram in the soil or scallion samples using an external standard calibration method. Procedural blanks and spiked blanks were included as quality control (QC) samples in each batch instrumental analysis. Recovery efficiency assays were performed by spiking standard solutions into control samples at 0.01 (MLOQ), 0.1 (10 MLOQ), and 1.0 (100 MLOQ, only soil) mg/kg, in triplicate. The mean and relative standard deviation (RSD) of the recovery efficiency were calculated to evaluate the accuracy and precision of the analytical method.

2.7. Dissipation Constant and Half-Life for Fluopyram in Soil and Scallions

The dissipation constants for fluopyram in soil and scallion were calculated using a first-order kinetic model using Equation (1) [7,17,18]:

$$C_t = C_0 \times e^{-\lambda t}, \tag{1}$$

where C_t is the concentration of fluopyram in soil or scallions at time t (day), C_0 is the initial concentration of fluopyram in soil or scallion at DAP 0, and λ is the dissipation constant. The half-life (DT$_{50}$) of fluopyram was then calculated using Equation (2) [7,18]:

$$DT_{50} = \ln(2)/\lambda = 0.693/\lambda, \tag{2}$$

The time-dependent residues of fluopyram in soil and scallions were evaluated using the F-test, regression equation, and regression coefficient (R^2). The mean and 95% confidence interval (95% CI) of the dissipation constant (λ) were calculated using regression analysis. Statistical analyses were performed using the statistical program, SPSS 18.0 (SPSS Inc., Arming, NY, USA).

2.8. Calculation of BCFs and Management Concentration in Soil

The concept of BCF was used to calculate the uptake rate of residual fluopyram from the soil into crops [17–19]. The BCF refers to the ratio of the concentration in the organism to the concentration in the environment, in the process of accumulating a specific pollutant in the organism. The BCF was calculated using Equation (3):

$$BCF = C_{plant}/C_{soil}, \tag{3}$$

where C_{plant} is the residual concentration in scallion at DAP 48, which indicated a full-grown (100% mature) scallion, and C_{soil} is the residual concentration in soil on the day of planting (DAP 0).

The management concentration in soil (MC$_{soil}$), which represents the concentration of fluopyram in the soil where the residual pesticide in the crop at harvest does not exceed the MRL, was calculated using Equation (4):

$$MC_{soil} = MRL_{plant}/BCF, \tag{4}$$

where the MRL$_{plant}$ for fluopyram in leaf-and-stem vegetable by unintentional contamination is 0.2 mg/kg [20].

3. Results and Discussion

3.1. Growth of Scallions during the Experiment

The growth characteristics of scallions are shown in Figure 1. Scallion length increased up to DAP 34, but showed no significant increase after DAP 41. Conversely, scallion weight steadily increased during the cultivation period to approximately 9-fold by the DAP 48, as compared to DAP 20. These results highlighted the general growth characteristic of the scallion: as harvest time approaches, the length of the scallion does not increase, but the plant becomes thicker and heavier.

3.2. Validation of the Analytical Method

The method validation was performed according to the European SANTE/12682/2019 guidelines [15]. During the analysis, no peak was detected at the retention time of fluopyram, indicating that there were no interferences affecting its detection. An analyte signal during ionization is enhanced or suppressed due to matrix components co-eluted with the analyte of interest, which is known as the matrix effect. Therefore, a matrix-matched calibration is necessary to compensate for the matrix effect during MS analysis. The MLOQ of fluopyram was calculated to be 0.01 mg/kg for soil and scallions.
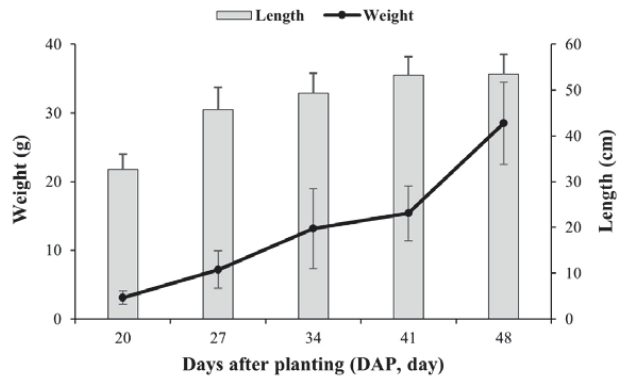
Figure 1. Growth characteristics of scallions during the cultivation period.

The linearity of the matrix-matched calibration curves was good, with $R^2 > 0.9996$ in soil and scallions, which satisfied the criteria of >0.98. As shown in Table 3, the average recovery efficiencies from soil and scallions were 71.3–96.3% with RSDs ranging from 0.4 to 2.2%, which was satisfactory with a recovery of 70–120% and reasonable RSDs $\leq$ 20%. These results demonstrated that the analytical method developed in this study had satisfactory precision and accuracy for quantifying fluopyram residues in soil and scallions.

Table 3. Recovery efficiencies for fluopyram in soil and scallions.

Matrix	Fortification Level (mg/kg)	Recovery (%, Mean $\pm$ SD [1])	MLOQ [2] (mg/kg)
Soil	0.01	71.3 $\pm$ 0.4	0.01
	0.1	90.1 $\pm$ 2.2	
	1.0	91.3 $\pm$ 1.2	
Scallion	0.01	87.5 $\pm$ 0.5	0.01
	0.1	96.3 $\pm$ 1.2	

[1] Mean $\pm$ standard deviation of triplicate samples. [2] Matrix-dependent limits of quantitation.

3.3. Dissipation of Fluopyram in Soil

To investigate the uptake/translocation of pesticide from soil to rotational crops, it is necessary to understand the residual characteristics in the soil by examining pesticide application during the cultivation of the preceding crops. According to the OECD guidelines [14], a suspension solution of fluopyram should be prepared at the maximum label rate (dilution factor 4000) and applied to bare soil for the maximum number of applications (three times). However, the guidelines recommend a single application of the pesticide suspension at the maximum seasonal rate, rather than multiple applications for practical purposes. Therefore, in this study, fluopyram was applied to soil at a treatment level of 0.06 g a.i./m^2. The OECD guidelines suggested plant-back intervals (PBIs) of 30 and 60 days. However, considering the domestic cropping system with a short uncultivated period, the PBI in this study was set at 30 days. The residual amount of fluopyram in soil was calculated in dry weight by correcting for moisture content. The moisture content of soil samples was in the range of 16.2–28.4%. The average residues at DAP 0 were 0.94 and 0.96 mg/kg in trials A and B, respectively, which decreased to 0.80 and 0.69 mg/kg at DAP 48, representing 84% and 72% of the initial residual amount, respectively. The DT$_{50}$ values of fluopyram in soil were 231 (95% CI, 139–347) days and 87 (95% CI, 63–173) days in trials A and B, respectively. These were 2.4–14.6 times longer than 15.8–24.8 days (watermelon) and 36 days (tomato and bell pepper) in soil during fruit vegetable cultivation [7,21]. Generally, pesticides degrade and dissipate in soil owing to biological factors, such as plants and microorganisms, and non-biological factors, including rainfall, irrigation, hydrolysis, and

photolysis [2,22]. However, our results showed that scallion cultivation gave no significant reduction in the fluopyram residue in the soil.

3.4. Uptake of Fluopyram by Scallions from Soil

The residual levels of fluopyram in scallions are shown in Table 4. Fluopyram residues at DAP 20 were 0.35 mg/kg and 0.22 mg/kg in trials A and B, respectively. As the plants reached maturity at DAP 48, residual levels decreased to 0.22 mg/kg and 0.15 mg/kg in trials A and B, which represented 61% and 69.5% of residues at DAP 20, respectively. The dissipation constants calculated using regression analysis were 0.014 (trial A) and 0.016 (trial B), respectively, and there was no significant difference between them (Figure 2A).

Table 4. Residues of fluopyram in field soil and scallions.

| Days after Planting (DAP) | Residue Levels (mg/kg, Mean $\pm$ SD [1]) | | | |
| | Soil | | Scallion | |
	Trial A	Trial B	Trial A	Trial B
0	0.94 $\pm$ 0.03	0.96 $\pm$ 0.04	-	-
20	-	-	0.35 $\pm$ 0.03	0.22 $\pm$ 0.01
27	-	-	0.28 $\pm$ 0.05	0.24 $\pm$ 0.02
34	0.86 $\pm$ 0.01	0.64 $\pm$ 0.02	0.27 $\pm$ 0.09	0.25 $\pm$ 0.03
41	-	-	0.27 $\pm$ 0.09	0.17 $\pm$ 0.01
48	0.80 $\pm$ 0.06	0.69 $\pm$ 0.01	0.22 $\pm$ 0.01	0.15 $\pm$ 0.01

[1] Mean $\pm$ standard deviation of triplicate samples.
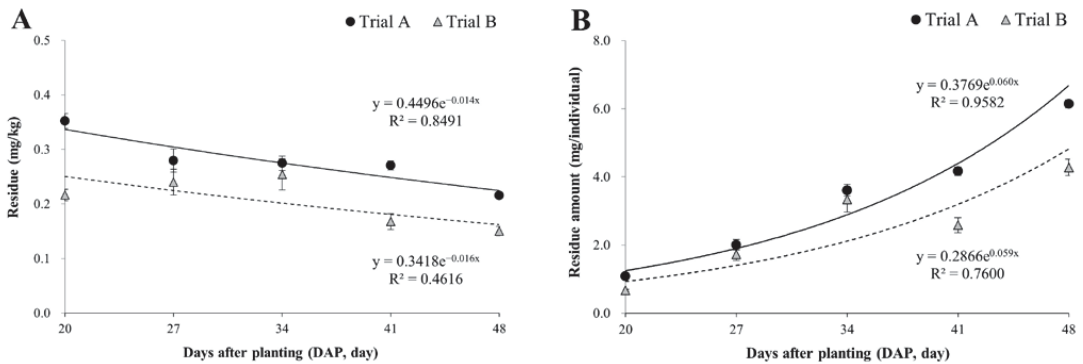
Figure 2. Time-dependent residual patterns of fluopyram in scallions. ((**A**) including dilution effect; and (**B**) excluding dilution effect).

Pesticide residue in crops decreases due to reduction factors such as respiration, volatilization, metabolism, and weight increase through growth [23,24]. In contrast to previous research indicating an increase in residual amounts of fluopyram in tomato and pepper leaves during the cultivation period [7], this study found that decreased fluopyram residual levels in scallions were primarily due to the dilution effect resulting from the 9-fold increase in weight over the 24-day growth period (Figure 1). The residual amount (mg/individual) was calculated to determine the dissipation characteristics, while excluding the dilution effect. As shown in Figure 2B, there was a 5.6 to 6.4-fold increase in individual residues during the 24-day growth period. These results indicated that fluopyram uptake by the roots was greater than dissipation by metabolism, respiration, and other processes. The water solubility and the octanol/water partition coefficient (log K_{ow}) of pesticides are important indicators of their mobility in soil and transportation in plants, since pesticides dissolve in the soil water, also known as the bioavailable portion of soil, and are taken up by plant roots and translocated to the aboveground tissues through

xylem [4]. Fluopyram is classified as readily soluble, with a water solubility of 16 mg/kg and hydrophobic with log K_{ow} of 3.3 [10]. Considering its physico-chemical properties, fluopyram has a higher tendency to accumulate in roots than to be transported from roots to shoots. However, the gradual increase in individual residue levels over time can be attributed to the stability of fluopyram, which does not degrade and instead accumulates in the plant tissue. Therefore, fluopyram has the potential to accumulate through uptake and translocation.

3.5. BCFs and Management Concentration of Fluopyram in Soil

The 95% confidence intervals of the BCF of scallion were determined from soil residues at DAP 0 and scallions at DAP 48, as shown in Table 5. The BCFs of scallions were in the range of 0.21–0.24 and 0.14–0.18 in trials A and B, respectively, which were lower than that of bell pepper leaves (0.32) and higher than that of tomato leaves (0.12) [7]. These results indicate that the uptake and accumulation capacity of fluopyram by scallions was intermediate between that of bell pepper leaves and tomato leaves.

Table 5. Bioconcentration factors (BCFs) of fluopyram calculated from residue estimates (95% confidence interval) in soil and scallions.

Trials	C_{soil} (mg/kg)	C_{plant} (mg/kg)	BCF
A	0.90–0.99	0.21–0.22	0.21–0.24
B	0.88–1.04	0.13–0.17	0.14–0.18

Based on the MRL in the crop and BCFs in this study, the management concentration in soil (MC_{soil}) was determined, which is the maximum tolerable level in soil caused by pesticides used during the cultivation of the preceding crop, thereby minimizing residual pesticide levels in rotational crops grown in contaminated soils and producing safe agricultural commodities. In the Republic of Korea, the MRL for fluopyram arising from unintentional contamination is set at 0.2 mg/kg for leaf-and-stem vegetables, including scallions. The minimum MC_{soil} for fluopyram was calculated as 0.83 mg/kg from the upper 95% confidence limit of the BCF. Therefore, the management concentration for fluopyram in the soil is proposed as less than 0.8 mg/kg. This threshold for fluopyram in the soil is likely to be set as a precautionary measure to ensure that scallions grown in soil contaminated with fluopyram will not be exposed to the MRL in scallions. If the concentration of fluopyram in the soil is found to be higher than the proposed management level of 0.8 mg/kg, appropriate measures should be taken to mitigate the associated risks. These measures may include delaying planting of seedlings, tillage, and soil dressing. These actions are generally taken to reduce the level of fluopyram in the soil to an acceptable level, in order to protect the rotational crops and the environment.

4. Conclusions

This study investigated the residue pattern of fluopyram, in terms of the bioconcentration factor, in soil and its uptake by scallions during greenhouse cultivation. Residues in the soil and scallions were measured using a modified QuEChERS method coupled with HPLC-MS/MS and validated according to the European SANTE/12682/2019 guidelines. Fluopyram residues in soil showed limited dissipation during cultivation, with a DT_{50} of 87–231 days. The DT_{50} values were found to be higher than that reported for other crops in the previous literature, indicating that fluopyram may be a persistent pollutant in the environment. Fluopyram in soil was taken up by scallions through the roots, but residual levels in scallions during cultivation decreased due to an increase in plant weight, which caused a dilution effect. The peak BCF was estimated as 0.24. Using the BCFs, the MC_{soil} was determined as 0.8 mg/kg to avoid exceeding the MRL (0.2 mg/kg) for scallions. Continuous monitoring and management of residual fluopyram in soil is necessary to

ensure compliance with MRLs, since this fungicide has the potential to persist for extended periods of time.

References

1. Kim, S.-S.; Kim, T.-H.; Lee, S.-M.; Park, D.-S.; Zhu, Y.-J.; Hur, J.-H. Mobility of pesticides in different slopes and soil collected from Gangwon alpine sloped-land under simulated rainfall conditions. *Korean J. Pest. Sci.* **2005**, *9*, 316–329.
2. Lee, K.-S. Behavior of pesticides in soil. *Korean J. Pest. Sci.* **2010**, *14*, 303–317.
3. Lee, J.-Y.; Noh, H.-H.; Lee, K.-H.; Park, H.-K.; Oh, J.-H.; Im, M.-H.; Kwon, C.-H.; Lee, J.-K.; Woo, H.-D.; Kwon, K.-S.; et al. Processing factors of azoxystrobin in processed ginseng products. *Korean J. Pest. Sci.* **2012**, *16*, 222–229. [CrossRef]
4. Wang, F.; Li, X.; Yu, S.; He, S.; Cao, D.; Yao, S.; Fang, H.; Yu, Y. Chemical factors affecting uptake and translocation of six pesticides in soil by maize (*Zea mays* L.). *J. Hazard Mater.* **2021**, *405*, 124269. [CrossRef] [PubMed]
5. Jeon, S.-O.; Hwang, J.-I.; Lee, S.-H.; Kim, J.-E. Uptake of boscalid and chlorfenapyr residues in soil into Korean cabbage. *Korean J. Pest. Sci.* **2014**, *18*, 314–320. [CrossRef]
6. Hwang, J.-I.; Lee, S.-E.; Kim, J.-E. Plant uptake and distribution of endosulfan and its sulfate metabolite persisted in soil. *PLoS ONE* **2015**, *10*, 11. [CrossRef] [PubMed]
7. Matadha, N.-Y.; Mohapatra, S.; Siddamallaiah, L.; Udupi, V.-R.; Gadigeppa, S.; Raja, D.-P. Uptake and distribution of fluopyram and tebuconazole residues in tomato and bell pepper plant tissues. *Environ. Sci. Pollut. Res.* **2019**, *26*, 6077–6086. [CrossRef] [PubMed]
8. Veloukas, T.; Karaoglanidis, G.-S. Biological activity of the succinate dehydrogenase inhibitor fluopyram against *Botrytis cinerea* and fungal baseline sensitivity. *Pest Man. Sci.* **2012**, *68*, 858–864. [CrossRef] [PubMed]
9. European Food Safety Authority. Conclusion on the peer review of the pesticide risk assessment of the active substance fluopyram. *EFSA J.* **2013**, *11*, 3052.
10. Turner, J.-A. *The Pesticide Manual*, 18th ed.; British Crop Production Council, Alton: Hamsphire, UK, 2018; pp. 527–528.
11. Ministry of Agricultural, Food and Rural Affairs. *Guide to the Correct Use of Pesticide by Item*; PES: Sejong, Republic of Korea, 2020. Available online: https://www.mafra.go.kr/bbs/PLS/351/331171/artclView.do (accessed on 23 March 2023).
12. Ministry of Agricultural. *Food and Rural Affairs. 2020 Status of Greenhouse Facilities for Vegetable Cultivation and Their Production performance*; Ministry of Agricultural: Sejong, Republic of Korea, 2021. Available online: https://www.mafra.go.kr/bbs/mafra/131/328839/artclView.do (accessed on 23 March 2023).
13. Rural Development Administration. *Comprehensive Laboratory Analysis Manual*; Rural Development Administration: Jeonju, Republic of Korea, 2017. Available online: https://lib.rda.go.kr/search/mediaView.do?mets_no=000000300087 (accessed on 23 March 2023).
14. Organisation for Economic Co-operation and Development. *Guidance Document on Residues in Rotational Crops*; Series on Pesticides No. 97 and Series on Testing & Assessment No. 279. ENV/JM/MONO(2018)9; Organisation for Economic Co-Operation and Development: Paris, France, 2018. Available online: https://www.oecd.org/chemicalsafety/guidance-document-on-residues-in-rotational-crops-99457f3f-en.htm (accessed on 23 March 2023).
15. European Commission. *Analytical Quality Control and Method Validation Procedures for Pesticide Residues Analysis in Food and Feed*; Document No. SANTE/12682/2019; European Commission Directorate General for Health and Food Safety: Brussels, Belgium, 2019. Available online: https://www.eurl-pesticides.eu/userfiles/file/EurlALL/AqcGuidance_SANTE_2019_12682.pdf (accessed on 23 March 2023).
16. Choi, H.; Moon, J.-K.; Kim, J.-H. Assessment of the exposure of workers to the insecticide imidacloprid during application on various field crops by a hand-held power sprayer. *J. Agric. Food Chem.* **2013**, *61*, 10642–10648. [CrossRef] [PubMed]
17. Li, Z. Approximate modeling of the uptake of pesticides by grass for grazing risk assessment and pasture management. *ACS Agric. Sci. Technol.* **2021**, *1*, 338–346. [CrossRef]
18. Yuan, X.; Lee, J.; Han, H.; Ju, B.; Park, E.; Shin, Y.-H.; Lee, J.-H.; Kim, J.-H. Translocation of residual ethoprophos and tricyclazole from soil to spinach. *Appl. Biol. Chem.* **2021**, *64*, 47. [CrossRef]

19. Choi, G.-H.; Lee, D.-Y.; Seo, D.-C.; Kim, L.; Lim, S.-J.; Ryu, S.-H.; Park, B.-J.; Kim, J.-H.; Kim, J.-H. Endosulfan plant uptake suppression effect on char amendment in oriental radish. *Water Air Soil Pollut.* **2018**, *229*, 24. [CrossRef]
20. Ministry for Food and Drug Safety. *Food Code*; Ministry for Food and Drug Safety: Cheongju, Republic of Korea, 2023. Available online: https://various.foodsafetykorea.go.kr/fsd/#/ext/Document/FC (accessed on 23 March 2023).
21. Dong, B.; Hu, J. Dissipation and residue determination of fluopyram and tebuconazole residues in watermelon and soil by GCMS. *Intern. J. Environ. Anal. Chem.* **2014**, *94*, 493–505. [CrossRef]
22. Pérez-Rodríguez, P.; Schmitt, A.-D.; Gangloff, S.; Masbou, J.; Imfelda, G. Plants affect the dissipation and leaching of anilide pesticides in soil mesocosms: Insights from compound-specific isotope analysis (CSIA). *Agric. Ecosyst. Environ.* **2021**, *308*, 107257. [CrossRef]
23. Fantke, P.; Gillespie, B.-W.; Juraske, R.; Jolliet, O. Estimating half-lives for pesticide dissipation from plants. *Environ. Sci. Technol.* **2014**, *48*, 8588–8602. [CrossRef] [PubMed]
24. Fu, D.; Zhang, S.; Wang, M.; Liang, X.; Xie, Y.; Zhang, Y.; Zhang, C. Dissipation behavior, residue distribution and dietary risk assessment of cyromazine, acetamiprid and their mixture in cowpea and cowpea field soil. *J. Sci. Food. Agric.* **2020**, *100*, 4540–4548. [CrossRef] [PubMed]

Article

Analysis of Endocrine Disrupting Nonylphenols in Foods by Gas Chromatography-Mass Spectrometry

Sang Mi Lee [1,†], Daeun Cheong [2,†], Meehye Kim [2] and Young-Suk Kim [2,*]

1   Department of Food and Nutrition, Inha University, Incheon 22212, Republic of Korea
2   Department of Food Science and Biotechnology, Ewha Womans University, Seoul 03760, Republic of Korea
*   Correspondence: yskim10@ewha.ac.kr; Tel.: +82-2-3277-3091
†   These authors contributed equally to this work.

Abstract: Nonylphenols (NPs) are classified as endocrine-disrupting chemicals (EDCs), which are known to cause disorders in the endocrine systems of organisms. Due to their high lipophilicity and low degradability, these harmful substances are known to accumulate and persist in the environment, and even enter into the food chain. Analytical methods of liquid–liquid extraction using solid-phase extraction for sample clean-up combined with gas chromatography/mass spectrometry were established to determine the presence of NPs in foods. This study aimed to develop and validate these methods using four food matrices representing high-fat and low-fat solid food, as well as high-fat and low-fat liquid food, groups. The single linear isomer 4-n-NP was used to validate the quantification of NPs, which exist in complex isomer mixtures. Our results showed good linearity, with correlation coefficients exceeding 0.998 for all four matrices. The limits of detection and quantification were 0.37–1.79 and 1.11–5.41 µg/kg, respectively. Recovery rates were 86.8–108.6% and 92.6–101.9% for intraday and interday assays, respectively, and the relative standard deviations (RSDs) were below 12% for both assays. The method was applied to analyze 1185 domestic food samples consumed by Koreans, with NPs detected at concentration ranges of 2.57–269.07 µg/kg. Results for each food type over wide concentration ranges indicated that these compounds are highly dependent on the area of cultivation, and are affected by the levels of those contaminants in different environments. The contents of NPs in foods from animal sources were generally higher than those from plant sources, in particular being higher in the intestines than in lean tissue. The present findings could form the basis for determining the level of dietary exposure to NPs and how each food source contributes to it in South Korea.

Keywords: nonylphenols; endocrine disrupting chemical; gas chromatography-mass spectrometry; food

1. Introduction

Nonylphenols (NPs) are persistent and hazardous endocrine-disrupting chemicals (EDCs), which are found in a variety of environmental matrices, including foods, human tissue samples, and blood [1]. EDCs can disrupt hormone biosynthesis, metabolism, or function by causing a disruption in normal homeostasis or reproduction [2]. These compounds interfere with the endocrine system by imitating or suppressing endogenous hormones, resulting in hormonal dysfunction and deleterious effects on living organisms. By competing with natural estrogen for estrogen receptor bindings, NP especially hinders the estrogenic balance in organisms [3]. NPs are a complex mixture of compounds composed of isomers with differently branched carbon side and linear chains, and there can, theoretically, be more than 200 constitutional isomers [4]. Linear 4-n-nonylphenol (4-n-NP) is the least active of the individual isomers, and its relative potency is known to increase with higher levels of nonyl-branching side chains [5]. Different degrading behaviors in these isomer forms of NP have been observed in soil and aquatic environments, with linear NPs degrading more rapidly than branched NPs [6].

Nonylphenol polyethoxylates (NPEOs) are nonionic surfactants that are widely used for detergent, pesticide, and emulsifier production. They are biodegraded into shorter chain compounds and NPs, which do not have ethoxyl groups, under certain conditions [7]. Effluents from sewage treatment plants, industrial discharges, and municipal waste streams are the main sources of these compounds in aquatic ecosystems. During sewage treatment, NPEOs are biodegraded by hydrolytic cleavage of ethoxylate groups into short-chain ethoxylates, and finally to alkylphenols, resulting in the formation of progressively more lipophilic and persistent metabolites. De-ethoxylated NP is more resistant to biodegradation than compounds with long-chain ethoxylates. NPs and NPEOs are persistent in aquatic environments, moderately bioaccumulative, and severely toxic to aquatic organisms, which means that their commercial manufacturing, processing, and distribution pose potential ecological threats.

Humans are exposed to NPs primarily through the intake of contaminated food and water. NPs are particularly known to be present in fish and shellfish due to their exposure to aquatic environments. NPs can also be introduced to soil used for producing crops and grazing livestock when sewage sludge is applied to agricultural land. Through these diverse pathways, NPs remain in the environment, enter the food chain, and finally accumulate in lipid-rich matrices including fish and edible oil [8]. NPs can accumulate in the internal organs of fish, reaching concentrations 10 to 100 times higher than those observed in the environment, due to their strong stability and solubility in lipids. They can then be readily transferred to humans through the food chain. Notably, NP bioaccumulation has been reported in humans, with accumulation values of 57 and 37 ng/g in the adipose tissue of humans and cadaver samples, respectively [9]. NPs were also found in every urine sample examined in a recent investigation conducted in Taiwan, with concentrations ranging from 0.65 to 6.69 ng/mL, demonstrating the human exposure to these types of EDCs [10].

Because of their low cost and high availability, traditional sample treatment techniques with long analysis times and waste production have been used to determine alkylphenols in samples. Conventional procedures, such as Soxhlet extraction, require analysis times from 10 to 48 h [11]. Alkylphenols have also been extracted from food and environmental samples using steam distillation. Despite steam distillation being known to be more simple than Soxhlet extraction, it is also laborious and time-consuming. To develop a simple and efficient method for analyzing NPs, particularly in high-fat food samples, solid-phase extraction (SPE) was combined with liquid–liquid extraction to reduce the isolation time for analytes. Due to its versatility, SPE has been widely used to separate and enrich NPEOs and their degradation products, NPs, from food and environmental matrices. Many SPE procedures have been devised using various sorbents with many variables, such as SPE sorbent and eluent types, potentially influencing the recovery of target compounds [12].

Since there was no literature on monitoring NP contents in foods from Korean markets, it was necessary to determine the concentrations of NPs in various food groups based on national consumption. Previous studies on NPs in foods are also scarce, although one of the major exposure routes to humans was oral food ingestion. The objective of the present study was to develop, optimize, and validate a simple, efficient, and sensitive integrated analysis method to determine NPs in high-fat and low-fat matrices. The established method was further applied to analyze the concentrations of NPs in 1185 food samples categorized as aquatic, livestock, and agricultural products.

2. Materials and Methods

2.1. Chemicals and Reagents

Nonylphenols (PESTANAL®, analytical standard, technical mixture, purity 96.8%) and 4-n-nonylphenol (PESTANAL®, analytical standard, purity 99.9%) were purchased from Sigma-Aldrich (Saint Louis, MO, USA). 4-n-nonylphenol RING-$^{13}C_6$ 100 µg/mL in nonane was purchased from Cambridge Isotope Laboratories (Tewksbury, MA, USA, purity 99.9%). Methylene chloride, acetonitrile, methanol, and hexane were acquired from J.T. Baker (Philipsburg, NJ, USA). Mega Bond Elut-C18 OH (1 g, 6 mL) was purchased from

Agilent (Santa Clara, CA, USA). Visiprep™ SPE Vacuum Manifold and disposable liners for SPE Vacuum Manifold were obtained from Supelco (Saint Louis, MO, USA).

2.2. Sample Selection and Preparation

The food samples for analysis were selected based on the "National Nutrition Statistics, Food Consumption Distribution" document published by the Korea Health Industry Development Institute (2017). Based on consumption rates and detection levels from previous studies, 79 food categories were chosen. Six major cities in Korea (Seoul, Busan, Incheon, Daegu, Daejeon, and Gwangju) were selected based on the population status data of the local government. Samples were all collected on the same day from marts and markets with high average annual sales in each city. Foods from each category were purchased from 15 different markets nationwide.

Food samples used for monitoring were analyzed in raw conditions, without having received treatments such as cooking or seasoning, and only the edible portions were separated and pretreated. Each sample was treated and homogenized using liquid nitrogen and a blender (Nutri Ninja Auto iQ, Hai Xin Technology), respectively. Each homogenized sample was placed and sealed in a separate HDPE bottle, then stored at –70°C in a deep freezer until the analysis.

2.3. Food Matrix Types

Food matrices were divided into high-fat and low-fat groups. The foods representing each matrix were as follows: high-fat solid, infant purée; high-fat liquid, olive oil; low-fat solid, enoki mushroom; and low-fat liquid, 7.00% ethanol solution. These matrices were selected based on the lipid contents from the standard guidelines of the Korean Total Diet Study by the Korean Ministry of Food and Drug Safety. Although 7% ethanol solution was not a real food, it was selected for the matrix of low fat liquid foods. The 7% ethanol content is in the range of commercial liquor products in Korea, which would represent alcoholic beverages. The additional advantage of its use would be less contamination of nonylphenols compared to other food matrices.

2.4. Preparation of Standards

A stock solution of 4-n-NP (1.00×10^3 µg/mL) was prepared by dissolving 0.01 g of 4-n-NP using 10.0 mL of methanol. A working solution (100 µg/mL) was prepared with a methanol dilution 10 times higher than the stock solution.

An internal standard 4-n-NP RING-$^{13}C_6$ (10.0 µg/mL in methanol) was prepared by diluting 1.00×10^2 µg/mL in nonane using methanol. Regarding the standard curve of the low-fat matrix, standard solutions of 4-n-NP were spiked at concentrations of 1.00×10^1, 2.00×10^1, 1.00×10^2, 5.00×10^2, and 1.00×10^3 ng/mL; for the standard curve of the high-fat matrix, standard solutions of 4-n-NP were spiked at concentrations of 1.00×10^2, 2.00×10^2, 5.00×10^2, 1.00×10^3, and 2.00×10^3 ng/mL.

2.5. Analysis Methods for Each Matrix

Analytical procedures for low-fat and high-fat matrices were based on the official ES 04613.1 method of the National Institute of Environmental Research (2017) and a modified version of another previous method [13].

For high-fat matrices, a 20.0-µL working solution of 4-n-NP RING-$^{13}C_6$ was added to 3.00 g of infant purée, along with 9.00 mL of acetonitrile. After vortexing the mixture for 1 min, the mixture was centrifuged at $1977 \times g$ at 0 °C for 5 min. The acetonitrile phase mixture was then collected. The mixture was extracted again using 9 mL of acetonitrile, as described above. The acetonitrile phase mixture was obtained and combined with the previously collected acetonitrile. After adding Mega Bond Elut-C18 OH combined with disposable liners to the Visiprep™ SPE Vacuum Manifold, the SPE cartridge was activated with 5.00 mL of both methylene chloride and acetonitrile. From this mixture, 3.00 mL of collected acetonitrile was extracted and poured into the activated cartridge. The analyte

was eluted with 5.00 mL of acetonitrile. The collected elution was completely evaporated using N_2 flow, and the residue was redissolved with 0.300 mL of hexane. The procedure described above was used to prepare 3.00 g of olive oil.

For low-fat matrices, a working solution of 10.0 µL of 4-n-NP RING-$^{13}C_6$ was added to 3.00 g of enoki mushroom in a separatory funnel. The mixture was added to 20.0 mL of methylene chloride for liquid–liquid extraction. The separatory funnel was agitated vigorously using a vertical shaker for 20 min. After separating the methylene chloride from the mixture, the collected elution was completely evaporated using N_2 flow. The dried residue was redissolved with 0.300 mL of methanol. The procedure described above was used to prepare 3.00 g of 7.00% ethanol solution.

2.6. Evaluation of Procedural Blanks

Due to the widespread usage of NP-containing substances, including consumer goods, NPs are often present in laboratory environments. These environments are also susceptible to contamination from external sources [5]. Both NPs and their parent compounds, NPEOs, are, therefore, ubiquitous in the environment due to the increasing production volumes of NPs in industry [14]. Special precautions are, therefore, required to prevent contamination during experiments [13]. NP residues were regularly present in the blank samples in this study to ensure that these compounds were not contaminated during the experiment procedure. To minimize contamination during the experiment and to properly control the procedural blank, glassware was mostly used throughout the experiments. Procedural blanks were analyzed to evaluate the analytical methods of the high-fat and low-fat matrices. The analytical procedure was identical to that illustrated above, except for the sample addition. Procedural blanks were analyzed using gas chromatography/mass spectrometry (GC-MS) as described below.

2.7. Instrument Analysis

The samples were analyzed using a 7890A gas chromatograph with a 5977B mass spectrometer. A DB-5ms capillary column was used for separation. Helium (99.9999% purity) was used as a carrier gas, with a 0.8 mL/min constant flow rate. Injection and ion source temperatures were set at 230 °C. The oven temperature program was as follows: initial temperature of 80 °C, 10 °C/min increase to 180 °C, 3 /min increase to 240 °C, and finally a post run at 250 °C for 15 min. The 1.0-µL sample volume was injected in splitless mode.

The mass spectrometer was operated in its SIM mode for quantification. The monitored fragment ions had m/z values of 121, 135, 149, and 163 for NP, m/z values of 107 and 220 for 4-n-NP, and m/z values of 113 and 226 for 4-n-NP RING-$^{13}C_6$.

The retention time and the qualifier and quantifier ions of each compound are listed in Table 1. The total ion chromatogram of analytes and the chromatogram of selected ions for 4-n-NP and 4-n-NP $^{13}C_6$ are shown in Figures 1 and 2, respectively.

Table 1. Mass spectral parameter of the analyzed compounds.

Compound	Abbreviation	Retention Times	Qualifier Ions	Quantifier Ions
Nonylphenol	NP	12.0–13.7	121, 149, 163	135
4-n-nonylphenol	4-n-NP	15.6	220	107
4-n-nonylphenol $^{13}C_6$ *	4-n-NP $^{13}C_6$	15.6	226	113

* Internal Standard.
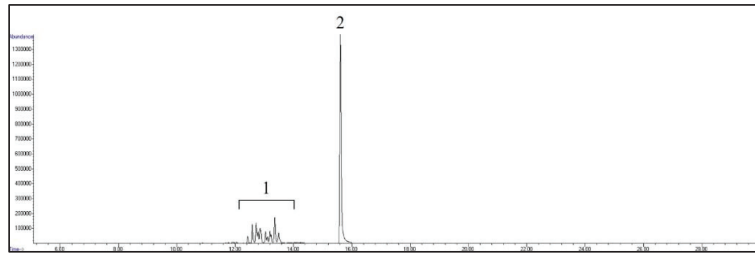
Figure 1. GC/MS total ion chromatogram of analytes. Peaks: 1, NPs; 2, 4-n-NP and 4-n-NP [13]C$_6$.
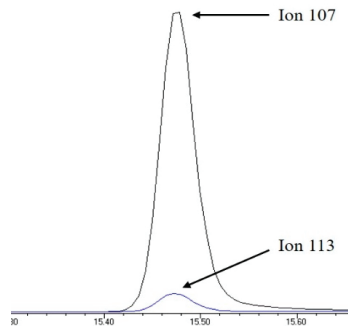
Figure 2. Selected ion chromatogram of quantifier ions for 4-n-NP and 4-n-NP [13]C$_6$.

2.8. Validation Method

NPs are frequently regarded as a single compound when their environmental occurrence, transit, removal, and toxicity are investigated. However, technical NPs comprise a mixture of over 100 isomers and congeners with different side chain lengths and branches [15]. The NP chromatogram presents more than 10 isomer peaks with various nonyl substituent branching configurations. Due to the characteristic of NPs being present in more than 100 isomers, some of the individual peaks can contain several isomers and are, therefore, not pure compounds. Furthermore, their compositions vary between manufacturers, and the concentration and exact type of each isomer are unknown [16]. The concentration and type for each isomer in standard branched NP chemicals used for the present investigation were also not identified.

Individual NPs are not commercially accessible, and the standard chemical is a mixture of isomers with alkyl groups with varying branches. Validation for the analysis and calibration curve, therefore, proceeded with 4-n-NP, a single linear compound whose concentration can be accurately determined, instead of branched NPs. The proposed analytical method was validated in terms of its linearity, accuracy, precision, and repeatability.

For high-fat matrices, the linearity of the calibration curve was determined at five points (n = 3), with concentrations of 4-n-NP ranging from 1.00×10^2 to 2.00×10^3 ng/mL at five points (1.00×10^2, 2.00×10^2, 5.00×10^2, 1.00×10^3, and 2.00×10^3 ng/mL), while for low-fat matrices, it ranged from 1.00×10^1 to 1.00×10^3 ng/mL at five points (1.00×10^1, 2.00×10^1, 1.00×10^2, 5.00×10^2, and 1.00×10^3 ng/mL). A calibration curve was obtained using the peak area and concentration ratio of 4-n-NP to 4-n-NP [13]C$_6$.

To determine the sensitivity of the method, the limit of detection (LOD) and limit of quantification (LOQ) were determined as follows:

$$\text{LOD} = 3.3\sigma/S \quad \text{LOQ} = 10\sigma/S$$

where S is the standard curve slope and σ is the RSD of the y-intercept.

Accuracy and precision were calculated as a percentage of spiked 4-n-NP in each matrix, and then compared with the AOAC guideline standard value (AOAC, 2012). Internal standards as well as 4-n-NP at three different concentrations were added to each sample. Intraday and interday precision and accuracy were validated by determining analytes in three replicates at the nominal concentrations on three consecutive days. The nominal concentrations were 5.00×10^2, 1.00×10^3, and 2.00×10^3 ng/mL for the high-fat matrices, and 1.00×10^2, 5.00×10^2, and 1.00×10^3 ng/mL for the low-fat matrices. Precision was calculated as the RSD by dividing the standard deviation by the mean, while measurement accuracy was determined by expressing the calculated concentration as a percentage of the nominal concentration.

2.9. Identification and Quantification of Branched NPs

NPs were identified by their retention times, and the quantifier and qualifier ions by standard chemicals. Branched NP concentrations were obtained by summing the isomers. For NP quantification in 1185 food samples, the calibration curve obtained using 4-n-NP and relative detected responses of linear and branched compounds was used. The relative response factor was calculated with respect to the area of corresponding analytes with equivalent amounts, in order to convert the concentration obtained using linear 4-n-NP into the total concentration of branched NP isomers. The recovery rates for conversion from 4-n-NP to NPs, which are both composed of isomers, were assumed to be identical, and only detected response values were considered [17].

2.10. Statistical Analysis

All experiments were performed once per sample without replications, and thus, we were unable show reproducibility and precision in the analysis of the samples, although our analytical method was validated as explained earlier. The values of NPs were presented as average $\pm$ standard deviation of independent data from 15 different samples for each food type. SPSS (version 12.0, Chicago, IL, USA) was used for statistical results.

3. Results and Discussion

3.1. Method Validation

The linearity of each matrix was verified at five 4-n-NP different concentrations. All four matrices had correlation coefficients exceeding 0.998. The LOD and LOQ values for 4-n-NP were 0.37–1.79 and 1.11–5.41 µg/kg, respectively. The low-fat matrices had lower LOD and LOQ values than the high-fat matrices. The LOD and LOQ values were comparable to or lower than those in the corresponding matrices of previous investigations, with values of 0.83 and 2.5 µg/kg, respectively, for vegetable oils, 1.3 and 4.4 µg/kg for baby food, 1.3 and 3.9 µg/kg for beverages, and 0.3 and 1.0 µg/kg for vegetables and fruits [2]. Table 2 lists the results for linearity, LOD, and LOQ.

Table 2. Linearity, LOD, and LOQ for 4-n-NP in food matrices.

Food Type	Matrix	Standard Curve	Linearity (R^2)	LOD (µg/kg)	LOQ (µg/kg)
High-fat	Infant puree	$y = 2.85\,x + 1.72 \times 10^{-1}$	9.98×10^{-1}	1.79	5.41
	Olive oil	$y = 2.95\,x + 8.98 \times 10^{-3}$	9.99×10^{-1}	6.39×10^{-1}	1.94
Low-fat	Enoki mushroom	$y = 1.96\,x + 5.04 \times 10^{-2}$	9.98×10^{-1}	3.66×10^{-1}	1.11
	7% ethanol	$y = 2.31\,x + 8.86 \times 10^{-2}$	9.99×10^{-1}	3.82×10^{-1}	1.16

The accuracies of the high-fat matrices were 91.8–108.6% and 94.6–101.9% for intraday and interday assays of 4-n-NP, respectively; the corresponding values for the low-fat matrices were 86.8–107.3% and 92.6–101.3%. The accuracies of the high-fat matrices were 1.80–9.68% and 5.42–6.43% for intraday and interday assays of 4-n-NP, respectively; the

corresponding values for the low-fat matrices were 0.67–11.83% and 1.65–10.45%. Table 3 lists the results for accuracy and precision.

Table 3. Accuracy and precision for 4-n-NP in four food matrices (*n* = 3).

Matrix	Nominal Concentration (ng/mL)	Intraday 1		Intraday 2		Intraday 3		Interday	
		Accuracy (%)	Precision (% RSD)	Accuracy (%)	Precision (% RSD)	Accuracy (%)	Precision (% RSD)	Accuracy (%)	Precision (% RSD)
Puree	500	97.2	7.68	92.8	7.19	93.9	6.05	94.6	6.43
	1000	95.9	4.12	93.0	4.95	101.0	5.23	96.6	5.53
	2000	103.7	7.16	97.7	4.07	104.2	3.41	101.9	5.42
Olive oil	500	97.1	9.68	91.8	4.25	97.7	2.51	95.5	6.23
	1000	95.4	2.00	97.7	7.72	99.8	7.10	97.6	5.74
	2000	98.0	2.64	108.6	1.80	97.4	2.98	101.3	5.80
Enoki mushroom	100	102.5	11.32	88.7	0.67	86.8	6.44	92.6	10.45
	500	107.3	6.45	99.8	11.83	93.9	6.12	100.3	9.36
	1000	92.9	5.88	97.9	8.19	103.3	4.68	98.0	7.16
7% EtOH	100	100.5	2.08	100.7	1.76	99.1	1.14	100.1	1.65
	500	102.8	2.72	99.3	4.60	101.9	3.80	101.3	3.61
	1000	100.3	4.30	99.6	1.50	101.0	1.63	100.3	2.49

3.2. Procedural Blanks

Procedural blanks were monitored regularly to inspect NP contamination sources during the experiments. The blank values for all matrices were meant to be lower than detectable levels for each matrix. In this study, the results of the procedural blank evaluation demonstrated that the blank NP values were all below the detection limit of the method.

3.3. NP Monitoring in Diverse Food Samples

The established analysis method was applied to 1185 food samples to determine NP concentrations. Results for each food group are listed in Table 4. NP contents appeared to be higher in aquatic products than in other food groups, such as agricultural and livestock products. Due to their lipophilic and bioaccumulative properties, alkylphenols remain in the fat tissue of animals throughout the food chain [8]. The NP levels of foods from animal sources were found to be higher than those from vegetables and fruits in Taiwan [8].

NP concentrations varied between species (Tables S1–S3). The concentration ranges for all aquatic products were wide, and the standard deviations were large even within the same food type. Many factors are expected to affect this heterogeneity of the NPs, including feeding patterns and metabolism, degrees of pollution levels in specific habitats, biotransformation, and excretion capabilities. Among these various factors, the habitat environments of each aquatic organism seemed to be a major cause of NP contamination. For example, eels collected from three distinct areas of lagoons and lakes in Poland had varying NP levels, demonstrating that NP concentrations in fish were highly dependent on the sampling area [18]. The alkylphenol concentrations in fish intestines were also closely related to how close sampling sites were to sewage treatment plants. The first sampling site downstream of a treatment plant had the highest NP levels, which declined as the distance from the plant increased. The number of samples was limited, and they were pretreated as pooled samples rather than individual liver samples, making specific correlations with environmental data unclear. However, NP concentrations appeared to follow a similar pattern as the ambient data [19]. Furthermore, different species of wild freshwater and marine fish from the same river or harbor had varying NP concentrations, implying that the potential of fish species for NP bioaccumulation may depend on habitat conditions, the metabolic activity of each aquatic organism, and their feeding strategy [20].

Table 4. Concentration of NPs in food groups.

Food Category	NPs (µg/kg)	
	Mean	Min~Max
Shellfish	21.27	N.D. *~72.80
Cephalopods	4.65	N.D.~41.89
Crustaceans	58.64	N.D.~252.65
Fresh water and saltwater fish	11.44	N.D.~68.78
Marine algae *	75.62	N.D.~269.07
Poultry	14.02	N.D.~50.59
Livestock	18.36	N.D.~227.06
Eggs	2.17	N.D.~7.36
Oils and fats	0.15	N.D.~1.14
Whole grains	7.34	3.26~23.08
Legumes	16.28	5.32~36.58
Root and tuber crops	34.70	9.54~69.27
Vegetables	19.88	2.68~123.91
Mushrooms	7.88	N.D.~39.22
Fruits	7.92	3.17~31.68
Nuts	3.82	N.D.~14.30

* N.D.: lower than the limit of detection.

NP concentrations in blue crabs, kelps, and seaweeds among marine algae were found to be relatively high, with mean levels around or higher than 100 µg/kg. Blue crabs, in particular, are known to be inhabitants of benthic environments and sediment dwellers, making them vulnerable to estrogenic chemicals that are substantially concentrated in the sediments below the water [21]. In sediment samples of the coast of Hong Kong, NPs were found in higher concentrations than in water samples, with average values ranging from 3–8 times higher [22]. Because these species experience direct contact with sediments, they are likely to absorb a considerable amount of NPs. In kelps and seaweeds, NPs would be enriched due to the absorption of these compounds, which is a similar tendency to the concentration of seaweed samples from China [23].

The present study performed NP analysis for each individual part of the cod and pollock fish, which revealed different concentrations. The NP contents in the intestines and eggs of cod and pollock were significantly higher than those in their flesh. The concentration distributions of each sample type are shown in Figure 3. A recent study found that the average content in flounder livers was 10.7 times higher than that in flounder muscles, while it was 4.3~19.1 times higher in eel livers than in eel muscles [18], which was a similar tendency to that found in the present study.

Our results indicate that NPs in fish flesh, which is primarily composed of muscles, are more stable and less varied than in the intestines, suggesting that these chemicals do not readily metabolize in the muscles. Low concentrations in the flesh may be attributed to their effective absorption and elimination by the liver and kidneys, as well as a lack of blood flow to the muscles. A smaller deviation in the concentrations of these compounds was observed in the flesh, which possibly indicates that NPs in fish muscles mostly come from the water. Chemical absorption from water is constant and unaffected by the diet or the availability of food for the fish. Because NPs are pollutants metabolized by fish, their levels in tissues vary depending on various factors, such as the routes and metabolic rates of NPs and the reproductive maturity and feeding behaviors of the fish [18]. This makes comparisons of the levels of these compounds between fish species or fish captured in different aquatic basins challenging.
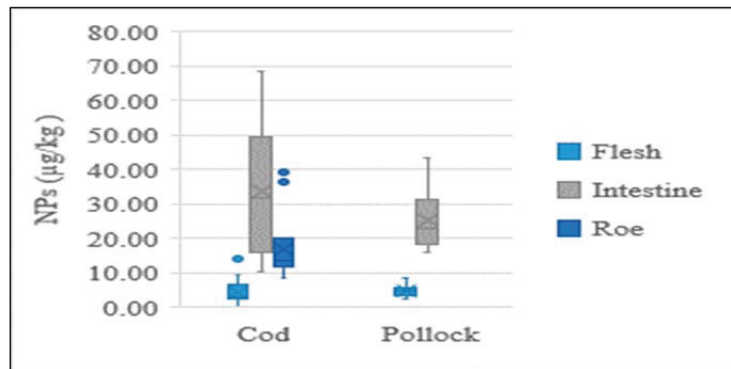
Figure 3. Average concentration of NPs in flesh, intestine, and roe of fish.

In a previous study, the total concentration of NP compounds analyzed in freshwater fish from other contaminated sites was as high as 5 µg/g (wet), while NPs in carps and yellow perches ranged from 18 to 2075 ng/g (wet). The presence of high quantities of NP compounds in fish suggest that they are persistent, hydrophobic, and bioaccumulative in aquatic organisms [24]. Once NPEOs enter the sediment, their degradation half-life is estimated to be approximately 60 years [25]. The presence of NPs in the environment will, therefore, continue to affect living organisms, which will consequently remain in the food chain as people consume food.

For livestock products, two key factors are expected to contribute to contamination of NPs: (1) bioaccumulation of compounds throughout the food chain and (2) migration from plastics used for packaging food products. The NP concentrations differed between the types of livestock and poultry products, and the differences were relatively large even within the same food type. Exposure to NPs of animals would mostly occur from food consumption. The amount of these compounds will, therefore, inevitably differ due to variations in the types and amounts of crops which each animal ingests. Furthermore, due to pollutant biomagnification in the food web, animals at the top of the chain are thought to have high levels of exposure to xenobiotics [26]. These chemicals are ingested mostly through their diets, especially for ruminants. A large proportion of cellulose can be found in crop residue and agroindustrial by-products such as straw in cereal and maize stover. These fibrous by-products are difficult for the rumens of ruminants to break down. Several feed additives capable of altering the fiber fermentation and digestion of ruminants are produced to enhance the ruminal environment for the purpose of promoting the efficiency of consuming roughage. As a result, nonionic surfactants can be used as feed additives for livestock. Tween 80, which contains NPEOs, is an example of a typical feed additive [27]. Our results indicated that beef had the highest average NP concentration among the analyzed livestock products. Since cows were the only ruminant in the livestock products analyzed in the present study, using NPs as feed additives was likely related to their high beef content.

Another route of NP contamination in foods is their packaging process. From plastic packaging materials in which NPs are added as antioxidants, for example, tris(nonylphenol) phosphate could migrate into foods [28]. Kawamura et al. investigated how much PVC stretch film migrated into fatty and nonfatty food types, and found that NPs moved into fatty foods at a higher rate than into nonfatty foods due to their lipophilic properties [29].

In addition to the lean meat portions of livestock, the intestines of cattle and pigs were also analyzed in the present study, considering their high rate of consumption by Koreans. NP levels were higher in intestines than in lean tissue, indicating a similar tendency to aquatic products. This could be explained by NPs having a stronger and greater affinity to tissues than intestines. Results of the distribution of concentrations for different edible portions of livestock are presented in Figures 4 and 5.
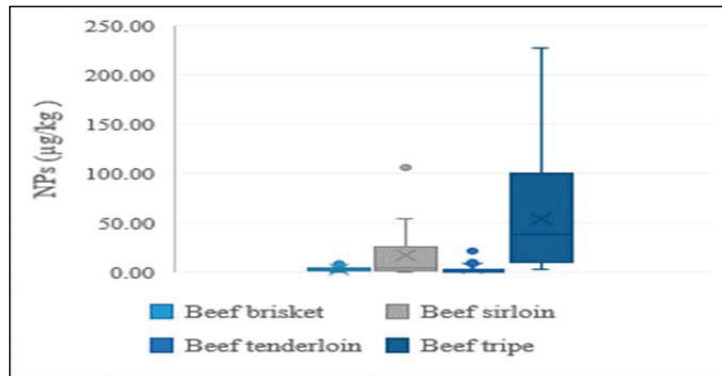
Figure 4. Average concentration of NPs in different edible parts of beef.
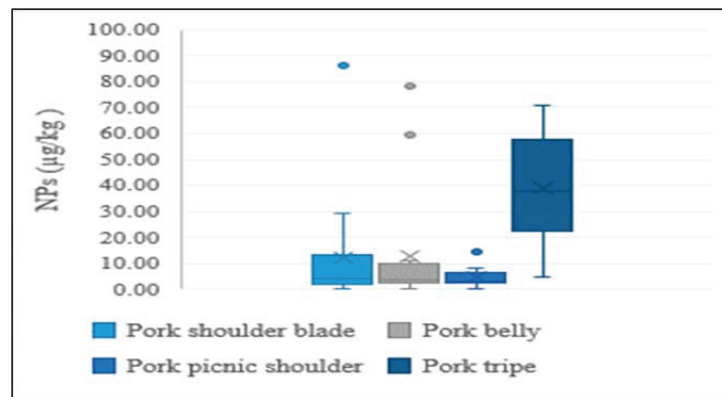
Figure 5. Average concentration of NPs in different edible parts of pork.

No previous study has compared the NP levels in the intestines and lean tissue of livestock. However, different internal tissues of birds, including ducks, were found to have a specific affinity to NPs. NPs accumulated the most in the muscles of each bird species, followed by the livers and kidneys. The various levels that accumulated in their livers and kidneys could possibly reflect differing degrees of excretion from the body due to a varied affinity to fatty tissues [26]. That tendency for bird intestines to accumulate NPs is expected to occur similarly in livestock products. When NPs are consumed through food or water, the intestine acts as a first barrier, absorbing and glucuronidating them. However, because the alkylphenol transport mechanism is hindered by its long alkyl chain, NP removal from the intestine is delayed, resulting in its accumulation in intestinal tissue. This NP accumulation causes its steady release into the bloodstream, which eventually reaches the liver. Although the liver can metabolize NPs, it also has a transport system that is restricted by long alkyl groups [30].

The lipid contents and NP concentrations of chicken and duck meat are listed in Table 5. Chicken breast had the lowest NP level, as well as the lowest lipid content, among types of chicken meat, with other portions with larger lipid contents having six-fold to nine-fold higher average NP levels. Additionally, the highest average NP concentration among poultry products was found in duck meat, which had the highest lipid content, possibly due to the aquatic environment being contaminated, and ducks being an aquicolous species [31].

Table 5. Lipid contents and NP concentrations for chicken and duck meat.

Food Samples	Lipid Contents (%) *	Average NP Level (µg/kg)
Chicken wings	10.5	13.0
Chicken breast	1.00	2.17
Chicken legs	7.70	19.8
Duck	21.0	21.1

* Lipid contents were referred to the food nutrition database of the Ministry of Food and Drug Safety (2019).

The presence of NPs in agricultural products purchased from markets has been observed to vary between regions, with its concentration differing between and within vegetable species. The distribution of concentrations for each food category of agricultural products is shown in Figure 6. The main factors expected to contribute to this large variation are as follows: the differences in the degree of contamination of sludge and soil used for cultivation, and the application of pesticide products containing varying amounts of NPEOs during cultivation.
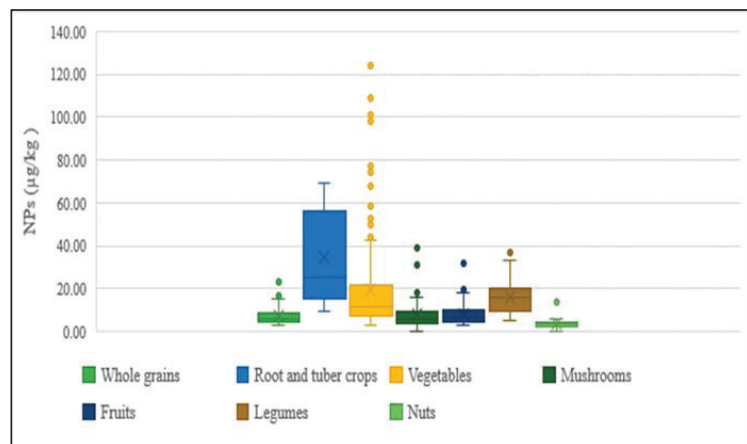
Figure 6. Concentration of NPs in agricultural products.

Applying sludge to agricultural land is a cost-effective technique for sewage disposal, and is one of the most common methods of sludge management. NPEOs are biodegraded in sewage treatment by the hydrolysis of ethoxylate groups, producing short-chain ethoxylates and NPs. Significant amounts of these breakdown products have been found in sewage effluents, surface waters, and sediments. Accumulation in sewage sludge induced the release of high NP concentrations into the environment once the sludge is applied to agricultural land. NPs may contact crops after being applied to soils, where they might be absorbed and accumulated through their root systems. A greater NP persistence in soil means a higher potential for crop uptake [32]. Furthermore, because of its hydrophobic property, NPs adsorb into solid organic particles in soil, and eventually bioaccumulate over time to produce large amounts [33].

NP breakdown in soil and water is influenced by factors such as oxygen availability and microbial activity, resulting in observations of substantial differences in NP persistence. The degradation of long-chain NPEOs begins with ethoxylate chains being cleaved into short chains, such as NP1EO and NP2EO. These short-chain ethoxylates further degrade into NPs, indicating that NPs are likely to accumulate due to polyethoxylate breakdown. The physical, chemical, and biological properties of individual soils ultimately control NP degradation and plant availability [32]. These results suggest that NP concentration

depends on the soil where crops are grown, which can have a wide range even within the same food type of agricultural products.

Another possible route for NPs reaching agricultural products is through adjuvants in pesticides. NPEOs are commonly used as nonionic surfactants in pesticide formulations due to their low cost and high performance. These surfactants are used in agricultural pesticides for various reasons, including increasing droplet spreading, lowering surface tension, lowering solvent evaporation rates, increasing residence duration on plant surfaces, and improving pesticide suspension and emulsion stability [33]. Using pesticides and fertilizers in agriculture can lead to NPEO degradation product accumulation with shorter-chain ethoxylate groups, such as NPs, on crop surfaces. Ethoxylate degradation to NPs could result in NP accumulation in fruits, vegetables, and cereals treated with pesticides. Furthermore, NPs can remain in the soil for months after sludge application, resulting in its uptake in plants [34]. NP residues are particularly shown to be primarily generated by pesticides used in the cultivation of leafy vegetables. High NP concentrations were observed in commercial pesticide products commonly used in China, significantly differing within a range of 138~1245 mg/kg [35].

Due to the varied concentrations of these compounds in different vegetables and crops, most samples were considered to be contaminated by NPs via diverse pathways at various stages of the food production process. Some of this contamination would derive from alkylphenol ethoxylates, which are utilized in disinfectants and pesticide formulations as nonionic surfactants and emulsifiers. NPEO degradation products could induce NP accumulation on the roots and other portions of vegetables and crops after being used in agriculture. Another possible source is degradation products such as NP residues from tris(nonylphenol) phosphate, a component of plastic, which could migrate into vegetables when applied by methods involving food contact [7]. Tris(nonylphenol) phosphate is produced when NPs react with phosphorous trichloride, which is applied as an antioxidant stabilizer. As a result, when the plastic is utilized in ways where it contacts food, NP residue degradation products or impurities from tris(nonylphenol) phosphate in the plastic may migrate into agricultural products [36].

4. Conclusions

Analytical methods were developed and validated for four different matrices to determine the NP concentrations in various foods. The linearity, sensitivity, accuracy, and precision results demonstrated that the methods established in this study are efficient for determining analytes in four different matrices with varied food compositions.

The results of the analyzed NPs in foods indicate that these compounds are ubiquitous in food products in Korea, suggesting the possibility of disrupting the endocrine systems of organisms. The monitoring of these substances should, therefore, be updated regularly in order to evaluate dietary exposure in humans. The separation and identification of branched NPs in a single run still represent a great challenge due to the coexistence of many different NP isomers. Further research should, therefore, be conducted, with a focus on increasing the separation of these isomers using sophisticated analytical methods, such as GC-MS/MS and GCxGC/MS.

Institutional Review Board Statement: Not applicable.

Informed Consent Statement: Not applicable.

Data Availability Statement: Data are contained within the article.

Conflicts of Interest: The authors declare no conflict of interest.

References

1. Günther, K.; Räcker, T.; Böhme, R. An Isomer-Specific Approach to Endocrine-Disrupting Nonylphenol in Infant Food. *J. Agri. Food Chem.* **2017**, *65*, 1247–1254. [CrossRef]
2. Lu, J.; Wu, J.; Stoffella, P.J.; Wilson, P.C. Analysis of Bisphenol A, Nonylphenol, and Natural Estrogens in Vegetables and Fruits Using Gas Chromatography–Tandem Mass Spectrometry. *J. Agri. Food Chem.* **2013**, *61*, 84–89. [CrossRef]
3. Grelska, A.; Noszczyńska, M. White rot fungi can be a promising tool for removal of bisphenol A, bisphenol S, and nonylphenol from wastewater. *Environ. Sci. Pollut. Res.* **2020**, *27*, 39958–39976. [CrossRef] [PubMed]
4. Raecker, T.; Thiele, B.; Boehme, R.M.; Guenther, K. Endocrine disrupting nonyl- and octylphenol in infant food in Germany: Considerable daily intake of nonylphenol for babies. *Chemosphere* **2011**, *82*, 1533–1540. [CrossRef] [PubMed]
5. Ringbeck, B.; Bury, D.; Hayen, H.; Weiss, T.; Brüning, T.; Koch, H.M. Determination of specific urinary nonylphenol metabolites by online-SPE-LC-MS/MS as novel human exposure biomarkers. *J. Chromatogr. B* **2021**, *1177*, 122794. [CrossRef] [PubMed]
6. Shan, J.; Jiang, B.; Yu, B.; Li, C.; Sun, Y.; Guo, H.; Wu, J.; Klumpp, E.; Schäffer, A.; Ji, R. Isomer-specific degradation of branched and linear 4-nonylphenol isomers in an oxic soil. *Environ. Sci. Technol.* **2011**, *45*, 8283–8289. [CrossRef]
7. She, Y.; Wang, J.; Zheng, Y.; Cao, W.; Wang, R.; Dong, F.; Liu, X.; Qian, M.; Zhang, H.; Wu, L. Determination of nonylphenol ethoxylate metabolites in vegetables and crops by high performance liquid chromatography–tandem mass spectrometry. *Food Chem.* **2012**, *132*, 502–507. [CrossRef]
8. Chen, G.; Ding, W.; Ku, H.; Chao, H.; Chen, H.; Huang, M.; Wang, S. Alkylphenols in human milk and their relations to dietary habits in central Taiwan. *Food Chem. Toxicol.* **2010**, *48*, 1939–1944. [CrossRef] [PubMed]
9. Vargas-Berrones, K.; Bernal-Jácome, L.; de León-Martínez, L.D.; Flores-Ramírez, R. Emerging pollutants (EPs) in Latin América: A critical review of under-studied EPs, case of study-Nonylphenol. *Sci. Total Environ.* **2020**, *726*, 138493. [CrossRef]
10. Chung, S.; Ding, W. Isotope-dilution gas chromatography-mass spectrometry coupled with injection-port butylation for the determination of 4-t-octylphenol, 4-nonylphenols and bisphenol A in human urine. *J. Pharm. Biomed. Anal.* **2018**, *149*, 572–576. [CrossRef]
11. Salgueiro-González, N.; Castiglioni, S.; Zuccato, E.; Turnes-Carou, I.; López-Mahía, P.; Muniategui-Lorenzo, S. Recent advances in analytical methods for the determination of 4-alkylphenols and bisphenol A in solid environmental matrices: A critical review. *Anal. Chim. Acta* **2018**, *1024*, 39–51. [CrossRef] [PubMed]
12. Li, C.; Jin, F.; Snyder, S.A. Recent advancements and future trends in analysis of nonylphenol ethoxylates and their degradation product nonylphenol in food and environment. *TrAC Trends Anal. Chem.* **2018**, *107*, 78–90. [CrossRef]
13. Wu, P.; Zhang, L.; Yang, D.; Zhang, J.; Hu, Z.; Wang, L.; Ma, B. Isotope dilution gas chromatography with mass spectrometry for the analysis of 4-octyl phenol, 4-nonylphenol, and bisphenol A in vegetable oils. *J. Sep. Sci.* **2016**, *39*, 904–909. [CrossRef]
14. Chokwe, T.B.; Okonkwo, J.O.; Sibali, L.L. Distribution, exposure pathways, sources and toxicity of nonylphenol and nonylphenol ethoxylates in the environment. *Water SA* **2017**, *43*, 529–542. [CrossRef]
15. Lu, Z.; Gan, J. Analysis, toxicity, occurrence and biodegradation of nonylphenol isomers: A review. *Environ. Int.* **2014**, *73*, 334–345. [CrossRef]
16. Eganhouse, R.P.; Pontolillo, J.; Gaines, R.B.; Frysinger, G.S.; Gabriel, F.L.; Kohler, H.E.; Giger, W.; Barber, L.B. Isomer-specific determination of 4-nonylphenols using comprehensive two-dimensional gas chromatography/time-of-flight mass spectrometry. *Environ. Sci. Technol.* **2009**, *43*, 9306–9313. [CrossRef]
17. Li, W.; Cohen, L.H. Quantitation of endogenous analytes in biofluid without a true blank matrix. *Anal. Chem.* **2003**, *75*, 5854–5859. [CrossRef] [PubMed]
18. Ruczyńska, W.; Szlinder-Richert, J.; Nermer, T. The occurrence and distribution of nonylphenols and nonylphenol ethoxylates in different species of fish. *Environ. Sci. Process. Impacts* **2020**, *22*, 1057–1070. [CrossRef]
19. Tavazzi, S.; Benfenati, E.; Barcelo, D. Accelerated solvent extraction then liquid chromatography coupled with mass spectrometry for determination of 4-t-octylphenol, 4-nonylphenols, and bisphenol A in fish liver. *Chromatographia* **2002**, *56*, 463–467. [CrossRef]
20. Lee, C.; Jiang, L.; Kuo, Y.; Chen, C.; Hsieh, C.; Hung, C.; Tien, C. Characteristics of nonylphenol and bisphenol A accumulation by fish and implications for ecological and human health. *Sci. Total Environ.* **2015**, *502*, 417–425. [CrossRef]
21. Lye, C.M.; Bentley, M.G.; Galloway, T. Effects of 4-nonylphenol on the endocrine system of the shore crab, *Carcinus maenas*. *Environ. Toxicol.* **2008**, *23*, 309–318. [CrossRef]
22. Xu, E.G.; Morton, B.; Lee, J.H.; Leung, K.M. Environmental fate and ecological risks of nonylphenols and bisphenol A in the Cape D'Aguilar Marine Reserve, Hong Kong. *Mar. Pollut. Bull.* **2015**, *91*, 128–138. [CrossRef] [PubMed]
23. Yang, C.; Zhao, J.; Wang, J.; Yu, H.; Piao, X.; Li, D. Water-based gas purge microsyringe extraction coupled with liquid chromatography for determination of alkylphenols from sea food Laminaria japonica Aresh. *J. Chromatogr. B* **2013**, *1300*, 38–42. [CrossRef]

24. Datta, S.; Loyo-Rosales, J.E.; Rice, C.P. A simple method for the determination of trace levels of alkylphenolic compounds in fish tissue using pressurized fluid extraction, solid phase cleanup, and high-performance liquid chromatography fluorescence detection. *J. Agri. Food Chem.* **2002**, *50*, 1350–1354. [CrossRef] [PubMed]

25. Shang, D.Y.; Macdonald, R.W.; Ikonomou, M.G. Persistence of nonylphenol ethoxylate surfactants and their primary degradation products in sediments from near a municipal outfall in the Strait of Georgia, British Columbia, Canada. *Environ. Sci. Technol.* **1999**, *33*, 1366–1372. [CrossRef]

26. Bodziach, K.; Staniszewska, M.; Falkowska, L.; Nehring, I.; Ożarowska, A.; Zaniewicz, G.; Meissner, W. Distribution paths of endocrine disrupting phenolic compounds in waterbirds (*Mergus merganser, Alca torda, Clangula hyemalis*) from the Southern Baltic. *Sci. Total Environ.* **2021**, *793*, 148556. [CrossRef]

27. Bina, B.; Mohammadi, F.; Amin, M.M.; Pourzamani, H.R.; Yavari, Z. Determination of 4-nonylphenol and 4-tert-octylphenol compounds in various types of wastewater and their removal rates in different treatment processes in nine wastewater treatment plants of Iran. *Chin. J. Chem. Eng.* **2018**, *26*, 183–190. [CrossRef]

28. Guenther, K.; Heinke, V.; Thiele, B.; Kleist, E.; Prast, H.; Raecker, T. Endocrine disrupting nonylphenols are ubiquitous in food. *Environ. Sci. Technol.* **2002**, *36*, 1676–1680. [CrossRef]

29. Kawamura, Y.; Ogawa, Y.; Mutsuga, M. Migration of nonylphenol and plasticizers from polyvinyl chloride stretch film into food simulants, rapeseed oil, and foods. *Food Sci. Nutr.* **2017**, *5*, 390–398. [CrossRef]

30. Daidoji, T.; Ozawa, M.; Sakamoto, H.; Sako, T.; Inoue, H.; Kurihara, R.; Hashimoto, S.; Yokota, H. Slow elimination of nonylphenol from rat intestine. *Drug Metab. Dispos.* **2006**, *34*, 184–190. [CrossRef] [PubMed]

31. Shao, B.; Han, H.; Li, D.; Ma, Y.; Tu, X.; Wu, Y. Analysis of alkylphenol and bisphenol A in meat by accelerated solvent extraction and liquid chromatography with tandem mass spectrometry. *Food Chem.* **2007**, *105*, 1236–1241. [CrossRef]

32. Sjöström, Å.E.; Collins, C.D.; Smith, S.R.; Shaw, G. Degradation and plant uptake of nonylphenol (NP) and nonylphenol-12-ethoxylate (NP12EO) in four contrasting agricultural soils. *Environ. Pollut.* **2008**, *156*, 1284–1289. [CrossRef]

33. De Bruin, W.; Kritzinger, Q.; Bornman, R.; Korsten, L. Occurrence, fate and toxic effects of the industrial endocrine disrupter, nonylphenol, on plants-a review. *Ecotoxicol. Environ. Saf.* **2019**, *181*, 419–427. [CrossRef] [PubMed]

34. Gyllenhammar, I.; Glynn, A.; Darnerud, P.O.; Lignell, S.; van Delft, R.; Aune, M. 4-Nonylphenol and bisphenol A in Swedish food and exposure in Swedish nursing women. *Environ. Int.* **2012**, *43*, 21–28. [CrossRef] [PubMed]

35. Fang, K.; Jiang, Z.; Wang, J.; She, Y.; Jin, M.; Jin, F.; Yang, M. Simulation of nonylphenol degradation in leafy vegetables using a deuterated tracer. *Environ. Sci. Process. Impacts* **2015**, *17*, 1323–1330. [CrossRef]

36. Mezcua, M.; Martínez-Uroz, M.A.; Gómez-Ramos, M.M.; Gómez, M.J.; Navas, J.M.; Fernández-Alba, A.R. Analysis of synthetic endocrine-disrupting chemicals in food: A review. *Talanta* **2012**, *100*, 90–106. [CrossRef] [PubMed]

Improved LC/MS/MS Quantification Using Dual Deuterated Isomers as the Surrogates: A Case Analysis of Enrofloxacin Residue in Aquatic Products

Yunyu Tang [1,†], Guangxin Yang [1,†], Essy Kouadio Fodjo [2], Shouying Wang [3], Wenlei Zhai [4], Wenshuai Si [3], Lian Xia [5] and Cong Kong [1,*]

[1] Key Laboratory of Control of Quality and Safety for Aquatic Products, Ministry of Agriculture and Rural Affairs, East China Sea Fisheries Research Institute, Chinese Academy of Fishery Sciences, Shanghai 200090, China

[2] Laboratory of Constitution and Reaction of Matter, UFR SSMT, Université Felix Houphouet Boigny, 22 BP 582 Abidjan 22, Côte d'Ivoire

[3] Institute for Agri-Food Standards and Testing Technology, Shanghai Academy of Agricultural Sciences, Shanghai 201403, China

[4] Institute of Quality Standard and Testing Technology, Beijing Academy of Agriculture and Forestry Science, Beijing 100097, China

[5] School of Chemistry and Chemical Engineering, Qufu Normal University, Qufu 273165, China

* Correspondence: kongc@ecsf.ac.cn

† These authors contributed equally to this work.

Abstract: Extensive and high residue variations in enrofloxacin (ENR) exist in different aquatic products. A novel quantitative method for measuring ENR using high-performance liquid chromatography–tandem mass spectrometry was developed employing enrofloxacin-d_5 (ENR-d_5) and enrofloxacin-d_3 (ENR-d_3) as isotope surrogates. This reduced the deviation of detected values, which results from the overpass of the linear range and/or the large difference in the residue between the isotope standard and ENR, from the actual content. Furthermore, high residue levels of ENR can be directly diluted and re-calibrated by the corresponding curve with the addition of high levels of another internal surrogate without repeated sample preparation, avoiding the overflow of the instrument response. The validation results demonstrated that the method can simultaneously determine ENR residues from MQL (2 µg/kg) to 5000 × MQL (method quantification limit) with recoveries between 97.1 and 106%, and intra-precision of no more than 2.14%. This method realized a wide linear calibration range with dual deuterated isomers, which has not been previously reported in the literature. The developed method was successfully applied to the analysis of ENR in different aquatic products, with ENR residue levels varying from 108 to 4340 µg/kg and an interval of precision in the range of 0.175~6.72%. These results demonstrate that batch samples with a high variation in ENR residues (over the linear range with a single isotope standard) can be detected by the dual isotope surrogates method in a single sample preparation process.

Keywords: enrofloxacin; dual isotope surrogates; enrofloxacin-d_3; contaminant detection; accurate quantification; aquatic animals

1. Introduction

Enrofloxacin (ENR) is a broad-spectrum antibiotic found in animals as a second-generation fluorinated quinolone. Because of its efficaciousness against common bacterial pathogens, ENR is applied in treating and preventing various bacterial diseases [1], including furunculosis, vibriosis, and bacterial kidney diseases in aquaculture [2–4]. At present, ENR is licensed for use at levels below maximum residue limits (MRL), set at 100 µg/kg for ENR and ciprofloxacin (CIP) in fish farming in China, the European Union, and Vietnam [5]. In the United States, no fluorinated quinolone has been approved for

use in food-producing animals (except in poultry) since 1997 [6]. Despite this constraint, ENR is extensively applied beyond the set limit value to control diseases in aquaculture, cattle, pigs, and poultry farms [7]. Recent reports have shown high detection rates of 11.4% and 50.4% of ENR residues in aquatic products in South Korea [8] and China [9], respectively. Residues range between N.D. and 785 µg/kg. This excessive use of ENR is the result of over-exploited domestic fisheries, with intensive and high-density culture being adopted to obtain high yields and profits. These activities lead to high antibiotic residues in treated aquatic animals, aquaculture-related sediments and soils, and natural water environments [10–12]. This, in turn, leads to potential exposure of human health to risks induced by the ultimate accumulation of ENR in humans and the alarmingly high issues related to antibiotic bacterial resistance [13]. Growing concerns about quality and safety necessitate the monitoring of ENR residues in aquatic products for the safety of human consumption.

The methods for quantitative determination of ENR in aquaculture have been extensively reported. Rapid detection with competitive indirect enzyme-linked immunosorbent assay (ELISA) was performed in field tests due to its easy operation and rapid analysis [14,15]. Furthermore, several studies reported the quantitation of ENR using high-performance liquid chromatography (HPLC) with fluorescence detectors [16,17]. On the other hand, high-performance liquid chromatography–tandem mass spectrometry (HPLC−MS/MS) was also extensively used for the determination of ENR in recent years [18,19]. Because of its high specificity and sensitivity, LC–MS/MS attracted much attention in various fields when applied to the analysis of antibiotics [20–23]. Generally, the pretreatment of ENR includes solvent extraction, followed by purification with liquid–liquid extraction or solid-phase extraction, concentration, and redissolution before analysis using LC–MS/MS assays. In most cases, the purification and concentration processes can cause the loss of the target analyte, resulting in decreased sensitivity in the detection method.

In order to solve this issue, and to obtain more accurate results, an isotope surrogate was introduced as the control of stochastic and/or systematic variation in analyte extraction and analysis [24,25]. Furthermore, the inaccuracy resulting from matrix effects and sample preparation can be effectively compensated by the addition of a fixed amount of isotope surrogate to each sample at the beginning of the process [26]. Therefore, ENR was extensively estimated using the isotope standard method with HPLC–MS/MS in most cases to obtain an accurate measurement. In previous reports, samples containing ENR with concentrations significantly above MRL, such as 785 µg/kg in loach [8], 148.4 µg/kg in carp [27], and 2200 µg/kg in grass carp [28], were found. These high residue values can be attributed to the overapplication of this antibiotic. However, the MS detector tends to produce unstable and imprecise results with the regular detection method, which might be caused by the range of the calibration curve, a high discrepancy between the analyte and the isotope surrogate, and/or the saturated response on the instrument [29]. According to our experience, the linear response range of ENR in the MS detector was not over 500 ng/mL in an actual sample test (Figure 1), as can be found in the recent literature [30,31]. Obviously, the response values of ENR at concentrations of more than 500 ng/mL do not follow the linear calibration curve and tend to be saturated (Figure 1).

Thus, ENR determination requies a repeated sample preparation to obtain more accurate results. It is noteworthy that the dilution of the original sample can reduce the response of MS to resolve the difficulty in MS saturation of the instrument, but the measured value of the diluted sample is still beyond the range of the calibration curve using the quantitative method with the isotope standard [32]. Moreover, the dilution of injection samples cannot resolve the enormous discrepancy in concentration between the analyte and the isotope surrogate to obtain stable and precise results. Therefore, the samples need to be further analyzed by changing the amount of added isotope surrogate and establishing a new procedure, as follows: (i) a new calibration curve is prepared to match the sample concentration; (ii) a repeated sample preparation should be performed with a reasonable

amount of added isotope surrogate [33]. However, the high amount of ENR may saturate the MS system detector, resulting in no suitable calibration curve. Consequently, the sample requires laborious re-preparation to resolve the linearity range of the calibration curve, saturation of the MS detector, and the vast discrepancy in concentration between the analyte and the isotope surrogate; this, therefore, increases the time spent on analysis and generates more hazards for the environment. Moreover, the repeatability and reproducibility of the determined results could be poor if a lower amount of isotope surrogate is used than the target ENR in the final solution to be analyzed [34]. This could occur even though the detection values fall within the range of the new calibration curve and the linear response range of the instrument. Therefore, it is necessary to develop a simple, fast, and reliable quantitative method for the analysis of ENR residue levels, which vary from low to high amount in aquatic animals. The use of two different levels of isotope surrogates can provide two ranges of calibration curves, which effectively extends the upper limit of the curve and leads to accurately quantitate the analyte at low and high concentrations, respectively. Moreover, the high addition level of the isotope surrogate can be diluted directly with solutions to adapt the instrument's response.
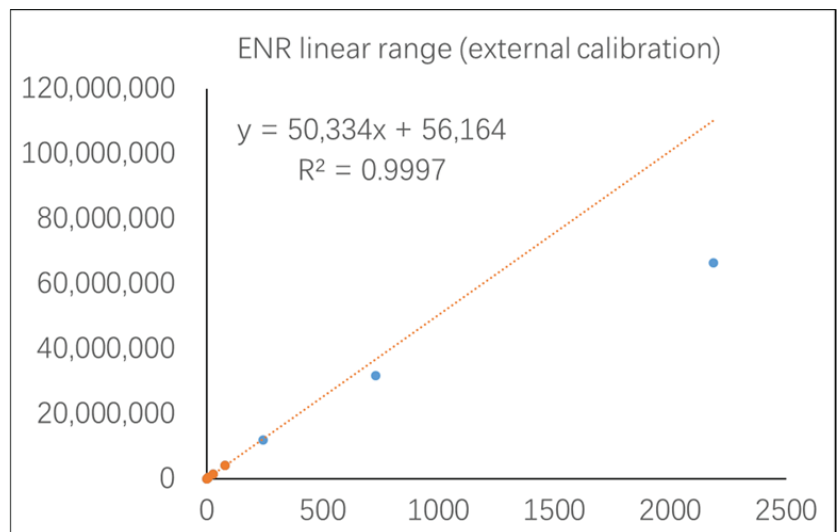
Figure 1. Linear range profile of ENR in the MS detector.

This detection strategy for use with an HPLC–MS instrument has not been proposed and validated in the previous literature. In this study, therefore, a new isotope standard, ENR-d_3, for ENR was synthesized and characterized by ^{1}HNMR and MS. We firstly established and validated a novel quantitative method for ENR in aquatic animals using two isotope surrogates with HPLC–MS/MS, achieving a wide range in the calibration curve, single-time sample preparation, direct dilution for the instrument limit, and accurate quantification from low to high residue levels. Moreover, the method involves easy sample preparation, high sensitivity, and a low amount of reagent. Finally, the new method was applied to the determination of ENR in actual positive samples for various aquatic species.

2. Materials and Methods

2.1. Experimental Materials

All reagents and chemicals used in this study were of analytical or chromatography grade. The enrofloxacin and enrofloxacin-d_5 standards (>95% purity) were obtained from Dr. Ehrenstorfer (Augsburg, Germany). The ciprofloxacin (CIP) and 1-bromoethane-2,2,2-d_3 were purchased from Shanghai AcmecBiochemical Co., Ltd. (Shanghai, China).

N,N-dimethylformamide (DMF) and triethylamine (Et$_3$N) were of analytical grade and obtained from Sinopharm Chemical Reagent Co., Ltd. (Shanghai, China). Methanol (MeOH), acetonitrile (MeCN), formic acid, ethyl acetate (EA), dichloromethane, acetic acid, and ammonium acetate of HPLC-grade were from Merck (Darmstadt, Germany). The certified reference material (CRM) (GBW 10167, Batch No. 1672107) was purchased from the Institute of Quality Standards and Testing Products for Agro-products of CAAS. The aquatic product samples were obtained from the local farmers' market in Shanghai, China. Ultrapure water (18.2 MΩ) was prepared in a Milli-Q water purification system (Millipore Co., Bedford, MA, USA).

2.2. Synthesis of ENR-d$_3$

The reaction was performed according to the synthesis route in Figure 2, which was optimized by a reported method [35]. To a solution of CIP (1.80 g, 5.4 mmol) in DMF (50 mL), Et$_3$N (1.20 g, 11.9 mmol) and 1-bromoethane-2,2,2-d$_3$ (0.78 g, 7.0 mmol) were added at room temperature. The reaction mixture was heated to 80 °C and further stirred for 2 h under an N$_2$ atmosphere. After cooling to room temperature, DMF was removed by a rotatory evaporator under reduced pressure at ca. 80 °C for about 30 min [36], and the residue was purified on a silica gel column using CH$_2$Cl$_2$:EA = 20:1 as the eluent, yielding the desired product (1.66 g, 85%) as a yellow solid. ^{1}H NMR spectra were obtained using a Bruker AM 400 MHz spectrometer (Bruker, Massachusetts, USA) at 298 K using tetramethylsilane (TMS) as the internal standard. HRMS measurements were performed using a Q-Orbitrap mass spectrometer (Q-exactive, Thermo Fisher, USA). ^{1}H NMR (400 MHz, D$_2$O): δ 8.47 (s, 1H), 7.86 (d, J = 8.8 Hz, 1H), 7.60 (d, J = 4.8 Hz, 1H), 3.65–3.59 (m, 1 H), 3.38–3.24 (m, 4H), 2.82–2.66 (m, 4H), 2.51–2.46 (m, 8H), 1.35–1.29 (m, 2H), 1.15–1.09 (m, 2H), 0.99–0.96 (m, 9H). HRMS (ESI, m/z): calcd for C$_{19}$H$_{20}$D$_3$FN$_3$O$_3$ ([M + H]$^+$), 363.1912; found, 363.1887.
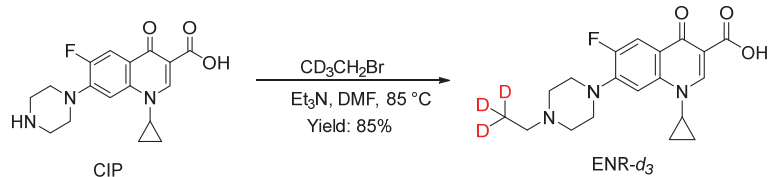
Figure 2. Synthetic route for the target compound.

The purity of ENR-d$_3$ was determined by LC–UV [37]. The LC–UV equipment consisted of an Agilent 1100 series with an autosampler injector (Agilent Technologies Inc., State of California, USA). UV detection was performed by a diode array detector (DAD) at a wavelength of 280 nm for ENR-d$_3$. The ENR was separated by chromatography on a Zorbax Eclipse XDB-C18 (150 mm × 4.6 mm i.d.; Agilent Technologies).

2.3. Sample Preparation

Stock solutions were prepared in methanol at 1 μg/mL for ENR and ENR-d$_5$, and 100 μg/mL for ENR-d$_3$. Further dilution was applied for recovery and calibration solutions. The blank samples were prepared using the muscle of grass carp obtained from a local supermarket in Shanghai (China). All blank samples were firstly screened to ensure that they were free of the antibiotics of interest. Two calibration curves (Curve 1 and 2) were established using a standard solution of different concentrations prepared with a blank matrix solution; the curves were fitted by linear regression with ENR-d$_5$ and ENR-d$_3$, respectively. For the plot of calibration Curve 1, the standard solutions were at 1, 3, 9, 27, 81, and 243 ng/mL of ENR, with 5 ng/mL of ENR-d$_5$ as the isotope standard for each point. For the plot of calibration Curve 2, the standard solutions were 27, 81, 243, 729, 2187, and 6561 ng/mL of ENR with 100 ng/mL of ENR-d$_3$. Considering that a high amount of ENR can saturate the MS system detector, the standard solutions of Curve 2 can be diluted 20 times to obtain good linearity for the subsequent quantification of the correspondingly

diluted sample solution. Finally, the actual concentrations of Curve 2 were 1.35, 4.05, 12.2, 36.4, 109, and 328 ng/mL of ENR with 5 ng/mL of ENR-d_3 for determination by LC–MS/MS.

The analyte was extracted following the optimized method in [29]. Briefly, a 5 g homogenized sample was weighed in a 50 mL centrifuge tube and added to 50 ng of ENR-d_5 (50 μL of solution of 1 μg/mL ENR-d_5 in methanol) and 1000 ng of ENR-d_3 (100 μL of solution of 10 μg/mL ENR-d_5 in methanol), respectively. An amount of 10 mL of acetonitrile–water solution (85:15, containing 1 mL/100 mL acetic acid) was then added, and the sample was vortex–mixed for 10 min. Afterward, the sample was extracted by ultrasonication for 10 min, and centrifuged (5000× *g*) for 5 min at 4 °C. Following this, a 1 mL aliquot was filtered through a 0.22 μm hydrophobic polytetrafluoroethylene (PTFE) membrane as solution 1 for analysis. Meanwhile, 50 μL of solution 1 was diluted with 950 μL of extraction solvent, and the obtained solution (solution 2) was used for analysis.

2.4. LC–MS/MS Analysis

A HPLC (LC-20A, Shimadzu Corporation, Japan) coupled with a Sciex Qtrap 5500 tandem quadrupole mass spectrometer (Danaher Corporation, Washington, DC, USA) with an electrospray ionization (ESI) source was used for the detection of ENR in the multiple reaction monitoring (MRM) mode. Chromatographic separation was performed on a C18 column (Agilent poreshell 120 EC-C18, 100 × 4.6 mm i.d., 2.7 μm, Agilent Technologies, Santa Clara, CA, USA) under a flow rate of 0.8 mL/min at 40 °C, with an injection volume of 2 μL [38]. Mobile phase A water (containing 1 mL/L of formic acid and 2 mmol/L ammonium acetate) and mobile phase B methanol were used for chromatography separation with the following gradient elution procedure: 15% B for 1.0 min, 15% B to 30% B over 2.5 min, 1.0 min at 30% B, ramping to 95% B over 2.0 min, held for 1.7 min at 95% B, followed by a return to 15% B within 0.1 min and 1.2 min at 15% B for re-equilibration.

The parameters for mass spectrometry include a spray voltage of 4500 V, a CUR pressure of 42 psi, GS1 and GS2 pressures of 55 psi, an ion source temperature at 550 °C, and CAD of the medium. MS/MS parameters for ENR, ENR-d_5, and ENR-d_3 are summarized in Table 1.

Table 1. MS/MS parameters and standard curves with two isotope surrogates.

Compounds	Precursor Ion (m/z) and Adduct	Product Ions (m/z) and Theoretical Fragments	CE (eV)	Calibration Curves	Linear Range (ng/mL)	r^2
ENR	360 ([M + H]$^+$)	316 * ($C_{18}H_{23}FN_3O^+$)	19	y = 0.295501 + 0.231345 * × (ENR-d_5)	1–243	0.9997
				y = 0.0231436 + 0.011281 * × (ENR-d_3)	27−6561	0.9996
		245 ($C_{14}H_{14}FN_2O^+$)	26	—	—	—
ENR-d_5	365 ([M + H]$^+$)	321 ($C_{18}H_{17}D_5FN_3O^+$)	19	—	—	—
ENR-d_3	363 ([M + H]$^+$)	319 ($C_{18}H_{20}D_3FN_3O^+$)	19	—	—	—

* Quantitative ion. CE, collision energy; r^2, coefficient of determination.

2.5. Method Validation

The method quantification limit (MQL) of 2 μg/kg was validated according to the Chinese Standard [39]. The calibration curves were prepared by the peak area ratios of ENR to the isotope standard plotted against the concentration. Recovery and accuracy were examined by comparing the measured concentrations from processed samples with different spiking levels. Intra- and inter-assay precision was assessed by relative standard deviation (RSD) of the measured positive samples. The RSD was calculated for all determi-

nations in a spiking experiment with three replicates. The content of ENR in the samples was calculated according to the following equation:

$$X = \frac{C \times V \times 1000}{m \times 1000}$$

where X (µg/kg) is the content of ENR in the samples; C (ng/mL) indicates the concentration of ENR detected in the samples; V (mL) is the volume of the extraction reagent; and m (g) stands for the weight of the sample.

The decision limit (CCα) and the detection capability (CCβ) of the method were obtained according to Commission Decision 2002/657/EC. We performed the measurement of noise on 20 blank samples (grass carp), with ENR-d_5 as the surrogate, and then the decision limit was obtained; this was greater than 3 times the signal-to-noise ratio from the blank sample. Furthermore, we spiked ENR in 20 blank samples (grass carp) at the concentration of CCα, and calculated the detection capability with the sum of CCα + 1.64 times the SD of within-laboratory reproducibility (n = 20).

3. Results and Discussion

3.1. ^{1}HNMR Spectra of ENR-d_3

ENR-d_5 is commonly used as an isotope standard for ENR. With the aim of obtaining a new stable isotope surrogate, ENR-d_3 was synthesized from commercial CIP and 1-bromoethane-2,2,2-d_3 via the S_N2 substitution reaction. The structure of ENR-d_3 was firstly characterized by ^{1}H NMR and MS analysis. For ^{1}H NMR (Figure 3), in comparison with CIP (Figure S1), 15 additional protons were observed; these can be attributed to the Et$_3$N salt existing with ENR-d_3 in the spectrum. In detail, the two proton signals in methylene linked to the CD$_3$ group were overlapped with six methylene proton signals of Et$_3$N at 2.51−2.46 ppm. The nine proton signals in the methyl group for Et$_3$N were at 0.99−0.96 ppm. All other signals were in good agreement with the original CIP. The m/z 363 in ENR-d_3 was obtained from product ion mass spectra (Figure S2), and the m/z 102 at the top of this figure shows the protonated Et$_3$N, which was also detected in the ENR-d_3 ^{1}HNMR spectra (Figure 3). Pure m/z 363 without an m/z 360 signal demonstrated the high purity of the synthesized ENR-d_3 without the presence of ENR. Moreover, the HPLC showed that the purity was >95% (Figure S3). Hence, the synthesized ENR-d_3 can be applied for HPLC−MS/MS analysis as an isotope surrogate.
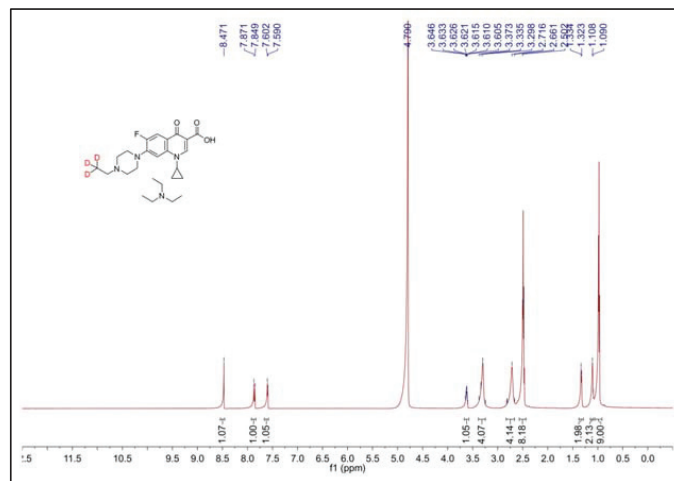
Figure 3. ^{1}H NMR spectrum of ENR-d_3.

3.2. Calibration Range and Deviation

With the aim of detecting ENR with a high variation in concentration in one batch of samples, two calibration curves were individually prepared using ENR-d_5 (5 ng/mL) and ENR-d_3 (100 ng/mL) as isotope surrogates with blank matrix solutions. The two isotope surrogates can compensate for extraction loss during the sample pretreatment and instrument measurement [40]. As shown in Figure 4, the calibration curves were tested for external calibration, and with ENR-d_5 and ENR-d_3 for internal calibration, respectively. It is clear that with such a wide calibration range, the external calibration did not produce a good coefficient of determination ($r^2 < 0.99$), while internal calibration with ENR-d_5 and ENR-d_3 allowed a satisfactory calibration of $r^2 > 0.999$. The internal calibration curves exhibited linearity with the ratio of the peak area of the analyte/ isotope standard (y) and the concentration of ENR (x). Firstly, the two calibration curves with different isotope surrogates covered a wide linear range of 1−6561 ng/mL. However, the measured concentration deviating from the specified amount was more than 10% above 243 ng/mL in the calibration curve with ENR-d_5 (Table S1). On the other hand, the deviations between the spiked and measured values were up to 32% and 111% at concentrations of 1 ng/mL and 3 ng/mL, respectively, in the curve with ENR-d_3 (Table S2). The deviations at different concentrations with two isotope surrogates demonstrated the difficulty of accomplishing accuracy when a large concentration difference between the isotope surrogates and the analyte is present. In our study, MQL was set as the first point of the calibration curve using ENR-d_5, varying from 1 to 243 ng/mL (2−486 µg/kg) with a coefficient of determination of 0.9997 (Table 1). For the calibration curve using ENR-d_3, the range for ENR was from 27 to 6561 ng/mL (54−13,122 µg/kg) with $r^2 = 0.9996$. As a result, the entire calibration curve, covering a wide quantification range from 2 to 13,122 µg/kg, was established for ENR detection.
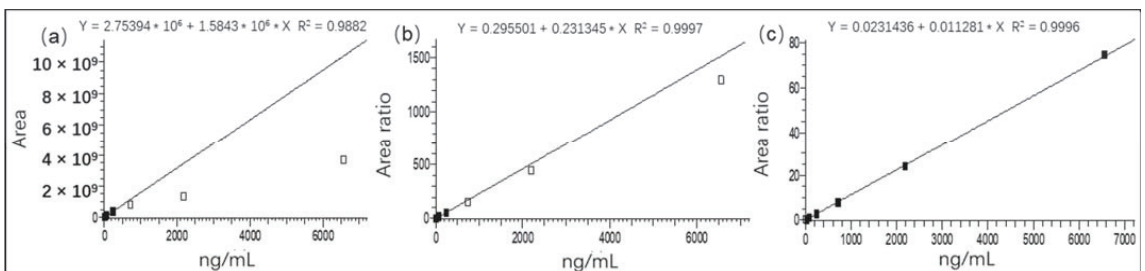
Figure 4. Calibration curves of ENR with the external method (**a**), ENR-d5 (**b**), and ENR-d3 (**c**) for internal calibration.

3.3. Method Validation

For the spiking experiments, the ENR standard was spiked in blank samples at 2, 6, 54, 486, 1458, and 4373 µg/kg, respectively, with the further addition of ENR-d_5 (50 ng) and ENR-d_3 (1000 ng) as isotope standards. Sample preparation was performed according to the above-mentioned procedure. Afterward, two solutions (solution 1 and solution 2) for each sample were measured by HPLC–MS/MS. Compared with the reported methods, our sample preparation process is obviously easier to operate without any enrichment [1] or clean up using SPE material [41], and/or hexane [42]. Furthermore, the sample can be directly diluted using the dual internal calibration method and then quantified using the isotope surrogate with a high concentration, which is feasible for accurate quantification of high residue samples without repeated sample preparation. Thus, it is time-efficient and requires less reagent and fewer consumables. Notably, linearity of the calibration curves was achieved regardless of whether ENR-d_5 was used at low or high levels of concentration. Similar results were observed for ENR-d_3. In other words, the concentrations of ENR-d_5 and ENR-d_3 can be interchanged with a similar good linearity of the calibration. The spiked

samples at 1458 and 4374 µg/kg were quantified using solution 2 with ENR-d_3 as the isotope standard. The residue at MQL of 2 µg/kg was obtained with ENR-d_5, and the CCα and CCβ were calculated to be 0.5 µg/kg and 1.5 µg/kg, respectively. As shown in Figure 5a, the blank sample shows a clean background signal with this method, and an excellent sensitivity is obtained (Figure 5b). The spiking experiment at 4374 µg/kg does not show a saturation response on the chromatogram (Figure 5c). Recovery ranging from 97.1% to 106% was observed at all levels of spiking samples (Table S3). Precision values evaluated by the RSD of the measurements of three positive samples in different matrices were found to be below 6.90% and 6.49% for intra- and inter-precision, respectively (Table S4 and S5). These results demonstrate that the new method was efficient during extraction, and fully satisfied the requirements of quantification for a broad ENR residue range. It is difficult to find a fish muscle CRM with high ENR residue levels. However, we conducted a test with our dual isotope surrogate method on a newly obtained CRM. The specified ENR residue level of the CRM was 62.5 ± 6.3 µg/kg. The residue level of this CRM could be quantified both with ENR-d_5 and ENR-d_3. By using the dual surrogate method, residue levels of 58.7 ± 2.3 µg/kg and 64.1 ± 1.2 µg/kg were obtained with the calibration curve prepared using ENR-d_5 and ENR-d_3, respectively. Moreover, we performed a spiked experiment on this positive sample with a high spiking amount, which was quantified using the dual isotope surrogate method. The result also shows a higher accuracy and stability with ENR-d_3 than with ENR-d_5 (Table 2). This demonstrates the good accuracy of the developed method. Furthermore, this method was compared with previous methods using mass spectrometry for testing for ENR residues in aquatic products, as shown in Table 3. Our method has comparable sensitivity and stability, but a much wider linear range through the use of dual isotope surrogates, which demonstrates the advantages of our method in the sample test for high ENR residue levels.
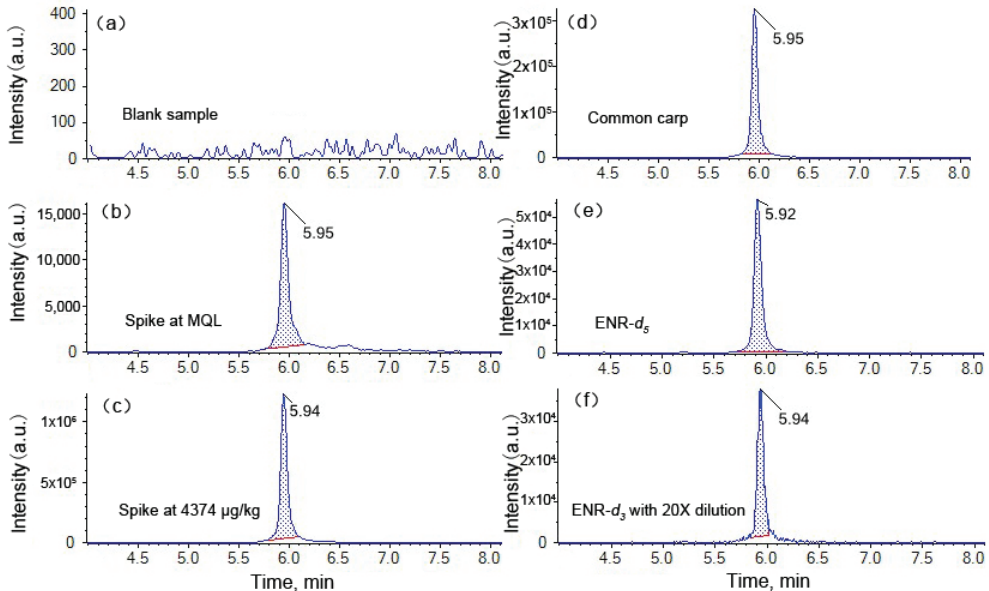
Figure 5. HPLC−MS/MS chromatograms: (**a**) blank sample (EIC of ENR); (**b**) blank samples spiked with ENR at an MQL of 2 µg/kg (EIC of ENR); (**c**) blank samples spiked with ENR at 4374 µg/kg (EIC of ENR); (**d**) positive sample, common carp (EIC of ENR); (**e**) EIC of ENR-d_5; (**f**) EIC of ENR-d_3 (samples in (**c,f**) were diluted at a ratio of 1:20).

Spike Amount (µg/kg)	ENR-d_5 as Internal Surrogate				ENR-d_3 as Internal Surrogate			
	Detected in Blank (µg/kg)	Detected After Spiking (µg/kg)	Recovery (%)	RSD (%)	Detected in Blank (µg/kg)	Detected After Spiking (µg/kg)	Recovery (%)	RSD (%)
10,000	58.7	7632	75.7	12.3	64.1	10,207	101	3.81

Table 3. Comparison of the developed method with previous reports of ENR residue tests using mass spectrometry.

Calibration Method	Instrument	Linear Range (µg/L)	LOQ (µg/kg)	Stability
Internal calibration	LC–MS/MS	0.2–100	1.0	6.7% (spiked at 2 µg/kg) [9]
External calibration	LC–MS/MS	12.5–75.0	12.5	9.2% (spiked at 25 µg/kg) [29]
External calibration	LC–MS/MS	0.5–600	0.5	3% (spike amount not mentioned) [8]
Internal calibration	LC-Q-Orbitrap MS	5–500	1.0	12.8% (spiked at 1 µg/kg) [1]
Internal calibration	LC–MS/MS	1–6561	2.0	2.14% (spiked at 2 µg/kg) (this study)

3.4. Application of Dual Isotope Surrogates to Aquatic Products

The proposed method was applied in the analysis of a batch of different aquatic products collected from commercial markets. A total of 47 out of 136 samples were detected as positive. Four samples were found to exceed the linear range of the calibration curve with ENR-d_5 as the surrogate. Three positive samples were then selected for validation of the method; these were a common carp (*Cyprinus carpio*), a bullfrog (*Lithobates catesbeiana (Shaw)*) and a bluntnose black bream (*Megalobrama amblycephala*), which showed a medium, high and significantly high concentration of ENR, respectively.

The ENR content in three aquatic products, determined using dual isotope surrogates, is summarized in Table 4. HPLC–MS/MS analyses show that the new isotope surrogate ENR-d_3 was successfully applied and detected in positive aquatic products. As a result, the detection of ENR was achieved using the two isotope surrogates, respectively. A slight difference in the detected concentrations and the RSD values between the two quantitative results was found. As shown in Table 4, ENR contents of 108 ± 7.25, 681 ± 35.7, and 3903 ± 433 µg/kg, using ENR-d_5 for quantitation, were detected in the bluntnose black bream, the common carp (Figure 5d), and the bullfrog, respectively. Meanwhile, the RSD values were found to be 6.72, 5.24, and 11.1%, respectively. It should be noted that the SD and RSD values of the common carp and bullfrog were relatively high, suggesting that the higher ENR concentrations were comparable with the added ENR-d_5. This effect results in relatively low repeatability and reproducibility of the measurement. On the other hand, all samples were measured with ENR at levels of 99.1 ± 0.173, 624 ± 4.95, and 4340 ± 21.2 µg/kg using ENR-d_3, respectively, and RSD values ranged from 0.175 to 0.794%. The response of ENR-d_3 in solution 2 was comparable with ENR-d_5 in solution 1 (Figure 5e,f). Clearly, the values of the two quantitative methods agreed well with each other. Meanwhile, the calculated SD and RSD values were much lower using the dual isotope surrogate method than those quantified by ENR-d_5 alone. It is worth noting that the ENR level in bluntnose black bream shows a discrepancy of around 8% between the result with ENR-d_5 and ENR-d_3. We assume that both results are suitable for quantitation with both ENR-d_5 and ENR-d_3. However, higher SD and RSD values were observed for ENR-d_5 as the isotope surrogate. This result may be interpreted by the variation in isotope surrogate loss through the preparation of the sample due to lower amounts of ENR-d_5. Therefore, the addition of more ENR-d_3 could improve the stability of quantitation due to the stable synchronous compensation effect for the analyte and isotope surrogate loss during sample preparation. On the other hand, the results of ENR-d_5 are not acceptable for formal reports, as they was obtained using a calculation curve where the linear range does not cover this value. The advantage of using dual deuterated isomers was not obvious for

the practical sample with only a low ENR residue. It does work and saves time for samples with a high ENR residue, especially when the result with single surrogates exceeds the linear range of the calibration curve. These observations suggest that the accuracy and precision of quantitative results can be achieved by choosing suitable isotope surrogates. Therefore, the experimental results demonstrate that using different levels of dual isotope surrogates could provide accurate and reproducible results in one preparation.

Table 4. Determination of ENR in three aquatic products using ENR-d_5 and ENR-d_3 as the isotope standards (n = 9).

Sample Type	ENR-d_5 as Isotope Surrogate		ENR-d_3 as Isotope Surrogate	
	Concentration $\pm$ SD (μg/kg)	RSD (%)	Concentration $\pm$ SD (μg/kg)	RSD (%)
Bluntnose black bream	108 $\pm$ 7.25	6.72	99.1 $\pm$ 0.173	0.175
Common carp	681 $\pm$ 35.7	5.24	624 $\pm$ 4.95	0.794
Bullfrog	3903 $\pm$ 433	11.1	4340 $\pm$ 21.2	0.489

4. Conclusions

In summary, ENR-d_3 was firstly synthesized as a new isotope surrogate to establish an accurate and fast quantitative method for measuring ENR residues in aquatic products with dual isotope surrogates (ENR-d_5 and ENR-d_3) using HPLC–MS/MS. The new method can be used to perform the determination of ENR with a wide linear range from 2 to 13,122 μg/kg in a single sample preparation with excellent sensitivity, accuracy, and precision. Moreover, a high residue level of ENR, which generally leads to the overflow of the instrument response, can be directly diluted and re-calibrated by the corresponding curve with a high addition level of the other internal surrogate without repeating sample preparation. Furthermore, it was also possible to reduce the deviation of the detected value caused by the vast concentration difference between the isotope standard and target analytes. The new method was applied for the determination of ENR in positive samples for various aquatic species showing the ENR values ranging from 99.1 to 4340 μg/kg. The new method was demonstrated to be time-efficient and easy to operate, providing a practical, accurate, and precise way to determine veterinary drug residues. It is especially suitable for batch samples with a wide range of residue variations and possible high residue content.

Author Contributions: Conceptualization, C.K. and G.Y.; methodology, C.K. and S.W.; validation, Y.T., W.S. and E.K.F.; formal analysis, Y.T. and G.Y.; investigation, Y.T. and G.Y.; resources, C.K.; writing—original draft preparation, Y.T.; writing—review and editing, C.K., W.Z. and E.K.F.; visualization, S.W. and L.X.; project administration, C.K.; funding acquisition, C.K. and G.Y.; All authors have read and agreed to the published version of the manuscript.

Data Availability Statement: The data presented in this study are available on request from the corresponding author.

Conflicts of Interest: The authors declare no conflict of interest.

References

1. Dai, J.; Wang, Y.; Lin, H.; Sun, Y.; Pan, Y.; Qiao, J.Q.; Lian, H.Z.; Xu, C.X. Residue screening and analysis of enrofloxacin and its metabolites in real aquatic products based on ultrahigh-performance liquid chromatography coupled with high resolution mass spectrometry. *Food Chem.* **2023**, *404*, 134757. [CrossRef] [PubMed]
2. Du, X.; Bayliss, S.C.; Feil, E.J.; Liu, Y.; Wang, C.; Zhang, G.; Zhou, D.; Wei, D.; Tang, N.; Leclercq, S.O.; et al. Real time monitoring of *Aeromonas salmonicida* evolution in response to successive antibiotic therapies in a commercial fish farm. *Environ. Microbiol.* **2019**, *21*, 1113–1123. [CrossRef] [PubMed]
3. Soto-Rodriguez, S.A.; Lozano-Olvera, R.; Abad-Rosales, S.M.; Martinez-Brown, J.M.; Ibarra-Castro, L. Susceptibility of Pacific white snook *Centropomus viridis to Vibrio* species. *Dis. Aquat. Org.* **2019**, *134*, 189–195. [CrossRef] [PubMed]
4. Delghandi, M.R.; El-Matbouli, M.; Menanteau-Ledouble, S. *Renibacterium salmoninarum*-The causative agent of bacterial kidney disease in salmonid fish. *Pathogens* **2020**, *9*, 845. [CrossRef] [PubMed]
5. Danyi, S.; Widart, J.; Douny, C.; Dang, P.K.; Baiwir, D.; Wang, N.; Tu, H.T.; Tung, V.T.; Phuong, N.T.; Kestemont, P.; et al. Determination and kinetics of enrofloxacin and ciprofloxacin in Tra catfish (*Pangasianodon hypophthalmus*) and giant freshwater prawn (*Macrobrachium rosenbergii*) using a liquid chromatography/mass spectrometry method. *J. Vet. Pharmacol. Ther.* **2011**, *34*, 142–152. [CrossRef] [PubMed]
6. Flores-Miranda, B.M.; Espinosa-Plascencia, A.; Gómez-Jiménez, S.; López-Zavala, A.A.; González-Carrillo, H.H.; Bermúdez-Almada, M.d.C. Accumulation and elimination of enrofloxacin and ciprofloxacin in tissues of shrimp *Litopenaeus vannamei* under laboratory and farm conditions. *ISRN Pharmaceutics* **2012**, *2012*, 374212. [CrossRef]
7. Morales-Gutiérrez, F.J.; Barbosa, J.; Barrón, D. Metabolic study of enrofloxacin and metabolic profile modifications in broiler chicken tissues after drug administration. *Food Chem.* **2015**, *172*, 30–39. [CrossRef]
8. Kang, H.S.; Lee, S.B.; Shin, D.; Jeong, J.; Hong, J.H.; Rhee, G.S. Occurrence of veterinary drug residues in farmed fishery products in South Korea. *Food Control* **2018**, *85*, 57–65. [CrossRef]
9. Hua, Y.Y.; Yao, Q.H.; Lin, J.; Li, X.; Yang, Y. Comprehensive survey and health risk assessment of antibiotic residues in freshwater fish in southeast China. *J. Food Compos. Anal.* **2022**, *114*, 104821. [CrossRef]
10. Cao, L.; Naylor, R.; Henriksson, P.; Leadbitter, D.; Metian, M.; Troell, M.; Zhang, W.B. China's aquaculture and the world's wild fisheries. *Science* **2015**, *347*, 133–135. [CrossRef]
11. Santos, L.; Ramos, F. Analytical strategies for the detection and quantification of antibiotic residues in aquaculture fishes: A review. *Trends Food Sci. Technol.* **2016**, *52*, 16–30. [CrossRef]
12. Quesada, S.P.; Paschoal, J.A.R.; Reyes, F.G.R. Considerations on the aquaculture development and on the use of veterinary drugs: Special issue for fluoroquinolones—A review. *J. Food Sci.* **2013**, *78*, 1321–1333. [CrossRef] [PubMed]
13. Griboff, J.; Carrizo, J.C.; Bonansea, R.I.; Valdés, M.E.; Wunderlin, D.A.; Amé, M.V. Multiantibiotic residues in commercial fish from Argentina. The presence of mixtures of antibiotics in edible fish, achallenge to health risk assessment. *Food Chem.* **2020**, *332*, 127380. [CrossRef] [PubMed]
14. Zhao, J.; Zhang, R.; Zhu, L.; Deng, H.; Li, F.; Xu, L.; Huan, J.; Sun, X.; Xu, Z. Establishment of a peptide-based enzyme-linked immunosorbent assay for detecting antibodies against PRRSV M protein. *BMC Vet. Res.* **2021**, *17*, 355. [CrossRef]
15. Yan, C.; Teng, J.; Liu, F.Y.; Yao, B.B.; Xu, Z.L.; Yao, L.; Chen, W. Signal amplified enzyme-linked immunosorbent assay with gold nanoparticles for sensitive detection of trace furaltadone metabolite. *Microchem. J.* **2020**, *159*, 105414. [CrossRef]
16. Zhang, W.W.J.; Zheng, G.; Yin, Y.; Zhu, X.; Shan, Q.; Yang, Y.; Ma, L.; Li, L.; Liu, S. Pharmacokinetics, tissue distribution, and depletion of enrofloxacin and its metabolite ciprofloxacin in the northern snake-head (*Channa argus*) following multiple oral administration. *Aquaculture* **2021**, *533*, 736183. [CrossRef]
17. Liu, Y.Z.G.; Sun, R.; Zhou, S.; Dong, J.; Yang, Y.; Yang, Q.; Xu, N.; Ai, X. Determination of pharmacokinetic parameters and tissue distribution characters of enrofloxacin and its metabolite ciprof-loxacin in *Procambarus clarkii* after two routes of administration. *Aquacult. Rep.* **2022**, *22*, 100939. [CrossRef]
18. Dickson, L.C. Performance characterization of a quantitative liquid chromatography–tandem mass spectrometric method for 12 macro-lide and lincosamide antibiotics in salmon, shrimp and tilapia. *J. Chromatogr. B* **2014**, *967*, 203–210. [CrossRef]
19. Monteiro, S.H.; Francisco, J.G.; Campion, T.F.; Pimpinato, R.F.; Andrade, G.C.R.M.; Garcia, F.; Tornisielo, V.L. Multiresidue antimi-crobial determination in Nile tilapia (*Oreochromis niloticus*) cage farming by liquid chromatography tandem mass spectrometry. *Aquaculture* **2015**, *447*, 37–43. [CrossRef]
20. Yu, R.; Chen, L.; Shen, R.; Li, P.; Shi, N.B. Quantification of ultratrace levels of fluoroquinolones in wastewater by molecularly imprinted solid phase extraction and liquid chromatography triple quadrupole mass. *Environ. Technol. Innov.* **2020**, *19*, 100919. [CrossRef]
21. Jadhav, M.R.; Pudale, A.; Raut, P.; Utture, S.; Ahammed Shabeer, T.P.; Banerjee, K. A unified approach for high-throughput quantitative analysis of the residues of multi-class veterinary drugs and pesticides in bovine milk using LC-MS/MS and GC-MS/MS. *Food Chem.* **2019**, *272*, 292–305. [CrossRef] [PubMed]
22. Hoff, R.B.M.L.; Deolindo, C.T.P.; Vargas, M.O.; Kleemann, C.R.; Daguer, H. Determination of 62 veterinary drugs in feeding stuffs by novel pressurized liquid extraction methods and LC-MS/MS. *J. Chromatogr. B* **2020**, *1152*, 122232. [CrossRef] [PubMed]
23. Geddes, E.J.; Li, Z.; Hergenrother, P.J. An LC-MS/MS assay and complementary web-based tool to quantify and predict compound accumulation in E. coli. *Nat. Protoc.* **2021**, *16*, 4833–4854. [CrossRef] [PubMed]

24. Wilkes, E.H.; Whitlock, M.J.; Williams, E.L. A data-driven approach for the detection of internal standard outliers in targeted LC-MS/MS assays. *J. Mass Spectrom. Adv. Clin. Lab* **2021**, *20*, 42–47. [CrossRef] [PubMed]

25. Burns, D.T.; Walker, M.J. Origins of the method of standard additions and of the use of an internal standard in quantitative instrumental chemical analyses. *Anal. Bioanal. Chem.* **2019**, *411*, 2749–2753. [CrossRef] [PubMed]

26. Kleigrewe, K.; Niehaus, E.M.; Wiemann, P.; Tudzynski, B.; Humpf, H.U. New approach via gene knockout and single-step chemical reaction for the synthesis of isotopically labeled fusarin C as an internal standard for the analysis of this fusarium mycotoxin in food and feed samples. *J. Agric. Food Chem.* **2012**, *60*, 8350–8355. [CrossRef]

27. Wang, H.X.; Ren, L.S.; Yu, X.; Hu, J.; Chen, Y.; He, G.S.; Jiang, Q.W. Antibiotic residues in meat, milk and aquatic products in Shanghai and human exposure assessment. *Food Control* **2017**, *80*, 217–225. [CrossRef]

28. Chen, H.; Liu, S.; Xu, X.R.; Diao, Z.H.; Sun, K.F.; Hao, Q.W.; Liu, S.S.; Ying, G.G. Tissue distribution, bioaccumulation characteristics and health risk of antibiotics in cultured fish from a typical aquaculture area. *J. Hazard. Mater.* **2018**, *343*, 140–148. [CrossRef]

29. Guidi, L.R.; Santos, F.A.; Ribeiro, A.C.; Fernandes, C.; Silva, L.H.; Gloria, M.B. A simple, fast and sensitive screening LC-ESI-MS/MS method for antibiotics in fish. *Talanta* **2017**, *163*, 85–93. [CrossRef]

30. Guidi, L.R.; Santos, F.A.; Ribeiro, A.; Fernandes, C.; Silva, L.H.M.; Gloria, M.B.A. Quinolones and tetracyclines in aquaculture fish by a simple and rapid LC-MS/MS method. *Food Chem.* **2018**, *245*, 1232–1238. [CrossRef]

31. Bajkacz, S.; Felis, E.; Kycia-Slocka, E.; Harnisz, M.; Korzeniewska, E. Development of a new SLE-SPE-HPLC-MS/MS method for the determination of selected antibiotics and their transformation products in anthropogenically altered solid environmental matrices. *Sci. Total Environ.* **2020**, *726*, 138071. [CrossRef] [PubMed]

32. de Groot, J.C.; Fiers, M.W.; van Ham, R.C.; America, A.H. Post alignment clustering procedure for comparative quantitative proteomics LC-MS data. *Proteomics* **2008**, *8*, 32–36. [CrossRef] [PubMed]

33. Gu, H.D.Z.Y.; DeMichele, M.; Zheng, N.; Zhang, Y.; Pillutla, R.; Zeng, J. Eliminating preparation of multisample external calibration curves and dilution of study samples using the multiple isotop-ologue reaction monitoring (MIRM) technique in quantitative LC-MS/MS bioanalysis. *Anal. Chem.* **2008**, *80*, 4200–4207. [CrossRef]

34. Heudi, O.B.S.; Zimmer, D.; Schmidt, J.; Bill, K.; Lehmann, N.; Bauer, C.; Kretz, O. Towards absolute quantification of therapeutic monoclonal antibody in serum by LC-MS/MS using isotope-labeled anti-body standard and protein cleavage isotope dilution mass spectrometry. *Anal. Chem.* **2019**, *91*, 8652–8659. [CrossRef]

35. Long, T.E.; Keding, L.C.; Lewis, D.D.; Anstead, M.I.; Withers, T.R.; Yu, H.D. Anionic fluoroquinolones as antibacterials against biofilm-producing Pseudomonas aeruginosa. *Bioorg. Med. Chem. Lett.* **2016**, *26*, 1305–1309. [CrossRef] [PubMed]

36. Svahn, O.B.E. Thermal stability assessment of antibiotics in moderate temperature and subcritical water using a pressurized dynamic flow-through system. *Int. J. Innov. Appl. Stud.* **2015**, *11*, 872–880.

37. Hermo, M.P.N.E.; Kır, S.; BarrÓn, D.; Barbosa, J. Improved determination of quinolones in milk at their MRL levels using LC–UV, LC–FD, LC–MS and LC–MS/MS and validation in line with regulation 2002/657/EC. *Anal. Chim. Acta* **2008**, *613*, 98–107. [CrossRef] [PubMed]

38. Chung, J.H.; Cho, K.; Kim, S.; Jeon, S.H.; Shin, J.H.; Lee, J.; Ahn, Y.G. Inter-laboratory validation of method to determine residual enrofloxacin in chicken meat. *Int. J. Anal. Chem.* **2018**, *2018*, 6019549. [CrossRef]

39. *No 1077-1-2008*; Announcement of the Ministry of Agriculture of the People's Republic of China. Simultaneous determination of 17 sulfonamides and 15 quinolones residues in aquatic by LC-MS/MS method. Ministry of Agriculture of the People's Republic of China: Beijing, China, 2008.

40. Vogeser, M.; Seger, C. Pitfalls associated with the use of liquid chromatography-tandem mass spectrometry in the clinical laboratory. *Clin. Chem.* **2010**, *56*, 1234–1244. [CrossRef]

41. Samanidou, V.; Evaggelopoulou, E.; Trotzmuller, M.; Guo, X.; Lankmayr, E. Multi-residue determination of seven quinolones antibiotics in gilthead seabream using liquid chromatography-tandem mass spectrometry. *J. Chromatogr. A* **2008**, *1203*, 115–123. [CrossRef]

42. Zhang, X.; Fang, C.; Huang, D.; Yang, G.; Tang, Y.; Shi, Y.; Kong, C.; Cao, P.; Cai, Y. Determination of 8 biogenic amines in aquatic products and their derived products by high-performance liquid chromatog-raphy-tandem mass spectrometry without derivatization. *Food Chem.* **2021**, *361*, 130044. [CrossRef] [PubMed]

MDPI

Article

Rapid Detection of Malathion, Phoxim and Thiram on Orange Surfaces Using Ag Nanoparticle Modified PDMS as Surface-Enhanced Raman Spectroscopy Substrate

Wenlei Zhai [1], Mingshuo Cao [1], Zhiyong Xiao [2], Dan Li [3] and Meng Wang [1,*]

[1] Institute of Quality Standard and Testing Technology, Beijing Academy of Agriculture and Forestry Sciences, Beijing 100097, China
[2] Beijing Center of AGRI-Products Quality and Safety, Beijing 100029, China
[3] School of Chemical and Environmental Engineering, Shanghai Institute of Technology, Shanghai 201418, China
* Correspondence: wangm@iqstt.cn

Abstract: Malathion, phoxim, and thiram are organophosphates and organosulfur pesticides widely used in agricultural products. The residues of these pesticides present a direct threat to human health. Rapid and on-site detection is critical for minimizing such risks. In this work, a simple approach was introduced using a flexible surface-enhanced Raman spectroscopy (SERS) substrate. The prepared Ag nanoparticles-polydimethylsiloxane (AgNPs-PDMS) substrate showed high SERS activity, good precision (relative standard deviation = 5.33%), and stability (30 days) after optimization. For target pesticides, the linear relationship between characteristic SERS bands and concentrations were achieved in the range of 10~1000, 100~5000, and 50~5000 µg L^{-1} with LODs down to 3.62, 41.46, and 15.69 µg L^{-1} for thiram, malathion, and phoxim, respectively. Moreover, SERS spectra of mixed samples indicated that three pesticides can be identified simultaneously, with recovery rates between 96.5 ± 3.3% and 118.9 ± 2.4%, thus providing an ideal platform for detecting more than one target. Pesticide residues on orange surfaces can be simply determined through swabbing with the flexible substrate before acquiring the SERS signal. This study demonstrated that the prepared substrate can be used for the rapid detection of pesticides on real samples. Overall, this method greatly simplified the pre-treatment procedure, thus serving as a promising analytical tool for rapid and nondestructive screening of malathion, phoxim, and thiram on various agricultural products.

Keywords: surface-enhanced Raman spectroscopy; organophosphates pesticide; thiram; malathion; phoxim; Ag nanoparticles; rapid detection

1. Introduction

Pesticides are widely used to protect plants from insects and diseases caused by bacteria and fungi in agricultural production all over the world. Among them, organophosphate insecticides, including malathion and phoxim, can effectively kill insects by targeting their nervous system [1]. Organosulfur fungicides such as thiram are also used for the preservation of fruits and vegetables [2]. Therefore, the combination of these pesticides is commonly used in agriculture [3]. However, the overuse of pesticides has already caused serious problems in terms of environmental pollution [4]. Moreover, their residues in agricultural products pose a direct threat to human health [5,6]. For example, there are reports of several health issues caused by thiram, with symptoms such as lethargy and motor disturbances [7]. Exposure to a high enough level of malathion could lead to various symptoms, including nausea, vomiting, muscle cramps, abdominal pain, and diarrhea [8]. Phoxim may have an acute effect on the nervous systems of humans and livestock through acetylcholinesterase inhibition [9]. Typical symptoms caused by phoxim are similar to malathion, and include nausea, vomiting, diarrhea, and so forth. Because of the potential

to cause those severe health issues, strict regulations have been introduced to minimize exposure to the aforementioned pesticides in many countries [10].

To better protect humans and livestock from the harmful effects of pesticides, it is urgently needed to develop effective analytical methods, especially those that can target mixed pesticides [11]. So far, malathion, phoxim, and thiram in agricultural products can be accurately measured using high-performance liquid chromatography (HPLC) [12], gas chromatography tandem mass spectrometry (GC-MS) [13], and liquid chromatography tandem mass spectrometry (LC-MS) [14]. However, these techniques require sophisticated and expensive instruments, as well as fully-trained technicians, to operate. The pre-treatment processes for food samples are also time-consuming [15]. In order to achieve rapid and on-site screening for these pesticides, many analytical methods have been developed in recent years, including electrochemical sensors [16,17], enzymatic inhibition-based sensors [18], enzyme-linked immunosorbent assay (ELISA) [19], lateral flow strip [20], surface-enhanced Raman spectroscopy (SERS) [21], microfluidics [22], and so forth. Among them, in recent decades SERS has been developed as a promising analytical platform for rapid and on-site detection of various target molecules [23,24]. Highly sensitive SERS detection depends on the enhancement of the Raman scattering signal generated from the localized surface plasmon resonance (LSPR) effect of Au or Ag nanomaterials. It presents unique advantages, including high sensitivity, instant data acquisition, highly specific molecular fingerprint from the SERS spectrum, low operating cost, and portability of devices [25,26]. Therefore, many SERS-based strategies have been reported for applications in the fields of food safety [27–29], environment monitoring [30], clinical diagnosis [31], security checking [32], and so forth.

In order to accomplish rapid and on-site detection of pesticides on agricultural products, a great deal of effort has been devoted to designing and fabricating Ag or Au nanomaterials as SERS substrates [33]. Recently, a new trend has been developed by combining a flexible substrate with SERS-active nanoparticles [34–36]. Simple sampling processes can be carried out by swabbing the target surface with the flexible substrate, while qualitative and even quantitative detection can be realized by SERS [37]. For example, a flexible SERS substrate was introduced by applying Au and Ag nanoparticles to an aluminum foil-based ZnO nanosheet. Extraction and identification of thiram on fruits and vegetables were accomplished using this substrate [38]. Apart from metal foils, polymer films have also been studied to fabricate flexible substrates for SERS [39]. Bai et al. spin-coated a monolayer of Ag island on a waterborne polyurethane emulsion film and applied the substrate for in-situ detection of thiram on apples [40]. In another study, a flexible Au nanostars/polydimethylsiloxane (PDMS) substrate was recently developed for in-situ determination of methyl parathion on fruit [41]. Wang et al. also reported the rapid detection of mixed chlorpyrifos and 2,4-dichlorophenoxyacetic acid residues on apple surfaces by using Ag colloid as a SERS substrate [42]. All these studies show the outstanding performance and great potential of applying a flexible substrate for fast and on-site SERS detection of pesticides on fruit surfaces. However, many studies still focus on a single type of pesticide, especially thiram, as the target [43,44]. New methods capable of rapidly determining mixed pesticides on one substrate are more desirable in practical applications [45].

Herein, we report the preparation of a flexible SERS substrate for the fast and simultaneous determination of three pesticides on orange surfaces. The proposed SERS substrate was fabricated by anchoring SERS-active Ag nanoparticles (AgNPs) on chemically modified PDMS thin film. The functionalization of PDMS and the surface density of AgNPs were optimized to minimize interference and achieve high SERS activity. Rhodamine 6G (R6G) was employed to evaluate the sensitivity, time stability, and signal uniformity of the prepared substrate. For pesticide detection, two organophosphate insecticides, malathion and phoxim, and the fungicide thiram were chosen as the targets. Qualitative and semi-quantitative measurement of each pesticide was established using a standard solution. Benefitting from the molecular fingerprint property of SERS spectra, the presence of each target compound can be identified according to the characteristic SERS bands, allowing

simultaneous identification of the mixture of three pesticides on orange surfaces. In general, this method provides a facile and affordable platform for rapid and on-site determination of different hazardous chemicals on the surfaces of food samples.

2. Materials and Methods

2.1. Chemicals and Reagents

Silver nitrate (AgNO$_3$, 99.7%) and R6G (95.0%) were purchased from Energy Chemical Co., Ltd. (Shanghai, China). Sodium citrate (99.0%) was purchased from Innochem Co., Ltd. (Beijing, China). PDMS Sylgard 184 was supplied by Dow Corning Corporation (Midland, MI, USA). (3-Aminopropyl) triethoxysilane (APTES, 99.0%) was obtained from Macklin Biochemical Co., Ltd. (Shanghai, China). Malathion (purity: 98.33%, expanded uncertainty: 0.48%), phoxim (purity: 97.26%, expanded uncertainty: 0.72%), and thiram (purity: 98.36%, expanded uncertainty: 0.56%) certified reference materials were purchased from LGC Standards GmbH (Wesel, Germany). Methanol and acetonitrile were supplied by Sinopharm Chemical Reagent Co., Ltd. (Shanghai, China). Deionized water was supplied by Titanchem Co., Ltd. (Shanghai, China) and used without further purification throughout the experiment.

2.2. Synthesis and Characterization of AgNPs

The AgNPs used in this study were synthesized following a modified Lee and Miesel protocol [46]. In brief, AgNO$_3$ (19 mg) was added to 100 mL of deionized water. The solution was heated to boiling point. Sodium citrate solution (2 mL, 10 g L^{-1}) was poured into the AgNO$_3$ solution under vigorous stirring. The reaction solution was kept at gentle boiling for 30 min under continuous heating. The color of the colloid turned from light yellow to gray during the reaction. After that, the obtained Ag colloid was cooled at room temperature and stored in a refrigerator. All glassware was cleaned and rinsed with deionized water multiple times before use.

Transmission electron microscopy (TEM) images and energy-dispersive X-ray spectrum of the synthesized AgNPs were recorded with a transmission electron microscope (Tecnai G2 F30, FEI Co., Ltd., Hillsboro, OR, USA). The UV-Vis absorption spectrum was collected using a multimode plate reader (EnVision, PerkinElmer Inc., Waltham, MA, USA).

2.3. Preparation of Amino-Functionalized PDMS Film

The flexible PDMS film was prepared by mixing 6 g of the main agent with 0.6 g auxiliary agent. The mixture was stirred with a glass rod and poured into a 9 cm plastic petri dish to form an even and thin fluid layer. It was then transferred to a vacuum oven to remove the bubbles and heated at 60 °C for 10 h. After solidification, the transparent PDMS film was cut into small slices of squares (~5 mm × 5 mm) for further use.

For the chemical modification of the PDMS film, a series of APTES ethanol solutions were prepared with different concentrations, from 0.002% to 2% (Vf). Square slices of the PDMS films were immersed in APTES solutions for 2 h. After that, the amino-functionalized PDMS was rinsed with deionized water multiple times before drying at room temperature.

2.4. Preparation of AgNPs-PDMS SERS Substrate

Ag colloids with different concentrations were prepared by concentrating or diluting the as-synthesized Ag colloid. In detail, the original Ag colloid (1 mL) was pipetted into centrifuge tubes and precipitated by centrifuging at 8000 rpm for 10 min (MiniSpin, Eppendorf, Hamburg, Germany). The supernatant was carefully drawn out using a pipette, and the remaining AgNPs were resuspended with 100 μL (Ag10×), 200 μL (Ag5×), 500 μL (Ag2×), 1 mL (Ag1×), and 2 mL (Ag0.5×) deionized water, respectively.

For the fabrication of AgNPs-PDMS substrate, Ag colloid (5 μL) was dropped on the amino-functionalized PDMS film. After drying under vacuum, a uniform circle of AgNPs was formed on the PDMS. The morphology of the prepared SERS substrate was characterized using a scanning electron microscope (Quanta 650FEG, FEI Co., Ltd., Hillsboro, OR, USA).

2.5. Optimization and Evaluation of AgNPs-PDMS SERS Substrate

SERS activity of the prepared AgNPs-PDMS substrate was investigated by incubating with different concentrations of R6G solutions (0.1 μg L^{-1}~1 mg L^{-1}). SERS spectra were collected using a Raman microscope system (DXR, Thermo Fisher Scientific Inc., Waltham, MA, USA) with optimized parameters: excited at 780 nm, scanning range between 500 and 1900 cm^{-1}, objective lens 10×, laser power 0.5 mW, integration time 2 s.

For evaluating signal uniformity, sixteen random spots on the substrate were chosen, and SERS spectra were collected after incubating with 100 μg L^{-1} R6G solution. Time stability was also examined by collecting the SERS spectrum every 5 days. The tested substrate was stored in a sealed tube filled with nitrogen gas after each measurement.

2.6. Semi-Quantitative Analysis of Three Pesticides and Determination of Intra-Batch and Inter-Batch Precision

Firstly, malathion and phoxim stork solutions with a concentration of 1000 mg L^{-1} were prepared by dissolving 1 μL of malathion and phoxim in 1.230 mL and 1.176 mL acetonitrile, respectively. Standard solutions with sixteen different concentrations (100, 50, 20, 10, 5, 2, 1 mg L^{-1} and 500, 200, 100, 50, 20, 10, 5, 2, 1 μg L^{-1}) were prepared by diluting the stork solution with corresponding amounts of solvent. Similarly, thiram stock solution was prepared by first weighing 10 mg thiram, dissolved in 10 mL methanol and diluted into solutions with sixteen different concentrations. Mixed solutions were prepared by mixing three standard solutions at different concentrations.

For semi-quantitative analysis of the three pesticides, SERS spectra of different concentrations of standard solutions were acquired with the following parameter setting: laser power 1 mW, integration time 5 s. In order to evaluate the intra-batch precision of this method, AgNPs-PDMS substrates fabricated in the same batch were used to record SERS spectra of 1000 μg L^{-1} thiram, malathion, and phoxim, respectively. Six SERS spectra were collected for each pesticide, and the relative standard deviation (RSD) of SERS intensity was calculated as the intra-batch precision. For inter-batch precision, six batches of AgNPs-PDMS substrates were prepared, then SERS spectra were recorded for each pesticide at the concentration of 1000 μg L^{-1}. The inter-batch precision was determined by calculation of the RSD of SERS signals generated from different batches of AgNPs-PDMS substrates.

2.7. Detection of Three Pesticides on Orange Surfaces

Thiram, malathion, and phoxim were tested on the surfaces of oranges from a local market to examine the performance of the AgNPs-PDMS substrate. Bought oranges were washed with water to clean the surface. Then, 10 μL mixed solution of pesticides at different concentrations (100 μg L^{-1} for thiram, 500 μg L^{-1} for malathion, 200 μg L^{-1} for phoxim) was spiked on the orange peel. After solvent evaporation, the spot was sprayed with a small amount of ethanol, pressed, and gently swabbed by the AgNPs-PDMS film to transfer pesticide residues onto the substrate. The SERS signal of the swabbed substrate was acquired for qualitative and semi-quantitative analysis. The Raman parameter setting was as follows: excitation wavelength and scanning range remained the same as before, laser power 3 mW, integration time 10 s.

2.8. Statistical Analysis

In this study, each sample was scanned three times, and the average signal was recorded as the SERS spectra. Baseline correction was performed using OMNIC 9 software (Thermo Fisher scientific Inc., Waltham, MA, USA). After that, spectral data were implemented in OriginPro 8 software (OriginLab Corporation, Northampton, MA, USA) for further analysis, including integration of the peak areas, linear fitting to obtain the regression equations, and calculation of relative standard deviation (RSD). The size distribution of the synthesized AgNPs was counted using ImageJ software (National Institutes of Health, Bethesda, MD, USA). All figures were plotted using OriginPro 8 software.

3. Results and Discussion

3.1. Characterization of the Synthesized AgNPs

In this study, TEM images, energy-dispersive X-ray, and UV-Vis spectroscopy were first used to characterize the synthesized AgNPs. As shown in Figure 1a, the AgNPs were well dispersed and the average size was measured as 70~80 nm. The energy-dispersive X-ray spectrum presented in Figure 1b confirmed the synthesized nanoparticles were composed of Ag. The UV-Vis absorption spectrum (see Figure 1b) showed a characteristic peak of AgNPs at 420 nm, which agreed well with previous literature reports [47]. The relatively narrow half band width of the absorption curve suggested the synthesized AgNPs had good size distribution [48].
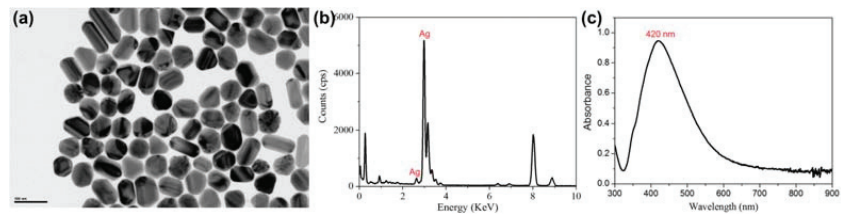
Figure 1. TEM image (**a**), energy-dispersive X-ray spectrum (**b**), and UV-Vis absorption spectrum (**c**) of the synthesized AgNPs. Scale bar in (**a**): 100 nm.

The surface of PDMS film exhibits a hydrophobic effect, making it undesirable for coating with aqueous Ag colloid. Therefore, chemical modification was carried out by simply incubating the PDMS film in an APTES ethanol solution. Presumably, a small number of hydroxyl groups on the PDMS surface enabled the formation of chemical bonds with APTES, resulting in amino functionalization of PDMS and reversing the hydrophobic property. After dropping 5 μL concentrated Ag colloid and drying in a vacuum, a small circle with metallic appearance was observed, as presented in the inset of Figure 2c and S1.
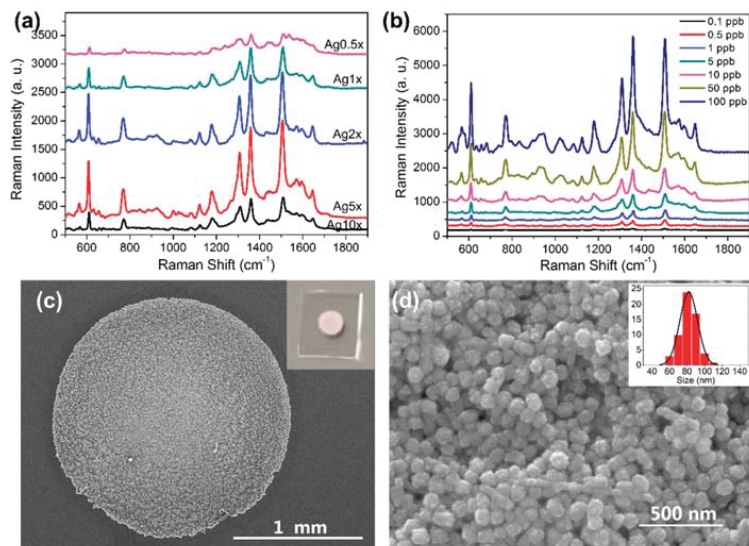
Figure 2. SERS spectra of R6G on AgNPs-PDMS substrates with various surface densities of AgNPs (**a**). SERS spectra of R6G (0.1~100 μg L^{-1}) on optimized AgNPs-PDMS substrate (**b**). SEM images of the optimized AgNPs-PDMS substrate under different scales (**c,d**). Inset of (**c**): photo of the prepared substrate. Inset of (**d**): statistical analysis of size distribution of the modified AgNPs.

3.2. Optimization and Characterization of AgNPs-PDMS Substrate

As the first step of modification, the amino functionalization process was optimized by adjusting the concentration of the APTES solution. PDMS slices were immersed in different concentrations of APTES ethanol solutions (0.002%, 0.005%, 0.01%, 0.02%, 0.05%, 0.1%, 0.2%, 0.5%, 1%, and 2%, Vf). After dropping Ag colloid and drying, it was observed that the minimum concentration of APTES was 0.01% for the successful formation of the circular AgNPs substrate (see Supplementary Materials, Figure S1), and it was established as the optimized condition for further experiments. Notably, by using a higher amount of APTES, the obtained AgNPs substrate was encapsulated with a thin layer of transparent coating in the SEM image (see Supplementary Materials, Figure S2), presumably caused by the self-polymerization of extra APTES [49]. In the SERS measurements, this coating material could prevent the access of target molecules to the proximity of AgNPs, resulting in poor sensitivity. Therefore, it is necessary to restrict the use of APTES to a minimum required level. Compared with a previous report, which required the treatment of PDMS with piranha solution before functionalization [41], this method simplifies the modification process and avoids the preparation and use of dangerous reagents.

After amino functionalization, the amount of AgNPs is another crucial factor to determine SERS activity. Thus, Ag colloids with different concentrations were prepared and evaluated. R6G has been extensively used as a probe molecule for SERS due to its excellent Raman properties [50]. In this study, it was also employed to investigate and optimize the performance of our substrate. As presented in Figure 2a, the SERS spectra of 100 µg L^{-1} R6G solution showed that PDMS modified with Ag5×, which was 5-fold concentrated from the original Ag colloid, produced the strongest SERS signal. The peak intensity at 1358 cm^{-1} was five times higher than Ag0.5×. This might be caused by the fully packed AgNPs through the concentrating process, which generate more "hot spot" nanostructures in SERS enhancement. The enhancement factor (EF) for R6G was calculated based on the widely adopted equation [51]:

$$EF = \frac{I_{SERS}/I_{bulk}}{N_{SERS}/N_{bulk}}$$

where I_{SERS} and I_{bulk} stand for peak intensities at 1358 cm^{-1} from both SERS and Raman spectrum of R6G, respectively. N_{SERS} and N_{bulk} represent the estimated number of molecules stroked by the laser on the SERS substrate and R6G powder. The calculation process is detailed in Supplementary Materials, Figure S3. As a result, the EF of the optimized substrate was estimated to be 1.64×10^5, which is sufficient to provide significant enhancement of Raman intensity from analytes adsorbed on the AgNPs-PDMS substrate [52].

In Figure 2b, SERS spectra of R6G with different concentrations are presented. The SERS intensity gradually increased with higher concentration of the tested solutions. As low as 0.1 µg L^{-1} of R6G can be detected using the AgNPs-PDMS substrate. This result indicates it is feasible to use this substrate for semi-quantitative analysis.

After optimization, the morphology of the optimized substrate was characterized via scanning electron microscopy (SEM). From the image shown in Figure 2c, we can observe that the diameter of the circle was approximately 2 mm. The zoomed in image shows AgNPs were densely distributed on the PDMS film (see Figure 2d). The approximate distance between AgNPs could lead to strong SERS enhancement due to the generation of "hot spots" for molecules trapped between the gaps of AgNPs [53]. Moreover, the relatively even distribution of aggregated AgNPs guarantees a uniform distribution of the SERS signal, which is also vital for reliable SERS measurement. Statistical analysis of the distribution of particle size is presented in the inset of Figure 2d. The result showed AgNPs with sizes between 80 and 90 nm are dominant, which agreed well with the observation of TEM image and UV-Vis spectrum.

3.3. Evaluation of Signal Uniformity and Stability

Apart from sensitivity, signal uniformity is another important aspect for assessing the performance of SERS substrates. In this experiment, 100 μg L^{-1} R6G was still used as the testing solution. As shown in Figure 3a, by measuring 16 randomly distributed points on the optimized substrate, signal intensity at 1358 cm^{-1} was analyzed, and the result showed the prepared substrate provided uniform enhancement of the Raman signal. The RSD was calculated as 5.33% (see Figure 3b), which is comparable with previous studies. In practical application, a SERS substrate with longer time stability has extra advantage. To evaluate the stability of our AgNPs-PDMS substrate, 100 μg L^{-1} R6G solution was dropped and dried. After recording the SERS spectrum, it was stored in a nitrogen environment and remeasured every 5 days. From Figure 3c,d, we can tell that the substrate showed relatively good stability, with 80% SERS activity preserved in the period of one month. Even though a decrease of SERS activity was observed, considering the easy to oxidize nature of Ag, the stability of this substrate is still acceptable [54]. In addition, benefitting from the easy to fabricate procedure and low cost, it is easy to resupply the substrate in large quantities.
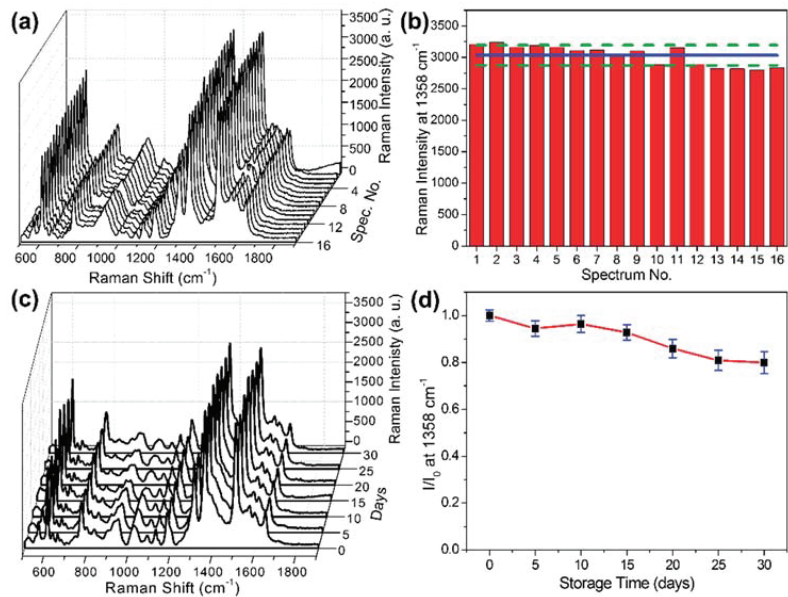
Figure 3. SERS spectra (**a**) and distribution of signal intensity (**b**) at 1358 cm^{-1} of R6G (100 μg L^{-1}) collected from 16 random points on optimized AgNPs−PDMS substrate. The solid line in b represents the average SERS intensity, and the dotted lines indicate the RSD. SERS spectra (**c**) and the ratio of intensities (**d**) at 1358 cm^{-1} of R6G (100 μg L^{-1}) acquired on optimized AgNPs-PDMS sub-strate stored in nitrogen atmosphere between 0 and 30 days.

3.4. Detection of Individual Pesticide on AgNPs-PDMS Substrate

The optimized substrate was employed to test standard solutions of thiram, malathion, and phoxim. Figure 4 presents the SERS spectra of different concentrations of thiram (a), malathion (c), and phoxim (e). The linear calibration plots of all three pesticides are also illustrated in Figure 4b,d,f, respectively. SERS detection of thiram has been extensively studied in previous reports [38,40,43,44]. In this study, thiram was chosen first for pesticide detection. As illustrated in Figure 4a, characteristic peaks at 558, 925, 1147, 1384, and 1513 cm^{-1} are identified and assigned in Table 1 according to Figure S4a and the literature [55]. In detail, the SERS band at 558 cm^{-1} corresponds to the stretching of the S−S bond. The broad peak at 925 cm^{-1} is the combination of the stretching mode of the

C=S double bond and CH$_3$N. The major signal at 1384 cm^{-1} is assigned to symmetric CH$_3$ deformation. The Raman shift of all these peaks matches well with previous literature reports. Among them, the peak at 1384 cm^{-1} provides the highest SERS intensity, thus it was chosen for semi-quantitative analysis. As presented in Figure 4b, for thiram between the concentrations of 10 and 1000 μg L^{-1}, the plotting of an integrated peak area at 1384 cm^{-1} against the logarithm of thiram concentrations presents a linear relationship, with a coefficient of determination (R^2) of 0.9665. This result demonstrates that the proposed substrate can be applied for qualitative and semi-quantitative detection of thiram at low levels. The limit of detection (LOD) is calculated as 3.62 μg L^{-1} using the widely adopted formula LOD = 3σ/S, in which σ represents the standard deviation of background signal and S stands for the slope of the linear calibration curve. For practical application, the maximum residue limit (MRL) for thiram in apple is 5 mg kg^{-1}, according to the national food safety standard (GB 2763-2019, China). Therefore, the sensitivity of this method is satisfied for thiram detection.
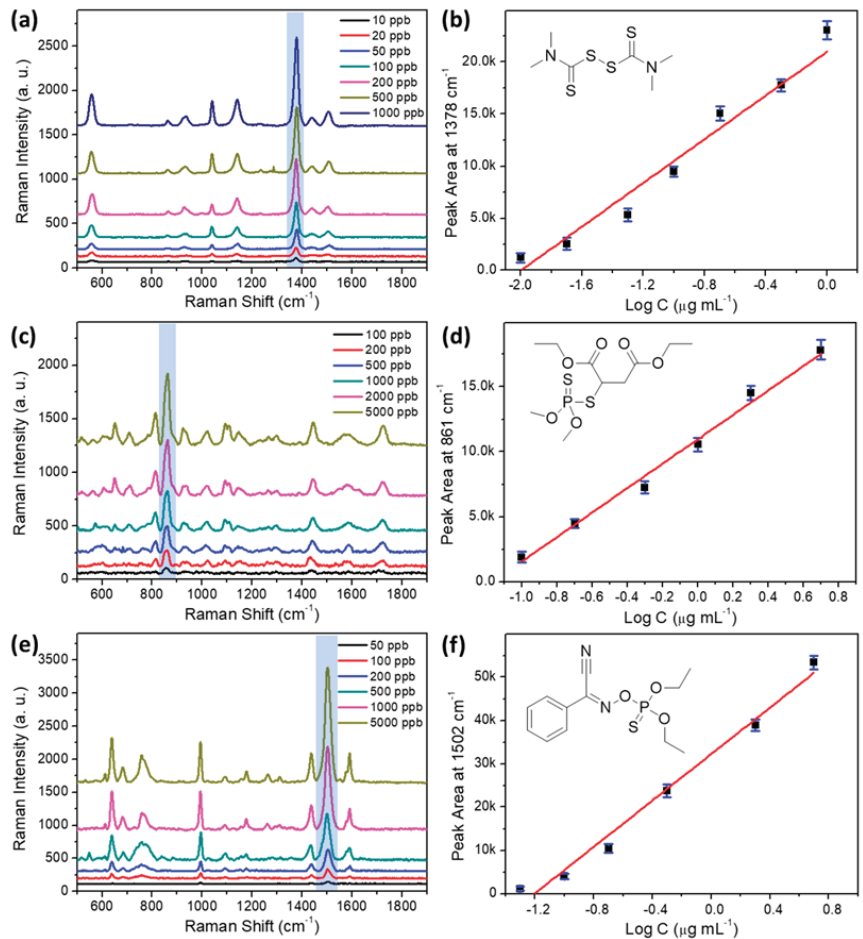
Figure 4. SERS spectra of different concentrations of thiram (**a**), malathion (**c**), and phoxim (**e**). Linear calibration plots between the integrated peak area and the logarithm of concentration for thiram (**b**), malathion (**d**), and phoxim (**f**). Inset of (**b**,**d**,**f**): molecular structure of thiram, malathion, and phoxim.

Table 1. Assignments of some characteristic bands in Raman and SERS spectra of three tested pesticides.

Analyte	Raman/cm^{-1}	SERS/cm^{-1}	Assignments
thiram	557	558 (m)	ν(S−S)
	973	925 (w)	ν(CH$_3$N); ν(C=S)
	1149	1147 (m)	ρ(CH$_3$); ν(C−N)
	1374	1384 (s)	δ_s(CH$_3$); ν(C−N)
	1396	1443 (w)	δ_{as}(CH$_3$)
	1455	1513 (m)	ν(C−N); δ(CH$_3$); ρ(CH$_3$)
malathion	716	709 (b, w)	ν(P=S); ν(P−O)
	824	815 (m)	γ(C−H)
	858	862 (s)	ν_s(C−O−C)
	1096	1094 (m)	ν(C−C)
	1164	1144 (w)	ν(P−S)
	1452	1444 (m)	ν_s(C−O)
	1736	1726 (m)	ν(C=C)
phoxim	750	758 (b, m)	ν(P=S)
	999	995 (m)	γ(C−H)
	1098	1092 (w)	γ(C−H)
	1182	1178 (w)	γ(C−H)
	1302	1264 (w)	δ_s(CH$_3$)
	1446	1437 (m)	ν_{as}(CH$_3$)
	1555	1502 (s)	ν(C$_6$H$_5$)
	1597	1591 (m)	ν(C$_6$H$_5$)

b—broad; s—strong; m—middle; w—weak; ν—stretching; δ—bending; ρ—rocking; γ—out-of-plane bending; ν_s—symmetric stretching; ν_{as}—asymmetric stretching; δ_s—symmetric bending; δ_{as}—asymmetric bending.

For organophosphates insecticides, malathion is tested first. The resulted SERS spectra are presented in Figure 4c. By comparing with the Raman spectrum of the reference material, it is confirmed that the recorded SERS signal is produced by SERS enhancement of malathion molecules (see Supplementary Materials, Figure S4b). The characteristic Raman band at 815 cm^{-1} is attributed to the out-of-plane bending of the C−H bond. The strong signal at 862 cm^{-1} is caused by the symmetric stretching mode of the C−O−C bond. The broad peak at 1144 cm^{-1} is generated from the stretching of the P−S bond. Finally, the two bands at 1444 and 1726 cm^{-1} are correlated with the stretching mode of the C−O and C=O bonds, respectively. The pattern of these characteristic peaks can be used for qualitative identification of malathion. For semi-quantitative detection, Figure 4d shows the linear fitting curve of data plotted between the logarithm of malathion concentration and integrated peak area at 862 cm^{-1}. As summarized in Table 2, a linear range of 100 to 5000 µg L^{-1} is achieved using this method, with a calculated LOD of 41.46 µg L^{-1}. Even though the sensitivity is not as high as thiram, probably due to the weak affinity between malathion molecules and the Ag substrate, it can still be useful for on-site inspection, considering the relatively high MRL of 4 mg kg^{-1} in oranges.

Phoxim is another target insecticide in this study due to its known toxicity, which is an acetylcholinesterase inhibitor that affects the human nervous system. According to GB 2763-2019, the MRLs of phoxim are set as 0.05 mg kg^{-1} in most fruits. Unlike thiram, SERS detection of phoxim has rarely been reported. Using an optimized AgNPs-PDMS substrate, SERS measurement of different concentrations of phoxim standard solutions were performed. Characteristic peaks can be observed on the acquired SERS spectra in Figure 4e. By comparing with the Raman spectrum of phoxim in Figure S4c, characteristic SERS bands can be identified. Among them, the broad peak at 758 cm^{-1} should be recognized as the stretching vibration of the P=S double bond. Peaks at 995, 1092, and 1178 cm^{-1} are all attributed to the in-plane bending of the C−H bond. Different from thiram and malathion, SERS spectra of phoxim showed characteristic stretching vibration signals of the phenyl ring at 1437, 1502, and 1591 cm^{-1}, which provide important information for distinguishing its signal in a mixed sample. For semi-quantitative detection, the strongest peak at 1502 cm^{-1} is used as a reference. A linear relationship is established between

the logarithm of concentrations and signal strength. The linear range is between 50 and 5000 µg L^{-1}, with LOD reaching 15.69 µg L^{-1}.

Table 2. Summary of validation parameters of the proposed method.

Parameters	Thiram	Malathion	Phoxim
Characteristic peak for semi-quantitative analysis (cm^{-1})	1378	861	1502
LOD (µg L^{-1})	3.62	41.46	15.69
Linear range (µg L^{-1})	10~1000	100~5000	50~5000
Regression equation	y = 11,226.81x + 21,852.76	y = 9556.87x + 11,017.77	y = 26,790.12x + 32,245.99
R^2	0.9665	0.9891	0.9805
Intra-batch precision (% RSD)	4.65	3.74	3.18
Inter-batch precision (% RSD)	8.27	5.96	7.03
Recovery rate (%) *	96.5 ± 3.3	104.6 ± 1.9	118.9 ± 2.4

* Recovery rates were calculated according to SERS spectra of the mixed samples.

As presented in Table 2, the R^2 of the calibration curves are in the range of 0.9665~0.9891 for the tested pesticides. Comparing with other quantitative analysis techniques such as GC-MS and LC-MS, the linearity of this method is relatively poorer. It might be caused by surface defects on the AgNPs-PDMS substrate, which give rise to uneven enhancement of the Raman signal. Nonetheless, the coefficients of determination achieved in this study are at the same level with previously reported SERS-based methods [41,42,56]. Considering that the priority of this study is to establish a method for the rapid screening of pesticide residues, the linearity of the regression equations should be acceptable for semi-quantitative SERS analysis.

To investigate the precision of this method for pesticide detection, a series of experiments was conducted by measuring the SERS spectra of each pesticide using substrates from the same and different batches. The results are summarized in Table 2. For the tested pesticides, the RSDs are between 3.18% and 4.65% for the SERS signals obtained from the same batch of AgNPs-PDMS substrates. In the case of inter-batch precision, SERS spectra from six different batches of substrates were collected, and the RSDs varies from 5.96% to 8.27%. These results indicate that consistent SERS measurements can be performed on different substrates, and the precision of this method is acceptable for rapid and on-site detection.

3.5. Detection of Mixed Pesticides on Orange Surface Using AgNPs-PDMS Substrate

After determining the calibration curve of each pesticide using the AgNPs-PDMS substrate, our next aim is to accomplish semi-quantitative detection of three pesticides simultaneously. A mixed solution of malathion (500 µg L^{-1}), thiram (100 µg L^{-1}), and phoxim (200 µg L^{-1}) was prepared and measured by SERS using the AgNPs-PDMS substrate. In Figure 5a, the characteristic peaks in the SERS spectrum of the mixed sample can be used for distinguishing each pesticide. As labeled in different colors, for each component there are at least two or three exclusive peaks without overlapping. In other words, benefiting from the molecular fingerprint property of SERS, the characteristic information of each pesticide can be extracted from the SERS signal of the mixed sample. According to integrated peak areas at 860, 1378, and 1506 cm^{-1}, the recovery rates were calculated as 104.6 ± 1.9%, 96.5 ± 3.3%, and 118.9 ± 2.4% for malathion, thiram, and phoxim, respectively. The recovery rate for phoxim is higher than expected, presumably due to slightly overlapping with the weak band of thiram at 1513 cm^{-1}. Nonetheless, this study confirms that the semi-quantitative analysis of three pesticides from a complex environment is feasible using this method.
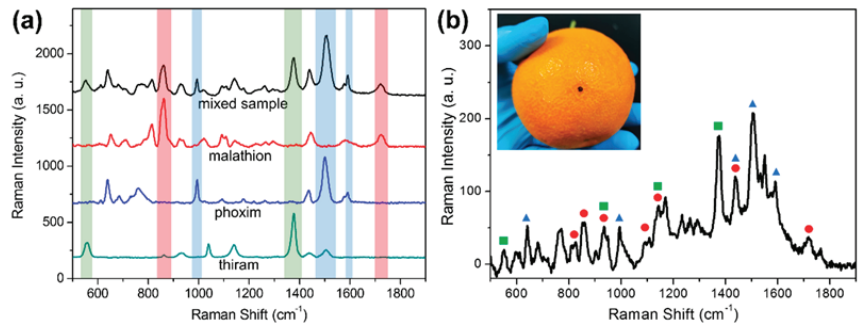
Figure 5. SERS spectra of mixed (black curve) and single pesticides (thiram, malathion, and phoxim) using an AgNPs-PDMS substrate (**a**). SERS spectrum of orange surface spiked with mixed pesticides after swab sampling using an AgNPs−PDMS substrate; characteristic SERS bands are labeled for each pesticide: thiram (green square), malathion (red circle), and phoxim (blue triangle) (**b**). Inset of (**b**): photo of performing swab sampling using the flexible SERS substrate.

Benefitting from the flexible property of the AgNPs-PDMS substrate, it is possible to transfer pesticide residues from the orange surface onto the substrate for SERS measurement. Comparing with other techniques, this method does not require the additional pre-treatment of oranges samples. In this work, a mixed solution of three pesticides was spiked onto the surface of oranges as the tested sample. After solvent evaporation, the orange surface was sprayed with the minimum amount of ethanol and covered by the AgNPs-PDMS substrate. As shown in the inset of Figure 5b, through gentle pressing and swabbing, adequate contact between the orange surface and the substrate was made, thus sampling of the spiked pesticides was completed. From the SERS spectrum presented in Figure 5b, it is obvious that the characteristic peaks of each pesticide can be identified. In detail, SERS signals at 552 and 1376 cm^{-1} are attributed to thiram; peaks at 811, 860, 1093, and 1718 cm^{-1} are assigned to malathion; and peaks at 640, 995, 1506, and 1591 cm^{-1} indicate the presence of phoxim. It is worth noting that no obvious matrix interferences can be observed in the SERS spectrum. Presumably, the surface of the tested orange did not break down owing to the swab sampling approach, resulting in an almost neglectable matrix effect for SERS measurements. This experiment demonstrates that it is feasible to conduct the rapid screening of mixed pesticides on orange surfaces using this flexible and low-cost SERS substrate.

4. Conclusions

In summary, a simple and robust method was proposed for the rapid screening of three pesticide residues on orange surfaces using SERS. Flexible SERS substrates were prepared by modifying AgNPs on amino-functionalized PDMS films. The optimized substrates showed high sensitivity, good uniformity, and stability. For pesticide detection, thiram, malathion, and phoxim were measured using this substrate. Linear relationships were established for each analyte, enabling semi-quantitative detection of these pesticides by SERS. Moreover, the simultaneous determination of three pesticides on orange surfaces was achieved by performing a swab sampling process. Compared with other methods, this approach allows rapid and nondestructive detection of mixed pesticides, with low-cost material and an easy to operate procedure. No extra treatment of samples is required before testing, and the substrate can be directly discarded after use. It is feasible to further extend this method for the rapid and on-site detection of other hazardous substances on various fruits.

References

1. Bajwa, U.; Sandhu, K.S. Effect of handling and processing on pesticide residues in food- a review. *J. Food Sci. Technol.* **2014**, *51*, 201–220. [CrossRef] [PubMed]
2. Zhu, G.-Y.; Chen, Y.; Wang, S.-Y.; Shi, X.-C.; Herrera-Balandrano, D.D.; Polo, V.; Laborda, P. Peel Diffusion and Antifungal Efficacy of Different Fungicides in Pear Fruit: Structure-Diffusion-Activity Relationships. *J. Fungi* **2022**, *8*, 547. [CrossRef] [PubMed]
3. Ma, M.; Chen, C.; Yang, G.; Li, Y.; Chen, Z.; Qian, Y. Combined cytotoxic effects of pesticide mixtures present in the Chinese diet on human hepatocarcinoma cell line. *Chemosphere* **2016**, *159*, 256–266. [CrossRef] [PubMed]
4. Mali, H.; Shah, C.; Raghunandan, B.H.; Prajapati, A.S.; Patel, D.H.; Trivedi, U.; Subramanian, R.B. Organophosphate pesticides an emerging environmental contaminant: Pollution, toxicity, bioremediation progress, and remaining challenges. *J. Environ. Sci.* **2023**, *127*, 234–250. [CrossRef]
5. Dara, D.; Drabovich, A.P. Assessment of risks, implications, and opportunities of waterborne neurotoxic pesticides. *J. Environ. Sci.* **2023**, *125*, 735–741. [CrossRef]
6. Bhanti, M.; Taneja, A. Contamination of vegetables of different seasons with organophosphorous pesticides and related health risk assessment in northern India. *Chemosphere* **2007**, *69*, 63–68. [CrossRef]
7. Kulyar, M.F.; Yao, W.; Mo, Q.; Ding, Y.; Zhang, Y.; Gao, J.; Li, K.; Pan, H.; Nawaz, S.; Shahzad, M.; et al. Regulatory Role of Apoptotic and Inflammasome Related Proteins and Their Possible Functional Aspect in Thiram Associated Tibial Dyschondroplasia of Poultry. *Animals* **2022**, *12*, 2028. [CrossRef]
8. Liu, Y.; Liu, S.; Zhang, Y.; Qin, D.; Zheng, Z.; Zhu, G.; Lv, Y.; Liu, Z.; Dong, Z.; Liao, X.; et al. The degradation behaviour, residue distribution, and dietary risk assessment of malathion on vegetables and fruits in China by GC-FPD. *Food Control* **2020**, *107*, 106754. [CrossRef]
9. Yang, N.; Zhou, X.; Yu, D.; Jiao, S.; Han, X.; Zhang, S.; Yin, H.; Mao, H. Pesticide residues identification by impedance time-sequence spectrum of enzyme inhibition on multilayer paper-based microfluidic chip. *J. Food Process Eng.* **2020**, *43*, e13544. [CrossRef]
10. Chen, Z.; Xu, Y.; Li, N.; Qian, Y.; Wang, Z.; Liu, Y. A national-scale cumulative exposure assessment of organophosphorus pesticides through dietary vegetable consumption in China. *Food Control* **2019**, *104*, 34–41. [CrossRef]
11. Mirres, A.C.; Silva, B.E.; Tessaro, L.; Galvan, D.; Andrade, J.C.; Aquino, A.; Joshi, N.; Conte-Junior, C.A. Recent Advances in Nanomaterial-Based Biosensors for Pesticide Detection in Foods. *Biosensors* **2022**, *12*, 572. [CrossRef] [PubMed]
12. Hejabri kandeh, S.; Amini, S.; Ebrahimzadeh, H. PVA/Stevia/MIL-88A@AuNPs composite nanofibers as a novel sorbent for simultaneous extraction of eight agricultural pesticides in food and vegetable samples followed by HPLC-UV analysis. *Food Chem.* **2022**, *386*, 132734. [CrossRef] [PubMed]
13. Yang, X.-B.; Ying, G.-G.; Kookana, R.S. Rapid multiresidue determination for currently used pesticides in agricultural drainage waters and soils using gas chromatography–mass spectrometry. *J. Environ. Sci. Health B* **2010**, *45*, 152–161. [CrossRef] [PubMed]
14. Li, R.; Zhu, B.; Hu, X.-p.; Shi, X.-y.; Qi, L.-l.; Liang, P.; Gao, X.-W. Overexpression of PxαE14 Contributing to Detoxification of Multiple Insecticides in Plutella xylostella (L.). *J. Agric. Food Chem.* **2022**, *70*, 5794–5804. [CrossRef]

15. Lee, S.-H.; Kwak, S.-Y.; Sarker, A.; Moon, J.-K.; Kim, J.-E. Optimization of a Multi-Residue Analytical Method during Determination of Pesticides in Meat Products by GC-MS/MS. *Foods* **2022**, *11*, 2930. [CrossRef]

16. Huo, D.; Li, Q.; Zhang, Y.; Hou, C.; Lei, Y. A highly efficient organophosphorus pesticides sensor based on CuO nanowires–SWCNTs hybrid nanocomposite. *Sens. Actuators B Chem.* **2014**, *199*, 410–417. [CrossRef]

17. Luo, R.; Feng, Z.; Shen, G.; Xiu, Y.; Zhou, Y.; Niu, X.; Wang, H. Acetylcholinesterase Biosensor Based On Mesoporous Hollow Carbon Spheres/Core-Shell Magnetic Nanoparticles-Modified Electrode for the Detection of Organophosphorus Pesticides. *Sensors* **2018**, *18*, 4429. [CrossRef]

18. Bedair, H.; Rady, H.A.; Hussien, A.M.; Pandey, M.; Apollon, W.; AlKafaas, S.S.; Ghosh, S. Pesticide Detection in Vegetable Crops Using Enzyme Inhibition Methods: A Comprehensive Review. *Food Anal. Methods* **2022**, *15*, 1979–2000. [CrossRef]

19. Fang, L.; Liao, X.; Jia, B.; Shi, L.; Kang, L.; Zhou, L.; Kong, W. Recent progress in immunosensors for pesticides. *Biosens. Bioelectron.* **2020**, *164*, 112255. [CrossRef]

20. Cheng, N.; Song, Y.; Fu, Q.; Du, D.; Luo, Y.; Wang, Y.; Xu, W.; Lin, Y. Aptasensor based on fluorophore-quencher nano-pair and smartphone spectrum reader for on-site quantification of multi-pesticides. *Biosens. Bioelectron.* **2018**, *117*, 75–83. [CrossRef]

21. Zhang, L.; Wang, B.; Zhu, G.; Zhou, X. Synthesis of silver nanowires as a SERS substrate for the detection of pesticide thiram. *Spectrochim. Acta Part A Mol. Biomol. Spectrosc.* **2014**, *133*, 411–416. [CrossRef] [PubMed]

22. Asgari, S.; Wu, G.; Aghvami, S.A.; Zhang, Y.; Lin, M. Optimisation using the finite element method of a filter-based microfluidic SERS sensor for detection of multiple pesticides in strawberry. *Food Addit. Contam. Part A* **2021**, *38*, 646–658. [CrossRef] [PubMed]

23. Xie, X.; Pu, H.; Sun, D.-W. Recent advances in nanofabrication techniques for SERS substrates and their applications in food safety analysis. *Crit. Rev. Food Sci. Nutr.* **2018**, *58*, 2800–2813. [CrossRef] [PubMed]

24. Wang, P.; Sun, Y.; Wang, L.; Li, X.; Liu, M.; Li, G. Facile Detection and Quantification of Acetamiprid Using a Portable Raman Spectrometer Combined with Self-Assembled Gold Nanoparticle Array. *Chemosensors* **2021**, *9*, 327. [CrossRef]

25. Ali, A.; Nettey-Oppong, E.E.; Effah, E.; Yu, C.Y.; Muhammad, R.; Soomro, T.A.; Byun, K.M.; Choi, S.H. Miniaturized Raman Instruments for SERS-Based Point-of-Care Testing on Respiratory Viruses. *Biosensors* **2022**, *12*, 590. [CrossRef]

26. Yu, H.; Wang, M.; Cao, J.; She, Y.; Zhu, Y.; Ye, J.; Wang, J.; Lao, S.; Abd El-Aty, A.M. Determination of Dichlorvos in Pears by Surface-Enhanced Raman Scattering (SERS) with Catalysis by Platinum Coated Gold Nanoparticles. *Anal. Lett.* **2022**, *55*, 427–437. [CrossRef]

27. Zhai, W.; You, T.; Ouyang, X.; Wang, M. Recent progress in mycotoxins detection based on surface-enhanced Raman spectroscopy. *Compr. Rev. Food Sci. Food Saf.* **2021**, *20*, 1887–1909. [CrossRef]

28. Han, C.; Zhai, W.; Wang, Y.; Cao, J.; Wang, M. A SERS aptasensor for rapid detection of aflatoxin B1 in coix seed using satellite structured Fe$_3$O$_4$@Au nanocomposites. *Food Control* **2022**, *142*, 109228. [CrossRef]

29. Yan, M.; Chen, G.; She, Y.; Ma, J.; Hong, S.; Shao, Y.; Abd El-Aty, A.M.; Wang, M.; Wang, S.; Wang, J. Sensitive and Simple Competitive Biomimetic Nanozyme-Linked Immunosorbent Assay for Colorimetric and Surface-Enhanced Raman Scattering Sensing of Triazophos. *J. Agric. Food Chem.* **2019**, *67*, 9658–9666. [CrossRef]

30. Li, D.-W.; Zhai, W.-L.; Li, Y.-T.; Long, Y.-T. Recent progress in surface enhanced Raman spectroscopy for the detection of environmental pollutants. *Microchim. Acta* **2014**, *181*, 23–43. [CrossRef]

31. Wu, L.; Dias, A.; Diéguez, L. Surface enhanced Raman spectroscopy for tumor nucleic acid: Towards cancer diagnosis and precision medicine. *Biosens. Bioelectron.* **2022**, *204*, 114075. [CrossRef] [PubMed]

32. Hakonen, A.; Andersson, P.O.; Stenbæk Schmidt, M.; Rindzevicius, T.; Käll, M. Explosive and chemical threat detection by surface-enhanced Raman scattering: A review. *Anal. Chim. Acta* **2015**, *893*, 1–13. [CrossRef] [PubMed]

33. Cheng, J.; Wang, P.; Su, X.-O. Surface-enhanced Raman spectroscopy for polychlorinated biphenyl detection: Recent developments and future prospects. *TrAC Trends Analyt. Chem.* **2020**, *125*, 115836. [CrossRef]

34. Prikhozhdenko, E.S.; Bratashov, D.N.; Gorin, D.A.; Yashchenok, A.M. Flexible surface-enhanced Raman scattering-active substrates based on nanofibrous membranes. *Nano Res.* **2018**, *11*, 4468–4488. [CrossRef]

35. Xu, K.; Zhou, R.; Takei, K.; Hong, M. Toward Flexible Surface-Enhanced Raman Scattering (SERS) Sensors for Point-of-Care Diagnostics. *Adv. Sci.* **2019**, *6*, 1900925. [CrossRef] [PubMed]

36. Kalachyova, Y.; Erzina, M.; Postnikov, P.; Svorcik, V.; Lyutakov, O. Flexible SERS substrate for portable Raman analysis of biosamples. *Appl. Surf. Sci.* **2018**, *458*, 95–99. [CrossRef]

37. Luo, J.; Wang, Z.; Li, Y.; Wang, C.; Sun, J.; Ye, W.; Wang, X.; Shao, B. Durable and flexible Ag-nanowire-embedded PDMS films for the recyclable swabbing detection of malachite green residue in fruits and fingerprints. *Sens. Actuators B Chem.* **2021**, *347*, 130602. [CrossRef]

38. Wang, M.; Yu, X.; Chang, Y.; Gao, C.; Chen, J.; Zhang, X.; Zhan, J. A 3D spongy flexible nanosheet array for on-site recyclable swabbing extraction and subsequent SERS analysis of thiram. *Microchim. Acta* **2019**, *186*, 458. [CrossRef]

39. Wang, T.-J.; Barveen, N.R.; Liu, Z.-Y.; Chen, C.-H.; Chou, M.-H. Transparent, Flexible Plasmonic Ag NP/PMMA Substrates Using Chemically Patterned Ferroelectric Crystals for Detecting Pesticides on Curved Surfaces. *ACS Appl. Mater. Interfaces* **2021**, *13*, 34910–34922. [CrossRef]

40. Bai, F.; Dong, J.; Qu, J.; Zhang, Z. Construction of flexible, transparent and mechanically robust SERS-active substrate with an efficient spin coating method for rapid in-situ target molecules detection. *Nanotechnology* **2021**, *32*, 385501. [CrossRef]

41. Ma, X.; Xie, J.; Wang, Z.; Zhang, Y. Transparent and flexible AuNSs/PDMS-based SERS substrates for in-situ detection of pesticide residues. *Spectrochim. Acta Part A Mol. Biomol. Spectrosc.* **2022**, *267*, 120542. [CrossRef] [PubMed]

42. Wang, L.; Ma, P.; Chen, H.; Chang, M.; Lu, P.; Chen, N.; Yuan, Y.; Chen, N.; Zhang, X. Rapid Determination of Mixed Pesticide Residues on Apple Surfaces by Surface-Enhanced Raman Spectroscopy. *Foods* **2022**, *11*, 1089. [CrossRef] [PubMed]

43. Wu, P.; Zhong, L.-B.; Liu, Q.; Zhou, X.; Zheng, Y.-M. Polymer induced one-step interfacial self-assembly method for the fabrication of flexible, robust and free-standing SERS substrates for rapid on-site detection of pesticide residues. *Nanoscale* **2019**, *11*, 12829–12836. [CrossRef] [PubMed]

44. Xie, T.; Cao, Z.; Li, Y.; Li, Z.; Zhang, F.-L.; Gu, Y.; Han, C.; Yang, G.; Qu, L. Highly sensitive SERS substrates with multi-hot spots for on-site detection of pesticide residues. *Food Chem.* **2022**, *381*, 132208. [CrossRef]

45. Li, J.; Yan, H.; Tan, X.; Lu, Z.; Han, H. Cauliflower-Inspired 3D SERS Substrate for Multiple Mycotoxins Detection. *Anal. Chem.* **2019**, *91*, 3885–3892. [CrossRef]

46. Li, D.; Qu, L.; Zhai, W.; Xue, J.; Fossey, J.S.; Long, Y. Facile On-Site Detection of Substituted Aromatic Pollutants in Water Using Thin Layer Chromatography Combined with Surface-Enhanced Raman Spectroscopy. *Environ. Sci. Technol.* **2011**, *45*, 4046–4052. [CrossRef]

47. Sikder, M.; Lead, J.R.; Chandler, G.T.; Baalousha, M. A rapid approach for measuring silver nanoparticle concentration and dissolution in seawater by UV–Vis. *Sci. Total Environ.* **2018**, *618*, 597–607. [CrossRef]

48. Moreno-Martin, G.; León-González, M.E.; Madrid, Y. Simultaneous determination of the size and concentration of AgNPs in water samples by UV–vis spectrophotometry and chemometrics tools. *Talanta* **2018**, *188*, 393–403. [CrossRef]

49. Zhai, W.-L.; Li, D.-W.; Qu, L.-L.; Fossey, J.S.; Long, Y.-T. Multiple depositions of Ag nanoparticles on chemically modified agarose films for surface-enhanced Raman spectroscopy. *Nanoscale* **2012**, *4*, 137–142. [CrossRef]

50. Qu, L.-L.; Li, D.-W.; Xue, J.-Q.; Zhai, W.-L.; Fossey, J.S.; Long, Y.-T. Batch fabrication of disposable screen printed SERS arrays. *Lab Chip* **2012**, *12*, 876–881. [CrossRef]

51. Qu, L.-L.; Geng, Z.-Q.; Wang, W.; Yang, K.-C.; Wang, W.-P.; Han, C.-Q.; Yang, G.-H.; Vajtai, R.; Li, D.-W.; Ajayan, P.M. Recyclable three-dimensional Ag nanorod arrays decorated with O-g-C3N4 for highly sensitive SERS sensing of organic pollutants. *J. Hazard. Mater.* **2019**, *379*, 120823. [CrossRef] [PubMed]

52. Banaee, M.G.; Crozier, K.B. Gold nanorings as substrates for surface-enhanced Raman scattering. *Opt. Lett.* **2010**, *35*, 760–762. [CrossRef] [PubMed]

53. Caldwell, J.D.; Glembocki, O.J.; Bezares, F.J.; Kariniemi, M.I.; Niinistö, J.T.; Hatanpää, T.T.; Rendell, R.W.; Ukaegbu, M.; Ritala, M.K.; Prokes, S.M.; et al. Large-area plasmonic hot-spot arrays: Sub-2 nm interparticle separations with plasma-enhanced atomic layer deposition of Ag on periodic arrays of Si nanopillars. *Opt. Express* **2011**, *19*, 26056–26064. [CrossRef] [PubMed]

54. Xia, D.; Jiang, P.; Cai, Z.; Zhou, R.; Tu, B.; Gao, N.; Chang, G.; He, H.; He, Y. Ag nanocubes monolayer-modified PDMS as flexible SERS substrates for pesticides sensing. *Microchim. Acta* **2022**, *189*, 232. [CrossRef]

55. Picone, A.L.; Rizzato, M.L.; Lusi, A.R.; Romano, R.M. Stamplike flexible SERS substrate for in-situ rapid detection of thiram residues in fruits and vegetables. *Food Chem.* **2022**, *373*, 131570. [CrossRef]

56. Li, L.; Chin, W.S. Rapid fabrication of a flexible and transparent Ag nanocubes@PDMS film as a SERS substrate with high performance. *ACS Appl. Mater. Interfaces* **2020**, *12*, 37538–37548. [CrossRef]

Preparation of Monoclonal Antibody against Pyrene and Benzo [a]pyrene and Development of Enzyme-Linked Immunosorbent Assay for Fish, Shrimp and Crab Samples

Shuangmin Wu [†], Huaming Li [†], Xiaoyang Yin, Yu Si, Liangni Qin, Hongfei Yang, Jiaxu Xiao and Dapeng Peng *

National Reference Laboratory of Veterinary Drug Residues (HZAU) and MOA Key Laboratory for the Detection of Veterinary Drug Residues in Foods, Huazhong Agricultural University, Wuhan 430070, China

* Correspondence: pengdapeng@mail.hzau.edu.cn; Tel.: +86-27-8728-7165; Fax: +86-27-8767-2232
† These authors contributed equally to this work.

Abstract: Polycyclic aromatic hydrocarbons (PAHs) are significant environmental and food pollutants that can cause cancer. In this work, a specific monoclonal antibody (mAb) to identify pyrene (PYR) and benzo [a]pyrene (BaP) was prepared, and an indirect competitive enzyme-linked immunoassay (ic-ELISA) was established to detect PYR and BaP residues in living aquatic products for the first time. The effects of complete antigens with different coupling ratios on the production of high-sensitivity mAb was explored. Under the optimal conditions, the IC_{50} value was 3.73 ± 0.43 µg/L (n = 5). The limits of detection (LODs) for PYR and BaP in fish, shrimp, and crab ranged from 0.43 to 0.98 µg/L. The average recoveries of the spiked samples ranged from 81.5–101.9%, and the coefficient of variation (CV) was less than 11.7%. The validation of the HPLC-FLD method indicated that the ELISA method set up in this experiment provided a trustworthy tool for PAHs residues detection in aquatic products.

Keywords: pyrene; benzo [a]pyrene; monoclonal antibody; enzyme-linked immunoassay; aquatic product

1. Introduction

PAHs, composed of two or more aromatic rings, are the most ubiquitous persistent organic hydrocarbons in the world [1]. The chemistry properties of PAHs (hydrophobicity, stability and carcinogenicity) will change as the ring number of PAHs increases [2,3]. The main source of PAHs is the incomplete combustion of organic materials such as fossil fuels, natural gas and wood, as well as human activities, including food processing, garbage incineration and automobile exhaust fumes [4–6]. PAHs can migrate with air and water for a long distance and accumulate in organisms, causing extensive and serious harm to human fitness and the ecological environment. Exposure to PAHs can cause a variety of adverse effects in humans and animals, including carcinogenicity, DNA damage, teratogenicity, mutagenicity and immunotoxicity [7–10]. Therefore, 16 PAHs have been classified as significant pollutants by the European Scientific Committee for Food (ECSCF) [11].

The pollution of PAHs in water environments is mainly caused by wastewater discharge and oil spills. For example, in 2010, the famous oil spill occurred in the Gulf of Mexico, and millions of tons of oil were released into the Gulf of Mexico [12]. China is a large aquaculture country, and its aquaculture production makes up more than 69% of the total global production. However, monitoring of major pollution sources in the national water environment in 2018 showed that PAHs were found in water, sediment and aquatic organisms. With the significant increase in industrial production and demand, the level of PAH-based pollutants in aquatic ecosystems has become strikingly high [13]. Owing to PAHs lipophilicity, they can easily accumulate in aquatic organisms and cause serious harm because their membranes are easily penetrated by PAHs [14]. It was reported that PAHs tend to accumulate in fatty aquatic products such as fish, shrimp and crabs. PAHs

can interfere with estrogen signaling pathways (especially 4- and 5-ring) [15,16]. PYR and BaP (Figure S1) are the main tetracyclic and pentacyclic compounds in PAHs, with strong persistence and harmfulness in the water environment. The residues in aquatic products are important factors affecting the quality and safety of aquaculture [17]. BaP is a residue marker of PAH pollution exposure due to its high carcinogenicity [18]. The European Commission has set limits of 2.0 μg/kg for fish, 5.0 μg/kg for crustaceans and cephalopods, and 10.0 μg/kg for shellfish [19].

Many chromatographic methods have been developed to monitor PAHs in different matrices, including GC–MS, LC-MS, and HPLC [20–22]. Although chromatographic methods have some advantages, the sample pretreatment is complicated and requires professional operators, making it unsuitable for on-site testing of a large number of samples. Immunoassays are more desirable because of their high sensitivity, time savings and low requirements for operators [23]. At present, ELISA is a widely used detection method in immunoassay, which is simple, fast and greatly improves the efficiency of residue analysis [24]. However, there are few studies on the ELISA methods of both PYR and BaP, and they mainly focus on the detection of environmental samples, such as water (lake water, tap water, drinking water) and air [25]. As far as we know, there is no reported immunoassay method for the PAHs residues assay in aquatic products.

In this work, a highly sensitivity mAb was prepared and an ELISA method was developed to detect PYR and BaP residues in fish, shrimp and crab without complex sample pretreatment. The effect of organic solvents on the sensitivity of ELISA was investigated. The accuracy of the ELISA is reliable compared to HPLC-FLD.

2. Materials and Methods

2.1. Chemicals and Reagents

Seventeen standard analytes of PAHs, namely, naphthalene, pyrene, fluorene, chrysene, benzo(k)fluoranthene, benzo(g, h, i) perylene, acenaphthylene, dibenzo(a, h)anthracene, acenaphthene, benzo(a)pyrene, phenanthrene, indeno(1, 2, 3-cd)pyrene, benzo(a)anthracene, fluoranthene, benzo(b)fluoranthene, anthracene and pyrene butyric acid, were purchased from Dr. Ehrenstorfer GmbH (Augsbury, Germany). Peroxidase-labelled goat anti-mouse immunoglobulins (HRP-IgG), OVA, serum-free cell freezing medium, Freund's complete adjuvant (FCA), BSA, hypoxanthine-aminopterin-thymidine (HAT), Freund's incomplete adjuvant (FIA) and PEG1450 were bought from Sigma (St. Louis, MO, USA). All other chemicals and organic solvents used were obtained from reagent grade or better.

2.2. Synthesis of Antigens

The synthesis method of the coating antigen and immunogen was appropriately improved by Meng et al. (2015) [15]. First, pyrene butyric acid (PBA) (110 mg), EDC (130 mg) and NHS (210 mg) were dissolved in 3 mL DMF. The solution was gently mixed at 4 °C overnight, which was called activated solution. BSA (70 mg) was dissolved in 9 mL of PBS (0.01 mol/L, pH = 7.4). Preparation of immunogen (PBA-BSA) with different coupling ratios: three glass bottles were used, and 3 mL BSA solution was added, respectively. Then, 400 μL, 600 μL, and 800 μL of activation solution was slowly added to the bottle successively and stirred at 4 °C for 10 h away from light. Three immunogens were represented by A_1, A_2 and A_3.

The coating antigen (PBA-OVA) was prepared using the same method as the immunogen. Briefly, OVA (90 mg) was dissolved in 12 mL PBS, the above activated solution (200 μL, 300 μL, 400 μL) was added to three glass bottles containing 4 mL OVA protein solution. These solutions were gently stirred at 4 °C for 12 h. Three coating antigens were represented by B1, B2 and B3. They were exhaustively dialyzed with 0.1M PBS at 4 °C for 5 days and the dialysate was changed every 12 hours. The antigens were collected and centrifuged at $10,000\times g$ for 5 min. The supernatant was obtained and stored in a −20 °C refrigerator for later use. Antigen synthesis was verified by 8453 UV–Visible spectrophotometer and the ratios of hapten/protein were estimated.

2.3. Immunization and Cell Fusion

All animal experiments were implemented in accordance with the animal ethics committee (HZAUMO-2021-0184) and following principles authorized by the Huazhong Agricultural University animal experiment center. Immunogens (A_1, A_2, A_3) and two different antigen doses (50 μg and 100 μg) were inoculated into Female Balb/c mice, 6 weeks old. For the first immunization, immunogens were mixed with FCA and given subcutaneous multipoint injection in the back or neck of mice. Subsequently, the immunogens emulsified with FIA were used to enhance immunization every 14 days. The serum titer and sensitivity were measured by ic-ELISA. A mouse with high serum titer and sensitivity was selected and immunized with immunogens without Freund's adjuvant for booster immunization. The mouse was euthanized and spleen cells were prepared for cell fusion. Activated SP2/0 myeloma cells and immunized spleen cells were fused at a ratio of 1:5~10 in 0.8 mL of 50% polyethylene glycol. The fusion cells were gently mixed in 1% HAT medium which contain feeder cells, then injected into 96-hole cell culture plates.

2.4. Generation of Hybridomas and Production of mAb

Hybridoma cells with highly sensitive ELISA positivity were cloned four times and expanded to screen the monoclonal cell line. Seven days later, the hybridoma cells (10^6) stably secreting PYR and BaP antibodies were intraperitoneally injected into mice which had been cleared by 0.5 mL FIA. The mice were executed humanly 7–10 days later, and the ascites was gathered and stored at −80 °C.

2.5. Assessment of mAb

The subtype of mAb was determined by an antibody type identification kit. The performance of the mAb were assessed by measuring the IC_{50} values and cross-reactivity (CR). The CR for 16 PAHs was tested using PYR as the target analyte to estimate the specificity of the mAb.

CR (%) = 100 × IC_{50} (PYR)/IC_{50} (other analogues).

2.6. ELISA Procedure

The operation procedure of indirect ELISA (i-ELISA) described in Peng et al. was used with some modifications [26]. Microculture plates were added PBA-OVA coating antigen (100 μL/well), incubated at 4 °C overnight. After being three times washed by PBST (0.05% Tween 20 in PBS, pH 7.4), 200μL of OVA-PBS (1% OVA in PBS) was added into every well and blocked for 1 h at 37 °C. Washed again, 100 μL antibody was added into every well, and the plates kept for 40 min at 37 °C. Washed again, HRP-IgG (1:6000 dilution in 0.1M PBS, 100 μL/well) was added to all wells and the plates was kept at 37 °C for 40min. After being washed four times, TMB substrate solution (100 μL/well) was added. After incubation at 37 °C in the dark for 15 min, 50 μL of 1 M H_2SO_4 was added to finish the reaction. The absorbance at 450 nm was determined by an automatic ELISA reader.

The operation procedure of indirect competitive ELISA (ic-ELISA) was in common with i-ELISA. The only difference was that the mAb and drug standard or sample (50 μL/well) were added to each well. The standard curve was established with logarithm of analyte concentration as the abscissa and the inhibition values (B/B_0) corresponding to each concentration as the ordinate.

2.7. Optimization of the ELISA Variables

2.7.1. The Coating Antigen and mAb Titers

The optimum coating antigen concentration and mAb dilution were verified. A series of concentrations of PBA-OVA (1, 2, 4, 8 μg/L) were coated on the plates, and the mAb of multiple dilution was successively added. The standard curve was established by the ic-ELISA method.

2.7.2. The Working Concentration of HRP-IgG

The effect of the working concentration of HRP-IgG on the performance of ic-ELISA was evaluated. Ninety-six-well microculture plates were coated with the most optimal combination of coating antigen and mAb dilution. The sensitivity of ELISA to various working concentrations of HRP-IgG was tested for assay optimization, which were diluted to 1:4000, 1:5000, 1:6000 and 1:7000 with PBS.

2.7.3. Incubation Time

The sensitivity was also greatly affected by the incubation time of antigen and antibody. Under the above determined conditions, the competition time was set to 25, 35, 45 and 55 min; the HRP-IgG incubation time was set to 30, 40, 50 and 60 min to explore the optimal incubation time.

2.7.4. Organic Solvents

To investigate the effect of different organic solvents on the binding ability of antigen and antibody, four solvents, DMF, acetone, acetonitrile and DMSO, were tested for assay optimization. Briefly, each solvent was diluted to 10%, 20%, 30% and 40% with PBS. Then, a series of PYR concentrations were prepared with the above dilution solvent, and standard curves were drawn according to the ic-ELISA steps.

2.8. Sample Preparation

Living aquatic products (fish, shrimp, crab) were obtained from local markets. The above samples were tested by HPLC-FLD and the negative samples were selected as blank samples. The pretreatment of the sample was as follows: the shell and viscera of fish, shrimp and crab samples were removed, three grams of homogenized samples were added into a 15 mL conical tube, 3 mL PBS buffer was added and agitated on a vortex mixer. Subsequently, 4 mL ethyl acetate and 2 mL acetonitrile were added, shaken thoroughly for 5 min and centrifuged at $5000\times g$ for 5 min. The supernatant was blown to near dry with nitrogen. Next, 1 mL 20% DMF-PBS (1:4, v:v) was used to dissolved the residue, and then 1 mL n-hexane was added and shaken acutely, static for 5 min and remove supernatant. The subnatant was detected by ic-ELISA.

2.9. Validation Test of ic-ELISA

The ELISA validation was as follows: 20 aquatic products samples purchased from different areas were detected by ic-ELISA. The LOD and LOQ were calculated from the sum of the 20 blank samples. The precision and accuracy were evaluated by analyzing the recovery and intra- and inter-assay variations (CV) via the repeated analysis of the spiked samples. Briefly, three different concentrations of PYR (2, 4, and 8 μg/L) were spiked into the blank samples, and three intra-batch tests and five inter-batch tests were employed for ELISA. The recovery and CV were calculated as follows: recovery (%) = (conc. measured/conc. spiked) $\times$ 100; CV (%) = sample standard deviation/sample average $\times$ 100%.

2.10. Comparison of ELISA and HPLC-FLD Analysis

Compared with HPLC-FLD, the reliability of the ELISA method was verified by the same positive samples. The positive samples were homogenized and pretreated and detected by ELISA and HPLC-FLD. The HPLC-FLD method was performed according to Godinho et al. [25].

3. Results and Discussion

3.1. Antigen Verification and Serum Antibody Monitoring

The design and synthesis of antigens are very important for promoting the immune response of mice and preparing mAb with high-affinity and high-sensitivity. PYR is a small molecule compound that lacks functional groups conjugated with proteins and has no immunogenicity. In this study, pyrene butyric acid (PBA) was used as a hapten to

synthesize artificial complete antigen. PAHs are composed of multiple benzene rings and have unique UV absorption spectra, so PBA hapten has multiple absorption peaks. The UV scanning spectra of immunogen PBA-BSA and coating antigen PBA-OVA are shown in Figures 1 and 2.
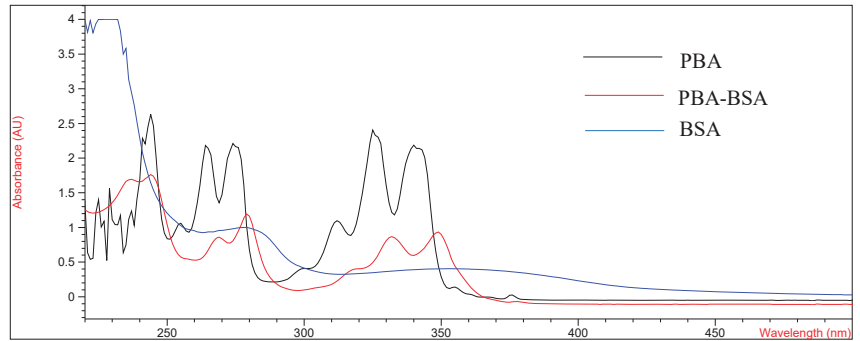
Figure 1. UV spectrum of BSA, PBA and PBA-BSA.
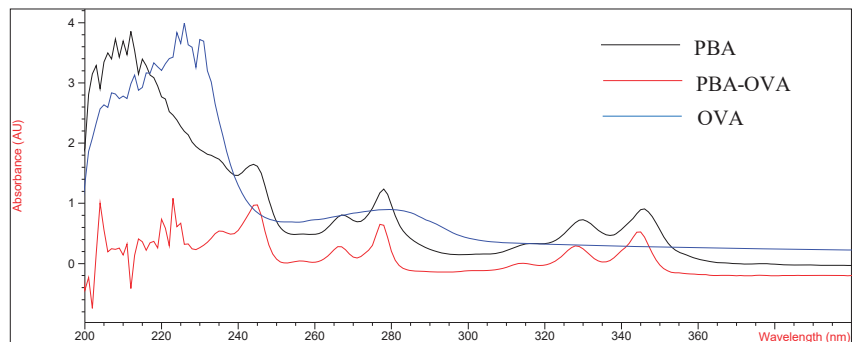
Figure 2. UV spectrum of OVA, PBA and PBA-OVA.

As shown in Figures 1 and 2, the UV absorption spectra of antigens changed significantly compared with those of carrier proteins (BSA, OVA) and PBA haptens and showed the characteristics of the absorption peaks of carrier proteins and haptens. The results showed that the PBA-BSA/OVA antigens were successfully synthesized. The estimated hapten/protein ratios of antigens were 8.1 (A_1), 12.8 (A_2), 18.3 (A_3), 9.4 (B_1), 11.7 (B_2), and 19.2 (B_3).

It has been reported that the immune effect of immunogens would be affected by the coupling rate of hapten and carrier proteins [27]. Therefore, we prepared antigens with different coupling ratios to explore their effects on the affinity and sensitivity of immunized mice. Three immunogens (A_1, A_2 and A_3) were used to immunize mice. The absorbance values and inhibition rates of antiserum under different coupling ratio antigens are shown in Table S1. It can be seen that in a certain range, the higher the hapten/protein ratio was, the better the serum titre and affinity of the antiserum were. This may be due to more haptens in the conjugate being exposed, which stimulated the mouse to produce more antibodies against PYR. Therefore, immunogen A_3 and coating antigen B_3 were the best combination.

3.2. Characterization of the mAbs

According to the antiserum results, the mouse with high sensitivity and inhibitory rate was selected for the cell fusion experiment. At present, PEG 4000 and PEG 1450 are commonly used for cell fusion. Due to the large molecular weight of PEG 4000, the cells lost water faster and fused more violently, causing cell injury. In contrast, the PEG 1450

fusion process was mild and achieved perfect results. After four subclones, PBA-BSA-A$_3$ was used as the immunogen, and four specific mAbs against PYR and BaP were obtained. They were named 4A3, 4D6, 5D8 and 6H4, and the results are provided in Table S2. The 4D6 mAb, which was selected for subsequent experiments because it exhibited the highest sensitivity, had an optimum dilution of 20,000 and an IC$_{50}$ of 5.3 ng/mL. The results of mouse monoclonal antibody type identification indicated that the antibody subtypes were all IgG$_1$ (Figure S2).

3.3. Optimization of the ELISA Variables

The concentrations of coating antigen and mAb, the incubation time of mAb and HRP-IgG, the working concentration of HRP-IgG and organic solvents were optimized, respectively. As shown in Table S3, the optimal concentrations of coating antigen and mAb were 2 µg/mL and 1:20,000, respectively. The optimal incubation times of the mAb and HRP-IgG were 35 min and 40 min, respectively. The optimal working concentration of HRP-IgG was 1:6000.

PAHs are hydrophobic lipophilic substances that are usually dissolved in organic solvents. It has been reported that the parameters of ELISA would be influenced by the organic solvent [28]. Therefore, acetone, DMF, acetonitrile and DMSO were selected for study in this experiment. The effect of organic solvents added to the ELISA reaction system on the antigen-antibody binding reaction should be as small as possible. Therefore, it was necessary to explore the binding ability of different concentrations of organic solvents. Organic solvents with different volume fractions (10%, 20%, 30% and 40%) in PBS buffer were used as drug standard diluents. During the experiment, we found that acetone was highly volatile. When incubated at 37 °C, the total amount of liquid in the wells decreased significantly, which affected the accuracy of the results, so it was excluded.

As shown in Figure 3, compared with acetonitrile, the OD$_{450}$ values of DMF and DMSO were relatively less affected. The use of organic cosolvents to improve the affinity and specificity of antibodies has also been supposed [29]. Then, the influence of concentrations of DMF and DMSO on the sensitivity of ELISA were investigated. When the volume fractions of DMF and DMSO were in the range of 10–40%, there was a large difference in sensitivity. In contrast, the IC$_{50}$ value of 20% DMF-PBS (1:4, v:v) was the lowest, which significantly improved the sensitivity of ic-ELISA (Table 1). Therefore, 20% DMF-PBS (1:4, v:v) was selected as a drug standard diluent.
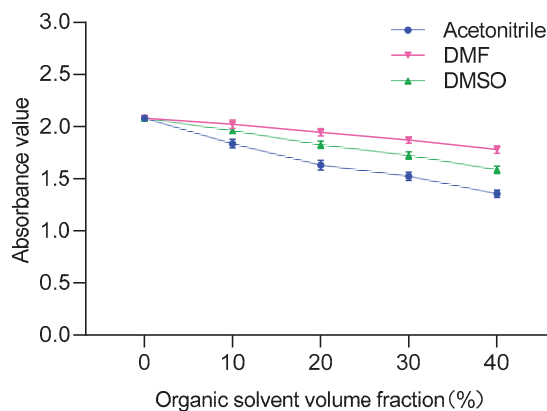
Figure 3. Comparison of different organic solvents.

Table 1. Comparison of different DMF and DMSO contents.

Organic Solvent (%)		Blank Hole OD$_{450}$ Value	IC$_{50}$ (µg/L)
DMF	10	1.872 ± 0.032	4.71 ± 0.31
	20	2.053 ± 0.031	3.37 ± 0.36
	30	2.113 ± 0.027	4.32 ± 0.28
	40	1.761 ± 0.041	3.91 ± 0.43
DMSO	10	1.972 ± 0.026	5.03 ± 0.37
	20	1.751 ± 0.043	5.74 ± 0.23
	30	1.721 ± 0.022	5.37 ± 0.28
	40	1.577 ± 0.034	6.62 ± 0.51

3.4. The Standard Curve and Cross-Reactivity

The PYR standard was diluted to 16.0, 8.0, 4.0, 2.0 and 1.0 µg/L. Under the above optimized conditions, the standard curve for PYR is shown in Figure 4. The equation was $y = -44.558x + 76.59$, ranging from 1 to 16 µg/L, $R^2 = 0.9929$, and the IC$_{50}$ was 3.73 ± 0.43 µg/L.
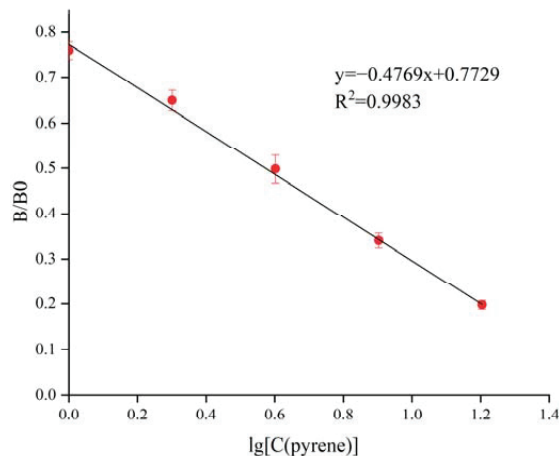
Figure 4. Standard curve for PYR in the ic-ELISA.

The specificity of developed ic-ELISA for PYR mAb was assessed by CR. The standards containing 16 PAHs were tested for CR using 4D6 mAb. The mAb exhibited high binding affinity with PYR (100%) and BaP (38%), low affinity with fluoranthene (8%) and negligible cross-reactivity (< 1%) with other PAHs (Table S4). This may be related to the structure of the hapten. The structures of PYR and BaP have the same four ring structures. Therefore, it is inevitable that antibodies prepared from PBA haptens cross with PYR and BaP. The CR results also confirmed our hypothesis. Previous studies on CR mainly focused on 2- to 5-ring PAHs [15,30,31]. However, this study mainly focused on 4- to 5-ring PAHs. Considering the CR for 16 PAHs, this mAb could specifically recognize PYR and BaP. Therefore, it can be used to set up an ic-ELISA kit to detect PYR and BaP in aquatic products.

3.5. Sample Preparation

In the establishment of the ELISA method, sample pretreatment is very important and is directly determined the accuracy of detection results. In recent years, the existing ELISA methods for PAHs detection have mainly concentrated on environmental samples, such as water (lake water, tap water, drinking water) and air [15,32,33]. However, there is no report on the detection of PAHs in aquatic products by ELISA. As a large country of aquatic products, it is imperative for China to detect PAHs in aquatic products. The ELISA method sensitivity is according to the specific binding ability of antigen and mAb, however, the

sensitivity is susceptible to interference by fat and protein in the sample. Therefore, the samples usually need to be pretreated (extracted, purified, concentrated or diluted) before analysis to reduce matrix interference. To improve the precision of detection, according to the chemical properties, the extraction method of PYR and BaP in aquatic products was explored.

First, the matrix effect was evaluated, and blank samples were directly pretreated with PBS as previously reported [33]. The results showed that the matrix effect was very severe, even false-positive. When organic solvent extraction was performed during sample pretreatment, the matrix effect problem was solved. In this study, several extraction buffers, including acetonitrile, ethyl acetate and ethyl acetate-acetonitrile (4:1; v:v), were used to investigate the extraction effect. It can be seen that a higher recovery rate was obtained by ethyl acetate-acetonitrile (4:1; v:v). Acetonitrile could not extract the drug, and the recovery of ethyl acetate was less than 70%. Therefore, ethyl acetate-acetonitrile (4:1; v:v) was selected as the extraction solvent for sample pretreatment.

3.6. IC-ELISA Performance for Aquatic Products

Based on the optimization of ic-ELISA conditions and sample pretreatment described above, 20 negative samples were collected for ELISA performance measurement. The LODs of the method for PYR and BaP in fish, shrimp and crab ranged from 0.43 to 0.54 µg/kg and 0.92 to 0.98 µg/kg, respectively. Meanwhile, the recoveries of PYR and BaP in fish, shrimp and crab were 81.5–101.9% and 84.9–94.0%, respectively, and the CV was less than 11.7% (Table 2). The minimum detection levels of PYR and BaP in aquatic products were far below the MRLs.

Table 2. The LODs, LOQs, CV and recoveries of PYR and BaP in aquatic products.

Analytes	Samples	LOD (µg/L)	LOQ (µg/L)	Spiked Drug (ng/L)	Recovery (%)	CV (%) (n = 25)
PYR	Fish	0.54	0.69	2	81.5 ± 5.3	6.5
				4	93.7 ± 5.6	6.0
				8	86.3 ± 5.5	6.4
	Shrimp	0.43	0.56	2	91.1 ± 4.9	5.4
				4	84.3 ± 3.6	4.3
				8	101.9 ± 5.8	5.7
	Crab	0.53	0.71	2	99.4 ± 9.2	9.3
				4	86.3 ± 4.4	5.1
				8	82.3 ± 5.7	6.9
BaP	Fish	0.98	1.15	2	89.2 ± 5.5	6.2
				4	84.9 ± 6.1	7.2
				8	86.2 ± 4.9	5.7
	Shrimp	0.92	1.12	2	86.3 ± 6.1	7.1
				4	94.0 ± 6.5	6.9
				8	91.6 ± 8.6	9.4
	Crab	0.96	1.22	2	85.5 ± 4.3	5.0
				4	87.1 ± 5.7	6.5
				8	85.9 ± 7.5	8.7

To validate the reliability of this experimental method, the ic-ELISA and HPLC-FLD methods were used to detect positive fish samples contaminated with PYR. The liquid chromatogram of PYR in the fish sample is shown in Figure S3. The results from the ic-ELISA were consistent with the results of HPLC-FLD, and the correlation coefficient was $R^2 = 0.9961$ (Figure 5). The results indicated that ic-ELISA can be used as an available tool for the detection of PYR and BaP in aquatic products samples.
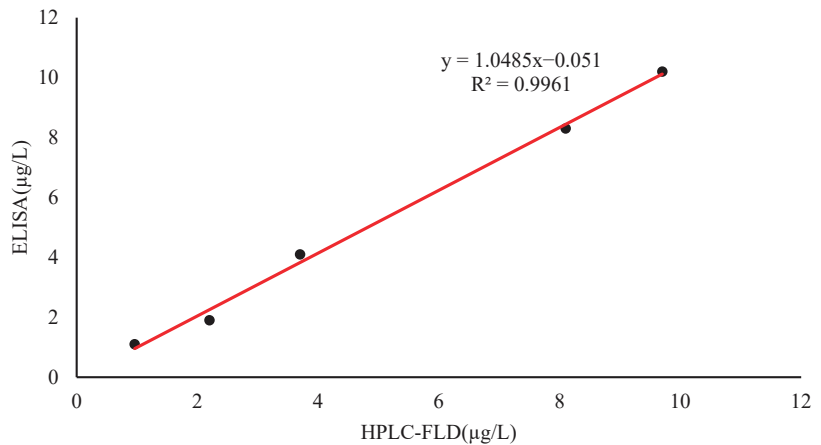
Figure 5. Correlation between ic-ELISA and HPLC-FLD for PYR determination of positive fish sample.

4. Comparison with Other Immunoassay Methods

Compared with other studies on immunoassay of PAHs, this study has the following advantages: firstly, this is the first study to establish an ELISA method for the detection of PYR and BaP in aquatic products, because most of the PAHS ELISA methods developed in recent years focus on environmental samples, such as water (lake water, tap water, drinking water) and air [15,32,33]. Secondly, although no new hapten was designed in this study, a monoclonal antibody with high sensitivity that can recognize PYR and BaP simultaneously was obtained by synthesizing complete antigens with different coupling ratios. Scharnweber et al. took BaP as the object to synthesize hapten. The procedure of this synthesis method is complicated, and hazardous chemical reagents such as toluene and pyridine are used in the synthesis of hapten, so it is difficult to control its harm to the environment and human beings in the synthesis process [29]. Finally, compared with the commercially available BaP kit of American REAGEN Company, the detection limit of this study is lower, and the pretreatment method is simpler.

5. Conclusions

In this study, antigens with different coupling ratios were synthesized and used to prepare a sensitive mAb, 4D6. The mAb showed high affinity for PYR (100%) and BaP (38%). Based on the mAb, a sensitive, efficient and reproducible ic-ELISA method was found and used for the determination of PYR and BaP residues in fish, shrimp and crab for the first time. The LODs of PYR and BaP in fish, shrimp and crab range between 0.43 and 0.98 μg/kg. Confirmation and relevance with HPLC-FLD showed the ic-ELISA method is a feasible tool. Therefore, the ic-ELISA method established in this experiment provided a practical tool for usual screening of PYR and BaP in aquatic products and supplemented the lack of an ELISA method in aquatic products. It lays a foundation for the development and application of PAHs residue detection kit in aquatic products. It has important academic value and practical significance to guarantee the quality of aquatic products.

References

1. Taioli, E.; Sram, R.J.; Garte, S.; Kalina, I.; Popov, T.A.; Farmer, P.B. Effects of polycyclic aromatic hydrocarbons (PAHs) in environmental pollution on exogenous and oxidative DNA damage (EXPAH project): Description of the population under study. *Mutat. Res.* **2007**, *620*, 1–6. [CrossRef] [PubMed]
2. Behera, B.K.; Das, A.; Sarkar, D.J.; Weerathunge, P.; Parida, P.K.; Das, B.K.; Thavamani, P.; Ramanathan, R.; Bansal, V. Polycyclic Aromatic Hydrocarbons (PAHs) in inland aquatic ecosystems: Perils and remedies through biosensors and bioremediation. *Environ. Pollut.* **2018**, *241*, 212–233. [CrossRef] [PubMed]
3. Xue, Z.; Zheng, X.; Yu, W.; Li, A.; Li, S.; Wang, Y.; Kou, X. Review—Research progress in detection technology of Polycyclic Aromatic Hydrocarbons. *J. Electrochem. Soc.* **2021**, *168*, 057528. [CrossRef]
4. Abbas, I.; Badran, G.; Verdin, A.; Ledoux, F.; Roumié, M.; Courcot, D.; Garçon, G. Polycyclic aromatic hydrocarbon derivatives in airborne particulate matter: Sources, analysis and toxicity. *Environ. Chem. Lett.* **2018**, *16*, 439–475. [CrossRef]
5. Gregoris, E.; Barbaro, E.; Morabito, E.; Toscano, G.; Donateo, A.; Cesari, D.; Contini, D.; Gambaro, A. Impact of maritime traffic on polycyclic aromatic hydrocarbons, metals and particulate matter in Venice air. *Environ. Sci. Pollut. Res. Int.* **2016**, *23*, 6951–6959. [CrossRef] [PubMed]
6. Liu, S.; Xia, X.; Yang, L.; Shen, M.; Liu, R. Polycyclic aromatic hydrocarbons in urban soils of different land uses in Beijing, China: Distribution, sources and their correlation with the city's urbanization history. *J. Hazard. Mater.* **2010**, *177*, 1085–1092. [CrossRef]
7. Diggs, D.L.; Huderson, A.C.; Harris, K.L.; Myers, J.N.; Banks, L.D.; Rekhadevi, P.V.; Niaz, M.S.; Ramesh, A. Polycyclic aromatic hydrocarbons and digestive tract cancers: A perspective. *J. Environ. Sci. Health C Environ. Carcinog. Ecotoxicol. Rev.* **2011**, *29*, 324–357. [CrossRef] [PubMed]
8. Jernström, B.; Gräslund, A. Covalent binding of benzo[a]pyrene 7,8-dihydrodiol 9,10-epoxides to DNA: Molecular structures, induced mutations and biological consequences. *Biophys. Chem.* **1994**, *49*, 185–199. [CrossRef]
9. Kim, K.H.; Jahan, S.A.; Kabir, E.; Brown, R.J. A review of airborne polycyclic aromatic hydrocarbons (PAHs) and their human health effects. *Environ. Int.* **2013**, *60*, 71–80. [CrossRef] [PubMed]
10. Olsson, A.C.; Fevotte, J.; Fletcher, T.; Cassidy, A.; t Mannetje, A.; Zaridze, D.; Szeszenia-Dabrowska, N.; Rudnai, P.; Lissowska, J.; Fabianova, E.; et al. Occupational exposure to polycyclic aromatic hydrocarbons and lung cancer risk: A multicenter study in Europe. *Occup. Environ. Med.* **2010**, *67*, 98–103. [CrossRef] [PubMed]
11. Karsunke, X.Y.; Pschenitza, M.; Rieger, M.; Weber, E.; Niessner, R.; Knopp, D. Screening and characterization of new monoclonal anti-benzo[a]pyrene antibodies using automated flow-through microarray technology. *J. Immunol. Methods* **2011**, *371*, 81–90. [CrossRef] [PubMed]
12. McNutt, M.K.; Camilli, R.; Crone, T.J.; Guthrie, G.D.; Hsieh, P.A.; Ryerson, T.B.; Savas, O.; Shaffer, F. Review of flow rate estimates of the Deepwater Horizon oil spill. *Proc. Natl. Acad. Sci. USA* **2012**, *109*, 20260–20267. [CrossRef] [PubMed]
13. Nwaichi, E.O.; Ntorgbo, S.A. Assessment of PAHs levels in some fish and seafood from different coastal waters in the Niger Delta. *Toxicol. Rep.* **2016**, *3*, 167–172. [CrossRef] [PubMed]
14. Ekere, N.R.; Yakubu, N.M.; Oparanozie, T.; Ihedioha, J.N. Levels and risk assessment of polycyclic aromatic hydrocarbons in water and fish of rivers Niger and Benue confluence Lokoja, Nigeria. *J. Environ. Health Sci. Eng.* **2019**, *17*, 383–392. [CrossRef] [PubMed]
15. Meng, X.Y.; Li, Y.S.; Zhou, Y.; Zhang, Y.Y.; Yang, L.; Qiao, B.; Wang, N.N.; Hu, P.; Lu, S.Y.; Ren, H.L.; et al. An enzyme-linked immunosorbent assay for detection of pyrene and related polycyclic aromatic hydrocarbons. *Anal Biochem.* **2015**, *473*, 1–6. [CrossRef]

16. van Lipzig, M.M.; Vermeulen, N.P.; Gusinu, R.; Legler, J.; Frank, H.; Seidel, A.; Meerman, J.H. Formation of estrogenic metabolites of benzo[a]pyrene and chrysene by cytochrome P450 activity and their combined and supra-maximal estrogenic activity. *Environ. Toxicol. Pharmacol.* **2005**, *19*, 41–55. [CrossRef] [PubMed]
17. Oliveira, M.; Ribeiro, A.; Hylland, K.; Guilhermino, L. Single and combined effects of microplastics and pyrene on juveniles (0+ group) of the common goby Pomatoschistus microps (Teleostei, Gobiidae). *Ecol. Indic.* **2013**, *34*, 641–647. [CrossRef]
18. Pschenitza, M.; Hackenberg, R.; Niessner, R.; Knopp, D. Analysis of benzo[a]pyrene in vegetable oils using molecularly imprinted solid phase extraction (MISPE) coupled with enzyme-linked immunosorbent assay (ELISA). *Sensors* **2014**, *14*, 9720–9737. [CrossRef] [PubMed]
19. Akpambang, V.O.; Purcaro, G.; Lajide, L.; Amoo, I.A.; Conte, L.S.; Moret, S. Determination of polycyclic aromatic hydrocarbons (PAHs) in commonly consumed Nigerian smoked/grilled fish and meat. *Food Addit. Contam. Part A Chem. Anal. Control Expo. Risk Assess.* **2009**, *26*, 1096–1103. [CrossRef] [PubMed]
20. Hassan, J.; Farahani, A. GC–MS Determination of PAHs in Fish Samples Following Salting-out-Assisted Solvent Extraction-Gel Permeation Chromatography. *Chromatographia* **2011**, *74*, 477. [CrossRef]
21. Pan, D.; Chen, C.; Yang, F.; Long, Y.; Cai, Q.; Yao, S. Titanium wire-based SPE coupled with HPLC for the analysis of PAHs in water samples. *Analyst* **2011**, *136*, 4774–4779. [CrossRef] [PubMed]
22. Zhou, Z.; Lu, J.; Wang, J.; Zou, Y.; Liu, T.; Zhang, Y.; Liu, G.; Tian, Z. Trace detection of polycyclic aromatic hydrocarbons in environmental waters by SERS. *Spectrochim. Acta. A Mol. Biomol. Spectrosc.* **2020**, *234*, 118250. [CrossRef] [PubMed]
23. Felemban, S.; Vazquez, P.; Moore, E. Future trends for in situ monitoring of Polycyclic Aromatic Hydrocarbons in water sources: The role of immunosensing techniques. *Biosensors* **2019**, *9*, 142. [CrossRef] [PubMed]
24. Peng, D.; Wang, Y.; Feng, L.; Cao, G.; Tao, Y.; Liu, Z.; Yuan, Z. Preparation of broadly specific monoclonal antibodies for simultaneous determination of fluoroquinolone residues in eggs. *Food Anal. Methods* **2016**, *9*, 3520–3531. [CrossRef]
25. Godinho, J.M.; Lawhorn, J.; Boyes, B.E. Rapid analysis of polycyclic aromatic hydrocarbons. *J. Chromatogr. A* **2020**, *1628*, 461432. [CrossRef]
26. Peng, D.; Ye, S.; Wang, Y.; Chen, D.; Tao, Y.; Huang, L.; Liu, Z.; Dai, M.; Wang, X.; Yuan, Z. Development and validation of an indirect competitive enzyme-linked immunosorbent assay for the screening of tylosin and tilmicosin in muscle, liver, milk, honey and eggs. *J. Agric. Food Chem.* **2012**, *60*, 44–51. [CrossRef]
27. Klaus, G.G.; Cross, A.M. The influence of epitope density on the immunological properties of hapten-protein conjugates: I. Characteristics of the immune response to hapten-coupled albumen with varying epitope density. *Cell Immunol.* **1974**, *14*, 226–241. [CrossRef]
28. Jiang, W.; Zhang, H.; Li, X.; Liu, X.; Zhang, S.; Shi, W.; Shen, J.; Wang, Z. Monoclonal antibody production and the development of an indirect competitive enzyme-linked immunosorbent assay for screening spiramycin in milk. *J. Agric. Food Chem.* **2013**, *61*, 10925–10931. [CrossRef]
29. Scharnweber, T.; Fisher, M.; Suchànek, M.; Knopp, D.; Niessner, R. Monoclonal antibody to polycyclic aromatic hydrocarbons based on a new benzo[a]pyrene immunogen. *Fresenius J. Anal. Chem.* **2001**, *371*, 578–585. [CrossRef]
30. Li, X.; Kaattari, S.L.; Vogelbein, M.A.; Vadas, G.G.; Unger, M.A. A highly sensitive monoclonal antibody based biosensor for quantifying 3-5 ring polycyclic aromatic hydrocarbons (PAHs) in aqueous environmental samples. *Sens. Bio-Sens. Res.* **2016**, *7*, 115–120. [CrossRef]
31. Spier, C.R.; Bromage, E.S.; Harris, T.M.; Unger, M.A.; Kaattari, S.L. The development and evaluation of monoclonal antibodies for the detection of polycyclic aromatic hydrocarbons. *Anal. Biochem.* **2009**, *387*, 287–293. [CrossRef] [PubMed]
32. Matschulat, D.; Deng, A.; Niessner, R.; Knopp, D. Development of a highly sensitive monoclonal antibody based ELISA for detection of benzo[a]pyrene in potable water. *Analyst* **2005**, *130*, 1078–1086. [CrossRef] [PubMed]
33. Ni, T.; Peng, D.; Wang, Y.; Pan, Y.; Xie, S.; Chen, D.; Wang, Y.; Tao, Y.; Yuan, Z. Development of a broad-spectrum monoclonal antibody-based indirect competitive enzyme-linked immunosorbent assay for the multi-residue detection of avermectins in edible animal tissues and milk. *Food Chem.* **2019**, *286*, 234–240. [CrossRef] [PubMed]

A Novel Metabolite as a Hapten to Prepare Monoclonal Antibodies for Rapid Screening of Quinoxaline Drug Residues

Wanyao Song [1,†], Mengyu Luo [1,†], Huaming Li [1], Jiaxu Xiao [1], Xiuping He [1], Jixiang Liang [1] and Dapeng Peng [1,2,3,4,*]

[1] National Reference Laboratory of Veterinary Drug Residues (HZAU), MOA Key Laboratory for the Detection of Veterinary Drug Residues in Foods, Huazhong Agricultural University, Wuhan 430070, China

[2] Shenzhen Institute of Nutrition and Health, Huazhong Agricultural University, Shenzhen 518000, China

[3] Shenzhen Branch, Guangdong Laboratory for Lingnan Modern Agriculture, Agricultural Genomics Institute at Shenzhen, Chinese Academy of Agricultural Sciences, Shenzhen 518000, China

[4] Genome Analysis Laboratory of the Ministry of Agriculture, Agricultural Genomics Institute at Shenzhen, Chinese Academy of Agricultural Sciences, Shenzhen 518000, China

[*] Correspondence: pengdapeng@mail.hzau.edu.cn; Tel.: +86-27-8728-7165

[†] These authors contributed equally to this work.

Abstract: Quinoxalines (Qx) are chemically synthesized antibacterial drugs with strong antibacterial and growth-promoting effects. Qx is heavily abused by farmers, resulting in large residues in animal-derived foods, which pose a serious threat to human health. Desoxyquinoxalines (DQx), which have the highest residue levels, have been identified as the major toxicant and have become a new generation of residue markers. In this study, we prepared monoclonal antibodies (mAb) based on a new generation metabolite (desoxymequindox, DMEQ) and establish an indirect competitive enzyme-linked immunosorbent assay (ic-ELISA) for the rapid determination of Qx residues in food. The mAb exhibited high sensitivity with half maximal inhibitory concentration (IC_{50}) and a linear range of 2.84 µg/L and 0.8–12.8 µg/L, respectively. Additionally, the cross-reactivity (CR) of the mAb showed that it recognized multiple DQx to varying levels. The limits of detection (LOD), limits of quantification (LOQ), and recoveries for the ic-ELISA assay of pork, swine liver, swine kidney, chicken, and chicken liver were 0.48–0.58 µg/kg, 0.61–0.90 µg/kg, and 73.7–107.8%, respectively, and the coefficients of variation (CV) were less than 11%. The results of the ic-ELISA showed a good correlation with LC–MS/MS in animal-derived foods. This suggests that this analytical method can be used for the rapid screening of QX residues.

Keywords: desoxymequindox; monoclonal antibody; ELISA; residue analysis

1. Introduction

Quinoxalines (Qx) are chemically synthesized antibacterial drugs that have a strong inhibitory effect on both gram-positive and gram-negative bacteria [1,2]. Due to the broad antimicrobial spectrum and obvious growth-promoting effects, Qx are used in excessive amounts by farmers as feed additives to obtain more economic benefits [3]. However, several studies have shown that Qx can cause toxic side effects such as trichothecation, photosensitivity, and adrenal cortical damage in livestock and poultry. More seriously, drug residues in animal-derived foods can pose a significant threat to the population directly consuming them [4–6]. According to the latest reports, the quinoxalines desoxymetabolites (desoxyquinoxalines, DQx) have the highest residues and have been identified as major toxicants. They will soon replace 3-methyl-quinoxaline-2-carboxylic acid (MQCA) and quinoxaline-2-carboxylic acid (QCA) as the new residue markers for Qx [1,7,8]. The chemical structures of Qx and the major DQx are shown in Figure 1. The Ministry of Agriculture and Rural Affairs of the People's Republic of China has stated that olaquindox (OLA), carbadox (CBX), and mequindox (MEQ) have been banned for use in food animals, and

the requirements for residue detection of quinoxalines have been increasing. In order to accurately monitor the residual hazards of Qx in animals and reduce the risk to human health, there is a need to develop a residue-monitoring method for DQx.
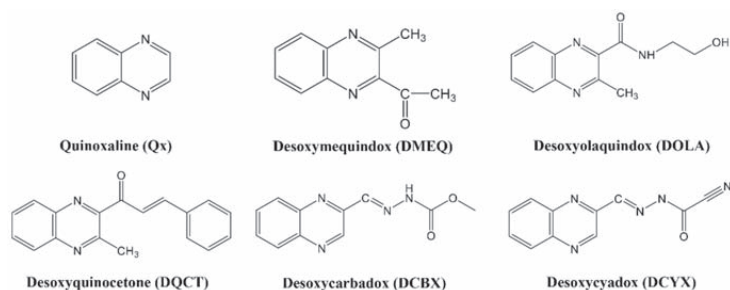
Figure 1. The chemical structures of Qx and the major DQx.

Currently, many detection assays have been reported but mainly for Qx prototypes or MQCA and QCA, which were previously identified as residue markers. Additionally, the detection of QX is mainly focused on instrumental detection assays, such as high-performance liquid chromatography (HPLC) [9,10] and liquid-chromatography tandem mass spectrometry (LC–MS/MS) [11,12]. Though the instrument-detection method has high sensitivity and precision, it requires rather expensive instruments, complicated technology, a long operation time, and low detection efficiency. In contrast, immunoassay methods, such as enzyme-linked immunosorbent assay (ELISA), are simple, convenient, sensitive, specific and inexpensive. ELISA has become an alternative analytical method or a meaningful complement, especially in the detection of large numbers of samples [13,14]. Current indirect competitive ELISAs (ic-ELISA) are all for Qx prototypes, MQCA, or QCA [15,16]. To the best of our knowledge, immunoassay assays for the residue detection of DQx have not been previously reported. The maximum residue limits (MRLs) for DQx are not legally standardized, leading to potential gaps in food safety. Therefore, it is important to develop a rapid and accurate detection method for DQx.

In this study, we propose to synthesize novel haptens against desoxymequindox (DMEQ) to fully expose the main part of DQx. The aim is to prepare monoclonal antibodies (mAb) against DQx and establish an ic-ELISA method to provide strong technical support for ensuring the food safety of animal origin and reducing the risk to human health.

2. Materials and Methods

2.1. Chemicals and Apparatus

Quinocetone (QCT), OLA, MEQ, CBX, cyadox (CYX), DMEQ, desoxyolaquindox (DOLA), desoxyquinocatone (DQCT), desoxycarbadox (DCBX), desoxycyadox (DCYX), N1-desoxycyadox (N1-DCYX), N4-desoxycyadox (N4-DCYX), MQCA, and QCA were purchased from Sigma (USA). N-acetylsulfanilyl chloride, p-aminobenzoic acid (PABA), carboxymethyl hydroxylamine (AOAA), N-hydroxysuccinimide, pyridine, bovine serumalbumin (BSA), human serum albumin (HSA), dimethyl sulfoxide (DMSO), ovalbumin (OVA), polyethylene glycol (PEG), hypoxanthine–aminopterin–thymidine (HAT) medium, hypoxanthine–thymidine (HT) medium, and peroxidase-labelled goat anti-mouse immunoglobulins (HRP-IgG) were purchased from Sigma-Aldrich (USA). Australian fetal bovine serum was purchased from Thermo Fisher Bioengineering Materials (Beijing, China). The SP2/0 mouse-tumor cell line was obtained from our laboratory. All other chemicals and organic solvents were of analytical grade or better. Female Balb/c mice (6–8 weeks old, NO. 42000600000485) were bought from Three Gorges University (Yichang, China) and quality-tested by the Hubei Provincial Center for Disease Control and Prevention (Wuhan, China).

A full-wavelength microplate reader (BioTek, Winooski, VT, USA) and a UV spectrophotometer (Model 8453) were purchased from Agilent Technologies, Inc. (Santa Clara, CA, USA).

2.2. Antigen Design and Preparation

2.2.1. Synthesis of Antigens MQCA–PABA–BSA/OVA

The synthesis protocol of MQCA–PABA–BSA/OVA is shown in Figure 2A. Briefly, MQCA (90.0 mg), dicyclohexylcarbodiimide (DCC, 110.0 mg), and N-hydroxysuccinimide (NHS, 55.0 mg) were dissolved with 1.2 mL of N, N-dimethylformamide (DMF), and the mixture was stirred at 4 °C overnight. After removing the precipitate by centrifugation at 6000× *g*, the supernatant was obtained, PABA (68.0 mg) was added, and the reaction was continued for 24 h with stirring. After centrifugation, the supernatant was collected and the solution became turbid after adding distilled water (10 mL). The precipitate obtained by filtering through filter paper is MQCA–PABA.
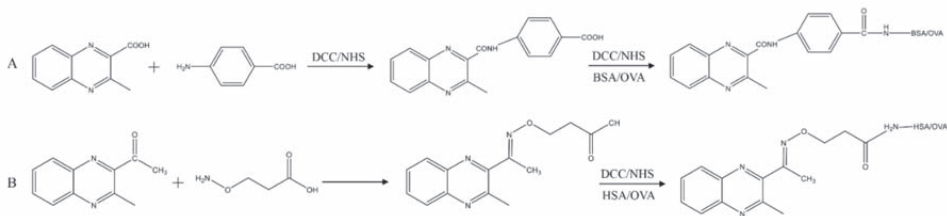
Figure 2. The synthesis protocol of MQCA–PABA–BSA/OVA (**A**) and DMEQ–AOAA–HSA/OVA (**B**).

Then, MQCA–PABA (30.0 mg), NHS (15.0 mg), and DCC (20.2 mg) were dissolved with 1.0 mL of DMF, and the mixture was stirred at 4 °C overnight. After centrifugation, the supernatant was added slowly with precipitate to the solution of 15 mL phosphate-buffered saline (PBS, 0.01 mol/L, pH 7.4) containing 66.0 mg BSA. The mixture was stirred for 24 h at 4 °C and then dialyzed in PBS for 5 d, and the dialysate was changed every 8 h. The dialyzed sample (MQCA–PABA–BSA) was collected and stored at −20 °C until use. The same principle can be followed to obtain MQCA–PABA–OVA.

2.2.2. Synthesis of Antigens DMEQ–AOAA–HSA/OVA

As shown in Figure 2B, AOAA (130.0 mg) was added to 6 mL of pyridine containing DMEQ (200.0 mg) and reacted at 60 °C for 6–8 h. Then, the pyridine was removed with a rotary evaporator, and 20 mL of saturated sodium bicarbonate solution and 50 mL of ethyl acetate were added. After shaking well, the aqueous layer was adjusted to pH 3 with hydrochloric acid and extracted twice with ethyl acetate. Finally, it was dried with anhydrous magnesium sulfate, and the filtrate was evaporated after filtration to obtain the solid: DMEQ–AOAA. The hapten was conjugated to the carrier protein in the same way as above, except that BSA was replaced with HSA. The haptens, carrier proteins, and conjugates were scanned under a UV spectrophotometer (200–400 nm) to determine the state of conjugation and to record the corresponding maximum absorption wavelength and absorption values. The relevant absorbance coefficient (K) was calculated from K = A/CL, and the conjugation ratio was calculated from [K(conjugation) − K(carrier protein)]/K(hapten).

2.3. Preparation of mAb

The preparation of mAb was performed according to that described in our laboratory by Peng et al. [17]. Briefly, sixteen female Balb/C mice were randomly divided into four groups for culture. Two immunogens (MQCA–PABA–BSA and DMEQ–AOAA–HSA) were immunized at a dose of 50 and 100 μg each. Then, serum titers and specificity were monitored by conventional ELISA procedures using MQCA–PABA–OVA and DMEQ–

AOAA–OVA as homologous and heterologous coating antigens, respectively [18]. The mice with the best titer and specificity were selected to obtain splenocytes in vitro and fused with mouse myeloma cells. Under screening by the ELISA method, positive monoclonal cell lines were obtained after subcloning the fused cells using the limited dilution method 3–5 times. Finally, mAb was prepared by ascites induction, purified using protein A affinity chromatography, and stored at −20 °C until use.

2.4. Development of ic-ELISA Analysis

First, the purified antibody was titrated with different coating antigens in a square matrix to find the best concentration so that the sensitivity of the ic-ELISA assay would be the highest [19]. Then, the gradient standard solutions of DMEQ (0.8, 1.6, 3.2, 6.4, and 12.8 µg/L) were analyzed by ic-ELISA using the optimal concentrations optimized as above. The absorbance values obtained (OD_{450nm}) were plotted against the corresponding concentrations in a standard calibration curve, and the concentration of DMEQ that produced half inhibition (IC_{50} value) was obtained from the results.

The extent of cross-reactivity (CR) of this mAb to different drugs was calculated by measuring the IC_{50} values of different structural analogs. Five DQx (DMEQ, DOLA, DQCT, DCYX, and DCBX) and six structural analogs (N1-DCYX, N4-DCYX, MQCA, MQCA–PABA, MEQ, and QCA) were used to determine the CR of the mAb. The IC_{50} values of all compounds were determined from the measured OD_{450nm} with the standard curve, and based on the IC_{50} values, the CR was calculated as follows:

$$CR\ (\%) = [IC_{50}\ (standard\ drug)/IC_{50}\ (analogues)] \times 100\%$$

2.5. Validation of ic-ELISA Analysis

Tissue samples of pork, swine liver, swine kidney, chicken, and chicken liver were purchased from local supermarkets. The homogenized samples (1 ± 0.05 g) were weighed, and 12 mL of extractant (ethyl acetate: acetonitrile = 1:1) was added to them. The mixture was mixed thoroughly for 3 min and then centrifuged at $4000\times g$ for 10 min at room temperature. The organic phase was pipetted, and 2 mL of the aqueous NaOH solution (0.5 mol/L) was added. After shaking for 5 min, all organic phases were blown dry under nitrogen at 40 °C in a water bath. Then, the residue was resuspended with 1 mL of the compound solution (PBS: methanol = 9:1) and diluted 16 times with PBS to be ready for ic-ELISA analysis.

The sensitivity of the ic-ELISA analysis for practical applications is determined by the detection of the actual samples. Twenty different blank samples (pork, swine liver, swine kidney, chicken, and chicken liver) that were confirmed to be free of drug residues by LC–MS/MS were performed to ic-ELISA analysis. The mean (C) of the concentrations and the standard deviation (SD) were calculated for all blank samples. The limit of detection (LOD) and limit of quantification (LOQ) of this ic-ELISA method were calculated according to LOD = C + 3 × SD and LOQ = C + 10 × SD.

To demonstrate the accuracy and precision of the ic-ELISA analysis, the recovery rate and coefficient of variation (CV) were evaluated as indicators. DMEQ standard solutions were added to different types of homogenized samples at final concentrations of 1 × LOQ, 2 × LOQ, and 4 × LOQ, with 5 replicates of each concentration. The samples were mixed well by vortexing and left to stand for 1 h to allow full absorption of the drug, followed by sample pretreatment and ic-ELSIA analysis. The calculating equation is as follows:

recovery = (actual concentration/spiked concentration) × 100%. CV = (SD/C) × 100%

To confirm the reliability of the developed ic-ELISA method, four spiked chicken samples were selected for comparison using ic-ELISA analysis and LC–MS/MS. The detailed procedures for LC–MS/MS analysis and sample preparation were performed according to the previous description [20]. Briefly, 10 mL of methanol-water (*v/v*, 5:95) and 20 mg of N-propyl ethylenediamine were added to the homogenized samples. They were vortexed

for 1 min and then centrifuged at 15,000× *g* for 10 min, and the supernatant was collected and filtered through a 0.22 μm membrane. A Thermo Hypersil Gold column (150 × 2.1 mm i.d., 5.0 μm) was used for LC–MS/MS analysis, and water-formic acid (*v/v*, 100:0.1) and acetonitrile were used for the mobile phases. For the analysis of spiked chicken samples by ic-ELISA and LC–MS/MS, correlation fitting curves were drawn to assess the correlation between the two methods.

3. Results and Discussion

3.1. Antigen Design and Characterization

In this study, quinoxaline haptens were designed with MQCA and DMEQ as the precursor substances and PABA and AOAA as the arms, respectively. The chemical structure of the precursor substances fully exposes the common structure of DQx and also carries reactive groups to facilitate the synthesis of hapten. Thus, the mAb prepared from such an immunogen could maximize the simultaneous recognition of multiple DQx. The haptens of MQCA–PABA and DMEQ–AOAA are small molecules that do not induce an immune response in the body and need to be conjugated with large proteins to be immunogenic. The prepared hapten was used as the basis for the synthesis of the conjugated product by the NHS active ester method. With the free carboxylic group, MQCA–PABA and DMEQ–AOAA were individually linked to proteins [21,22]. BSA and OVA, which served as the most common candidates of carrier protein, were adopted for the assay.

The spectra of the hapten, carrier protein, and conjugates were scanned using a UV–Vis spectrophotometer. The ultraviolet absorbance spectra of MQCA–PABA–BSA (λmax, 279 nm, 324 nm), MQCA–PABA–OVA (λmax, 280 nm, 322 nm), DMEQ–AOAA–HSA (λmax, 321 nm), and DMEQ–AOAA–OVA (λmax, 281 nm) were different from the carrier protein of the BSA (λmax, 279 nm) and OVA (λmax, 279 nm), and from the haptens of MQCA–PABA (λmax, 322 nm) and DMEQ–AOAA (λmax, 321 nm), which confirmed that the antigens were successfully synthesized (Figure 3). The estimated conjugation ratios of MQCA–PABA–BSA, MQCA–PABA–OVA, DMEQ–AOAA–HSA, and DMEQ–AOAA–OVA were 16.9, 10.7,17.8, and 11.3, respectively, obtained from the absorbance calculation analysis.

UV spectrum of BSA, MQCA-PABA and MQCA-PABA–BSA

UV spectrum of HSA, DMEQ-AOAA and DMEQ-AOAA-HSA

UV spectrum of OVA, MQCA-PABA and MQCA-PABA-OVA

UV spectrum of OVA, DMEQ-AOAA and DMEQ-AOAA-OVA
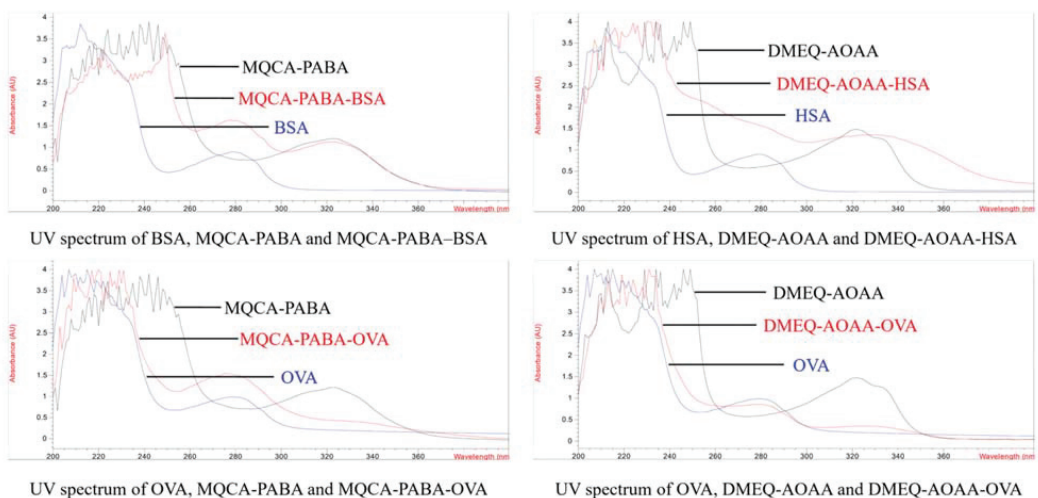
Figure 3. UV absorption peak spectra of 4 different antigens at 200–400 nm.

3.2. Characterization of mAb

The immunogens MQCA–PABA–BSA and DMEQ–AOAA–HSA were inoculated into mice to produce mAb. After the third injection, the specificity and titer of the immunized mouse antisera were determined using homologous and heterologous coatings, respectively

(Table 1). The analysis in the table shows that DMEQ–AOAA–HSA showed poor specificity as an immunogen, both in homologous and heterologous coating. The immunogen MQCA–PABA–BSA with the coating antigen MQCA–PABA–OVA showed high titers but poor specificity against DMEQ. However, DMEQ–AOAA–OVA showed a better inhibition rate as a coating antigen for heterologous analysis. Therefore, splenocytes from mice immunized with MQCA–PABA–BSA were fused with myeloma cells. In the process of preparing an antibody, we similarly found that the heterologous coating antigen DMEQ–AOAA–OVA was more suitable for ic-ELISA than the homologous coating antigen MQCA–PABA–OVA. After multiple cell subcloning, a single strain of hybridoma cells 1A3 showed better recognition of DMEQ. Therefore, this cell line was selected for the production of monoclonal antibodies.

Table 1. The titer and specificity of the antiserum.

Immunogen	Coating Antigen	Titre (1:X × 10^3)				B/B0 [1] Values (DMEQ, 100 µg/L)			
		Mouse 1	Mouse 2	Mouse 3	Mouse 4	Mouse 1	Mouse 2	Mouse 3	Mouse 4
MQCA–PABA–BSA	MQCA–PABA–OVA	2	1.5	12	3.5	0.846	0.965	0.815	0.902
	DMEQ–AOAA–OVA	1	0.8	2	1.5	0.516	0.469	0.568	0.766
DMEQ–AOAA–HSA	MQCA–PABA–OVA	2	3	1.8	1.5	0.851	0.921	0.956	0.827
	DMEQ–AOAA–OVA	3.5	5	4	3	0.790	0.873	0.884	0.919

[1] B is the absorbance value of DMEQ addition, and B0 is the absorbance value of PBS addition of equal amount.

First, the obtained antibodies were optimized for the ic-ELISA conditions. The results showed that the ratio of 1:2000 mAb and 6.0 µg/mL of the coating antigen (DMEQ–AOAA–OVA) worked best, and the rest of the experiments were performed under this condition. As shown in Figure 4, the standard curve was fitted with the logarithmic value of DMEQ concentration as the *X*-axis and B/B0 as the *Y*-axis. The standard curve ranged from 0.8–12.8 µg/L, and the IC_{50} value was 2.84 µg/L based on the DMEQ standard solution. In Table 2, it can be seen that the CR of mAb showed varying levels of cross-reactivity to MQCA–PABA (44%), DOLA (27%), MQCA (2%), DQCT (1.3%), and QCA (1%) but showed no measurable CR (CR < 0.1%) with DCBX, DCYX, N1-DCYX, N4-DCYX, and MEQ.
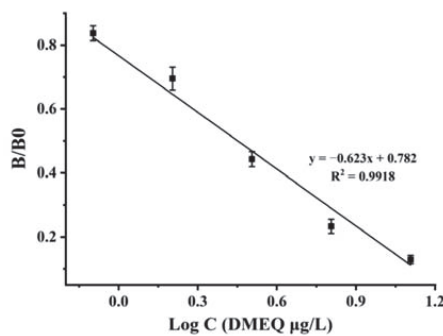
Figure 4. The standard curve of ic-ELISA.

Table 2. The cross-reactivity of mAb to different analytes.

Competitor	IC$_{50}$ (µg/L)	CR (%)
DMEQ	2.84	100
MQCA–PABA	6.45	44
DOLA	10.52	27
MQCA	142	2
DQCT	218	1.3
QCA	284	1
DCBX	>1000	<0.1
DCYX	>1000	<0.1
N1-DCYX	>1000	<0.1
N4-DCYX	>1000	<0.1
MEQ	>1000	<0.1

3.3. Performance of the ic-ELISA Analysis

Simple sample pretreatment will directly affect the analytical results of the ELISA. A large number of compounds in the sample matrix often have a strong interfering effect on the assay [19]. In previous studies, ethyl acetate was added to animal tissues for extraction and needed to be incubated for 2 h. After nitrogen blowing, it was degreased with hexane and diluted with PBS. Other studies showed that samples can be extracted by sodium hydroxide and acetonitrile, and diluted with diluent (methanol: PBS = 5:95) [23,24]. In this study, sodium hydroxide, ethyl acetate and acetonitrile were selected for the rapid extraction of DMEQ from the actual samples. This extraction method is faster and more efficient than previous methods.

To characterize the detection performance of the assay, we measured the LODs, LOQs, accuracy, and precision of the assay. Table 3 shows the results of 20 different blank samples, with the LODs and LOQs of samples ranging from 0.47–0.58 µg/kg and 0.61–0.90 µg/kg, respectively. The recoveries of the above samples spiked with DMEQ at the levels of 1 × LOQ, 2 × LOQ, and 4 × LOQ are listed in Table 3, which were in the range of 73.7% to 107.8%. The CVs were less than 10.8%, and we can find that the swine and chicken livers have the highest CVs. This is due to the different metabolic pathways of MEQ in different species and the differences in the enzymes involved [25,26]. All of the above results indicate that the analytical method developed in this study is highly sensitive, with good sample pretreatment and a low coefficient of variation.

Table 3. LOD, LOQ, and CVs of the samples spiked with DMEQ.

Sample	LOD (µg/kg)	LOQ (µg/kg)	Spiked Level (µg/kg)	Recovery (%)	CV$_{intra-assay}$ (%, n^{1} = 3)	Mean Recovery ± SD (%)	CV$_{inter-assay}$ (%, n^{1} = 9)
Pork	0.47	0.61	0.6	93.3–95.7	<10.8	94.7 ± 1.2	1.3
			1.2	87.5–101.8	<9.7	94.3 ± 7.2	7.6
			2.4	86.3–89.8	<9.3	88.6 ± 2.0	2.3
Swine liver	0.58	0.90	0.9	89.6–104.0	<7.6	99.0 ± 8.2	8.2
			1.8	89.0–97.9	<10.1	94.4 ± 4.7	5.0
			3.6	95.9–107.8	<4.5	100.6 ± 6.3	6.2
Swine kidney	0.55	0.77	0.75	80.8–86.1	<8.9	82.9 ± 5.7	6.9
			1.5	79.3–94.8	<8.8	85.6 ± 8.8	10.3
			3.0	73.7–80.8	<6.0	78.2 ± 4.5	5.8
Chicken	0.52	0.74	0.75	82.4–99.5	<8.3	89.2 ± 9.1	10.2
			1.5	93.7–99.2	<6.6	96.0 ± 2.9	3.0
			3.0	81.3–89.5	<7.8	85.1 ± 4.1	4.8
Chicken liver	0.54	0.77	0.75	93.9–99.7	<5.1	97.2 ± 4.6	4.7
			1.5	76.4–82.9	<2.7	79.3 ± 3.2	4.0
			3.0	91.2–101.1	<8.2	97.0 ± 7.5	7.7

[1] "*n*" means the number of parallel detection.

In order to determine the stability of this method, a study was investigated to correlate the stability of the coating antigen, the antibodies, and the DMEQ standard used in the assay system. The coated enzyme plates and the prepared antibodies were placed in a 37 °C thermostat and taken out for ELISA validation on days 0, 2, 4, 6, and 8, respectively. The stability of the method was evaluated using the titer and the IC_{50} value of the analysis as evaluation criteria. The results in Figure 5A,B show that the titer of the enzyme plate and the antibody remained above 80%, and the IC_{50} fluctuated within 20% after 8 d of storage at 37 °C. According to the empirical Arrhenius equation, this implies that the enzyme plates and antibodies can be stored for at least 12 months at 4 °C. We also measured the IC_{50} of the standard concentration of DMEQ at 4 °C every month. The results showed that the standard solution of DMEQ can still be stored at 4 °C for at least 6 months and keep the IC_{50} stable (Figure 5C).
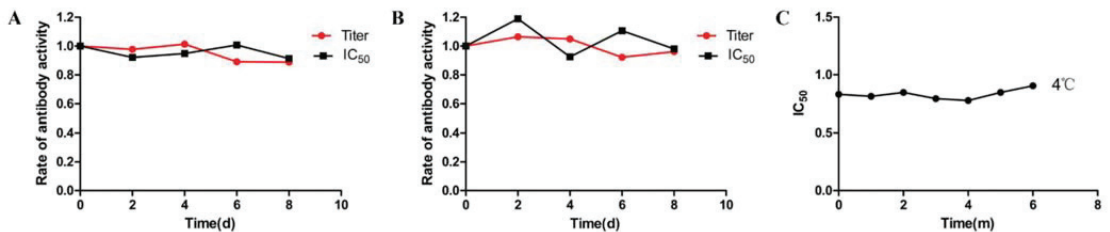
Figure 5. Stability testing of DMEQ–AOAA–OVA coating antigen (**A**), antibody (**B**), and DMEQ standard solution (**C**).

In addition, the reliability of the method was verified by analyzing the four spiked chicken samples (0.5, 1.0, 2.0, and 4.0 µg/kg) by ic-ELISA and LC–MS/MS, respectively. Figure 6 shows the fitted correlation coefficient (R^2) of 0.9973 between this analytical method and the instrumental analysis results in chicken. This demonstrates the reliability of the established ic-ELISA method for DMEQ, which provides strong technical support for the monitoring of Qx drug residues in food.
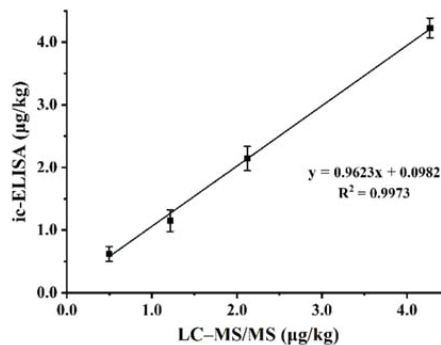
Figure 6. Correlation of LC–MS/MS and ic-ELISA for the analysis of spiked chicken samples.

4. Conclusions

In this study, we creatively synthesized a novel hapten to generate mAb against DQx. Based on the mAb, we firstly developed an ic-ELISA method to detect the residues of Qx in animal-derived foods, which was rapid, accurate, and sensitive. The simple analytical method reduces the sample pretreatment time, ensures higher efficiency, and meets the requirements for Qx residue analysis. The prepared mAb and the developed ic-ELISA method can monitor the residues of Qx in animal-derived foods to ensure food safety and human health.

References

1. Liu, Z.Y.; Huang, L.L.; Chen, D.M.; Yuan, Z.H. Metabolism of mequindox in liver microsomes of rats, chicken and pigs. *Rapid Commun. Mass Spectrom.* **2010**, *24*, 909–918. [CrossRef] [PubMed]
2. Liu, Q.Y.; Lei, Z.X.; Gu, C.Q.; Guo, J.C.; Yu, H.R.; Fatima, Z.N.; Zhou, K.X.; Shabbir, M.A.B.; Maan, M.K.; Wu, Q.H.; et al. Mequindox induces apoptosis, DNA damage, and carcinogenicity in Wistar rats. *Food Chem. Toxicol.* **2019**, *127*, 270–279. [CrossRef]
3. Liu, Q.Y.; Lei, Z.X.; Wu, Q.; Awais, I.; Shabbir, M.A.B.; Ahmed, S.; Fatima, Z.; Wang, X.; Pan, Y.H.; Xie, S.Y.; et al. The Reproductive Toxicity of Mequindox in a Two-Generation Study in Wistar Rats. *Front. Pharmacol.* **2018**, *9*, 870. [CrossRef] [PubMed]
4. Ihsan, A.; Wang, X.; Liu, Z.Y.; Wang, Y.L.; Huang, X.J.; Liu, Y.; Yu, H.; Zhang, H.F.; Li, T.T.; Yang, C.H.; et al. Long-term mequindox treatment induced endocrine and reproductive toxicity via oxidative stress in male Wistar rats. *Toxicol. Appl. Pharm.* **2011**, *252*, 281–288. [CrossRef] [PubMed]
5. Ihsan, A.; Wang, X.; Tu, H.G.; Zhang, W.; Dai, M.H.; Peng, D.P.; Wang, Y.L.; Huang, L.L.; Chen, D.M.; Mannan, S.; et al. Genotoxicity evaluation of Mequindox in different short-term tests. *Food Chem. Toxicol.* **2013**, *51*, 330–336. [CrossRef] [PubMed]
6. Liu, Q.Y.; Lei, Z.X.; Wu, Q.; Huang, D.Y.; Xie, S.Y.; Wang, X.; Pan, Y.H.; Yuan, Z.H. Mequindox Induced Genotoxicity and Carcinogenicity in Mice. *Front. Pharmacol.* **2018**, *9*, 361. [CrossRef] [PubMed]
7. Huang, L.L.; Yin, F.J.; Pan, Y.H.; Chen, D.M.; Li, J.; Wan, D.; Liu, Z.L.; Yuan, Z.H. Metabolism, Distribution, and Elimination of Mequindox in Pigs, Chickens, and Rats. *J. Agric. Food Chem.* **2015**, *63*, 9839–9849. [CrossRef]
8. Tan, H.L.; Pan, Y.H.; Chen, D.M.; Tao, Y.F.; Zhou, K.X.; Liu, Z.L.; Yuan, Z.H.; Huang, L.L. Discovery of the Marker Residue of Olaquindox in Pigs, Broilers, and Carp. *J. Agric. Food Chem.* **2019**, *67*, 6603–6613. [CrossRef] [PubMed]
9. Wu, Y.J.; Wang, Y.L.; Huang, L.; Tao, Y.F.; Yuan, Z.H.; Chen, D.M. Simultaneous determination of five quinoxaline-1,4-dioxides in animal feeds using ultrasonic solvent extraction and high-performance liquid chromatography. *Anal. Chim. Acta* **2006**, *569*, 97–102. [CrossRef]
10. He, Q.Q.; Fang, B.H.; Su, Y.J.; Zeng, Z.L.; Yang, J.W.; He, L.M.; Zeng, D.P. Simultaneous determination of quinoxaline-1,4-dioxides in feeds using molecularly imprinted solid-phase extraction coupled with HPLC. *J. Sep. Sci.* **2013**, *36*, 301–310. [CrossRef]
11. You, Y.L.; Song, L.T.; Li, Y.S.; Wu, Y.T.; Xin, M. Simple and Fast Extraction-Coupled UPLC-MS/MS Method for the Determination of Mequindox and Its Major Metabolites in Food Animal Tissues. *J. Agric. Food Chem.* **2016**, *64*, 2394–2404. [CrossRef]
12. Li, Y.S.; Liu, K.L.; Beier, R.C.; Cao, X.Y.; Shen, J.Z.; Zhang, S.X. Simultaneous determination of mequindox, quinocetone, and their major metabolites in chicken and pork by UPLC-MS/MS. *Food Chem.* **2014**, *160*, 171–179. [CrossRef]
13. Le, T.; Xu, J.; He, H.Q.; Niu, X.D.; Chen, Y.; Jia, Y.Y. Development and validation of an enzyme-linked immunosorbent assay for rapid detection of multi-residues of five quinoxaline-1,4-dioxides in animal feeds. *Food Agric. Immunol.* **2013**, *24*, 457–466. [CrossRef]
14. Le, T.; Zhu, L.Q.; Shu, L.H.; Zhang, L. Simultaneous determination of five quinoxaline-1,4-dioxides in animal feeds using an immunochromatographic strip. *Food Addit. Contam. A* **2016**, *33*, 244–251. [CrossRef] [PubMed]
15. Cheng, L.L.; Shen, J.Z.; Wang, Z.H.; Jiang, W.X.; Zhang, S.X. A sensitive and specific ELISA for determining a residue marker of three quinoxaline antibiotics in swine liver. *Anal. Bioanal. Chem.* **2013**, *405*, 2653–2659. [CrossRef] [PubMed]
16. Cheng, L.L.; Shen, J.Z.; Wang, Z.H.; Zhang, Q.D.; Dong, X.Y.; Wu, C.; Zhang, S.X. Rapid Screening of Quinoxaline Antimicrobial Growth Promoters and Their Metabolites in Swine Liver by Indirect Competitive Enzyme-Linked Immunosorbent Assay. *Food Anal. Method* **2013**, *6*, 1583–1591. [CrossRef]
17. Peng, D.P.; Wang, Y.L.; Feng, L.; Cao, G.C.; Tao, Y.F.; Liu, Z.L.; Yuan, Z.H. Preparation of Broadly Specific Monoclonal Antibodies for Simultaneous Determination of Fluoroquinolone Residues in Eggs. *Food Anal. Method* **2016**, *9*, 3520–3531. [CrossRef]
18. Chen, X.J.; Li, Z.Z.; Guo, J.Y.; Li, D.M.; Gao, H.L.; Wang, Y.; Xu, C.L. Simultaneous screening for marbofloxacin and ofloxacin residues in animal-derived foods using an indirect competitive immunoassay. *Food Agric. Immunol.* **2017**, *28*, 489–499. [CrossRef]
19. Peng, D.P.; Ye, S.Q.; Wang, Y.L.; Chen, D.M.; Tao, Y.F.; Huang, L.L.; Liu, Z.L.; Dai, M.H.; Wang, X.Q.; Yuan, Z.H. Development and Validation of an Indirect Competitive Enzyme-Linked Immunosorbent Assay for the Screening of Tylosin and Tilmicosin in Muscle, Liver, Milk, Honey and Eggs. *J. Agric. Food Chem.* **2012**, *60*, 44–51. [CrossRef]

20. Yang, H.C.; He, L.M.; Liu, Y.H.; Bian, K.; Hu, F.Y.; Fang, B.H. Determination of Quinoxalines and Their Two Main Metabolites in Environmental Water Samples by Liquid Chromatography-Tandem Mass Spectrometry. *Anal. Lett.* **2014**, *47*, 1421–1433. [CrossRef]

21. Lowry, O.H.; Rosebrough, N.J.; Farr, A.L.; Randall, R.J. Protein Measurement with the Folin Phenol Reagent. *J. Biol. Chem.* **1951**, *193*, 265–275. [CrossRef]

22. Bradford, M.M. A rapid and sensitive method for the quantitation of microgram quantities of protein utilizing the principle of protein-dye binding. *Anal. Biochem.* **1976**, *72*, 248–254. [CrossRef]

23. Han, X.Y.; Sheng, F.; Kong, D.X.; Wang, Y.L.; Pan, Y.H.; Chen, M.; Tao, Y.F.; Liu, Z.L.; Ahmed, S.; Yuan, Z.H.; et al. Broad-spectrum monoclonal antibody and a sensitive multi-residue indirect competitive enzyme-linked immunosorbent assay for the antibacterial synergists in samples of animal origin. *Food Chem.* **2019**, *280*, 20–26. [CrossRef] [PubMed]

24. Sheng, W.; Zhang, B.; Zhao, Q.X.; Wang, S.; Zhang, Y. Preparation of a Broad-Spectrum Heterocyclic Aromatic Amines (HAAs) Antibody and Its Application in Detection of Eight HAAs in Heat Processed Meat. *J. Agric. Food Chem.* **2020**, *68*, 15501–15508. [CrossRef]

25. Li, Y.; Li, L.X.; Shen, J.Z.; Zhang, S.X.; Feng, P.S.; Wu, H.X.; Wu, C.M. Comparative Metabolism of Mequindox in Liver Microsomes, Hepatocytes, and Intestinal Microflora of Chicken. *Anal. Lett.* **2012**, *45*, 1749–1763. [CrossRef]

26. Liu, Q.Y.; Lei, Z.X.; Dai, M.H.; Wang, X.; Yuan, Z.H. Toxic metabolites, Sertoli cells and Y chromosome related genes are potentially linked to the reproductive toxicity induced by mequindox. *Oncotarget* **2017**, *8*, 87512–87528. [CrossRef] [PubMed]

Article

Two-Dimensional Liquid Chromatography Method for the Determination of *Gelsemium* Alkaloids in Honey

Xiao Ma [1,2], Meng-Ting Zuo [1,2], Xue-Jia Qi [1,2], Zi-Yuan Wang [1,2] and Zhao-Ying Liu [1,2,*]

1   College of Veterinary Medicine, Hunan Agricultural University, Changsha 410128, China
2   Hunan Engineering Technology Research Center of Veterinary Drugs, Hunan Agricultural University, Changsha 410128, China
*   Correspondence: liu_zhaoying@hunau.edu.cn; Tel./Fax: +86-731-84618042

Abstract: Toxic Chinese medicine residues in honey pose a serious threat to consumer health. *Gelsemium* is one of the nine ancient poisons, making the whole plant virulent. The residue of *Gelsemium* alkaloid in honey causes poisoning from time to time. Therefore, it is very important to establish a method for the detection of *Gelsemium* alkaloids in honey. In this study, a method of solid phase extraction (SPE) with two-dimensional liquid chromatography (2D-LC) was developed for the first time for the simultaneous determination of *Gelsemium* alkaloids in honey, including gelsemine, koumine and humantenmine. First, the honey samples were purified by a PRS cation exchange column and extracted with 5% ammoniated methanol. Then, we verified the methodological indicators, which were in line with the Codex Guideline requirements. The verification results are as follows: matrix-matched calibrations indicated that the correlation coefficients were higher than 0.998. The recovery was in the range of 81%–94.2% with an intraday precision (RSD) of ≤5.0% and interday RSD of ≤3.8%. The limit of detection for the three alkaloids was 2 ng/g. The limits of quantification for gelsemine and koumine were 5 ng/g, and humantenmine was 20 ng/g. This method can be applied to the monitoring of *Gelsemium* alkaloids in honey.

Keywords: honey; two-dimensional liquid chromatography; koumine; humantenmine; *Gelsemium*; toxicity

1. Introduction

Honey is a natural sweet substance formed by mixing nectar or honeydew collected by bees and their own secretions [1]. It is a mixture of water and sugar and is rich in nutrients such as amino acids, minerals and essential trace elements and vitamins [2–4]. In our country, honey is a kind of medicine and food with a long history. "Shennong Materia Medica Classic" records that honey has many effects such as beneficial gas filling, pain relief and detoxification. Modern pharmacological studies have shown that honey has a variety of biological activities, such as anti-inflammatory, antioxidant, immune regulation and wound repair [5]. Due to its nutritional value and pharmacological activity, there is a great market demand. According to the data of the Food and Agriculture Organization of the United Nations, China is the world's largest producer of bee culture and bee products, ranking first in the world in both the total number of bee colonies and the output of bee products [6]. There are about 300,000 beekeepers, 9.2 million bee colonies and about 500,000 tons of honey on the market [7]. However, some toxic substances are frequently introduced into honey products during the gathering honey process [8]. Therefore, the exact composition and contaminants in any batch of honey depend on the crops around the hives [9]. As early as 2000 years ago, many Greek soldiers accidentally ate the "mad honey", resulting in a poisoning incident [10,11]. In recent years, in Yunnan, Guizhou and other places, incidents of accidentally eating toxic honey have also occurred [12–14]. It has been proven that honey poisoning is mainly caused by nectariferous plants, including

Gelsemium elegans, *Common Threewingnut Root*, *Tripterygium hypoglaucum* and so on [15,16]. Therefore, it is very important to establish a method for the detection of toxic ingredients in honey.

Gelsemium elegans is a whole herb of the genus Mackeraceae, and it ranks first among the nine poisons in ancient China. Whole plants are highly toxic to nectariferous plants. According to their different distribution areas, the snout can be roughly divided into three categories. One is the *Gelsemium sempervirens,* mainly distributed in the south of the United States to Central America; another one is the *Asia Gelsemium*. Current research shows that a total of 121 indole alkaloids have been found in *Asia Gelsemium* [17]. According to the skeleton structure of the compounds, they are mainly divided into six categories of alkaloids, including gelsemine-type, koumine-type, gelsedine-type, humantenine-type, yohimbine-type and sarpagine-type alkaloids. According to a report, koumine has the highest content of indole alkaloids, which belongs to the koumine-type; this is followed by gelsemine, which belongs to the gelsemine-type. The most toxic indole alkaloid is humantenmine, which belongs to the most toxic alkaloid in *Gelsemium,* which belongs to the gelsedine-type [18–20]. In recent years, there have been many cases of poisoning caused by ingestion of *Gelsemium* honey. On the one hand, *Gelsemium* honey poisoning can lead to strong and rapid poisoning reactions, such as dyspnea and convulsions, and even death. On the other hand, there is no specific detoxification drug. Therefore, it is necessary to establish a rapid, sensitive method for the detection of the phytotoxin *Gelsemium* alkaloid in honey, Which it is very important for the prevention and diagnosis of *Gelsemium* poisoning.

At present, there are only methodological studies of gelsemine, koumine and humantenmine in biological and plant samples [21–23]. Detection methods for *Gelsemium* poisoning are also limited to biological samples, such as blood and urine [24,25]. However, there are few reports on alkaloid detection in honey. Recently, the solid-phase extraction method (SPE), QuEChERs method (Quick, Easy, Cheap, Effective, Rugged, Safe) and the liquid–liquid extraction (LLE) method have been used for the determination of toxic substance residues in honey. Honey is an extraordinarily complex matrix containing more than three hundred chemicals, and it is rich in proteins and lipids [26]. Each sample of honey has a specific set of twenty-five ingredients because it comes from a different plant [27]. Thus, honey substrates require complex and extensive pre-treatment to eliminate or reduce the matrix effects. The traditional LLE method has complicated steps and requires many expensive organic solvents. It takes 150–180 min to process a sample, and the extraction recovery rate of polar substances in honey is low [28]. Pau Calatayud et al. compared the effects of SPE, QuEChERs and LLE on the extraction recovery of 52 pesticides in honey, and the results showed that SPE was superior to QuEChERs in terms of precision and accuracy. In addition, the plasma effect of SPE was lower than that of QuEChERs [29]. Therefore, the SPE method has more advantages for the pretreatment of the honey matrix than other methods.

It has been reported that liquid chromatography–tandem mass spectrometry (LC–MS) was used to detect the alkaloids in honey, including gelsemine and koumine [30]. However, due to the cost of mass spectrometry and the high requirement for the laboratory, the general laboratory cannot meet the requirements. Recently, our team established a two-dimensional liquid chromatography (2D-LC) method for *Gelsemium* in biological samples [31]. On this basis, this study aims to establish a 2D-LC method for the simultaneous determination of three standards of *Gelsemium* alkaloids (gelsemine, koumine and humantenmine) in honey samples. This method provides a technical means for the detection of *Gelsemium* alkaloids in food species of animal origin and can be used for the rapid detection of nectariferous plant poisoning events and the traceability of alkaloids.

2. Materials and Methods

2.1. Chemicals and Reagents

The standard products, including gelsemine (CAS#: 1803-14-9, purity: 99.28%), koumine (CAS#: 1807-14-8, purity: 99.84%) and humantenmine (CAS#: 2106-30-8, pu-

rity: 99.63%), were purchased from Must (Chengdu, China). A PRS cation exchange column (500 mg, 3 mL) was purchased from Welch (Shanghai, China). A Waters Oasis HLB column (3 cc, 60 mg, 30 μm) was purchased from Waters (Shanghai, China). Methanol and acetonitrile of HPLC grade were purchased from Merck Co. (Darmstadt, Germany). Ammonium dihydrogen phosphate, phosphoric acid and ammonia were purchased from Kemiou (Tianjin, China). Ultra-pure water with a resistivity of <18.2 MΩ cm was prepared from a Milli-Q water purification system (Millipore, Bedford, MA, USA). The blank honey sample was purchased from various supermarkets. Thirty honey samples were collected from farmers' markets in Hunan, Guizhou, Yunnan and Fujian Provinces from January 2022 to May 2022.

2.2. Preparation of Standard Solutions

Standard stock solutions of gelsemine, koumine and humantenmine were prepared with methanol at a concentration of 1 mg/mL and stored at −20 °C. The working solution of gelsemine, koumine and humantenmine was compounded by diluting the standard stock solution with methanol. Moreover, working solutions of gelsemine, koumine and humantenmine were added to blank honey to compound quality control (QC) samples. All QC samples were stored at −20 °C.

2.3. Sample Preparation Step

Honey (1.0 g) was mixed with 5 mL of water and vortexed for 2 min. Alkaloid was isolated using PRS cation exchange cartridges preconditioned with 5 mL of methanol and 5 mL of Milli-Q water. The mixed sample was passed through the PRS cartridges at a flow rate of less than 5 mL/min. Then, the PRS cartridges were rinsed with 10 mL of Milli-Q water and all effluent was discarded. The retained alkaloid was eluted with 8 mL of 5% ammoniated methanol. The eluate was evaporated to 0.5 mL using a gentle steam of nitrogen. Then, the sample was transferred quantitatively with methanol into a 1 mL volumetric flask, obtaining a final extract in 100% methanol. One milliliter of the extract was filtered through a 0.22-μm microbore cellulose membrane for 2D-LC analysis.

2.4. D-LC Analysis

The 2D-LC system was composed of an ACK 3200 column oven from ANAX with a fully automatic two-dimensional chromatographic coupling instrument (Changsha, China) and an LC-20AT high-performance liquid chromatograph from Shimadzu (Kyoto, Japan), which included a high-pressure LC-20AT pump (PUMP-B), two low-pressure gradient chromatography LC-20AT pumps (PUMP-A and PUMP-C), a CBM-20A system controller, a SIL-20A autosampler equipped with a 1000 μL injection loop and an SPD-20A UV detector.

The 2D-LC system used a heart-cutting transfer mode between the LC1 column and the LC2 column. The samples were first separated in 1D LC (LC1 column) mode to eliminate the interference of most impurities. The second step is the MC mode, in which the target material is transferred to the intermediate column after heart-cutting, where it is enriched. In the third step, the target was transferred to 2D LC (LC2 column) for further separation and, finally, UV detection. The mode switching in the whole process is done by LabSolutions LC Workstation V ER.5. The workstation corresponding to each mode can be highly automated to complete the corresponding work.

The first-dimensional (1D) liquid chromatography separation column was a strong cation exchange column (ASTON SXI 3.5 × 25 mm i.d.; particle size, 5 μm, Changsha, China). The middle column was a bonded phenyl column (SN-MA 4.6 × 10 mm i.d.; particle size, 5 μm, Changsha, China). The second-dimensional (2D) chromatography column was a reversed-phase column (SBR-2A 4.6 × 10 mm i.d.; particle size, 5 μm, Changsha, China). The mobile phase of PUMP-A was a 27:10:63 ($v/v/v$) solution of 80:20 (v/v) acetonitrile/water-10 mmol/L ammonium dihydrogen phosphate buffer (pH = 7.5)–10 mmol/L ammonium dihydrogen phosphate buffer (pH = 3.0). The PUMP-B mobile phase was water. The PUMP-C mobile phase was a 35:46:16.4:1.6:1 ($v/v/v/v/v$)

solution of water–acetonitrile–methanol–85% phosphoric acid–acetic acid (pH = 7.0). The temperature of the column was maintained at 40 °C, and the injection volume was 500 µL. The flow rate of PUMP-A is 1.2 mL/min; the PUMP-C flow rate is 1 mL/min. The detector wavelengths were 254 nm and 263 nm.

2.5. Method Validation Procedure

The method was validated according to the Codex guidelines [32] and the parameters included linearity, specificity, accuracy, precision, limit of quantification (LOQ), limit of detection (LOD), stock solution stability and sample stability. For the calibration curve, linearity was evaluable by a seven-point detection matrix-matched calibration curve. For gelsemine and koumine, the concentrations were 5, 20, 50, 100, 200, 500 and 1000 ng/g; for humantenmine, the concentrations were 20, 40, 100, 200, 400, 800 and 1000 ng/g. The standard curve was constructed with an added concentration (X) as the abscissa and peak area (Y) as the ordinate.

Recovery was determined by four concentration added levels of QC samples, including QCLL (1 × LOQ), QCL (3 × LOQ), QCM (6 × LOQ) and QCH (30 × LOQ) (n = 6) detection. Precision is measured by intraday precision and interday precision, usually expressed as RSD values. Intraday and interday precision is the result of the repeated analysis of honey QC samples at four supplemental concentrations (n = 6) for one day (intraday precision) and three consecutive days (intraday precision).

The LOD and LOQ were calculated by preparing a sample of honey at the lowest concentration and calculating the S/N 3 and 10 times. The method specificity was evaluated by comparing multiple blank matrix samples with blank matrix spiked samples (blank honey matrix supplemented with gelsemine, koumine and humantenmine).

The standard stock solution stability was measured by the standard deviation (RSD) of four different time nodes, which were measuring the stock solution at −20 °C for 0 d, 7 d, 30 d and 60 d (n = 6). The working solution was diluted from the standard reserve solution to near the lower limit and upper limit of quantification, respectively.

The sample stability was measured by the standard deviation (RSD) of four honey samples at different concentration levels, which were freeze–thawed three times at room temperature (25 °C) for 24 h and frozen for 30 d at −20 °C (n = 6).

3. Results and Discussion

3.1. Optimization of Chromatographic Separation

The essence of the 2D-LC is through the LC1 flow of the target material and the matrix extraction column separation, which removes the impurities, then the elution target substances are enriched in the capture column for a further transfer, and then enter the LC2 flow path for detection through the analysis column. Among them, the interception window width of the LC1 flow path extraction column for the target substance and the LC2 peak separation degree are the key factors determining the transfer recovery rate, peak shape and time length of the two-dimensional analysis. This directly affects the accuracy, sensitivity and detection limit of the two-dimensional liquid chromatography detection method.

Our laboratory has previously established a two-dimensional liquid phase detection method for *Gelsemium* alkaloids in pig plasma, tissue and urine. Referring to the method described by Liu et al., we optimized the mobile phase and time program on this basis [31]. The interception window was 0.7–4.2 min when the mobile phase was an acetonitrile–phosphate solution. Excessive window width would cause a loss in the process of target material transfer, and more impurities would be transferred to the analysis column, resulting in a poor impurity removal effect. Eventually, the transfer recovery rate will be reduced, column efficiency will be reduced and the impurities will affect the target analysis. Only using methanol or acetonitrile and water as a mobile phase could not separate the three target substances well. Therefore, in order to adjust the viscosity and strength of the mobile phase and improve the separation effect and selectivity, we added methanol

based on the original acetonitrile–water as the mobile phase for fine tuning, and the separation degree was improved, but the target peak tailing was relatively serious. Thus, to improve the peak shape, methanol acetonitrile water was used as the mobile phase, and 1.6% phosphoric acid (85%)–1% acetic acid was added to improve the peak shape and reduce tailing. However, the peak time of humantenmine is 0.6 min, which may lead to the failure of the interception of the target substance. Finally, the peak time of humantenmine was delayed by adding auxiliary water. Finally, the LC1 time program was determined to be 0–0.4 min with 1.2 L/min auxiliary water, and the interception window was 1.3–3.2 min. The LC2 mobile phase was adjusted to avoid the overlap of the peak times of the three target substances and to maintain a good separation degree. By adjusting the flow rate ratio of bottle-A (organic phase), bottle-B (water phase—alkali) and bottle-C (water phase—acid) in pump A, the peak time is delayed when the water phase increases, and the increase in the water phase—alkali ratio will lead to wider peak deformation. Therefore, by controlling the ratio of alkali and increasing the ratio of acid, the three target peaks can achieve a better separation and a good peak shape can be obtained. Finally, the flow rate ratio of pump-A was determined to be A:B:C = 27%:10%:63%. The optimized time program is shown in Table 1.

Table 1. Time program for 2D-LC detection of three alkaloids.

t/min	Time Program Setting				
	0.00–1.20	1.20–3.20	3.21–3.8	3.81–4.7	4.70–17.0
Column connection	The 1D column is disconnected from the MC column	The 1D column is disconnected from the MC column	The 1D column is connected to the MC column	The MC column is connected to the 2D column	The MC column is disconnected from the 2D column
Major function	Complete sample on-line enrichment	Perform the first-dimension chromatography separation	The target component is transferred to the MC column	The target component is transferred to 2D column	The further two-dimensional separation of target components

3.2. SPE Column Selection

We chose the solid phase extraction column (e.g., the HLB column and PRS cation exchange column) commonly used in alkaloid detection methods [33,34]. The HLB column is filled with a synthetic ultra-low pressure rapid reverse-phase chromatography filler, like the C18 column, which is suitable for the extraction of non-polar to moderately polar acidic, neutral and basic compounds. HLB columns are often used in the detection of complex substrates such as blood, urine and food. The PRS strong cation exchange column is based on the strong cation exchange being adsorbent. The main functional group is sulfonyl propyl, which has two ways of cation exchange and reverse phase retention. The retention mechanism is mainly related to strong cation exchange, while polarity is a secondary effect. It is suitable for the extraction of basic compounds. Therefore, we chose an HLB column and a PRS cation exchange column to investigate the effect of the pretreatment. Under the same pretreatment conditions (5 mL of methanol and 5 mL of Milli-Q water.), the HLB column showed poor retention of koumine and humantenmine, while the PRS column showed a high sensitivity and retention of koumine and humantenmine. The reason is that the cationic group of alkaloids can exchange with the positive ion [H] + of the PRS column, while the retention of the HLB column to the substance with greater polarity was poor. As shown in Figure 1, a cation exchange column was selected, and a solid phase extraction column (PRS) was used for sample extraction and purification; thus, a good peak shape and separation will be obtained.
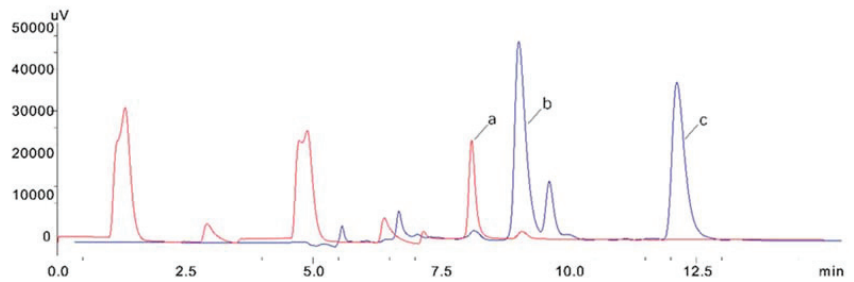
Figure 1. Comparison between the PRS cation exchange column (blue) and HLB solid phase extraction column (red). (**a**) Gelsemine, (**b**) koumine and (**c**) humantenmine.

3.3. Optimization Flush Solvent

On the one hand, honey is a highly complex sugar mixture, and approximately 95% of the ingredients are sugar. On the other hand, the SPE column we used would adsorb substances with a larger polarity, so we chose to wash out the adsorbed impurities with water or methanol. Because the material is alkaloids, methanol leaching can lead to the loss of the target substance, reducing the extraction of the recovery. The sugar in honey is easily soluble in water. Therefore, water was selected as the flush solvent first, and then the amount of flush solvent was investigated. The results of rinsing with 5, 10 and 15 mL of water were investigated. The results are shown in Figure 2. The impurity removal effect of flushing with 15 mL of water is good, which is conducive to the recovery of gelsemine but will cause the loss of koumine and humantenmine, while flushing with 10 mL of water could completely elute saccharides and achieve a good recovery of the target components. However, the flushing effect of the 5 mL volume was significantly lower than that of the 10 mL volume. Combining the above results, 10 mL of water was selected to wash away the interference.
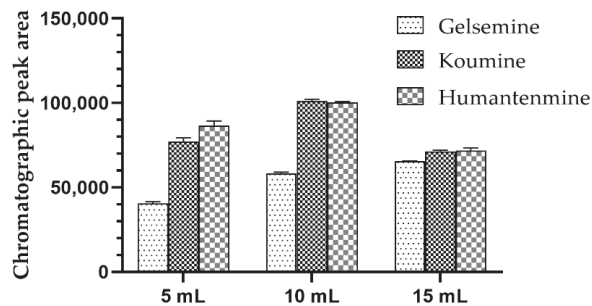
Figure 2. Comparison of the effects of 5 mL, 10 mL and 15 mL of flush solvent.

3.4. Optimization Elution Solvent

Because the target substance is alkaloid, it was converted into a free alkaloid under alkaline conditions. The organic reagent can be made alkaline by adding the appropriate amount of ammonia water. We compared 1% ammoniated methanol with 5% ammoniated methanol. The eluting effect of the 1% ammoniated methanol was no different from that of the methanol. The eluting effect of the 5% aminoacylated methanol was obvious due to the 1% aminoacylated methanol. To better dissolve alkaloids in organic solvents, the 5% ammoniated methanol was selected for elution, and then the amount of elution solvent was investigated [30]. The target substance was eluted with 3 mL, 5 mL and 8 mL solvents. The effect of the elution solvent amount on the extraction recovery of the target substance was observed. With the increase in the amount of elution solvent, the recovery rate improved significantly. When the elution solvent was 3 mL, the recovery rate of leucosin and leucosin

was about 65%, when the elution solvent was 5 mL, the recovery rate of leucosin and leucosin increased to 70%–75% and when the elution solvent volume reached 8 mL, the recovery rate was over 80%, which met the experimental requirements. The results are shown in Figure 3. More elution solvent can elute the target substance completely, but organic reagents are harmful to the body, so, after comprehensive consideration, 8 mL of the 5% ammoniated methanol was finally selected as the elution solvent in the spirit of cost savings and on the premise that the extraction recovery meets the experimental requirements.
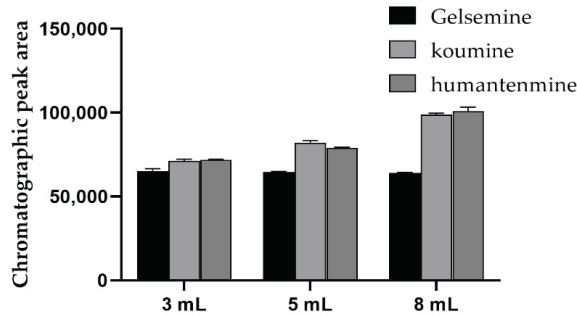
Figure 3. Comparison of elution effects with 3 mL, 5 mL and 8 mL of elution solvent.

3.5. Method Validation Results

There was a good linear relationship between the concentration of gelsemine in honey and koumine in honey in the range of 5–1000 ng/g, and humantenmine in the range of 20–1000 ng/g. The linear correlation coefficients R2 were all higher than 0.998 when the injection amount was 500 μL. The extraction recoveries were in the range of 81%–94.2% with an intraday RSD, and the interday RSD were all less than 5%. The accuracy and precision parameters met the methodological requirements. The LOQ of gelsemine and koummine was 5 ng/g, and the LOQ of humantenmine was 20 ng/g (Figure 4). The LOD of gelsemine, koummine and humantenmine was 2 ng/g. In 2D-LC, the retention times of the three alkaloids were approximately 7.28 min, 8.30 min and 11.30 min. The peak shapes of the three alkaloids were good, and there was no interference near the target peak. The sample stability results were in the range of 1.1%–10.16% (Table 2). The standard stock solution stability results were in the range of 0.2%–2.3% (Table 3). The method has good linearity, recovery, accuracy, precision, durability and specificity. These results indicate that this method can be used for the detection of snout toxicity in honey samples, reduce the risk of snout poisoning and can also be applied to the clinical detection of honey poisoning events. What's more, it also provides a theoretical basis and technical reference for the establishment of detection methods for other Chinese herbal medicines or toxic ingredients in honey.

Table 2. Results of linear range, correlation coefficient, LOD, recovery, accuracy, precision and sample stability.

Alkaloid	Added Concentration (ng/g)	Linear Range (ng/g)	Linearity (r2)	LOD (ng/g)	LOQ (ng/g)	Recovery (%)	Intraday RSD (%)	Interday RSD (%)	Short-Term RSD (%)	Freeze–Thaw RSD (%)	Long-Term RSD (%)
Gelsemine	QCLL					87.1	3.4	3.0	2.0	1.5	8.6
	QCL	5–1000	0.9998	2	5	94.2	1.9	2.0	1.2	4.5	3.1
	QCM					82.2	5.0	3.2	3.8	2.1	1.5
	QCH					83	3.6	3.8	2.4	1.8	4
Koumine	QCLL					92.9	3.4	2.0	2.9	1.2	4.3
	QCL	5–1000	0.9985	2	5	88.0	1.1	2.5	1.2	4.3	8.1
	QCM					89.4	3.8	3.8	5.4	5.8	10.2
	QCH					81	1.6	1.6	1.6	1.5	3.2

Alkaloid	Added Concentration (ng/g)	Linear Range (ng/g)	Linearity (r2)	LOD (ng/g)	LOQ (ng/g)	Recovery (%)	Intraday RSD (%)	Interday RSD (%)	Short-Term RSD (%)	Freeze–Thaw RSD (%)	Long-Term RSD (%)
Humantenmine	QCLL	20–1000	0.9999	2	20	81.5	3.9	3.0	3.7	7.1	7.4
	QCL					82.8	3.8	3.5	1.1	2.1	5.5
	QCM					83.4	3.1	1.9	6.1	4.4	2.3
	QCH					81.3	2.3	2.6	1.5	2.4	2.4
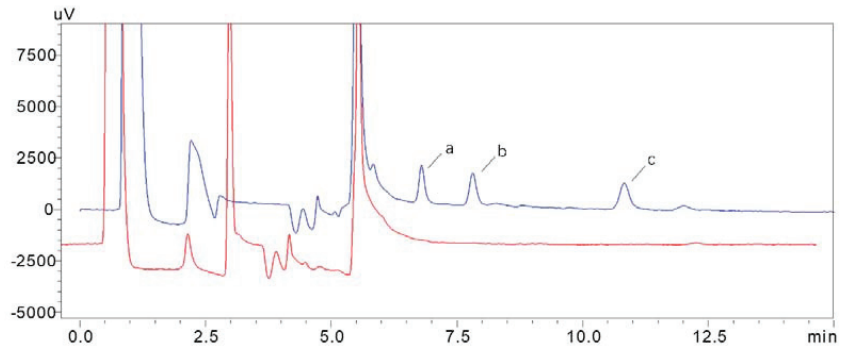
Figure 4. 2D-LC of blank samples (red) and added sample (bule-20 ng/g) (**a**) gelsemine, (**b**) koumine and (**c**) humantenmine.

Table 3. Results of standard stock solution stability.

Alkaloid	Added Concentration (ng/g)	0 d RSD (%)	7 d RSD (%)	30 d RSD (%)	60 d RSD (%)
Gelsemine	20	1.2	0.6	1.4	1.0
	900	0.4	1.0	1.5	1.3
Koumine	20	2.0	1.2	1.6	2.3
	900	0.9	0.6	1.1	1.7
Humantenmine	50	1.0	2.1	0.7	0.9
	900	0.2	1.2	1.6	2.0

3.6. Analysis of Actual Honey Samples

Thirty actual honey samples were collected from south China, where hookworm is widely distributed. Thirty honey samples were analyzed to assess the feasibility of the method. The results showed that there was no gelsemine, koumine or humantenmine residue in any of the 30 honey samples, which may be because our sampling time was from January to May, so we had not yet reached the full-bloom stage of the Gelsemium flower, or because the alkaloid content in the honey was very low and did not reach the detection limit of the method. In conclusion, according to our test results, there is a high probability that the honey on the market will not cause poisoning, but the overall evaluation of its safety needs more sample sizes and more test data of samples at different times.

3.7. Methods to Compare

Due to the high sensitivity and precision of LC-MS/MS, the current detection methods for toxic substances in honey mostly rely on LC-MS/MS but the laboratory requirements for LC-MS/MS are relatively high, so it is difficult to use and expensive to maintain. However, the long detection time and low sensitivity of liquid chromatography are not enough to meet the needs of detection. Two-dimensional liquid chromatography has the advantages of a short detection time, simple operating system, large injection volume and high sensitivity. Therefore, we compared the previously established LC-MS/MS and 2D-LC methods for

simultaneous quantification of gelsemine, koumine and humantenmine in pig plasma and tissue. Some methods for detecting toxic alkaloids in honey include LC-MS/MS, HPLC and UHPLC-MS [30,35–37]. The 2D-LC method established by us for the simultaneous detection of gelsemine, koumine and humantenmine in honey has a slightly higher limit of quantification than LC-MS/MS, but it is superior to the two methods in accuracy, precision and stability.

4. Conclusions

In this study, a 2D-LC method for the simultaneous quantification of gelsemine, koumine and humantenmine in honey was established at first. It is optimized based on the SPE method, with a lower matrix influence, limit of quantitation and better accuracy and precision. This method has the advantages of a short detection time and high specificity. Compared with mass spectrometry and high-performance liquid chromatography, this method has a lower cost than mass spectrometry and a higher sensitivity than high-performance liquid chromatography. This method can be applied to the clinical detection and tracing of nectariferous plant poisoning. In summary, this method has wide application prospects in the clinical detection and tracing of nectariferous plant poisoning.

Author Contributions: The experiments were conceived and designed by Z.-Y.L.; the experiments were performed by X.M.; the samples were prepared by X.-J.Q. and M.-T.Z.; the detected method was provided by Z.-Y.W.; data were analyzed and interpreted by X.M., X.-J.Q. and M.-T.Z.; the manuscript was drafted by M.-T.Z. and critically edited by Z.-Y.L. All authors have read and agreed to the published version of the manuscript.

Data Availability Statement: Data are contained within the article.

Conflicts of Interest: The authors declare no conflict of interest.

References

1. *GB 14963-2011*; National food safety standard Honey. Ministry of Health P. R. China: Beijing, China, 2011.
2. Ajibola, A.; Chamunorwa, J.; Erlwanger, K. Nutraceutical values of natural honey and its contribution to human health and wealth. *Nutr. Metab.* **2012**, *9*, 61. [CrossRef] [PubMed]
3. Dezmirean, G.I.; Mărghitaş, L.A.; Dezmirean, D.S. Honey Like Component of Functional Food. *Sci. Pap. Anim. Sci. Biotechnol.* **2011**, *44*, 406–411.
4. Stefan, B.; Tomislav, J.; Robert, S.; Peter, G. Honey for nutrition and health: A review. *J. Am. Coll. Nutr.* **2008**, *27*, 677–689.
5. Rehman, M.U.; Majid, S. Therapeutic Applications of Honey and Its Phytochemicals. Springer: Singapore, 2020.
6. Food and Agriculture Organization of the United Nations. Statistical Information—FAO Statistical Database [EB/OL]. Available online: http://www.fao.org/statistics/zh (accessed on 20 June 2021).
7. National Bureau of Statistics. National Data [EB/OL]. Available online: https://data.stats.gov.cn (accessed on 20 June 2021).
8. Xiang, H.; Zhou, Y.J.; Huang, P.L.; Yu, C.N.; Liu, J.; Liu, L.Y.; He, P. Lethal poisoning with Gelsemium elegans in Guizhou, China. *Public Health* **2016**, *136*, 185–187. [CrossRef]
9. Aliferis, K.A.; Tarantilis, P.A.; Harizanis, P.C.; Alissandrakis, E. Botanical discrimination and classification of honey samples applying gas chromatography/mass spectrometry fingerprinting of headspace volatile compounds. *Food Chem.* **2009**, *121*, 856–862. [CrossRef]
10. Gunduz, A.; Turedi, S.; Uzun, H.; Topbas, M. Mad honey poisoning. *Am. J. Emerg. Med.* **2006**, *24*, 595–598. [CrossRef]
11. Biberoğlu, S.; Biberoğlu, K.; Komsuoğlu, B. Mad honey. *JAMA* **1988**, *259*, 1943. [CrossRef]
12. Liu, Z.; Zhang, Q.; Li, J.; Ruan, Y.; Yang, Y.; Su, W.; Peng, M.; Wan, Q.; Zhao, J. Analysis of wild honey poisoning events from 2010 to 2019 in Yunnan Province. *J. Food Saf. Qual.* **2020**, *11*, 9063–9067. [CrossRef]
13. Chen, S.; Huang, X.; Zhang, Q.; Liu, Z.; Zhao, S.; Wan, R.; Wang, Y.; Zhang, X. The analysis of main toxic alkaloids in honey from distribution areas of toxic nectariferous plant in Yunnan. *J. Chin. Inst. Food Sci. Technol.* **2018**, *18*, 330–337. [CrossRef]
14. Zhou, W.; Lin, L.; Wei, X. Investigation on the source plants of toxic honey powder and honey poisoning in Guizhou Province. *Apic. China* **2017**, *68*, 38–39.

15. Tan, K.; Guo, Y.H.; Nicolson, S.W.; Radloff, S.E.; Song, Q.S.; Hepburn, H.R. Honeybee (*Apis cerana*) foraging responses to the toxic honey of *Tripterygium hypoglaucum* (Celastraceae): Changing threshold of nectar acceptability. *J. Chem. Ecol.* **2007**, *33*, 2209–2217. [CrossRef] [PubMed]

16. Edgar, J.A.; Roeder, E.; Molyneux, R.J. Honey from plants containing pyrrolizidine alkaloids: A potential threat to health. *J. Agric. Food Chem.* **2002**, *50*, 2719–2730. [CrossRef] [PubMed]

17. Jin, G.; Su, Y.; Liu, M.; Xu, Y.; Yang, J.; Liao, K.; Yu, C. Medicinal plants of the genus Gelsemium (Gelsemiaceae, Gentianales)–a review of their phytochemistry, pharmacology, toxicology and traditional use. *J. Ethnopharmacol.* **2014**, *152*, 33–52. [CrossRef]

18. Liu, M.; Shen, J.; Liu, H.; Xu, Y.; Su, Y.; Yang, J.; Yu, C. Gelsenicine from Gelsemium elegans attenuates neuropathic and inflammatory pain in mice. *Biol. Pharm. Bull.* **2011**, *34*, 1877–1880. [CrossRef]

19. Sun, L.; Lei, L.; Fang, F.; Yang, S.; Wang, J. Inhibitory effect of koumine on splenocyte proliferation and humoral immune response in mice. *Pharmacol. Clin. Chin. Mater. Med.* **1999**, *15*, 10–12.

20. Zhang, L.; Lin, J.; Zhong, W. Advances in chemical constituents and pharmacology of Gelsemium elegans. *J. Chin. Med. Mater.* **2003**, *26*, 451–453. [CrossRef] [PubMed]

21. Yang, K.; Long, X.; Liu, Y.; Chen, F.; Liu, X.; Sun, Z.; Liu, Z. Development and in-house validation of a sensitive LC-MS/MS method for simultaneous quantification of gelsemine, koumine and humantenmine in porcine plasma. *J. Chromatogr. B Anal. Technol. Biomed. Life Sci.* **2018**, *1076*, 54–60. [CrossRef]

22. Ji, S.-J.; Liu, W. Simultaneous determination of Koumine Gelsemine, and Gelsenicine in biological samples by LC-MS/MS. *J. Forensic Med.* **2017**, *33*, 141–147.

23. Lin, W.; Sun, L.; Liu, H.; Zhao, N.; Meng, F. Simultaneous determination of three alkaloids in extracts from gelsemium elegans benth. by HPLC. *Chin. J. Pharmacovigil.* **2017**, *14*, 161–164.

24. Feng, T.; Tao, S.; Ruan, S.; Li, X.; Lin, D. Emergency detection of a food poisoning by gelsemine GC-MS technology. *Mod. Food* **2021**, *6*, 156–160. [CrossRef]

25. Zhong, S. Determination of Phytotoxins in Biological Samples by Quechers-HPLC-MS/MS Method. Master's Thesis, People's Public Security University of China, Beijn, China, 2020.

26. Kujawski, M.W.; Namieśnik, J. Challenges in preparing honey samples for chromatographic determination of contaminants and trace residues. *TrAC Trends Anal. Chem.* **2008**, *27*, 785–793. [CrossRef]

27. Zhang, Y.; Li, X.Q.; Li, H.M.; Zhang, Q.H.; Gao, Y.; Li, X.J. Antibiotic residues in honey: A review on analytical methods by liquid chromatography tandem mass spectrometry. *Trends Anal. Chem.* **2018**, *110*, 344–356. [CrossRef]

28. Gałuszka, A.; Migaszewski, Z.; Namieśnik, J. The 12 principles of green analytical chemistry and the SIGNIFICANCE mnemonic of green analytical practices. *TrAC Trends Anal. Chem.* **2013**, *50*, 78–84. [CrossRef]

29. Calatayud-Vernich, P.; Calatayud, F.; Simo, E.; Pico, Y. Efficiency of QuEChERS approach for determining 52 pesticide residues in honey and honey bees. *MethodsX* **2016**, *3*, 452–458. [CrossRef]

30. Dalong, L.; Hua, W.; Chaojie, C.; Jialiang, Z.; Yongcheng, Y. Determination of Gelsemine and Koumine in Honey by liquid Chromatography-tandem mass spectrometry. *Food Ind.* **2020**, *41*, 297–300.

31. Liu, S.S.; Yang, K.; Sun, Z.L.; Zheng, X.; Bai, X.; Liu, Z.Y. A novel two-dimensional liquid chromatography system for the simultaneous determination of three monoterpene indole alkaloids in biological matrices. *Anal. Bioanal. Chem.* **2019**, *411*, 3857–3870. [CrossRef]

32. Codex Alimentarius Commission. *Codex Guidelines for the Establishment of a Regulatory Programme for Control of Veterinary Drug Residues in Foods. Part III Attributes of Analytical Methods for Residue of Veterinary Drugs in Foods16*; Codex Alimentarius Commission, CAC: Rome, Italy, 1993; Volume 16, p. 41.

33. Huang, D.; Zhao, X.; Liu, X.; Chao, R. Determination of Five Aminoalcohol-diterpenoid Alkaloids in the Lateral Root of Aconitum carmichaeli by HPLC-ELSD with SPE. *J. Chromatogr. Sci.* **2017**, *55*, 940–945. [CrossRef] [PubMed]

34. Brian, K. Determination of Ephedra Alkaloids and Synephrine in Dietary Supplements via Strong Cation-Exchange SPE and LC-MS/MS Detection. *LC GC Eur.* **2017**, *30*, 696.

35. Li, C.; Dan, W.; Shuang, Z.; Jiangling, Z.; Yunfeng, Z. Determination of five pyrrolizidine alkaloids in honey by ultra high performance liquid chromatography-tandem triple quadrupole mass spectrometry. *Environ. Chem.* **2014**, *33*, 1971–1977.

36. Mudge, E.M.; Jones, A.M.P.; Brown, P.N. Quantification of pyrrolizidine alkaloids in North American plants and honey by LC-MS: Single laboratory validation. *Food Addit. Contam. Part A Chem. Anal. Control Expo. Risk Assess.* **2015**, *32*, 2068–2074. [CrossRef]

37. Ling, Y.; Li-Li, D.; Xiu-ling, W.; Zhang-Ji, H.; Min, L.; Jun-chun, W. Determination of caffeine in honey by HPLC coupled with Ultrasound-assisted dispersive Liquid-Liquid microextraction. *Phys. Test. Chem. Anal. (Part B Chem. Anal.)* **2015**, *51*, 897–901.

Article

PCDD/Fs and DL-PCBs in Chinese Mitten Crab (*Eriocheir sinensis*) and Its Farming Environment in Shanghai, China

Ya Li Wang [1,2,3], Si Ying Fei [1,2,3], Tian Wei Wang [1,2,3], Xue Ting Liu [1,2,3], Xiao Nin Gao [1,2,3], Hao Tian Wu [1,2,3] and Kun Hu [1,2,3,*]

1   National Demonstration Center for Experimental Fisheries Science Education, Shanghai Ocean University, Shanghai 201306, China
2   National Pathogen Collection Center for Aquatic Animals, Shanghai Ocean University, Shanghai 201306, China
3   Key Laboratory of Freshwater Aquatic Genetic Resources, Ministry of Agriculture, Shanghai Ocean University, Shanghai 201306, China
*   Correspondence: khu@shou.edu.cn

Abstract: Most polychlorinated dibenzo-p-dioxins and dibenzofurans (PCDD/Fs) and dioxin-like polychlorinated biphenyls (DL-PCBs) in the human body are acquired from dietary intake. The chronic exposure of humans to PCDD/Fs and DL-PCBs is a major health concern, and these compounds are strictly controlled in many areas. This study measured the levels of PCDD/Fs and DL-PCBs in Chinese mitten crab (*Eriocheir sinensis*) farms in Shanghai and determined potential sources. The mean concentrations of PCDD/Fs and DL-PCBs in the studied crab samples were 264.20 ± 260.14 and 506.25 ± 226.80 pg/g ww (wet weight), respectively. The range of the toxic equivalent (TEQ) for the total PCDD/Fs and DL-PCBs in the crab samples was 1.20–29.04 pg TEQ/g ww. Further analysis revealed that the TEQ input to crabs in aquacultural water was 1.6 times higher than the TEQ in edible crab parts. Aquatic plants, shore plants, and feed contributed about 0.05% of the total TEQ input to crabs. The TEQ contribution from sediment was 317 times that found in edible crab parts, and sediment may be the most prevalent source of PCDD/Fs and DL-PCBs in farm crabs. The evaluation of the Shanghai market crab revealed different levels of PCDD/Fs and DL-PCBs. The TEQs for the mean PCDD/F and DL-PCB levels were 1.55 ± 1.96 and 1.05 ± 0.55 pg TEQ/g ww, respectively. The tolerable daily intake (TDI) levels of adults and children were lower than the prescribed range (1–4 pg TEQ/kg (weight)·d), indicating no significant chronic or acute ingestion risk for adults and children.

Keywords: persistent organic pollutant; PCDD/Fs; DL-PCBs; high-resolution gas chromatography and high-resolution mass spectrometry (HRGC/HRMS); *Eriocheir sinensis*; bioaccumulation

1. Introduction

Polychlorinated dibenzo-p-dioxins and dibenzofurans (PCDD/Fs) are a group of halogenated aromatic hydrocarbons that exhibit high toxic potential and that include polychlorinated dibenzo-dioxins (PCDDs) and polychlorinated dibenzo-furans (PCDFs), comprising a total of 210 congeners [1]. They typically accumulate in the air, soil, sediment, fish, human adipose tissue, and milk [2,3]. Dioxin-like polychlorinated biphenyls (DL-PCBs) are persistent organic pollutants that remain in the environment for long periods of time [4]. They are hailed as the most hazardous elements for human health and were enlisted during the Stockholm Convention owing to their high carcinogenicity [5]. DL-PCBs have a lipophile and stable chemical structure, making them resistant to degradation [6]. They are introduced into the aquatic environment, tend to settle in the sediment, enter the food chain via numerous routes, and accumulate in living organisms [7]. The International Agency for Research on Cancer (IARC) has classified PCDD/Fs and DL-PCBs as "Group I human carcinogens " [8]. As inducements, PCDD/Fs and DL-PCBs have become research

hotspots. Previous studies revealed that the by-products of industrial manufacturing processes involving chlorine remain the major sources of PCDD/Fs and DL-PCBs, which are strongly associated with natural heat [9]. Subsequently, their footprints have also been found in the North and South Poles and may play a significant role in migration processes, posing a serious threat to the earth's ecological environment [10,11]. In the atmosphere, PCDD/Fs and DL-PCBs may be transported into the ocean and rivers via environmental deposition and may affect the health of aquatic animals. The PCDD/Fs and DL-PCBs are widely distributed in the aquatic environment and accumulate in aquatic organisms, being integrated into the food chain [12]. Hyo-bang Moon et al. [13] recorded the highest levels of PCDD/Fs and DL-PCBs residues in crustaceans followed by fish. Dietary intake is believed to be the main route of human exposure to dioxins, accounting for more than 90% of total human exposure [5]. They may be present in one's diet, as it is possible for them to be passed up through the food chain and to accumulate in humans at the top. At the same time, the presence of these compounds in the human body leads to serious health concerns due to their toxicity, indirectness, stability, and generational hereditary. They can also interfere with the immune, reproductive, and nervous systems and render a carcinogenic impact on human beings [6]. Therefore, food safety issues related to dioxins are attracting more and more attention. The tolerable daily intake (TDI) levels recommended by the World Health Organization (WHO) at a 1990 dioxin conference in the Netherlands were 10 pg TEQ/(kg (weight)·d) [14]. Since then, following the emergence of new epidemiological data and data regarding the significant effects of dioxins on neurological development and the endocrine system, the WHO experts consulted these data and re-evaluated their stance on dioxins, determining a new allowable TDI range of 1–4 pg TEQ/(kg (weight)·d) to ensure the safety of food and to build health barriers [15].

The Chinese mitten crab (*Eriocheir sinensis*) is a common freshwater crab, accounting for 18% of shrimp crab culture. They are widely distributed from Northern China to South Korea, existing in freshwater as juveniles and adults. Upon reaching sexual maturity, this crab migrates to brackish water to mate, lay eggs, and hatch, and it then returns to its freshwater habitat [16]. Its delicious meat, richness in unsaturated fatty acids, unique pleasant aroma, and delicious taste have promoted the Chinese mitten crab as a popular aquatic product. In 2021, global sales of the Chinese mitten crab market reached hundreds of millions of dollars, providing a substantial advantage to the marine industry. However, according to Taiwan's Food and Drug Administration, in October 2018, Taiwan had imported about 196 tons of Chinese mitten crab from the mainland, 40 tons of which contained more dioxin than standard levels, accounting for 20% of the total product (https://www.mohw.gov.tw/cp-16-44846-1.html (accessed on 21 January 2022). The sampling limit was four times higher than the maximum of 27 pq/g TEQ/g ww (more than 6.5 pq/g TEQ/g (wet weight)). In October 2017, the dioxin content of Chinese mitten crab from Hunan province exceeded the standard limit. Among them, 4.114 tons of hairy crabs constituted 4.1 pg/g of dioxin, and 4.455 tons of hairy crabs were found to constitute 12.1 pg/g of dioxin and PCBs, seriously affecting crab sales (https://www.ereying.com/articles/83.html (accessed on 27 January 2022).

The accumulation of contaminants in aquatic organisms is closely related to the food chain and its culture environment [17]. Studies have shown that animal feed remains one of the primary sources of pollution, and contaminated animal feed or feed additives may lead to food contamination [18,19]. In 1999, dioxin contamination was found in chicken feed in Belgium [20]; in the USA, livestock, aquaculture, and poultry feed exceeded dioxin limits from 2002 to 2003, and this revealed that dioxins enter the food chain via feed, potentially contributing to dioxin accumulation [21]. Other studies have shown that soil is the source of dioxin contamination in eggs from free-range hens on Polish farms [22]. As omnivorous animals, mixed feed is the primary source of nutrition for Chinese mitten crabs. Moreover, Chinese mitten crabs also eat aquatic plants and benthic animals. Contaminants in sediment might be the source of dioxins in samples of these crabs [23]. Some substances, such as

water bodies, food residues, and feces, will eventually form sediments, which may lead to dioxin accumulation and contamination in sediments and the development of secondary pollution [24]. Sediment is also a feeding route for crabs, so the chemical constituents in sediment can affect crab health. For Chinese mitten crab, the cultural environment has gained gradual prominence in its growth and development. The wide variety of substances consumed by Chinese mitten crabs indicates that the sources of dioxins and biphenyls may be complex and that the food and culture environment of Chinese mitten crabs may be contributing factors.

Currently, the sources of PCDD/Fs and DL-PCBs found in Chinese mitten crab in Shanghai are not clearly understood. This study investigated the PCDD/F and DL-PCB contents in Chinese mitten crabs and the potential sources of these contaminants. The amount of pollution found in Chinese mitten crab on the market was analyzed to provide a scientific basis for targeted prevention and control measures, public scientific consumption, and essential support to ensure the healthy breeding and sustainable development of livestock, poultry, and aquatic products.

2. Materials and Methods

2.1. Crab Sampling

Chinese mitten crabs were obtained from various farms situated in the Qingpu and Chongming districts of Shanghai (Table 1). Among the sampling sites, three were in the Qingpu district and three were in the Chongming district (Figure 1). A total of 90 crabs were collected, 15 at each sampling site, and each crab was the commercial standard size of about 100.2 ± 5.6 g. In addition, Chinese mitten crab samples sold in fresh markets around Shanghai were also procured for further testing and evaluation. A total of 555 crabs were collected, 15 at each sampling site, and each crab was about 101.6 ± 3.6 g. The sampling information for the market crabs is shown in Table S1 and Figure 1. After arriving at the lab, the samples were freeze-dried and stored in a refrigerator at $-20\ ^\circ$C.

Table 1. Farm crab sampling site information.

Name of Farm	Latitude and Longitude	Number
Shanghai Ruijie Aquaculture Professional Cooperative	31°0′40″ N, 121°2′45″ E	RJ
Nanxin Village farm	31°31′11″ N, 121°41′20″ E	NXC
Shanghai Mahe Product Professional Cooperative	31°0′1.54″ N, 121°0′44″ E	MH
Shanghai Zihao Industrial Development Company Limited	31°35′4″ N, 121°39′14″ E	ZH
Shanghai Yufeng Aquaculture Professional Cooperative	31°36′37″ N, 121°39′0″ E	YF
Shanghai Huikang Aquaculture professional cooperative	31°31′12″ N, 121°41′21″ E	HK
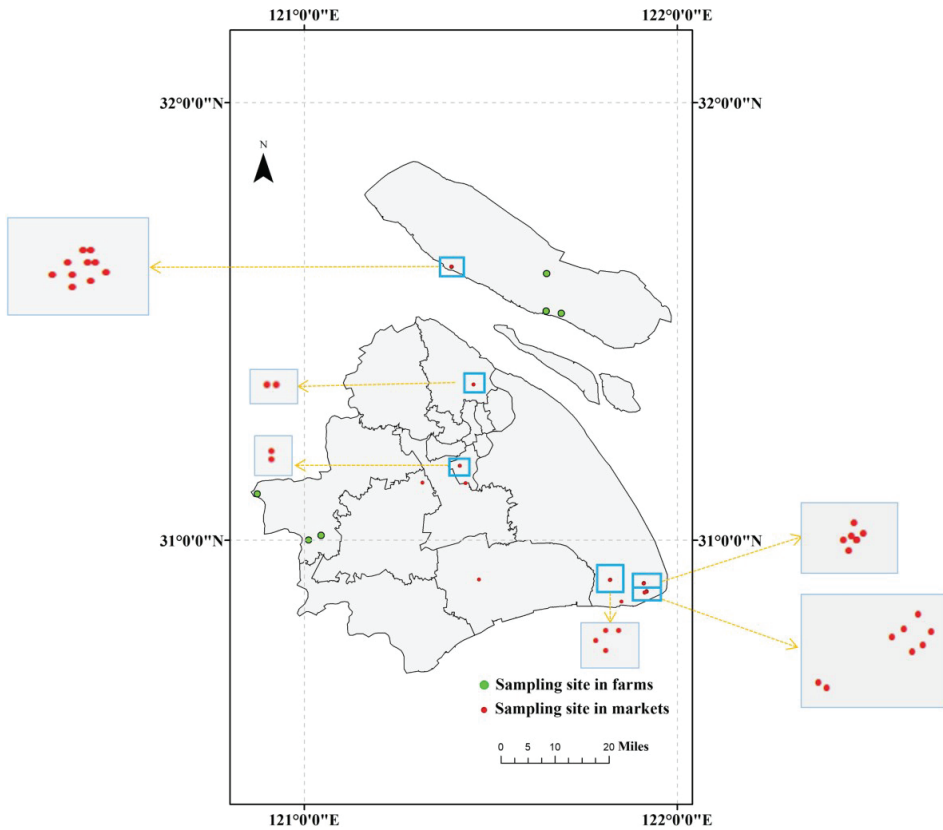
Figure 1. Crab sampling sites in Shanghai.

2.2. Sampling of Potential Sources of PCDD/Fs and DL-PCBs

To determine the primary sources of the PCDD/Fs and DL-PCBs found in Chinese mitten crabs, various crab culture processes, including sediment (-CJW), culture water (-YS), aquatic grass (-SC), shore plants (-ZW), and feed (-SL), were collected. We collected 6 replicates of sediment samples from 6 farms (each not less than 1 kg dw). Comprehensive samples were taken from 6 different locations with the crab farms' pool aquaculture water (every 20 L), feed samples (each not less than 500 g ww), aquatic plants (each not less than 1 kg ww), and shore plants (each not less than 1 kg ww). The corresponding farm information is shown in Table 1.

2.3. PCDD/Fs and DL-PCBs Detection Method

The chromatographic method used in this experiment is currently the internationally recognized standard method for dioxin detection and analysis and mainly uses a combination of high-resolution gas chromatography and high-resolution mass spectrometry (HRGC/HRMS) [25]. This study adopts the method outlined by the National Food Safety Standard for the determination of toxic equivalent of dioxins and their analogs in food (GB 5009.205-2013) for sample analysis [26]. High-resolution gas chromatography, high-resolution mass spectrometry, and a gas chromatography column (HRGC-HRMS, Agilent, Palo Alto, CA, USA) with a resolution of no less than 10,000 were used in this experiment. The contents of 17 2,3,7,8-substituted polychlorinated dibenzo-dioxins (PCDDs) and polychlorinated dibenzo-furans (PCDFs) and 12 dioxin-like polychlorinated biphenyls (DL-PCBs) and their toxic equivalents (TEQs) were analyzed. Details of these 29 compounds are

shown in Table S2. Quantitative internal standard: $^{13}C_{12}$-labeled solution of the internal standard for the quantification of PCDD/Fs and PCBs compounds; internal standard of recovery: $^{13}C_{12}$-labeled solution of internal standard for the recovery of PCDD/F and PCB compounds (Wellington Laboratory, Guelph, ON, Canada). Details of these internal standards are shown in Tables S3 and S4.

2.4. Sample Preparation

The collected samples were packaged in light-protected aluminum foil and brown glass bottles, transported to the laboratory at the Shanghai Academy of Agricultural Sciences at a low temperature, and stored at −20 °C. The collected water samples were adsorbed on a resin chromatography column containing XAD-2 (Serva, Sparks, NV, USA) and were stored in the dark after drying. Before sample processing, the edible parts, sediments, feed, aquatic plants, and shore plant samples that were collected from the Chinese river crab farms were crushed and ground in a freeze dryer (Pilot-4LD, Beijing Biocool, Beijing, China). The samples were mixed well with the appropriate amount of internal standard before extraction (details of quantitative internal standard in Table S3). After that, using accelerated solvent extraction (Dionex ASE300, Thermo Fisher Scientific, Waltham, MA, USA)), 200 mL of n-hexane: dichloromethane (1:1, volume ratio) (GR, Sigma, Ronkonkoma, NY, USA) was used for solvent extraction. All of the extracts produced from the feed and crab samples needed to be pickled 3 times with 30 mL of concentrated sulfuric acid (GR, Sinopharm Chemical, Beijing, China) to remove any lipids. They also needed to then be rinsed with 50 mL of deionized water three times to neutralize the acidity, and anhydrous sodium sulfate (GR, Kermel, Tianjin, China) was then used on the samples to remove moisture. The samples were then set aside. Finally, all of the extracts were concentrated using a rotary evaporator (R-210V, Buchi, Hendrik-Ido-Ambacht, Sweden), and the concentrates were purified using a series of adsorption chromatography columns, such as acidic silica gel columns, composite silicone columns, and alkaline alumina columns (Thermo, Waltham, MA, USA). The eluate of each component obtained after purification and separation was concentrated from 1 mL to 2 mL using a rotary evaporator and by increasing the nitrogen concentration (Organomation, Berlin, MA, USA), and the eluates were then transferred to a sample bottle filled with a 0.2 mL lined tube and concentrated to about 20 μL, and the appropriate amount of internal standard required for recovery was added to each component (the amounts of internal standard required for recovery are shown in Table S4) for on-machine detection.

2.5. Instrumentation and Measurements

The PCDD/F and DL-PCB contents in the samples were determined using the coupled HRGC-HRMS method. Different GC columns should be used for different targets. Detailed information regarding the chromatographic conditions is shown in Table 2.

Table 2. Chromatographic condition information.

Instrumental Conditions	PCDD/Fs Detection	DL-PCBs Detection
DB-5 ms column	60 m × 0.25 mm × 0.25 μm	60 m × 0.25 mm × 0.25 μm
Inlet temperature	280 °C	290 °C
Transmission line temperature/interface temperature	310 °C	290 °C
Column temperature	120 °C (hold for 1 min); ramp up to 220 °C at 43 °C/min (hold for 15 min); ramp up to 250 °C at 2.3 °C/min, ramp up to 260 °C at 0.9 °C/min, ramp up to 310 °C at 20 °C/min (hold for 9 min)	80 °C (hold for 2 min); ramp up to 150 °C at 15 °C/min; ramp up to 270 °C at 2.5 °C/min (hold for 3 min), ramp up to 330 °C at 15 °C/min (hold for 1 min)
Carrier gas flow rate	1.2 mL/min	1.2 mL/min

The GC conditions were optimized to achieve high sensitivity with rapid and accurate separation. After condition optimization, the same GC conditions were optimized for standard solution, blank, IPR and OPR, and sample determination. The mass spectrometer was tuned using a reference gas (PFK or FC43) to monitor m/z 330.9792 or other PFK fragment ions in the m/z 300 to 350 mass range to achieve a mass spectrometer resolution of 10,000 (10% peak-to-valley). During the study, the amount of reference gas entering the HRMS was regulated to ensure that the chosen signal intensity of the locking mass number did not exceed 10% of the detector's whole range. The mass shift of the mass spectrometer was corrected using the PFK's (or another reference gas') locking mass number. The method of adding recovery rate internal standard was used to perform quality control on the analysis and determination of the samples, and a certain amount and standard solution were added before the samples were processed to determine the recovery rate to correct the error caused by the losses incurred during sample processing and the change in the sample amount during analysis. We excluded test results that were not included in the recovery rate to ensure the reliability of the results. At the same time, blank experiments were performed during sample handling to prevent contamination.

2.6. Statistical Analysis

Toxicity equivalent (TEQ) calculations are based on the revised WHO-TEF values from 2005. All of the TEQ concentrations are reported according to upper, median, and lower limits. The TEQs of the PCDD/Fs and DL-PCBs in Chinese mitten crab were calculated according to Formulas (1)–(6):

$$TEQ_i = TEF \times c_i \tag{1}$$

$$TEQ_{PCDDs} = \Sigma TEF_{iPCDDs} \times c_{iPCDDs} \tag{2}$$

$$TEQ_{PCDFs} = \Sigma TEF_{iPCDDFs} \times c_{iPCDFs} \tag{3}$$

$$TEQ_{PCDD/Fs} = TEQ_{PCDDs} + TEQ_{PCDFs} \tag{4}$$

$$TEQ_{DL-PCBs} = \Sigma TEF_{iDL-PCBs} \times c_{iDL-PCBs} \tag{5}$$

$$TEQ_{(PCDD/Fs + DL-PCBs)} = TEQ_{PCDD/Fs} + TEQ_{DL-PCBs} \tag{6}$$

where TEQ_i—dioxin toxic equivalent (*TEQ*) of the congeners of *PCDD/Fs* or *DL-PCBs* in food in micrograms per unit kg (µg/kg); TEF_i— toxicity equivalent factors of congeners in *PCDD/Fs* or *DL-PCBs*; c_i—concentrations of *PCDD/Fs* or *DL-PCBs* congeners in food in micrograms per kilogram (µg/kg); the remaining subscripts are specific combinations of *PCDD/Fs* or *DL-PCBs*.

3. Results and Analysis

3.1. The Concentration of PCDD/Fs and DL-PCBs in Farm Crabs

A total of 17 PCDD/Fs and 12 DL-PCBs were detected in the edible parts of the sampled crabs, and the PCDD/F and DL-PCB concentrations in the crab samples from the different farms varied greatly. Detailed results are shown in Table S5. The mean PCDD/F and DL-PCB concentrations of the crab samples were 264.20 ± 260.14 and 506.25 ± 226.80 pg/g ww, respectively. The PCDD/F concentrations ranged from 20.45 to 686.64 pg/g ww, with OCDD having the greatest concentration (612.75 pg/g ww), accounting for 38.7%, followed by 1,2,3,4,6,7,8-HpCDD at 549.05 pg/g ww, accounting for 34.6% (Figures 2A and 3A). The DL-PCB concentrations ranged from 246.51 to 894.47 pg/g ww, with the highest concentration of 2,3′,4,4′,5-PeCB (1573.97 pg/g ww) accounting for 51.8%, followed by 2,3,3′,4,4′-PeCB (86.63 pg/g ww), which accounted for 19.8% (Figures 2B and 3B). The remaining PCDD/F and DL-PCB congeners in the crab samples accounted for less than 10%.
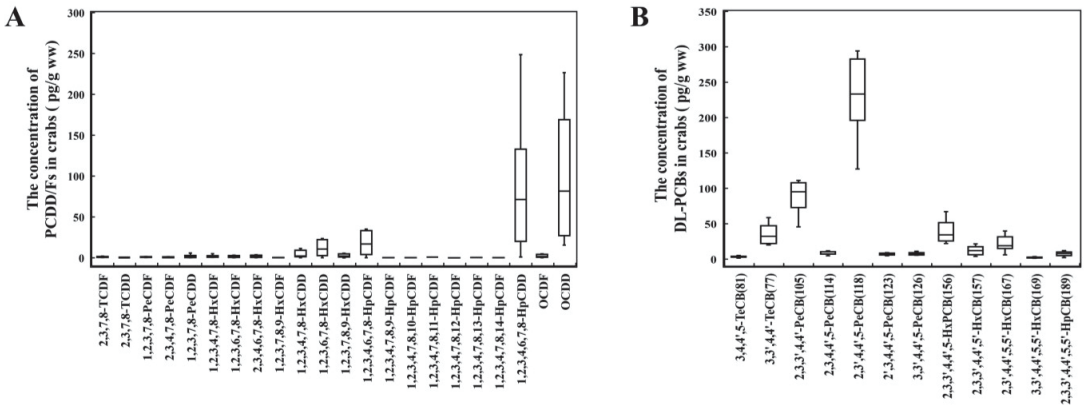
Figure 2. Concentrations of PCDD/Fs (**A**) and DL-PCBs (**B**) in farmed Chinese mitten crabs (*n* = 90).
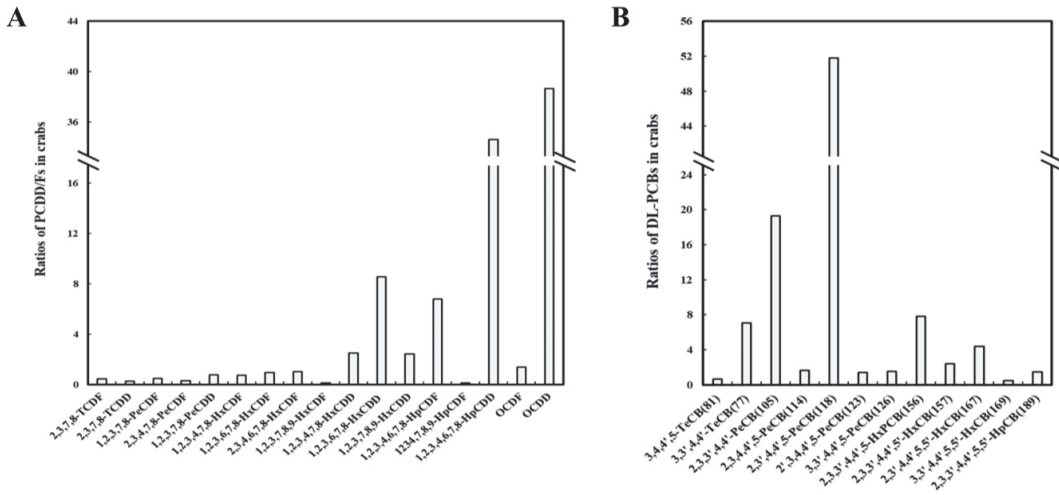
Figure 3. Ratios of PCDD/Fs (**A**) and DL-PCBs (**B**) in farmed Chinese mitten crabs.

The TEQs of the total PCDD/F and DL-PCB levels in the crab samples ranged from 1.20 to 29.04 pg TEQ/g ww, and the mean was 9.37 pg TEQ/g ww. Similarly, the TEQ range for the PCDD/Fs was 0.54–27.86 pg TEQ/g, and the mean was 8.50 pg TEQ/g ww; the TEQ range for the DL-PCBs was 0.60–1.18 pg TEQ/g ww, and the mean was 0.87 pg TEQ/g ww. The TEQs of the PCDD/Fs and DL-PCBs in the crabs from three farms (MH, RJ, and NXC) were higher than the standard limits (3.5 pg/g for PCDD/Fs and 6.5 pg/g for the total PCDD/Fs and dl-PCBs) [27]. The TEQs of the PCDD/Fs and DL-PCBs in the farm crab samples are shown in Supplementary Table S7.

3.2. The Concentration of PCDD/Fs and DL-PCBs in Market Crabs

The PCDD/F and DL-PCB contents in 37 crab samples from fresh markets in Shanghai were determined, and the specific results are shown in Table S8. The concentration range and average level of PCDD/Fs in these crab samples were 223.62–1934.88 and 24.27 ± 53.05 pg/g ww, respectively. The concentration range and mean values of the DL-PCBs were 228.85–2163.32 pg/g ww and 628.19 ± 375.48 pg/g ww, respectively. OCDD (375.48 pg/g ww) and 1,2,3,4,6,7,8-HpCDD (3.98 pg/g ww) were the most abun-

dant PCDD/Fs. For the DL-PCBs, 2,3′,4,4′,5-PeCB (321.68 pg/g ww) and 2,3,3′,4,4′-PeCB (115.10 pg/g ww) exhibited the highest abundance (Figure 4).
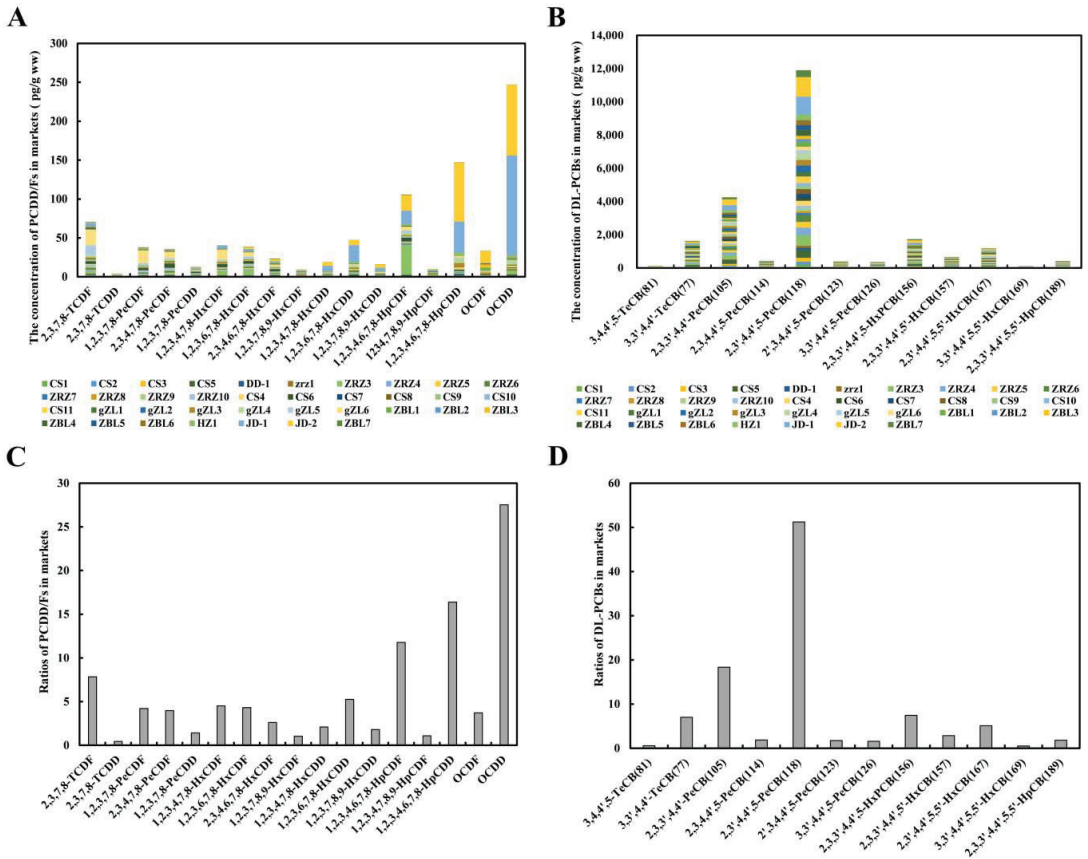
Figure 4. Concentrations of PCDD/F (**A**) and DL-PCB (**B**) in Chinese mitten crabs from markets (*n* = 555). PCDD/F (**C**) and DL-PCB (**D**) ratios in Chinese mitten crabs from markets.

The PCDD/F and DL-PCB detection rates in the market crab samples were 100%, and in some samples, the TEQ ranges of the PCDD/Fs and DL-PCBs exceeded the relevant limits [27]. The total PCDD/F and DL-PCB TEQ levels in the market crab samples ranged from 0.33 to 10.80 pg TEQ/g, and the mean was 2.67 pg TEQ/g. The total PCDD/F TEQs ranged from 0.11 to 8.80 pg TEQ/g, and the mean was 1.56 pg TEQ/g. The total DL-PCB TEQs ranged from 0.23 to 2.35 pg TEQ/g, and the mean was 1.11 pg TEQ/g. TEQs of the total PCDD/F and DL-PCB contents in 8% of the samples were higher than the relevant limit (6.5 pg TEQ/g for the total PCDD/Fs and DL-PCBs) [27]. The TEQ of the PCDD/Fs in 14% of the samples was higher than the relevant limit (3.5 pg TEQ/g for PCDD/Fs) [27]. The TEQs of the total PCDD/Fs and DL-PCBs found in market crabs are shown in Table S6. TEFs were used to determine the TEQ distribution of individual congeners. 1,2,3,7,8-PeCDD; 2,3,4,7,8-PeCDF; and 2,3,7,8-TCDF contributed 22%, 19%, and 12%, respectively, and the TEQs of the remaining congeners accounted for less than 10%. Among the DL-PCBs, 3,3′,4,4′,5-PeCB (89%) are the main contributors to the TEQs of the DL-PCBs, followed by 3,3′,4,4′,5,5′-HxCB (8%) and 2,3′,4,4′,5-PeCB (0.8%). The toxicity equivalent factors of the 17 PCDD/Fs and 12 DL-PCBs were determined according to the WHO-TEF standards (Table S2) that were revised by WHO in 2005.

3.3. The Concentration of PCDD/Fs and DL-PCBs in Potential Sources

To determine the major sources of PCDD/Fs and DL-PCBs in crabs, we further examined the concentrations of PCDD/Fs and DL-PCBs in each stage of crab farming. For specific results, see Table S5. The potential sources of dioxins consist of feed, including fishmeal, soybean meal, rapeseed meal, cottonseed meal, soybean phospholipid oil, dihydrogen calcium phosphate, and other chemicals to suit the crab's development requirements. In addition, other sources included water and plants from farmed crab ponds, plants on the shore of farmed crab ponds, and sediments at the bottom of farmed crab ponds.

Some substances in aquaculture water, such as impurities, food residues, and feces, eventually turn into sediments that may be more susceptible to contamination. The experimental results showed that the concentrations of PCDD/Fs and DL-PCBs in sediment were the highest on the farms, with concentrations ranging from 109.02 to 35,301.67 pg/g dw. The mean of the PCDD/F and DL-PCB concentrations in the sediment samples was 13,050.71 ± 14,855.84 pg/g dw. The concentration of the PCDD/Fs and DL-PCBs in aquaculture water ranged from 8.30 to 574.71 pg/L, with a mean concentration of 211.27 ± 217.07 pg/L. The concentrations of the PCDD/Fs and DL-PCBs in aquatic plants ranged from 3.28 to 419.12 pg/g ww, with a mean concentration of 139.83 ± 159.68 pg/g ww. The concentrations of the PCDD/Fs and DL-PCBs in shore plants ranged from 2.17 to 194.30 pg/g ww, with a mean concentration of 52.48 ± 76.80 pg/g ww. The concentration of the PCDD/Fs and DL-PCBs in feed ranged from 7.26 to 68.37 pg/g dw, with a mean concentration of 40.22 ± 23.19 pg/g dw.

The TEQs of the potential sources of PCDD/Fs and DL-PCBs are shown in Table S7. On the farms, sediments showed the highest TEQs, ranging from 0.48 to 31.51 pg TEQ/g dw. The total TEQs of the PCDD/Fs and DL-PCBs in aquaculture water, aquatic plants, and shore plants ranged from 0.23 to 1.06 pg TEQ/L, from 0.05 to 0.83 pg TEQ/g ww, and from 0.06 to 0.34 pg TEQ/g ww, respectively. The TEQs of the PCDD/Fs and DL-PCBs in feed ranged from 0.22 to 0.60 pg TEQ/g dw, in compliance with EU limit regulation EU NO 277/2012 (feed) (the maximum residue limit was 1.75 pg TEQ/g for PCDD/Fs and 5.5 pg TEQ/g for PCDD/Fs + DL-PCBs). The total TEQs of the PCDD/Fs and DL-PCBs from the three farms in Qingpu district (MH, RJ, and NXC) were greater than those found in the three farms in Chongming district (YF, HK, and ZH) (Figure 5).
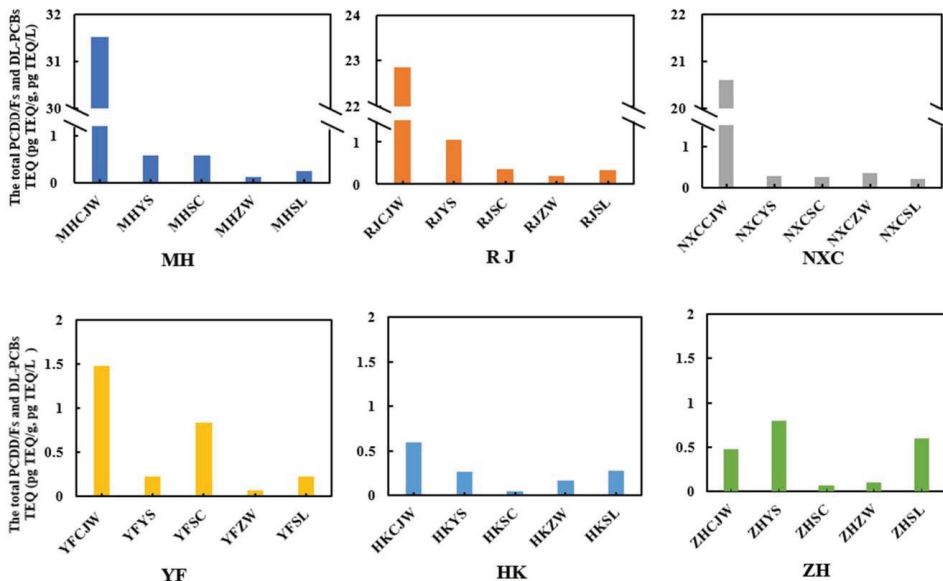
Figure 5. The total PCDD/F and DL-PCB TEQs in the potential sources.

The congeners of PCDD/Fs and DL-PCBs in the potential sources and in the crabs were similarly distributed. OCDD and 1,2,3,4,6,7,8-HpCDD were dominant in aquaculture water, aquatic plants, and, especially, in sediments. 2,3′,4,4′,5-PeCB was abundant in sediment, aquaculture water, and feed. Different congeners contribute differently to the TEQ in different samples. For PCDD/Fs, 1,2,3,4,6,7,8-HpCDD had the highest TEQ in sediment, aquatic plants, and aquaculture water, with contribution rates of 39%, 32%, and 21%, respectively. In addition, in feed, 1,2,3,7,8-PeCDD contributed to 40%. For the DL-PCBs, 3,3′,4,4′,5-PeCB made the most dominant contributions in almost all of the samples, followed by 3,3′,4,4′,5,5′-HxCB, which is consistent with our conclusion that 3,3′,4,4′,5-PeCB (90%) and 3,3′,4,4′,5,5′-HxCB (9%) predominate in crab samples.

3.4. Bioaccumulation of PCDD/Fs and DL-PCBs in Crabs

Sediments, aquacultural water, aquatic plants, shore plants, and feed can all enter crabs, so pollutants from each aquacultural process can accumulate in crabs, posing a threat to our health. The above results showed that the DL-PCBs to PCDD/Fs concentration ratio in farm crabs was 191.62%. In sediments, aquacultural water, aquatic plants, shore plants, and feed, the DL-PCB to PCDD/F concentration ratios were 0.20%, 2.72%, 2.22%, 13.36%, and 2553.51%, respectively. In contrast, the concentrations of PCDD/Fs were higher in sediments, aquacultural water, aquatic plants, and shore plants than in crabs, while the concentrations of DL-PCBs were lower in sediments, aquacultural water, aquatic plants, and shore plants than in crabs (Figure S1). These results indicate that crabs bioaccumulate DL-PCBs more readily than PCDD/Fs and that raw materials used in feed may be contaminated with DL-PCBs.

To determine the key link responsible for the accumulation of pollutants in crabs, we conducted a correlation analysis of the residual pollutants in crabs and the potential sources, and the correlation coefficient R was used to measure the relationship between the crabs and potential sources. The correlation coefficient between crabs and sediment was 0.89 (R > 0.8), showing a strong correlation, while the correlation coefficient between crabs and aquaculture water was 0.28, showing a weak correlation and suggesting that the accumulation of PCDD/Fs and DL-PCBs in crabs in aquaculture mainly comes from sediments (Figure 6). PCDD/Fs and DL-PCBs can enter crabs through feed, water, aquatic plants, and shore plants; remain in crab tissues through distribution and metabolism; are excreted in feces and urine; and further migrate into sediments, increasing the exposure of crabs to pollutants.
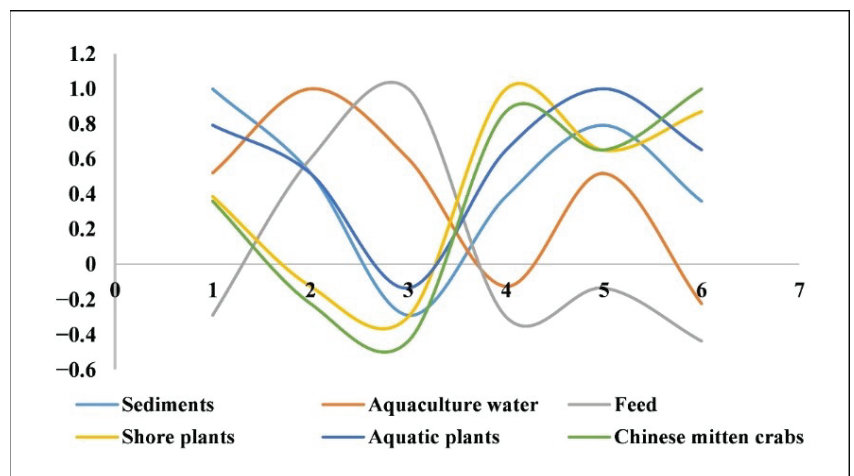
Figure 6. Correlation analysis of the residual pollutants in Chinese mitten crabs and the potential sources.

4. Discussion

On 27 November 2020, the International Agency for Research on Cancer (IARC) updated its latest list of carcinogens, and both 2,3′,4,4′,5-PeCB (118) and 2,3,3′,4,4′-PeCB (105) were classified as class I carcinogens. The findings of the current study revealed that the highest proportions of PCB-118 and PCB-105 were found in farm crabs (51.8% and 19.8%) and in market crabs (51.2% and 18.3%). Compared to PCDD/Fs, DL-PCBs were abundantly produced and used in the past, and they are relatively difficult to degrade under the influence of physical and chemical factors [28]. The most decent explanation for the above statement may be that the presence of residual PCB-118 and PCB-105 in crab may make DL-PCBs more stable. In one study, Grazia Barone et al. [1] found that PCB-118 was dominant in bluefin tuna samples. Wang X. et al. [29] reported that PCB-118 and PCB-105 were predominant in all of the fish samples they studied. Similarly, Danae Costopoulou et al. [30] also found that the main congener for monoorthmic PCBs produced in Greece was PCB-118 followed by PCB-105. These results align with our experiment's key finding, which state that PCB-118 and PCB-105 comprise the dominant concentrations and closely related to their ability to enrich organisms.

OCDD and 1,2,3,4,6,7,8-HpCDD are polychlorinated dibenzo-p-dioxins (PCDDs) as well as the dominant PCDD/F congener [31,32]. Battisti Sabrina et al. [33] found that OCDD was the most abundant PCDD/F congener in dairy products collected in the Latium region of Italy (2011–2017). L. P. Fang et al. [34] found that fish tissues contained a relatively large amount of OCDD, accounting for 54% of the total PCDD/F congeners. Our results showed that OCDD was dominant in both farm crabs (38.7%) and market crabs (12.7%), concordant with the above scholars' conclusions, our results suggest that OCDD has a strong enrichment capacity. Milena Dömötörová et al. [35] observed that 1,2,3,4,6,7,8-HpCDD was the second most abundant congener in most of the soil samples considered in their study. Kim K.S. et al. [36] found that 1,2,3,4,6,7,8-HpCDD was predominant in all of their soil samples. Regarding this substance, Loganathan B.G. et al. [37] observed the same pattern of HpCDD accumulation in sediment and mussel tissues. Our results showed that 1,2,3,4,6,7,8-HpCDD is the second highest PCDD/F congener in crabs (34.6% in farm crabs and 10.0% in market crabs) after OCDD.

We then conducted further research on content and analyzed the sources of PCDD/Fs and DL-PCBs in crabs to search for possible sources. Our results showed that the means of the TEQs of the PCDD/Fs and PCBs in crabs, sediments, aquacultural water, aquatic plants, shore plants, and feed were 9.37 pg TEQ/g, 12.92 pg TEQ/g, 0.53 pg TEQ/L, 0.28 pg TEQ/g, 0.17 pg TEQ/g, and 0.32 pg TEQ/g. We referred to Han Ying's [38] method to evaluate all of the substances that hairy crabs may ingest in a 1-hectare (ha) crab pond. In crab ponds, every hectare produces about 50 kg of Chinese mitten crab, and the edible portion accounts for about 26% of the crabs' weight. As a result, the production of crab meat and roe (crab paste) per hectare of crab pond is about 13 kg/ha, implying that the PCDD/Fs and DL-PCBs TEQ in crab meat and roe (crab paste) per hectare of crab pond is approximately 122 ng TEQ/ha. The recovery rate of hairy crabs was assumed to be 70% per hectare of crab pond, and a TEQ of 52 ng was found in dead crabs. A mean feed dose of 95 kg/ha resulted in a PCDD/Fs and DL-PCBs input of 30 ng TEQ/ha. The coverage rate of aquatic plants and shore plants in crab ponds was about 50% per hectare, or about 0.265 kg; the water (aquacultural water) content at a depth of 0.8 m was about 534 m^3; the sediment weight of the 0.1 m disturbed layer was about 4269 kg. The total TEQ exposure of PCDD/Fs and DL-PCBs was 0.12 ng/ha, 283 ng/ha, and 55,155 ng/ha. We found that the amount of PCDD/Fs and PCBs input into crab ponds is much higher than that output to crabs. The TEQ of the PCDD/Fs and DL-PCB input to crabs in aquacultural water was 1.6 times higher than the TEQ in edible crab parts. Aquatic plants, shore plants, and feed contributed about 0.05% of the total TEQ inputs to crabs. Without considering biological processes, the TEQ contribution from sediment was 195 times that from aquacultural water. Therefore, sediment is considered the major contributor to PCDD/Fs and DL-PCBs in Chinese mitten crabs. All of the external substances added in the cultivation of crab culture can settle into

the sediment, affecting the historical concentration of pollutants in the sediment, increasing the exposure risk of hairy crab to pollutants.

The results showed that the total TEQ of PCDD/Fs and DL-PCBs in Shanghai's Qingpu district, China, were significantly higher than in Shanghai's Chongming district, China (Figure 5). This situation may be closely related to the surrounding industrial environment. The three aquaculture farms in Qingpu district were all raised by the Taipu River. Hong Yao et al. [39] found that a large amount of wastewater containing heavy metals was discharged into the Taihu Basin every year. The Taipu River, an important tributary of the Taihu Basin, is similarly plagued by wastewater contamination, which might be one of the explanations for the elevated levels of dioxins and dioxin-like PCBs in farms in the Qingpu district. To supplement the experimental results, we detected the level of pollutants in the soil around farms in the Qingpu and Chongming districts. The findings revealed that the level of pollutants in the soil near the farms in Qingpu district (4.89 pg TEQ/g dw in MH, 19.07 pg TEQ/g dw in RJ, 3.78 pg TEQ/g dw in NXC) was higher than that near the farms in Chongming district (1.00 pg TEQ/g dw in YF, 0.89 pg TEQ/g dw in HK, 0.86 pg TEQ/g dw in ZH). The pollutants migrated into crab farms over a long period of time, which further indicated that the crab farms in Qingpu district had high levels of pollutants. Detailed results are shown in Supplementary Tables S9 and S10.

Our above investigation on market crab revealed that the average residual value of dioxins and dioxin-like PCBs in crabs was 0.0027 pg TEQ/kg. Based on the average daily consumption of adults (60 kg) and children (13.1 kg) of 3 crabs and 1 crab (at an average weight of 100 g per crab), the TDIs of adults and children would be 0.0135 pg TEQ/g (weight)·d and 0.0206 pg TEQ/g (weight)·d, respectively, lower than the prescribed range, indicating no significant chronic ingestion risk for adults and children (WHO experts determined that the TDI range of total PCDD/Fs and PCBs was 1–4 pg TEQ/kg (weight)·d) [15]. The TDIs for adults and children were 0.054 pg TEQ/g (weight)·d and 0.0824 pg TEQ/g (weight)·d when calculated with the maximum residual value of 0.0108 pg TEQ/kg, respectively, both of which were below the prescribed range, indicating that there was no significant risk of acute ingestion in adults and children. Taking into account the above data analysis and the daily quota determined by the WHO, the consumption of Chinese mitten crabs does not seem to pose a threat to health. However, given the persistence and bioaccumulation of such pollutants, the excessive consumption of aquatic products may increase the burden of dioxin-type pollutants in the body. Therefore, it is recommended that the government increase its detection of pollutants, that individuals eat normal amounts of aquatic products, and that certain restrictions be imposed on the consumption of aquatic products. Although there may be some uncertainties and limitations, the study provides a valuable assessment of the health risks associated with PCDD/Fs and DL-PCBs exposure in Chinese river crabs.

5. Conclusions

The PCDD/F and DL-PCB contents in crabs from the market and from farms in Shanghai were investigated. It was found that crabs bioaccumulate DL-PCBs more readily than PCDD/Fs. As the main source, the total TEQ exposure to PCDD/Fs and DL-PCBs in sediments was 55,155 ng/ha. The PCDD/F and DL-PCB contents in crabs was generally safe, and crabs had a strong enrichment ability for 2,3′,4,4′,5-PeCB (118), 2,3,3′,4,4′-PeCB (105), OCDD, and 1,2,3,4,4,6,7,8-HpCDD. A health and safety assessment based on market crab samples showed no significant chronic or acute ingestion risk for adults and children, suggesting that eating crab several times a year may not cause PCDD/Fs and DL-PCBs to exceed safe limits. Finally, by further studying the PCDD/F and DL-PCB contents in the farming process, the PCDD/Fs and DL-PCBs in crabs mainly come from sediments. Therefore, regular sediment treatment can effectively reduce the exposure of crabs to pollutants.

References

1. Barone, G.; Storelli, A.; Garofalo, R.; Mallamaci, R.; Quaglia, N.C.; Storelli, M.M. Pcbs and Pcdd/Fs in Bluefin Tuna: Occurrence and Dietary Intake. *Int. J. Environ. Res. Public Health* **2018**, *15*, 911. [CrossRef] [PubMed]
2. Franchina, F.A.; Lazzari, E.; Scholl, G.; Focant, J.F. Assessment of a New Gc-Ms/Ms System for the Confirmatory Measurement of Pcdd/Fs and (N)Dl-Pcbs in Food under Eu Regulation. *Foods* **2019**, *8*, 302. [CrossRef] [PubMed]
3. Park, J.W.; Kurosawa, S.; Aizawa, H.; Hamano, H.; Harada, Y.; Asano, S.; Mizushima, Y.; Higaki, M. Dioxin Immunosensor Using Anti-2,3,7,8-Tcdd Antibody Which Was Produced with Mono 6-(2,3,6,7-Tetrachloroxanthene-9-Ylidene) Hexyl Succinate as a Hapten. *Biosens. Bioelectron.* **2006**, *22*, 409–414. [CrossRef] [PubMed]
4. Kumar, N.; Ramirez-Ortiz, D.; Solo-Gabriele, H.M.; Treaster, J.B.; Carrasquillo, O.; Toborek, M.; Deo, S.; Klaus, J.; Bachas, L.G.; Whitall, D.; et al. Environmental PCBs in Guánica Bay, Puerto Rico: Implications for Community Health. *Environ. Sci. Pollut. Res. Int.* **2016**, *23*, 2003–2013. [CrossRef] [PubMed]
5. Wu, W.L.; Deng, X.L.; Zhou, S.J.; Liang, H.; Yang, X.F.; Wen, J.; Li, X.M.; Zhang, C.Z.; Zhang, Y.H.; Zou, F. Levels, Congener Profiles, and Dietary Intake Assessment of Polychlorinated Dibenzo-P-Dioxins/Dibenzofurans and Dioxin-Like Polychlorinated Biphenyls in Beef, Freshwater Fish, and Pork Marketed in Guangdong Province, China. *Sci. Total Environ.* **2018**, *615*, 412–421. [CrossRef] [PubMed]
6. Yang, J.H.; Lee, H.G.; Park, K.Y. Development of Human Dermal Epithelial Cell-Based Bioassay for the Dioxins. *Chemosphere* **2008**, *72*, 1188–1192. [CrossRef]
7. Han, Y.; Liu, W.; Zhu, W.; Rao, K.; Xiao, K.; Gao, L.; Su, G.; Liu, G. Sources of Polychlorinated Dibenzo-P-Dioxins and Dibenzofurans, and Biphenyls in Chinese Mitten Crabs. *Chemosphere* **2018**, *196*, 522–530. [CrossRef]
8. Dibenzo, I.P. Iarc Working Group on the Evaluation of Carcinogenic Risks to Humans: Polychlorinated Dibenzo-Para-Dioxins and Polychlorinated Dibenzofurans. Lyon, France, 4–11 February 1997. *IARC Monogr. Eval. Carcinog. Risks Hum.* **1997**, *69*, 1–631.
9. Gilpin, R.K.; Wagel, D.J.; Solch, J.G. Production, Distribution, and Fate of Polychlorinated Dibenzo-P-Dioxins, Dibenzofurans, and Related Organohalogens in the Environment. *Dioxins Health* **2003**, 55–87. [CrossRef]
10. Addison, R.F.; Ikonomou, M.G.; Fernandez, M.P.; Smith, T.G. Pcdd/F and Pcb Concentrations in Arctic Ringed Seals (Phoca Hispida) Have Not Changed between 1981 and 2000. *Sci. Total Environ.* **2005**, *351–352*, 301–311. [CrossRef]
11. Li, H.W.; Wu, Y.L.; Lee, W.J.; Chang-Chien, G.P. Fate of Polychlorinated Dibenzo-P-Dioxins and Dibenzofurans in a Fly Ash Treatment Plant. *J. Air Waste Manag. Assoc.* **2007**, *57*, 1024–1031. [CrossRef] [PubMed]
12. Gao, L.; Zhang, Q.; Zhang, B.; Liu, W.; Xiao, K. Polychlorinated Dibenzo-P-Dioxins and Dibenzofurans in Water and Six Fish Species from Dongting Lake, China. *Chemosphere* **2014**, *114*, 150–157. [CrossRef] [PubMed]
13. Moon, H.B.; Ok, G. Dietary Intake of Pcdds, Pcdfs and Dioxin-Like Pcbs, Due to the Consumption of Various Marine Organisms from Korea. *Chemosphere* **2006**, *62*, 1142–1152. [CrossRef] [PubMed]

14. Consultation on assessment of the health risk of dioxins; re-evaluation of the tolerable daily intake (TDI): Executive sum-mary. *Food Addit. Contam.* **2000**, *17*, 223–240. [CrossRef] [PubMed]
15. FAO/WHO. Joint FAO/WHO Expert Committee on Food Additives. Fifty-Seventh Meeting, Rome, 5–14 June 2001. Summary and Conclusions. Food and Agriculture Organization of the United Nations and the World Health Organization. 2001. Available online: http://www.who.int/pcs/jecfa/Summaries.htm (accessed on 24 January 2022).
16. Malik, A.; Kim, C.B. Role of Transportome in the Gills of Chinese Mitten Crabs in Response to Salinity Change: A Meta-Analysis of Rna-Seq Datasets. *Biology* **2021**, *10*, 39. [CrossRef]
17. Camacho-Chab, J.C.; Castañeda-Chávez, M.D.R.; Chan-Bacab, M.J.; Aguila-Ramírez, R.N.; Galaviz-Villa, I.; Bartolo-Pérez, P.; Lango-Reynoso, F.; Tabasco-Novelo, C.; Gaylarde, C.; Ortega-Morales, B.O. Biosorption of Cadmium by Non-Toxic Extracellular Polymeric Substances (Eps) Synthesized by Bacteria from Marine Intertidal Biofilms. *Int. J. Environ. Res. Public Health* **2018**, *15*, 314. [CrossRef]
18. Kim, M.; Kim, S.; Yun, S.J.; Kwon, J.W.; Son, S.W. Evaluation of Pcdd/Fs Characterization in Animal Feed and Feed Additives. *Chemosphere* **2007**, *69*, 381–386. [CrossRef]
19. Hayward, D.G.; Bolger, P.M. Tetrachlorodibenzo-P-Dioxin in Baby Food Made from Chicken Produced before and after the Termination of Ball Clay Use in Chicken Feed in the United States. *Environ. Res.* **2005**, *99*, 307–313. [CrossRef]
20. Guruge, K.S.; Seike, N.; Yamanaka, N.; Miyazaki, S. Polychlorinated Dibenzo-P-Dioxins, -Dibenzofurans, and Biphenyls in Domestic Animal Food Stuff and Their Fat. *Chemosphere* **2005**, *58*, 883–889. [CrossRef]
21. Mikolajczyk, S.; Warenik-Bany, M.; Pajurek, M. Dioxins and Pcbs in Freshwater Fish and Sediments from Polish Lakes. *Food Addit. Contam. Part B Surveill.* **2022**, *15*, 159–167. [CrossRef]
22. Piskorska-Pliszczynska, J.; Mikolajczyk, S.; Warenik-Bany, M.; Maszewski, S.; Strucinski, P. Soil as a Source of Dioxin Contamination in Eggs from Free-Range Hens on a Polish Farm. *Sci. Total Environ.* **2014**, *466–467*, 447–454. [CrossRef] [PubMed]
23. Tan, J.; Lu, X.; Fu, L.; Yang, G.; Chen, J. Quantification of Cl-Pahs and Their Parent Compounds in Fish by Improved Ase Method and Stable Isotope Dilution Gc-Ms. *Ecotoxicol. Environ. Saf.* **2019**, *186*, 109775. [CrossRef] [PubMed]
24. Environmental Mutagenesis and Genomics Society 50th Annual Meeting. *Environ. Mol. Mutagen.* **2019**, *60* (Suppl. 1), 1–91. [CrossRef]
25. Liao, Z.; Biao, L.M.; Qiang, L.J.; Zhen, P.; Yang, C. Advances in the Trace Determination of Dioxins in Foods. *Food Res. Dev.* **2011**, *32*, 231–235.
26. *GB 5009.205-2013*; Determination of Toxic Equivalencies of Dioxin and Dioxin-Like Compound in Foods. Domestic—National Standard—State Administration for Market Regulation CN-GB, National Health and Family Planning Commission of the People's Republic of China: Beijing, China, 2013.
27. Hoogenboom, R.L.; Kotterman, M.J.; Nieuwenhuizen, M.H.; van der Lee, M.K.; Mennes, W.C.; Jeurissen, S.M.; van Leeuwen, S.P. Dioxins, Pcbs and Heavy Metals in Chinese Mitten Crabs from Dutch Rivers and Lakes. *Chemosphere* **2015**, *123*, 1–8. [CrossRef]
28. Gresner, P.; Zielinski, M.; Ligocka, D.; Polanska, K.; Wasowicz, W.; Gromadzinska, J. Environmental Exposure to Persistent Organic Pollutants Measured in Breast Milk of Lactating Women from an Urban Area in Central Poland. *Environ. Sci. Pollut. Res. Int.* **2021**, *28*, 4549–4557. [CrossRef]
29. Wang, X.; Zhang, H.; Zhang, L.; Zhong, K.; Shang, X.; Zhao, Y.; Tong, Z.; Yu, X.; Li, J.; Wu, Y. Assessment on Dioxin-Like Compounds Intake from Various Marine Fish from Zhoushan Fishery, China. *Chemosphere* **2015**, *118*, 163–169. [CrossRef]
30. Costopoulou, D.; Vassiliadou, I.; Leondiadis, L. Pcdds, Pcdfs and Pcbs in Farmed Fish Produced in Greece: Levels and Human Population Exposure Assessment. *Chemosphere* **2016**, *146*, 511–518. [CrossRef]
31. Bulle, C.; Bertrand, F.; Samson, R.; Deschenes, L. Sensitivity Study of an Ocdd Environmental Fate Screening Model in Soils in the Presence of Pcp Wood-Preserving Oil. *Chemosphere* **2008**, *73*, S149–S157. [CrossRef]
32. Correa, O.; Rifai, H.; Raun, L.; Suarez, M.; Koenig, L. Concentrations and Vapor–Particle Partitioning of Polychlorinated Dibenzo-P-Dioxins and Dibenzofurans in Ambient Air of Houston, Tx. *Atmospheric. Environ.* **2004**, *38*, 6687–6699. [CrossRef]
33. Battisti, S.; Scaramozzino, P.; Boselli, C.; Busico, F.; Berretta, S.; Sala, M.; Neri, B. A Retrospective Study on Dioxins and Dioxin-Like Polychlorinated Biphenyls in Milk and Dairy Products from the Latium Region (Italy) over a 7-Year Study Period (2011–2017). *Environ. Sci. Pollut. Res. Int.* **2022**, *Online ahead of print*. [CrossRef]
34. Fang, L.P.; Zheng, M.H.; Zhang, B.; Liu, W.B.; Gao, L.R. Profiles of Polychlorinated Dibenzo-P-Dioxins and Dibenzofurans in Fish Livers and Gills from Dongting Lake, China. *Bull. Environ. Contam. Toxicol.* **2007**, *79*, 45–48. [CrossRef]
35. Domotorova, M.; Sejakova, Z.S.; Kocan, A.; Conka, K.; Chovancova, J.; Fabisikova, A. Pcdds, Pcdfs, Dioxin-Like Pcbs and Indicator Pcbs in Soil from Five Selected Areas in Slovakia. *Chemosphere* **2012**, *89*, 480–485. [CrossRef]
36. Kim, K.S.; Lee, S.C.; Kim, K.H.; Shim, W.J.; Hong, S.H.; Choi, K.H.; Yoon, J.H.; Kim, J.G. Survey on Organochlorine Pesticides, Pcdd/Fs, Dioxin-Like Pcbs and Hcb in Sediments from the Han River, Korea. *Chemosphere* **2009**, *75*, 580–587. [CrossRef]
37. Loganathan, B.G.; Kumar, K.S.; Masunaga, S.; Sajwan, K.S. Polychlorinated Dibenzo-P-Dioxins, Dibenzofurans, and Dioxin-Like Polychlorinated Biphenyls in Sediment and Mussel Samples from Kentucky Lake, USA. *Arch. Environ. Contam. Toxicol.* **2008**, *54*, 20–30. [CrossRef]
38. Han, Y.; Liu, W.B.; Xing, Y.; Gao, L.R.; Gui-Jin, S.U. Study on Exposure Levels of Dioxin-Like Persistent Organic Pollutants in Chinese Hairy Crabs. *J. Food Saf. Qual.* **2018**, *9*, 4302–4307.
39. Yao, H.; Zhuang, W.; Qian, Y.; Xia, B.; Yang, Y.; Qian, X. Estimating and Predicting Metal Concentration Using Online Turbidity Values and Water Quality Models in Two Rivers of the Taihu Basin, Eastern China. *PLoS ONE* **2016**, *11*, e0152491. [CrossRef]

Article

Residues of Pesticides and Heavy Metals in Polish Varietal Honey

Monika Kędzierska-Matysek [1], Anna Teter [1,*], Piotr Skałecki [1], Barbara Topyła [1], Piotr Domaradzki [1], Ewa Poleszak [2] and Mariusz Florek [1]

[1] Department of Quality Assessment and Processing of Animal Products, University of Life Sciences in Lublin, Akademicka 13, 20-950 Lublin, Poland

[2] Chair and Department of Applied and Social Pharmacy, Laboratory of Preclinical Testing, Medical University of Lublin, Chodźki Street 1, 20-093 Lublin, Poland

* Correspondence: anna.teter@up.lublin.pl

Abstract: The levels of chemical pollutants were determined in 30 samples of varietal honey from southeastern Poland, including 223 pesticides (insecticides, herbicides, fungicides, acaricides, plant growth regulators, and veterinary drugs) and 5 heavy metals (Pb, Cd, Hg, Cu, and Zn). In 10% of the samples, no pesticide residues were found. The most frequently identified pesticides were thiacloprid (90% of the samples, max 0.337 mg/kg), acetamiprid (86.6%, max 0.061 mg/kg), carbendazim (60%, max 0.049 mg/kg), DMF (56.6%, max 0.038 mg/kg), total amitraz (53.3%, max 0.075 mg/kg), thiamethoxam (26.6%, max 0.004 mg/kg), thiacloprid-amide (13.3%, max 0.012 mg/kg), dimethoate (10%, max 0.003 mg/kg), azoxystrobin (10%, max 0.002 mg/kg), tebuconazole (6.66%, max 0.002 mg/kg), and boscalid (3.33%, max 0.001 mg/kg). The acceptable limits for the compounds were not exceeded in any sample. The Pb content ranged between 0.044 and 0.081 mg/kg. The concentration of Hg and Cd did not exceed 5.0 µg/kg and 0.02 mg/kg, respectively. The honey variety significantly ($p < 0.01$) influenced the content of Cu, which ranged from 0.504 (rapeseed honey) to 1.201 mg/kg (buckwheat). A similar tendency ($p > 0.05$) was observed for the Zn content, which ranged from 0.657 mg/kg (linden) to 2.694 mg/kg (buckwheat). Honey produced in southeastern Poland was shown to be safe for human consumption.

Keywords: honey; pesticide residues; QuEchERS; fungicide; insecticide; veterinary drugs

1. Introduction

Honey, due to its high nutritional value and numerous health-promoting properties, is a valuable component of the daily diet. The chemical composition of honey is varied and depends mainly on the region where it is produced, the soil conditions, and the water and air quality, which affect the quality of the food sources for bees, including the presence and level of chemical pollutants [1]. The health risks associated with honey consumption stem from the presence of pesticide residues (including active substances and their metabolites), antibacterial substances (including antibiotics), and heavy metals. Another source of risk in honey is microbial contaminants [2]. These substances come mainly from the environment, whose cleanliness depends largely on human activity. Antibacterial substances are used to prevent and fight diseases in broods and bees, and pesticides are meant to protect crop plants against fungi (fungicides), insects (insecticides), and weeds (herbicides). The use of pesticides in agriculture is essential to obtaining high yields, but results in the contamination of the soil, water, air, and also the flowers from which bees collect nectar and pollen, the natural components of honey [3]. These agents negatively affect both bees and people, causing changes in the endocrine and nervous systems [4]. Detailed information on the potential sources of the contamination of honeys (e.g., heavy metals, airborne particulate matter, and agrochemical pesticides) was provided by Cunningham et al. [5].

Therefore, the monitoring of their levels in food products is crucial for ensuring consumer health safety.

Colony collapse disorder (CCD) threatens the health of beehives worldwide, but scientists still struggle to identify the specific causes. In view of the important ecological and economic value of bees, there is a need to monitor and maintain healthy bee stocks. In the framework of the Farm to Fork Strategy, one of the main priorities of the European Commission is the 50% reduction of the overall use of (and risk from) chemical pesticides by 2030, especially for the most hazardous ones. In addition, the EU Pollinators Initiative objectives state that by 2030, the scientific knowledge about the magnitude, causes, and consequences of the insect pollinator decline will have improved, that the main known causes of this decline will be addressed and managed, and that the societal awareness and collaboration amongst stakeholders will have strengthened [6]. In response to a mandate from the European Parliament's Committee for the Environment, Public Health, and Food Safety (ENVI), The European Food Safety Authority (EFSA) devised an integrated framework for the environmental risk assessment (ERA) of multiple stressors in honey bees (MUST-B). These stressors range from chemicals such as plant protection products, other types of chemicals (e.g., biocides), biological agents (e.g., *Varroa*, *Nosema*), and other elements (e.g., food availability, weather conditions, and beekeeping management practices) in managed honey bees [7].

Among the compounds recognized as toxic for pollinating insects, an important group is the neonicotinoid insecticides, widely used in agriculture and with a share of about one third of the global insecticide market. Neonicotinoids act on nicotinic acetylcholine receptors (nAChRs) in the central nervous system of the honeybee and other pollinating insects, which impairs their learning and memory functions, causing them to not look for food [8] and thus leading to their elimination [9]. The most commonly used insecticides are imidacloprid and acetamiprid [10].

The Agency for Toxic Substances and Disease Registry [11] lists polychlorinated biphenyls, dimethoate, and metals such as lead, mercury, cadmium, zinc, and copper as harmful substances. Fakhri et al. [12], based on a meta-analysis of the results of 45 studies, estimated the overall rank order of nine potentially toxic elements (PTE) according to their concentrations in honey (Fe > Mn > Pb > Cr > Cu > Ni > Cd > As > Hg) as well as their rank according to their hazard quotient (HQ: Pb > Cd > Mn > Fe >Ni > As > Cu > Hg > Cr). Lead (Pb) and cadmium (Cd), due to their carcinogenic and cytotoxic properties, are regarded as the most toxic heavy metals. Lead, mainly from car exhaust, is not transported by plants, but can pollute the air and subsequently nectar and honeydew. Cadmium from the metallurgical industry and combustion plants is transferred from the soil to plants; thus, it can contaminate nectar and honeydew [13]. The predominant source of lead, cadmium, mercury, and arsenic is industrial contamination, i.e., exhaust gases and fumes, as well as pesticides and synthetic fertilizers. Oroian et al. [14] showed that information on the level of heavy metals in honey can be used to determine its botanical origin, with an about 81% accuracy, and its geographic origin, but with only a 21% accuracy.

One of the effects of human activity on the environment may be the presence of unacceptable chemical residues and drugs in the honey made by bees. The presence of these compounds is a significant challenge in monitoring the quality of honey. Taking into account human exposure to the effects of active substances and their potential cumulative and synergistic effects, maximum residue levels (MRL) have been established. Foodstuffs, including honey, are safe for human health or life if their content of these compounds does not exceed the acceptable limits [15]. The maximum residue levels of pesticides in food are regulated by Regulation (EC) No 396/2005 of the European Parliament and of the Council [16], and the levels of veterinary agents by Regulation (EC) No 37/2010 [17]. In Poland, honey is monitored in accordance with the Regulation of the Minister of Agriculture and Rural Development [18]. Specifically, it is tested for the presence of antibacterial substances, including sulphonamides and quinolones; medicinal products (carbamates and pyrethroids); chemical pollutants such as organochlorine pesticides, polychlorinated

biphenyls (PCB), and organophosphate pesticides; and toxic elements. Changing hazards, however, make it necessary to study new unsafe chemical compounds as they appear.

Testing for the presence of chemical contaminants in honey can provide important data on the presence of these contaminants in the environment. The honey bee (*Apis mellifera* L.) and its products are currently also used as bioindicators of environmental contamination. These insects fly around nectar plants growing up to 4 km away from the hive, but they can cover distances even up to 12 km, accumulating pollutants present in the air, soil, and water [19]. For this reason, honey can serve as an indicator material for evaluating the contamination of the environment from which bees have collected nectar for making honey.

The aim of the study was to assess the safety of honey from southeastern Poland based on the levels of residues of pesticides, including organochlorine and organophosphate insecticides, herbicides, and fungicides; plant growth regulators; acaricides; and others, as well as the content of copper and zinc and the presence of these toxic heavy metals: lead, cadmium, and mercury.

2. Materials and Methods

2.1. Material

The study was conducted on 30 samples of honey produced in 2019 from nectar and honeydew sources located in the Lublin region (southeastern Poland). The material comprised 10 samples of multifloral honey (MF), 6 samples of linden honey (LI), 5 samples of rapeseed honey (RS), 5 samples of buckwheat honey (BW), and 4 samples of honeydew honey (HD). Honey samples represented the locally produced honey from apiaries located in 8 districts from different parts of the Lubelskie voivodship: northern (Bialski district (BW $n = 2$, LI $n = 1$, RS $n = 1$, MF $n = 1$)), southern (Zamojski (MF $n = 2$, HD $n = 1$) and Biłgoraj (HD $n = 1$, LI $n = 1$, BW $n = 2$) districts), eastern (Włodawa (MF $n = 2$, LI $n = 2$, HD $n = 1$) and Chełmski (MF $n = 2$, RS $n = 1$) districts), western (Puławy (LI $n = 2$, HD $n = 1$) and Opole (MF $n = 2$, RS $n = 1$, BW $n = 1$) districts), and central (Lubelski district RS $n = 2$, MF $n = 1$). The apiaries were located in agricultural farmlands without concentrations of industry. The honey was purchased directly from beekeepers just after harvesting (from May to August) and stored in glass jars at 20 °C (± 2 °C) out of direct sunlight.

2.2. Determination of Pesticide Residues

Pesticide residues in the honey were determined by the QuEChERS (quick, easy, cheap, effective, rugged, and safe) method using chromatographs coupled with tandem mass spectrometers (LC-MS/MS and GC-MS/MS) [20]. The honey was tested for the presence of 223 substances: 93 insecticides, 57 herbicides, 57 fungicides, 9 acaricides, 4 veterinary drugs, and 3 plant growth regulators (a detailed list of the compounds analysed is presented in Table 1).

Table 1. List of analysed compounds.

Category of Use	Compound *
Herbicides	6-chloro-4-hydroxy-3-phenyl pyridazine (metabolite of Pyridate), 6-hydroxy bentazone (metabolite of bentazone), Acetochlor, Amidosulfuron, Asulam, Bentazone, Bifenox, Quinochlamine, Chizalofop-P-ethyl, Chizalofop-P-tefuryl, Chlomazone, Chlorosulfuron, Chlortoluron, Chloridazon, Cycloxydim, Desmedipham, Diflufenican, Dimethachlor, Etofumesate, Fenmedipham, Phenoxaprop-P-ethyl, Flazasulfuron, Florasulam, Fluazifop-P-butyl, Flufenacet, Flurochloridone, Foramsulfuron, Isoproturon, Iodosulfuron-methyl-sodium, Carbetamide, Carfentrazone-ethyl, Kletodim, Lenacyl, Linuron, Metamitron, Metazachlor, Metolachlor-S, Metribuzin, Metsulfuron-methyl, Mesosulfuron-methyl, Mesotrione, Napropamide, Nicosulfuron, Pendimethalin, Pethoxamide, Propachizafop, Propoxycarbazone sodium, Propyzamide, Prosulfocarb, Rimsulfuron, Sulfosulfuron, Sulcotrione, Tembotrione, Tepraloxydim, Terbutylazine, Thifensulfuron-methyl, Tralkoxydim

Table 1. *Cont.*

Category of Use	Compound *
Insecticides	2,4′-DDT, 4,4′-DDD, 4,4′-DDE, 4,4′-DDT, 4,4-Methoxychlor, Acetamiprid, Aldrin, alpha-Cypermethrin, alpha-Endosulfan, alpha-HCH, azinphos-ethyl, azinphos-methyl, beta-Cyfluthrin, beta-Endosulfan, beta-HCH, Bifenthrin, Chlorantraniliprole, Chlorfenvinphos, Chlorpyriphos-methyl, Chlorpyriphos, cis-Chlordane, cis-Heptachlor epoxide, cis-Permethrin, Deltamethrin, Diazinon, Dieldrin, Diflubenzuron, Dimethoate, Endrin, Esfenvalerate, Etofenprox, Etoprophos, Fenitrothion, Fention, Fention-sulfone (metabolite of fenthion), Fention-sulfoxide (metabolite of fenthion), Fipronil, Fipronil-desulfinyl (metabolite of fipronil), Fipronil-carboxamide (metabolite of fipronil), Fipronil-sulfide (metabolite of fipronil), Fipronil-sulfone (fipronil metabolite), Flonicamid, Phoxim, Phosalon, Fosmet, HCB, Heptachlor, Heptenofos, Imidacloprid, Imidacloprid-olefin (imidacloprid metabolite), Imidacloprid-urea derivative (imidacloprid metabolite), Indoxacarb, Clothianidin, Lambda-Cyhalothrin, Lindane (gamma-HCH), Malathion, Methiocarb sulphone (methiocarb metabolite), Methiocarb sulfoxide (methiocarb metabolite), Methiocarb, Methoxyfenozide, Methidathion, MITC (Methyl isothiocyanate) (metabolite of Metam and Dazomet), Nitenpyram, Oxychlordane, Parathion ethyl, Parathion methyl, Pyrimiphos ethyl, Pyrimiphos methyl, Pyrimicarb, Pyrimicarb-desmethyl (metabolite of Pyrimicarb), Pyriproxyfen, Profenofos, Resmethrin, Endosulfan sulphate (metabolite of fipronil), Spirodiclofen, Spirotetramat, Spirotetramat-enol (spirotetramat metabolite), Spirotetramat-enol glucoside (spirotetramat metabolite), Spirotetramat-keto hydroxy (spirotetramat metabolite) tau-Fluvalinate, Tebufenozide, Teflubenzuron, Tefluthrin, Tetramethrin, Thiacloprid, Thiacloprid-amide (metabolite of thiacloprid), Thiamethoxam, trans-Chlordane, trans-Heptachlor epoxide, trans-Permethrin, Triazinphos, zeta-Cypermethrin
Fungicides	Azoxystrobin, Bixafen, Boscalid, Bupirimate, Quinoxyfen, Chlorothalonil, Chymexazole, Cyflufenamide, Cyazofamid, Cymoxanil, Cyprodinil, Cyproconazole, Difenoconazole, Dimethomorph, Dimoxystrobin, Epoxiconazole, Fenbuconazole, Fenhexamid, Fenpropidin, Fenpropimorph, Fluchinkonazole, Fludioxonil, Flusilazole, Flutriafol, Imazalil, Ipconazole, Iprodione, Isopyrazam, Carbendazim, Carboxin, Kresoxim-methyl, Mandipropamid, Mepanipyrm, Metalaxyl-M (Metalaxyl), Metconazole, Metrafenone, Myclobutanil, Pencycuron, Picoxystrobin, Pyrimethanil, Proquinazid, Prochloraz, Propamocarb, Propiconazole, Prothioconazole-desthio (a metabolite of prothioconazole), Pyraclostrobin, Pyrazophos, Silthiopham, Spiroxamine, Tebuconazole, Tetraconazole, Thiophanate-methyl, Triadimefon, Triadimenol, Trifloxystrobin, Triticonazole, Vinclozolin
Acaricides	Bifenazate, Bromopropylate, Etoxazole, Fenazaquin, Fenpyroximate, Hexithiazox, Clofentezine, Propargit, Tebufenpyrad
Veterinary drugs	Cymiazole, DMF (2,4-dimethylphenylformamide) (amitraz metabolite), DMPF (*N*-(2,4-dimethylphenyl)-*N*′-methylformamidine) (amitraz metabolite), Coumaphos
Plant growth regulators	Chlorpropham, IBA (Indolylbutyric acid), NAD (1-Naphthylacetamide)

* The limits of quantification (LOQ) of the substances are given in Supplementary Table S1.

2.2.1. LC-MS/MS

The Agilent series 1260 HPLC system was used for the analyses. The substances were separated on a Luna 3 μm Phenyl-Hexyl 150 mm × 2.0 mm column (Phenomenex, Torrance, NJ, USA) using water with 5 mM ammonium formate and acetonitrile as the mobile phase. The flow rate was 400 μL/min and the column was thermostated at 50 °C. Gradient elution was used. The injection volume was 2 μL, and the total LC analysis time was 40 min. Spectrometric analysis was performed using the AB Sciex QTRAP® 6500 LC-MS/MS system (Framingham, MA, USA) with the Turbo Spray ion drive with positive ionization and positive and negative ionization. The spray voltage was set to 5000 V and −4500 V for positive and negative ionization, respectively. The source temperature was set to 550 °C. Nitrogen was used as the curtain gas (20 psi), collision gas (medium), and ion source gases, nebulizer gas (50 psi) and heating gas (55 psi). Analyst 1.6.2 software (AB Sciex, Framingham, MA, USA) was used to control the LC-MS/MS system and to archive the data.

2.2.2. GC-MS/MS

A GC-MS/MS system with an Agilent 7890A+ gas chromatograph (Palo Alto, CA, USA), 7693B autosampler, split/splitless injector, and 7000B tandem mass spectrometry detector with an electron ionization source was used for the analysis. Chromatographic separation was carried out on an HP-5 MS UI capillary column (30 m × 0.25 mm ID, 0.25 μm, Agilent Technologies, Palo Alto, CA, USA) using helium with 99.9999% purity as the carrier gas (constant flow 0.9 mL/min). The injection volume was 1 μL. The following furnace temperature program was used: initial temperature 80 °C held for 1 min, increased by 40 °C/min to 200 °C, 2.3 °C/min to 210 °C (held for 5 min), and increased by 10 °C/min

to 320 °C. The analysis time was 38 min. The remaining conditions were as follows: inlet temperature was 280 °C, transfer line temperature was 295 °C, source temperature was 300 °C, MS1 and MS2 quadrupole temperatures were 150 °C, collision gas flow rate (N_2) was 1.5 mL/min, and quenching gas flow rate (He) was 2.25 mL/min. Mass Hunter B.07.01 software was used to control the GC-MS/MS system and to archive the data.

2.3. Determination of Heavy Metals (Pb, Cd, Hg, Cu, and Zn)

The levels of Cd and Pb in the digest solution of honey were determined according to Kędzierska-Matysek et al. [21] by inductively coupled plasma mass spectrometry (Varian MS-820ICP Mass Spectrometer). The gas used to create the plasma was argon (Messer) with 99.999% purity. No reaction chamber (CRI) was used in the analysis. The following settings were used: plasma flow at 16 dm^3/min, nebulizer flow at 0.98 dm^3/min, RF power of 1.38 kW, and sampling depth of 6.5 mm. The following isotopes of the elements were used: ^{114}Cd, ^{206}Pb, ^{207}Pb, and ^{208}Pb.

Levels of Cu and Zn were analysed with a Varian SpectrAA 240 FS atomic absorption flame spectrometer (Fast Sequential Atomic Absorption Spectrometer, Varian Australia Pty Ltd., Mulgrave, Australia). The following settings were used for Cu: absorption—324.8 nm, slit width—0.5 nm, lamp current—4 mA. The corresponding settings for Zn were 213.9 nm, 1.0 nm, and 5 mA. The atomizer was a slit burner 100 mm in length operating on a stoichiometric acetylene/air gas mixture. During the analysis of Pb, Cd, Cu, and Zn, quality control was carried out by measuring blank samples and the certified reference material NCS ZC 73014 Tea. The results were expressed as mg/kg fresh weight.

Mercury content was determined using an AMA 254 atomic absorption spectrometer. The analysis was performed without mineralization, which limited the risk of contamination of the sample. Before each measurement, the apparatus was cleaned with air and deionized water.

2.4. Data Analysis

All statistical analyses were performed using Statistica ver. 13 (TIBCO Software Inc., Palo Alto, CA, USA). The parametric and nonparametric descriptive statistics are presented in the tables and figures. The influence of honey variety on concentration of metals was verified by the Kruskal–Wallis test (comparison of multiple independent groups). Statistical differences between means at confidence levels of 95% and 99% ($p < 0.05$ and $p < 0.01$, respectively) were considered significant.

3. Results and Discussion

3.1. Pesticide Residues

Among the 223 pesticides analysed in the honey samples (Table 1), 11 substances were identified, including 5 insecticides (acetamiprid, thiacloprid, thiacloprid-amide, thiamethoxam, and dimethoate), 4 fungicides (carbendazim, azoxystrobin, tebuconazole, and boscalid), and 2 pharmacologically active substances used in veterinary medicine (DMF and total amitraz) (Table 2). No residues of herbicides, plant growth regulators, or acaricides were found in the honey samples. Only three samples were free of pesticide residues, but it should be noted that there was no sample in which the acceptable level of any of the substances was exceeded.

Table 2. List of substances identified in honey (V—Veterinary drugs, F—Fungicides, I—Insecticides; II—Moderately hazardous, U—Unlikely to present acute hazard; LOQ—Limit of quantification (mg/kg), MRL—Maximum residue level (mg/kg)).

Compound	Category of Use	WHO Category [22]	Chemical Group	LOQ	MRL	Positive Samples	
						n	%
Acetamiprid	I	II	cyano-substituted neonicotinoid	0.001	0.05	26	86.66
Carbendazim	F	U	benzimidazole	0.001	1	18	60.00
Thiacloprid	I	II	cyano-substituted neonicotinoid	0.001	0.2	27	90.00
DMF (*N*-2,4-Dimethylphenyl-formamide)	V	-	-	0.005	-	17	56.66
Total amitraz	V	II	-	-	-	16	53.33
Thiacloprid-amide	I	II	cyano-substituted neonicotinoid	0.005	-	4	13.33
Thiamethoxam	I	II	nitro-substituted neonicotinoid	0.001	-	8	26.66
Dimethoate	I	II	organophosphate	0.001	-	3	10.00
Azoxystrobin	F	U	strobilurin methoxyacrylate	0.001	0.05	3	10.00
Tebuconazole	F	II	triazole	0.001	0.05	2	6.66
Boscalid	F	U	anilide pyridine-carboxamide	0.001	0.05	1	3.33

3.1.1. Insecticides

Thiacloprid was detected in 90% of honey samples (max 0.337 mg/kg), acetamiprid in 86.7% (max 0.061 mg/kg), carbendazim in 60% (max 0.049 mg/kg), DMF in 56.7% (max 0.038 mg/kg), amitraz in 53.3% (max for total 0.075 mg/kg), thiamethoxam in 26.7% (max 0.004 mg/kg), thiacloprid-amide in 13.3% (max 0.012 mg/kg), dimethoate in 10% (max 0.003 mg/kg), azoxystrobin in 10% (max 0.002 mg/kg), tebuconazole in 6.66% (max 0.002 mg/kg), and boscalid in 3.33% (max 0.001 mg/kg) (Table 3). All the samples of rapeseed honey contained residues of thiacloprid, acetamiprid, and carbendazim (0.0702 mg/kg, 0.0300 mg/kg and 0.0242 mg/kg), and all the samples of multifloral honey contained thiacloprid and acetamiprid (0.1062 mg/kg and 0.0150 mg/kg) (Table 4). The highest degree of contamination with pesticides was noted for multifloral honey (0.1646 mg/kg in total) and rapeseed honey (0.1498 mg/kg), while buckwheat (0.0324 mg/kg), honeydew (0.0125 mg/kg), and linden (0.0268 mg/kg) honey were less contaminated with pesticides. All the samples of buckwheat honey were contaminated with the neonicotinoid insecticide thiacloprid (0.0122 mg/kg). Mitchell et al. [19], in an analysis of the presence of five commonly used neonicotinoids (acetamiprid, clothianidin, imidacloprid, thiacloprid, and thiamethoxam) in 198 samples of honey from various parts of the world, showed the regional differences in the use of different types of pesticides. Imidacloprid was predominant in honey from Africa and South America, acetamiprid in samples from Asia, thiamethoxam in honey from Oceania and North America, and thiacloprid in European honey. Under the Commission Implementing Regulation (EU) No 2020/23 [23], the approval of thiacloprid as an active substance was not renewed, and stores of it were to be used by 3 February 2021. At the same time, the European Food Safety Authority (EFSA) indicated a problem raising serious concern associated with the contamination of groundwater by the metabolites of thiacloprid [24]. All the suggested applications of thiacloprid entail the risk of exceeding the acceptable limit (0.1 μg/L) of the metabolites M30, M34, and M46 in drinking water. These metabolites are assumed to have the same carcinogenic properties as the original active substance (thiacloprid), which—according to Regulation (EC) No 1272/2008 of the European Parliament and of the Council [25] (amended by Commission Regulation (EU) 2019/521 [26])—is a category 2 carcinogen. This category includes agents, mixtures, and groups of agents for which there is sufficient evidence of carcinogenicity in humans as well as those for which there is no evidence of carcinogenicity in humans, but where there is evidence of carcinogenicity in experimental animals. In addition, thiacloprid is classified as a category 1B reproductive toxin. This group includes compounds presumed to adversely affect reproduction in humans based on experiments in animals.

Table 3. Descriptive statistics of pesticide residues (mg/kg) detected in honey.

	Compoud	Mean	Median	Min	Max	25th Percentile	75th Percentile
1	Acetamiprid	0.0127	0.0065	<LOQ	0.0610	0.0020	0.0160
2	Carbendazim	0.0074	0.0020	<LOQ	0.0490	0.0000	0.0130
3	Thiacloprid	0.0527	0.0240	<LOQ	0.3370	0.0040	0.0520
4	DMF	0.0061	0.0030	<LOQ	0.0380	0.0000	0.0100
5	Total Amitraz	0.0112	0.0050	<LOQ	0.0750	0.0000	0.0160
6	Thiacloprid-Amide	0.0013	0.0000	<LOQ	0.0120	0.0000	0.0000
7	Thiamethoxam	0.0005	0.0000	<LOQ	0.0040	0.0000	0.0010
8	Dimethoate	0.0002	0.0000	<LOQ	0.0030	0.0000	0.0000
9	Azoxystrobin	0.0001	0.0000	<LOQ	0.0020	0.0000	0.0000
10	Tebuconazole	0.0001	0.0000	<LOQ	0.0020	0.0000	0.0000
11	Boscalid	0.0000	0.0000	<LOQ	0.0010	0.0000	0.0000

Table 4. Descriptive statistics of pesticide residues (mg/kg) detected in varietal honeys (RS—rapeseed; MF—multifloral; BW—buckwheat; HD—honeydew; LI—linden).

	Compound	Honey	Mean	Median	Min	Max	25th Percentile	75th Percentile	Positive Samples	
									n	%
1	Acetamiprid	RS	0.0300	0.030	0.009	0.061	0.015	0.035	5	100.0
2	Carbendazim	RS	0.0242	0.020	0.007	0.049	0.014	0.031	5	100.0
3	Thiacloprid	RS	0.0702	0.053	0.043	0.118	0.044	0.093	5	100.0
4	DMF	RS	0.0072	0.003	<LOQ	0.027	0.002	0.004	4	80.0
5	Total Amitraz	RS	0.0144	0.006	<LOQ	0.054	0.004	0.008	4	80.0
6	Thiacloprid-Amide	RS	0.0016	0.000	<LOQ	0.008	0.000	0.000	1	20.0
7	Thiamethoxam	RS	0.0012	0.001	<LOQ	0.002	0.001	0.002	4	80.0
8	Azoxystrobin	RS	0.0004	0.000	<LOQ	0.002	0.000	0.000	1	20.0
9	Tebuconazole	RS	0.0004	0.000	<LOQ	0.002	0.000	0.000	1	20.0
10	Boscalid	RS	0.0002	0.000	<LOQ	0.001	0.000	0.000	1	20.0
	Total		**0.1498**							
1	Acetamiprid	MF	0.0150	0.009	0.001	0.042	0.003	0.026	10	100.0
2	Carbendazim	MF	0.0060	0.002	<LOQ	0.028	0.000	0.013	6	60.0
3	Thiacloprid	MF	0.1062	0.042	0.004	0.337	0.015	0.178	10	100.0
4	DMF	MF	0.0122	0.011	<LOQ	0.038	0.007	0.014	9	90.0
5	Total Amitraz	MF	0.0216	0.018	<LOQ	0.075	0.006	0.028	8	80.0
6	Thiacloprid-Amide	MF	0.0031	0.000	<LOQ	0.012	0.000	0.008	3	30.0
7	Thiamethoxam	MF	0.0004	0.000	<LOQ	0.002	0.000	0.000	2	20.0
8	Azoxystrobin	MF	0.0001	0.000	<LOQ	0.001	0.000	0.000	1	10.0
	Total		**0.1646**							
1	Acetamiprid	BW	0.0086	0.004	<LOQ	0.020	0.004	0.015	4	80.0
2	Carbendazim	BW	0.0056	0.004	<LOQ	0.018	0.000	0.006	3	60.0
3	Thiacloprid	BW	0.0122	0.005	0.002	0.027	0.003	0.024	5	100.0
4	DMF	BW	0.0012	0.000	<LOQ	0.006	0.000	0.000	1	20.0
5	Total Amitraz	BW	0.0024	0.000	<LOQ	0.012	0.000	0.000	1	20.0
6	Thiamethoxam	BW	0.0010	0.000	<LOQ	0.004	0.000	0.001	2	40.0
7	Dimethoate	BW	0.0014	0.002	<LOQ	0.003	0.000	0.002	3	60.0
	Total		**0.0324**							
1	Acetamiprid	HD	0.0023	0.001	<LOQ	0.007	0.000	0.005	2	50.0
2	Carbendazim	HD	0.0003	0.000	<LOQ	0.001	0.000	0.001	1	25.0
3	Thiacloprid	HD	0.0025	0.001	<LOQ	0.008	0.000	0.005	2	50.0
4	DMF	HD	0.0025	0.000	<LOQ	0.010	0.000	0.005	1	25.0
5	Total Amitraz	HD	0.0050	0.000	<LOQ	0.020	0.000	0.010	1	25.0
	Total		**0.0125**							
1	Acetamiprid	LI	0.0047	0.002	<LOQ	0.016	0.001	0.007	5	83.3
2	Carbendazim	LI	0.0018	0.002	<LOQ	0.005	0.000	0.003	3	50.0
3	Thiacloprid	LI	0.0160	0.015	<LOQ	0.032	0.003	0.031	5	83.3
4	DMF	LI	0.0013	0.000	<LOQ	0.005	0.000	0.003	2	33.3
5	Total Amitraz	LI	0.0027	0.000	<LOQ	0.010	0.000	0.006	2	33.3
6	Azoxystrobin	LI	0.0002	0.000	<LOQ	0.001	0.000	0.000	1	16.6
7	Tebuconazole	LI	0.0002	0.000	<LOQ	0.001	0.000	0.000	1	16.6
	Total		**0.0268**							

The contamination of honey with neonicotinoid insecticides largely depends on the apiary's location in an agricultural area transformed by human activity [9]. A comparison was made of 90 samples of honey from western France, obtained from an apiary located on a plain and surrounded by crops and from another apiary situated in a bocage environment

(fields surrounded by shrubs and trees). The levels of thiacloprid and thiamethoxam were higher in the honey from the apiary in the plain (11.6 ng/g and 2 ng/g) than in the honey from the bocage (9.1 ng/g and not detected). On the other hand, the maximum level of acetamiprid in the honey from the bocage (112.8 ng/g) was higher than in the honey from the plain (51.9 ng/g).

Our study found no residues of organochlorine insecticides in the honey samples. Wilczyńska and Przybyłowski [27], on the other hand, detected eight organochlorine insecticides in honey from Poland, including HCH and *p,p′*-DDT (about 60% of samples), *p,p*-methoxychlor (29% of samples), and aldrin (21% of samples). Organochlorine pesticides are especially hazardous in agriculture due to their persistence and bioaccumulation in the environment, and their residues are identified in honey in various parts of the world.

Ruiz-Toledo et al. [28] demonstrated the presence of a wide spectrum of organochlorine compounds in honey from Mexico (in the state of Chiapas), despite the fact that their use has been banned there since 2000. At least one organochlorine pesticide was present in more than 90% of honey samples—the most frequently identified were heptaclor (44% of samples), γ-HCH (36%), DDT (19%), endrin (18%), and DDE (11%).

The EFSA [24] reported that among 1301 samples of honey and other bee products evaluated in 2019, 78.7% were free of pesticide residues, and 20.4% of samples contained residues at the maximum level (MRL) or lower. The MRL was exceeded in 0.9% of samples. In total, 27 pesticides were quantified: most frequently thiacloprid (173 samples), acetamiprid (49 samples), amitraz (37 samples), dimoxystrobin (29 samples), azoxystrobin (27 samples), glyphosate (17 samples), coumaphos (10 samples), and flonicamid (10 samples). The MRL was exceeded for amitraz (four samples), glyphosate (two samples), and in one sample each for acetamiprid, bromide ion, thiacloprid, azoxystrobin, boscalid, and chlorfluazuron.

El-Nahhal [29] identified residues of 92 pesticides in honey from 27 countries, including 6 substances belonging to toxicity class IA (extremely hazardous), 8 from class IB (highly hazardous), 42 from class II (moderately hazardous), 35 from class III (slightly hazardous), and one from class IV (not posing a serious threat). The hazard indices (HI) indicated a high potential health risk from honey consumption.

Bargańska et al. [30], in an analysis of residues of 30 pesticides in honey from northern Poland (Pomerania), detected them in 29% of samples. In five samples (11%), the MRL was exceeded for bifenthrin (14.5 ng/g), fenpyroximate (16.3 ng/g), methidathion (25.7 ng/g), spinosad (20.6 ng/g), thiamethoxam (20.2 ng/g), and triazophos (20.3 ng/g). The organophosphate pesticide profenofos, which was not found in the present study, was detected as well (from <LOQ to 17.2 ng/g). In turn, Gaweł et al. [20] monitored 155 samples of Polish honey for the potential presence of 207 pesticide residues from 2015–2017. A total of 21 pesticides were identified: thiacloprid, acetamiprid, carbendazim, DMF and DMPF (amitraz metabolites), azoxystrobin, tebuconazole, dimethoate, boscalid, coumaphos, cyproconazole, flutriafol, tau-fluvalinate, tetraconazole, diazinon, dimoxystrobin, *p,p′*-DDD, difenoconazole, lindane, propiconazole, and prothioconazole-desthio. The most frequently detected pesticides were two cyano-substituted neonicotinoids—thiacloprid and acetamiprid—and carbendazim, which were found in 68%, 55%, and 38% of honey samples, respectively. In the present study, the presence of residues of these substances was detected in 90%, 87%, and 60% of samples. Moreover, Gaweł et al. [20] reported acetamiprid concentrations in honey ranging from 0.001 to 0.13 mg/kg and thiacloprid concentrations from 0.001 to 0.2 mg/kg. The maximum content of acetamiprid in the present study (0.061 mg/kg) was half of that reported in the cited study, while that of thiacloprid (0.337 mg/kg) was higher.

3.1.2. Fungicides

In the present study, the most frequently identified fungicide was carbendazim (present in 60% of samples), followed by azoxystrobin (10%), tebuconazole (6.66%), and boscalid (3.33% samples). Similarly, Gaweł et al. [20] showed the presence of the fungi-

cides carbendazim (38%), azoxystrobin (11%), tebuconazole (10%), and boscalid (5%) in Polish honey, as well as other fungicides that were not detected in our study, including cyproconazole (6%), flutriafol (5%), tetraconazole (3%), dimoxystrobin, difenoconazole, propiconazole, and prothioconazole-desthio (1% each).

Only two honey samples contained both a triazole fungicide (tebuconazole) and cyano-substituted neonicotinoids (acetamiprid and thiacloprid). This combination of pesticide residues increases the toxicity of cyano-substituted neonicotinoids [31]. The degradation of cyano-substituted neonicotinoids (acetamiprid and thiacloprid) takes longer than in the case of nitro-substituted neonicotinoids (thiamethoxam, clothianidin, and imidacloprid).

3.1.3. Residues of Veterinary Drugs

The veterinary drugs whose residues were identified in the present study were DMF (*N*-2,4-Dimethylphenyl-formamide) and amitraz (total). Amitraz is used in apiaries against parasitic mites *Varroa destructor*, which are carriers of pathogenic viruses such as Acute Bee Paralysis Virus (ABPV) and Deformed Wing Virus (DWV) [32]. O'Neal et al. [33], however, showed that Amitraz has certain limitations, because exposure to this compound can adversely affect bees' resistance to viral infections. Amitraz and its metabolites significantly alter the heart rate of the honey bee, most likely through interactions with octopamine receptors. A sublethal dose of amitraz can affect the detoxification, cyclic adenosine monophosphate (cAMP)-dependent protein kinase, immunity, antioxidant capacity, and the development of honeybee queens [34]. Amitraz is not a highly stable substance; in addition to amitraz itself, products of its degradation may be found, such as DMPF (*N*-(2,4-dimethylphenyl)-*N*′-methylformamide) and DMF (2,4-dimethylformanilide) [35].

3.2. Concentration of Metals

Honey is a plant and animal product that contains macro- and microelements as well as heavy metals (Pb, Cd, Hg, Cu, and Zn). Their concentrations vary depending on regional and environmental conditions, seasonal differences, and beekeeping and agricultural techniques [36].

Mercury is considered to be the most toxic heavy metal in the environment [37]. In the present study, the LOQ for Hg (5.0 μg/kg) was not exceeded in the honey. Brodziak-Dopierała et al. [38] detected the presence of Hg in 32 honeys from different parts of Poland (on average 0.37 μg/kg). The highest Hg content was noted in honeydew honey (1.55 μg/kg) and the lowest in goldenrod honey (0.02 μg/kg). In honey from Romania, the average Hg level was 0.908 μg/kg, ranging from 0.369 μg/kg to 2.154 μg/kg [14].

The level of elements in honey is associated with pollution in the area in which bees fly around honey plants. According to EC Regulation 1881/2006 [39], honey (as a food product) must meet the requirements for the maximum level of Pb (0.10 mg/kg). However, no limit has been established for Cd [36]. Tomczyk et al. [40] tested levels of Cd and Pb in successive links of the food chain (soil-plant-bee-honey) and showed that bees are susceptible to their bioaccumulation but at the same time are a biological barrier preventing the transfer of these elements to honey.

In the present study, the lowest Pb content was noted in honeydew honey (0.044 mg/kg) and the highest in linden (0.080 mg/kg) and rapeseed (0.081 mg/kg) honey (Figure 1). Due to the considerable variation in the Pb concentration in the honey samples, the differences were not confirmed statistically. The acceptable Pb concentration was exceeded in four honey samples, including one sample of rapeseed honey (0.107 mg/kg), two samples of linden honey (0.158 and 0.114 mg/kg), and one sample of multifloral honey (0.191 mg/kg). Piven et al. [2] reported a higher Pb content in Ukrainian honey (from the Odessa region), with the highest concentration noted in sunflower honey (0.24 mg/kg) and the lowest in multifloral honey (0.13 mg/kg). According to the authors, the high Pb level in honey was caused by the proximity of the apiaries to traffic routes. Aghamirlou et al. [41] reported a Pb content of 0.45 mg/kg in multifloral honey from Iran. An excessive

Pb content in honey poses a threat to people mainly due to its neurotoxic and nephrotoxic effects [42].
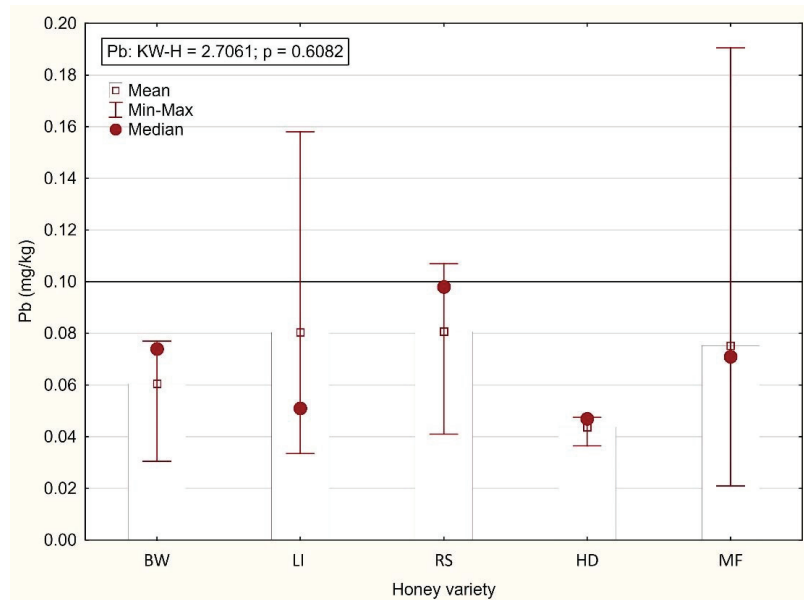
Figure 1. Content of Pb (mg/kg) in varietal honeys (BW—buckwheat; LI—linden; RS—rapeseed; HD—honeydew; MF—multifloral).

The Cd content in the present study did not exceed the LOQ of 0.02 mg per kg of honey, except for one sample of linden honey (0.0215 mg/kg). Piven et al. [2] reported Cd at a level of 0.03 mg/kg in sunflower honey from the Odessa region (Ukraine). Aghamirlou et al. [41] detected Cd at a level of 0.013 mg/kg in multifloral honey from Iran.

The Cu content in the honey was significantly influenced by the variety ($p = 0.0013$) (Figure 2). The Cu content was significantly the highest in buckwheat honey (1.201 mg/kg) and the lowest in rapeseed, linden, and multifloral honey (0.504–0.579 mg/kg). Dżugan et al. [43], in an analysis of Polish varietal honeys from the Podkarpacie region (southeastern Poland), showed a lower average Cu content in multifloral (0.21 mg/kg), rapeseed (0.05 mg/kg), linden (0.20 mg/kg), and honeydew (0.03 mg/kg) honey, and the highest Cu content in buckwheat honey (0.86 mg/kg), as in the present study. Tarapatskyy et al. [44], in honey obtained in Pogórze Karpackie (southern Poland), reported a Cu content similar to the levels found in the present study in multifloral (0.410 mg/kg), linden (0.460 mg/kg), and honeydew (0.960 mg/kg) honey.

The honey variety did not affect the Zn level, although it was highest in buckwheat honey (2.694 mg/kg) compared with the other varieties (0.657–1.500 mg/kg) (Figure 3). Dżugan et al. [43] reported similar results for Zn in honey varieties, with the exception of honeydew honey, in which the level was twice as high as in our study (2.33 mg/kg). Similarly, in the study by Tarapatskyy et al. [44], the Zn level in honeydew honey from Pogórze Karpackie (Poland) was twice as high as in the present study, while its content in buckwheat honey was only a third as high. In general, the literature reports indicate a considerable variation in the content of the elements analysed (macro- and microelements and toxic metals) in European varietal honeys from Poland [21,45,46], Slovakia [44,47], Romania [14], and Turkey [36,48]. The contamination of honey with toxic metals is mainly associated with industry and agriculture [45]. Numerous studies supply valuable information on the effect of the environment on the quality of honey produced in industrial areas.

Honey obtained from industrialized areas or near major roads has been shown to have higher concentrations of heavy metals.
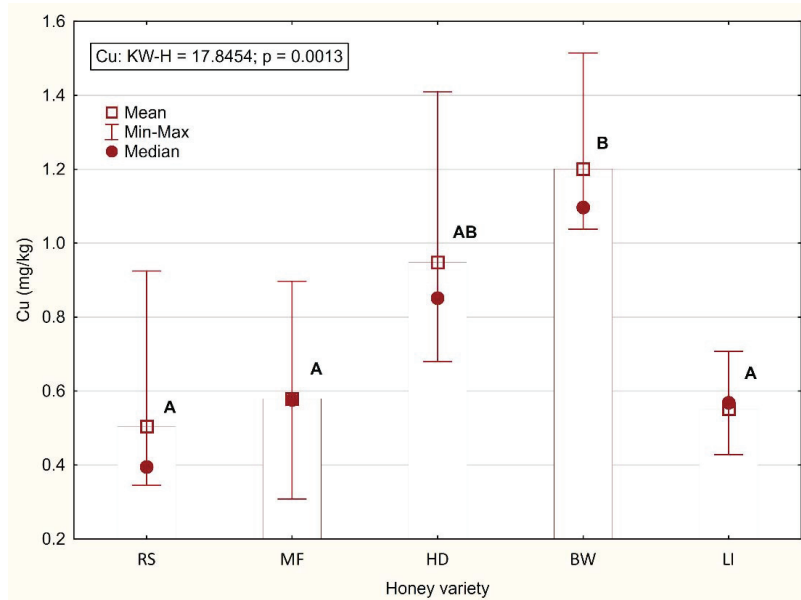
Figure 2. Content of Cu (mg/kg) in varietal honeys (RS–rapeseed; MF–multifloral; HD—honeydew; BW—buckwheat; LI—linden). Means with different letters (A, B) differ significantly (*p* < 0.01).
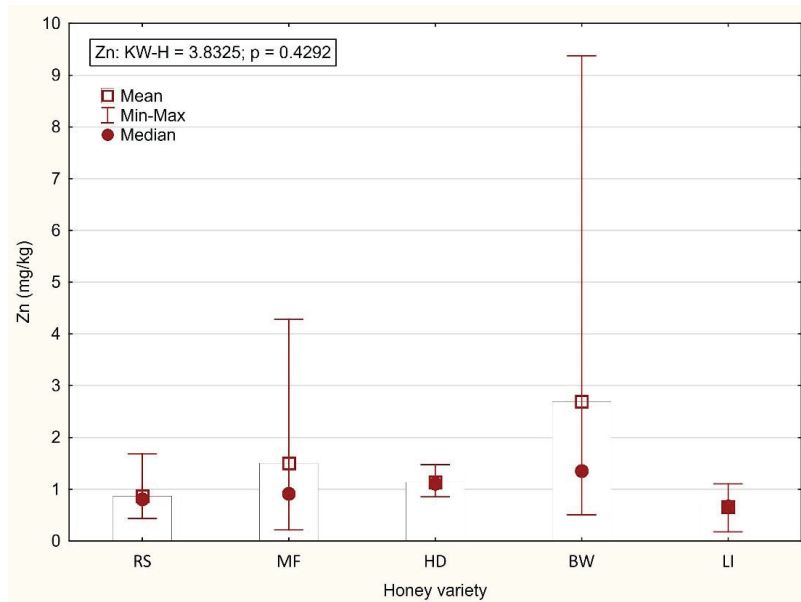
Figure 3. Content of Zn (mg/kg) in varietal honeys (RS—rapeseed; MF—multifloral; HD—honeydew; BW—buckwheat; LI—linden).

Bartha et al. [49] analysed the content of heavy metals (Pb, Cd, Zn, and Cu) in multifloral honey produced in an industrial area of Romania, considered to be one of the most polluted regions of Eastern Europe (the town of Copșa Mică and its vicinity). The spread of pollutants emitted by the local industrial platform resulted from the topography of the area, where the main air masses are directed towards the corridors of the rivers Târnava Mare and Visa. Apiaries situated in the valley channeling pollutants from the industrial platform were shown to be more susceptible to the bioaccumulation of Pb than those situated in side valleys further from the source of pollution. The Cd concentration in the honey decreased exponentially with an increasing distance between the apiary and the pollution source, while the Cu concentrations increased linearly. The median for the elements was high: Pb—1.49 mg/kg, Cd—2.20 mg/kg, Zn—20.40 mg/kg, and Cu—3.70 mg/kg. According to Klym and Stadnytska [50], the content of heavy metals increased with the degree of the impact of industry on the environment. The levels of Zn, Cu, Pb, and Cd were the highest in honey from forested and steppe areas, lower in honey from foothills, and the lowest in mountainous areas of the Carpathian region. Dobrzański et al. [51] found that the Pb limit was exceeded in 75% of the samples of honey from apiaries located in a copper-producing region but did not observe elevated levels of Cd. The honey in the present study contained much lower levels of residues of these elements.

4. Conclusions

The presence of pesticide residues was detected in 90% of the analysed samples, but the concentrations did not exceed acceptable residue levels (Regulation (EC) No 396/2005 of the European Parliament and of the Council [16]). The residues of 11 substances were identified, including 5 insecticides (acetamiprid, thiacloprid, thiacloprid-amide, thiamethoxam, and dimethoate), 4 fungicides (carbendazim, azoxystrobin, tebuconazole, and boscalid) and 2 pharmacologically active substances used in veterinary medicine (DMF and total amitraz). The most frequently identified substances were thiacloprid, acetamiprid, and carbendazim.

The analysis of heavy metals showed that the honey from apiaries located in southeastern Poland is safe for human consumption. The levels of the toxic heavy metals mercury and cadmium did not exceed the maximum level that is safe for human health. The average lead content in the varietal honey also did not exceed the accepted limit of 0.10 mg/kg. The concentrations of Zn and Cu did not deviate from those reported in the literature for specific honey varieties.

To summarise the results of the research, the honey produced in southeastern Poland was shown to be safe for human health and consumption. The quality control of honey for the presence of chemical contaminants is crucial to the evaluation of the health safety of the product.

Data Availability Statement: Data will be made available upon reasonable request by the corresponding author.

Conflicts of Interest: The authors declare no conflict of interest.

References

1. Mititelu, M.; Udeanu, D.I.; Nedelescu, M.; Neacsu, S.M.; Nicoara, A.C.; Oprea, E.; Ghica, M. Quality Control of Different Types of Honey and Propolis Collected from Romanian Accredited Beekeepers and Consumer's Risk Assessment. *Crystals* **2022**, *12*, 87. [CrossRef]
2. Piven, O.T.; Khimych, M.S.; Salata, V.Z.; Gutyj, B.V.; Naidich, O.V.; Skrypka, H.A.; Koreneva, Z.B.; Dvylyuk, I.V.; Gorobey, O.M.; Rud, V.O. Contamination of heavy metals and radionuclides in the honey with different production origin. *Ukr. J. Ecol.* **2020**, *10*, 405–409. [CrossRef]
3. Oymen, B.; Aşır, S.; Türkmen, D.; Denizli, A. Determination of multi-pesticide residues in honey with a modified QuEChERS procedure followed by LC-MS/MS and GC-MS/MS. *J. Apic. Res.* **2022**, *61*, 530–542. [CrossRef]
4. Hernández, A.F.; González-Alzaga, B.; López-Flores, I.; Lacasaña, M. Systematic reviews on neurodevelopmental and neurodegenerative disorders linked to pesticide exposure: Methodological features and impact on risk assessment. *Environ. Int.* **2016**, *92*, 657–679. [CrossRef] [PubMed]
5. Cunningham, M.M.; Tran, L.; McKee, C.G.; Polo, R.O.; Newman, T.; Lansing, L.; Griffiths, J.S.; Bilodeau, G.J.; Rott, M.; Guarna, M.M. Honey bees as biomonitors of environmental contaminants, pathogens, and climate change. *Ecol. Indic.* **2022**, *134*, 108457. [CrossRef]
6. Auteri, D.; Devos, Y.; Fabrega, J.; Pagani, S.; Rortais, A.; de Seze, G.; Heppner, C.; Hugas, M. Advancing the Environmental Risk Assessment of Chemicals to Better Protect Insect Pollinators (IPol-ERA). *EFSA Support. Publ.* **2022**, *19*, e200505. [CrossRef]
7. More, S.J.; Auteri, D.; Rortais, A.; Pagani, S. EFSA is working to protect bees and shape the future of environmental risk assessment. *EFSA J.* **2021**, *19*, e190101. [CrossRef]
8. Rolke, D.; Fuchs, S.; Grünewald, B.; Gao, Z.; Blenau, W. Large-scale monitoring of effects of clothianidin-dressed oilseed rape seeds on pollinating insects in Northern Germany: Effects on honey bees (*Apis mellifera*). *Ecotoxicology* **2016**, *25*, 1648–1665. [CrossRef]
9. Paradis, D.; Bérail, G.; Bonmatin, J.M.; Belzunce, L.P. Sensitive analytical methods for 22 relevant insecticides of 3 chemical families in honey by GC-MS /MS and LC-MS/MS. *Anal. Bioanal. Chem.* **2014**, *406*, 621–633. [CrossRef]
10. Scripcă, L.A.; Amariei, S. The Influence of Chemical Contaminants on the Physicochemical Properties of Unifloral and Multifloral Honey. *Foods* **2021**, *10*, 1039. [CrossRef]
11. The Agency for Toxic Substances and Disease Registry (ATSDR). *Priority List of Hazardous Substances*; ATSDR: Atlanta, GA, USA, 2019. Available online: https://www.atsdr.cdc.gov/spl/resources (accessed on 29 June 2022).
12. Fakhri, Y.; Abtahi, M.; Atamaleki, A.; Raoofi, A.; Atabati, H.; Asadi, A.; Miri, A.; Shamloo, E.; Alinejad, A.; Keramati, H.; et al. The concentration of potentially toxic elements (PTEs) in honey: A global systematic review and meta-analysis and risk assessment. *Trends Food Sci. Technol.* **2019**, *91*, 498–506. [CrossRef]
13. Ciobanu, O.; Rădulescu, H. Monitoring of heavy metals residues in honey. *Res. J. Agric. Sci.* **2016**, *48*, 9–13.
14. Oroian, M.; Prisacaru, A.; Hretcany, E.C.; Stroe, S.G.; Leahu, A.; Buculei, A. Heavy Metals Profile in Honey as a Potential Indicator of Botanical and Geographical Origin. *Int. J. Food Prop.* **2016**, *19*, 1825–1836. [CrossRef]
15. De Souza, A.P.F.; Petrarca, M.H.; de Campos Braga, P.A.; Rodrigues, N.R.; Reyes, F.G. Analysis of insecticide residues in honey by liquid chromatography tandem mass spectrometry using QuEChERS optimized by the Plackett Burman design. *CYT—J. Food* **2021**, *19*, 326–332. [CrossRef]
16. European Comission. Regulation (EC) No 396/2005 of the European Parliament and of the Council of 23 February 2005 on Maximum residue levels of pesticides in or on food and feed of plant and animal origin and amending Council Directive 91/414/EEC. *Off. J. Eur. Union* **2005**, *L70*, 1–16.
17. European Comission. Commission Regulation (EU) No 37/2010 of 22 December 2009 on Pharmacologically Active Substances and Their Classification Regarding Maximum Residue Limits in Foodstuffs of Animal Origin. *Off. J. Eur. Union* **2009**, *L15*, 1–72.
18. Minister of Agriculture and Rural Development. Regulation of 21 June 2017 on the Monitoring of Prohibited Substances, Chemical and Biological Residues, Medicinal Products and Radioactive Contamination. *J. Laws* **2017**, *1246*, 1–12.
19. Mitchell, E.A.; Mulhauser, B.; Mulot, M.; Mutabazi, A.; Glauser, G.; Aebi, A. A worldwide survey of neonicotinoids in honey. *Science* **2017**, *358*, 109–111. [CrossRef]
20. Gaweł, M.; Kiljanek, T.; Niewiadowska, A.; Semeniuk, S.; Goliszek, M.; Burek, O.; Posyniak, A. Determination of neonicotinoids and 199 other pesticide residues in honey by liquid and gas chromatography coupled with tandem mass spectrometry. *Food Chem.* **2019**, *282*, 36–47. [CrossRef]
21. Kędzierska-Matysek, M.; Teter, A.; Stryjecka, M.; Skałecki, P.; Domaradzki, P.; Rudaś, M.; Florek, M. Relationships linking the colour and elemental concentrations of blossom honeys with their antioxidant activity: A chemometric approach. *Agriculture* **2021**, *11*, 702. [CrossRef]
22. World Health Organization. *WHO Recommended Classification of Pesticides by Hazard and Guidelines to Classification*, 2019th ed.; World Health Organization: Geneva, Switzerland, 2020; pp. 85–96.

23. European Comission. Commission Implementing Regulation (EU) 2020/23 of 13 January 2020 Concerning the Non-Renewal of the Approval of the Active Substance Thiacloprid, in Accordance with Regulation (EC) No 1107/2009 of the European Parliament and of the Council Concerning the Placing of Plant Protection Products on the Market, and Amending the Annex to Commission Implementing Regulation (EU) No 540/2011. *Off. J. Eur. Union* **2020**, *L8*, 8–11.

24. Cabrera, L.C.; Pastor, P.M. The 2019 European Union report on pesticide residues in food. *EFSA J.* **2021**, *19*, e06491. [CrossRef]

25. European Parliament. Regulation (EC) No 1272/2008 of the European Parliament and of the Council of 16 December 2008 on Classification, Labelling and Packaging of Substances and Mixtures, Amending and Repealing Directives 67/548/EEC and 1999/45/EC, and Amending Regulation (EC) No 1907/2006. *Off. J. Eur. Union* **2008**, *L353*, 1–1355.

26. European Parliament. Regulations Commission Regulation (EU) 2019/521 of 27 March 2019 Amending, for the Purposes of its Adaptation to Technical and Scientific Progress Regulation (EC) No 1272/2008 of the European Parliament and of the Council on Classification, Labelling and Packaging of Substances and Mixtures. *Off. J. Eur. Union* **2019**, *L86*, 1–36.

27. Wilczyńska, A.; Przybyłowski, P. Residues of organochlorine pesticides in Polish honeys. *Apiacta* **2007**, *42*, 16–24.

28. Ruiz-Toledo, J.; Vandame, R.; Castro-Chan, R.A.; Penilla-Navarro, R.P.; Gómez, J.; Sánchez, D. Organochlorine Pesticides in Honey and Pollen Samples from Managed Colonies of the Honey Bee *Apis mellifera* Linnaeus and the Stingless Bee *Scaptotrigona mexicana* Guérin from Southern, Mexico. *Insects* **2018**, *9*, 54. [CrossRef]

29. El-Nahhal, Y. Pesticide residues in honey and their potential reproductive toxicity. *Sci. Total Environ.* **2020**, *741*, 139953. [CrossRef]

30. Bargańska, Ż.; Ślebioda, M.; Namieśnik, J. Pesticide residues levels in honey from apiaries located of Northern Poland. *Food Control* **2013**, *31*, 196–201. [CrossRef]

31. Biddinger, D.J.; Robertson, J.L.; Mullin, C.; Frazier, J.; Ashcraft, S.A.; Rajotte, E.G.; Neelendra, K.J.; Vaughn, M. Comparative Toxicities and Synergism of Apple Orchard Pesticides to *Apis mellifera* (L.) and *Osmia cornifrons* (Radoszkowski). *PLoS ONE* **2013**, *8*, e72587. [CrossRef]

32. Locke, B.; Thaduri, S.; Stephan, J.G.; Low, M.; Blacquière, T.; Dahle, B.; Le Conte, Y.; Neumann, P.; de Miranda, J.R. Adapted tolerance to virus infections in four geographically distinct *Varroa destructor*-resistant honeybee populations. *Sci. Rep.* **2021**, *11*, 12359. [CrossRef]

33. O'Neal, S.T.; Brewster, C.C.; Bloomquist, J.R.; Anderson, T.D. Amitraz and its metabolite modulate honey bee cardiac function and tolerance to viral infection. *J. Invertebr. Pathol.* **2017**, *149*, 119–126. [CrossRef] [PubMed]

34. Chaimanee, V.; Pettis, J.S. Gene expression, sperm viability, and queen (*Apis mellifera*) loss following pesticide exposure under laboratory and field conditions. *Apidologie* **2019**, *50*, 304–316. [CrossRef]

35. Chaimanee, V.; Johnson, J.; Pettis, J.S. Determination of amitraz and its metabolites residue in honey and beeswax after Apivar®treatment in honey bee (*Apis mellifera*) colonies. *J. Apic. Res.* **2022**, *61*, 213–218. [CrossRef]

36. Altunatmaz, S.S.; Tarhan, D.; Aksu, F.; Ozsobaci, N.P.; Or, M.E.; Barutçu, U.B. Levels of Chromium, Copper, Iron, Magnesium, Manganese, Selenium, Zinc, Cadmium, Lead and Aluminium of honey varieties produced in Turkey. *Food Sci. Technol. Campinas* **2019**, *39*, 392–397. [CrossRef]

37. Jaishankar, M.; Tseten, T.; Anbalagan, N.; Mathew, B.B.; Beeregowda, K.N. Toxicity, mechanism and health effects of some heavy metals. *Interdiscip. Toxicol.* **2014**, *7*, 60–72. [CrossRef]

38. Brodziak-Dopierała, B.; Mendak-Oleś, P.; Fischer, A. Occurrence of mercury in various types of honey. *Med. Srod.* **2020**, *23*, 39–43. [CrossRef]

39. Commission of the European Communities. Commission Regulation (EC) No 1881/2006 of 19 December 2006 Setting Maximum Levels for Certain Contaminants in Foodstuffs. *Off. J. Eur. Union* **2006**, *L364*, 5–24.

40. Tomczyk, M.; Zaguła, G.; Puchalski, C.; Dżugan, M. Transfer of some toxic metals from soil to honey depending on bee habitat conditions. *Acta Univ. Cibiniensis Ser. E Food Technol.* **2020**, *24*, 49–59. [CrossRef]

41. Aghamirlou, H.M.; Khadem, M.; Rahmani, A.; Sadeghian, M.; Mahvi, A.H.; Akbarzadeh, A.; Nazmara, S. Heavy metals determination in honey samples using inductively coupled plasmaoptical emission spectrometry. *J. Environ. Health Sci. Eng.* **2015**, *13*, 39. [CrossRef]

42. European Food Safety Authority. Lead dietary exposure in the European population. *EFSA J.* **2012**, *10*, 2831. [CrossRef]

43. Dżugan, M.; Zaguła, G.; Wesołowska, M.; Sowa, P.; Puchalski, C. Levels of toxic and essential metals in varietal honeys from Podkarpacie. *J. Elem.* **2017**, *22*, 1039–1048. [CrossRef]

44. Tarapatskyy, M.; Sowa, P.; Zaguła, G.; Dżugan, M.; Puchalski, C. Assessment of the Botanical Origin of Polish Honeys Based on Physicochemical Properties and Bioactive Components with Chemometric Analysis. *Molecules* **2021**, *26*, 4801. [CrossRef] [PubMed]

45. Formicki, G.; Greń, A.; Stawarz, R.; Zyśk, B.; Gał, A. Metal Content in Honey, Propolis, Wax, and Bee Pollen and Implications for Metal Pollution Monitoring. *Pol. J. Environ. Stud.* **2013**, *22*, 99–106.

46. Roman, A.; Popiela, E. Studies of chosen toxic elements concentration in multiflower bee honey. *Potravin. Slovak J. Food Sci.* **2011**, *5*, 67–69. [CrossRef]

47. Kacaniová, M.; Knazovicka, V.; Melich, M.; Fikselova, M.; Massanyi, P.; Stawarz, R.; Hascik, P.; Pechociak, T.; Kuczkowska, A.; Putała, A. Environmental concentration of selected elements and relation to physicochemical parameters in honey. *J. Environ. Sci. Health Part A* **2009**, *44*, 414–422. [CrossRef]

48. Tutun, H.; Kahraman, H.A.; Aluc, Y.; Avci, T.; Ekici, H. Investigation of some metals in honey samples from West Mediterranean region of Turkey. *Vet. Res. Forum* **2019**, *10*, 181–186. [CrossRef]

49. Bartha, S.; Taut, I.; Goji, G.; Vlad, I.A.; Dinulică, F. Heavy Metal Content in Polyfloral Honey and Potential Health Risk. A Case Study of Copșa Mică, Romania. *Int. J. Environ. Res. Public Health* **2020**, *17*, 1507. [CrossRef]

50. Klym, O.; Stadnytska, O. Concentrations of heavy metals in multifloral honey from the different terrestrial ecosystems of the Carpathians. *Acta Sci. Pol. Zootech.* **2019**, *18*, 11–14. [CrossRef]

51. Dobrzański, Z.; Roman, A.; Górecka, H.; Kołacz, R. Content of hazardous elements and macro- and micronutrients in bee honeys from areas of industrial pollution. *Bromatol. Chem. Toksykol.* **1994**, *27*, 157–160. (In Polish)

Analysis of Fungal Microbiomes in Edible Medicinal Morindae Officinalis Radix and Alpiniae Oxyphyllae Fructus Using DNA Metabarcoding

Wenjun Jiang [1,†], Xuyu Chen [2,†], Mengyue Guo [1], Jingsheng Yu [1], Meihua Yang [1] and Xiaohui Pang [1,*]

[1] Institute of Medicinal Plant Development, Chinese Academy of Medical Sciences & Peking Union Medical College, Beijing 100193, China; wenjunjiang0927@gmail.com (W.J.); guomy0908@hotmail.com (M.G.); yujsimplad@hotmail.com (J.Y.); mhyang@implad.ac.cn (M.Y.)

[2] Hainan Provincial Key Laboratory of Resources Conservation and Development of Southern Medicine, Hainan Branch of the Institute of Medicinal Plant Development, Chinese Academy of Medical Sciences & Peking Union Medical College, Haikou 570311, China; chenxuyu-11@163.com

* Correspondence: xhpang@implad.ac.cn

† These authors contributed equally to this work.

Abstract: Morindae Officinalis Radix (MOR) and Alpiniae Oxyphyllae Fructus (AOF) have been widely used as dietary supplements and traditional herbal medicines for centuries. Fungal and mycotoxin contamination in MOR and AOF has been reported recently. In this study, fungi in MOR and AOF are first investigated using DNA metabarcoding, and the differences in fungal microbiome between moldy and non−moldy samples are analyzed. The results show that Ascomycota is the most prevailing fungus at the phylum level in MOR and AOF with relative abundances of 49.53–94.32% and 14.81–81.85%, respectively. *Penicillium* (1.86–76.14%), *Cladosporium* (1.82–56.65%), and *Trichoderma* (0.12–19.71%) are the dominant genera in MOR. *Penicillium* (0.27–56.06%), *Papiliotrema* (0.04–51.71%), and *Cladosporium* (3.08–44.41%) are the dominant genera in AOF. Two potential toxigenic fungi were detected, namely, *Trichoderma atroviride* and *Fusarium equiseti*. Moreover, the differences in fungal communities between moldy and non−moldy samples were monitored. In conclusion, DNA metabarcoding can be used to assess the fungal microbiome in edible medicinal herbs, thereby providing a basis for ensuring food safety and drug efficacy.

Keywords: Morindae Officinalis Radix; Alpiniae Oxyphyllae Fructus; DNA metabarcoding; fungal microbiome; toxigenic fungi

1. Introduction

Chinese herbal medicines (CHMs), which are widely used for clinical treatment and daily healthcare, have undoubtedly played a significant role in medical and healthcare industries. About 70–80% of the global population depends on herbal medicinal products in their primary healthcare [1]. The global market of medicinal plants is growing and expected to reach USD 5 trillion by 2050 [2]. The popularity of herbal products is increasing as they are considered natural or harmless [2]. Unfortunately, fungal contamination in CHMs is a concern. Since the sources of CHMs are diversified and the planting and processing are decentralized, CHMs may be contaminated by fungi at any link of the complex traditional Chinese medicine industry chain if good manufacturing procedures are not followed, and even mycotoxins may be produced by potential toxigenic fungi under suitable conditions. Cases of fungal and mycotoxin contamination associated with CHMs have been constantly reported worldwide and have attracted considerable global attention. A study on microbial contamination in 132 herbal medicines and 18 water samples used in the preparation of herbal medicines from northern Brazil showed that 31% of tested samples exceeded the safety limits for fungal growth [3]. Keter et al. assessed the risk of fungi in 100 herbal

products from the Kenyan market, and the results revealed that 69% of the samples did not meet the requirements about microbial limits shown in Pharmacopoeia. Among these, *Aspergillus* and *Penicillium* were dominant [4]. In Latvia, Reinholds et al. investigated the contamination profile of multi−mycotoxin and fungi in 140 *Camellia sinensis* and 26 herbal teas; 87% of the tea samples were positive for fungi and 42% had 1 to 16 mycotoxins, for instance, ochratoxin A (OTA), deoxynivalenol, and aflatoxins (AFs) [5]. A Poland investigation on the occurrence of OTA and fumonisins in 79 herbs and spices showed that 31% of the samples were positive for fumonisins and 49% for OTA [6]. Another investigation on the fungal and multi−mycotoxin contamination in 48 root herbs marketed in China determined that all samples were affected by fungal contamination; 37.5% were positive for AFs and 16.67% for OTA [7]. Moldy CHMs affect drug efficacy, pose threats to consumer health, affect the export trade, and cause economic losses.

Morindae Officinalis Radix (MOR, Bajitian in Chinese), namely, the dried root of *Morinda officinalis* How. (Rubiaceae), has long been used as a tonic herbal medicine for tonifying the kidney, strengthening sinew and bone, and dispelling wind−dampness [8]. MOR is also a popular dietary supplement for daily healthcare (e.g., bone protection and gynecological and andrological healthcare) [9]. The constituents extracted from MOR, e.g., anthraquinones, oligosaccharides, polysaccharides, and iridoid glycosides, have various bioactive activities, including anti-osteoporosis, anti-depressant, pro-fertility, immune-regulatory, anti-inflammation, and antioxidant effects [10–14]. Alpiniae Oxyphyllae Fructus (AOF, Yizhi in Chinese), a famed edible medicinal herb, is from the dried, ripe fruit of *Alpinia oxyphylla* Miq. AOF has the functions of warming the kidney to secure essence to reduce urination, and warming the spleen to check diarrhea and constrain spittle [8]. Contemporary research shows the presence of sesquiterpenes, polysaccharides, diarylheptanoids, flavonoids, and volatile oils in AOF [15]. AOF and its extracts exhibit neuroprotective, anti-ulcer, anti-inflammatory, and anti-hyperuricemic effects, and have been used for the treatment of dementia, ulceration, and tumors [16–18]. The consumption and demand for MOR and AOF are high, owing to their outstanding pharmaceutical properties and edible values. MOR and AOF are mainly produced in Hainan, Guangdong, and Guangxi provinces, as well as in other tropical and subtropical regions of China [19], in which the climate situation contributes to the development of fungi and the production of mycotoxins [20]. MOR and AOF are easily affected by the contamination of fungi without obeying proper harvest, processing, transportation, and storage procedures. Therefore, it is necessary to comprehensively and efficiently investigate the fungal contamination before the use of MOR and AOF. Contamination of fungi is challenging to identify because of their complex morphological and taxonomic characteristics. Thus, a method that simultaneously and effectively analyzes fungal microbiomes in MOR and AOF is urgently desired.

DNA metabarcoding, an emerging culture-independent technique, refers to high-throughput multispecies (or higher-level taxon) identification using the total and typically degraded DNA extracted from an environmental sample (i.e., soil, water, and feces) [21]. It has a wide range of applications in the study of fungal ecology and provides new insights into fungal microbiomes in different environments. The internal transcribed spacer (ITS) region of rDNA was recommended as a universal DNA barcode marker for fungi [22]. Most amplicon sequencing studies of fungal diversity have focused on ITS1 or ITS2 sublocus [23]. In this study, we first use DNA metabarcoding to characterize the fungal microbiomes in MOR and AOF, and compare the differences between moldy and non−moldy samples.

2. Materials and Methods

2.1. Sampling

A total of 18 samples, including MOR and AOF, were collected from herbal markets in Hainan, Guangdong, and Guangxi. The samples were divided into two groups, according to the species (i.e., MOR and AOF), and four groups based on the presence or absence of macroscopic molds (i.e., MM and MA are the moldy MOR and AOF samples, respectively;

NM and NA are the non-moldy MOR and AOF samples, respectively). The details of all samples are shown in Table 1.

Table 1. Voucher information and GenBank accession numbers of the samples.

Name	Sample ID	Group	Moldy	Group	Source	GenBank Accession No.
Morindae Officinalis Radix	MCK1	MOR	No	NM	Haikou, Hainan	SAMN19591296
Morindae Officinalis Radix	MCK2	MOR	No	NM	Haikou, Hainan	SAMN19591297
Morindae Officinalis Radix	MCK3	MOR	No	NM	Haikou, Hainan	SAMN19591298
Morindae Officinalis Radix	GDM1	MOR	Yes	MM	Qingping, Guangdong	SAMN19591299
Morindae Officinalis Radix	GDM2	MOR	Yes	MM	Qingping, Guangdong	SAMN19591300
Morindae Officinalis Radix	GDM3	MOR	Yes	MM	Qingping, Guangdong	SAMN19591301
Morindae Officinalis Radix	GXM1	MOR	Yes	MM	Yulin, Guangxi	SAMN19591302
Morindae Officinalis Radix	GXM2	MOR	Yes	MM	Yulin, Guangxi	SAMN19591303
Morindae Officinalis Radix	GXM3	MOR	Yes	MM	Yulin, Guangxi	SAMN19591304
Alpiniae Oxyphyllae Fructus	ACK1	AOF	No	NA	Haikou, Hainan	SAMN19591305
Alpiniae Oxyphyllae Fructus	ACK2	AOF	No	NA	Haikou, Hainan	SAMN19591306
Alpiniae Oxyphyllae Fructus	ACK3	AOF	No	NA	Haikou, Hainan	SAMN19591307
Alpiniae Oxyphyllae Fructus	HNA1	AOF	Yes	MA	Qingping, Guangdong	SAMN19591308
Alpiniae Oxyphyllae Fructus	HNA2	AOF	Yes	MA	Qingping, Guangdong	SAMN19591309
Alpiniae Oxyphyllae Fructus	HNA3	AOF	Yes	MA	Qingping, Guangdong	SAMN19591310
Alpiniae Oxyphyllae Fructus	GXA1	AOF	Yes	MA	Yulin, Guangxi	SAMN19591311
Alpiniae Oxyphyllae Fructus	GXA2	AOF	Yes	MA	Yulin, Guangxi	SAMN19591312
Alpiniae Oxyphyllae Fructus	GXA3	AOF	Yes	MA	Yulin, Guangxi	SAMN19591313

2.2. DNA Extraction

About 3 g of MOR (the dried root) or AOF (the dried ripe fruit) samples was transferred into a 50 mL sterilized centrifuge tube and mixed with 20 mL of sterilized water, and shaken for 20 min by a vortex mixer. Then, the mixture was filtered by Millipore filter membrane (50 mm diameter, 0.2 μm pore size). Total DNA was extracted by the cetyltrimethyl ammonium bromide method [24].

2.3. Polymerase Chain Reaction (PCR) Amplification and High-Throughput Sequencing (HTS)

The ITS1 region of the fungi was amplified with the primer pairs ITS1F (5′-CTTGGTCA TTTAGAGGAAGTAA-3′) [25] and ITS2R (5′-GCTGCGTTCTTCATCG ATGC-3′) [26]. PCR was performed on initial denaturation at 95 °C for 5 min, 34 cycles of denaturation at 95 °C for 45 s, 50 s annealing at 58 °C, 60 s elongation at 72 °C, and 10 min extension at 72 °C. The PCR product was detected by 2% agarose gel electrophoresis and purified using the Universal DNA Purification Kit (DP214) (TIANGEN Biotech Co., Ltd., Beijing, China). Then, the amplicons were sequenced on the IonS5™XL platform (Thermofisher, Waltham, MA, USA). Raw reads were submitted to the National Center for Biotechnology Information Sequence Read Archive database under the accession numbers SAMN19591296–SAMN19591313.

2.4. Data Analysis

Low-quality regions of the sequences were removed by Cutadapt (version 1.9.1) [27], and then the barcode and primer sequences were cut off to obtain the raw reads. Chimeric sequences were removed using USEARCH (version 8.1.1861) [28], and clean reads were clustered into operational taxonomic units (OTUs) at a 97% similarity level by UPARSE (version 7.1) [29]. OTUs were annotated according to the UNITE database ranging from kingdom to species level [30] and verified via manual search. Five metrics, Shannon, Chao 1, ACE, Simpson, and Good's coverage, were calculated by QIIME (version 1.9.1) [31] to assess alpha diversity. Statistical differences between MOR and AOF were examined by analysis of similarity (ANOSIM). Principal coordinate analysis (PCoA) on the basis of the Bray–Curtis distance matrix was applied to estimate the difference in the fungal community of samples from different species. The linear discriminant analysis effect

size (LEfSe) algorithm (LDA score = 4.0) was performed to distinguish the differentially abundant taxa between two groups [32]. Samples were hierarchically clustered by the unweighted pair group method with arithmetic mean (UPGMA) based on unweighted UniFrac distances. R tools (version 2.15.3) were applied to plot the rarefaction curves, heat map, and Venn diagram.

3. Results

3.1. Diversity Analysis of Fungal Microbiomes in MOR and AOF Samples

A total of 1,413,703 valid ITS1 sequences with an average length of 235 bp were obtained from 18 samples. The sequences were clustered into 579 OTUs (≥97% similarity, Table S1). Venn analysis exhibited that 91 and 76 OTUs were, respectively, unique for AOF and MOR groups, and the remaining 412 OTUs were common in the two groups (Figure 1a). Moreover, 282 OTUs were shared by 4 groups, and 23, 34, 43, and 28 OTUs were, respectively, unique for NM, MM, NA, and MA groups (Figure 1b). With the number of sequences sampled increasing, the rarefaction curves of all samples were parallel to the *x*-axis, which indicates the reliability of the sequencing depth employed (Figure 1c). The 5 alpha-diversity indices were employed to analyze the richness, diversity, and coverage of fungal microbiomes in 18 samples (Table 2). The Good's coverage was over 99.8%, which shows that the sampling depth satisfies the analysis requirements. In the MOR group, the ACE and Chao 1 indices of GDM were the highest, and the community richness was the highest. In contrast, GXM had the lowest community richness. The community diversity of GDM samples was the highest with the highest Shannon and Simpson indices. GXM had the lowest community diversity. Similarly, HNA and ACK in the AOF group had the highest community diversity and community richness, respectively. PCoA analysis showed that AOF and MOR groups were distinguishable (Figure 1d).
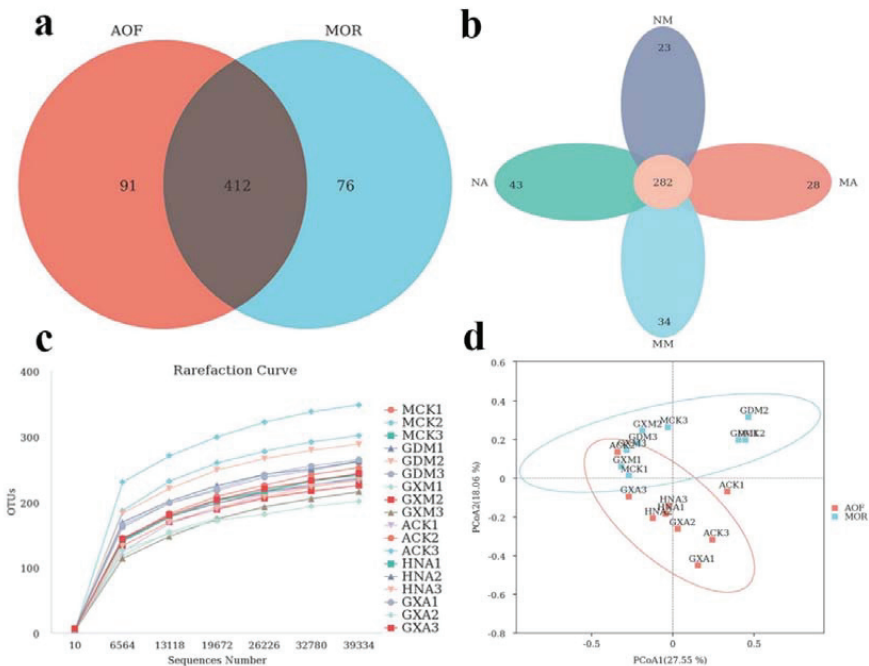
Figure 1. Analysis of fungal diversity in MOR and AOF samples. (**a**) Venn diagram of OTUs in the MOR and AOF groups; (**b**) Venn diagram of OTUs in the moldy and non-moldy samples; (**c**) Rarefaction curves for OTUs in all samples; and (**d**) PCoA diagram. of fungal compositions in samples.

Table 2. Alpha-diversity indices of samples.

Sample No.	Shannon	Simpson	Chao1	Ace	Goods_Coverage
MCK1	4.055	0.857	249.794	257.651	0.999
MCK2	3.791	0.779	364.441	354.497	0.998
MCK3	3.971	0.865	269.150	282.910	0.999
GDM1	4.412	0.910	315.250	297.879	0.998
GDM2	4.618	0.902	321.588	323.193	0.999
GDM3	4.068	0.840	347.370	333.659	0.998
GXM1	3.269	0.721	274.000	280.869	0.998
GXM2	3.441	0.751	243.077	253.748	0.999
GXM3	3.098	0.679	280.278	294.317	0.998
ACK1	3.122	0.740	349.241	330.054	0.998
ACK2	3.403	0.766	290.250	300.323	0.998
ACK3	4.050	0.745	424.241	402.027	0.998
HNA1	3.706	0.843	294.286	309.556	0.998
HNA2	4.886	0.931	315.038	308.207	0.999
HNA3	3.786	0.803	273.933	276.385	0.999
GXA1	3.476	0.712	311.838	322.078	0.998
GXA2	3.398	0.761	238.037	244.68	0.999
GXA3	4.064	0.839	257.500	269.869	0.999

3.2. Composition of Fungal Microbiomes in MOR and AOF Samples

In the MOR group, the dominant phylum was Ascomycota with a relative abundance of 49.53–94.32%, whereas the other phyla were low in abundance (Figure 2a). Eurotiomycetes, Dothideomycetes, and Sordariomycetes were dominant at the class level, accounting for 2.09–78.91%, 1.88–57.02%, and 0.60–20.37% of the fungal reads, respectively (Figure 2b). At the order level, Capnodiales was predominant in MCK1, GDM3, GXM1, GXM2, and GXM3, whereas Eurotiales was predominant in MCK2, MCK3, GDM1, and GDM2 (Figure 2c). Further taxonomical classification demonstrated that Aspergillaceae (1.90–76.73%) was the most dominant at the family level, followed by Cladosporiaceae (1.83–56.78%) and Trichocomaceae (0.12–20.45%, Figure 2d). At the genus level, *Penicillium* (1.86–76.14%), *Cladosporium* (1.82–56.65%), *Trichoderma* (0.12–19.71%), *Monascus* (0.00–19.35%), and *Talaromyces* (0.18–19.71%) were the top 5 genera with the highest relative abundance (Figure 3a). The top 20 abundant genera were visualized using a heatmap, which showed the relative abundance of fungal genera in different samples (Figure 3b).

In the AOF group, Ascomycota was the most abundant phylum representing 14.81–81.85%, followed by Basidiomycota (0.36–52.57%, Figure 4a). At the class level, Eurotiomycetes (0.57–56.84%), Tremellomycetes (0.11–51.81%), and Dothideomycetes (3.13–46.37%) were prevalent (Figure 4b). Among the 39 orders detected, Eurotiales, Tremellales, and Capnodiales were dominant with the relative abundances of 0.41–56.29%, 0.09–51.78%, and 3.11–46.30%, respectively (Figure 4c). At the family level, the dominant fungi in samples ACK1 and HNA3 were Aspergillaceae (56.17%) and Rhynchogastremataceae (51.71%), respectively. Cladosporiaceae was dominant in the rest of the samples representing 5.71–46.30% (Figure 4d). *Penicillium* (0.27–56.06%), *Papiliotrema* (0.04–51.71%), and *Cladosporium* (3.08–44.41%) were dominant at the genus level (Figure 5a). *Candida* was the subdominant genus in the ACK1 with the relative abundance of 11.95%, while it accounted for low levels in other samples (0.00–4.51%). A heatmap of the 20 most abundant genera is presented in Figure 5b.
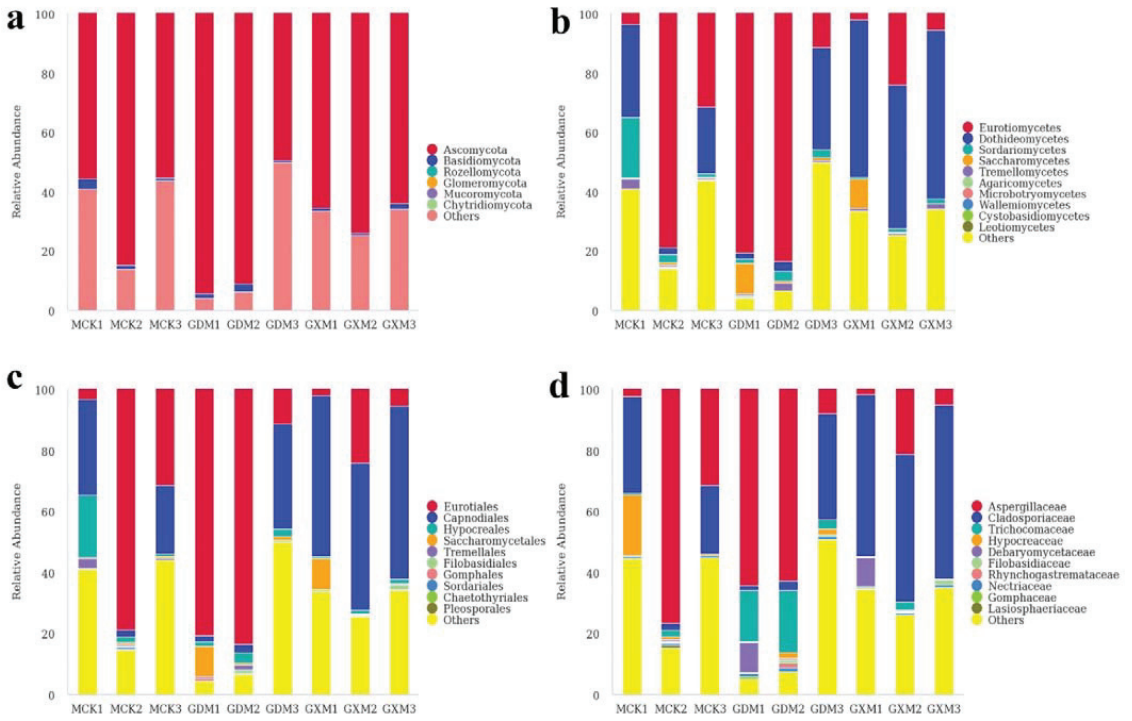
Figure 2. Fungal composition of the MOR samples at the phylum (**a**), class (**b**), order (**c**), and family (**d**) levels.
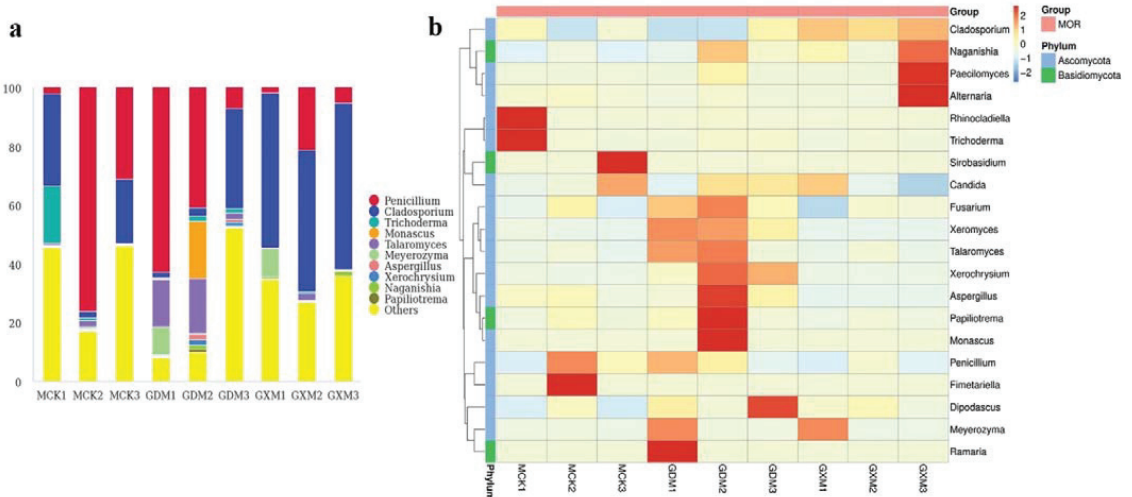
Figure 3. Composition analyses of the fungal microbiomes in the MOR samples. (**a**) Fungal composition in MOR samples at genus level; (**b**) Heatmap of the top 20 genera in MOR samples.
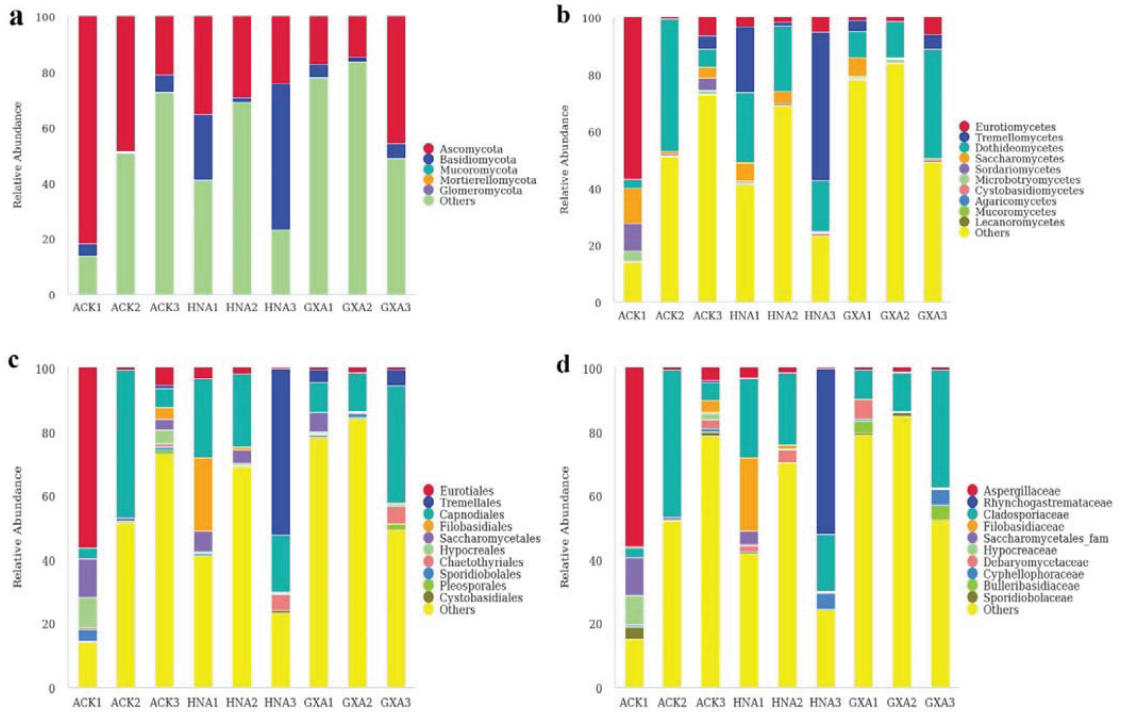
Figure 4. Fungal composition of the AOF samples at the phylum (**a**), class (**b**), order (**c**), and family (**d**) levels.
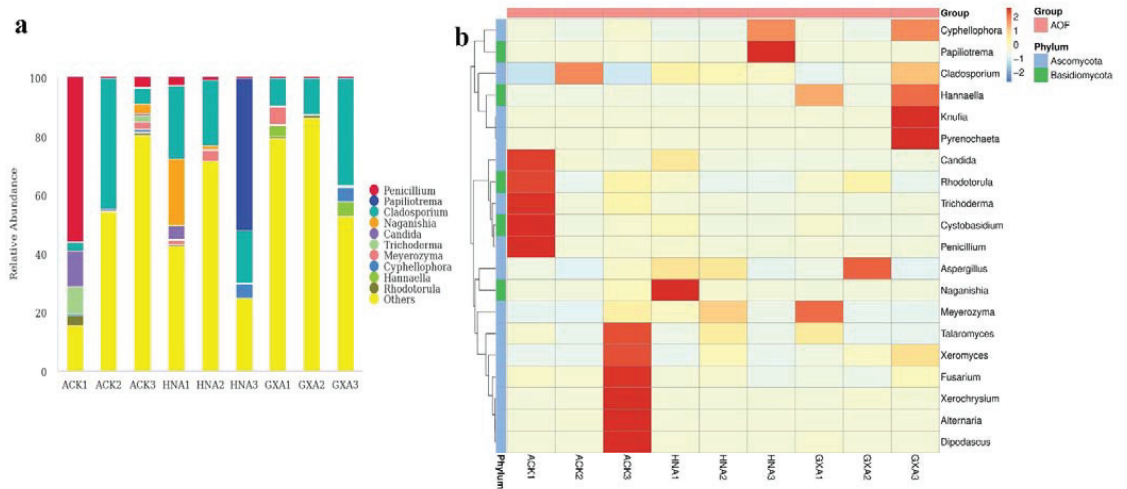
Figure 5. Composition analyses of the fungal microbiomes in the AOF samples. (**a**) Fungal composition in AOF samples at genus level; (**b**) Heatmap of the top 20 genera in AOF samples.

It is worth noting that a potential toxigenic fungus, namely, *Trichoderma atroviride*, was detected in all samples. Furthermore, another potential toxigenic fungus (*Fusarium equiseti*) was detected in four non-moldy samples (MCK1, MCK2, ACK1, and ACK3). The species and relative abundance of harmful fungi in each sample are shown in Supplementary Table S2.

3.3. Comparison of Fungal Microbiomes in MOR and AOF

ANOSIM analysis was applied to test the difference between the two groups; the results show that MOR and AOF express statistical differences in fungal microbiomes ($R = 0.2$, $p = 0.009$, Figure 6a). LEfSe analysis was performed to calculate the differences in fungal taxa from the phylum to species level between different groups (LDA score = 4.0). In contrast to AOF samples, MOR samples had more abundant Ascomycota, but had less Basidiomycota. The relative abundance of the Aspergillaceae family was much higher in MOR samples, whereas Amanitaceae was more abundant in AOF samples. *Penicillium* and *Talaromyces* were detected more frequently in MOR samples, whereas *Amanita* was more abundant in AOF samples (Figure 6b).
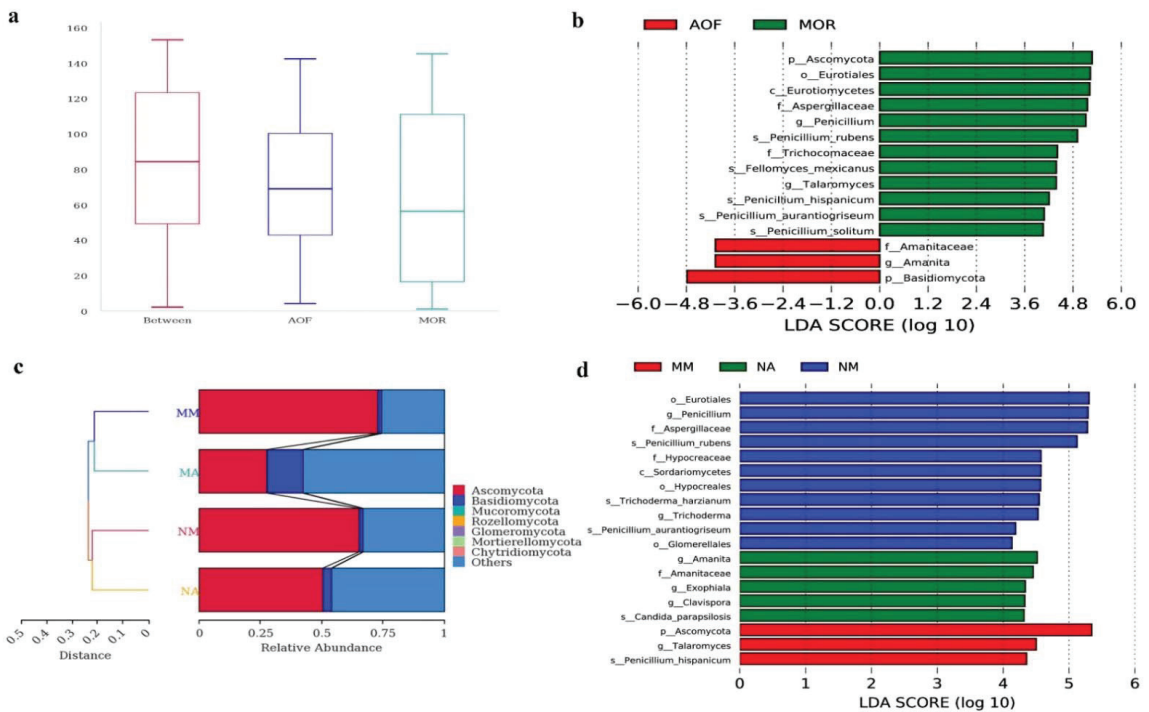
Figure 6. Comparison of fungal microbiomes in the MOR and AOF samples. (**a**) Evident difference in fungal microbiomes between the MOR and AOF groups based on ANOSIM; (**b**) Differentially abundant fungal taxa between the MOR and AOF groups; (**c**) UPGMA clustering based on unweighted UniFrac distance analysis; and (**d**) Differentially abundant fungal taxa between the moldy and non–moldy samples.

As for the moldy and non-moldy samples, the result of hierarchical clustering analysis indicates that samples are clustered according to the presence or absence of macroscopic molds (Figure 6c). LEfSe analysis showed that none of the fungal taxa was found to be enriched in the MA group. In the NM group, three orders (Eurotiales, Hypocreales, and Glomerellales), two families (Aspergillaceae and Hypocreaceae), and two genera (*Penicillium* and *Trichoderma*) were enriched. In the NA group, one family (Amanitaceae) and three genera (*Amanita*, *Exophiala*, and *Clavispora*) were enriched. Moreover, *Talaromyces* was enriched in the MM group (Figure 6d).

4. Discussion

4.1. The Necessity of Characterizing Fungal Microbiomes in MOR and AOF Samples

MOR and AOF are derived from the roots and fruits of plants, respectively. They are susceptible to fungal contamination during pre- and post-harvest processes owing to the lack of standard management. In our study, all 18 samples were contaminated with fungi. The relative abundances of fungi were varied in different samples. Ascomycota, Eurotiomycetes, Eurotiales, and Aspergillaceae were generally dominant at the phylum, class, order, and family levels in AOF and MOR samples, respectively. In general, *Penicillium* and *Cladosporium* were the dominant genera. In our previous studies, the predominant genus in four seed herbs (Platycladi Semen, Myristicae Semen, and Cassiae Semen) was *Aspergillus* [33–35]. The relationship between dominant fungi and herbs has not been well explained, owing to the complex factors that influence the fungal community. The storage conditions and matrix composition of CHMs may be responsible for the difference in fungal microbiomes between MOR and AOF. Moreover, the fungal microbiomes between moldy and non-moldy samples are different. All samples were clustered based on the presence or absence of visible molds in UPGMA, thus indicating the meaningfulness of grouping. *Cladosporium* and *Penicillium* were dominant in moldy and non-moldy samples, respectively.

Notably, all samples were contaminated with a potential toxigenic fungus, namely, *Trichoderma atroviride*. Additionally, four non-moldy samples were contaminated with another toxigenic fungus (*Fusarium equiseti*). Trichothecenes and zearalenone, which disturb hormonal balance and cause numerous diseases in the reproductive system, can be produced by *F. equiseti* [36,37]. The findings of our study are consistent with another study; potential mycotoxin-producing fungi were detected in non-moldy and moldy Ziziphi Spinosae Semen samples [38]. Similarly, Wei et al. detected AFs and OTA in six moldy and nine non-visible moldy *Glycyrrhiza uralensis* samples collected from China [39]. Therefore, the safety assessment of CHMs should not depend on whether macroscopic molds are present or not. Characterizing fungal microbiomes, especially potential toxigenic fungi, in MOR and AOF samples is essential, which is providing an early warning for mycotoxin contamination.

4.2. DNA Metabarcoding Is a Powerful Tool for the Analysis of Fungal Diversity in CHMs

Mycotoxins, the toxic secondary metabolites, can lead to numerous health problems and even death in just small intakes, and they are mainly produced by *Penicillium*, *Aspergillus*, and *Fusarium* [40]. Mycotoxins cannot degrade during storage and are difficult to remove from CHMs because of their thermostability [41,42]. Moreover, considerable transfer rates of AFs and OTA have been observed from herbal medicines to decoctions and pose a threat to consumer health [43,44]. Comprehensive and efficient fungi identification in CHMs is an important basis for preventing fungal and mycotoxin contamination. Current assessment methods for fungal contamination in CHMs are based on fungal isolation and culture, which may affect the real extent of fungal diversities because of the difficulty to cultivate and isolate certain microorganisms. The application of DNA metabarcoding could overcome this limitation and better reveal the fungal diversity. For example, Xia et al. found that 55 genera in Chinese Cordyceps that were not observed by culture-dependent methods were identified through Illumina Miseq sequencing [45]. Similarly, another study indicated that the number of fungi in Coix Seed detected by HTS was considerably greater than that by potato dextrose agar medium [46]. In addition, DNA metabarcoding also overcomes some of the limitations of a culture-dependent approach (e.g., time-consuming and complicated procedure). It could be used as an effective tool for the simultaneous characterization of numerous microbial species. In previous studies, DNA metabarcoding has been successfully applied in the investigation of fungal contamination in Platycladi Semen [33], Myristicae Semen [34], and Cassiae Semen [35]. In the present study, DNA metabarcoding efficiently analyzed the fungal microbiomes in MOR and AOF. Thus, it can serve as a powerful tool for identifying fungi in CHMs.

5. Conclusions

The fungal microbiomes in MOR and AOF were first investigated by DNA metabarcoding. The results highlight the effectiveness of the technique to analyze fungal diversity in CHMs and the need for the surveillance of marketed herbs to guarantee quality. This study provided an early warning for subsequent potential mycotoxin biosynthesis and can serve as a basis for the safe use of edible medicinal herbs.

References

1. Chan, K. Some aspects of toxic contaminants in herbal medicines. *Chemosphere* **2003**, *52*, 1361–1371. [CrossRef]
2. Ghisleni, D.D.M.; Braga, M.D.S.; Kikuchi, I.S.; Braşoveanu, M.; Nemţanu, M.R.; Dua, K.; Pinto, T.D.J.A. The Microbial Quality Aspects and Decontamination Approaches for the Herbal Medicinal Plants and Products: An in-Depth Review. *Curr. Pharm. Des.* **2016**, *22*, 4264–4287. [CrossRef] [PubMed]
3. de Sousa Lima, C.M.; Fujishima, M.A.T.; de Paula Lima, B.; Mastroianni, P.C.; de Sousa, F.F.O.; da Silva, J.O. Microbial contamination in herbal medicines: A serious health hazard to elderly consumers. *BMC Complement. Med. Ther.* **2020**, *20*, 17. [CrossRef] [PubMed]
4. Keter, L.; Too, R.; Mwikwabe, N.; Mutai, C.; Orwa, J.; Mwamburi, L.; Ndwigah, S.; Bii, C.; Korir, R. Risk of Fungi Associated with Aflatoxin and Fumonisin in Medicinal Herbal Products in the Kenyan Market. *Sci. World J.* **2017**, *2017*, 1892972. [CrossRef] [PubMed]
5. Reinholds, I.; Bogdanova, E.; Pugajeva, I.; Alksne, L.; Stalberga, D.; Valcina, O.; Bartkevics, V. Determination of Fungi and Multi-Class Mycotoxins in Camelia sinensis and Herbal Teas and Dietary Exposure Assessment. *Toxins* **2020**, *12*, 555. [CrossRef] [PubMed]
6. Waśkiewicz, A.; Beszterda, M.; Bocianowski, J.; Goliński, P. Natural occurrence of fumonisins and ochratoxin A in some herbs and spices commercialized in Poland analyzed by UPLC–MS/MS method. *Food Microbiol.* **2013**, *36*, 426–431. [CrossRef] [PubMed]
7. Su, C.; Hu, Y.; Gao, D.; Luo, Y.I.; Chen, A.J.; Jiao, X.; Gao, W. Occurrence of Toxigenic Fungi and Mycotoxins on Root Herbs from Chinese Markets. *J. Food Prot.* **2018**, *81*, 754–761. [CrossRef]
8. Chinese Pharmacopeia Commission. *Pharmacopoeia of People's Republic of China (Part 1)*; China Medical Science Press: Beijing, China, 2020; pp. 83, 303.
9. Yip, K.; Xu, J.; Zhou, S.; Lau, Y.; Chen, Q.; Tang, Y.; Yang, Z.; Yao, Z.; Ding, P.; Chen, H.; et al. Characterization of Chemical Component Variations in Different Growth Years and Tissues of Morindae Officinalis Radix by Integrating Metabolomics and Glycomics. *J. Agric. Food Chem.* **2019**, *67*, 7304–7314. [CrossRef]
10. Liang, J.; Liang, J.; Hao, H.; Lin, H.; Wang, P.; Wu, Y.; Jiang, X.; Fu, C.; Li, Q.; Ding, P.; et al. The Extracts of Morinda officinalis and Its Hairy Roots Attenuate Dextran Sodium Sulfate-Induced Chronic Ulcerative Colitis in Mice by Regulating Inflammation and Lymphocyte Apoptosis. *Front. Immunol.* **2017**, *8*, 905. [CrossRef]
11. Song, B.; Wang, F.; Wang, W. Effect of Aqueous Extract from Morinda officinalis F. C. How on Microwave-Induced Hypothalamic-Pituitary-Testis Axis Impairment in Male Sprague-Dawley Rats. *Evid. Based Complement. Altern. Med.* **2015**, *2015*, 360730. [CrossRef]
12. Chi, L.; Khan, I.; Lin, Z.; Zhang, J.; Lee, M.Y.S.; Leong, W.; Hsiao, W.L.W.; Zheng, Y. Fructo-oligosaccharides from Morinda officinalis remodeled gut microbiota and alleviated depression features in a stress rat model. *Phytomedicine* **2020**, *67*, 153157. [CrossRef] [PubMed]

13. Zhang, Z.; Zhang, Q.; Yang, H.; Liu, W.; Zhang, N.; Qin, L.; Xin, H. Monotropein isolated from the roots of Morinda officinalis increases osteoblastic bone formation and prevents bone loss in ovariectomized mice. *Fitoterapia* **2016**, *110*, 166–172. [CrossRef] [PubMed]

14. Zhang, J.H.; Xin, H.L.; Xu, Y.M.; Shen, Y.; He, Y.Q.; Hsien-Yeh; Lin, B.; Song, H.T.; Yang, H.Y.; Qin, L.P.; et al. Morinda officinalis How. A comprehensive review of traditional uses, phytochemistry and pharmacology. *J. Ethnopharmacol.* **2018**, *213*, 230–255. [CrossRef] [PubMed]

15. Qing, Z.J.; Yong, W.; Hui, L.Y.; Yong, L.W.; Long, L.H.; Ao, D.J.; Xia, P.L. Two new natural products from the fruits of Alpinia oxyphylla with inhibitory effects on nitric oxide production in lipopolysaccharide-activated RAW264.7 macrophage cells. *Arch. Pharm. Res.* **2012**, *35*, 2143–2146. [CrossRef] [PubMed]

16. Li, Y.H.; Chen, F.; Wang, J.F.; Wang, Y.; Zhang, J.Q.; Guo, T. Analysis of nine compounds from Alpinia oxyphylla fruit at different harvest time using UFLC-MS/MS and an extraction method optimized by orthogonal design. *Chem. Cent. J.* **2013**, *7*, 134. [CrossRef] [PubMed]

17. An, L.J.; Guan, S.; Shi, G.F.; Bao, Y.M.; Duan, Y.L.; Jiang, B. Protocatechuic acid from Alpinia oxyphylla against MPP+-induced neurotoxicity in PC12 cells. *Food Chem. Toxicol.* **2006**, *44*, 436–443. [CrossRef]

18. Shi, G.F.; An, L.J.; Jiang, B.; Guan, S.; Bao, Y.M. Alpinia protocatechuic acid protects against oxidative damage in vitro and reduces oxidative stress in vivo. *Neurosci. Lett.* **2006**, *403*, 206–210. [CrossRef] [PubMed]

19. Jiang, K.; Huang, D.; Zhang, D.; Wang, X.; Cao, H.; Zhang, Q.; Yan, C. Investigation of inulins from the roots of Morinda officinalis for potential therapeutic application as anti-osteoporosis agent. *Int. J. Biol. Macromol.* **2018**, *120*, 170–179. [CrossRef]

20. Zhao, X.; Wei, J.; Zhou, Y.; Kong, W.; Yang, M. Quality evaluation of Alpinia oxyphylla after Aspergillus flavus infection for storage conditions optimization. *AMB Express* **2017**, *7*, 151. [CrossRef]

21. Taberlet, P.; Coissac, E.; Pompanon, F.; Christian, B.; Eske, W. Towards next-generation biodiversity assessment using DNA metabarcoding. *Mol. Ecol.* **2012**, *21*, 2045–2050. [CrossRef]

22. Schoch, C.L.; Seifert, K.A.; Huhndorf, S.; Robert, V.; Spouge, J.L.; Levesque, C.A.; Chen, W. Nuclear ribosomal internal transcribed spacer (ITS) region as a universal DNA barcode marker for Fungi. *Proc. Natl. Acad. Sci. USA* **2012**, *109*, 6241–6246. [CrossRef] [PubMed]

23. Nilsson, R.H.; Anslan, S.; Bahram, M.; Wurzbacher, C.; Baldrian, P.; Tedersoo, L. Mycobiome diversity: High-throughput sequencing and identification of fungi. *Nat. Rev. Microbiol.* **2019**, *17*, 95–109. [CrossRef] [PubMed]

24. Huang, X.; Duan, N.; Xu, H.; Xie, T.N.; Xue, Y.R.; Liu, C.H. CTAB-PEG DNA Extraction from Fungi with High Contents of Polysaccharides. *Mol. Biol.* **2018**, *52*, 718–726. [CrossRef]

25. Gardes, M.; Bruns, T.D. ITS primers with enhanced specificity for basidiomycetes—Application to the identification of mycorrhizae and rusts. *Mol. Ecol.* **1993**, *2*, 113–118. [CrossRef] [PubMed]

26. White, T.J.; Bruns, T.; Lee, S.; Taylor, J. Amplification and Direct Sequencing of Fungal Ribosomal Rna Genes for Phylogenetics. In *PCR Protocols*; Innis, M.A., Gelfand, D.H., Sninsky, J.J., White, T.J., Eds.; Academic Press: San Diego, CA, USA, 1990; pp. 315–322.

27. Martin, M. Cutadapt removes adapter sequences from high-throughput sequencing reads. *EMBnet J.* **2021**, *1*, 10–12. [CrossRef]

28. Edgar, R.C. Search and clustering orders of magnitude faster than BLAST. *Bioinformatics* **2010**, *26*, 2460–2461. [CrossRef]

29. Edgar, R.C. UPARSE: Highly accurate OTU sequences from microbial amplicon reads. *Nat. Methods* **2013**, *10*, 996–998. [CrossRef]

30. Nilsson, R.H.; Larsson, K.H.; Taylor, A.; Bengtsson-Palme, J.; Jeppesen, T.S.; Schigel, D.; Kennedy, P.; Picard, K.; Glockner, F.O.; Tedersoo, L.; et al. The UNITE database for molecular identification of fungi: Handling dark taxa and parallel taxonomic classifications. *Nucleic Acids Res.* **2019**, *47*, D259–D264. [CrossRef]

31. Caporaso, J.G.; Kuczynski, J.; Stombaugh, J.; Bittinger, K.; Bushman, F.D.; Costello, E.K.; Fierer, N.; Pẽa, A.G.; Goodrich, J.K.; Gordon, J.I.; et al. QIIME allows analysis of high-throughput community sequencing data. *Nat. Methods* **2010**, *7*, 335–336. [CrossRef]

32. Segata, N.; Izard, J.; Waldron, L.; Gevers, D.; Miropolsky, L.; Garrett, W.S.; Huttenhower, C. Metagenomic biomarker discovery and explanation. *Genome Biol.* **2011**, *12*, R60. [CrossRef]

33. Yu, J.; Guo, M.; Jiang, W.; Yang, M.; Pang, X. Assessment of the Microbiome and Potential Aflatoxin Associated with the Medicinal Herb Platycladus orientalis. *Front Microbiol.* **2020**, *11*, 582679. [CrossRef] [PubMed]

34. Jiang, W.; Guo, M.; Yang, M.; Mantri, N.; Chen, X.; Pang, X. High-throughput analysis of fungal communities in Myristicae Semen. *LWT Food Sci. Technol.* **2020**, *128*, 109499. [CrossRef]

35. Guo, M.; Jiang, W.; Yang, M.; Dou, X.; Pang, X. Characterizing fungal communities in medicinal and edible Cassiae Semen using high-throughput sequencing. *Int. J. Food Microbiol.* **2020**, *319*, 108496. [CrossRef] [PubMed]

36. Kowalska, K.; Habrowska-Gorczynska, D.E.; Piastowska-Ciesielska, A.W. Zearalenone as an endocrine disruptor in humans. *Environ. Toxicol. Pharmacol.* **2016**, *48*, 141–149. [CrossRef] [PubMed]

37. Barros, G.; Zanon, M.S.; Palazzini, J.M.; Haidukowski, M.; Pascale, M.; Chulze, S. Trichothecenes and zearalenone production by Fusarium equiseti and Fusarium semitectum species isolated from Argentinean soybean. *Food Addit. Contam. Part A Chem. Anal. Control Expo. Risk Assess.* **2012**, *29*, 1436–1442. [CrossRef] [PubMed]

38. Guo, M.; Jiang, W.; Luo, J.; Yang, M.; Pang, X. Analysis of the Fungal Community in Ziziphi Spinosae Semen through High-Throughput Sequencing. *Toxins* **2018**, *10*, 494. [CrossRef]

39. Wei, R.; Qiu, F.; Kong, W.; Wei, J.; Yang, M.; Luo, Z.; Qin, J.; Ma, X. Co-occurrence of aflatoxin B1, B2, G1, G2 and ochrotoxin A in Glycyrrhiza uralensis analyzed by HPLC-MS/MS. *Food Control* **2013**, *32*, 216–221. [CrossRef]

40. Prouillac, C.; Koraichi, F.; Videmann, B.; Mazallon, M.; Rodriguez, F.; Baltas, M.; Lecoeur, S. In vitro toxicological effects of estrogenic mycotoxins on human placental cells: Structure activity relationships. *Toxicol. Appl. Pharmacol.* **2012**, *259*, 366–375. [CrossRef]
41. Zinedine, A.; Soriano, J.M.; Molto, J.C.; Manes, J. Review on the toxicity, occurrence, metabolism, detoxification, regulations and intake of zearalenone: An oestrogenic mycotoxin. *Food Chem. Toxicol.* **2007**, *45*, 1–18. [CrossRef]
42. Kong, W.; Wei, R.; Logrieco, A.F.; Wei, J.; Wen, J.; Xiao, X.; Yang, M. Occurrence of toxigenic fungi and determination of mycotoxins by HPLC-FLD in functional foods and spices in China markets. *Food Chem.* **2014**, *146*, 320–326. [CrossRef]
43. Nian, Y.; Wang, H.; Ying, G.; Yang, M.; Wang, Z.; Kong, W.; Yang, S. Transfer rates of aflatoxins from herbal medicines to decoctions determined by an optimized high-performance liquid chromatography with fluorescence detection method. *J. Pharm. Pharmacol.* **2018**, *70*, 278–288. [CrossRef] [PubMed]
44. Shim, W.B.; Ha, K.S.; Kim, M.G.; Kim, J.S.; Chung, D.H. Evaluation of the transfer rate of ochratoxin a to decoctions of herbal medicines. *Food Sci. Biotechnol.* **2014**, *23*, 2103–2108. [CrossRef]
45. Xia, F.; Chen, X.; Guo, M.Y.; Bai, X.H.; Liu, Y.; Shen, G.R.; Li, Y.L.; Lin, J.; Zhou, X.W. High-throughput sequencing-based analysis of endogenetic fungal communities inhabiting the Chinese Cordyceps reveals unexpectedly high fungal diversity. *Sci. Rep.* **2016**, *6*, 33437. [CrossRef] [PubMed]
46. Luo, X.; Li, H.; Jiang, D.; Meng, J.; Zhang, F.; Xu, Q.; Chen, X.; Liu, C.; Yang, Y. Analysis of Fungi on Coix (Coix lacryma-jobi) Seed and the Effect of Its Aqueous Extract on the Growth of Aspergillus flavus. *J. Food Prot.* **2019**, *82*, 1775–1782. [CrossRef]

Impact of Potentially Toxic Compounds in Cow Milk: How Industrial Activities Affect Animal Primary Productions

Sergio Forcada [1,*], Mario Menéndez-Miranda [1], Carlos Boente [2], José Luis Rodríguez Gallego [3], José M. Costa-Fernández [4], Luis J. Royo [1,5] and Ana Soldado [4,*]

[1] Regional Service for Agrofood Research and Development (SERIDA), P.O. Box 13, 33300 Villaviciosa, Asturias, Spain

[2] Atmospheric Pollution Laboratory, CIQSO-Center for Research in Sustainable Chemistry, Associate Unit CSIC-University of Huelva, Campus El Carmen s/n, 21071 Huelva, Huelva, Spain

[3] Environmental Biogeochemistry & Raw Materials Group and INDUROT, Campus de Mieres, University of Oviedo, C/Gonzalo Gutiérrez Quirós s/n, 33600 Mieres, Asturias, Spain; jgallego@uniovi.es

[4] Department of Physical and Analytical Chemistry, Faculty of Chemistry, University of Oviedo, Avda. Julián Clavería 8, 33006 Oviedo, Asturias, Spain; jcostafe@uniovi.es

[5] Department of Functional Biology, Genetics, University of Oviedo, Avda. Julián Clavería 6, 33006 Oviedo, Asturias, Spain

* Correspondence: sforcada@serida.org (S.F.); soldadoana@uniovi.es (A.S.)

Abstract: Potentially toxic elements (PTEs) and polycyclic aromatic hydrocarbons (PAHs) frequently coexist in soils near industrial areas and sometimes in environmental compartments directly linked to feed (forage) and food (milk) production. However, the distribution of these pollutants along the dairy farm production chain is unclear. Here, we analyzed soil, forage, and milk samples from 16 livestock farms in Spain: several PTEs and PAHs were quantified. Farms were compared in terms of whether they were close to (<5 km) or far away from (>5 km) industrial areas. The results showed that PTEs and PAHs were enriched in the soils and forages from farms close to industrial areas, but not in the milk. In the soil, the maximum concentrations of PTEs reached 141, 46.1, 3.67, 6.11, and 138 mg kg^{-1} for chromium, arsenic, cadmium, mercury, and lead, respectively, while fluoranthene (172.8 µg kg^{-1}) and benzo(b)fluoranthene (177.4 µg kg^{-1}) were the most abundant PAHs. Principal component analysis of the soil PTEs suggested common pollution sources for iron, arsenic, and lead. In the forage, the maximum contents of chromium, arsenic, cadmium, mercury, and lead were 32.8, 7.87, 1.31, 0.47, and 7.85 mg kg^{-1}, respectively. The PAH found in the highest concentration in the feed forage was pyrene (120 µg kg^{-1}). In the milk, the maximum PTE levels were much lower than in the soil or the feed forages: 74.1, 16.1, 0.12, 0.28, and 2.7 µg kg^{-1} for chromium, arsenic, cadmium, mercury, and lead, respectively. Neither of the two milk samples exceeded the 20 µg kg^{-1} limit for lead set in EU 1881/2006. Pyrene was the most abundant PAH found in the milk (39.4 µg kg^{-1}), while high molecular weight PAHs were not detected. For PTEs, the results showed that soil–forage transfer factors were higher than forage–milk ratios. Our results suggest that soils and forages around farms near industries, as well as the milk produced from those farms, have generally low levels of PTE and PAH contaminants.

Keywords: pollution; soil; forage; milk; polycyclic aromatic hydrocarbon; potentially toxic element

1. Introduction

Cow milk is considered a nearly complete food because of its high content of protein, fat, and essential minerals, yet the potential presence of contaminants in milk constitutes a health concern. This is particularly true in light of the fact that cow milk is one of the main constituents of the daily diet in many countries, especially for vulnerable groups, infants, and elderly people [1]. Guidelines from the European Union Common Agricultural Policy aim to ensure a high level of food safety and animal health through coherent "farm to fork"

measures and adequate monitoring. This necessitates exhaustive characterization of farms at different levels of the production chain.

In the case of dairy farms, this characterization includes the milk and even the soil where crops are cultivated for animal forage (feed forage). Many dairy farms in northern Spain, for example, produce their own forage crops as a traditional practice [2], and forage-based animal nutrition depends strongly on local geographical conditions [3]. The growth of cities and industrial expansion means that many farms lie near cities or industrial zones that emit pollutants into the atmosphere and wastewater. This increases the risk of soil contamination, potentially compromising animal food safety. In fact, hazardous compounds in the soil can pose a risk to animals and to humans who consume animal-derived products [4,5].

Potentially toxic elements (PTEs), mainly heavy metals and metalloids, pose a growing hazard in the environment [6]. Those elements named as heavy metals are referred to by their high atomic mass and density. Their persistence in the soil, reflecting their resistance to degradation, makes them the most dangerous group of inorganic contaminants. While the PTEs iron (Fe), cobalt (Co), copper (Cu), manganese (Mn), molybdenum (Mo), and zinc (Zn) are essential for humans and cattle in trace amounts, they are toxic at higher concentrations [7,8]. The PTEs arsenic (As), mercury (Hg), cadmium (Cd), and lead (Pb) are considered toxic even at low concentrations and can cause serious illness if they accumulate in an organism [8]. PTEs can enter the food chain by first entering the soil from the atmosphere or as a result of irrigation with polluted water or deposition of animal manure, agrochemicals, and inorganic fertilizers [8,9], as well as wastewater filtration derived from industrial activities [10]. It appears that PTEs can enter forage crops and then the milk of dairy cattle that feed on that forage [9,11,12].

In addition to PTEs, polycyclic aromatic hydrocarbons (PAHs) are also widespread pollutants in soil, water, air, and plants [13–15]. They primarily result from the incomplete combustion or pyrolysis of organic materials, through incineration or industrial activities [4]. The U.S. Environmental Protection Agency categorizes 16 PAHs as priority pollutants due to their mutagenic and carcinogenic properties. PAHs can enter plants from the soil [16] and then transfer to the milk of dairy cows that eat the plants as forage, ultimately passing to humans who drink the milk [17–19]. In addition, the lipophilicity of PAHs may facilitate their accumulation in milk [20]. Considering this, the European Union has established maximum permissible limits for certain PAHs in certain foods likely to contain these contaminants. An example is milk and follow-on milk intended for infants, with a maximum permissible content of 1 μg L^{-1} of benzo(a)pyrene or 1 μg L^{-1} of the sum of benzo(a)pyrene, benzo(a)anthracene, benzo(b)fluoranthene, and chrysene [21].

PTEs and PAHs frequently coexist in soils in proximity to highways and certain industries, such as the smelting and mining industries [22,23]. Therefore, it is quite important to assess the risk that milk produced from dairy farms near these areas may be contaminated with PAHs and PTEs. Northern Spain provides a good study area, since many dairy farms are located close to active industrial facilities. Here, we quantified several PTEs and PAHs of concern in soil, forage, and milk samples on farms near and farther from industrial areas in northern Spain, and we evaluated the transfer of these contaminants into milk.

2. Materials and Methods

2.1. Reagents

Ultrapure water ($\geq$18 MΩ-cm resistivity; $\leq$5 μg L^{-1} TOC) was obtained from a Milli-Q IQ 7000 purification system (Merck Millipore, Darmstadt, Germany). Elemental calibration solutions for inductively coupled plasma mass spectrometry (ICP-MS) were obtained from HPS (North Charleston, Charleston, SC, USA) and were prepared as 1 g L^{-1} solutions in 1% nitric acid. All dilutions were performed with analytical-grade 65% nitric acid (Suprapur®) or 30% hydrochloric acid (Merck, Darmstadt, Germany). Our analytical procedures were validated using the following Certified European Reference Materials

(IRMM, Geel, Belgium): "ERM-CC141 Loam soil", "ERM-CD281 Rye grass", and "ERM-BD151 Skimmed milk powder".

2.2. Sample Collection

Soil, milk, and forages (fresh or silage, depending on the farm stock) were sampled at 16 dairy farms, each of which had no more than 40 heads of cattle. As the studied area comprises multiple pollution sources, 10 farms were classified as close to industries (having one or more pollution sources less than 5 km away), while 6 farms were grouped as far (located 5 km or more from each pollution source). This 5 km distance was chosen to provide a compromise between the total farms sampled—those at maximum distance (classified as far) and those near to industries. Sampling on each farm was performed in autumn, spring, and summer in order to assess reproducibility. The soil samples from the upper layer soil (20 cm) were collected in three random points per cropland with a Dutch auger of 5 cm inner diameter. Once in the laboratory, the samples were air-dried at room temperature, crumbled, finely crushed, and sieved through a 2 mm screen [9,11,24]. Forage samples consisted of grass-based fodder and they were either fresh or preserved as silage (grass chopped and packaged without air to facilitate the fermentation process and minimize nutrient losses, for use as animal feed). Forage samples were collected at three points in the trough, then pooled to a total mass of around 1 kg. Milk samples (1 L) were collected directly from the tank after stirring. Figure 1 summarizes the sample collection and processing.
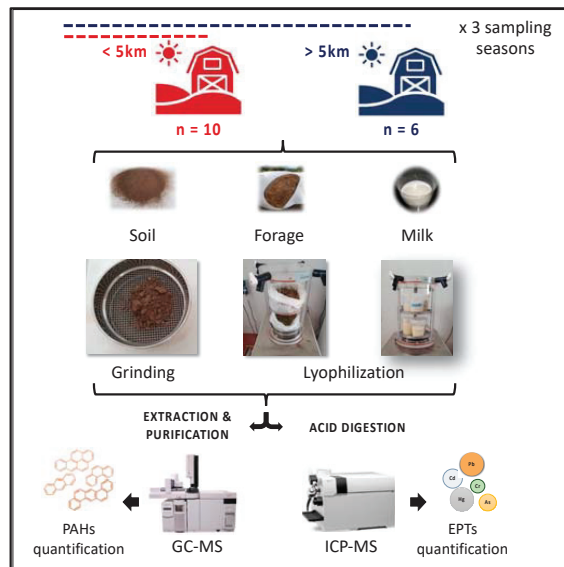
Figure 1. Sampling collection and processing of soil, forage, and tank milk from the selected farms.

2.3. Sample Preparation

Soil samples were dried, ground, and sieved through a 2 mm sieve. Freshly collected samples of forage, silage, and total mixed rations were freeze-dried in a Coolsafe Pro 100-9 system (Labogene, Allerød, Denmark), ground, and stored at room temperature until analysis. Milk was freeze-dried under the same conditions and stored at −80 °C until analysis (see Figure 1). Samples were analyzed within a maximum time of six months.

2.4. Determination of Inorganic Elements in Soil, Forage, and Milk by ICP-MS

Procedures to quantify inorganic elements were based on official methods for trace element determination by ICP-MS: ISO/TS 16965:2013, EN 17053:2018 and ISO 15151:2018

for soils, animal feed, and milk, respectively. All of them were self-optimized and validated in our laboratory by using different European reference materials (Joint Research Centre, EU): loam soil (ERM CD-141), rye grass (ERM CD-281), and skimmed milk powder (ERM BD-151). Accuracy, reproducibility, and optimization of these procedures are detailed in Appendix A.

Samples of soil (0.1 g), forage (0.5 g), or milk powder (0.5 g) were digested in 8 mL of aqua regia (HCl:HNO$_3$ 3:1) in closed polytetrafluoroethylene vessels using an Ethos One microwave digestion system (Milestone Srl., Sorisole, BG, Italy), as described in Table A2. The digested solution was filtered through a 0.22 μm syringe filter (Merck Millipore, Billerica, MA, USA), then diluted to 40 mL with ultrapure water in the case of forage and milk samples [overall dilution, 1:80 (*w/v*)] or 20 mL in the case of soil samples. An aliquot (1 mL) of diluted soil samples was then diluted to 10 mL [overall dilution, 1:2000 (*w/v*)].

Standard metal solutions were prepared daily. Solutions of Na, K, Mg, and Ca were prepared from a multi-elemental stock solution (1000 μg mL^{-1}), while solutions of Cr, Zn, Fe, Cu, As, Se, Cd, and Pb were added from individual stock solutions (1000 μg mL^{-1}). All standards were prepared in 1% HNO$_3$. Internal standards (HPS, North Charleston, Charleston, SC, USA) were as follows: ^{45}Sc for Na, K, Ca, and Mg; ^{72}Ge for Cr, Fe, Cu, Zn, Se, and As; ^{103}Rh for Cd; and ^{193}Ir for Hg and Pb. Samples were analyzed per duplicate.

The content of inorganic elements in the soil and forage samples was calculated in terms of dry weight, while the content of inorganic elements in the milk was calculated in terms of wet weight after applying a correction factor based on mean water content (88%) [25]. The assay procedures were validated per triplicate for the three sample matrices using the Certified European Reference Materials, as set out in Section 2.1. Elements whose concentrations were not reported in the reference materials were spiked into the materials. Recoveries in ryegrass ranged from 93% for Cd to 114% for Ca, while those in skimmed milk powder ranged from 88% for Pb to 113% for Cr (Table A2).

2.5. Determination of PAHs in Soil, Forage, and Milk by Gas Chromatography–Tandem Mass Spectrometry (GC-MS/MS)

Soil samples (10 g) were extracted with dichloromethane:acetone [1:1 (*v/v*)] in a Soxtherm system (Gerhardt, Bonn, Germany). The extracts were cleaned with silica gel, then concentrated by rotary evaporation (Heidolph, Schwabach, Germany). PAH concentrations were determined after injection into a 7890A GC System coupled to a 5975C Inert XL MSD with a Triple-Axis Detector (Agilent Tech., Santa Clara, CA, USA), following EPA Method 8272, with modifications. The samples were run on a capillary column DB-5ms with a length of 30 m, an inner diameter of 0.25 mm, and a film thickness of 0.25 μm (Agilent Tech. Santa Clara, CA, USA), with He as the carrier gas at 1 mL min^{-1}. The initial oven temperature of 70 °C was held for 2 min; ramped up to 220 °C at 20 °C min^{-1}, then to 270 °C at 10 °C min^{-1}, where it was held for 1 min; ramped up to 290 °C at 10 °C min^{-1}, where it was held for 1 min; and finally ramped up to 300 °C at 10 °C min^{-1}, where it was held for 7 min. The total run time of GC separation was 30 min The gas chromatography injector was operated in splitless mode for 2 min, and its temperature was maintained at 260 °C. The mass spectrometer was operated in electron ionization mode (EI) at 70 eV and calibrated daily by auto-tuning with perfluorotributylamine (PFTBA). PAH calibration standards (AccuStandard, New Haven, CT, USA) were used. Blanks (one for every five samples), duplicate samples, and cross correlation were used for quality assurance and quality control (QA/QC) purposes. RSD for individual PAHs was below 10% in all cases. The following species (*m/z*) were quantified: 128 (naphthalene), 152 (acenaphthylene), 153 and 154 (acenapthene), 165 and 166 (fluorene), 178 (anthracene/phenanthrene), 202 (fluoranthene/pyrene), 228 (benzo(a)anthracene/chrysene), 252 (benzo(b)fluoranthene/benzo(k)fluoranthene), 276 (indene(1,2,3-c,d)pyrene/benzo(g,h,i)perylene), and 278 (benzo(a,h)anthracene). In Appendix A, the most representative chromatogram of soil samples has been included.

Forage and milk samples were treated according to the "QuEChERS" extraction method, with some modifications [26]. Briefly, samples (10 g) were extracted with 30 mL

acetonitrile and vortexed at 3000 rpm for 1 min. A total of 4 g anhydrous MgSO$_4$ and 1 g NaCl were added and immediately vortexed for 1 min, then 50 µL of an internal standard solution were added and the mixture was vortexed for another 30 s. The mixture was centrifuged at 2800× *g* for 5 min at room temperature and the supernatant was purified by a dispersive solid-phase extraction method [26]. An aliquot of supernatant (5 mL) was transferred to a flat-bottomed flask, concentrated in a 40 °C water bath until near-drying, and dissolved in 5 mL of cyclohexane [26]. An aliquot of 1 µL was injected into a 7890B gas chromatograph (Agilent Tech.) equipped with a Select PAH CP7462 capillary column with a length of 30 m, an inner diameter of 0.25 mm, and a film thickness of 0.15 µm. He was used as carrier gas at 2 mL min^{-1}. The initial oven temperature of 70 °C was held for 0.7 min, ramped up to 180 °C at 85 °C min^{-1} and then to 230 °C at 3 °C min^{-1}, where it was held for 7 min; ramped up to 280 °C at 28 °C min^{-1}, where it was held for 10 min; and, finally, ramped up to 350 °C at 14 °C min^{-1}, where it was held for 3 min. The total run time of GC separation was 60 min. The GC injector was operated in splitless mode for 1 min and its temperature was maintained at 300 °C. The compounds were detected using a 7000D mass spectrometer (Agilent Tech.), which was operated in electron ionization mode (EI) at 70 eV. The following m/z ratios were monitored: 178 (anthracene/phenanthrene), 202 (fluoranthene/pyrene), 228 (benzo(a)anthracene/chrysene), 252 (benzo(b)fluoranthene/benzo(k)fluoranthene/benzo(a)pyrene), 276 (benzo(g,h,i)-perylene/Indene(1,2,3-c,d)pyrene), and 278 (benzo(a,h)anthracene). Each sample was analyzed per duplicate. The method was validated using five internal standards (AccuStandard, New Haven, CT, USA), prepared by adding isotopically labelled PAHs to sample extracts. Concentrations of PAHs in the samples were determined by comparing their peak areas to those of the internal standards.

2.6. Data Treatment and Statistical Analyses

Univariate statistical descriptors (mean, median, coefficient of variation, minimum, and maximum) were calculated for the concentrations of PTEs and PAHs in each type of sample. The variation (%) in the mean concentration for each metal or PAH between the close and far groups of farms was calculated using the following expression:

$$Variation(\%) = \frac{mean_{close}}{mean_{far}} \cdot 100 \tag{1}$$

Principal component analysis was performed for soil data to identify anthropogenic or natural factors associated with the concentrations of contaminants. Factors were extracted using the Kaiser/Gutmann criterion and varimax rotation, reflecting recommendations and our own experience [27–29].

The soil–forage transfer factor (TF$_{sf}$) and forage–milk transfer factor (TF$_{fm}$) for the inorganic elements were calculated as follows:

$$TF_{sf} = c_f/c_s \tag{2}$$

$$TF_{fm} = c_m/c_f \tag{3}$$

where C$_f$, C$_s$, and C$_m$ are the median concentrations in the forage, soil and milk, respectively. SPSS 24 (IBM, Armonk, NY, USA) was used for all statistical analyses.

3. Results and Discussion

3.1. PTEs and PAHs in the Soil

The results of the soil analyses are summarized in Table 1. Descriptive statistics are detailed for each element (including PTEs and essential minerals) and PAHs analyzed. The soils closer (<5 km) to industrial areas contained higher content of PTEs and heavy weight PAHs than those located farther away (>5 km).

Table 1. Comparison of metals and polycyclic aromatic hydrocarbons in soils from farms located <5 or >5 km from industrial areas.

	Farms < 5 km from Industrial Areas (*n* = 10)				Farms > 5 km from Industrial Areas (*n* = 6)				Total Median	V (%)	RBSSL
	Mean	Median	Min	Max	Mean	Median	Min	Max			
Inorganic elements											
Na (g kg^{-1})	3.10	2.81	0.08	9.55	3.24	2.95	0.35	14.6	2.94	−5	-
Mg (%)	0.44	0.22	0.08	1.34	0.32	0.17	0.1	0.79	0.20	27	-
K (%)	0.77	0.64	0.24	2.11	0.63	0.53	0.34	1.7	0.59	19	-
Ca (%)	0.73	0.55	0.1	2.34	0.62	0.35	0.14	2.3	0.43	15	-
Cr (mg kg^{-1})	35.1	24.4	2.7	141.5	24.8	22.2	8.0	56.0	23.3	29	-
Fe (%)	2.58	1.92	0.85	6.09	1.54	1.45	0.9	2.32	1.76	40	-
Cu (mg kg^{-1})	20.8	19.9	4.6	56.0	17.0	11.0	7.1	71.8	15.4	18	55
Zn (mg kg^{-1})	261	232	30	506	96	61	33	256	176	63	455
As (mg kg^{-1})	17.8	11.3	4.9	46.1	10.3	10.4	4.3	14.5	11.1	42	40
Se (mg kg^{-1})	1.75	1.59	1.1	3.09	1.42	1.43	0.95	1.86	1.50	19	25
Cd (mg kg^{-1})	1.41	1.16	0.21	3.67	0.39	0.32	0.18	1.24	0.71	73	2
Hg (mg kg^{-1})	0.97	0.41	0.06	6.11	0.57	0.19	0.06	3.2	0.39	41	1
Pb (mg kg^{-1})	52	48	13	138	25	24	15	43	34	51	70
Polycyclic aromatic hydrocarbons (µg kg^{-1})											
Naphthalene	2.75	<0.1	<0.1	13.86	1.45	<0.1	<0.1	5.61	3.73	47	1000
Acenaphthylene	1.54	0.98	<0.1	7.69	1.23	0.71	<0.1	5.23	1.02	20	-
Acenaphthene	0.63	<0.1	<0.1	7.81	0.81	0.55	<0.1	2.59	1.19	−28	6000
Fluorene	2.36	2.03	<0.1	9.61	1.06	1.13	<0.1	2.47	1.41	55	5000
Anthracene	28.8	25.9	0.67	85.2	17.5	12.8	2.78	49.19	20.83	39	45,000
Phenanthrene	4.86	3.33	<0.1	22.95	3.59	1.12	<0.1	17.11	2.76	26	-
Fluoranthene	57.9	45.7	2.7	172.8	28.9	18.8	4.4	109.5	34.6	50	8000
Pyrene	38.5	30.5	1.4	100.6	24.0	15.1	3.7	94.6	25.7	38	6000
Benzo(a) anthracene	36.7	26.0	3.7	95.4	15.5	9.1	3.2	58.3	19.7	58	200
Crysene	48.2	35.5	4.1	116.4	18.6	10.3	3.1	55.7	27.4	61	20,000
Benzo(b) fluoranthene	83.2	61.7	8.0	177.4	35.0	22.2	7.0	108.8	52.4	58	200
Benzo(k) fluoranthene	25.2	17.5	2.3	56.1	9.5	4.8	1.5	27.5	14.2	62	2000
Benzo(a)pyrene	45.4	30.3	3.8	105.3	16.7	8.8	2.9	50.0	22.3	63	20
Indene(1,2,3-c,d)pyrene	30.5	26.6	<0.1	81.9	7.4	<0.1	<0.1	38.8	32.4	76	300
Dibenz(a,h) anthracene	10.4	6.1	<0.1	47.5	1.2	<0.1	<0.1	9.4	10.7	89	30
Benzo(g,h,i) perylene	39.7	29.8	6.5	91.7	13.2	8.6	3.6	42.9	21.3	67	-

Max: maximum; min: minimum; *n*: number of farms; V: close-far variation; <0.1: not detected; RBSSL: risk-based soil-screening level.

The similitude between the mean and the median is a preliminary indicator of normal distribution. The variation (V%) revealed an enrichment of PTEs and PAHs in soils closer to industrial areas (Table 1), with the highest value for dibenzo(a,h)anthracene (89%). The enrichment of Zn, Cd, and Pb was consistent with the known metal emissions from current and past industrial activities in this region of northern Spain [30,31]. PAHs with a molecular weight higher than that of fluoranthene were also enriched in the soil closer to industrial areas, except for pyrene (38%), and these results are consistent with studies of soils near industrial areas in northern Spain [32,33]. The enrichment of these high molecular weight PAHs is concerning, as these are the most persistent PAHs in the environment. In addition, these data are consistent with previous studies on soils located near to the industrial areas [32–35].

To assess the risk that the observed levels of pollutants may pose for humans and the environment, we compared the measured levels to so-called "risk-based soil screening levels" (RBSSLs) [36], which are based on toxicity parameters for different uses of soil (Table 1). We applied the most restrictive values for "other uses" of soil, which include farming [36].

In the soils close to industries, Cu, Zn, As, Cd, Hg, and Pb exceeded the threshold limits by at least 100%. For instance, the mean concentration of Hg (0.97 mg kg^{-1}), one of the most toxic elements, was close to its RBSSL (1 mg kg^{-1}). In the case of soils located more than 5 km away from industrial areas, thresholds were occasionally exceeded only for Cu and Hg, and mean values were much lower than RBSSLs. In the case of PAHs, the concentration of benzo(a)pyrene in the soils closer to industries (45.4 µg kg^{-1}) was more than twice the RBSSL (20 µg kg^{-1}), while it was notably lower in the soils farther away (16.7 µg kg^{-1}). More specifically, the soils from N1, N2, and N3 dairy farms showed levels of benzo(a)pyrene above their ML, with 85.9, 61.4, and 78.7 ug kg^{-1}, respectively. These three farms are located less than 2 km from the steel industry and less than 5 km from the zinc industry. Similar enrichment in heavy-molecular-weighted PAHs has been previously reported in soils located less than 2 km from a Cu smelting industry [37]. These results suggest that livestock near industrial areas may be exposed to above-threshold levels of several pollutants when they feed on forage cultivated on local soils.

To identify potential pollution sources, principal component analysis was performed using all the samples, irrespective of their location (Table 2). Four principal components explained 83% of the initial variance with high communality values. PTEs such as As and Pb were quite well represented by principal component 1, which was also associated with high Fe and Se load, suggesting the presence of an anthropogenic source that was probably related to the steel industry (Fe) and/or coal-combustion (Fe and Se) power plants [27,38]. This component 1 was also associated with natural iron oxy-hydroxides, which may explain the presence of As. The elements with higher loads in the second principal component were Mg, Ca, and K, which were probably associated with natural sources, such as calcareous and clayey materials. In the third principal component, a remarkable association was observed among high concentrations of PAHs, Zn, and Cd, consistent with emissions from the Zn smelting industry [32]. The correlation between Zn and heavy molecular-weighted PAHs has been also observed in soils near Cu smelting industries [37]. The high levels of PAHs and the contribution of Pb in the third component, together with the absence of PAHs in the other two components, may indicate heavy-traffic pollution as another source [39]. The fourth principal component was linked to Na and Cr, both naturally occurring elements.

Table 2. Principal component data matrix (rotated) for potentially toxic elements and polycyclic aromatic hydrocarbons (PAHs) in soils.

Element	Principal Component				Communality
	1	2	3	4	
As	0.922	0.125	0.158	0.019	0.891
Se	0.862	0.242	0.125	0.126	0.833
Fe	0.781	0.432	0.257	−0.006	0.862
Pb	0.719	−0.020	0.626	0.050	0.913
Mg	0.211	0.944	−0.017	0.059	0.939
Ca	−0.006	0.926	0.190	0.151	0.917
K	0.398	0.788	−0.101	0.357	0.917
Cu	0.306	0.727	0.489	0.099	0.872
Zn	0.320	0.265	0.838	0.136	0.893
Sum PAHs	−0.035	0.044	0.807	−0.154	0.678

Table 2. *Cont.*

Element	Principal Component				Communality
	1	2	3	4	
Cd	0.449	−0.063	0.791	0.171	0.861
Hg	0.093	0.207	0.539	0.464	0.557
Na	−0.095	0.138	0.029	0.887	0.816
Cr	0.460	0.180	0.032	0.616	0.625
% VE	45.840	63.970	73.852	82.653	

VE: Variance explained (cumulative).

3.2. PTEs and PAHs in Forage

Table 3 shows the concentration (mean, median, minimum, and maximum) and the percentage of variation between mean (and median) concentration of inorganic elements and PAHs in the forages produced near to (<5 km) and farther from (>5 km) the point-sources of pollution. The concentrations of PTEs and PAHs in the forage were generally lower than those measured in the soils, suggesting limited transfer from soils to plants [27]. This could be explained by the low bioavailability of PTEs in the soils of the industrial areas [27], and perhaps by low deposition from the atmosphere.

Table 3. Comparison of potentially toxic metals and polycyclic aromatic hydrocarbons in feed from farms <5 or >5 km from industrial areas.

	Farms < 5 km from Industrial Areas ($n = 10$)				Farms > 5 km from Industrial Areas ($n = 6$)				Total Median	V (%)	ML
	Mean	Median	Min	Max	Mean	Median	Min	Max			
Inorganic elements											
Na (g kg^{-1})	3.61	3.9	0.44	6.48	2.71	2.92	0.2	5.68	3.16	25	-
Mg (g kg^{-1})	2.32	2.34	1.2	3.15	2.28	1.94	1.32	4.15	2.30	2	-
K (g kg^{-1})	17.5	15.13	4.91	40.95	15.56	13.2	10.07	29.59	13.75	11	-
Ca (g kg^{-1})	7.72	7.63	3.05	10.52	8.23	7.74	5.42	16.05	7.63	−7	-
Cr (mg kg^{-1})	7.56	6.51	1.57	19.12	8.04	5.58	0.96	32.76	6.07	−6	-
Fe (g kg^{-1})	1.28	0.92	0.24	7.63	0.68	0.48	0.12	2.55	0.82	47	-
Cu (mg kg^{-1})	8.86	7.41	4.44	18.96	10.58	9.4	5.12	22.8	7.48	−19	-
Zn (mg kg^{-1})	89.8	76.3	22.9	216.1	43.9	36.2	24.7	87.2	61.7	51	-
As (mg kg^{-1})	0.8	0.53	0.15	3.94	0.85	0.3	0.06	7.87	0.42	−7	2 [a]
Se (µg kg^{-1})	300	209	50	1077	287	242	38	729	220	4	-
Cd (µg kg^{-1})	318	192	39	1313	94	87	10	314	115	70	1000 [b]
Hg (µg kg^{-1})	38.9	27.3	11.4	114.3	39.2	7.9	3.0	471.1	20.1	−1	100 [a]
Pb (mg kg^{-1})	1.83	1.5	0.23	7.85	1.48	0.87	0.2	5.69	1.10	19	10 [a]
Polycyclic aromatic hydrocarbons (µg kg^{-1})											
Phenanthrene	7.68	7.4	3.3	14.7	6.69	6.9	3.5	10.4	7.1	13	-
Fluoranthene	15.2	14.3	4.5	37.4	10.4	7.1	1.8	26.1	10.6	32	-
Pyrene	34.0	23.9	3.4	120	23.5	15.7	1.1	75.3	19.6	31	-
Benzo(a)anthracene	3.17	1.9	<0.1	31.3	0.05	<0.1	<0.1	0.9	1.9	98	-
Crysene	5.8	3.45	1.2	51.9	1.11	1.2	<0.1	2.5	2.1	81	-
Benzo(b)fluoranthene	6.91	3.2	1.5	71.3	0.68	<0.1	<0.1	3.2	2.1	90	-
Benzo(k)fluoranthene	2.8	1.5	<0.1	30	0.07	<0.1	<0.1	1.2	1.7	98	-
Benzo(a)pyrene	4.28	2.15	<0.1	48.7	0.06	<0.1	<0.1	1	2.3	99	-
Indene(1,2,3-c,d)pyrene	3.92	1.9	0.9	41.6	0.24	<0.1	<0.1	1.5	1.6	94	-
Dibenz(a,h)anthracene	0.68	<0.1	<0.1	10.2	<0.1	<0.1	<0.1	<0.1	1.4	100	-
Benzo(g,h,i)perylene	4.76	2.25	1	54.9	0.19	<0.1	<0.1	1.5	1.9	96	-

Max: maximum; min: minimum; *n*: number of farms; V: close–far variation; <0.1: not detected; ML: maximum level according to EU regulations; [a] (EU 2019/1869); [b] (EU 1275/2013).

The number of pollutants enriched closer to the industry was smaller in the forage than in the soil (Tables 1 and 3), although in both types of samples, Zn, Cd, and PAHs with at least four aromatic rings were enriched closer to industrial areas. This enrichment in high-molecular-weight PAHs in the soils and plants can be partially explained by the "distillation effect" [40]: high molecular weight PAHs in the atmosphere deposit onto surfaces closer to their source, whereas low-molecular weight PAHs diffuse farther before deposition. The levels of PAHs found in forage samples (1–20 $\mu g\,kg^{-1}$ dry weight) were lower than those reported in 2003 in grasslands near roads with high-traffic intensity [20], but they were similar to those in forages from urban and rural farms [19].

Forage (fresh forage or silage) is the primary source of essential mineral supply to cattle in sustainable farms [7]. The essential trace minerals are required in the diet of the animals, as they play fundamental roles in their organisms, such as the roles of enzyme cofactors, catalyzers of metabolic reactions, and so on [7]; however, they become potentially toxic at high concentrations, so the National Research Council (NRC, United States) has established tolerable limits for these elements in the cattle diet. Nearly all the essential trace minerals (Zn, Cu, Se, and Cr) were below the maximum tolerable limits that the NRC recommends for cattle [41]. The only exception was Fe, whose median concentration (920 $mg\,kg^{-1}$ dry weight) in farms near industries exceeded the tolerable level of 500 $mg\,kg^{-1}$, which was much higher than the concentration found in farms far away from industrial areas.

Among the PTEs, Cd and Pb showed respective median concentrations of 0.115 and 1.10 $mg\,kg^{-1}$ in the forage, which were below the levels in forage produced near industrial activities in Romania [11] or India [42] but above the levels on commercial farms in England [43]. The maximal content of As (7.87 $mg\,kg^{-1}$), Cd (1.31 $mg\,kg^{-1}$), and Hg (0.47 $mg\,kg^{-1}$) in the forage exceeded the maximum levels (ML) for animal feed based on European Union regulations [44,45]. More specifically, one farm exceeded the ML of Cd (N1, see Table A1) with 1.31 $mg\,kg^{-1}$. In that sense, other farms near industries (N2 and N3) also had high levels of Cd (>0.6 $mg\,kg^{-1}$), although they did not exceed its ML. In contrast, the As concentration in the forages was above its ML in farm F4 (7.87 $mg\,kg^{-1}$), which is more than 20 km away from point pollution sources (Table A1), and in the close-to-industry farms N1 (3.94 $mg\,kg^{-1}$) and N4 (2.19 $mg\,kg^{-1}$). Again, the Hg concentration exceed its ML in farm F4 (0.47 $mg\,kg^{-1}$) and in the close-to-industry farms N4 (1.13 $mg\,kg^{-1}$) and N7 (1.14 $mg\,kg^{-1}$). Thus, As and Hg might not be enriched near industrial facilities, which is similar to what we observed in the soil. These results suggest that As and Hg, in particular, may have a natural occurrence.

Regarding PAHs, EU legislation has not established a ML in animal feed for these compounds. However, the most concerning PAH is benzo(a)pyrene, whose concentrations were higher in the forages produced in farm N2 (48.7 $\mu g\,kg^{-1}$), which is located 0.4 km from the steel industry (Table A1). Together with benzo(a)pyrene, the forage from this farm also contained higher concentrations of the rest of PAHs.

3.3. PTEs and PAHs in Milk

Table 4 provides a comparison between the concentrations of inorganic elements and PAH found in the milk produced in farms close to and farther from industries. In addition, similarly to the soil and the forage, the variation in the mean (and median) concentration between both locations was calculated for each pollutant to assess its enrichment in the milk, depending on industrial proximity.

Table 4. Comparison of metals and polycyclic aromatic hydrocarbons in milk from farms < 5 or > 5 km from industrial areas.

	Farms < 5 km from Industrial Areas (*n* = 10)				Farms > 5 km from Industrial Areas (*n* = 6)				Total Median	V (%)	ML
	Mean	Median	Min	Max	Mean	Median	Min	Max			
Inorganic elements											
Na (g kg^{-1})	0.39	0.39	0.29	0.52	0.41	0.41	0.34	0.50	0.40	−5	-
Mg (g kg^{-1})	0.11	0.11	0.08	0.13	0.12	0.11	0.1	0.15	0.11	−8	-
K (g kg^{-1})	1.66	1.69	1.37	1.89	1.71	1.72	1.51	1.97	1.70	−3	-
Ca (g kg^{-1})	1.15	1.15	1	1.27	1.23	1.21	1.16	1.53	1.19	−7	-
Cr (µg kg^{-1})	8.56	3.09	<0.07	74.1	5.14	1.09	<0.07	44.2	1.88	40	-
Fe (mg kg^{-1})	0.27	0.18	0.05	1.22	0.25	0.19	0.08	1.19	0.18	9	-
Cu (µg kg^{-1})	36.6	36.0	19.6	58.6	42.9	43.4	26.5	73.6	40.2	−17	-
Zn (mg kg^{-1})	3.52	3.46	2.92	4.24	4.04	4.12	3.02	5.57	3.67	−15	-
As (µg kg^{-1})	2.77	1.62	1.23	16.01	1.83	1.7	1.26	3.91	1.65	34	-
Se (µg kg^{-1})	28.7	25.8	17.7	54.0	28.6	27.3	12.6	55.5	27.2	1	-
Cd (µg kg^{-1})	0.03	0.02	<0.002	0.12	0.02	0.02	<0.002	0.03	0.019	38	-
Hg (µg kg^{-1})	0.03	<0.01	<0.01	0.28	0.01	<0.01	<0.01	0.17	<0.01	59	-
Pb (µg kg^{-1})	1.17	0.95	0.2	2.7	0.54	0.51	<0.06	1.44	0.70	54	20 [a]
Polycyclic aromatic hydrocarbons (µg kg^{-1})											
Phenanthrene	1.18	1.11	0.16	3.04	1.1	0.89	0.41	3.55	1.07	7	-
Fluoranthene	1.91	1.1	0.22	7.22	1.44	0.92	0.32	6.29	1.03	25	-
Pyrene	7.73	3.49	0.43	39.4	5.8	3.6	0.64	20.0	3.55	25	-

Max: maximum; min: minimum; V: close-far variation; ML: Maximum Level according to EU regulations; *n*: number of farms. [a]: (CE 1881/2006).

The concentrations of PTEs in the milk were low, regardless of whether the farms were near to or farther from industrial areas. Hg and Pb showed substantial enrichment (50%) in farms closer to industries, while Cr, As, and Cd showed weaker enrichment (35%). These results are consistent with previous studies showing that the milk of cows on farms near industrial areas contained elevated contents of Cd [46] and Pb [47]. Nevertheless, the levels of Cd and Pb in milk were considerably higher in those studies than in the present work. Indeed, the levels of Cd in 11% of our milk samples and the level of Hg in 63% of our milk samples were below the limit of detection of our methodology (see Table 4). None of the milk samples exceeded the maximum recommended limit of 20 µg kg^{-1} for Pb [48] (The European Union has not established limits in milk or dairy products for the other metals that we analyzed). None of our samples exceeded the maximum level of 2.6 µg kg^{-1} for Cd, as recommended by the International Dairy Federation [49]. Perhaps these PTEs could be accumulated in the liver, kidney, or lung bovine organs, as previously stated [50].

The presence of PAHs in the milk was addressed to a lesser extent than the presence of PTEs; however, some works have reported PAH concentrations in milk from cows raised in industrial or in rural areas [4,18,19]. The presence of PAHs in milk can occur not only after ingestion of soil when livestock graze in fields, but also via feed (pasture or silage) when livestock is confined indoors [4].

We detected only three PAHs in the milk, and all three had low molecular weight: phenanthrene, fluoranthene, and pyrene. Their concentrations were similar to those reported in rural areas of France [18,19]. In contrast to the enrichment that we observed in the soil and the forage, we did not observe such enrichment in the milk, which was similar to a report comparing PAH levels in milk from rural or urban areas in France [19]. These results suggest that PAHs are not efficiently transferred into milk at such levels of pollution, as previously reported in a controlled experiment with goats, where C^{14} PAHs were added to the diet [51].

3.4. Transfer Factors between Soil and Forage and between Forage and Milk

Table 5 provides the soil–forage transfer factor (TF_{sf}) and forage–milk transfer factor (TF_{fm}) for the inorganic elements.

In general, TF_{sf} ratios were higher than TF_{fm} ratios. Previous studies also reported very low forage–milk transfer of heavy metals, with values as low as 1:500 [52], implying that mammary glands act as barriers to prevent the entry of PTEs [53]. Na, K, Ca, and Mg had higher TF_{sf} and TF_{fm}, probably reflecting that they are major essential elements. TF_{sf} values were above 1 for these elements, indicating a higher concentration of these minerals in the forage than in the soil. TFs varied across studies (Table 5), probably reflecting the complex influences on these factors, including plant species, soil properties, and dry matter intake by the animals [11]. Moreover, these TF_{sf} could be affected by the sampling procedure, so it is necessary to remark that these data were obtained by collecting three subsamples in each location.

Table 5. Soil–forage (TF_{sf}) and forage–milk (TF_{fm}) transfer factors for potentially toxic metals.

	TF_{sf}				TF_{fm}			
	Present Study			**Literature**	**Present Study**			**Literature**
	Mean ± SD	**Range**	**Median**		**Mean ± SD**	**Range**	**Median**	
Na	20.4 ± 50.9	0.65–401	12.80		0.227 ± 0.329	0.047–1.973	0.1212	
K	3.0 ± 2.4	0.62–11.5	2.517		0.118 ± 0.054	0.042–0.345	0.1185	
Ca	2.2 ± 1.8	0.24–7.14	1.626		0.157 ± 0.058	0.076–0.41	0.1538	
Mg	1.1 ± 0.8	0.1–3.77	1.062		0.051 ± 0.019	0.032–0.107	0.0483	
Cr	0.47 ± 0.76	0.023–3.95	0.232	(0.01–0.1) [54]	0.002 ± 0.007	0–0.046	0.0004	
Fe	0.005 ± 0.006	0.00–0.033	0.004		0.0005 ± 0.0005	0.00003–0.0017	0.0002	
Cu	0.74 ± 0.53	0.082–2.02	0.682	0.07 [11] (0.1–1) [54]	0.0048 ± 0.0024	0.0014–0.0125	0.0048	0.04 [11]
Zn	0.54 ± 0.37	0.048–1.85	0.460	0.092 [11] (1–10) [54]	0.074 ± 0.045	0.016–0.173	0.0636	0.117 [11]
As	0.099 ± 0.28	0.003–1.84	0.033	(0.01–0.1) [54]	0.0074 ± 0.0077	0.0002–0.038	0.0050	
Se	0.187 ± 0.146	0.026–0.602	0.141	(0.1–10) [54]	0.0010 ± 0.001	0–0.005	0.0007	0.037 [11]
Cd	0.338 ± 0.407	0.011–2.31	0.235	0.06 [11] (1–10) [54]	0.0002 ± 00003	0–0.0013	0.0001	0.021 [11]
Hg	0.125 ± 0.202	0.002–0.48	0.041	(0.01–0.1) [54]	0.001 ± 0.005	0–0.029	0.0000	
Pb	0.062 ± 0.087	0.002–1.0799	0.029	0.005 [11] 0.01–0.1 [54]	0.0010 ± 0.001	0–0.005	0.0007	0.037 [11]

SD: standard deviation.

The TF_{sf} values in our work followed the trend Zn ≈ Cu > Cd >> Pb, showing some discrepancies with previous work in the transfer of Cu and Zn [11,54], but consistent with a report that Zn and Cu accumulate to a much greater extent than Cd in edible plant parts [55]. Our trend is also consistent with the lower transfer of Pb from soil to plants observed in previous work, which led investigators to propose that this metal enters the human food chain via an alternative water–forage–milk pathway [9]. The TF_{fm} values in our work followed the trend Zn > Cu > Pb > Cd, consistent with previous studies in Romania [11]. In contrast to that work, however, PTE concentrations in the present study were orders of magnitude larger in the forage than in the milk.

4. Conclusions

Our results suggest that PTEs and high-molecular-weight PAHs are enriched in soils near industrial areas, and that this enrichment led to somewhat elevated levels in the forage but not dangerously high levels in the milk (lower than the EU legislation maximum permitted level) from cows feeding on that forage. These results suggest that there is no risk for humans consuming cow's milk from these areas. Principal component analysis suggested that the sources of soil pollutants may be related to anthropogenic factors linked to industrial activity, as well as to natural soil mineralogy, as found in principal component

1 for As, Pb, Fe, and Se, emitted because of coal combustion of power plants or the steel industry. The calculated forage–milk transfer factors proved to be minimal for the most toxic elements (Cd, Hg, and Pb), with values lower than 10^{-3}. Further, the content of PAHs and PTEs decreased along the soil–forage–milk food chain and only low molecular weight PAHs were detected in the milk. Future work should examine the fate of PTEs and PAHs in soils and farm-produced forage, as well as meat production and the health implications for cattle.

Author Contributions: Conceptualization, C.B., J.L.R.G., L.J.R., J.M.C.-F. and A.S. methodology, A.S., M.M.-M. and S.F.; validation, S.F., M.M.-M., A.S. and L.J.R.; formal analysis, S.F., C.B. and J.L.R.G.; investigation, A.S. and S.F.; resources, J.M.C.-F., L.J.R., S.F. and A.S.; data curation, S.F. and C.B.; writing—original draft preparation, S.F.; writing—review and editing, M.M.-M., C.B., J.L.R.G., L.J.R., J.M.C.-F. and A.S.; visualization, A.S. and S.F.; supervision, A.S. and J.L.R.G.; funding acquisition, L.J.R., J.M.C.-F. and A.S. All authors have read and agreed to the published version of the manuscript.

Data Availability Statement: The data presented in this study are available on request from the corresponding author.

Conflicts of Interest: The authors declare no conflict of interest.

Appendix A

Distance from sampling positions to the industry are detailed in Table A1. Experimental conditions and validation data of PTEs analysis procedure are included in Tables A2–A5 of this Appendix.

Table A1. Distance from farm to industry.

Farm Code	Distance (km)					Group
	Zinc	Chemical Fiber	Steel (1)	Steel (2)	Thermal Power Plant	
N1	3.0	5.7	1.9	14	14	Near
N2	5.0	4.1	0.4	12	13	Near
N3	3.4	5.6	1.9	14	14	Near
N4	10	3.7	4.0	6.8	7.2	Near
N5	9.3	0.8	3.4	8.7	10	Near
F1	51	44	45	34	35	Far
N6	7.1	4.0	4.6	13	15	Near
N7	10	4.6	6.6	12	14	Near
N8	5.9	2.8	2.0	12	13	Near
N9	14	5.0	7.2	5.3	7.7	Near
N10	17	9.4	10	0.98	2.3	Near
F2	30	21	24	16	17	Far
F3	27	18	21	13	14	Far
F4	39	32	33	22	23	Far
F5	3.0	5.7	1.9	14	14	Far
F6	5.0	4.1	0.4	12	13	Far

N: Near; F: Far.

Table A2. Temperature gradient program used in the acid digestion of soil, forage, and milk.

Time (min)	Power (W)	Temperature (°C)
3	900	95
10	900	160
3	900	185
15	900	185

For each element analyzed by ICP-MS, the LOD and LOQ were calculated as 3 and 10 times the standard deviation (SD) of ten blank samples, respectively.

Table A3. Instrumental limit of detection (LOD), limit of quantification (LOQ), and calibration range for inorganic elements quantification by using inductively coupled plasma mass spectrometry.

	LOD	LOQ	Calibration Range
Na mg L^{-1}	0.025	0.083	10–200
Mg mg L^{-1}	0.001	0.003	10–200
K mg L^{-1}	0.132	0.440	10–200
Ca mg L^{-1}	0.216	0.720	10–200
Cr µg L^{-1}	0.100	0.333	10–5000
Fe µg L^{-1}	0.800	2.667	10–5000
Cu µg L^{-1}	0.325	1.083	1–50
Zn mg L^{-1}	0.002	0.007	0.01–5
As µg L^{-1}	0.010	0.033	0.1–50
Se µg L^{-1}	0.092	0.305	1–50
Cd µg L^{-1}	0.001	0.003	0.1–50
Hg µg L^{-1}	0.018	0.060	0.1–10
Pb µg L^{-1}	0.017	0.057	0.1–50

Repeatability of extraction procedure from replicates of certified European reference materials was calculated according to the following expression:

$$RSD_r = \frac{\sqrt{\frac{\sum(x_1-x_2)^2}{n-1}}}{\bar{x}} \cdot 100$$

where x_1 and x_2 are the measured values for duplicates, n is the number of total measures, and $\bar{x}$ is the average concentration of the element in all the samples.

Table A4. Relative standard deviation (RSD) values of soil, ryegrass, and milk powder.

	% Relative Standard Deviation (Repeatability *n* = 3)		
	Soil	Rye Grass	Milk Powder
Na	13.73	1.64	4.42
Mg	2.16	2.26	4.10
K	4.78	1.76	3.53
Ca	2.55	1.18	2.69
Cr	8.75	4.67	23.19
Fe	1.64	5.89	6.13
Cu	1.75	4.63	8.54
Zn	5.02	4.08	3.52
As	2.03	6.77	12.83
Se	4.05	3.31	7.42
Cd	4.67	5.70	5.07
Hg	2.81	2.14	7.76
Pb	2.63	4.65	4.71

In Table A5, validation statistics are included. Note that for Na, Mg, K, and Ca (ERM CD-281 "Rye-grass") there was no availability of uncertainty values because these inorganic elements were included as additional material information in the ERM CD-281 report. As detailed in this report, the results were obtained from "*semi-quantitative screening analysis using ICP-SFMS (. . .). The elements were determined using 18 scans over the mass range, resulting in a total measurement time of 300 s. The results are an average of triplicate measurements*".

Table A5. Method validation statistics for ERM-CC141 (loam soil), ERM-CD 281 (rye grass), and ERM BD-151 (skimmed milk powder) analysis by ICP-MS.

	ERM CD-141 "Loam Soil"			ERM CD-281 "Rye Grass"			ERM BD-151 "Skimmed Milk Powder"		
	Cert.	Det. ($n = 3$)	Rec, %	Cert.	Det. ($n = 3$)	Rec, %	Cert.	Det. ($n = 3$)	Rec, %
g kg^{-1}									
Na	-	-	-	(4) [3]	4.07 ± 0.07	102	4.19 ± 0.23	4.39 ± 0.07	105
Mg	-	-	-	(1.6)	1.67 ± 0.03	104	1.26 ± 0.07	1.36 ± 0.03	107
K	-	-	-	(34)	36.3 ± 0.6	107	17 ± 0.8	17.8 ± 0.3	104
Ca	-	-	-	(6.3)	7.2 ± 0.1	114	13.9 ± 0.7	14.1 ± 0.2	101
mg kg^{-1}									
Cr	31 ± 4	46 ± 3	149	24.8 ± 1.3	25.4 ± 0.5	102	0.19 [2]	0.214 ± 0.005	113
Fe	-	-	-	-	-	-	53 ± 4	49.9 ± 0.7	94
Cu	12.4 ± 0.9	12.0 ± 0.1	96	10.2 ± 0.5	10.1 ± 0.2	99	5 ± 0.23	4.52 ± 0.11	90
Zn	50 ± 4	58 ± 1.3	117	30.5 ± 1.1	29.3 ± 0.5	96	44.9 ± 2.3	40.6 ± 0.9	90
As	7.5 ± 1.4	9.6 ± 1.2	128	0.042 ± 0.01	0.046 ± 0.002	109	-	-	-
Se	-	-	-	0.092 [1]	0.097 ± 0.008	105	0.19 ± 0.04	0.176 ± 0.011	93
Cd	0.25 ± 0.04	0.27 ± 0.01	106	0.120 ± 0.007	0.111 ± 0.004	93	0.106 ± 0.013	0.100 ± 0.003	94
Hg	0.080 ± 0.008	0.087 ± 0.010	108	0.016 ± 0.002	0.018 ± 0.001	112	0.52 ± 0.04	0.475 ± 0.010	91
Pb	32.2 ± 1.4	35.4 ± 1.2	110	1.67 ± 0.11	1.63 ± 0.03	97	0.207 ± 0.014	0.183 ± 0.004	88

[1] Selenium was added to rye grass ERM before acid digestion. [2] Chromium was added to skimmed milk powder ERM before acid digestion. [3] Data between brackets indicate approximate values.

PAH quantification was carried out by using GC-MS. A representative chromatogram of a soil sample was included in Figure A1.
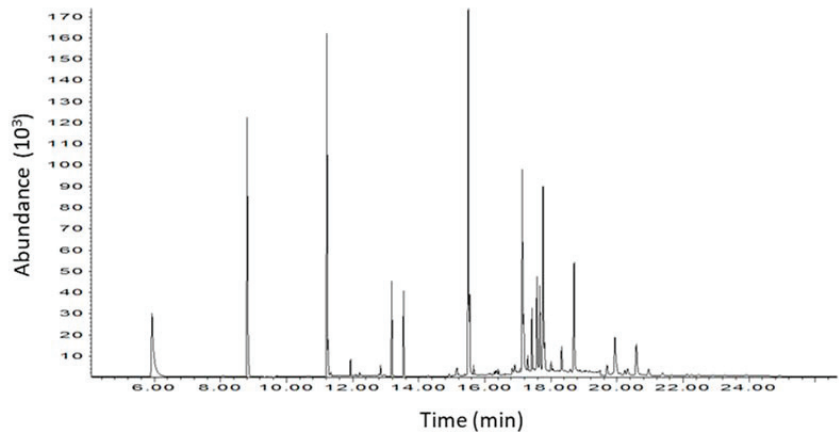
Figure A1. Merged-SIM chromatogram of PAHs found in a representative sample of soil collected in the vicinity of the industrial areas. Concentrations found in µg·kg^{-1} (main peaks): naphthalene (1.04), acenaphthylene (0.71), acenaphthene (0.64), Fluorene (0.61), phenanthrene (9.73), anthracene (0.89), fluoroanthene (10.23), pyrene (7.98), benzo(a)anthracene (5.06), chrysene (7.06), benzo(k)fluoroanthene (14.68), benzo(b)fluoroanthene (3.43), benzo(a)pyrene (5.62), and benzo(g,h,i)perylene (5.44).

References

1. Foroutan, A.; Guo, A.C.; Vazquez-Fresno, R.; Lipfert, M.; Zhang, L.; Zheng, J.; Badran, H.; Budinski, Z.; Mandal, R.; Ametaj, B.N.; et al. Chemical Composition of Commercial Cow's Milk. *J. Agric. Food Chem.* **2019**, *67*, 4897–4914. [CrossRef] [PubMed]
2. Doltra, J.; Villar, A.; Moros, R.; Salcedo, G.; Hutchings, N.J.; Kristensen, I.S. Forage Management to Improve On-Farm Feed Pro-duction, Nitrogen Fluxes and Greenhouse Gas Emissions from Dairy Systems in a Wet Temperate Region. *Agric. Syst.* **2018**, *160*, 70–78. [CrossRef]
3. Orjales, I.; Herrero-Latorre, C.; Miranda, M.; Rey-Crespo, F.; Rodríguez-Bermúdez, R.; López-Alonso, M. Evaluation of Trace Element Status of Organic Dairy Cattle. *Animal* **2018**, *12*, 1296–1305. [CrossRef]
4. Gutiérrez, R.; Vega, S.; Ortiz, R.; Pérez, J.J.; Schettino, B. Presence of PAHs in Milk of Industrial Farms from Tizayuca, Hidalgo, Mexico. *J. Environ. Sci. Health-B Pestic. Food Contam. Agric. Wastes* **2015**, *50*, 317–321. [CrossRef] [PubMed]
5. Crawshaw, R. Animal Feeds, Feeding Practices and Opportunities for Feed Contamination: An Introduction. In *Animal Feed Contamination: Effects on Livestock and Food Safety*; Fink-Gremmels, J., Ed.; Woodhead Publishing Limited: Cambridge, UK, 2012.
6. Boente, C.; Albuquerque, M.T.D.; Fernández-Braña, A.; Gerassis, S.; Sierra, C.; Gallego, J.R. Combining raw and compositional data to determine the spatial patterns of potentially toxic elements in soils. *Sci. Total Environ.* **2018**, *631–632*, 1117–1126. [CrossRef]
7. Arthington, J.D.; Ranches, J. Trace Mineral Supplementation of Grazing Beef Cattle. *Animals* **2021**, *11*, 2767. [CrossRef]
8. Singh, R.; Gautam, N.; Mishra, A.; Gupta, R. Heavy Metals and Living Systems: An Overview. *Indian J. Pharmacol.* **2011**, *43*, 246–253. [CrossRef] [PubMed]
9. Zhou, X.; Zheng, N.; Su, C.; Wang, J.; Soyeurt, H. Relationships between Pb, As, Cr, and Cd in Individual Cows' Milk and Milk Composition and Heavy Metal Contents in Water, Silage, and Soil. *Environ. Pollut.* **2019**, *255*, 113322. [CrossRef]
10. Wilkinson, J.M.; Hill, J.; Phillips, C.J.C. The Accumulation of Potentially-Toxic Metals by Grazing Ruminants. *Proc. Nutr. Soc.* **2003**, *62*, 267–277. [CrossRef]
11. Miclean, M.; Cadar, O.; Levei, E.A.; Roman, R.; Ozunu, A.; Levei, L. Metal (Pb, Cu, Cd, and Zn) Transfer along Food Chain and Health Risk Assessment through Raw Milk Consumption from Free-Range Cows. *Int. J. Environ. Health Res.* **2019**, *16*, 5–7. [CrossRef]
12. Cui, Y.J.; Zhu, Y.G.; Zhai, R.H.; Chen, D.Y.; Huang, Y.Z.; Qiu, Y.; Liang, J.Z. Transfer of Metals from Soil to Vegetables in an Area near a Smelter in Nanning, China. *Environ. Int.* **2004**, *30*, 785–791. [CrossRef] [PubMed]
13. Kováts, N.; Hubai, K.; Sainnokhoi, T.A.; Teke, G. Biomonitoring of Polyaromatic Hydrocarbon Accumulation in Rural Gardens Using Lettuce Plants. *J. Soils Sediments* **2021**, *21*, 106–117. [CrossRef]
14. Foan, L.; Sablayrolles, C.; Elustondo, D.; Lasheras, E.; González, L.; Ederra, A.; Simon, V.; Santamaría, J.M. Reconstructing Historical Trends of Polycyclic Aromatic Hydrocarbon Deposition in a Remote Area of Spain Using Herbarium Moss Material. *Atmos. Environ.* **2010**, *44*, 3207–3214. [CrossRef]
15. Chen, Y.; Wang, C.; Wang, Z. Residues and Source Identification of Persistent Organic Pollutants in Farmland Soils Irrigated by Effluents from Biological Treatment Plants. *Environ. Int.* **2005**, *31*, 778–783. [CrossRef] [PubMed]
16. Meng, L.; Qiao, M.; Arp, H.P.H. Phytoremediation Efficiency of a PAH-Contaminated Industrial Soil Using Ryegrass, White Clover, and Celery as Mono- and Mixed Cultures. *J. Soils Sediments* **2011**, *11*, 482–490. [CrossRef]
17. Costera, A.; Rychen, G.; Feidt, C.; Soligot, C.; Jurjanz, S. Ruminal Disappearance of PAHs in Contaminated Grass Using the Nylon Bag Technique. *Agron. Sustain. Dev.* **2010**, *30*, 769–775. [CrossRef]
18. Grova, N.; Feidt, C.; Crépineau, C.; Laurent, C.; Lafargue, P.E.; Hachimi, A.; Rychen, G. Detection of Polycyclic Aromatic Hydrocarbon Levels in Milk Collected Near Potential Contamination Sources. *J. Agric. Food Chem.* **2002**, *50*, 4640–4642. [CrossRef]
19. Grova, N.; Laurent, C.; Feidt, C.; Rychen, G.; Laurent, F. Gas Chromatography-Mass Spectrometry Study of Polycyclic Aromatic Hydrocarbons in Grass and Milk from Urban and Rural Farms. *Eur. J. Mass Spectrom.* **2000**, *6*, 457–460. [CrossRef]
20. Crépineau, C.; Rychen, G.; Feidt, C.; Le Roux, Y.; Lichtfouse, E.; Laurent, F. Contamination of Pastures by Polycyclic Aromatic Hydrocarbons (PAHs) in the Vicinity of a Highway. *J. Agric. Food Chem.* **2003**, *51*, 4841–4845. [CrossRef]
21. Commission Regulation (EU) No 835/2011 of 19 August 2011 Amending Regulation (EC) No 1881/2006 as Regards Maximum Levels for Polycyclic Aromatic Hydrocarbons in Foodstuffs. 2011. Available online: https://eur-lex.europa.eu/LexUriServ/LexUriServ.do?uri=OJ:L:2011:215:0004:0008:En:PDF (accessed on 12 December 2022).
22. Liang, X.; Zhu, L.; Zhuang, S. Sorption of Polycyclic Aromatic Hydrocarbons to Soils Enhanced by Heavy Metals: Perspective of Molecular Interactions. *J. Soils Sediments* **2016**, *16*, 1509–1518. [CrossRef]
23. Gunawardena, J.; Egodawatta, P.; Ayoko, G.A.; Goonetilleke, A. Role of Traffic in Atmospheric Accumulation of Heavy Metals and Polycyclic Aromatic Hydrocarbons. *Atmos. Environ.* **2012**, *54*, 502–510. [CrossRef]
24. Baizán, S.; Vicente, F.; Martínez-Fernández, A. Management Influence on the Quality of an Agricultural Soil Destined for Forage Production and Evaluated by Physico-Chemical and Biological Indicators. *Sustainability* **2021**, *13*, 5159. [CrossRef]
25. McCarthy, O.J.; Singh, H. Physico-chemical Properties of Milk. In *Advanced Dairy Chemistry*; McSweeney, P., Fox, P., Eds.; Springer: New York, NY, USA, 2009. [CrossRef]
26. Li, H.; Zhu, D.; Lu, X.; Du, H.; Guan, S.; Chen, Z. Determination and Risk Assessment of Sixteen Polycyclic Aromatic Hydrocarbons in Vegetables. *J. Environ. Sci. Health-Toxic/Hazard. Subst. Environ. Eng.* **2017**, *53*, 116–123. [CrossRef]
27. Boente, C.; Matanzas, N.; García-González, N.; Rodríguez-Valdés, E.; Gallego, J.R. Trace elements of concern affecting urban agriculture in industrialized areas: A multivariate approach. *Chemosphere* **2017**, *183*, 546–556. [CrossRef]

28. Reimann, C.; Filzmoser, P.; Garrett, R.G.; Dutter, R. *Statistical Data Analysis Explained. Applied Environmental Statistics with R*; Wiley & Sons Ltd.: Chichester, West Sussex, UK, 2008; 343p.

29. Borůvka, L.; Vacek, O.; Jehlička, J. Principal component analysis as a tool to indicate the origin of potentially toxic elements in soils. *Geoderma* **2005**, *128*, 289–300. [CrossRef]

30. Gallego, J.R.; Ortiz, J.E.; Sánchez-Palencia, Y.; Baragaño, D.; Borrego, Á.G.; Torres, T. A multivariate examination of the timing and accumulation of potentially toxic elements at las conchas bog (NW Spain). *Environ. Pollut.* **2019**, *254*, 113048. [CrossRef] [PubMed]

31. Sierra, C.; Boado, C.; Saavedra, A.; Ordóñez, C.; Gallego, J.R. Origin, patterns and anthropogenic accumulation of potentially toxic elements (PTEs) in surface sediments of the Avilés estuary (Asturias, northern Spain). *Mar. Pollut. Bull.* **2014**, *86*, 530–538. [CrossRef]

32. Baragaño, D.; Ratié, G.; Sierra, C.; Chrastný, V.; Komárek, M.; Gallego, J.R. Multiple pollution sources unravelled by environmental forensics techniques and multivariate statistics. *J. Hazard. Mater.* **2022**, *424*, 127413. [CrossRef]

33. Boente, C.; Baragaño, D.; Gallego, J.R. Benzo[a]pyrene sourcing and abundance in a coal region in transition reveals historical pollution, rendering soil screening levels impractical. *Environ. Pollut.* **2020**, *266*, 115341. [CrossRef]

34. Velea, T.; Gherghe, L.; Predica, V.; Krebs, R. Heavy metal contamination in the vicinity of an industrial area near Bucharest. *Environ. Sci. Pollut. Res.* **2009**, *16*, 27–32. [CrossRef]

35. Su, C.; Meng, J.; Zhou, Y.; Bi, R.; Chen, Z.; Diao, J.; Huang, Z.; Kan, Z.; Wang, T. Heavy Metals in Soils From Intense Industrial Areas in South China: Spatial Distribution, Source Apportionment, and Risk Assessment. *Front. Environ. Sci.* **2022**, *10*, 820536. [CrossRef]

36. Official Bulletin of the Principality of Asturias No. 91 of 21 April 2014 Setting the Generic Reference Levels for Heavy Metals in Soils from the Principality of Asturias. 2014. Available online: http://sede.612asturias.es/bopa/2014/04/21/2014e06617.pdf (accessed on 12 December 2022).

37. Bandowe, B.A.M.; Shukurov, N.; Leimer, S.; Kersten, M.; Steinberger, Y.; Wilcke, W. Polycyclic aromatic hydrocarbons (PAHs) in soils of an industrial area in semi-arid Uzbekistan: Spatial distribution, relationship with trace metals and risk assessment. *Environ. Geochem. Health* **2021**, *43*, 4847–4861. [CrossRef] [PubMed]

38. Lage, J.; Wolterbeek, H.; Almeida, S.M. Contamination of surface soils from a heavy industrial area in the North of Spain. *J. Radioanal. Nucl. Chem.* **2016**, *309*, 429–437. [CrossRef]

39. Querol, X.; Viana, M.; Alastuey, F.; Amato, F.; Moreno, T.; Castillo, S.; Pey, J.; de la Rosa, J.; Sánchez de la Campa, A.; Artíñano, B.; et al. Source origin of trace elements in PM from regional background, urban and industrial sites of Spain. *Atmos. Environ.* **2007**, *41*, 7219–7231. [CrossRef]

40. Bryselbout, C.; Henner, P.; Carsignol, J.; Lichtfouse, E. Polycyclic Aromatic Hydrocarbons in Highway Plants and Soils. Evidence for a Local Distillation Effect. *Analusis* **2000**, *28*, 290–293. [CrossRef]

41. National Research Council & National Academies of Sciences, Engineering, and Medicine. *Nutrient Requirements of Beef Cattle*, 8th ed.; The National Academies Press: Washington, DC, USA, 2016. [CrossRef]

42. Yasotha, A.; Dabadé, D.S.; Singh, V.P.; Sivakumar, T. Risk Assessment of Heavy Metals in Milk from Cows Reared around Industrial Areas in India. *Environ. Geochem. Health* **2021**, *43*, 1799–1815. [CrossRef]

43. Nicholson, F.A.; Chambers, B.J.; Williams, J.R.; Unwin, R.J. Heavy Metal Contents of Livestock Feeds and Animal Manures in England and Wales. *Bioresour. Technol.* **1999**, *70*, 23–31. [CrossRef]

44. Commission Regulation (EU) No 1275/2013 of 6 December 2013 Amending Annex I to Directive 2002/32/EC of the European Parliament and of the Council as Regards Maximum Levels for arsenic, cadmium, lead, nitrites, volatile mustard oil and Harmful Botanical Impurities. 2013. Available online: https://eur-lex.europa.eu/eli/reg/2013/1275/oj (accessed on 12 December 2022).

45. Commission Regulation (EU) No 2019/1869 of 7 November 2019 Amending and Correcting Annex I to Directive 2002/32/EC of the European Parliament and of the Council as Regards Maximum Levels for Certain Undesirable Substances in Animal Feed. 2019. Available online: https://eur-lex.europa.eu/legal-content/EN/TXT/?uri=uriserv:OJ.L_.2019.289.01.0032.01.ENG (accessed on 12 December 2022).

46. Griboff, J.; Baroni, M.V.; Horacek, M.; Wunderlin, D.A.; Monferran, M.V. Multielemental + isotopic Fingerprint Enables Linking Soil, Water, Forage and Milk Composition, Assessing the Geographical Origin of Argentinean Milk. *Food Chem.* **2019**, *283*, 549–558. [CrossRef]

47. Patra, R.C.; Swarup, D.; Kumar, P.; Nandi, D.; Naresh, R.; Ali, S.L. Milk Trace Elements in Lactating Cows Environmentally Exposed to Higher Level of Lead and Cadmium around Different Industrial Units. *Sci. Total Environ.* **2008**, *404*, 36–43. [CrossRef]

48. Commission Regulation (EU) No 1881/2006 of 19 December 2006 Setting Maximum Levels for Certain Contaminants in Foodstuffs. 2006. Available online: https://eur-lex.europa.eu/LexUriServ/LexUriServ.do?uri=OJ:L:2006:364:0005:0024:EN:PDF (accessed on 12 December 2022).

49. Werner, H. Metal Contaminants in Milk and Milk Products. *Bull. Int. Dairy Fed.* **1978**, *105*, 9–12.

50. Miedico, O.; Iammarino, M.; Paglia, G.; Tarallo, M.; Magiacotti, M.; Chiaravalle, A.E. Environmental monitoring of the area surrounding oil wells in Val d'Agri (Italy): Element accumulation in bovine and ovine organs. *Environ. Monit. Assess.* **2016**, *188*, 338. [CrossRef] [PubMed]

51. Grova, N.; Feidt, C.; Laurent, C.; Rychen, G. [14C] Milk, urine and faeces excretion kinetics in lactating goats after an oral administration of [14C] polycyclic aromatic hydrocarbons. *Int. Dairy J.* **2002**, *12*, 1025–1031. [CrossRef]

52. Blüthgen, A. Contamination of Milk from Feed. *Bull. Int. Dairy Fed.* **2000**, *356*, 43–47.
53. Nag, S.K. Contaminants in Milk: Routes of Contamination, Analytical Techniques and Methods of Control. In *Improving the Safety and Quality of Milk*; Griffiths, M.W., Ed.; Woodhead Publishing Limited: Cambridge, UK, 2010; Volume 1, pp. 146–178.
54. Kloke, A.; Sauerbeck, D.R.; Vetter, H. The Contamination of Plants and Soils with Heavy Metals and the Transport of Metals in Terrestrial Food Chains. In *Changing Metal Cycles and Human Health*; Nriagu, O.J., Ed.; Springer: Berlin/Heidelberg, Germany, 1984; Volume 28, pp. 113–141. [CrossRef]
55. Puschenreiter, M.; Horak, O. Influence of Different Soil Parameters on the Transfer Factor Soil to Plant of Cd, Cu and Zn for Wheat and Rye. *Bodenkultur* **2000**, *51*, 3–10.

Article

The Effect of Household Food Processing on Pesticide Residues in Oranges (*Citrus sinensis*)

Perihan Yolci Omeroglu [1,2,*]**, Busra Acoglu Celik** [1] **and Elif Koc Alibasoglu** [1]

1   Department of Food Engineering, Faculty of Agriculture, Gorukle Campus, Bursa Uludag University, Bursa 16059, Turkey
2   Science and Technology Application and Research Center (BITUAM), Gorukle Campus, Bursa Uludag University, Bursa 16059, Turkey
*   Correspondence: pyomeroglu@uludag.edu.tr; Tel.: +90-542-423-78-29

Abstract: In this study, the effect of various household food-processing methods (washing, peeling, processing into jam and fruit juice, freezing, storage) on pesticide residues (abamectin, buprofezin, ethoxazole, imazalil, and thiophanate-methyl) in oranges was investigated. Residue analyses were performed by quick-easy-cheap-efficient-rugged-safe (QuEChERS) extraction and liquid chromatography coupled with triple quadrupole mass spectrometry (LC-MS/MS) analysis. The limit of quantification of the method for each pesticide was 10 µg/kg. Physicochemical properties of the pesticides and the type of the food process had a considerable effect on the fate of pesticide residue. Pesticide residues were mostly dispersed on orange peels and washing with tap water decreased the residue levels by 26–84%. The amount of residue in oranges was reduced by 63–100% during fruit juice processing, while residues were removed by 90–100% after jam processing. Pesticides with a high octanol–water coefficient were absorbed by the wax of the orange peel, therefore they remained on the peel and could not easily be removed by washing. Moreover, pesticides with lower water solubility did not diffuse easily through the fruit juices from the pulp section of the fruit. The processing factor was greater than 1 for the separation of the orange peel and less than 1 for the washing step and jam and fruit juice productions.

Keywords: pesticide residues; orange; household food processing; processing factor

1. Introduction

Orange (*Citrus sinensis*) is one of the most popular and most-grown citrus families in the world. According to the Turkish Mediterranean Exporters' Association, the citrus group took first place in Turkish total fruit and vegetable exports between 2017 and 2018 (405.2 million tons) [1]. Valencia is the most important orange variety grown in Turkey, and its farming has been increasing rapidly in recent years. Its most important feature is that it can be grown and harvested up to the late months of the spring. The peel of the fruit is slightly rough and moderately thick and the inner skin is thick and contains few seeds. Orange is a good source of vitamins, flavonoids, terpenes, potassium, and calcium, and fulfills most of the daily need for vitamin C for consumers. Orange can be consumed fresh or processed domestically or industrially into jam, marmalade, or fruit juice, in addition to its frozen and dried forms [2]. Orange peel is used as a flavoring agent in the pastry sector and essential oils extracted from the peels are used in the cosmetics industry.

Since citrus fruits are cultivated in warm and subtropical climates where unwanted pests and wild herbs are common, it is normal agricultural practice to use pesticides to increase the yield of the crop [3]. However, excessive and unprescribed spraying and early harvesting can leave residues in the product, which may adversely affect the safety of the food consumed. Pesticide residue levels in foods must be safe for consumers, so national and international authorities have set maximum residue limits (MRL) for fresh fruits and vegetables, animal products, and feeds [4] (EC 2005). Processing factor (P_F) is defined as

the ratio of pesticide residue level in processed food to the pesticide residue level in the raw agricultural commodity (RAC). Processing factors are taken into account when verifying the compliance of residues in processed products with the MRL of agricultural commodities and to refine dietary exposure intake with respect to residues in processed products [5–7]. The studies reported in the literature revealed that pesticide residues in RACs can be decreased or increased as a result of the processes applied during the preparation of the products for consumption both at industrial and household-scale productions, including washing, peeling, freezing, heating, and drying [8–11].

Although oranges and their products are widely consumed throughout the world, the fate of the pesticide residues during the processing of oranges has been revealed in a limited number of studies in the literature [2,3,12–14]. The panel of experts on Pesticide Residues in Food and the Environment and the WHO Core Assessment Group on Pesticide Residues reported processing factors for different type of pesticides in food commodities. The reports included processing factors of pasteurized or canned orange juice, canned orange marmalade, dried orange peel oil, dried orange pulp, and chopped fresh orange peel, for different type of pesticides including buprofezin, dimethoate fenpyroximate, fluensulfone, imizalil metalxyl, mandipropamid, omethate, and pydiflumetofen [14]. Since processing effects depend on the physicochemical properties of the pesticide in addition to the type of the process and the matrix, processing factors should be individually determined for each pesticide, process, and matrix combination [5,15]. Therefore, there is still a need for further studies on the other common pesticides and household processing of oranges. In the light of the needs in the literature, we aimed to study the effects of various household food processing techniques (washing with tap water, peeling, pulping, processing to jam or fruit juice, storage of frozen grated peels for a certain period of time) on the initial concentration of abamectin, buprofezin, etoxazole, imazalil, and thiophanate-methyl residues in oranges. The pesticides were selected among the authorized commercial pesticides commonly used for local farming applications of citrus in Turkey.

2. Materials and Methods

2.1. Sampling

The oranges used in the study were purchased from the local market in Bursa in 2018, it was indicated that oranges were cultivated from Antalya region in Turkey in the same year [2].

Prior to analysis, samples were kept in the cold storage room at 5–7 °C and 90–95% relative humidity. Before pesticide treatment at laboratory conditions, three laboratory samples (C) were allocated as blank samples. It was found that control samples contained only one pesticide (imazalil) at 0.01 mg/kg level [2].

The moisture level of the control samples "C" was measured as 94.05% (MA150 Sartorius, Göttingen, Germany). The weights of each orange unit in laboratory sample "C" varied between 223 g and 246 g. Therefore, orange samples were defined as medium-sized products according to legal regulations. In this manner, in total 30–35 kg of orange samples were used, to make approximately 1 kg laboratory samples (at least 10 units for raw orange samples) depending on the type of the process [16].

2.2. Pesticide Treatment

The orange samples used in the scope of this study were immersed in to the solutions of the commercial formulations at the laboratory [17–19]. Therefore, a homogeneous distribution was provided between and within each unit of laboratory samples and a detectable amount of residue was obtained [2].

Commercial formulations of abamectin, buprofezin, etoxazole, imazalil, and thiophanate-methyl were purchased from a local seller. The physicochemical properties of the active ingredients were provided in Figure 1. The commercial formulations of the pesticides were Asmition (18 g/L, emulsified concentrate), Korfezin (400 g/L, suspension concentrate), Sorides (500 g/L, emulsified concentrate), Emtop (60%, wetted powder), and Novamite

(110 g/L, suspension concentrate), respectively. Their recommended dose for 100 mL during good agricultural practices were 25 mL, 35–65 mL, 25 mL, 400 mL, and 60 g, respectively. To obtain pesticide residue levels in the raw agricultural commodity (RAC) higher than the limit of quantification of the method, it is permissible to apply more formulations than the recommended dose [15]. Therefore, approximately one to four times the recommended dose of the formulations (indicated on the prospectus) were taken and diluted in 10 L of water in a plastic containers (15–20 L) providing a homogenous distribution of the mixture. To treat all orange samples at the same time for 30 min, a proper number of the plastic containers with 10 L of mixture solutions were prepared. Subsequently, all samples were sun dried for 3–4 h. Three laboratory samples were allocated from the dried samples as "RAC" samples. From the remaining samples, three laboratory samples were separated for each of the processes as explained below. Dried samples were stored at +4 °C for 1 day until further analysis [2].
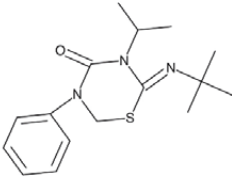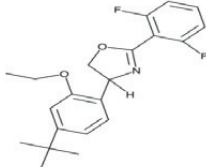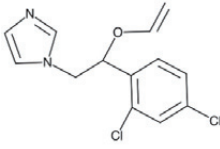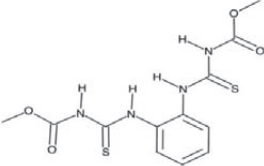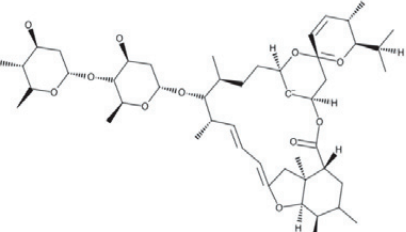
Buprofezin

➤ logP = 3.8
➤ Solubility in water = 0.9 mg/L (25 °C)
➤ Vapor pressure = 0.042 mPa
➤ Contact and Insecticide
➤ MRL for orange = 1 mg/kg

Etoxazole

➤ logP = 5.6
➤ Solubility in water = 0.07 mg/L (20 °C)
➤ Vapor pressure = 7.0 mPa
➤ Contact and Acaracide
➤ MRL for orange = 0.1 mg/kg

Imazalil

➤ logP = 3.82
➤ Solubility in water = 180 mg/L (25 °C)
➤ Vapor pressure = 0.158 mPa
➤ Systemic and Fungicide
➤ MRL for orange = 5 mg/kg

Thiophanate-Methyl

➤ logP = 1.5
➤ Solubility in water = 26.6 mg/L (25 °C)
➤ Vapor pressure = 9.0×10^{-3} mPa
➤ Contact and Fungicide
➤ MRL for orange = 6 mg/kg

Abamectin

➤ logP = 4.4
➤ Solubility in water = 1.21 mg/L (25 °C)
➤ Vapor pressure= 1.5×10^{-9} mPa
➤ Semi-Systemic and Insecticide
➤ MRL for orange = 0.015 mg/kg

Figure 1. Physicochemical structure and mode of action for the active ingredient (pesticide). MRL represents maximum residue level (EC 2005).

2.3. Household Processing

2.3.1. Washing (W)

Washing was the initial step for all household processing applied in the scope of this study. Orange samples were rubbed by hand under flowing tap water at 10 °C for 1–2 min.

2.3.2. Peeling: Separation of Peel (P) and Pulp (PU)

The peel and white flesh of the orange samples were separated from the fruit pulp with a knife. Peel/fruit weight ratios (%) ranged between 29% and 35%. The moisture content of the samples prior to peeling and the peel were 5.33 g H_2O/g sample in dry base and 15.81 g H_2O/ sample in dry base, respectively.

2.3.3. Frozen Grated Peels (GP)

The peel separated from the fruit were grated and stored at −20 °C for three months. In order to investigate the effect of storage period on the fate of the residue, the amount of residue in the frozen grated peels were determined monthly.

2.3.4. Fruit Juice (FJ)

Orange samples were divided into two sections to make fresh fruit juice by a home-based processer. The mean pH value of the juices was determined as 2.82 ± 0.05 (Mettler Toledo Seven compact pH/Ion pH meter, Colombus, OH, USA).

2.3.5. Homemade Jam (HJ)

The jam production was based on a local recipe. The peels of the orange samples were gently grated and removed. In order to remove the bitterness of the outer thin layer on the fruit pulp, the pulps were boiled in water 3 times for 15 min. For each time, boiling water was replaced with fresh. Then, the fruits were sliced into 2-cm-thick cubes with a knife. Sugar syrup was prepared by dissolving sugar in water at 1:1 concentration (w/w) followed by boiling for 30 min. Orange juice (1 mL) was added to the syrup at the end of the boiling step. The fruits were added in to the syrup and cooked at 95 °C for 30 min until the jam reached a proper consistency. The hot jam was put into the glass jars. Subsequently, the jars were turned upside down for cap sterilizations and kept in this form until they were cool. pH of the jam was measured as 3.45 ± 0.06 and water-soluble dry matter (Brix) was determined as 72.65 ± 0.64/100 g (RA-500 Model Kyoto Electronics Manufacturing Co. Ltd., Kyoto, Japan).

Samples were stored at −20 °C until further analysis.

2.4. Pesticide Residue Analysis

Acetonitrile, glacial acetic acid, methanol, formic acid (with a quality of sufficient purity that is free of interfering compounds in LC/MS/MS) were obtained from Merck (Germany). Neat reference standards with purity >99% were obtained from Dr. Ehrenstorfer (Germany). Deionized pure water was used (Milli Q purification system, Merck, Germany) for the analysis. The standard solutions were prepared with 1% acetic acid acetonitrile and stored at −18 °C. Regarding chopping of the laboratory samples, each unit of the laboratory samples was divided into four, and two cross sections were homogenized until a final particle size of 2–3 mm was obtained (RechtGM 200, Haan, Germany). On the other hand, the laboratory sample coded as HJ was entirely homogenized, and the laboratory samples FJ and GP were not subjected to homogenization. Two analytical portions from each analytical sample were taken and stored for one month at −20 °C in capped polypropylene sample vials until further analysis was performed.

The QuEChERS (fast, easy, cheap, effective, robust, and safe) extraction method was applied [20]. The details of the method, including LC-MS/MS identification and equipment parameters, were provided by Acoglu and Yolci Omeroglu [2].

All household processes were repeated three times, and pesticide residue analyses including LC-MS/MS injections were performed in duplicates for each analytical sample. Results were presented as mean ± standard error.

2.5. Processing Factor

The processing factor (P_F) can be calculated by Equation (1) [5,15]. A factor less than 1 or higher than 1 is an indication of a decrease or concentration, respectively.

$$P_F = \frac{B}{RAC} \tag{1}$$

where *B* refers to the residue level in the processed orange samples (W, P, PU, FJ, HJ, and GP). When the amount of pesticide residue in the processed product (*B*) was lower than the limit of quantification of the method (LOQ), the processing factor was determined by replacing *B* with the LOQ level in the Equation (1). Consequently, the processing factor was expressed with an asterisk "<" [5,7,21].

The effect of processing on pesticide residue concentration was evaluated by the calculation of the reduction ratio or concentration ratio (C_R) as given in Equation (2) [22];

$$C_R \ (\%) = \frac{RAC - B}{RAC} \times 100 \tag{2}$$

3. Results and Discussion

3.1. Reliability of the Analytical Method

The method used in the scope of the study was validated and approved by the Association of Official Agricultural Chemists (AOAC) as a standardized method [20]. Therefore, the method was verified at our laboratory conditions with a minimum requirement to obtain the provision of objective evidence that a given item fulfils specified requirements [23].

The standard analysis method applied in the scope of the study for the pesticide residue analyses was verified at 10 µg/kg to 60 µg/kg levels for high acid and water-containing foods and foods with high sugar and low water activity in accordance with the European SANTE/11312/2021 Guidance Document [24]. The following parameters were evaluated in the scope of the verification study: linearity, limit of quantification (LOQ), trueness (in terms of recovery), precision (repeatability and interim precision-intra-laboratory reproducibility), and measurement uncertainty.

The quantification and linearity of the method were evaluated during method verification study using matrix-matched calibration curves. Non-treated control orange samples were extracted as blank samples according to the extraction method described previously and the extracts were fortified with multi-standard working solutions at seven concentrations in a range between 2 µg/L and 80 µg/L. Moreover, during the analysis of the processed samples in the scope of the study (Table 1), multi-level calibration curves were constructed to cover the response of the pesticide residue in the sample at concentrations ranging between 10 µg/kg and 4000 µg/kg. The concentrations of pesticide active substances in samples were calculated in µg/kg using the weighted linear calibration curve functions with regression coefficients (R^2) > 0.9999.

As a result, mean recovery (%), repeatability (% CV_r), and intra-laboratory reproducibility (% CV_i) of the method ranged between 98.54–107.60%, 0.82–14.06%, and 1.56–16.23%, respectively (Figure 2). In addition, a blank sample was spiked with pesticides at the level of 10 µg/kg for each batch of analysis (*n* = 9), and the average recovery ratio was obtained in the range of 91% to 108%. LOQ was 10 µg/kg. The method performance parameters were compatible with the criteria set in the SANTE guideline [24].

Table 1. Effect of household processing of orange on the concentration of pesticide residue and processing factors ($n = 3$).

Process	Abamectin		Buprofezin		Ethoxazole		Imazalil		Thiophanate-Methyl	
	C (mg/kg)	P_F	C (mg/kg)	P_F	C (mg/kg)	P_F	C (mg/kg)	P_F	C (mg/kg)	P_F
Raw agricultural commodity (RAC)	0.030 ± 0.004	-	0.189 ± 0.047	-	0.082 ± 0.025		2.113 ± 0.475		0.110 ± 0.030	
Washing	0.020 ± 0.003	0.663 ± 0.115	0.136 ± 0.023	0.720 ± 0.121	0.050 ± 0.001	0.616 ± 0.011	1.643 ± 0.271	0.776 ± 0.127	0.019 ± 0.003	0.173 ± 0.028
Peeling; Separation of peel	0.080 ± 0.012	2.68 ± 0.42	0.650 ± 0.091	3.43 ± 0.48	0.396 ± 0.025	4.83 ± 0.307	2.963 ± 0.366	1.40 ± 0.176	0.404 ± 0.041	3.67 ± 0.37
Peeling; Separation of pulp	<LOQ	<0.330	0.080 ± 0.014	0.423 ± 0.076	<LOQ[1]	<0.120	0.453 ± 0.011	0.216 ± 0.005	0.015 ± 0.005	0.146 ± 0.005
Fruit juice	<LOQ	<0.330	0.037 ± 0.001	0.200 ± 0.001	<LOQ[1]	<0.120	0.580 ± 0.001	0.270 ± 0.001	0.039 ± 0.316	0.363 ± 0.063
Homemade jam	<LOQ	<0.330	0.019 ± 0.005	0.103 ± 0.028	<LOQ[1]	<0.120	0.105 ± 0.008	0.050 ± 0.001	<LOQ[1]	<0.090
Frozen storage of grated peels (1st month)	0.090 ± 0.017	2.83 ± 0.58	0.840 ± 0.036	4.60 ± 1.04	0.466 ± 0.030	6.07 ± 1.92	3.866 ± 0.075	1.90 ± 0.487	0.520 ± 0.051	4.88 ± 0.29
Frozen storage of grated peels (2nd month)	0.069 ± 0.011	2.32 ± 0.39	0.686 ± 0.025	3.62 ± 0.13	0.436 ± 0.005	5.33 ± 0.08	3.753 ± 0.254	1.78 ± 0.121	0.486 ± 0.127	3.53 ± 0.77
Frozen storage of grated peels (3rd month)	0.032 ± 0.011	1.11 ± 0.43	0.533 ± 0.020	2.81 ± 0.11	0.393 ± 0.152	4.80 ± 0.19	2.846 ± 0.06	1.35 ± 0.02	0.390 ± 0.085	3.26 ± 1.73

[1] LOQ: limit of determination, 0.01 mg/kg, residue amount (B) is taken as 0.010 mg/kg when calculating the processing factor for these processes (Scholtz vd., 2017).
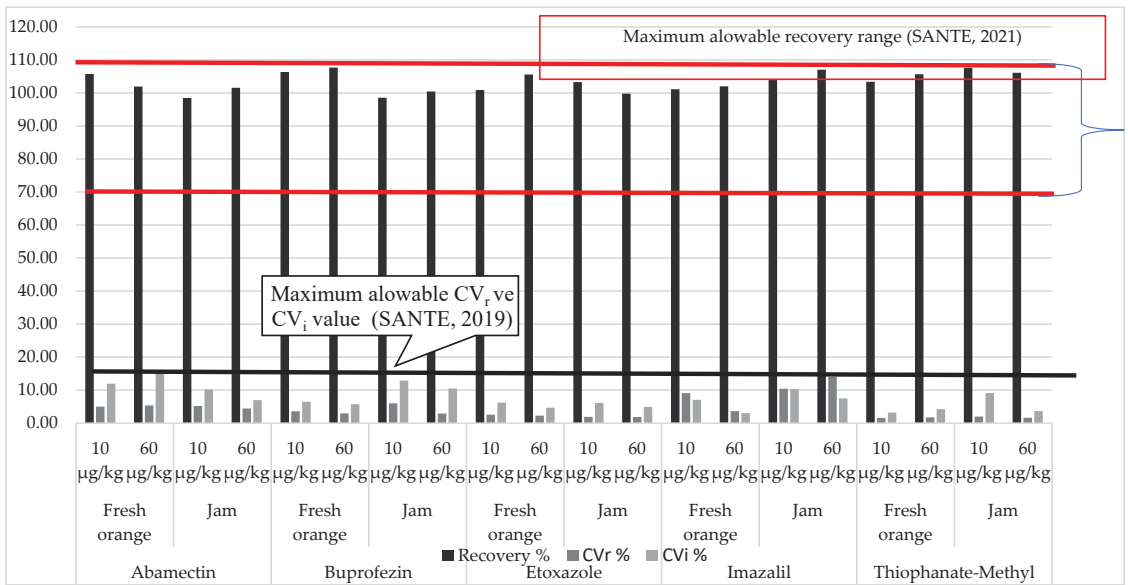
Figure 2. Method verification results (SANTE 2021).

Uncertainty is defined as a non-negative parameter characterizing the dispersion of the quantity values being attributed to a measurement based on the information used. There are two basic approaches to estimate measurement uncertainty, namely the bottom-up and top-down approaches. The top-down approach can be based on the method validation/verification and inter-quality-control laboratory dataset obtained within a laboratory. Combined measurement uncertainty arising from laboratory operations ($u_{Laboratory}$) can be estimated from the square root of the quadratic sum of the random component (u_{Rw}) and the systematic component (u_{Bias}):

$$u_{Laboratory} = \sqrt{u_{Rw}^2 + u_{Bias}^2}$$ (3)

u_{Rw} is the coefficient of variation of within-laboratory reproducibility which reflects all variation under routine conditions. u_{Bias} is the root mean square of the individual bias values and obtained from recovery studies [25,26]. As shown in Figure 3, the relative standard combined uncertainty arises from laboratory operations ranging between 0.1% and 19.21%, which corresponds to 0.2–38.42% of the expanded combined uncertainty at a 95% confidence level (k = 2). Those values comply with the maximum default relative expanded measurement uncertainty set as 50% in the European SANTE/11312/2021 Guidance Document [24].

3.2. Effect of Household Food Processing on Residue Content of Orange

The concentration of the residue in RAC should be higher than the limit of quantification (LOQ) of the analytical methods [15]. After the dipping of the orange samples into the commercial formulations in laboratory conditions, it was observed that the amount of pesticide residue in the treated orange samples (TC) ranged from 0.030 mg/kg to 3.753 mg/kg (Table 1), therefore the criteria set by OECD guideline was met in the scope of the study. Processing factors were calculated with Equation (1) and shown in Table 1.
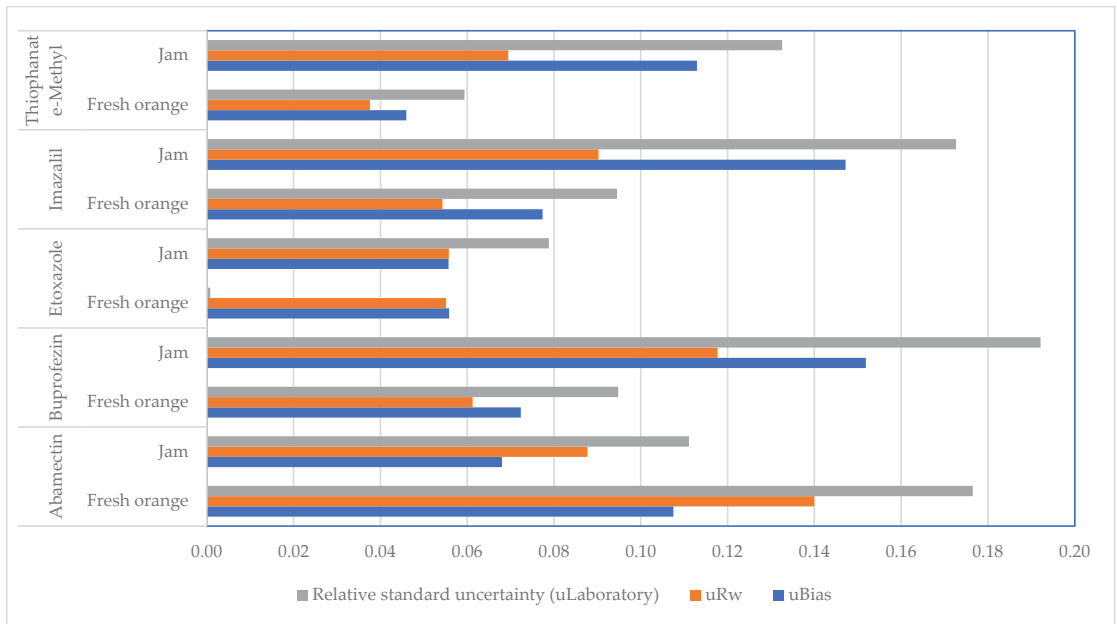
Figure 3. Uncertainty components (SANTE 2021).

3.2.1. Washing (W)

Washing is the pretreatment in any type of food processing. It was observed that the washing process under tap water reduced the initial concentration of the residues in oranges by 26–84%, and processing factors ranged between 0.173 and 0.776. Consistently with our findings, other studies reported in the literature prevailed that pesticide residue decreased because of the washing of fruits and vegetables [2,27,28].

Li et al. [3] reported that washing of oranges with tap water reduced the residues of carbendazim, abamectin, imidacloprid, prochloraz, and cypermethrin by 43.6–85.4%. Another other study reported by Kwon et al. [29] revealed that the residues of chlorothalonil, oxadixyl, and thiophanate-methyl in tomatoes decreased by 92%, 52%, and 84%, respectively, after washing for 10 s. Acoglu and Yolci Omeroglu [2] investigated the effect of different washing agents on the fate of pesticides in orange. After washing oranges by dipping them into cold water (<10 °C) for 20 min, pesticide residues of abamectin, buprofezin, etoxazole, imazalil, and thiophanate-methyl decreased by 3–68%. In the current study, the additional hand rubbing operations eased the removal of pesticides during the washing of oranges.

After the washing step, the highest reduction (84%) was obtained for thiophanate-methyl, which has the lowest octanol/water partition coefficient (LogP) value among the other pesticides (Figure 1). The lowest reduction ratios (31–38%), achieved for abamectin, buprofezin, and etoxazole, can be attributed to their lower water solubility and higher LogP values compared to others. The octanol/water partition coefficient (LogP) of pesticides is the ratio of the solubility of a compound in octanol (a nonpolar solvent) to its water (a polar solvent) solubility [2]. Even though imazalil has a high water solubility (180 g/mL) 26% of the initial concentration was reduced after washing with tap water by hand. Romeh et al. [30] stated that the nature of the harvested crops was effective on the pesticide residue content of the final product. They demonstrated that pesticides can dry on the surface of the fruit and can be absorbed by the outer waxy structure. In this context, although imazalil has a systemic action and should diffuse through the inner part of the fruit, it deposited on the outer oily layer of the peel due to its high octanol–water coefficient as 3.82.

In the same context, most of the studies demonstrated that pesticides with low LogP values can be easily washed away from the crop surface compared to the pesticides with high LogP values [2,11]. Polat and Tiryaki [28] observed that the reduction effects of different washing processes for capia pepper was related to the physicochemical properties of the pesticide (including mainly water solubility and an octanol–water coefficient). Similarly, Vass et al. [31] observed that 2% of the imazalil residue in lemon was reduced by washing with cold water.

3.2.2. Peeling: Separation of Peel and Pulp

Peeling is the first step during the processing of many fruits and vegetables. It is an effective method to cut out the outer layers or skins of fruits and some vegetables and to reduce pesticide residues. It is also reported that chemical, mechanical, steam, or freezing peeling processes can provide a significant removal of residues depending on the chemical nature of the pesticides and environmental conditions [9,32].

In the scope of this study, it was concluded that the average initial concentration of the residues increased by 83% to 270% for obtaining the peel (P). As a result of the separation of the orange peels from the fruit pulp (PU), abamectin and etoxazole residues were not detected in the pulp, while a decrease was observed in the concentration of buprofezin, imazalil, and thiophanate-methyl by 57%, 73%, and 86%, respectively. In the same manner, processing factors for peel and pulp ranged between 1.40 and 4.83 and <0.120 and 0.423, respectively. In line with our observations, Yolci Omeroglu et al. [33] reported that the residue concentration of benomyl, which is a systemic fungicide, decreased by 41% to 83% by peeling. Li et al. [3] concluded that immidacloprid, carbendazim, abamectin, and cypermethrin residues were mostly distributed on peel of the orange. They reported that 7.5 to 17.9% of the initial residues diffused through the pulp of the fruit. Kwon et al. [29] observed that peeling process decreased the chlorothalonil, oxadixyl, and thiophanate-methyl concentration in tomato by 96%, 60%, and 93%, respectively.

After the peeling process, the pesticide residues remained on the peel layer of the fruit and mass transfer of the residues from peel to the pulp occurred at a lower diffusivity rate. This can be attributed to the physicochemical properties of the pesticides investigated in the scope of the study. Since thiophanate-methyl, etoxazole, and abamectin are contact and semi-systemic pesticides, they retained on the peel and did not diffuse through the pulp section of the fruit. In the same context, as a systemic pesticide imazalil was expected to diffuse completely through the pulp of the fruits, but its diffusion to the pulp section occurred on a limited scale. This can be attributed to its high octanol-water coefficient. Pesticides with high octanol–water coefficients (logP) (Figure 1) can be easily absorbed by the wax on the orange peel and cannot be removed from the peel easily [28,32]. Similarly, studies reported in the literature emphasize that the peeling process significantly decreased pesticide residues in fruits by peeling, and the reduction ratio was mainly based on the physicochemical properties of the active ingredients [27,32,34,35].

3.2.3. Processing in to Fruit Juice (FJ)

The transition of pesticide residues from fruit to fruit juice depends on the distribution of the residue between peel and pulp in addition to their physicochemical properties. Residues are also reduced by the steps in the fruit juice production process, including clarification steps such as centrifugation or filtration [8,31].

As shown at Table 1, while abamectin and etoxazole residues were not detected in fruit juice, buprofezin, imazalil, and thiophanate-methyl residues decreased by 93%, 79%, and 63% respectively. Processing factor ranged between <0.120 and 0.363. Similarly, Li et al. [3] found that imidacloprid, abamectin, cypermethrin, and prochloraz residues decreased by 46.5%, 46.0%, 94.7%, and 81.0%, respectively, by obtaining orange juice from fresh oranges.

During the processing of oranges into fruit juice it was observed that highest reduction ratio was obtained for the pesticides with low water solubility (abamectin and etoxazole), while most of the residue concentration of the pesticides with higher solubility (thiophanate-

methyl and imazalil) transferred into the juice. These findings can be attributed to the distribution of the pesticide residues between fruit peel/pulp and juice, depending on their water solubility [36].

3.2.4. Frozen Storage of Grated Peels (GP)

Freezing is a commonly used food preservation method, as it slows down the chemical reactions that affect food quality, and retain flavor, texture, and nutritional quality of the final products better than other methods [31]. Orange peels can be stored as frozen forms to be evaluated as a by-product, to prolong its shelf life without any deterioration in its physicochemical structure, and can be used as an ingredient in pastry products.

In the scope of the study, pesticide residues in GP were significantly higher ($p < 0.05$) than the residue levels of the control orange samples (TC) (Table 1). Comparing the residue level of the frozen grated peels with the fresh peels (P), it was observed that there was a significant difference ($p < 0.05$), except for in abamectin. It can be related to the difference between the structure of the GP and P samples. GP was obtained by grating the top layer of the peel which did not contain any trace of the mesocarb section. As a result of a three-month storage periods, it was observed that pesticide residues in GP decreased significantly ($p < 0.05$). Therefore, it was concluded that the storage period affected the residue concentrations. Processing factors changed between 1.91 and 6.07, 1.780 and 5.33, 1.11 and 4.80, after the first, second, and third month of the frozen storage periods, respectively. Similarly, Ögüt et al. [37] reported that diazinon, parathion-methyl, captan, methidathion, cypermethrin, and deltamethrin residues in frozen cherries decreased during storage. The other studies reported in the literature supported these findings [37,38]

3.2.5. Homemade Jam Processing (HJ)

Jams and marmalades are products in which fruits are made to be durable by high-heat treatment with the addition of sugar. As shown in Table 1, abamectin, etoxazole, and thiophanate-methyl residues were not detected in orange jam, while buprofezin and imazalil decreased significantly by 90% and 95% considering their initial levels. Consequently, processing factors were obtained (between 0.05 and <0.330). Within the scope of the study, in order to process orange jam, boiling was carried out as a pre-treatment step. During the boiling step, boiling water was replaced with fresh water three times. At the last step, cooking was carried out by adding fresh water and sugar to the fruits. Therefore, the reduction of pesticide residue levels in the jam could be attributed to the removal of water-soluble pesticides with boiling water [8,32,39,40], evaporation, decomposition, heat degradation, time, and the temperature of the heat treatment process applied for cooking [41,42]. Hendawi et al. [43] reported that imidacloprid residue decreased by about 15% with the processing of strawberries, in which the boiling of the fruit and removal of boiling water was not applied, in contrast to our study. Lozowicka et al. [42] revealed that thiophanate-methyl residue decreased by a ratio of 82% and difenoconazole decreased by 29% during the production of black currant jam. Therefore, it can be stated that there may be a difference in the reduction rate according to the jam cooking technique and the physicochemical structure of the pesticide residue in the product.

4. Conclusions

The fate of pesticides during various household and industrial processes depends on the type of processing methods, the physicochemical properties of the pesticides, and the nature of the product. Pesticides with high octanol–water coefficients were absorbed by the wax of the orange peel, therefore they remained on the peel and could not easily be removed by the washing step. Moreover, pesticides with lower water solubility did not diffuse easily through the fruit juices from the pulp section of the fruit. The processing factor was greater than 1 for the separation of the orange peel and less than 1 for the washing step and jam and fruit juice production. The compliance of residues in processed commodities with MRLs set for RAC should be assessed by taking into account the processing factor

values. Furthermore, processing factors are essential to estimate residues in processed commodities for conducting dietary risk assessment. Therefore, it is essential to reveal the processing factors with scientific studies in order to make legal arrangements. It should be indicated that the dipping of the crops into commercial formulations of the pesticides under laboratory conditions does not reflect real processing effects. Therefore, to obtain more accurate processing factors, in future studies field treatment of the crops should be applied. In field-treated crops, pesticides may penetrate into different sections of the plants based on the pre-harvest interval. Absorption and translocation of the pesticide through the crops may affect the fate of the pesticide throughout the processing. Consequently, this study can be taken as a case study and more extensive studies should be carried out for different type of foods and different type of processing methods with field-treated crops.

References

1. Anonymous. Yaş Meyve Ve Sebze Sektörü Türkiye Geneli Değerlendirme Raporu. *Akdeniz İhracatçılar Birliği.* **2018**. Available online: http://www.akib.org.tr/files/downloads/ArastirmaRaporlari/YSM/ocak-2018.pdf (accessed on 18 June 2022).
2. Acoglu, B.; Yolci Omeroglu, P. Effectiveness of Different Type of Washing Agents on Reduction of Pesticide Residues in Orange (*Citrus sinensis*). *LWT* **2021**, *147*, 111690. [CrossRef]
3. Li, Y.; Jiao, B.; Zhao, Q.; Wang, C.; Gong, Y.; Zhang, Y.; Chen, W. Effect of Commercial Processing on Pesticide Residues in Orange Products. *Eur. Food Res. Technol.* **2012**, *234*, 449–456. [CrossRef]
4. European Commission (EC). *Regulation (EU) No 396/2005 on Maximum Residue Levels of Pesticides in or on Food and Feed of Plant and Animal Origin, and Amending Council Directive 91/414/EEC*; European Commission (EC): Luxembourg, 2005; pp. 1–16.
5. Scholz, R.; Herrmann, M.; Michalski, B. Compilation of Processing Factors and Evaluation of Quality Controlled Data of Food Processing Studies. *J. Verbrauch. Leb.* **2017**, *12*, 3–14. [CrossRef]
6. European Commission (EC). Information Note on Article 20 of Regulation (EC) No 396/2005 as Regards Processing Factors, Processed and Composite Food and Feed. (SANTE/10704/2021). Available online: https://food.ec.europa.eu/system/files/2022-02/pesticides_mrl_guidelines_proc_imp_sante-2021-10704.pdf (accessed on 6 October 2022).
7. FAO. Submission and Evaluation of Pesticide Residues Data for the Estimation of Maximum Residue Levels in Food and Feed, Plant Production and Protection Paper 225, Third Edition. 2016. Available online: https://www.fao.org/3/i5452e/I5452E.pdf (accessed on 6 October 2022).
8. Dordevic, T.; Durovic-Pejcev, R. Food Processing as a Means for Pesticide Residue Dissipation. *Pestic. Phytomed.* **2017**, *31*, 89–105. [CrossRef]
9. Chung, S.W.C. How Effective Are Common Household Preparations on Removing Pesticide Residues from Fruit and Vegetables? A Review. *J. Sci. Food Agric.* **2018**, *98*, 2857–2870. [CrossRef]
10. El-Sayed, E.; Hassan, H.; Abd El-Raouf, A.; Salman, S.N. Investigation of the Effects of Household Processing on the Reduction Rate of Chlorpyrifos, Metalaxyl and Diazinon Residues in Orange Fruit Investigation of the Effects of Household Processing on the Reduction Rate of Chlorpyrifos, Metalaxyl and Diazino. *Hell. Plant Prot. J.* **2021**, *14*, 64–75. [CrossRef]
11. Li, C.; Li, C.; Yu, H.; Cheng, Y.; Xie, Y.; Yao, W.; Guo, Y.; Qian, H. Chemical Food Contaminants during Food Processing: Sources and Control. *Crit. Rev. Food Sci. Nutr.* **2021**, *61*, 1545–1555. [CrossRef]
12. Kusvuran, E.; Yildirim, D.; Mavruk, F.; Ceyhan, M. Removal of Chloropyrifos Ethyl, Tetradifon and Chlorothalonil Pesticide Residues from Citrus by Using Ozone. *J. Hazard. Mater.* **2012**, *241–242*, 287–300. [CrossRef]
13. Cámara, M.A.; Cermeño, S.; Martínez, G.; Oliva, J. Removal Residues of Pesticides in Apricot, Peach and Orange Processed and Dietary Exposure Assessment. *Food Chem.* **2020**, *325*, 126936. [CrossRef]

14. FAO and WHO Reports. Pesticide Residues in Food—Joint FAO/WHO Meeting on Pesticide Residues. Rome. 2022. Available online: https://www.fao.org/pest-and-pesticide-management/guidelines-standards/faowho-joint-meeting-on-pesticide-residues-jmpr/reports/en (accessed on 6 October 2022).

15. OECD. OECD Guideline for the Testing of Chemicals. Magnitude of the Pesticide Residues in Processed Commodities. 2008. Available online: http://www.oecd.org/env/ehs/pesticidesbiocides/publicationsonpesticideresidues.htm (accessed on 19 June 2022).

16. European Commission (EC). Commission Directive 2002/63/EC of 11 July 2002 establishing Community methods of sampling for the official control of pesticide residues in and on products of plant and animal origin and repealing Directive 79/700/EEC. *OJEC* **2002**, *187*, 30–45.

17. Hassan, H.; Elsayed, E.; El-Raouf, A.E.R.A.; Salman, S.N. Method Validation and Evaluation of Household Processing on Reduction of Pesticide Residues in Tomato. *J. Consum. Prot. Food Saf.* **2019**, *14*, 31–39. [CrossRef]

18. Heshmati, A.; Hamidi, M.; Nili-Ahmadabadi, A. Effect of Storage, Washing, and Cooking on the Stability of Five Pesticides in Edible Fungi of Agaricus Bisporus: A Degradation Kinetic Study. *Food Sci. Nutr.* **2019**, *7*, 3993–4000. [CrossRef]

19. Ruengprapavut, S.; Sophonnithiprasert, T.; Pongpoungphet, N. The Effectiveness of Chemical Solutions on the Removal of Carbaryl Residues from Cucumber and Chili Presoaked in Carbaryl Using the HPLC Technique. *Food Chem.* **2020**, *309*, 125659. [CrossRef]

20. AOAC. Official Method 2007.01: Pesticide Residues in Foods by Acetonitrile Extraction and Partitioning with Magnesium Sulfate. *J. AOAC Int.* **2007**, *90*, 485–520.

21. FAO. *Pesticide Residue in Food*; FAO Plant Protection Paper, No.163; FAO: Rome, Italy, 2000.

22. Bian, Y.; Wang, J.; Liu, F.; Mao, B.; Huang, H.; Xu, J.; Li, X.; Guo, Y. Residue Behavior and Removal of Iprodione in Garlic, Green Garlic, and Garlic Shoot. *J. Sci. Food Agric.* **2020**, *100*, 4705–4713. [CrossRef]

23. Magnusson, B.; Ornemak, U. (Eds.) *Eurachem Guide: The Fitness for Purpose of Analytical Methods—A Laboratory Guide to Method Validation*, 2nd ed.; EUURACHEM: London, UK, 2014; Available online: www.eurachem.org (accessed on 6 October 2022).

24. SANTE. European Commision (EC) Director General for Food and Health Safety. Guidance Document on Analytical Quality Control and Validation Procedures for Pesticide Residues Analysis in Food and Feed, Document No: SANTE 11312/2021. 2021. Available online: https://food.ec.europa.eu/system/files/2022-02/pesticides_mrl_guidelines_wrkdoc_2021-11312.pdf (accessed on 1 June 2022).

25. Ellison, S.L.R.; Williams, A. (Eds.) *Eurachem/CITAC Guide: Quantifying Uncertainty in Analytical Measurement*, 3rd ed.; Eurachem/CITAC: Teddington, UK, 2012; ISBN 978-0-948926-30-3. Available online: www.eurachem.org (accessed on 4 October 2020).

26. Magnusson, B.; Näykki, T.; Hovind, H.; Krysell, M.; Sahlin, E. Handbook for Calculation of Measurement Uncertainty in Environmental Laboratories; 2017. Nordtest Report TR 537 (ed. 4). Available online: www.nordtest.info (accessed on 4 June 2022).

27. Bonnechere, A.; Hanot, V.; Bragard, C.; Bedoret, T.; Loco, J.V. Effect of Household and Industrial Processing on the Levels of Pesticide Residues and Degradation Products in Melons. *Food Addit. Contam. Part A* **2012**, *29*, 1058–1066. [CrossRef]

28. Polat, B.; Tiryaki, O. Assessing Washing Methods for Reduction of Pesticide Residues in Capia Pepper with LC-MS/MS. *J. Environ. Sci. Health Part B Pestic. Food Contam. Agric. Wastes* **2019**, 1–10. [CrossRef]

29. Kwon, H.; Kim, T.K.; Hong, S.M.; Se, E.K.; Cho, N.J.; Kyung, K.S. Effect of Household Processing on Pesticide Residues in Field-Sprayed Tomatoes. *Food Sci. Biotechnol.* **2015**, *24*, 1–6. [CrossRef]

30. Romeh, A.A.; Mekky, T.M.; Ramadan, R.A.; Hendawi, M.Y. Dissipation of Profenofos, Imidacloprid and Penconazole in Tomato Fruits and Products. *Bull. Environ. Contam. Toxicol.* **2009**, *83*, 812–817. [CrossRef]

31. Vass, A.; Korpics, E.; Dernovics, M. Follow-up of the Fate of Imazalil from Post-Harvest Lemon Surface Treatment to a Baking Experiment. *Food Addit. Contam. Part A* **2015**, *32*, 1875–1884. [CrossRef]

32. Kaushik, G.; Satya, S.; Naik, S.N. Food Processing a Tool to Pesticide Residue Dissipation—A Review. *Food Res. Int.* **2009**, *42*, 26–40. [CrossRef]

33. Yolci Omeroglu, P.; Ambrus, Á.; Boyacioglu, D.; Majzik, E.S. A Case Study to Assess the Sample Preparation Error in Pesticide Residue Analysis. *Food Anal. Methods* **2015**, *8*, 474–482. [CrossRef]

34. Han, Y.; Dong, F.; Xu, J.; Liu, X.; Li, Y.; Kong, Z.; Liang, X.; Liu, N.; Zheng, Y. Residue Change of Pyridaben in Apple Samples during Apple Cider Processing. *Food Control* **2014**, *37*, 240–244. [CrossRef]

35. Andrade, G.C.R.M.; Monteiro, S.H.; Francisco, J.G.; Figueiredo, L.A.; Rocha, A.A.; Tornisielo, V.L. Effects of Types of Washing and Peeling in Relation to Pesticide Residues in Tomatoes. *J. Braz. Chem. Soc.* **2015**, *26*, 1994–2002. [CrossRef]

36. Özel, E.; Tiryaki, O. Elma ve Işlenmiş Ürünlerinde Imidacloprid ve Indoxacarb Kalıntılarının Belirlenmesi. *Bitki Koruma Bülteni Plant Prot. Bull.* **2019**, *59*, 23–32. [CrossRef]

37. Öğüt, S.; Canbay, H.S.; Yilmazer, M.; Üniversitesi, A.M.; Yüksekokulu, A.S. Dondurularak Saklanan Kirazlardaki Pestisit Kalıntı Miktarlarının Zamanla Değişimi Changes in Pesticide Residue Amounts on Frozen Cherries Over Time. *Süleyman Demirel Üniversitesi Fen Bilim. Enstitüsü Derg. (Suleyman Demirel Univ. J. Nat. Appl. Sci.)* **2014**, *18*, 72–77.

38. Chauhan, R.; Monga, S.; Kumari, B. Dissipation and Decontamination of Bifenthrin Residues in Tomato (*Lycopersicon esculentum* Mill). *Bull. Environ. Contam. Toxicol.* **2012**, *89*, 181–186. [CrossRef] [PubMed]

39. Oliva, J.; Cermeño, S.; Cámara, M.A.; Martínez, G.; Barba, A. Disappearance of Six Pesticides in Fresh and Processed Zucchini, Bioavailability and Health Risk Assessment. *Food Chem.* **2017**, *229*, 172–177. [CrossRef] [PubMed]

40. Medina, M.B.; Munitz, M.S.; Resnik, S.L. Effect of Household Rice Cooking on Pesticide Residues. *Food Chem.* **2021**, *342*, 128311. [CrossRef] [PubMed]

41. Bajwa, U.; Sandhu, K.S. Effect of Handling and Processing on Pesticide Residues in Food—A Review. *J. Food Sci. Technol.* **2014**, *51*, 201–220. [CrossRef] [PubMed]

42. Lozowicka, B.; Jankowska, M.; Kaczynski, P. Behaviour of Selected Pesticide Residues in Blackcurrants (*Ribes nigrum*) during Technological Processing Monitored by Liquid-Chromatography Tandem Mass Spectrometry. *Chem. Pap.* **2016**, *70*, 545–555. [CrossRef]

43. Hendawi, M.Y.; Romeh, A.A.; Mekky, T.M. Effect of Food Processing on Residue of Imidacloprid in Strawberry Fruits. *J. Agric. Sci. Technol.* **2013**, *15*, 951–959.

foods

Article

Comparative Transcriptome Analysis to Investigate the Immunotoxicity Mechanism Triggered by Dimethomorph on Human Jurkat T Cell Lines

Yun-Cheng Li [1,2], Shu-Yan Liu [2], Fan-Bing Meng [2], Shu-Hui Xu [2], Jing Qiu [1], Yong-Zhong Qian [1,*], Yan-Yang Xu [1] and Yun Li [1]

[1] Institute of Quality Standards and Testing Technology for Agro-Products, Chinese Academy of Agricultural Sciences, Beijing 100081, China

[2] College of Food and Biological Engineering, Chengdu University, Chengdu 610106, China

* Correspondence: qianyongzhong@caas.cn; Tel.: +86-10-82106515

Abstract: Dimethomorph (DMM) is a broad-spectrum fungicide used globally in agricultural production, but little is known regarding the immunotoxicity of DMM in humans. In this study, the immunotoxicity of DMM on human Jurkat T cells was evaluated in vitro. The results indicated that the half-effective concentration (EC_{50}) of DMM for Jurkat cells was 126.01 mg/L (0.32 mM). To further elucidate the underlying mechanism, transcriptomics based on RNA sequencing for exposure doses of EC_{25} (M21) and EC_{10} (L4) was performed. The results indicated that compared to untreated samples (Ctr), 121 genes (81 upregulated, 40 downregulated) and 30 genes (17 upregulated, 13 downregulated) were significantly differentially regulated in the L4 and M21 samples, respectively. A gene ontology analysis indicated that the significantly differentially expressed genes (DEGs) were mostly enriched in the negative regulation of cell activities, and a KEGG pathway analysis indicated that the DEGs were mainly enriched in the immune regulation and signal transduction pathways. A quantitative real-time PCR for the selected genes showed that compared to the high-dose exposure (M21), the effect of the low-dose DMM exposure (L4) on gene expression was more significant. The results indicated that DMM has potential immunotoxicity for humans, and this toxicity cannot be ignored even at low concentrations.

Keywords: dimethomorph; Jurkat T cells; immunotoxicity; transcriptomics; RNA sequencing

1. Introduction

With the deterioration of the environment and the growth of the population, a good public health environment and adequate food supplies have increasingly become stumbling blocks for the development of human society [1–3]. Pesticides play an important role in controlling insect-borne diseases and developing agricultural production [2,4,5]. The ideal pesticide is effective against targeted diseases and insect pests without harming the human body; however, this seems difficult to achieve [6]. Mounting evidence has shown that pesticide residues can impact human health through environmental and food contamination [2], even at very low levels of exposure [4]. Therefore, a comprehensive understanding of pesticide toxicities is essential to the rational application of pesticides.

Numerous pesticide toxicity assessments have been carried out in recent years, but most of them are focused on general toxicity (acute toxicity, subchronic or subacute toxicity, chronic toxicity, etc.), endocrine toxicity, neurotoxicity, and "mutagenesis, carcinogenesis, teratogenesis" effects [7–10]. However, when a chemical compound is stated to be toxic, it does not necessarily mean that it induces the death of cells; effects may not result in cytotoxicity but alteration of cell function, leading to a detrimental outcome [11]. Among them, the immune system is the first line of defense against foreign hazardous chemicals within the human body. Thus, the immune response triggered by pesticides may be closely associated with the

predisposition to different types of disease because the immune system mutually and closely interacts with all body organs [12,13]. Therefore, immunotoxicity evaluations of pesticide residues are very important for a comprehensive pesticide residue risk assessment that can guide agricultural production. Traditional immunotoxicity is usually evaluated through animal experiments for studying the specific antigen immune response, immune function, and so on. However, animal experiments are time consuming and require a lot of animal materials, and the use of animals is an important ethical and political issue [14]. Therefore, animal alternative methods (such as in vitro cell experiment) combined with bioinformatics has the potential to provide more comprehensive knowledge on the toxicological mechanism of chemicals in biological systems than more traditional approaches [15].

Dimethomorph (4-[3-(4-chlorophenyl)-3-(3-4-dimethox-yphenyl) acryloyl] morpholine, DMM), a cinnamic acid derivative, is a broad-spectrum fungicide globally used in agricultural production to prevent gray mold, powdery and downy mildews, crown and root rots, and late blight [16,17]. Since the use of DMM is very extensive, some reports in recent years have shown that the content of water, soil, and agricultural products of DMM range from ng/kg to mg/kg [18] and pose a certain risk to living organisms, including aquatic organisms, birds, and mammals [19,20]. Therefore, numerous studies have been performed to determine the dissipation and residue of DMM in vegetables, fruits, and their processed products [19–22]. More importantly, many studies have demonstrated that DMM is toxic to some soil and water microflora, birds, and mammals, even at very low concentrations [18,20]. Although the Environmental Protection Agency (EPA) reports show that DMM has low toxicity to humans, there has been insufficient knowledge regarding the toxicity and toxicity mechanisms of DMM pesticides in humans, especially immunotoxicity. In addition, owing to the continual and prolonged exposure of dimethomorphs, previous studies have indicated that fungal species have developed resistance and become insensitive to lower concentrations of DMM [16]. In order to fight fungal infection, a higher concentration of DMM is sprayed in fields, resulting in an increase in residues within agricultural products, as high as 7 mg/kg, which has been detected in vegetables. Meanwhile, a previous study also suggested that DMM is extremely resistant to hydrolysis and has a long half-life in the ecosystem [18]. Therefore, it is necessary to study the toxicity and mechanism of DMM in order to provide some reference for its risk assessment.

In the present study, the in vitro immunotoxicity of DMM in humans was investigated by using the human Jurkat T cell line, an in vitro model system frequently used in immunotoxicity evaluation due to its well-established reliability [23]. In addition, a comparative transcriptome analysis was applied to reveal the underlying immunotoxicity mechanism of DMM. To our knowledge, this is the first study to focus on the immunotoxicity of DMM to human immune cells, and the results provide a reference for the risk assessment of DMM.

2. Materials and Methods

2.1. Chemicals and Reagents

Dimethomorph (DMM, 99.9% purity) was obtained from A Chemtek Inc. (Worcester, MA, USA). The human T-lymphocyte cell line (Jurkat T cells) was obtained from the American Type Culture Collection (ATCC, Manassas, VI, USA); this cell line was derived from the peripheral blood of human T-lymphocyte leukemia cells. Acetone (HPLC grade) was purchased from Merck & Co. (Darmstadt, Germany). RPMI-1640 medium, penicillin/streptomycin, phosphate-buffered saline (PBS), and fetal bovine serum (FBS) were all purchased from HyClone (Logan, UT, USA). The Cell Counting Kit-8 was purchased from Dojindo (Kumamoto, Japan). The Annexin V-FITC/PI detection kit was purchased from Abbkine (Wuhan, China). The Mycoplasma Stain Kit was purchased from Sigma Aldrich (St Louis, Missouri, MO, USA), the TruSeq™ RNA Sample Preparation Kit was purchased from Illumina (San Diego, CA, USA), and the PrimeScript RT Reagent Kit was purchased from Beyotime Biotechnology (Shanghai, China). Unless otherwise specified, the reagents used in this study were of analytical grade.

2.2. Jurkat Cell Culture

As DMM has low solubility in water, an 11,000 mg/L stock solution of dimethomorph was prepared in acetone without FBS and maintained at −20 °C [24]. Final concentrations of DMM in the assay were achieved by their dilution in the culture medium. The final acetone concentration in the medium was less than 0.1% (v/v). The Jurkat cells were inoculated in RPMI-1640 medium containing 10% (v/v) heat-inactivated FBS, 100 U/mL of penicillin sodium, and 100 μg/mL of streptomycin solution, and incubated in a humidified atmosphere containing 5% CO_2 at 37 °C. The cells were kept at the logarithmic phase by passages at 2–3 d intervals. The absence of mycoplasma was routinely checked using the Mycoplasma Stain Kit [25].

2.3. Cell Viability Assay

Cell viability was assayed according to a previous study with some modifications [26]. Briefly, activated Jurkat T cells were diluted to 2×10^5 cells/mL using fresh medium, pipetted into 100 μL of the cell dilutions, seeded in a 96-well multiplate, and treated for 36 h with DMM at final concentrations of 0.5, 5, 25, 50, 100, 250, and 500 mg/L. The final acetone concentration of each well was adjusted to the same concentration and less than 0.1%, which exerted no effect on cell viability. A blank group (without pesticide and cells) and a control group (containing cells, equivalent solvent but without pesticide) were included. Cell viability was determined by the Cell Counting Kit-8 (CCK-8), according to the manufacturer's instructions. Absorbance was measured at 450 nm in a ReadMax 500F enzyme-labeled instrument (Shanpu Biotechnology Co., Ltd., Shanghai, China). Cell viability was calculated using Equation (1).

$$\text{Cell viability} = \frac{A_t - A_b}{A_c - A_b} \tag{1}$$

where A_t is the absorbance of the test group, A_b is the absorbance of the blank group, and A_c is the absorbance of the control group. Concentration–response curves were plotted, and the half maximal effective concentration (EC_{50}) values were then calculated using a sigmoidal dose–response curve equation [27].

2.4. Cell Apoptosis Analysis

Cell apoptosis was assessed by using an Annexin V-FITC/PI detection kit. Activated Jurkat T cells were diluted to 2×10^5 cells/mL using fresh medium, pipetted into 4 mL of the cell dilutions, seeded in a 6-well multiplate, and treated for 36 h with DMM at final concentrations of EC_{50}, EC_{25}, EC_{10}, and the control group. The cells were collected and washed to remove the medium, resuspended in binding buffer, and incubated with Annexin V-FITC solution and PI solution at normal temperature for 15 min. Apoptotic cells were analyzed by a MoFlo Astrios[EQ] flow cytometer (Beckman Coulter, Inc., Brea, CA, USA) [28].

2.5. Transcriptome Analysis

2.5.1. RNA Extraction and High-Throughput Sequencing

The Jurkat T cells were seeded in a 75 cm² cell culture bottle with 60 mL of medium at an initial concentration of 1.2×10^7 cells/bottle and treated for 36 h with DMM at final concentrations of 4 mg/L (EC_{10}) and 21 mg/L (EC_{25}). The cells were collected for transcriptome analysis. Total RNA was isolated using the TRIzol® reagent (Thermo Fisher, Waltham, MA, USA), according to the manufacturer's protocol, and genomic DNA was removed using DNase I (TaKaRa, Dalian, China). Then, RNA quality was determined by a 2100 Bioanalyzer (Agilent Technologies, Santa Clara, CA, USA) and quantified using an ND-2000 (NanoDrop, Wilmington, DE, USA). Only high-quality RNA samples (OD260/280 = 1.8~2.2, OD260/230 ≥ 2.0, RIN ≥ 6.5, 28S:18S ≥ 1.0, >1 μg) were used to construct a sequencing library.

The RNA transcriptome library was prepared following the TruSeq[TM] RNA sample preparation kit. Libraries were size selected for cDNA target fragments of 300 bp on 2% Low

Range Ultra Agarose, followed by PCR amplification using Phusion DNA polymerase (NEB, Ipswich, MA, USA) for 15 PCR cycles. After quantification by TBS380, a paired-end RNA sequencing library was obtained by using a Nova Seq 6000 sequencer (2×150 bp read length).

2.5.2. Read Mapping and Differential Expression Analysis

The raw paired-end reads were clipped and quality controlled by SeqPrep https://github.com/jstjohn/SeqPrep (accessed on 10 January 2022) and Sickle https://github.com/najoshi/sickle (accessed on 10 January 2022) with the default parameters. The clean reads of each sample were sequenced and aligned with the specified reference genome Homo_sapien, http://asia.ensembl.org/Homo_sapiens/Info/Index (accessed on 23 January 2022). The mapped reads of each sample were assembled by StringTie https://ccb.jhu.edu/software/stringtie/index.shtml t = example (accessed on 23 January 2022) in a reference-based approach [29].

To identify the differential expression genes (DEGs) between the two different samples, the expression level of each transcript was calculated according to the fragments per kilobase of exon per million mapped fragments (FPKM) method. RSEM http://deweylab.biostat.wisc.edu/rsem/ (accessed on 20 March 2020) [30] was used to quantify gene abundances. A differential expression analysis was performed using DESeq2 [31] with $|\log_2 FC| > 1.3$, and a $Q_{value} \leq 0.05$ was considered to indicate significantly differentially expressed genes. Functional enrichment analyses, including gene ontology (GO) and Kyoto Encyclopedia of Genes and Genomes (KEGG) analyses, were implemented to find significantly enriched DEGs in GO terms and metabolic pathways at a Bonferroni-corrected $P_{value} \leq 0.05$ compared with the whole-transcriptome background [32].

2.6. Quantitative Real-Time PCR

Four genes that were significantly differentially expressed were selected for QRT-PCR analysis, and GAPDH was used as the reference gene. The primers were designed with Primer-BLAST http://www.ncbi.nlm.nih.gov/tools/primer-blast/ (accessed on 3 November 2020) and are presented in Supplementary Table S1. Total RNA was reverse-transcribed using the PrimeScript RT Reagent Kit with gDNA Eraser. The reactions were prepared on a StepOne Plus^TM Real-time PCR detection system (ABI, Boston, MA, USA) with a total volume of 10 μL: 3 μL of 1:2 diluted template, 1 μL of each primer (5 μM), and 5 μL of $2\times$ Fast SYBR® Green Master Mix (ABI, Boston, MA, USA). Baseline, threshold cycles (Ct), and statistical analyses were automatically determined using the StepOne Plus^TM Software version 2.3 (ABI, Boston, MA, USA).

2.7. Statistical Analysis

The cell viability assay was tested in three independent experiments with five biological replicates; the cell apoptosis analysis was tested in three independent experiments; the transcriptome analysis was tested in three independent experiments with three biological replicates. Data are expressed as the mean $\pm$ SD of three independent experiments. All statistical analyses were performed using SPSS version 18.0 software (IBM). The values were compared with a one-way ANOVA followed by Duncan's test. $p < 0.05$ was considered statistically significant.

3. Results and Discussion

3.1. Effect of Dimethomorph on Cell Viability

The action mechanism of DMM is to destroy the cell wall membrane, causing the decomposition of the sporangium wall and inducing pathogen death [33]. However, the immunotoxicity of DMM on the human body and its mechanism has not received much attention. In the process of in vitro cytotoxicity evaluation, cell proliferation is an important marker for the evaluation of cytotoxicity [34]. The assessment of cellular activity was based on the ability of these cells to metabolize water-soluble tetrazole-8 (WST-8) of CCK-8 and convert it to orange formazan via mitochondrial dehydrogenase. Cell viability was

determined by the extent of WST-8 cleavage by mitochondrial dehydrogenases in DMM-exposed cells and controls [35]. Figure 1A shows the viability of Jurkat cells after exposure to different concentrations of DMM. Compared to the control group (with 0.1% acetone but without DMM addition), the cell activity decreased with an increasing DMM concentration, showing a concentration-dependent trend. In the EC_{50}, EC_{25}, and EC_{10} treatment groups, the Jurkat cells calculated by nonlinear curve fitting were 126.01 mg/L (0.32 mM), 21.37 mg/L (0.06 mM), and 4.12 mg/L (0.01 mM), respectively (Figure 1B). When the cells were exposed to the EC_{50}, EC_{25}, and EC_{10} treatment groups, the cell activities were consistent with the expected results (97.8%, 81.8%, and 53.4%, respectively) (Figure 1C), which could be used in subsequent apoptosis experiments.
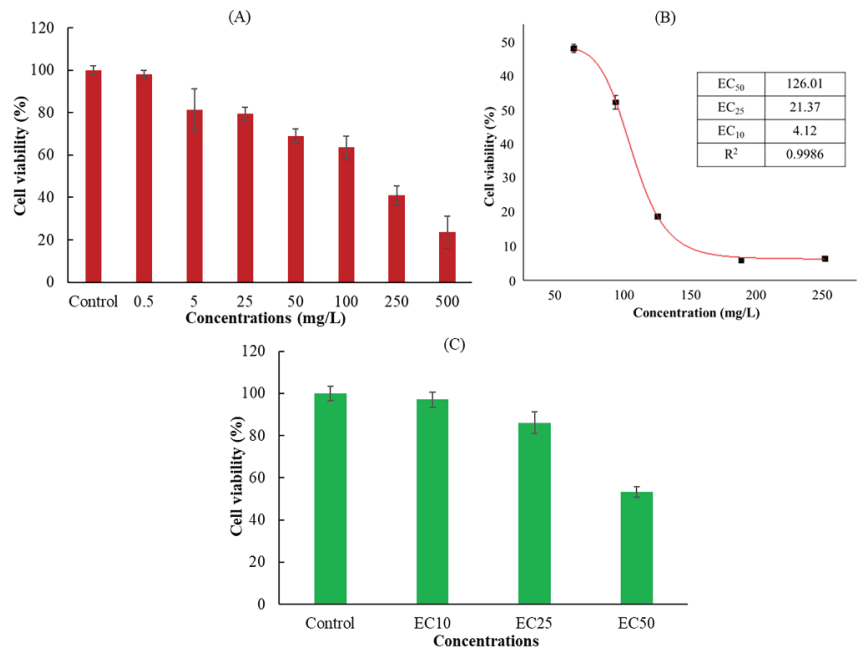
Figure 1. Effect of dimethomorph on Jurkat T cells viability. (**A**) Jurkat cells exposed for 36 h at different DMM concentrations or controls. (**B**) Nonlinear curve fitting results of different effective concentration (EC) using the results of (**A**). (**C**) Jurkat T cells exposed for 36 h to EC_{50}, EC_{25}, EC_{10} DMM, or controls. Cell viability is presented as a percentage compared to the control. The results shown are the mean ± SD from triplicate exposures.

3.2. Effect of DMM on Cell Apoptosis

Previous studies have indicated that cell apoptosis or programmed cell death is closely linked to cell proliferation in mammalian cells [36], and the Annexin-V/PI staining assay is a simple and effective method to detect apoptosis at a very early stage [3]. From the results of Figure 2A–D, there was no significant change in apoptosis between EC_{10} and the control group, but with the increasing DMM concentration, the ratio of the late apoptotic cells for the EC_{25} and EC_{50} treatments increased 1.93-, 4.37-fold higher than that of the control. The results indicated that DMM caused the apoptosis of Jurkat T cells in a concentration-dependent manner, which is consistent with the results predicted in the cell viability experiment, and could be used in subsequent experiments.

3.3. RNA Extraction and Quality Evaluation

In the in vitro immunotoxicity screening test using Jurkat T cells, DMM was found to have significant immunotoxicity. Therefore, we further systematically evaluated the

immunotoxicity of DMM on human Jurkat T cells, and the mechanism of action was also expounded by using comparative transcriptomics. To fully elucidate the underlying mechanism, a transcriptome analysis based on RNA-seq was performed. During transcriptomic studies, selecting a proper pesticide exposure concentration is very important, because too high a concentration could cause cell death, and too low a concentration might not be cytotoxic [37]. As shown in Figure 3A and Table 1, when the exposure concentration was EC_{50}, the RNA bonds were unclear, and the RIN was below 8, which indicated that the total RNA degraded to a degree that it was not suitable for transcriptome analysis [38]. The RNA bonds under the EC_{25} treatment (named M21), the EC_{10} treatment (named L4), and the control (named Ctr) were clear, and there was no contamination of other impurities. The RIN values were higher than 9.5, which indicates good RNA quality. Moreover, according to the procedure of the ISO 10993-5 standard, a tested material that is incubated for at least 24 h with precultured cells and has a decreased viability of under 70% of the control is considered cytotoxic [39]. As shown in Figure 1, the cell viability under the EC_{10} and EC_{25} treatments exposure was 97.8% and 81.8%, respectively, which indicated that samples M21 and L4 could be used in the following transcriptomic analysis.

Table 1. RNA quality assessment.

Samples	Concentration(ng/μL)	Content (μg)	OD260/280	OD260/230	RIN
H126-1	115.00	4.03	2.05	2.11	7.40
H126-2	112.00	3.92	2.03	2.01	7.80
H126-3	96.20	3.37	2.04	2.10	7.60
M21-1	1545.90	54.11	2.02	2.21	10.00
M21-2	1731.70	60.61	2.01	2.18	9.90
M21-3	1678.50	58.75	2.01	2.17	10.00
L4-1	2141.30	74.95	1.99	2.14	10.00
L4-2	2090.50	73.17	1.99	2.13	10.00
L4-3	2133.00	74.66	2.00	2.13	9.50
Ctr-1	2020.60	70.72	2.00	2.15	9.90
Ctr-2	1862.20	65.18	2.01	2.17	9.60
Ctr-3	1892.30	66.23	2.01	2.18	9.90

RIN: RNA Integrity Number.

3.4. RNA Sequencing Data Assessment

In this study, a total of 77.76 Gb of high-quality clean reads were obtained after the unqualified reads were filtered out. The clean reads of each sample in each group reached more than 7.63 Gb, and the sequencing error rate was less than 0.025%. The Q30 base accounted for more than 94.18% and the GC content ranged from 49.4% to 50.36% (Table 2). The statistics indicate that the quality of the sequencing is high enough for further analysis. As shown in Figure 3B, the correlation coefficients between samples (Ctr group, L4 group, and M21 group) were higher than 99%, and the phylogenetic tree analysis results demonstrated that the Ctr group was different from the L4 group and the M21 group, but there was a high correlation between the control group and the L4 group. These results are consistent with expectations, so the results revealed good reliability among the samples [40].

Table 2. Statistics and quality estimation of RNA-seq reads.

Sample	Raw Reads	Clean Reads	Clean Bases	Error Rate (%)	Q20 (%)	Q30 (%)
Ctr_1	69321808	68648290	10248272849	0.0247	98.15	94.41
Ctr_2	56231964	55657530	8295729777	0.0249	98.07	94.21
Ctr_3	62512340	61926524	9209389908	0.0245	98.25	94.67
L4_1	65369620	64580756	9635172686	0.0244	98.26	94.71
L4_2	51616818	51120046	7630992231	0.0246	98.21	94.57
L4_3	58748206	58167602	8680297728	0.0249	98.08	94.18
M21_1	52328192	51754638	7726615557	0.0249	98.07	94.23
M21_2	56519460	56045588	8350478112	0.0241	98.4	95.03
M21_3	54012066	53454568	7983424171	0.0248	98.1	94.31
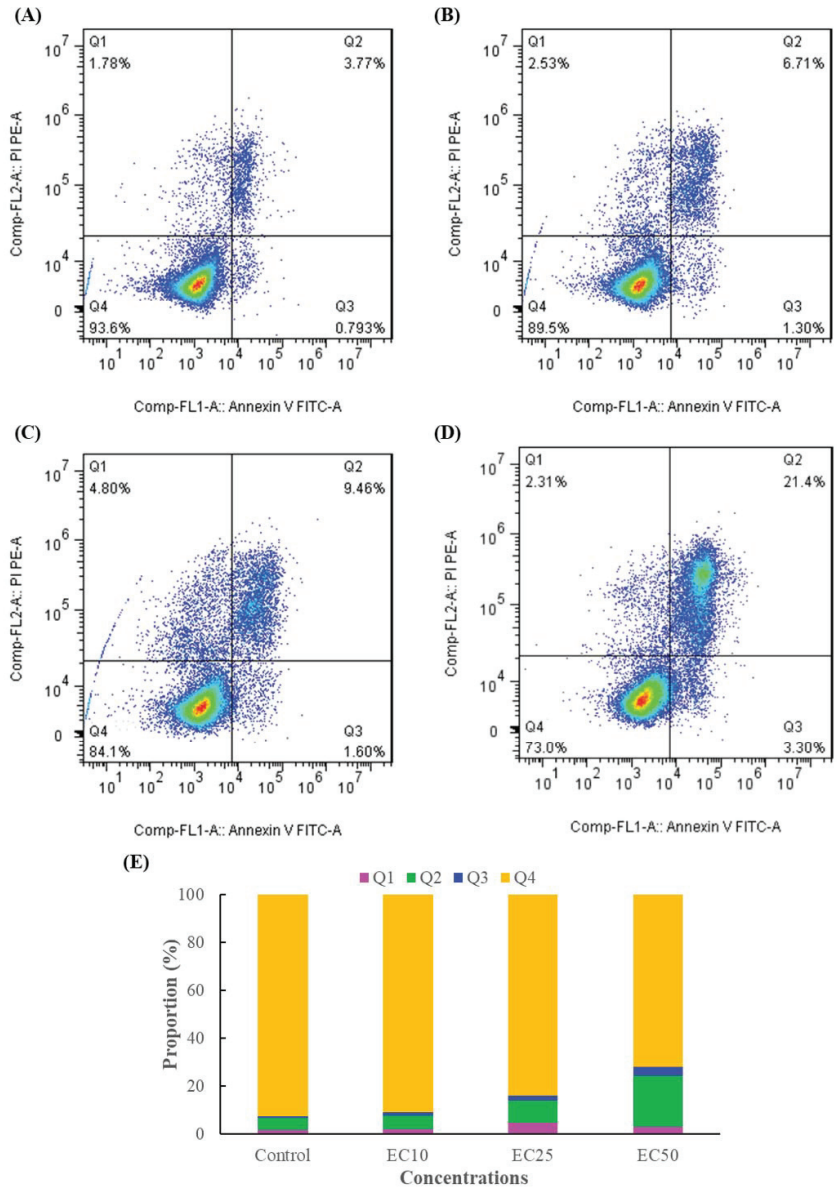
Figure 2. DMM-induced apoptosis in Jurkat T cells. (**A**): Control, (**B**): EC_{10}, (**C**): EC_{25}, (**D**): EC_{50}, (**E**): statistics of the apoptosis data of three independent experiments. Q1, Q2, Q3, and Q4 of the flow cytometry graph indicate dead cells, late apoptotic cells, early apoptotic cells, and normal cells, respectively.

3.5. Gene Expression Overview

As shown in Figure 4A, a total of 15,721 genes were identified through RNA sequencing, and 14,193 genes were co-expressed in the Ctr, L4, and M21 samples. A principal component analysis (PCA) was performed to assess the transcriptomics of the different samples. Figure 4B reveals that the Ctr, L4, and M21 samples were well divided into three characteristic groups by PCA, which indicated that there were significant differences in the

transcriptomics between the groups [41]. Further analysis indicated that compared to the Ctr samples, 121 genes (81 upregulated, 40 downregulated) and 30 genes (17 upregulated, 13 downregulated) were significantly differentially regulated in the L4 and M21 samples, respectively (Figure 4C,D, Tables S2 and S3). The results indicated that DMM can significantly interfere with the gene expression of Jurkat T cells, even at a low dose (4.12 mg/L L4 group). This result is consistent with that of the toxicity test shown in Figure 1. Previous studies showed that the highest dimethomorph residue was 6.8 mg/kg for leafy vegetables and stalk and stem vegetables and 6.11 mg/kg for *Dendrobium officinale* [42,43]. Considering the cytotoxicity and transcriptomic results of our study, the immunotoxicological effects of DMM should be emphasized.
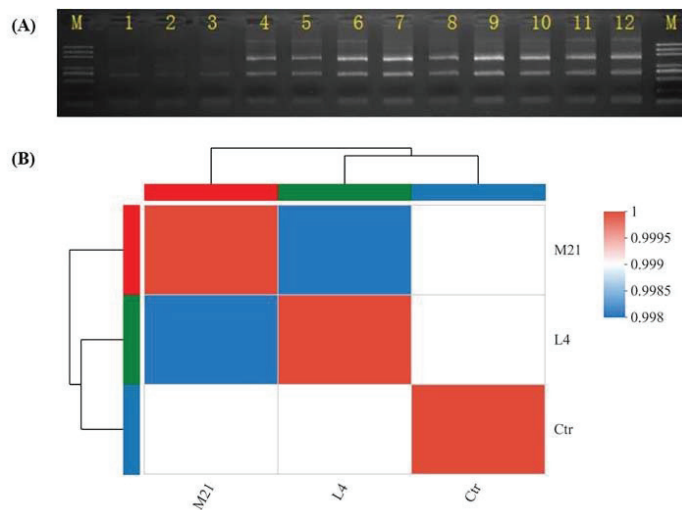
Figure 3. RNA electropherogram (**A**) and sample correlations based on RNA sequencing (**B**). (**A**): M, marker; 1–3, EC_{50} group; 4–6, EC_{25} group; 7–9, EC_{10} group; 10–12, control group.

3.6. Gene Ontology (GO) Analysis of Differentially Expressed Genes (DEGs)

A GO enrichment analysis can be used to reveal the functional characteristics of differentially expressed genes (DEGs). GO terms are widely used to classify genes into the categories of cellular component (CC), molecular function (MF), and biological process (BP) [44]. As shown in Figure 5A, the GO enrichment analysis indicated that the DEGs were mostly enriched in biological processes (involving 31 BPs, $P_{adjust} \leq 0.05$) (Supplementary Table S4), and many of them were involved in the negative regulation of cell activities, such as the negative regulation of biological processes, cellular processes, and cell development, which indicated that DMM has negative toxic effects on Jurkat T cells. Moreover, many genes were also involved in the immune regulation of cell biological processes, such as lymphocyte activation and differentiation, T cell activation and differentiation, leukocyte differentiation, and negative regulation of the T cell apoptotic process. Most of the genes were downregulated in comparison to L4 vs. Ctr or M21 vs. Ctr (such as *RAG1*, *HDAC9*, *SOX4*, and *CD7*). However, only 12 genes (*AC138035.1*, *AP002990.1*, *BMP10*, *CHI3L2*, *DNTT*, *LINC01355*, *MME*, *MSH4*, *PAXIP1-AS1*, *PTPN3*, *SERPINB2*, and *TDRD9*) were upregulated, and four genes (*AL121594.1*, *CD40LG*, *EGR1*, and *SH3BP5*) were downregulated simultaneously in comparison to both L4 vs. Ctr and M21 vs. Ctr (Figure 5B). Among them, two important genes, *EGR1* and *CD40LG*, related to immune regulation were downregulated in both comparisons to L4 vs. Ctr and M21 vs. Ctr. Human CD40LG protein is a transmembrane protein and the ligand of CD40. It belongs to the tumor necrosis factor gene superfamily and is involved in immune-related pathways of breast cancer. The gene *CD40LG* plays critical roles in the regulation of the activation and differentiation of B cells

and the maturation of dendritic cells [45]. The gene *EGR1* (early growth response 1) is an important transcription factor that is widely expressed in many cell types and participates in important physiological processes of human cells [46]. A previous study indicated that *EGR1* serves as a tumor suppressor in cancers, such as prostate tumors and gastric tumors [47]. The downregulation of these genes may indicate that DMM exposure reduces the immune resistance of the body, even at a low concentration.
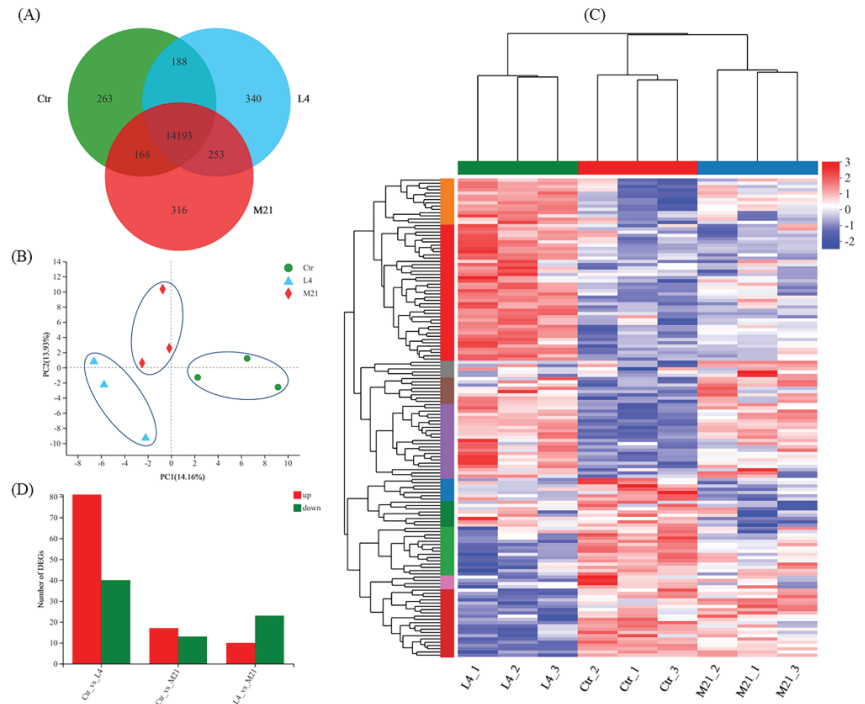
Figure 4. Venn diagram (**A**) and principal component analysis (PCA) for the differentially expressed genes (**B**). Hierarchical clustering analysis (HCA) of significantly differentially expressed genes (**C**) and statistics of the significantly differentially expressed genes (**D**) for each comparison.

3.7. KEGG Enrichment Analysis of DEGs

KEGG is a database for the systematic analysis of gene function and genome information, which can be used as a whole network to study gene and expression information [48]. As shown in Figure 5C and Supplementary Table S5, the significant DEGs were mainly enriched in 11 KEGG pathways ($P_{value} \leq 0.05$), and most of them were related to immune regulation and signal transduction. Among them, the hematopoietic cell lineage, hematopoietic cell lineage, the FoxO signaling pathway, and the cytokine-cytokine receptor interaction are closely related to the occurrence of cancer in humans. Cytokines are crucial intercellular regulators and mobilizers of cells engaged in innate and adaptive inflammatory host defenses, cell growth, differentiation, cell death, angiogenesis, and development and repair processes aimed at the restoration of homeostasis [49]. FOXO (Forkhead Box O) is a subgroup of Fox transcription factors that are considered to play a key role as tumor suppressors in a variety of cancers [50]. Complement and coagulation cascades could interact with systemic lupus erythematosus (SLE), and this interaction may lead to aggravation of the disease, which is more obvious in inflamed patients [51]. In the complement and coagulation cascades pathway, the expression of the important gene *SERPINB2* was increased in both L4 vs. Ctr and M21 vs. Ctr. A previous study showed that the protein SerpinB2 is substantially upregulated under multiple inflammatory conditions, and dys-

regulated expression and polymorphisms are associated with several human inflammatory diseases [52]. The above results further indicated that DMM exposure reduces the immune resistance of the body, even at a low concentration. DMM has certain immunotoxicity to the human body. Even low-dose exposure can cause immune reactions and cause potential harm to the body.
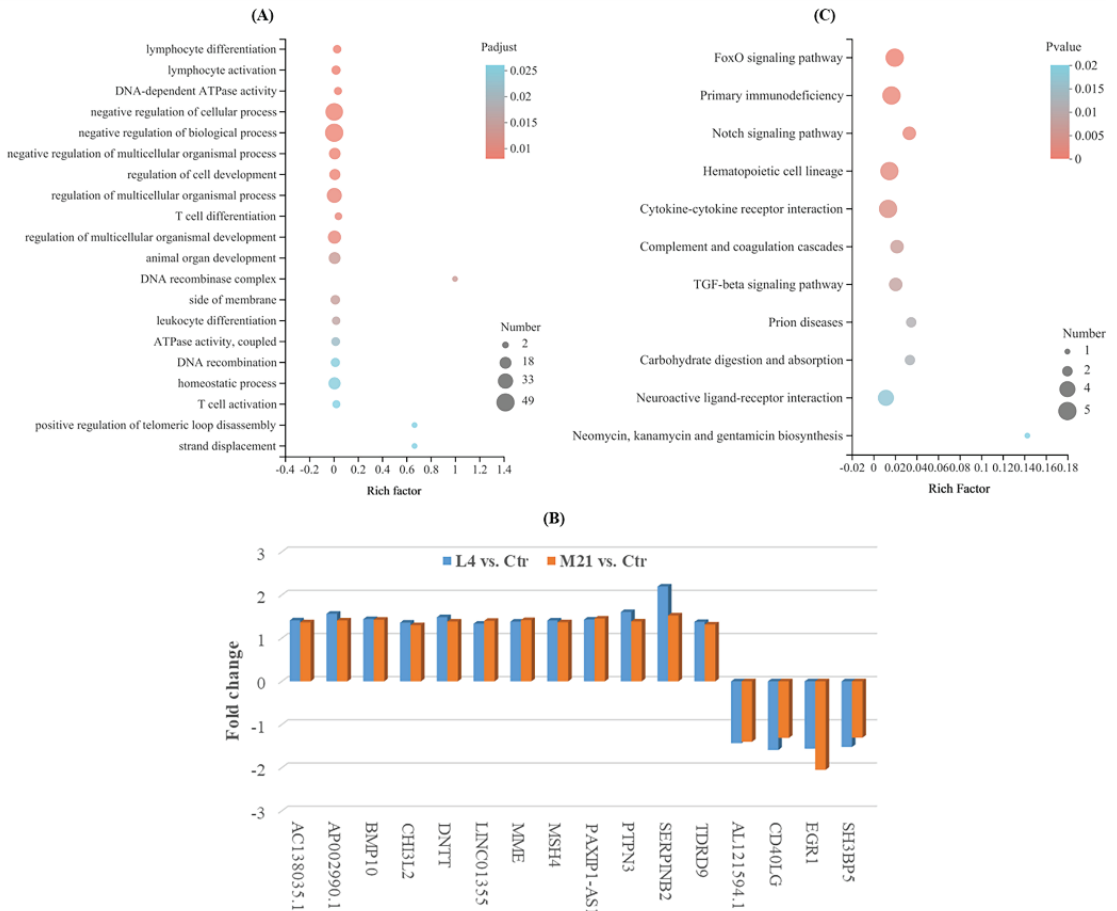
Figure 5. Gene ontology enrichment analysis for the significantly differentially expressed genes (**A**), simultaneously significantly different expressed genes for both comparison of L4 vs. Ctr and M21 vs. Ctr (**B**), and KEGG enrichment analysis for the significantly differentially expressed genes (**C**).

3.8. Target Gene Screening and Quantitative Real-Time PCR Validation

To validate the results obtained from the transcriptome analysis, four important genes related to immune regulation were selected. As shown in Figure 6, there was general accordance between the RNA sequence and the real-time qPCR data for all the tested genes (*CD40LG* and *EGR1* downregulated, *SERPINB2* and *RAG1* upregulated), although the fold changes differed between the analytical methods. Compared to the high concentration exposure (M21), the effect of the low concentration DMM exposure (L4) on gene expression was more significant. Therefore, the low-dose chronic toxicity of DMM needs to be further studied.
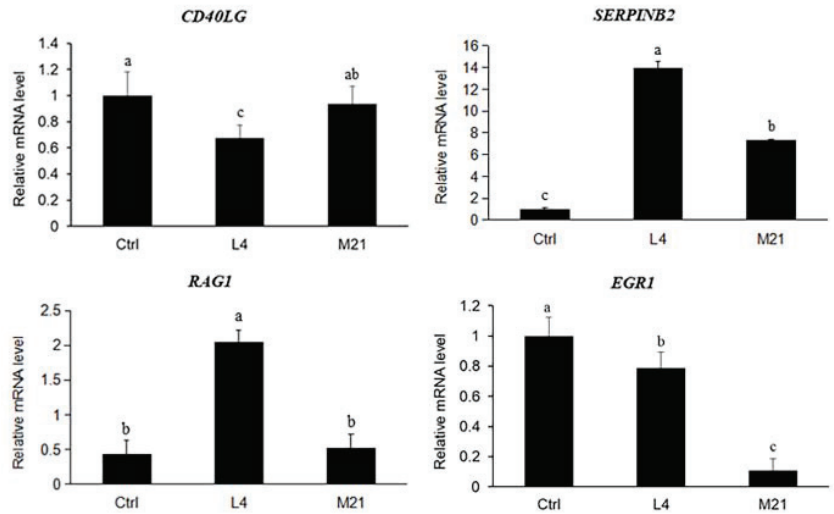
Figure 6. Quantitative real-time PCR results for the selected genes. Data are expressed as the mean ± SD from triplicate exposures. Different letters on the different bars indicate significant differences ($p < 0.05$).

4. Conclusions

This study demonstrated that when exposed to DMM, human Jurkat T cells' activity decreased with increasing DMM concentration, and the half-effective concentration (EC_{50}) of DMM for Jurkat cells was 126.01 mg/L (0.32 mM). There was no significant change in apoptosis between EC_{10} and the control samples, but the ratio of the late apoptotic cells for the EC_{25} and EC_{50} treatments increased 1.93-, 4.37-fold higher than that of the control. Transcriptomics based on RNA sequencing indicated that compared to untreated samples (Ctr), 121 genes (81 upregulated, 40 downregulated) and 30 genes (17 upregulated, 13 downregulated) were significantly regulated when exposed to EC_{10} (L4) and EC_{25} (M21), respectively. GO and KEGG analyses indicated that the DEGs were mostly involved in immune regulation and signal transduction pathways. The quantitative RT-PCR for the selected genes showed that the effect of low-dose DMM on gene expression was more significant than that of high-dose exposure. The results suggested that DMM exposure may cause immune system disturbance, and thus, negatively affect body health. In future, the in vivo experiments are necessary to further verify the immunotoxicity and target genes triggered by DMM.

Institutional Review Board Statement: Not applicable.

Informed Consent Statement: Not applicable.

Data Availability Statement: The data presented in this article are available on reasonable request, from the corresponding author.

Conflicts of Interest: The authors declare no conflict of interest.

References

1. Lawler, S.P. Environmental safety review of methoprene and bacterially-derived pesticides commonly used for sustained mosquito control. *Ecotox. Environ. Safe.* **2017**, *139*, 335–343. [CrossRef]
2. Tudi, M.; Ruan, H.D.; Wang, L.; Lyu, J.; Sadler, R.; Connell, D.; Chu, C.; Phung, D.T. Agriculture development, pesticide application and its impact on the environment. *Int. J. Environ. Res. Pub. He.* **2021**, *18*, 1112. [CrossRef] [PubMed]
3. Ji, C.Y.; Magnuson, J.T.; Zhang, W.; Zhao, M.R. New insight into the enantioselective cytotoxicity of cypermethrin: Imbalance between cell cycle and apoptosis. *J. Hazard. Mater.* **2021**, *403*, 123893. [CrossRef]
4. Kim, K.H.; Kabir, E.; Jahan, S.A. Exposure to pesticides and the associated human health effects. *Sci. Total Environ.* **2017**, *575*, 525–535. [CrossRef]
5. Fu, H.Y.; Tan, P.; Wang, R.J.; Li, S.N.; Liu, H.Z.; Yang, Y.; Wu, Z.L. Advances in organophosphorus pesticides pollution: Current status and challenges in ecotoxicological, sustainable agriculture, and degradation strategies. *J. Hazard. Mater.* **2022**, *424*, 127494. [CrossRef] [PubMed]
6. Aktar, W.; Sengupta, D.; Chowdhury, A. Impact of pesticides use in agriculture: Their benefits and hazards. *Interdiscipl. Toxicol.* **2009**, *2*, 1–12. [CrossRef] [PubMed]
7. Ma, M.M.; Chen, C.; Yang, G.L.; Wang, Y.H.; Wang, T.C.; Li, Y.; Qian, Y.Z. Combined anti-androgenic effects of mixtures of agricultural pesticides using *in vitro* and in silico methods. *Ecotox. Environ. Safe.* **2019**, *186*, 109652. [CrossRef] [PubMed]
8. Arab, A.; Mostafalou, S. Neurotoxicity of pesticides in the context of CNS chronic diseases. *Int. J. Environ. Health R.* **2021**, *32*, 2718–2755. [CrossRef] [PubMed]
9. Lerro, C.C.; Freeman, L.E.B.; DellaValle, C.T.; Andreotti, G.; Hofmann, J.N.; Koutros, S.; Parks, C.G.; Shrestha, S.; Alavanja, M.C.R.; Blair, A.; et al. Pesticide exposure and incident thyroid cancer among male pesticide applicators in agricultural health study. *Environ. Int.* **2021**, *146*, 106187. [CrossRef]
10. Damalas, C.A.; Eleftherohorinos, I.G. Pesticide exposure, safety issues, and risk assessment indicators. *Int. J. Environ. Res. Public Health* **2011**, *8*, 1402–1419. [CrossRef] [PubMed]
11. Dhouib, I.; Jallouli, M.; Annabi, A.; Marzouki, S.; Gharbi, N.; Elfazaa, S.; Lasram, M.M. From immunotoxicity to carcinogenicity: The effects of carbamate pesticides on the immune system. Environ. *Sci. Pollut. R.* **2016**, *23*, 9448–9458. [CrossRef] [PubMed]
12. Naasri, S.; Helali, I.; Aouni, M.; Mastouri, M.; Harizi, H. N-acetylcysteine reduced the immunotoxicity effects induced *in vitro* by azoxystrobin and iprodione fungicides in mice. *Environ. Toxicol.* **2021**, *36*, 562–571. [CrossRef] [PubMed]
13. Lee, G.H.; Choi, K.C. Adverse effects of pesticides on the functions of immune system. Comp. *Biochem. Phys. C* **2020**, *235*, 108789.
14. Hochstenbach, K.; Leeuwen, D.M.V.; Gmuender, H.; Stølevik, S.B.; Nygaard, U.C.; Løvik, M.; Granum, B.; Namork, E.; van Delft, J.H.M.; van Loveren, H. Transcriptomic profile indicative of immunotoxic exposure: *In Vitro* studies in peripheral blood mononuclear cells. *Toxicol. Sci.* **2010**, *118*, 19–30. [CrossRef]
15. Dos Santos, S.C.; Sa-Correia, I. Yeast toxicogenomics: Lessons from a eukaryotic cell model and cell factory. *Curr. Opin. Biotech.* **2015**, *33*, 183–191. [CrossRef] [PubMed]
16. Rao, T.N.; Balaji, A.P.B.; Panagal, M.; Parvatamma, B.; Selvaraj, B.; Panneerselvam, S.; Aruni, W.; Subramanian, K.; Renuga, P.S.; Pandian, S. Nanoremediation of dimethomorph in water samples using magnesium aluminate nanoparticles. *Environ. Technol. Inno.* **2020**, *20*, 101176. [CrossRef]
17. Wang, C.X.; Zhang, Q.M.; Wang, F.F.; Liang, W.X. Toxicological effects of dimethomorph on soil enzymatic activity and soil earthworm (*Eisenia fetida*). *Chemosphere* **2017**, *169*, 316–323. [CrossRef]
18. Zhang, C.; Li, J.; Wu, X.; Long, Y.; An, H.; Pan, X.; Li, M.; Dong, F.; Zheng, Y. Rapid degradation of dimethomorph in polluted water and soil by *Bacillus cereus* WL08 immobilized on bamboo charcoal-sodium alginate. *J. Hazard. Mater.* **2020**, *398*, 122806. [CrossRef]
19. Lin, S.; Tang, T.; Cang, T.; Yu, S.Q.; Ying, Z.T.; Gu, S.J.; Zhang, Q. The distributions of three fungicides in vegetables and their potential health risks in Zhejiang, China: A 3-year study (2015–2017). *Environ. Pollut.* **2020**, *267*, 115481. [CrossRef]
20. Yang, L.P.; Zheng, Q.; Lin, S.; Wang, Y.Q.; Zhu, Q.Z.; Cheng, D.M.; Chen, J.J.; Zhang, Z.X. Dissipation and residue of dimethomorph in potato plants produced and dietary intake risk assessment. *Int. J. Environ. Anal. Chem.* **2020**, *102*, 1332–1344. [CrossRef]
21. Shabeer, A.; Banerjee, T.P.K.; Jadhav, M.; Girame, R.; Utture, S.; Hingmire, S.; Oulkar, D. Residue dissipation and processing factor for dimethomorph, famoxadone and cymoxanil during raisin preparation. *Food Chem.* **2015**, *170*, 180–185. [CrossRef]
22. Kabir, M.H.; Abd El-Aty, A.M.; Rahman, M.M.; Chung, H.S.; Lee, H.S.; Kim, M.R.; Chang, B.J.; Wang, J.; Shin, H.C.; Shim, J.H. Residual dynamic and risk assessment of dimethomorph in Swiss chard grown at two different sites. *Biomed. Chromatogr.* **2018**, *32*, e4053. [CrossRef] [PubMed]

23. Shao, J.; Berger, L.F.; Hendriksen, P.J.M.; Peijnenburg, A.A.C.M.; van Loveren, H.; Volger, O.L. Transcriptome-based functional classifiers for direct immunotoxicity. *Arch. Toxicol.* **2014**, *88*, 673–689. [CrossRef] [PubMed]
24. Hsu, C.C.; Xu, J.B.; Brinkhof, B.; Wang, H.; Cui, Z.F.; Huang, W.E.; Ye, H. A single-cell Raman-based platform to identify developmental stages of human pluripotent stem cell-derived neurons. *PNAS* **2020**, *117*, 18412–18423. [CrossRef]
25. Escriva, L.; Jennen, D.; Caiment, F.; Manyes, L. Transcriptomic study of the toxic mechanism triggered by beauvericin in Jurkat cells. *Toxicol. Lett.* **2018**, *284*, 213–221. [CrossRef] [PubMed]
26. Li, Y.-C.; Luo, Y.; Meng, F.-B.; Li, J.; Chen, W.-J.; Liu, D.-Y.; Zou, L.-H.; Zhou, L. Preparation and characterization of feruloylated oat β-glucan with antioxidant activity and colon-targeted delivery. *Carbohyd. Polym.* **2022**, *279*, 119002. [CrossRef]
27. Zhang, J.K.; Williams, T.D.; Abdallah, M.A.E.; Harrad, S.; Chipman, J.K.; Viant, M.R. Transcriptomic and metabolomic approaches to investigate the molecular responses of human cell lines exposed to the flame retardant hexabromocyclododecane (HBCD). *Toxicol. Vitro* **2015**, *29*, 2116–2123. [CrossRef] [PubMed]
28. Meng, F.-B.; Gou, Z.-Z.; Li, Y.-C.; Zou, L.-H.; Chen, W.-J.; Liu, D.-Y. The efficiency of lemon essential oil-based nanoemulsions on the inhibition of *Phomopsis* sp. and reduction of postharvest decay of kiwifruit. *Foods* **2022**, *11*, 1510. [CrossRef]
29. Pertea, M.; Pertea, G.M.; Antonescu, C.M.; Chang, T.C.; Mendell, J.T.; Salzberg, S.L. StringTie enables improved reconstruction of a transcriptome from RNA-seq reads. *Nat. Biotechnol.* **2015**, *33*, 290–295. [CrossRef]
30. Wang, Y.P.; Hu, Z.K.; Ye, N.; Yin, H.F. IsoSplitter: Identification and characterization of alternative splicing sites without a reference genome. *RNA* **2021**, *27*, 868–875. [CrossRef]
31. Love, M.I.; Huber, W.; Anders, S. Moderated estimation of fold change and dispersion for RNA-seq data with DESeq2. *Genome Biol.* **2014**, *15*, 550. [CrossRef] [PubMed]
32. Anders, S.; Huber, W. Differential expression analysis for sequence count data. *Genome Biol.* **2010**, *11*, R106. [CrossRef] [PubMed]
33. Yang, L.H.; Zhou, X.G.; Deng, Y.C.; Gong, D.X.; Luo, H.F.; Zhu, P. Dissipation behavior, residue distribution, and dietary risk assessment of fluopimomide and dimethomorph in taro using HPLC-MS/MS. *Environ. Sci. Pollut. R.* **2021**, *28*, 43956–43969. [CrossRef] [PubMed]
34. Alessandra, V.; Vincenzo, L.M.; Alessandro, V.; Antonio, D.S. Rectal neuroendocrine cell proliferation in a patient with ulcerative colitis treated with adalimumab. *Eur. J. Gastroen. Hepat.* **2021**, *33*, 766–768.
35. Zheng, Q.; Lin, Z.; Li, X.; Xin, X.; Wu, M.; An, J.; Gui, X.; Li, T.; Pu, H.; Li, H.; et al. Inflammatory cytokine IL6 cooperates with CUDR to aggravate hepatocyte-like stem cells malignant transformation through NF-κB signaling. *Sci. Rep.* **2016**, *6*, 36843. [CrossRef] [PubMed]
36. Huang, J.F.; Shui, K.J.; Li, H.Y.; Hu, M.Y.; Zhong, G.H. Antiproliferative effect of azadirachtin A on *Spodoptera litura* Sl-1 cell line through cell cycle arrest and apoptosis induced by up-regulation of p53. *Pestic. Biochem. Phys.* **2011**, *99*, 16–24. [CrossRef]
37. Wang, X.L.; Qiu, J.; Xu, Y.Y.; Liao, G.Q.; Jia, Q.; Pan, Y.C.; Wang, T.C.; Qian, Y.Z. Integrated non-targeted lipidomics and metabolomics analyses for fluctuations of neonicotinoids imidacloprid and acetamiprid on Neuro-2a cells. *Environ. Pollut.* **2021**, *284*, 117327. [CrossRef] [PubMed]
38. Gallego Romero, I.; Pai, A.A.; Tung, J.; Gilad, Y. RNA-seq: Impact of RNA degradation on transcript quantification. *BMC Biol.* **2014**, *12*, 42. [CrossRef] [PubMed]
39. *ISO10993-10995*; Biological Evaluation of Medical Devices-Part5: Tests for in vitro Cytotoxicity. International Organization for Standardization: Geneva, Switzerland, 2009.
40. Fan, H.; Lv, Z.P.; Gan, L.P.; Ning, C.; Li, Z.; Yang, M.H.; Zhang, B.B.; Song, B.C.; Li, G.; Tang, D.Z.; et al. A Novel lncRNA regulates the toll-like receptor signaling pathway and related immune function by stabilizing FOS mRNA as a competitive endogenous RNA. *Front. Immunol.* **2019**, *10*, 838. [CrossRef] [PubMed]
41. Meng, F.-B.; Zhou, L.; Li, J.-J.; Li, Y.-C.; Wang, M.; Zou, L.-H.; Liu, D.-Y.; Chen, W.-J. The combined effect of protein hydrolysis and *Lactobacillus plantarum* fermentation on antioxidant activity and metabolomic profiles of quinoa beverage. *Food Res. Int.* **2022**, *157*, 111416. [CrossRef] [PubMed]
42. Park, D.W.; Kim, K.G.; Choi, E.A.; Kang, G.R.; Kim, T.S.; Yang, Y.S.; Moon, S.J.; Ha, D.R.; Kim, E.S.; Cho, B.S. Pesticide residues in leafy vegetables, stalk and stem vegetables from South Korea: A long-term study on safety and health risk assessment. *Food Addit. Contam. A* **2016**, *33*, 105–118. [CrossRef]
43. Xu, Z.; Li, L.; Xu, Y.; Wang, S.; Zhang, X.; Tang, T.; Yu, J.; Zhao, H.; Wu, S.; Zhang, C.; et al. Pesticide multi-residues in *Dendrobium officinale* Kimura et Migo: Method validation, residue levels and dietary exposure risk assessment. *Food Chem.* **2021**, *343*, 128490. [CrossRef] [PubMed]
44. Kwok, M.L.; Meng, Q.; Hu, X.L.; Chung, C.T.; Chan, K.M. Whole-transcriptome sequencing (RNA-seq) study of the ZFL zebrafish liver cell line after acute exposure to Cd^{2+} ions. *Aquat. Toxicol.* **2020**, *228*, 105628. [CrossRef] [PubMed]
45. Yuan, M.Q.; Pei, J.Y.; Li, R.H.; Tian, L.R.; He, X.; Li, Y.P. CD40LG as a prognostic molecular marker regulates tumor microenvironment through immune process in breast cancer. *Int. J. Gen. Med.* **2021**, *14*, 8833–8846. [CrossRef] [PubMed]
46. Sukhatme, V.P.; Cao, X.M.; Chang, L.C.; Tsai-Morris, C.H.; Stamenkovich, D.; Ferreira, P.C.; Cohen, D.R.; Edwards, S.A.; Shows, T.B.; Curran, T.; et al. A zinc finger-encoding gene coregulated with c-fos during growth and differentiation, and after cellular depolarization. *Cell* **1988**, *53*, 37–43. [CrossRef]
47. Wang, B.; Guo, H.F.; Yu, H.Q.; Chen, Y.; Xu, H.Y.; Zhao, G. The role of the transcription factor EGR1 in cancer. *Front. Oncol.* **2021**, *11*, 642547. [CrossRef] [PubMed]

48. Hu, Z.G.; Cao, J.T.; Liu, G.Y.; Zhang, H.L.; Liu, X.L. Comparative transcriptome profiling of skeletal muscle from black muscovy duck at different growth stages using RNA-seq. *Genes* **2020**, *11*, 1228. [CrossRef] [PubMed]

49. Oppenheim, J.J. Cytokines: Past, Present, and Future. *Int. J. Hematol.* **2001**, *74*, 3–8. [CrossRef]

50. Ma, Z.; Xin, Z.; Hu, W.; Jiang, S.; Yang, Z.; Yan, X.; Li, X.; Yang, Y.; Chen, F. Forkhead box O proteins: Crucial regulators of cancer EMT. *Semin. Cancer Biol.* **2018**, *50*, 21–31. [CrossRef]

51. Liang, Y.; Xie, S.B.; Wu, C.H.; Hu, Y.; Zhang, Q.; Li, S.; Fan, Y.G.; Leng, R.X.; Pan, H.F.; Xiong, H.B.; et al. Coagulation cascade and complement system in systemic lupus erythematosus. *Oncotarget* **2018**, *9*, 14862–14881. [CrossRef]

52. Schroder, W.A.; Major, L.; Suhrbier, A. The Role of SerpinB2 in Immunity. *Crit. Rev. Immunol.* **2011**, *31*, 15–30. [CrossRef]

Effectiveness of Different Washing Strategies on Pesticide Residue Removal: The First Comparative Study on Leafy Vegetables

So-Jin Yang †, Sujin Mun †, Hye Jin Kim †, Sue Ji Han, Do Woo Kim, Bae-Sik Cho, Ae Gyeong Kim and Duck Woong Park *

Health and Environment Research Institute of Gwangju, 584, Mujin-daero, Seo-gu, Gwangju 61954, Korea
* Correspondence: vetpo2005@korea.kr; Tel.: +82-62-613-7681; Fax: +82-62-613-7689
† These authors contributed equally to this work.

Abstract: Leafy vegetables are used in various cuisines worldwide; however, as they cannot be peeled and their leaf surface area is large, the risk of retaining pesticide residues on these vegetables is relatively higher than on others. To our knowledge, this is the first comparative study to reveal the effect of removing pesticide residues from five artificially contaminated leafy vegetables (lettuce, perilla leaves, spinach, crown daisy, and ssamchoo (*Brassica lee* ssp. *namai*)) using different removal methods. The percent reduction range for each method was 43.7–77.0%, and the reduction range for the five leafy vegetables was 40.6–67.4%. Lettuce had the highest reduction ($67.4 \pm 7.3\%$), whereas ssamchoo had the lowest reduction ($40.6 \pm 12.9\%$). Spinach and crown daisy showed no significant difference in their reductions. Based on reduction by method, running water ($77.0 \pm 18.0\%$) and boiling ($59.5 \pm 31.2\%$) led to the highest reduction, whereas detergent ($43.7 \pm 14.5\%$) led to the lowest reduction. The reductions of chlorfenapyr, diniconazole, indoxacarb, fludioxonil, pyraclostrobin, and lufenuron in the leafy vegetables were lower with blanching and boiling than with other methods ($p < 0.05$). These results highlight the importance of thoroughly washing leafy vegetables to lower the intake of pesticide residues before cooking.

Keywords: pesticide residue; leafy vegetable; ssamchoo; boiling; detergent

1. Introduction

Despite their toxicity, pesticides are widely used to protect crops against insects, weeds, fungi, and other pests. Accordingly, pesticides are indispensable for food productivity and quality [1]. The application of pesticides may result in residues on vegetables, and these specified derivatives can induce adverse health effects (acute and chronic effects, such as reproductive harm, carcinogenicity, neurological toxicity, and cell dysplasia) [2,3]. Therefore, excessive consumption of residual pesticides via raw or processed vegetables is dangerous for consumers and thus warrants an effective removal strategy.

Globally, studies have been conducted to derive methods that can be utilized for pesticide residue removal from various types of vegetables. Many studies have used methods, such as peeling/trimming, washing/rinsing, soaking, and blanching/boiling, mainly for fruits and fruiting vegetables [4–12]. Tomatoes, oranges, cucumbers, and strawberries have been mainly employed in these studies. However, as these fruits can be peeled and washed relatively easily, it is comparatively simple to remove pesticide residues on these fruits compared to those on vegetables, especially leafy vegetables. Notably, the pesticides analyzed in these studies were limited to those used in fruits and fruiting vegetables. The removal of pesticide residues from the outer skin of certain fruits and fruiting vegetables by peeling or trimming is reported to be the most efficient approach to reduce pesticide residues [13]. However, it is difficult to apply these methods to leafy vegetables, as they cannot be peeled or trimmed. Therefore, the removal method of various

pesticides from vegetables must be investigated. As leafy vegetables cannot be peeled, they are relatively difficult to clean; only attached dust, insects, and foreign substances can be removed. In addition, owing to the large surface area of these vegetables, pesticide residues are likely to remain on their surfaces [14].

Leafy vegetables are used in various cuisines worldwide. Hence, an efficient method is required to remove pesticide residues from leafy vegetables in households. Among all methods, washing (tap water) is known as the most common and efficient method of pesticide residue removal in general households [15]. However, as many pesticides are hydrophobic, washing with tap water is inefficient for pesticide residue removal [16]. Cooking is known to be effective at removing some volatile pesticides but is ineffective at removing less volatile pesticides [11]. Therefore, depending on the characteristics of pesticides, various removal methods should be used. In particular, a removal method suitable for the characteristics of pesticides with a high frequency of use and high detection rate is necessary [13].

Several studies investigated the removal of pesticide residues from leafy vegetables. For example, washing spinach with tap water removed 0–48% of boscalid, deltamethrin, iprodione, mancozeb, and propamocarb [17]; washing Chinese cabbage with electrolyzed water removed 32–38% of chlorpyrifos, prothiofos, and deltamethrin; and blanching (5 min at 88 °C) spinach removed 0–72% of boscalid, deltamethrin, iprodione, mancozeb, and propamocarb [17,18]. However, studies using these methods, particularly washing with water, are scarce and are limited to only a few leafy vegetables.

In general, different methods are used to remove pesticide residues, including washing or blanching, in South Korea and other countries. Accordingly, studies comparing the effectiveness of removing various pesticide residues from various leafy vegetables are warranted. The objective of this study was to evaluate the effectiveness of various methods used in households to remove pesticide residues from agricultural products. Agricultural products, particularly leafy vegetables, were selected based on long-term research results obtained in the largest production area of leafy vegetables in South Korea and Food Safety Management Guidelines for 2021: lettuce, perilla leaves, spinach, crown daisy, and ssamchoo (*Brassica lee* ssp. *namai*) (Figure 1). The pesticides used were azoxystrobin, chlorantraniliprole, chlorfenapyr, diniconazole, fludioxonil, imidacloprid, indoxacarb, lufenuron, pyraclostrobin, and thiamethoxam [19,20].
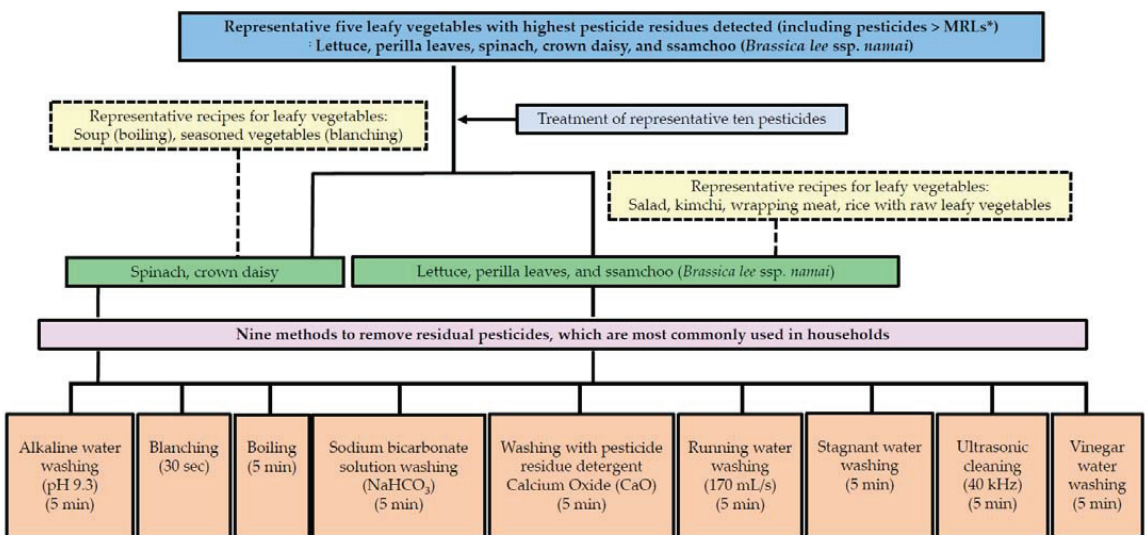
*: MRLs (Maximum Residue Levels) in Food Code (Ministry of Food and Drug Safety, Korea)

Figure 1. Sampling and processing scheme.

Leafy vegetables are widely consumed in Asia in (1) salad, (2) kimchi, (3) seasoned vegetables, (4) meat wrapping, and (5) vegetable soup. Herein, nine pesticide residue removal methods were selected (alkaline electrolyzed water washing, blanching, boiling, sodium bicarbonate solution washing, washing with detergent, tap water washing-running water, tap water washing-stagnant water, ultrasonic cleaning, and vinegar water washing) for comparison (Figure 1).

To the best of our knowledge, the removal efficiency of the selected pesticides in vegetables, especially leafy vegetables, remains largely unknown. The aim of this study was to determine the effectiveness of nine pesticide residue removal methods on the removal of pesticide residues from leafy vegetables.

2. Materials and Methods

2.1. Standards, Reagents, and Materials

The following ten pesticides with high detection rates on leafy vegetables were selected: azoxystrobin, chlorantraniliprole, chlorfenapyr, diniconazole, fludioxonil, imidacloprid, indoxacarb, lufenuron, pyraclostrobin, and thiamethoxam (Table 1) [19,20].

Table 1. The main properties of ten pesticides.

Pesticides [1] (CAS No.)	Leafy Vegetables [2]	MRL [3] (mg/kg)	Molecular Weight	Water Solubility at 20 °C (mg/L)	Log P [4]	Melting Point (°C)	Henry's Constant at 25 °C (Pa m^3 mol^{-1})
Azoxystrobin (131860-33-8)	Perilla leaves, aster scaber, danggi leaf (Korean angelica root leaf)	20	403.4	6.7	2.5	116	7.40×10^{-9}
Chlorantraniliprole (500008-45-7)	Spinach, chives	5.0	483.2	0.88	2.86	209	3.2×10^{-9}
Chlorfenapyr (122453-73-0)	Crown daisy, lettuce, danggi leaf	5.0	407.6	0.112	4.83	101	5.81×10^{-4}
Diniconazole (83657-24-3)	Ssamchoo (*Brassica lee* ssp. *namai*), perilla leaves, crown daisy	0.3	326.2	4	4.3	145	4.00×10^{-2}
Fludioxonil (131341-86-1)	Crown daisy	15	248.2	1.8	4.12	199.8	5.40×10^{-5}
Imidacloprid (138261-41-3)	Perilla leaves, pepper leaves	3.0	255.7	610	0.57	144	1.7×10^{-10}
Indoxacarb (173584-44-6)	Spinach, danggi leaf	3.0	527.8	0.2	4.65	88.1	6.00×10^{-5}
Lufenuron (103055-07-8)	Spinach, crown daisy, lettuce, mustard green	5.0	511.2	0.046	5.12	169.1	3.41×10^{-2}
Pyraclostrobin (175013-18-0)	Perilla leaves, chives	15	387.8	1.9	3.99	63.7	5.31×10^{-6}
Thiamethoxam (153719-23-4)	Crown daisy, curled mallow	5.0	291.7	4100	−0.13	139.1	4.70×10^{-10}

[1] Pesticides with high nonconformity and detection rate in the previous study and Food Safety Management Guidelines for 2021 [19,20]. [2] Main leafy vegetables with the highest detection of each pesticide in the previous study and Food Safety Management Guidelines for 2021 [19,20]. [3] MRL of leafy vegetable set by the Ministry of Food and Drug Safety, South Korea [21]. [4] The values of Log P are octanol-water partition coefficient at pH 7, 20 °C.

2.1.1. Pesticides

The pesticides were purchased as three commercially available formulations (suspension concentrate; SC, water-dispersible granule; WG, and emulsifiable concentrate; EC). Diniconazole (SC, 5% active ingredient) was purchased from Dongbang agro Co., Ltd. (Seoul, South Korea). Chlorfenapyr (SC, 10% a.i.) was purchased from Shin Young agro Co., Ltd. (Seoul, South Korea). Imidacloprid (SC, 8% a.i.) was obtained from Bayer Crop Science (Seoul, South Korea). Thiamethoxam (WG, 10% a.i.), chlorantraniliprole (SC, 2.7% a.i.), fludioxonil (SC, 20% a.i.), and lufenuron (EC, 5% a.i.) were purchased from Syngenta Korea (Seoul, South Korea). Indoxacarb (WG, 5% a.i.) was purchased from Hanearl Science (Gangwon-do, Taebaek-si, South Korea). Azoxystrobin (SC, 21.7% a.i.) and pyraclostrobin (SC, 20% a.i.) were purchased from Chunjiinbiotec (Gangwon-do, Taebaek-si, South Korea).

2.1.2. Standards

Lufenuron (purity: 100%), the pesticide standard, was provided by the Institute of Kemidas (Gyeonggi-do, Gunpo-si, South Korea). The purities of the nine pesticide standards (azoxystrobin, chlorantraniliprole, chlorfenapyr, diniconazole, fludioxonil, imidacloprid, indoxacarb, pyraclostrobin, and thiamethoxam) ranged from 98 to 100%; these standards were obtained from Accustandard (New Haven, CT, USA).

2.1.3. Reagents

The extraction salt kit (4 g $MgSO_4$, 1 g NaCl, 0.5 g disodium citrate sesquihydrate, and 1 g trisodium citrate dehydrate) and dispersive solid phase extraction (dSPE) kit (25 mg primary secondary amine and 150 mg $MgSO_4$) were purchased from Chromatific (Heidenrod, Germany). Acetonitrile, methanol (Merck, Darmstadt, Germany), formic acid (purity: 99%) (Wako, Osaka, Japan), and ammonium acetate (purity: 99%) (Sigma-Aldrich, St. Louis, MO, USA) were of liquid chromatography grade. Vegetable detergent (CaO, 100%), alkaline water (water 99.99%, calcium hydroxide 0.005%, magnesium hydroxide 0.005%) (pH 9.3), vinegar, and sodium bicarbonate were obtained from Ecobiotec Co., Ltd. (Gyeonggi-do, Hwaseong-si, South Korea), Auskorea Co., Ltd. (Gyeonggi-do, Seongnam-si, South Korea), Daesang Corp. (Seoul, South Korea), and LG Household & Health Care Ltd. (Seoul, South Korea), respectively.

2.2. Sample Preparation and Washing Treatments

The following five leafy vegetables with the highest rate of pesticide detection were selected: lettuce, perilla leaves, spinach, crown daisy, and ssamchoo [19,20]. The samples were randomly purchased from the Gakhwa Agricultural Products Wholesale Market (Gwangju, South Korea) in 2021. Samples of the five leafy vegetables were pre-analyzed and determined to be free of previous residues prior to the experiment and stored at 4 °C prior to analysis. The pesticides used to prepare the contaminated samples were administered according to the doses recommended by the manufacturer. The recommended doses were 20 mL/20 L for diniconazole and indoxacarb and 10 mL/20 L for chlorfenapyr, azoxystrobin, imidacloprid, chlorantraniliprole, fludioxonil, and lufenuron. The recommended amounts of thiamethoxam and pyraclostrobin were 10 g/20 L and 6.7 g/20 L, respectively. The concentration of the 10 pesticides in the mixed solution ranged from 13.5–108.5 mg/L. Leafy vegetables were soaked in 20 L of mixed pesticide and treated for 10 s to ensure even application of the pesticide. Contaminated leafy vegetables were air-dried in a fume hood for 15 h at room temperature. Subsequently, 100 g of the contaminated leafy vegetables was randomly collected to detect the initial residual amount. The contaminated samples were washed using nine methods. The treatment time was set to 5 min, which is the mid-point of the treatment time used in previous studies, and was unified, except for blanching (30 s), to compare the washing effect [13]. Each process was repeated five times.

(a) Running tap water: Samples (100 g) were rinsed under running tap water for 5 min. The running rate of the tap water was controlled at 170 mL/s.

(b)   Stagnant tap water/alkaline water: Samples (100 g) were soaked in a bucket containing 2 L of stagnant tap water and alkaline water for 5 min.

(c)   Ultrasonic cleaning: Samples (100 g) were placed in an ultrasonic cleaner bath (Bransonic CPX8800H-E, Branson, MO, USA) containing stagnant water (2 L). The ultrasonic cleaner was maintained at 40 kHz for 5 min (the frequency of commercially available household ultrasonic cleaners).

(d)   5% vinegar, 2% sodium bicarbonate, and vegetable detergent in water: Samples (100 g) were soaked in a bucket containing 2 L of 5% vinegar, 2% sodium bicarbonate, and vegetable detergent (1.5 g/2 L) in water for 5 min.

(e)   Blanching/boiling: Samples (100 g) were placed into a bucket and 2 L of boiling water (100 °C) for 30 s and 5 min, respectively.

2.3. Extraction and Analysis of the Pesticide Residues

The extraction was performed using the QuEChERS (Quick, Easy, Cheap, Effective, Rugged, Safe) method [21]. Briefly, the washed samples (100 g) were homogenized and processed using a blender. Thereafter, 10 g of the sample was placed in 50 mL centrifuge tubes and mixed with 10 mL of acetonitrile. The tube was sealed and vigorously shaken in a shaker (VIBA X.30, Collomix, Gaimersheim, Germany) for 1 min. The extraction salt kit was subsequently added. The mixture was shaken vigorously for 1 min and then centrifuged (Avanti J-15R, Beckman Coulter, Brea, CA, USA) at $4000 \times g$ for 10 min. A 1 mL aliquot of the supernatant was transferred to a 2 mL centrifuge tube containing a dSPE kit. The 2 mL centrifuge tube was then shaken for 1 min and centrifuged (Microfuge 20R, Beckman Coulter, Brea, CA, USA) for 5 min at $10,000 \times g$. Finally, the supernatant was filtered through a 0.2 μm membrane into a chromatography vial for analysis.

2.4. Chromatographic Analysis

2.4.1. Gas Chromatography-Tandem Mass Spectrometry (GC-MS/MS) Analysis

The pesticides (chlorfenapyr, diniconazole, and indoxacarb) were analyzed using an Agilent 7000D GC/TQ with a 7890 B gas chromatograph and a 7693A autosampler (Agilent Technologies, Santa Clara, CA, USA). Chromatographic separation was achieved on a DB-5MS UI column (0.25 mm I.D. × 30 m, 0.25 μm) (Agilent Technologies, Santa Clara, CA, USA). The oven temperature program was as follows: 200 °C hold for 0.1 min, increased to 250 °C at a rate of 40 °C/min, and increased to 300 °C at a rate of 60 °C/min and hold for 5 min. One microliter of the sample was injected in splitless mode. The total running time was 7.18 min. Helium gas was used as the carrier gas at a constant flow rate of 1.5 mL/min. Triple quadrupole MS was applied in dynamic multiple reaction monitoring mode with electron ionization at 70 eV. The GC-MS/MS parameters are summarized in Table 2. The ion source and transfer line temperatures were set at 250 and 280 °C, respectively. The MassHunter quantitative analysis software (version 10.1) (Agilent Technologies, Santa Clara, CA, USA) was used for data processing.

Table 2. Experimental parameters of ten pesticides by GC-MSMS and LC-MSMS.

Pesticide	Retention Time (min)	Precursor Ion (*m/z*)	Product Ion (*m/z*)	Collision Energy (eV)
GC-MSMS				
Chlorfenapyr	2.74	247 328	227 247	15 15
Diniconazole	2.90	268	136 232	45 15
Indoxacarb	5.59	203	106 134	25 15
LC-MSMS				
Azoxystrobin	8.85	404	372 344	21 35
Chlorantraniliprole	8.62	484	453 286	27 21
Fludioxonil	9.14	266	229 158	23 50
Imidacloprid	5.89	256	209 212	25 17
Lufenuron	12.87	509	339 326	15 30
Pyraclostrobin	11.48	388	163 194	39 18
Thiamethoxam	5.57	292	211 132	17 35

2.4.2. Liquid Chromatography-Tandem Mass Spectrometry (LC-MS/MS) Analysis

The pesticides (azoxystrobin, chlorantraniliprole, fludioxonil, imidacloprid, lufenuron, pyraclostrobin, and thiamethoxam) were analyzed using a nanospace NASCA (OSAKA SODA, Tokyo, Japan) liquid chromatograph with a QTRAP 4500 detector (AB Sciex, Framingham, MA, USA). The target pesticides were separated on a CAPCELL CORE C18 column (2.1 mm I.D. × 150 mm, 2.7 μm) (OSAKA SODA, Tokyo, Japan) maintained at 40 °C. The mobile phase was 5 mM ammonium acetate in water with 0.1% formic acid (phase A) and 5 mM ammonium acetate in methanol with 0.1% formic acid (phase B). The following gradient was employed: 95:5 (A:B) (0–1 min), 40:60 (1–3 min), 0:100 (3–13 min), and held for 18 min, and finally maintained at 95:5 (18.1–25 min). The flow rate was 200 μL/min. Two microliters of the final extracted sample solution were injected into the system. The analysis time was 26.05 min. Quantification and identification of the target compounds were carried out in multiple reaction monitoring mode. Electrospray ionization was conducted in positive ion mode (ESI+) and negative ion mode (ESI−) at capillary voltages of 5500 and −4500 V, respectively, and evaporation of solvents with synthetic air at 450 °C. Table 2 summarizes the LC-MS/MS parameters.

2.5. Method Validation

The analytical method was validated according to the SANTE/12682/2019 guidelines on validation procedures for pesticide residue analysis in food and feed [22]. The limits of detection (LODs) and limits of quantitation (LOQs) were estimated using signal-to-noise (S/N) ratios of 3 and 10, respectively. The analytical method was validated for each matrix, and the linearity of the matrix-matched calibration curve was determined at five concentrations (0.01, 0.025, 0.05, 0.075, and 0.1 mg/kg). Recovery was estimated at three concentrations (0.01, 0.05, and 0.1 mg/kg) by spiking ten standard pesticides into a blank sample.

2.6. Statistical Analysis

All data analyses were performed using SPSS Statistics, Version 27.0 (IBM, Armonk, NY, USA). For each washing method, the mean and standard deviation of the data from the repeated experiments were determined. The significance of all data was determined using ANOVA, and Tukey's test was used as a post-hoc analysis technique. Differences between treatments were established at a significance level of $p < 0.05$. Pearson's correlation test was conducted to estimate the effect of washing methods and properties of pesticide on the decline pattern. Correlation analysis and principal component analysis (PCA) were performed to determine the correlation between the pesticide physicochemical parameters, pesticide percent reduction, and effectiveness of each washing method.

3. Results

3.1. Method Validation

In general, method validation was performed using each matrix. Table 3 shows the standard curve coefficients (R^2), average recoveries, and relative standard deviations for the pesticides studied using each matrix. The LOQs for the ten pesticides (azoxystrobin, chlorantraniliprole, chlorfenapyr, diniconazole, fludioxonil, imidacloprid, indoxacarb, lufenuron, pyraclostrobin, and thiamethoxam) were defined as the concentrations produced from a S/N ratio of 10. The estimated LOD and the LOQ were 0.001–0.003 and 0.002–0.009 mg/kg, respectively. The LOQ was lower than the maximum residue limit (MRL) set by the Ministry of Food and Drug Safety of the South Korea (Table 1). Identical linearities with determination coefficients ($R^2 > 0.999$) were obtained from matrix-matched calibration of the blank and each matrix. The recovery rates were satisfactory, ranging from 87 to 115%, with an RSD of <8%. The RSD for five leafy vegetables never exceeded 20% according to the acceptance and rejection criteria of the SANTE guidelines. All mean values for recovery were within the acceptable range (70–120%).

Table 3. Regression coefficient (R^2), LOQs, and average recoveries for ten pesticides in five leafy vegetables (n = 5).

Pesticide	Linearity (R^2), 0.01–0.1 mg/kg	LOQ (mg/kg)	Average Recovery					
			0.01 mg/kg		0.05 mg/kg		0.1 mg/kg	
			%	%RSD	%	%RSD	%	%RSD
Lettuce								
Azoxystrobin	0.9993	0.004	102.1	3.3	105.7	4.8	102.8	2.3
Chlorantraniliprole	0.9996	0.005	100.5	4.0	100.6	3.4	100.5	3.1
Chlorfenapyr	0.9999	0.003	102.7	3.1	113.1	1.7	103.8	1.4
Diniconazole	1.0000	0.002	105.3	0.7	109.0	0.5	104.8	0.8
Fludioxonil	0.9995	0.005	86.8	2.3	92.7	2.5	90.6	3.0
Imidacloprid	0.9999	0.005	88.0	2.2	91.1	2.1	88.5	2.9
Indoxacarb	0.9993	0.005	104.8	4.1	114.6	2.9	115.4	1.9
Lufenuron	0.9999	0.003	97.6	4.7	102.2	5.1	100.9	4.1
Pyraclostrobin	0.9992	0.009	102.7	1.9	104.5	1.8	103.0	1.9
Thiamethoxam	0.9999	0.002	87.4	3.3	90.0	1.0	87.9	3.2

Table 3. *Cont.*

Pesticide	Linearity (R²), 0.01–0.1 mg/kg	LOQ (mg/kg)	Average Recovery					
			0.01 mg/kg		0.05 mg/kg		0.1 mg/kg	
			%	%RSD	%	%RSD	%	%RSD
Perilla leaves								
Azoxystrobin	0.9998	0.006	98.8	6.5	102.1	5.8	96.8	2.8
Chlorantraniliprole	0.9999	0.006	98.6	5.7	96.4	6.9	93.5	4.0
Chlorfenapyr	1.0000	0.004	105.2	6.4	99.5	1.1	99.9	3.5
Diniconazole	1.0000	0.003	102.1	3.2	100.1	1.7	99.0	1.7
Fludioxonil	0.9999	0.009	98.8	5.3	96.2	5.5	103.3	5.1
Imidacloprid	0.9998	0.003	98.1	0.5	96.1	2.2	96.6	1.9
Indoxacarb	0.9999	0.004	98.6	4.6	98.1	3.8	104.2	3.0
Lufenuron	0.9999	0.006	97.2	2.4	96.2	3.3	97.0	4.9
Pyraclostrobin	0.9999	0.005	96.7	2.2	96.9	2.3	100.7	3.5
Thiamethoxam	0.9999	0.006	96.0	1.5	95.1	3.0	95.3	2.0
Spinach								
Azoxystrobin	0.9999	0.002	100.5	1.2	93.0	3.2	96.9	3.8
Chlorantraniliprole	0.9998	0.002	100.4	4.8	95.2	3.4	101.5	2.0
Chlorfenapyr	0.9999	0.004	100.0	5.5	99.0	1.0	101.0	0.7
Diniconazole	0.9997	0.003	103.1	1.3	99.1	1.4	99.6	1.0
Fludioxonil	0.9998	0.003	102.6	1.4	100.3	2.2	94.5	2.7
Imidacloprid	0.9999	0.004	99.0	1.8	102.9	3.3	98.6	1.2
Indoxacarb	0.9994	0.002	99.0	5.0	97.9	3.3	97.6	0.9
Lufenuron	0.9999	0.004	99.7	4.4	101.9	4.2	94.7	2.3
Pyraclostrobin	0.9999	0.003	102.5	3.9	97.8	2.2	104.1	4.2
Thiamethoxam	0.9999	0.002	99.9	1.5	95.9	2.8	100.2	4.7
Crown daisy								
Azoxystrobin	0.9999	0.003	102.6	2.0	101.4	1.9	102.0	1.7
Chlorantraniliprole	0.9999	0.004	95.8	1.9	102.7	1.8	102.6	2.2
Chlorfenapyr	0.9999	0.003	101.8	3.3	101.5	2.2	99.4	0.9
Diniconazole	0.9999	0.002	102.0	0.9	100.2	2.3	102.0	0.6
Fludioxonil	0.9998	0.006	99.5	6.4	102.8	5.3	98.1	4.7
Imidacloprid	0.9999	0.004	97.3	4.0	96.2	4.5	100.8	4.0
Indoxacarb	0.9998	0.007	102.7	5.7	96.1	5.2	100.7	2.7
Lufenuron	0.9999	0.002	88.2	7.5	98.6	1.8	98.0	1.5
Pyraclostrobin	0.9999	0.007	95.1	2.9	95.5	1.2	94.1	2.2
Thiamethoxam	1.0000	0.006	93.2	3.9	96.0	3.0	98.9	1.9
Ssamchoo								
Azoxystrobin	0.9997	0.003	93.2	1.3	95.4	1.9	95.8	4.8
Chlorantraniliprole	0.9999	0.002	95.5	3.5	97.1	4.7	98.4	4.0
Chlorfenapyr	1.0000	0.005	99.9	3.0	99.5	1.6	99.1	1.3
Diniconazole	0.9999	0.006	101.4	1.2	99.7	0.9	98.8	0.6
Fludioxonil	0.9998	0.002	89.7	2.0	103.1	5.1	90.8	0.9
Imidacloprid	0.9999	0.002	97.8	1.9	101.6	3.4	100.3	5.0
Indoxacarb	0.9996	0.006	101.2	4.6	99.1	3.6	100.3	1.4
Lufenuron	1.0000	0.002	96.9	1.8	96.5	1.3	95.5	2.9
Pyraclostrobin	0.9999	0.002	98.6	3.2	99.7	2.7	100.4	3.1
Thiamethoxam	0.9999	0.002	90.2	2.3	93.2	1.6	95.7	1.3

3.2. Differences in Efficiency by Type of Leafy Vegetable and Removal Method for the Reduction of Pesticide Residues

In this study, ten pesticides with high detection rates were administered to five leafy vegetables. Thereafter, nine removal methods were applied. As various washing methods are applied for various dishes in Asian countries, including China and South Korea, a representative method for removing pesticide residues from leafy vegetables was tested. Since leafy vegetables are intended to be consumed following these treatments, their structure must remain more or less intact to maintain consumer acceptance. Figure S1 depicts images revealing the effect of the treatment on the appearance of the leafy vegetables. Except for blanching and boiling, all methods preserved the structural integrity of the leafy vegetables. Blanched or boiled leafy vegetables are consumed as soup or seasoned vegetables; therefore, consumers could accept them even if their structure is not retained.

The initial residue values for the pesticides found on artificially contaminated samples are outlined in Table S1: lettuce (4.45–34.81 mg/kg), perilla leaves (5.74–42.97 mg/kg), spinach (4.52–37.04 mg/kg), crown daisy (4.02–29.67 mg/kg), and ssamchoo (2.95–27.96 mg/kg). The reductions in the pesticide amount in the five vegetables are summarized in Table 4. The reduction range for the five leafy vegetables was 40.6–67.4%. The average reductions for each sample appeared in the following order: lettuce (67.4 ± 7.3%) > perilla leaves (59.8 ± 10.2%) > spinach (55.1 ± 13.8%) and crown daisy (54.3 ± 11.5%) > ssamchoo (40.6 ± 12.9%). Spinach and crown daisy showed no significant difference in their reductions. Lettuce had the highest reduction (57.5% (detergent)–82.5% (running water)), whereas ssamchoo had the lowest reduction (28.0% ($NaHCO_3$)–59.7% (running water)). Overall, the reductions for each method were as follows: running water (77.0 ± 18.0%), boiling (59.5 ± 31.2%), alkaline water (56.4 ± 18.0%), blanching (54.9 ± 25.9%), ultrasonic cleaning (52.8 ± 18.7%), $NaHCO_3$ (52.0 ± 19.2%), stagnant water (51.4 ± 16.4%), vinegar (51.2 ± 18.3%), detergent (43.7 ± 14.5%). Washing with running water led to the highest removal efficiency among all methods, whereas washing with detergent led to the lowest removal efficiency.

Table 4. Reduction of pesticide residues in five leafy vegetables using nine methods (means ± SD, n = 5).

Treatment	% Reduction					
	Lettuce	Perilla Leaves	Spinach	Crown Daisy	Ssamchoo	Mean
Alkaline water	72.0 ± 1.9	67.8 ± 1.2	50.3 ± 4.5	49.9 ± 4.8	42.0 ± 7.9	56.4 ± 18.0 [bc]
Blanching	68.4 ± 1.8	56.7 ± 3.9	49.3 ± 3.6	47.9 ± 5.4	52.3 ± 2.3	54.9 ± 25.9 [cd]
Boiling	66.5 ± 4.9	44.0 ± 3.3	65.6 ± 4.3	65.9 ± 2.9	55.4 ± 7.0	59.5 ± 31.2 [b]
$NaHCO_3$	66.7 ± 2.9	63.5 ± 1.8	47.1 ± 5.7	54.8 ± 2.7	28.0 ± 8.6	52.0 ± 19.2 [d]
Detergent	57.5 ± 2.3	45.8 ± 5.1	43.9 ± 8.3	38.6 ± 4.5	32.6 ± 2.7	43.7 ± 14.5 [e]
Running water	82.5 ± 1.3	76.3 ± 4.5	87.8 ± 2.1	78.5 ± 0.8	59.7 ± 4.1	77.0 ± 18.0 [a]
Stagnant water	59.0 ± 2.7	63.1 ± 4.8	50.0 ± 4.6	50.9 ± 3.4	33.7 ± 8.4	51.4 ± 16.4 [d]
Ultrasonic cleaning	68.0 ± 0.9	62.1 ± 1.0	49.7 ± 2.0	52.9 ± 2.0	31.2 ± 7.4	52.8 ± 18.7 [cd]
Vinegar	65.7 ± 2.2	58.6 ± 5.2	51.8 ± 6.4	49.1 ± 3.4	30.9 ± 4.5	51.2 ± 18.3 [d]
Mean	67.4 ± 7.3 [A]	59.8 ± 10.2 [B]	55.1 ± 13.8 [C]	54.3 ± 11.5 [C]	40.6 ± 12.9 [D]	-

The different letters indicate significant different ($p < 0.05$) and comparison of means were formed using Tukey's test.

3.3. Comparison of the Removal Efficiency of Each Pesticide Residue

The reductions of each pesticide in the five leafy vegetables using the nine methods are shown in Figure 2. Table S1 presents the numerical results. The initial residual values of pesticides found in artificially contaminated samples were 27.96–42.97 mg/kg (azoxystrobin), 2.95–5.74 mg/kg (chlorantraniliprole), 11.54–16.27 mg/kg (chlorfenapyr), 10.95–15.56 mg/kg (diniconazole), 21.64–39.28 mg/kg (fludioxonil), 8.54–16.03 mg/kg (imidacloprid), 8.72–20.76 mg/kg (indoxacarb), 4.88–9.04 mg/kg (lufenuron), 16.65–26.95 mg/kg (pyraclostrobin), and 9.27–17.35 mg/kg (thiamethoxam). As pesticide treatment was not performed in the field, the initial pesticide residues exceeded the MRL in most cases.

The experimental conditions were not identical to those of the crop-growing environment, which served as a limitation. Therefore, it was difficult to treat pesticides according to the growth stage, harvest time, and frequency of use of crops, and these changes could not be reflected in the results. Although we excluded these factors, the pesticides were assumed to be administered at their maximum value. Furthermore, this study sought to identify the cleaning effect of various cleaning methods.
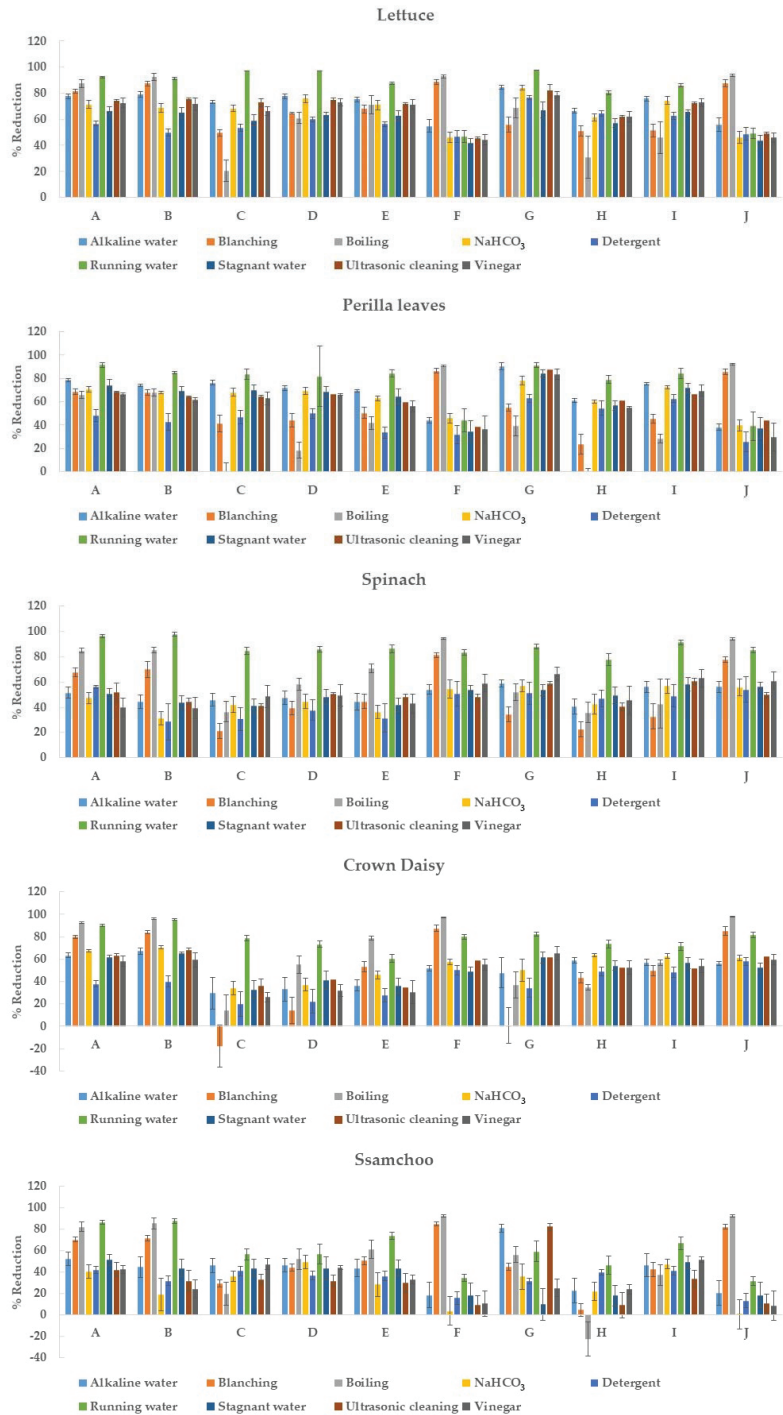
Figure 2. Comparison of removal efficiency of each pesticide in five leafy vegetables (n = 5). A: azoxystrobin, B: chlorantraniliprole, C: chlorfenapyr, D: diniconazole, E: fludioxonil, F: imidacloprid, G: indoxacarb, H: lufenuron, I: pyraclostrobin, and J: thiamethoxam.

The average reductions of each pesticide appeared in the following order: azoxystrobin (66.2 ± 7.6%) > chlorantraniliprole (63.3 ± 11.5%) > indoxacarb (61.2 ± 14.1%) > pyraclostrobin (58.1 ± 8.2%) > thiamethoxam (54.0 ± 15.2%), imidacloprid (53.6 ± 13.7%), fludioxonil (53.5 ± 11.0%), and diniconazole (53.3 ± 12.9%) > chlorfenapyr (46.0 ± 13.8%) and lufenuron (45.1 ± 16.0%). For the overall reduction by pesticide, azoxystrobin had the highest reduction (66.2%), whereas lufenuron had the lowest reduction (45.1%). A reduction difference of approximately 20% was found between the highest and lowest values for each pesticide. The reduction efficiencies of thiamethoxam, imidacloprid, fludioxonil, and diniconazole were not significantly different. Furthermore, lufenuron and chlorfenapyr were not significantly different.

3.4. Statistical Analysis of the Physicochemical Parameters and Removal Efficiency of Ten Pesticides

According to the correlation analysis (Table 5), the dominant physicochemical parameter affecting the reduction of pesticide residues during thermal processing (blanching and boiling) was log *P* (negative correlation) and that for the running water washing method was water solubility (negative correlation). PCA was performed to better understand the correlation between various physicochemical parameters of pesticides and pesticide reduction in each of the nine removal methods. Figure 3 shows the PCA results of the nine methods and their characteristic results. Of note, the relationship between the molecular weight, polarity (log *P*), water solubility, melting point, Henry's constant of the pesticides, and reduction is discussed below for each method of pesticide residue removal. Score plots were obtained for each removal method using PCA. The first and second principal components (PC1 and PC2, respectively) were selected according to the Kaiser's rule of selecting principal components with eigenvalues greater than 1 (Figure 3a–i1). PC1 and PC2 were further analyzed.

Table 5. Correlation analysis between nine washing methods and properties of pesticide.

Treatment	Pearson's r				
	Molecular Weight	Water Solubility	Log *P*	Melting Point	Henry's Constant
Alkaline water	0.627	−0.515	0.475	−0.373	−0.213
Blanching	−0.454	0.512	−0.920 **	0.317	−0.451
Boiling	−0.467	0.476	−0.866 **	0.300	−0.476
NaHCO$_3$	0.535	−0.607	0.606	−0.520	0.049
Detergent	0.603	−0.249	0.366	−0.589	0.160
Running water	0.550	−0.672 *	0.573	−0.033	−0.064
Stagnant water	0.495	−0.555	0.469	−0.271	−0.081
Ultrasonic cleaning	0.616	−0.406	0.430	−0.411	−0.180
Vinegar	0.592	−0.539	0.585	−0.592	−0.046

* $p < 0.05$; ** $p < 0.01$.
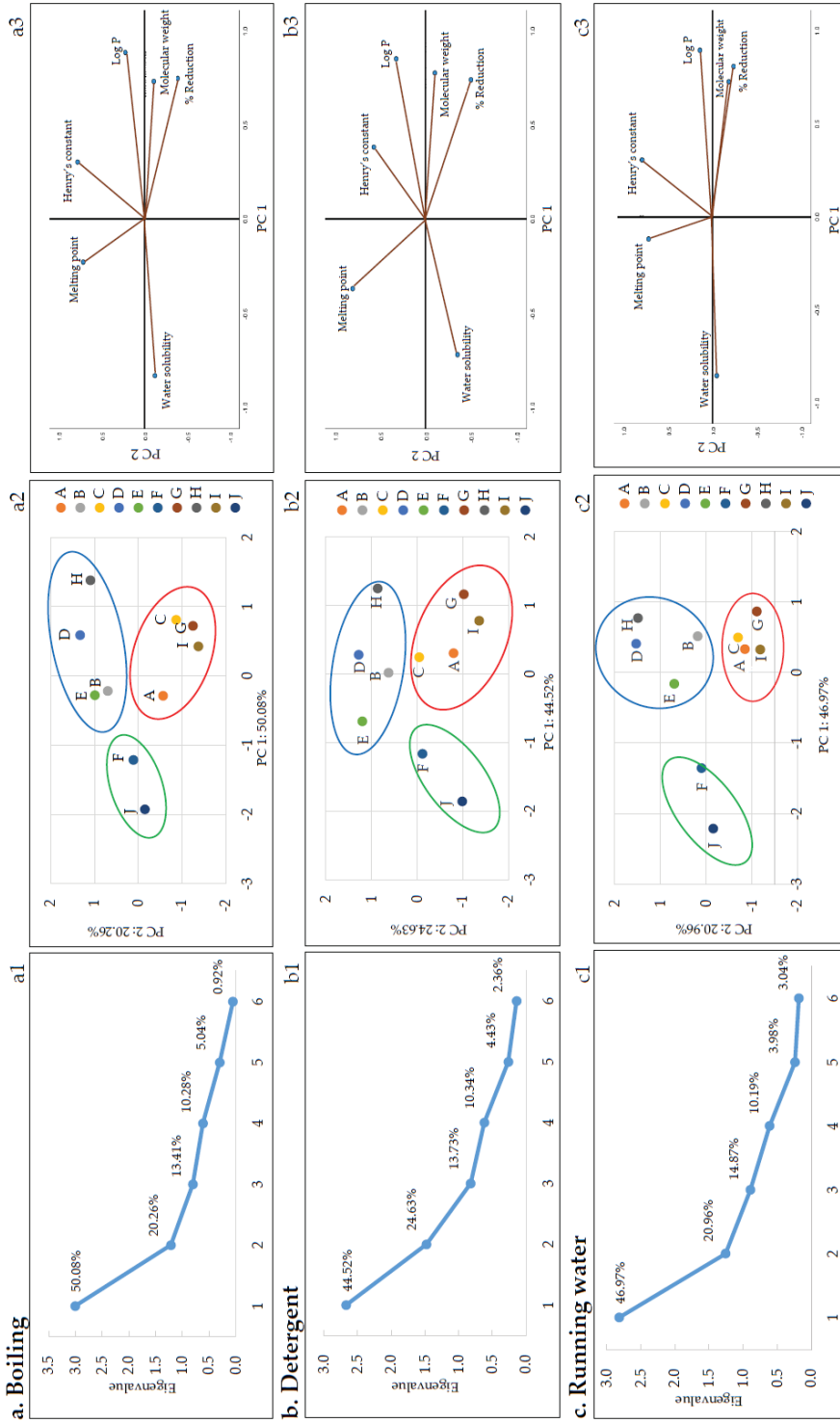
Figure 3. *Cont.*
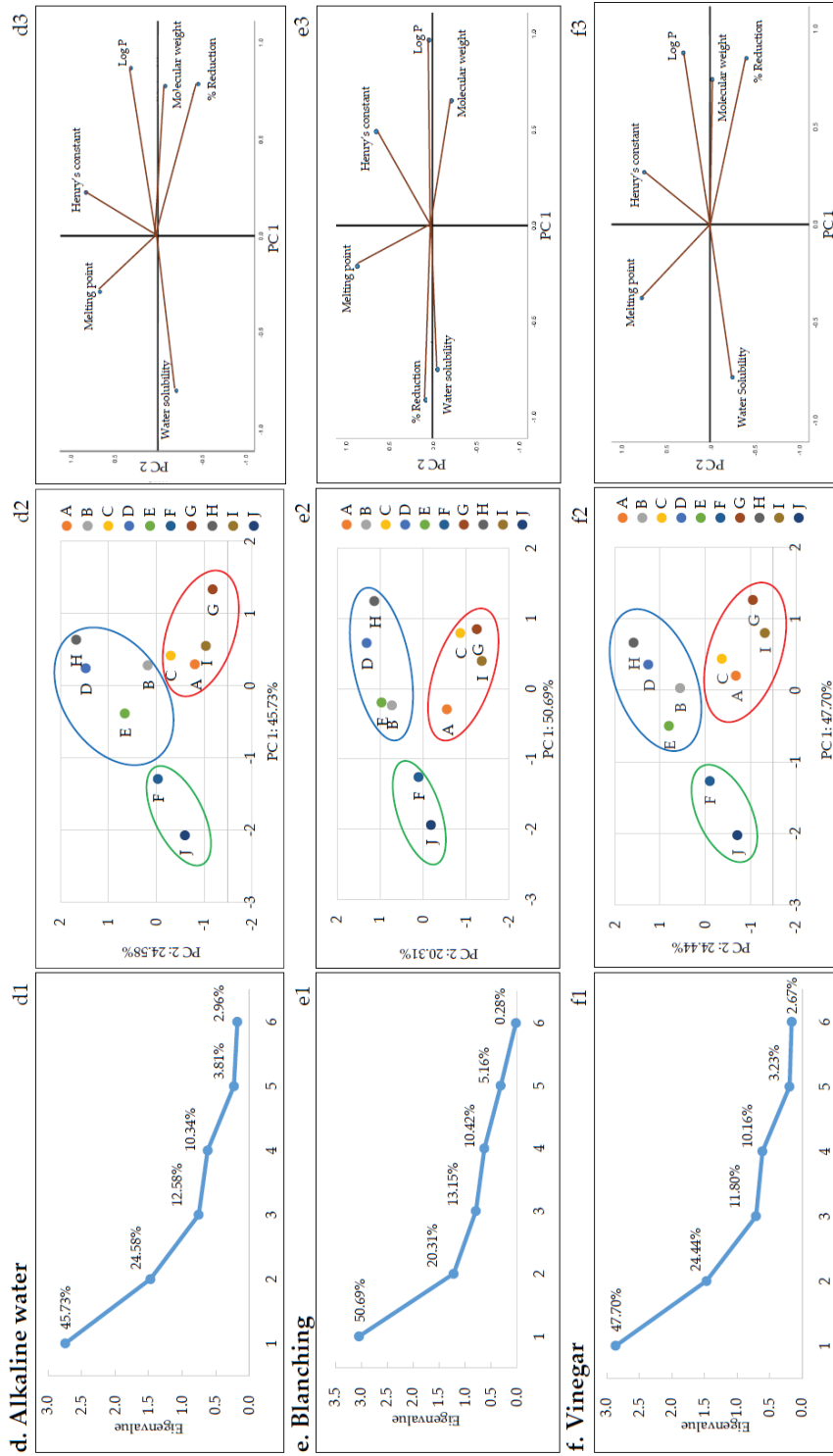
Figure 3. *Cont.*
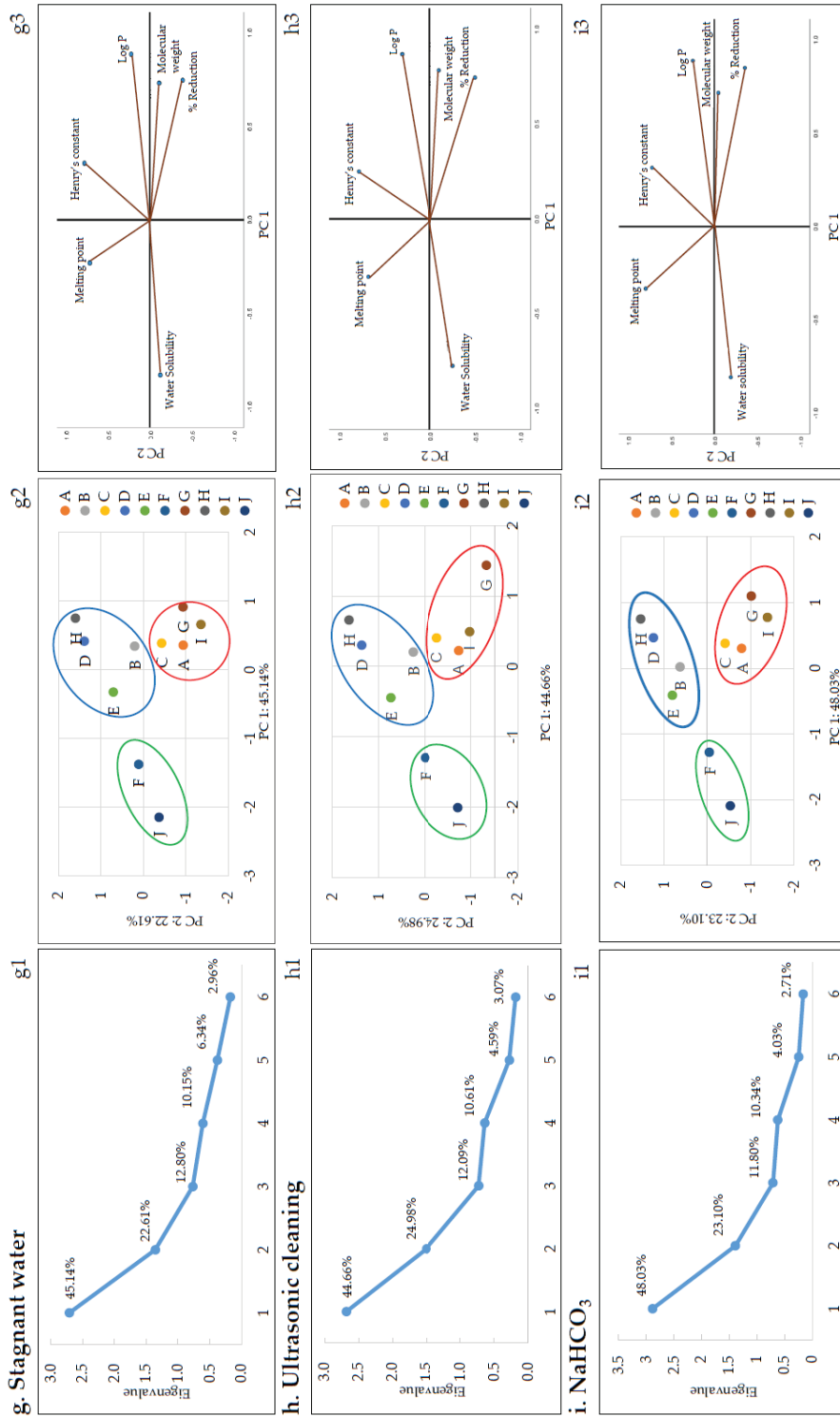
Figure 3. The plots of PCA: The scree (**a**–**i1**), score (**a**–**i2**), and loading (**a**–**i3**) plots. A: Azoxystrobin, B: Chlorantraniliprole, C: Chlorfenapyr, D: Diniconazole, E: Fludioxonil, F: Imidacloprid, G: Indoxacarb, H: Lufenuron, I: Pyraclostrobin, and J: Thiamethoxam.

Score plots and loading plots revealed that the PC1 and PC2 accounted for more than 68% of the total variance in PCA. The two significant principal components accounted for a proportion of the total variation: running water: 67.93% (PC1: 46.97% and PC2: 20.96%), boiling: 70.3% (PC1: 50.08% and PC2: 20.26%), detergent: 69.14% (PC1: 44.52% and PC2: 24.63%), alkaline water: 70.3% (PC1: 45.73% and PC2: 24.58%), blanching: 71.0% (PC1: 50.69% and PC2: 20.31%), vinegar: 72.14% (PC1: 47.70% and PC2: 24.44%), stagnant water: 67.76% (PC1: 45.14% and PC2: 22.61%), ultrasonic cleaning: 69.64% (PC1: 44.66% and PC2: 24.98%), and NaHCO$_3$: 71.12% (PC1: 48.03% and PC2: 23.10%). The pesticides were categorized based on the scores and loadings and grouped into three clusters, as shown in Figure 3a–i2. Each group consisted of the following pesticides: first pesticides group (imidacloprid and thiamethoxam), second pesticides group (chlorantraniliprole, diniconazole, fludioxonil, and lufenuron), and third pesticides group (azoxystrobin, chlorfenapyr, indoxacarb, and pyraclostrobin). Imidacloprid and thiamethoxam, classified into the first group, displayed similar reduction patterns in all methods based on Figures 2 and 3. The first group had log *P* less than 1 and high water solubility, and the second and third groups had log *P* greater than 1 and low water solubility.

4. Discussion

4.1. Differences in Efficiency Based on the Type of Leafy Vegetable and Removal Method for the Reduction of Pesticide Residues

In this study, the reduction range for five leafy vegetables was 40.6–67.4% (Table 4). Previous studies revealed the effectiveness of pesticide residue removal from fruits and fruiting vegetables. When tomatoes and cucumbers were washed for 1 min, over 83–100% of the pesticide residues (dimethoate and profenofos) were removed. When okra (*Abelmoschus esculentus*) was washed for 1 min, malathion was almost completely removed. Up to 70–100% of azoxystrobin, acrinathrin, and kresoxim-methyl were removed when zucchini was washed (intensive) [23,24]. In China, when the kumquat (*Citrus japonica*) was washed with tap water for 5 min, the average reduction of the 10 pesticides (chlorpyrifos, myclo-butanil, tebuconazole, bifenthrin, lambda-cyhalothrin, beta-cypermethrin, esfenvalerate, difenoconazole, imidacloprid, and acetamiprid) was 25%. Furthermore, when spinach was washed in the same manner, the average removal efficiency was 11%. The reduction of the pesticide amount in spinach was lower than that in kumquat for the ten pesticides (chlorpyrifos, myclobutanil, tebuconazole, bifenthrin, lambda-cyhalothrin, beta-cypermethrin, esfenvalerate, difenoconazole, acetamiprid, and imidacloprid) [25]. The removal efficiency of leafy vegetables was relatively lower than that of fruits, as they are consumed without peeling. Removing the skin of fruits is known to have the greatest pesticide removal efficiency [13]. Peeling mangoes has been reported to completely remove fenthion, dimethoate, cypermethrin, and fenvalerate [26]. Based on a comprehensive review of the results of this study and other studies, it is concluded that leafy vegetables tend to have lower pesticide reduction than fruits and fruiting vegetables.

Spinach washed with running water (87.8%) and ssamchoo treated with NaHCO$_3$ (28.0%) showed a three-fold difference in reduction (Table 4). Overall, leafy vegetables (perilla leaves and lettuce; average reduction, 63.6%) with a large leaf surface area had a higher reduction than those with a small surface area (spinach and crown daisy; average reduction, 54.7%) (*p* < 0.05); this is because each removal method is considered to have high efficiency over a large area [27]. However, although ssamchoo is a leafy vegetable with broad leaves, such as lettuce and perilla leaves, it has a different aspect ratio (lowest reduction on average). This finding indicates that the reduction may differ depending on the area and surface characteristics (wax amounts on the cuticle, curvature of the surface, etc.) of each agricultural product, despite the similar shape of leafy vegetables. Ssamchoo was developed in 1998 through the interspecies hybridization of Chinese cabbage and cabbage. Accordingly, ssamchoo is a new vegetable with completely different ecological characteristics, shapes, and genetic compositions from Chinese cabbage or cabbage [28].

Washing is the most effective method for removing pesticide residues from agricultural products in households and commercial processing [17]. The removal efficiency of pesticide residues by washing is affected by various elements (including the nature of sample, such as thickness, type, wax amounts on the cuticle, and surface area; pesticide characteristics; retention time of various pesticide residues; and washing methods) [11,29–31]. Despite these various factors, washing is the most effective treatment for leafy vegetables. In a study by Kim, washing crown daisy with a commercial detergent (0.5%) was found to reduce pesticide residues by 71.3–87.9%, owing to their ability to dissolve non-polar pesticides. Furthermore, when washed with NaCl (1%), vinegar (5%), and charcoal (1%), the reductions were 80.4–87.3%, 76.9–89.0%, and 78.5–88.2%, respectively. However, the reduction was lower than that of washing with water (80.2–90.5%) [32].

The reductions caused by the other eight methods were lower than those caused by washing with running water. The reduction efficiencies of alkaline water, blanching, vinegar, NaHCO$_3$, stagnant water, and ultrasonic cleaning were approximately 51.2–56.4%. The removal efficiency was in the following order: running water > boiling > vinegar, stagnant water, and NaHCO$_3$ > detergent ($p < 0.05$). Washing with detergent led to the lowest removal efficiency (43.7 ± 14.5) among all methods (Table 4). Other studies reported results different from those found in this study. Washing cucumber with micron calcium solution was more effective than washing with tap water, alkaline electrolyzed water (pH 10.50 and 12.35), or sodium bicarbonate. Washing with micron calcium solution for 20 min caused a greater loss of ten pesticides in cucumber, leading to a removal efficiency of 60% on average [25]. This difference might be due to the differences in agricultural products, processing times, and pesticides.

In Asian food culture, many foods (vegetable soup, seasoned vegetables) are consumed following the boiling or blanching of leafy vegetables. Residual pesticides in agricultural products are considered non-residue, as they decompose upon heating and cooking. However, according to the results of this study, blanching and boiling caused 54.9% and 59.5% reductions, respectively, which were lower than those induced by washing ($p < 0.05$). This finding highlights the importance of cooking after sufficient washing of leafy vegetables.

4.2. Comparison of the Removal Efficiency of Each Pesticide Residue

As mentioned earlier, ssamchoo had the lowest pesticide reduction among the five leafy vegetables, which might be due to the following two pesticides: imidacloprid (3.5–92.1%, average 31.8%) and thiamethoxam (0.2–92.0%, average 30.7%). Imidacloprid and thiamethoxam also had relatively low reductions in the perilla leaves and lettuce. For other pesticides, washing with running water was the most effective. However, imidacloprid and thiamethoxam had significantly higher removal efficiencies with boiling and blanching than those with other methods (Figure 2). This finding can be explained by the fact that an increase in temperature during heating affects the hydrolysis of pesticide compounds [33]. In addition, the removal patterns of the two pesticides were similar for the five leafy vegetables; this is due to the characteristics of each pesticide component. Imidacloprid and thiamethoxam are neonicotinoid-based insecticides, with higher water solubility compared to that of other pesticides, and are non-volatile substances with a log *P* value of <1 and high polarity.

The reductions in chlorfenapyr and lufenuron contents using the blanching and boiling methods tended to be lower than those of other pesticides ($p < 0.05$). In crown daisy, the residual amounts of chlorfenapyr after blanching were higher than their initial values. In addition, the residual level of lufenuron increased in perilla leaves and ssamchoo after boiling. Similarly, Yang et al. reported that the residual level of acetamiprid increased in green chilis after boiling and stir-frying (reduction: approximately 80%) [34]. This finding might be due to the concentration of pesticides as a result of moisture evaporation via heating in an open environment [35]. In a study by Lozowicka et al., the concentration of most pesticides was significantly reduced after 5 min of the boiling process used to prepare strawberry jam. However, pyrethroids (alpha-cypermethrin, deltamethrin,

and lambda-cyhalothrin) had a processing factor (PF) of 1 or more (when the PF is 1 or more, the residual pesticide amount is higher than the initial amount). The solubility of alpha-cypermethrin, deltamethrin, and lambda-cyhalothrin was low, at 0.004, 0.0002, and 0.005 mg/L, respectively [36]. The authors judged that the removal of pesticide residues during the heat treatment process would be influenced by the strong adsorption of the pesticides onto plant tissues and the solubility of the pesticides in water. Similarly, in this study, the residual amount of the pesticides chlorfenapyr and lufenuron was higher than the initial amount in the boiling process, and these pesticides had relatively low solubility (0.112 mg/L and 0.046 mg/L, respectively) compared to other pesticides (Table 1). Therefore, it is judged that the characteristics of the pesticides, such as the solubility as well as evaporation of water during the boiling process, may have influenced the residual amount.

Diniconazole had the lowest reduction after lufenuron and chlorfenapyr ($p < 0.05$). Diniconazole was characteristically and mainly detectable in ssamchoo [20]. Therefore, diniconazole must be removed from ssamchoo prior to consumption. When ssamchoo grows too large, it is less commercialized. Therefore, diniconazole is used to control the growth of ssamchoo to a moderate size. Diniconazole is a broad-spectrum triazole fungicide that acts as a plant growth regulator, decreasing the height and leaf area in bean plants when applied to roots [37,38]. In this study, the reduction of diniconazole contents in ssamchoo using different methods showed the following trend: running water (56.7%) and boiling (51.9%) > detergent (36.2%) > ultrasonic cleaning (31.6%) ($p < 0.05$). Overall, the reduction in pesticide residues in ssamchoo was low; washing with running water and boiling proved to be the most effective, especially for the removal of diniconazole from ssamchoo. The ultrasonic method and detergents led to the lowest reductions. Therefore, both washing and boiling are recommended for ssamchoo.

The reduction amounts of chlorfenapyr, diniconazole, indoxacarb, fludioxonil, pyraclostrobin, and lufenuron in all leafy vegetables were low after blanching and boiling ($p < 0.05$). Crown daisy and spinach are consumed as vegetables after blanching in boiling water or as soup after boiling for a long time. Therefore, crown daisy and spinach must be cooked after washing to sufficiently remove these pesticides.

In a previous study from 2005 to 2019, the MRL of leafy vegetables in South Korea was highly exceeded for diniconazole and lufenuron. The detection amount of diniconazole in ssamchoo and perilla leaves was 0.4–6.6 mg/kg and 0.7–2.4 mg/kg, and the MRL was 0.3 mg/kg. Furthermore, the detection amount exceeding the MRL (5.0 mg/kg) of lufenuron in spinach and crown daisy was 0.4–3.8 mg/kg and 0.3–2.1 mg/kg [20]. When running water was used for washing, the reduction of diniconazole from ssamchoo and perilla leaves (ssamchoo, 56.7%; perilla leaves, 81.8%) was highest (Table S1). The reduction of lufenuron in these two leafy vegetables (spinach, crown daisy) was also the highest when running water was employed as the washing method (spinach—77.9%, crown daisy—73.4%). In previous studies, leafy vegetables that do not meet the MRL were not harmful to health based on a risk assessment (risk index ranged from 0.001 to 7.6%) [20]. However, washing with running water before ingestion can reduce pesticide residues to levels below the MRL concentration.

4.3. Statistical Analysis between Physicochemical Parameters and Removal Efficiency of Ten Pesticides

As mentioned earlier, correlation analysis (Table 5) revealed that the dominant physicochemical parameter affecting the rate of pesticide residue removal during heat treatment (blanching and boiling) was log *P* (negative correlation). As depicted in Table 1, the log *P* values of chlorfenapyr, diniconazole, indoxacarb, fludioxonil, pyraclostrobin, and lufenuron ranged between 3.99 and 5.12, and the log *P* values of azoxystrobin, chlorantraniliprole, imidacloprid, and thiamethoxam ranged between −0.13 and 2.86. Therefore, the pesticide residues for chlorfenapyr, diniconazole, indoxacarb, fludioxonil, pyraclostrobin, and lufenuron, which have relatively high log *P* values, could not be easily removed. Similarly, Nagayama reported that the log *P* value and reduction were inversely proportional based

on an analysis of the residual pesticide amount after blanching or making jam using agricultural products collected from the market [39]. Reichman et al. reported volatility changes owing to phase distribution according to Henry's constant when a pesticide is placed in a wet medium. Therefore, in their soil test, the highest volatilization rate of trifluralin was reported to correspond to the highest Henry's constant [40]. Similarly, in a study by Kwon, the reduction in pesticide residues by boiling water was proportional to Henry's constant of pesticides [27]. However, by comparing the pesticide residue reduction and Henry's constant, a proportional relationship with Henry's constant was not found. The dominant variables in the PCA plot were water solubility and Log P (Figure 3a–i3). These two variables are the important variables that have the greatest influence on PC1.

5. Conclusions

A comparative study was conducted to determine the effectiveness of removing ten pesticide residues from five leafy vegetables artificially contaminated with pesticides using nine removal methods. The reduction range for each method was 43.7–77.0% and that for five leafy vegetables was 40.6–67.4%. Lettuce had the highest reduction ($67.4 \pm 7.3\%$), whereas ssamchoo had the lowest reduction ($40.6 \pm 12.9\%$). Spinach and crown daisy showed no significant difference in their reductions. On average, removal using running water ($77.0 \pm 18.0\%$) and boiling ($59.5 \pm 31.2\%$) led to the highest reduction, whereas using detergent ($43.7 \pm 14.5\%$) led to the lowest reduction. The reductions in chlorfenapyr, diniconazole, indoxacarb, fludioxonil, pyraclostrobin, and lufenuron in the five leafy vegetables were lower following blanching and boiling than that following the other methods. High log P values (3.99–5.12, which is greater than 1) were considered to be one of the causes of this result. Therefore, to increase the removal efficiency of these pesticide residues, the vegetable must be boiled and blanched after sufficient washing. Further research on various leafy vegetables associated with high consumption of pesticides should be conducted based on our results, as leafy vegetables have a high risk of pesticide residue contamination.

Author Contributions: S.-J.Y.: Methodology, analysis, interpretation of data, writing the original draft, statistical analysis, and visualization. S.M.: Methodology, validation, analysis, and interpretation of the data, statistical analysis, and visualization. H.J.K.: Methodology, validation, investigation, analysis, and interpretation of the data. S.J.H.: Methodology, investigation, analysis, and interpretation of the data. D.W.K.: Methodology, investigation, analysis, and interpretation of the data. B.-S.C.: Supervision, writing—review, and editing. A.G.K.: Methodology, supervision, visualization, analysis, and interpretation of data. D.W.P.: Conception and design of the study, methodology, writing—original draft, analysis and interpretation of data, visualization. All authors have read and agreed to the published version of the manuscript.

Institutional Review Board Statement: Not applicable.

Informed Consent Statement: Not applicable.

Data Availability Statement: Data is contained within the article or supplementary materials and is available upon reasonable request from the corresponding author.

Conflicts of Interest: The authors declare no conflict of interest.

References

1. Jardim, A.N.O.; Caldas, E.D. Brazilian monitoring programs for pesticide residues in food-Results from 2001 to 2010. *Food Control* **2012**, *25*, 607–616. [CrossRef]
2. IPCS (International Programme on Chemical Safety). INCHEM (Internationally Peer Reviewed Chemical Safety Information). Available online: https://inchem.org/documents/jmpr/jmpmono/v075pr40.htm (accessed on 6 September 2021).
3. SDWF (Safe Drinking Water Foundation). Pesticides and Water Pollution. Available online: https://www.safewater.org/fact-sheets-1/2017/1/23/pesticides (accessed on 6 September 2021).
4. Abou-Arab, A.A.K. Behavior of pesticides in tomatoes during commercial and home preparation. *Food Chem.* **1999**, *65*, 509–514. [CrossRef]
5. Bonnechère, A.; Hanot, V.; Bragard, C.; Bedoret, T.; Loco, J.V. Effect of household and industrial processing on the levels of pesticide residues and degradation products in melons. *Food Addit. Contam. Part A* **2012**, *29*, 1058–1066. [CrossRef] [PubMed]
6. Cámara, M.A.; Cermeño, S.; Martínez, G.; Oliva, J. Removal residues of pesticides in apricot, peach and orange processed and dietary exposure assessment. *Food Chem.* **2020**, *325*, 126936. [CrossRef] [PubMed]
7. Chai, M.K.; Tan, G.H. Headspace solid-phase microextraction for the evaluation of pesticide residue contents in cucumber and strawberry after washing treatment. *Food Chem.* **2010**, *123*, 760–764.
8. Christensen, H.B.; Granby, K.; Rabølle, M. Processing factors and variability of pyrimethanil, fenhexamid and tolylfluanid in strawberries. *Food Addit. Contam.* **2003**, *20*, 728–741. [CrossRef]
9. Cengiz, M.F.; Certel, M.; Karakaş, B.; Göçmen, H. Residue contents of captan and procymidone applied on tomatoes grown in greenhouses and their reduction by duration of a pre-harvest interval and post-harvest culinary applications. *Food Chem.* **2007**, *100*, 1611–1619. [CrossRef]
10. Liu, N.; Dong, F.S.; Liu, X.G.; Xu, J.; Li, Y.B.; Han, Y.T.; Zhu, Y.L.; Cheng, Y.P.; Chen, Z.L.; Tao, Y.; et al. Effect of household canning on the distribution and reduction of thiophanate-methyl and its metabolite carbendazim residues in tomato. *Food Control* **2014**, *43*, 115–120. [CrossRef]
11. Randhawa, M.A.; Anjum, F.M.; Ahmed, A.; Randhawa, M.S. Field incurred chlorpyrifos and 3,5,6-trichloro-2-pyridinol residues in fresh and processed vegetables. *Food Chem.* **2007**, *103*, 1016–1023. [CrossRef]
12. Wang, Z.; Huang, J.; Chen, J.; Li, F. Effectiveness of dishwashing liquids in removing chlorothalonil and chlorpyrifos residues from cherry tomatoes. *Chemosphere* **2013**, *92*, 1022–1028. [CrossRef]
13. Chung, S.W.C. How effective are common household preparations on removing pesticide residues from fruit and vegetables? A review. *J. Sci. Food Agric.* **2018**, *98*, 2857–2870. [CrossRef] [PubMed]
14. Farha, W.; El-Aty, A.M.A.; Rahman, M.M.; Jeong, J.H.; Shin, H.C.; Wang, J.; Shin, S.S.; Shim, J.H. Analytical approach, dissipation pattern, and risk assessment of pesticide residue in green leafy vegetables: A comprehensive review. *Biomed. Chromatogr.* **2018**, *32*, e4134. [CrossRef]
15. Chavarri, M.J.; Herrera, A.; Ariño, A. Pesticide residues in field-sprayed and processed fruits and vegetables. *J. Sci. Food Agric.* **2004**, *84*, 1253–1259. [CrossRef]
16. Qi, H.; Huang, Q.; Hung, Y.C. Effectiveness of electrolyzed oxidizing water treatment in removing pesticide residues and its effect on produce quality. *Food Chem.* **2018**, *239*, 561–568. [CrossRef]
17. Bonnechère, A.; Hanot, V.; Jolie, R.; Hendrickx, M.; Bragard, C.; Bedoret, T.; Loco, J.V. Effect of household and industrial processing on levels of five pesticide residues and two degradation products in spinach. *Food Control* **2012**, *25*, 397–406. [CrossRef]
18. Sung, J.M.; Park, K.J.; Lim, J.H.; Jeong, J.W. Removal effects of microorganism and pesticide residues on chinese cabbages by electrolyzed water washing. *Korean J. Food Sci. Technol.* **2012**, *44*, 628–633. [CrossRef]
19. Ministry of Food and Drug Safety (MFDS) Korea. *Food Safety Management Guidelines for 2021*; Ministry of Food and Drug Safety: Cheongju-si, Korea, 2021; pp. 470–473.
20. Park, D.W.; Yang, Y.S.; Lee, Y.U.; Han, S.J.; Kim, H.J.; Kim, S.H.; Kim, J.P.; Cho, S.J.; Lee, D.V.; Song, N.J.; et al. Pesticide residues and risk assessment from monitoring programs in the largest production area of leafy vegetables in South Korea: A 15-year study. *Foods* **2021**, *15*, 425. [CrossRef]
21. Ministry of Food and Drug Safety (MFDS) Korea. Food Code. Available online: https://www.mfds.go.kr/brd/m_211/view.do?seq=14626 (accessed on 30 September 2021).
22. European Comission. Guidance Document on Analytical Quality Control and Method Validation Procedures for Pesticides Residues Analysis in Food and Feed. 2019. Available online: https://www.eurl-Pesticides.eu/userfiles/file/EurlALL/AqcGuidance_SANTE_2019_12682.pdf (accessed on 8 October 2021).
23. Aguilera, A.; Valverde, A.; Camacho, F.; Boulaid, M.; García-Fuentes, L. Effect of household processing and unit to unit variability of azoxystrobin, acrinathrin and kresoxim methyl residues in zucchini. *Food Control* **2012**, *25*, 594–600. [CrossRef]
24. Wallis, R.L.; Smith, F.F.; Wheeler, H.G.; Gaylor, E.A. Malathion residues on vegetable, berry and tobacco crops. *J. Econ. Entomol.* **1957**, *50*, 362–364. [CrossRef]
25. Wu, Y.; An, Q.; Li, D.; Wu, J.; Pan, C. Comparison of different home/commercial washing strategies for ten typical pesticide residue removal effects in kumquat, spinach and cucumber. *Int. J. Environ. Res. Public Health* **2019**, *16*, 472. [CrossRef]
26. Awasthi, M.D. Determination of insecticide residues on mango by washing and peeling. *J. Food Sci. Technol.* **1993**, *30*, 132–133.
27. Kwon, H.Y.; Lee, H.D.; Kim, J.B.; Jin, Y.D.; Moon, B.C.; Park, B.J.; Son, K.A.; Kwon, O.K.; Hong, M.K. Reduction of pesticide residues in field-sprayed leafy vegetables by washing and boiling. *J. Food Hyg. Saf.* **2009**, *24*, 182–187.

28. Doopedia. *Brassica lee* ssp. *namai*, Korean Cabbage. Available online: http://www.doopedia.co.kr/doopedia/master/master.do?_method=view&MAS_IDX=101013000898618/ (accessed on 6 September 2021).

29. Krol, W.J.; Arsenault, T.L.; Pylypiw, H.M.; Incorvia Mattina, M.J. Reduction of pesticide residues on produce by rinsing. *J. Agric. Food Chem.* **2000**, *48*, 4666–4670. [CrossRef] [PubMed]

30. Ling, Y.; Wang, H.; Yong, W.; Zhang, F.; Sun, L.; Yang, M.L.; Wu, Y.N.; Chu, X.G. The effects of washing and cooking on chlorpyrifos and its toxic metabolites in vegetables. *Food Control* **2011**, *22*, 54–58. [CrossRef]

31. López-Fernández, O.; Rial-Otero, R.; Simal-Gándara, J. Factors governing the removal of mancozeb residues from lettuces with washing solutions. *Food Control* **2013**, *34*, 530–538. [CrossRef]

32. Kim, S.W.; El-Aty, A.M.; Choi, J.H.; Lee, Y.J.; Lieu, T.T.B.; Chung, H.S.; Musfiqur Rahman, M.; Choi, O.J.; Shin, H.C.; Rhee, G.S.; et al. Contributing effect of various washing procedures and additives on the decline pattern of diethofencarb in crown daisy, a model of leafy vegetables. *Food Chem.* **2016**, *201*, 153–159. [CrossRef]

33. Holland, P.T.; Hamilton, D.; Ohlin, B.; Skidmore, M.W. Effects of storage and processing on pesticide residues in plant products. IUPAC Reports on Pesticides (31). *Pure Appl. Chem.* **1994**, *66*, 335–356. [CrossRef]

34. Yang, A.; Park, J.H.; El-Aty, A.M.A.; Choi, J.H.; Oh, J.H.; Do, J.A.; Kwon, K.S.; Shim, K.H.; Choi, O.J.; Shim, J.H. Synergistic effect of washing and cooking on the removal of multi-classes of pesticides from various food samples. *Food Control* **2012**, *28*, 99–105. [CrossRef]

35. Keikotlhaile, B.M.; Spanoghe, P.; Steurbaut, W. Effects of food processing on pesticide residues in fruits and vegetables: A meta-analysis approach. *Food Chem. Toxicol.* **2010**, *48*, 1–6. [CrossRef]

36. Bozena, L.; Jankowska, M.; Hrynko, I.; Kaczynski, P. Removal of 16 pesticide residues from strawberries by washing with tap and ozone water, ultrasonic cleaning and boiling. *Environ. Monit. Assess.* **2016**, *188*, 51. [CrossRef]

37. Yoshida, Y.; Aoyama, Y.; Takano, H.; Kato, T. Stereo-selective interaction of enantiomers of diniconazole, a fungicide, with purified P-45014DM from yeast. *Biochem. Biophys. Res. Commun.* **1986**, *137*, 513–519. [CrossRef]

38. Fletcher, R.A.; Hofstra, G.; Gao, J.G. Comparative fungitoxic and plant growth regulating properties of triazole derivatives. *Plant Cell Physiol.* **1986**, *27*, 367–371.

39. Nagayama, T. Behavior of residual organophosphorus pesticides in foodstuffs during leaching or cooking. *J. Agric. Food Chem.* **1996**, *44*, 2388–2393. [CrossRef]

40. Reichman, R.; Mahrer, Y.; Wallach, R. A combined soil atmosphere model for evaluating the fate of surface applied pesticides. 2. The effect of varying environmental conditions. *Environ. Sci. Technol.* **2000**, *34*, 1321–1330. [CrossRef]

Article

Effect of Cooking Methods on Amphenicols and Metabolites Residues in Livestock and Poultry Meat Spiked Tissues

Manli Wu [1,2,3,4], **Xin Cheng** [5], **Xinyi Wu** [1,2,3,4], **Hang Qian** [1,2,3,4] **and Wei Wang** [1,2,3,4,*]

1   College of Food Science and Technology, Nanjing Agricultural University, Nanjing 210095, China
2   National Center of Meat Quality and Safety Control, Nanjing Agricultural University, Nanjing 210095, China
3   Key Laboratory of Animal Products Processing, Ministry of Agriculture and Rural Affairs, Nanjing 210095, China
4   Jiangsu Collaborative Innovation Center of Meat Production and Processing, Quality and Safety Control, Nanjing Agricultural University, Nanjing 210095, China
5   The Center for Agri-Food Quality & Safety, Ministry of Agriculture and Rural Affairs, Beijing 100125, China
*   Correspondence: wangwei821220@njau.edu.cn; Tel.: +86-25-8439-5650

Abstract: Foods of animal origin, as nutritional supplements, are usually consumed after cooking, but residues of amphenicols in fresh raw meat threaten human health. Therefore, this study was designed to evaluate the effects of boiling, deep-frying and microwave processing under different time conditions on the residue levels of amphenicols and metabolites in livestock and poultry meat. Antibiotic-free pork, beef, lamb and chicken samples were spiked with chloramphenicol (CAP), thiamphenicol (TAP), florfenicol (FF) and florfenicol amine (FFA) standard solutions and made into homogeneous meat blocks. These positive mock meat blocks were processed using three different cooking methods, and the analyses were performed by ultra-high-performance liquid chromatography-tandem mass spectrometry (UHPLC-MS/MS). The results showed that cooking methods, time and food matrices were the main factors influencing the changes in amphenicols and metabolites residues in livestock and poultry meat. With the increase in cooking time, boiling processing was the most effective in reducing the four drug residues in livestock and poultry meat matrices, followed by deep-frying, while microwaving caused an increase in drug residue concentrations. Although boiling and frying processes are effective strategies to reduce amphenicols and metabolites residues in meat, it cannot be assumed that these residues can always decrease to levels that are safe for consumer health, especially when the drug residue concentrations in raw meat are above the maximum residue limits (MRLs). Therefore, it is not reliable to remove residues of amphenicols and metabolites from food by cooking. The solution to the food safety problem of veterinary drug residues must start from the breeding source and accelerate the implementation of antibiotic reduction, antibiotic substitution and antibiotic-free farming.

Keywords: livestock and poultry meat; cooking methods; amphenicols; metabolites; residues

1. Introduction

Livestock and poultry meat, rich in protein, fat, minerals and vitamins, is an important source of nutrients for the human body [1]. In recent years, livestock and poultry farming have grown rapidly worldwide. However, the industry is facing problems such as bacterial, viral and parasitic infections. If not given prompt treatment, they may lead to the occurrence of zoonotic diseases during the breeding process or through the food chain and cause severe economic losses. Thus, antibiotics are widely used in animal production to prevent and treat bacterial diseases, as well as to promote growth and improve feed utilization. They provide convenience to modern intensive farming and can meet the demand for livestock and poultry production and market consumption [2].

Amphenicols, mainly including chloramphenicol (CAP), thiamphenicol (TAP) and florfenicol (FF), are a class of highly potent and economic antibiotics with broad-spectrum

antimicrobial activities that are widely used in livestock and poultry breeding and production [3,4]. The first generation of amphenicols, CAP, has many toxic side effects and can disrupt the body's hematopoietic function and trigger aplastic anemia (a condition in which the bone marrow fails to produce enough new cells to replenish the blood cells). It has been banned by China, the European Union, the United States and other countries and organizations for treating food-producing animals [5]. The para-nitro group on the aromatic ring of CAP is the leading group that causes aplastic anemia. As a derivative of CAP, TAP replaces the *p*-nitro (-NO$_2$) of CAP with *p*-methylsulfonyl (-SO$_2$CH$_3$). The two have a similar antibacterial spectrum and antibacterial effect, but TAP is much less toxic than CAP. FF is a third-generation amphenicol drug obtained by replacing the C-3 hydroxyl group (-OH) of TAP with the fluorine atom. The presence of the fluorine atom reduces the number of sites for the acetylation of CAP and TAP by bacteria, thus enhancing the acetylation effect of the drug against bacterial resistance. FF has better antimicrobial activity, resistance and safety than TAP and CAP and is an animal-specific broad-spectrum antibiotic. The metabolic response of FF in the tested animals is shown in Figure 1, with the main metabolite being florfenicol amine (FFA) [6]. TAP and FF have completely replaced the use of CAP in food animals due to their excellent antibacterial effect and higher safety. Unfortunately, these antibiotics are often used irrationally, resulting in excessive residues in the tissues of the animals to be consumed, posing a significant challenge to food safety [7,8]. To protect consumers from potential health-related problems, many countries and organizations have established maximum residue limits (MRLs) for amphenicols in animal-origin foods (Table 1).

Table 1. Maximum residue limits (MRLs) for amphenicols and metabolites in animal-derived foods.

Compound	Species	Target Tissue	MRL (µg/kg)		
			China	U.S.	EU
CAP	All species	All tissues			
TAP	All species	All tissues	50		50
FF (sum of FF and FFA)	Porcine	Skin and fat	500		500
		Muscle	300	200	300
		Liver	2000	2500	2000
		Kidney	500		500
	Bovine	Muscle	200	300	200
		Liver	3000	3700	3000
		Kidney	300		300
	Ovine caprine	Muscle	200		200
		Liver	3000		3000
		Kidney	300		300
	Poultry	Skin and fat	200		200
		Muscle	100		100
		Liver	2500		2500
		Kidney	750		750

CAP: chloramphenicol; TAP: thiamphenicol; FFA: florfenicol amine; U.S.: the United States; EU: the European Union.

To date, food safety risk assessment, market supervision and the import/export certification of veterinary drug residues in livestock and poultry meat have been carried out on unprocessed products. However, most animal-derived foods are ordinarily cooked or processed prior to consumption to improve their nutrient digestibility, palatability and shelf-life [8]. Studies have shown that cooking not only affects nutrients such as protein and fat in livestock and poultry meat but also leads to changes in drug residue concentrations, chemical structures and their solubility in the tissues [9–11]. Therefore, to accurately assess the dietary exposure levels of drug residues, it is crucial to study the impacts of cooking methods on the residues of amphenicols and metabolites in livestock and poultry meat.

Currently, there is minimal research on the changes in amphenicol antibiotic residues in livestock and poultry meat processing at home and abroad. The available studies also have problems, such as the single selection of meat species and cooking methods and unsystematic studies.
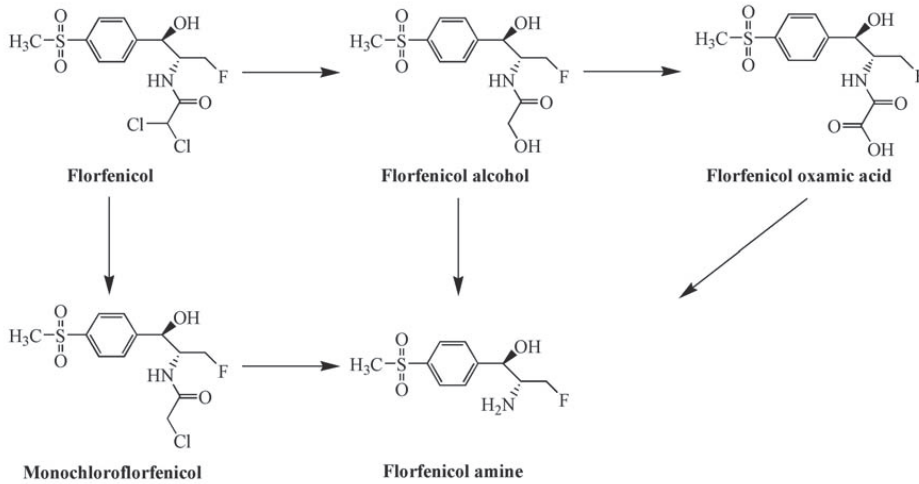
Figure 1. Florfenicol (FF) metabolic pathways.

In this study, we added certain concentrations of CAP, TAP, FF and FFA standard solutions to the muscle of negative livestock and poultry (pig, cattle, sheep and chicken) and made meat blocks that were 18 g in size, had good drug homogeneity and were processed to simulate domestic cooking such as boiling, deep-frying and microwaving. Our aim was to assess the effects of three processing methods under different temporal conditions on the residue levels of amphenicols and metabolites in livestock and poultry meat. The development of this study may provide some data basis and theoretical support for the accurate assessments of meat safety and the risk of dietary exposure to amphenicol antibiotics.

2. Materials and Methods

2.1. Samples

Fresh raw livestock and poultry meat (pork, beef, lamb and chicken) were provided by the Supervision, Inspection and Testing Center for Quality of Meat-Products, Ministry of Agriculture and Rural Affairs (Nanjing, China). All samples tested negative for residues of amphenicols and metabolites before the experiment.

2.2. Chemicals and Reagents

Standards of CAP, TAP, FF, FFA and CAP-D5 (purity $\geq$99.50%) were obtained from Dr. Ehrenstorfer GmbH (Augsburg, Germany). FFA-D3 standard (purity $\geq$99.50%) was purchased from Toronto Research Chemicals (North York, ON, Canada). HPLC-grade solvents, including methanol, acetonitrile (ACN), ethyl acetate and n-hexane, were supplied by Merck Company (Darmstadt, Germany). HPLC-grade acetone, formic acid and guaranteed reagent grade ammonium hydroxide were provided by Sinopharm Chemical Reagent Co., Ltd. (Shanghai, China). Ultrapure water was supplied by the Sartorius-Arium pro system (Sartorius AG, Goettingen, Germany).

Individual standard stock solutions (1 mg/mL) of CAP, TAP, FF, FFA, CAP-D5 and FFA-D3 were prepared in methanol and stored at -20 °C for six months. CAP-D5 and FFA-D3 were used as internal standards. The combined standard working solution at a concentration of 10 µg/mL for each analyte was prepared by mixing equal volumes of

the individual standard stock solution of CAP, TAP, FF and FFA with a concentration of 1 mg/mL and diluting with methanol. The mixed internal standard working solution at the concentration of 1.0 μg/mL was prepared by diluting the internal standard stock solutions (1 mg/mL) with methanol. The abovementioned standard working solutions were stored at −20 °C for up to three months.

2.3. Preparation of Positive Mock Samples

Fresh negative pork, beef, lamb and chicken samples with fat and connective tissue removed were weighed and then homogenized by the addition of standards of amphenicols and metabolites, respectively. Where CAP was spiked at 20 μg/kg in the four kinds of livestock and poultry meat, TAP, FF and FFA were spiked at twice the MRLs specified in the Chinese standard GB 31650-2019 "National food safety standard—Maximum residue limits for veterinary drugs in foods" (Table 2) [12]. Next, the spiked and homogenized meat mash was prepared into cuboid meat blocks with a length × width × height of about 25 mm × 25 mm × 33 mm and a mass of about 18 g for subsequent cooking.

Table 2. Spiked concentrations of amphenicols and metabolites in positive mock samples.

Matrix	Concentration (μg/kg)			
	CAP	TAP	FF	FFA
Pork	20	100	300	300
Beef	20	100	200	200
Lamb	20	100	200	200
Chicken	20	100	100	100

2.4. Cooking Operations

According to the cooking method of this experiment, the positive simulated livestock and poultry meat blocks of each matrix (pork, beef, lamb and chicken) were divided into three groups of 21 portions each. Before further treatment, three pieces of meat blocks were randomly selected from each group to verify the spiking homogeneity of the positive mock samples. The remaining pieces were used for boiling, deep-frying and microwave processing, respectively.

2.4.1. Boiling

The boiling process was performed at 100 °C in a water bath (TW20, Julabo Laborthechnik GmbH, Seelbach, Germany) for 5, 10, 15, 20 and 25 min, respectively, and then it was allowed to cool naturally to room temperature (22 ± 2 °C) before being weighed and subsequently detected and analyzed within one day. Three parallel experiments were conducted at each time point, with the unprocessed meat blocks serving as the control group.

2.4.2. Deep-Frying

The meat pieces were fried with edible oil at 180 °C, turned over every 30 s, taken out at 1, 2, 3, 4 and 5 min, respectively, and allowed to cool naturally to room temperature (22 ± 2 °C) before being weighed and subsequently detected and analyzed within one day. Three parallel experiments were conducted at each time point, with the unprocessed meat blocks serving as the control group.

2.4.3. Microwaving

The microwaving operation was carried out in a turntable domestic microwave oven (P70D20TL-D4, Guangdong Galanz Microwave Electrical Appliances Manufacturing Co., Ltd., Guangdong, China). The meat pieces were cooked under full power (700 W, 2450 MHz) for 0.25, 0.50, 0.75, 1.00 and 1.25 min, respectively, and allowed to cool naturally to room temperature (22 ± 2 °C) before being weighed and subsequently detected and analyzed

within one day. Three parallel experiments were conducted at each time point, with the unprocessed meat blocks serving as the control group.

The changes in the residual concentrations of amphenicols and metabolites in the livestock and poultry meat blocks after cooking were calculated as follows:

$$\Delta T\ (\%) = \left| \frac{C_P - C_0}{C_0} \right| \times 100 \tag{1}$$

where C_0 (μg/kg) is the initial concentration of drug residues in the uncooked livestock and poultry pieces; C_p (μg/kg) is the concentration of drug residues in the cooked livestock and poultry pieces.

2.5. Sample Preparation and Analysis

2.5.1. Sample Preparation

The extraction and purification of amphenicols and metabolites from livestock and poultry meat were performed using our self-built method [13]. Briefly, pork, beef, lamb and chicken samples were chopped and homogenized at 10,000 r/min using an HM6300 intelligent homogenizer (Lab Precision Beijing Technology Co., Ltd., Beijing, China). After homogenization, 5 g (accuracy, 0.01 g) of each livestock and poultry meat sample were placed in a 50 mL centrifuge tube. Then, 10 μL of 1.0 μg/mL mixed internal working standard solution and 15 mL of ethyl acetate with 2% ammonia were added and vortexed for 1 min. The mixture was centrifuged at 4 °C for 5 min at 10,621 g in a refrigerated centrifuge (D-16C, Sartorius Lab Instruments GmbH & Co. KG, Goettingen, Germany), and the supernatant was collected. The extraction operation was repeated with another 15 mL of ethyl acetate with 2% ammonia, and the supernatants were combined. The supernatants were evaporated to dryness at 40 °C with a nitrogen evaporator (N-EVAPTM-112, Organomation Associates Inc., Berlin, MA, USA). Subsequently, the residue was reconstituted with 5 mL of acetone: n-hexane (1:9, *v/v*), purified by a CNW Si solid-phase extraction (SPE) column and defatted with ACN-saturated hexane. Finally, the solution was filtered through a 0.22 μm filter membrane and injected into the ultra-high-performance liquid chromatography-tandem mass spectrometry (UHPLC-MS/MS) system analysis.

2.5.2. UHPLC-MS/MS Conditions

The separation and quantification of the four amphenicols and metabolites were performed on a Thermo Scientific Vanquish ultra-high-performance liquid chromatography instrument coupled with a Thermo Scientific TSQ Quantis mass spectrometer (Thermo Fisher Scientific, Waltham, MA, USA). A Waters Acquity UPLC HSS C18 (2.1 mm × 50 mm, 1.8 μm) was used as the analytical column, with a Waters Acquity UPLC HSS C18 VanGuard precolumn (2.1 mm × 5 mm, 1.8 μm) attached to the front end. The column temperature was 40 °C, and the injection volume was 2.0 μL. Gradient elution, with water and ACN as mobile phases, was carried out at a constant flow rate of 0.3 mL/min. The starting mobile phase composition was 4:96 (ACN/water) at 0 min. It was switched to 96:4 after 4 min and held for 2 min, returning to the initial conditions at 10 min.

The MS/MS was equipped with an ESI source and scanned in positive ion (PI) and negative ion (NI) mode switching. CAP, TAP, FF and CAP-D5 were analyzed in NI mode, while FFA and FFA-D3 were analyzed in PI mode. The detection mode was selective reaction monitoring. The ESI source was operated with the following capillary voltages: 3.5 kV in PI mode, 2.5 kV in NI mode; sheath gas: 50 Arb; auxiliary gas: 10 Arb; ion transfer tube temperature: 325 °C; and evaporator temperature: 350 °C. The specific mass spectrometry parameters of amphenicols and metabolites are shown in Table 3. Under these conditions, the limits of detection and limits of quantification for all four analytes were below 1.5 μg/kg and 5.0 μg/kg, respectively, with good precision (RSD < 9.0%) and accuracy (recovery > 72.0%). This means that the extraction and purification procedures used in this experiment are effective and that the UHPLC-MS/MS conditions are applicable to detecting residues of amphenicols and metabolites in livestock and poultry meat samples.

The linear working ranges of the current quantitative method were 5.0–50.0 µg/kg for CAP, 1–100 µg/kg for TAP and 5–300 µg/kg for FF and FFA, at which concentration ranges the changes in the peak area were proportional to the changes in the drug concentrations ($R^2 > 0.9990$ for CAP, TAP, FF and FFA).

Table 3. Mass spectrometry parameters of amphenicols and metabolites.

Compound	Reaction Mode	Precursor Ion (*m/z*)	Product Ion (*m/z*)	Collision Voltage (V)	Radio-Frequency Voltage (V)
CAP	−	321	257	16.94	146
			152 *	10.23	146
CAP-D5	−	326	157	16.94	146
TAP	−	354	290 *	20.08	164
			185	12.39	164
FF	−	356	185 *	31.87	141
			119	19.17	141
FFA	+	248	230 *	24.52	97
			130	12.88	97
FFA-D3	+	251	233	12.88	97

*: quantitative ion; −: negative ion reaction mode; +: positive ion reaction mode.

2.6. Statistical Analysis

Data acquisition was performed using TraceFinder software (version number: 4.1.31.9, Thermo Fisher Scientific, Waltham, MA, USA). Three parallels were carried out for each experiment, and the data were expressed as the mean ± standard deviation. Statistical analysis was performed using SAS software (version number: 6.2.9200, SAS Institute Inc., Cary, NC, USA), and the significant influence of different cooking methods or times on the concentrations of amphenicols and metabolites in livestock and poultry meat blocks were analyzed by one-way analysis of variance (ANOVA) and Duncan's multiple comparisons. A $p < 0.05$ was considered to be statistically significant. The figures were plotted using OriginPro 2022 software (OriginLab, Northampton, MA, USA).

3. Results and Discussion

3.1. Homogeneity Analysis of Positive Simulated Samples

Studies related to the effect of thermal processing on drug residues have shown significant differences in the percentage of thermal degradation of amphenicols in model solutions (water), spiked tissues and incurred samples, and their degradation products vary. To provide reliable information on the stability of residues of amphenicols for food safety risk assessments, Tian [14] suggested that incurred samples should be systematically implemented rather than spiked tissues to study the impact of cooking on drug residues. However, the subject of this experiment was livestock and poultry meat, and positive samples contaminated with amphenicols and metabolites from the market were difficult to collect. Furthermore, livestock and poultry animals bioaccumulate slowly, and it is also challenging to obtain contamination through controlled laboratory conditions. Therefore, in this study, positive mock samples could only be obtained by adding amphenicols and metabolites standards to negative livestock and poultry meat samples.

In order to ensure the consistency of the target compound concentrations in the meat blocks used for subsequent cooking, the homogeneity analysis of positive mock samples was carried out in this experiment, and the results are shown in Table 4. The one-way ANOVA showed $p > 0.05$ for the measured concentrations of amphenicols and metabolites in pork, beef, lamb and chicken blocks, indicating that the differences in drug concentrations between meat nuggets were insignificant. That is, the meat nuggets prepared by this experimental method had a good homogeneity and could meet the requirements for subsequent cooking.

Table 4. Homogeneity analysis of amphenicols and metabolites added to livestock and poultry meat blocks.

Matrix	Compound	Group	Concentration (μg/kg)				*p*-Value
			No. 1	No. 2	No. 3	Average	
Pork	CAP	P-1 P-2 P-3	20.12 20.72 18.05	18.18 19.73 19.99	19.60 18.51 21.35	19.58	0.89
	TAP	P-1 P-2 P-3	107.28 91.91 110.56	113.02 91.25 95.66	94.49 112.76 103.77	102.30	0.73
	FF	P-1 P-2 P-3	308.13 288.18 296.31	302.82 301.16 277.32	292.61 292.05 286.97	293.95	0.18
	FFA	P-1 P-2 P-3	314.81 287.32 294.91	312.97 295.51 296.31	310.16 306.97 309.97	303.21	0.09
Beef	CAP	B-1 B-2 B-3	19.89 18.46 18.33	20.12 19.43 19.90	19.97 21.33 20.30	19.75	0.85
	TAP	B-1 B-2 B-3	99.38 91.91 95.61	93.05 101.25 96.60	99.50 102.21 97.46	97.44	0.84
	FF	B-1 B-2 B-3	190.30 198.22 196.01	200.80 205.55 197.65	199.90 205.34 201.98	199.53	0.31
	FFA	B-1 B-2 B-3	194.87 197.92 197.13	210.69 192.11 198.90	201.79 204.15 206.31	200.43	0.71
Lamb	CAP	L-1 L-2 L-3	18.31 18.50 20.01	18.47 19.88 19.62	20.34 20.95 20.86	19.66	0.45
	TAP	L-1 L-2 L-3	103.25 97.44 96.21	101.34 98.22 97.60	96.85 101.75 102.31	99.44	0.76
	FF	L-1 L-2 L-3	196.56 189.97 202.67	200.60 204.78 198.46	199.40 203.11 200.90	199.61	0.90
	FFA	L-1 L-2 L-3	197.48 201.19 203.46	198.90 196.40 200.79	201.50 204.10 200.90	200.52	0.57
Chicken	CAP	C-1 C-2 C-3	22.30 20.60 19.90	20.10 19.87 21.10	20.60 20.70 20.10	20.59	0.58
	TAP	C-1 C-2 C-3	100.50 104.20 98.66	99.90 103.60 95.98	101.70 97.86 101.30	100.41	0.36
	FF	C-1 C-2 C-3	99.50 101.60 97.40	102.88 103.00 96.80	99.65 100.90 100.10	100.20	0.07
	FFA	C-1 C-2 C-3	104.60 103.92 101.30	97.00 98.00 99.70	100.90 104.30 102.10	101.31	0.87

Positive simulated meat blocks of each matrix (pork, beef, lamb and chicken) were divided into three groups corresponding to the subsequent boiling, deep-frying and microwaving treatment groups. The three groups for pork were numbered P-1, P-2 and P-3, respectively. The three groups for beef were numbered B-1, B-2 and B-3, respectively. The three groups for lamb were numbered L-1, L-2 and L-3. The three groups for chicken were numbered C-1, C-2 and C-3. No. 1, No. 2 and No. 3 were the three meat blocks randomly selected from each group.

3.2. Processing Quality Loss of Livestock and Poultry Meat

The effects of boiling, deep-frying and microwave processing on the quality loss of livestock and poultry meat are shown in Figure 2. The mass loss of livestock and poultry meat during boiling showed an overall trend of rising and then leveling off with time. After 20 min of boiling, the quality of pork, beef, lamb and chicken remained stable ($p > 0.05$). During deep-frying and microwave processing, livestock and poultry meat quality loss continued to increase over time ($p < 0.05$). The quality losses of pork, beef, lamb and chicken were 39.89%, 44.95%, 42.61% and 32.60% and 39.98%, 47.34%, 44.76% and 36.91% at 25 min of boiling and 5 min of deep-frying, respectively, and the degree of loss was similar for both. At 1.25 min of microwaving, the quality loss of the four livestock and poultry meat species reached 29.82%, 50.19%, 50.26% and 45.41%, respectively. Compared with boiling and deep-frying, the quality loss rate was faster in microwaves. The reason is that microwaves can heat the whole material simultaneously, which results in a violent heating process, rapid temperature rise and faster water evaporation, thus causing the most severe quality loss in a short time. The determination of the quality loss index should facilitate the understanding of the effect of subsequent cooking on the concentration of drug residues in livestock and poultry meat.
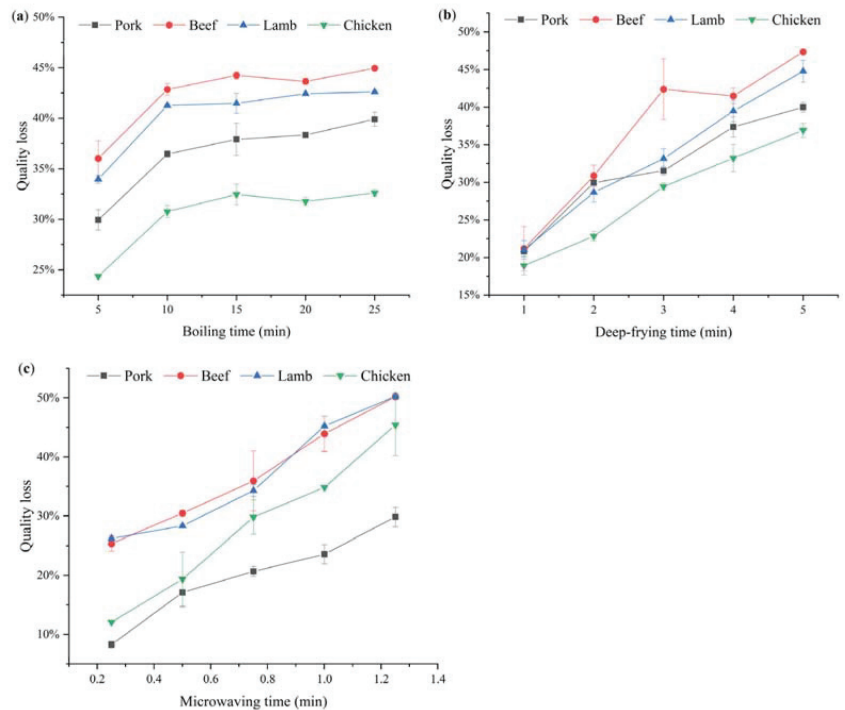
Figure 2. Processing quality loss of livestock and poultry meat. (**a**) Boiling; (**b**) Deep-frying; (**c**) Microwaving.

3.3. Effect of Cooking Time on Residues of Amphenicols and Metabolites in Livestock and Poultry Meat

The residue levels of amphenicols and metabolites in the meat blocks of livestock and poultry cooked by boiling for varying time periods are presented in Table 5. It can be seen from the table that the residue concentrations of CAP, TAP, FF and FFA in pork, beef, lamb and chicken gradually decreased with the prolonged boiling time. Within 25 min, the depletion rates of the four drugs were 38.55–75.75% in pork, 47.60–100% in beef, 20.18–100% in lamb and 39.31–50.19% in chicken. This is consistent with the results

reported by Shakila et al. [15] and Filazi et al. [10], which showed that boiling reduced CAP residues in shrimps and FF and FFA residues in eggs, and the loss was strongly correlated with heating time. In addition, Table 5 also shows that the elimination rates of the four drugs in different livestock and poultry meat matrices were different during the boiling process. CAP, TAP and FF were removed faster in beef and lamb and relatively slower in pork and chicken, while FFA was removed faster in beef, pork and chicken and was removed the slowest in lamb.

Table 5. Effect of boiling time on residues of amphenicols and metabolites in livestock and poultry meat.

Compound	Time (min)	Concentration (µg/kg) [Reduction Rate (%)]			
		Pork	**Beef**	**Lamb**	**Chicken**
CAP	0	19.30 ± 1.00 [a]	19.99 ± 0.12 [a]	19.04 ± 1.13 [a]	21.00 ± 1.15 [a]
	5	20.37 ± 0.86 [a] (−5.54)	14.64 ± 1.62 [b] (26.76)	19.33 ± 0.63 [a] (−1.52)	19.80 ± 1.80 [a] (5.71)
	10	13.04 ± 0.73 [b] (32.44)	3.43 ± 0.34 [c] (82.84)	6.29 ± 0.76 [b] (66.96)	16.82 ± 0.70 [b] (19.90)
	15	10.24 ± 1.05 [c] (46.94)	0.92 ± 0.65 [d] (95.40)	2.01 ± 0.34 [c] (89.44)	15.57 ± 0.11 [b] (25.86)
	20	7.36 ± 0.46 [d] (61.87)	0.00 ± 0.00 [e] (100.00)	0.32 ± 0.12 [d] (98.32)	11.30 ± 0.32 [c] (46.19)
	25	4.68 ± 0.54 [e] (75.75) *	0.00 ± 0.00 [e] (100.00)	0.00 ± 0.00 [d] (100.00)	10.46 ± 1.13 [c] (50.19) *
TAP	0	104.93 ± 9.49 [a]	97.31 ± 3.69 [a]	100.48 ± 3.29 [a]	100.70 ± 0.92 [a]
	5	88.85 ± 2.92 [b] (15.32)	76.44 ± 5.53 [b] (21.45)	67.28 ± 0.34 [b] (33.04)	83.50 ± 8.66 [b] (17.08)
	10	77.53 ± 2.22 [c] (26.11)	32.43 ± 0.33 [c] (66.67)	39.75 ± 3.85 [c] (60.44)	73.84 ± 1.96 [c] (26.67)
	15	69.96 ± 1.35 [d] (33.33)	16.29 ± 1.31 [d] (83.26)	23.17 ± 0.24 [d] (76.94)	70.80 ± 4.16 [c] (29.69)
	20	55.00 ± 1.37 [e] (47.58)	7.13 ± 2.58 [e] (92.67)	11.77 ± 0.70 [e] (88.29)	56.22 ± 0.91 [d] (44.17)
	25	51.59 ± 2.60 [e] (50.83) *	3.70 ± 1.12 [e] (96.20)	6.11 ± 0.64 [f] (93.92)	58.70 ± 3.07 [d] (41.71) *
FF	0	301.19 ± 7.89 [a]	197.00 ± 5.82 [a]	198.85 ± 2.07 [a]	100.68 ± 1.91 [a]
	5	286.97 ± 7.54 [a] (4.72)	114.19 ± 4.97 [b] (42.04)	185.27 ± 8.69 [b] (6.83)	82.63 ± 4.71 [b] (17.93)
	10	220.32 ± 0.51 [b] (26.85)	37.53 ± 2.26 [c] (80.95)	83.78 ± 5.34 [c] (57.87)	71.80 ± 0.65 [c] (28.68)
	15	188.13 ± 9.59 [c] (37.54)	12.70 ± 3.59 [d] (93.55)	38.13 ± 3.10 [d] (80.82)	65.95 ± 2.67 [d] (34.50)
	20	142.46 ± 1.93 [d] (52.70)	3.70 ± 1.91 [e] (98.12)	12.22 ± 0.09 [e] (93.85)	51.73 ± 1.97 [e] (48.62)
	25	118.41 ± 4.60 [e] (60.69) *	2.30 ± 1.62 [e] (98.83)	4.56 ± 1.45 [e] (97.71)	51.52 ± 2.23 [e] (48.83) *
FFA	0	312.65 ± 2.34 [a]	202.45 ± 7.93 [a]	199.29 ± 2.04 [a]	100.83 ± 3.80 [a]
	5	265.97 ± 14.91 [b] (14.93)	130.20 ± 10.82 [b] (35.69)	207.13 ± 8.47 [a] (−3.93)	100.62 ± 14.12 [a] (0.21)
	10	244.29 ± 2.32 [c] (21.86)	117.30 ± 18.61 [bc] (42.06)	197.65 ± 4.55 [a] (0.82)	98.52 ± 7.92 [a] (2.29)
	15	212.98 ± 2.88 [d] (31.88)	111.86 ± 11.21 [bc] (44.75)	181.69 ± 7.05 [ab] (8.83)	84.83 ± 3.05 [ab] (15.87)
	20	215.14 ± 10.48 [d] (31.19)	106.62 ± 5.62 [c] (47.34)	150.78 ± 7.46 [b] (24.34)	80.22 ± 10.65 [ab] (20.44)
	25	192.12 ± 13.04 [e] (38.55) *	106.09 ± 19.02 [c] (47.60)	159.07 ± 6.05 [b] (20.18)	61.19 ± 2.12 [b] (39.31) *

Different lowercase letters in the same column indicate significant differences ($p < 0.05$) in the concentration of the same compound in the same species of livestock and poultry meat between different boiling times. * indicates that the drug residue concentrations do not meet the requirements of non-detectable (CAP) or lower than MRLs (TAP, FF (sum of FF and FFA)), as stipulated by the Chinese standard GB 31650-2019 and (EU) No 37/2010 after boiling.

The effects of different deep-frying times on the residue levels of the four amphenicols and metabolites in livestock and poultry meat are shown in Table 6. The residue concentrations of CAP and TAP in pork, beef, lamb and chicken showed a decreasing or first increasing and then decreasing trend with frying time, while FF and FFA showed a decreasing trend in all four livestock and poultry meats. These findings indicate that the effect of heat treatment on amphenicols and metabolites is matrix-dependent. In addition, the reason for the elevated CAP and TAP residue concentrations in some livestock and poultry meat at the beginning of the deep-frying process may be related to the rapid water loss and evaporation from the meat at the initial stage with less drug loss [16]. Residue concentrations of CAP, TAP, FF and FFA in pork decreased by 6.70–41.29% within 5 min of frying, while those in beef, lamb and chicken decreased by 43.07–61.14%, 5.45–57.16% and 15.20–40.27%, respectively. One notable result worth emphasizing was that all four drugs were removed at the fastest rate in beef during deep-frying, as in the case of boiling. The reason may be that beef has a high water content, and heating results in the most

severe loss of quality (Figure 2) due to the disruption of its water-retaining protein spatial structure, the tightening of myogenic fibers and reduced water-binding capacity [17,18]. It is known that the decrease in the water binding capacity of meat increases drug degradation [19]. Therefore, it can be speculated that the highly reduced contents of amphenicols and metabolites in beef may be at least partially attributed to the significant decrease in the water-binding capacity of the meat caused by heating. In addition, the thermal treatment itself can affect the drug's chemical structure and its solubility in tissues [9].

Table 6. Effect of deep-frying time on residues of amphenicols and metabolites in livestock and poultry meat.

Compound	Time (min)	Concentration (µg/kg) [Reduction Rate (%)]			
		Pork	Beef	Lamb	Chicken
CAP	0	19.65 ± 1.11 [bc]	19.74 ± 1.46 [a]	19.78 ± 1.23 [b]	20.39 ± 0.45 [a]
	1	25.18 ± 0.25 [a] (−28.14)	19.83 ± 1.18 [a] (−0.46)	22.38 ± 0.68 [a] (−13.14)	20.79 ± 0.41 [a] (−1.96)
	2	20.71 ± 0.51 [b] (−5.39)	13.81 ± 0.19 [b] (30.04)	17.72 ± 0.41 [c] (10.41)	19.09 ± 0.79 [ab] (6.38)
	3	19.74 ± 1.18 [bc] (−0.46)	14.16 ± 0.22 [b] (28.27)	14.51 ± 0.09 [d] (26.64)	18.94 ± 1.03 [ab] (7.11)
	4	18.81 ± 0.87 [c] (4.27)	9.57 ± 0.77 [c] (51.52)	12.52 ± 0.94 [e] (36.70)	18.36 ± 1.17 [b] (9.96)
	5	15.53 ± 0.71 [d] (20.97) *	8.40 ± 0.23 [c] (57.45) *	10.50 ± 0.61 [f] (46.92) *	17.29 ± 0.07 [b] (15.20) *
TAP	0	98.64 ± 12.23 [b]	98.46 ± 5.69 [a]	99.14 ± 2.30 [c]	101.89 ± 3.50 [a]
	1	112.67 ± 2.93 [a] (−14.22)	72.35 ± 4.16 [b] (26.52)	121.14 ± 3.60 [ab] (−22.19)	93.12 ± 9.72 [ab] (8.61)
	2	101.25 ± 0.32 [b] (−2.65)	65.32 ± 0.29 [bc] (33.66)	124.10 ± 0.74 [a] (−25.18)	87.18 ± 4.16 [bc] (14.44)
	3	107.32 ± 0.88 [b] (−8.80)	63.23 ± 0.46 [c] (35.78)	112.92 ± 3.02 [b] (−13.90)	79.28 ± 3.04 [cd] (22.19)
	4	100.55 ± 3.74 [b] (−1.94)	52.00 ± 6.87 [d] (47.19)	96.58 ± 5.27 [c] (2.58)	72.45 ± 0.46 [de] (28.89)
	5	92.03 ± 2.36 [c] (6.70) *	41.30 ± 2.38 [e] (58.05)	93.74 ± 1.77 [c] (5.45) *	61.35 ± 1.95 [e] (39.79) *
FF	0	293.80 ± 6.66 [a]	203.04 ± 4.17 [a]	199.29 ± 8.11 [a]	101.83 ± 1.07 [a]
	1	298.03 ± 9.48 [a] (−1.44)	165.75 ± 10.10 [b] (18.37)	159.73 ± 9.09 [b] (19.85)	83.15 ± 0.13 [b] (18.34)
	2	266.83 ± 9.51 [b] (9.18)	118.85 ± 0.26 [c] (41.46)	133.21 ± 3.41 [c] (33.16)	76.62 ± 0.21 [b] (24.76)
	3	251.20 ± 7.70 [c] (14.50)	115.11 ± 1.74 [c] (43.31)	113.79 ± 3.44 [d] (42.90)	75.91 ± 4.61 [b] (25.45)
	4	245.61 ± 3.32 [c] (16.40)	87.78 ± 6.67 [d] (56.77)	99.77 ± 1.73 [e] (49.94)	82.14 ± 9.93 [b] (19.34)
	5	208.57 ± 4.55 [d] (29.01) *	78.91 ± 5.40 [d] (61.14)	85.38 ± 3.14 [e] (57.16) *	80.40 ± 8.67 [b] (21.04) *
FFA	0	296.60 ± 9.87 [a]	198.06 ± 6.02 [a]	200.56 ± 3.89 [a]	102.07 ± 3.53 [a]
	1	285.17 ± 3.26 [b] (3.85)	198.81 ± 2.97 [a] (−0.38)	206.53 ± 5.50 [a] (−2.98)	82.21 ± 9.59 [ab] (19.46)
	2	239.38 ± 12.25 [c] (19.29)	160.87 ± 3.50 [ab] (18.78)	176.47 ± 6.06 [ab] (12.01)	60.34 ± 9.00 [b] (40.88)
	3	230.31 ± 12.66 [cd] (22.35)	146.54 ± 0.90 [ab] (26.01)	175.74 ± 16.52 [ab] (12.38)	79.34 ± 11.32 [ab] (22.27)
	4	220.12 ± 1.35 [d] (25.79)	121.13 ± 1.65 [b] (38.84)	168.28 ± 12.08 [bc] (16.09)	64.79 ± 8.90 [b] (36.52)
	5	174.13 ± 14.67 [e] (41.29) *	112.75 ± 2.89 [b] (43.07)	141.71 ± 6.47 [c] (29.34) *	60.97 ± 10.53 [b] (40.27) *

Different lowercase letters in the same column indicate significant differences ($p < 0.05$) in the concentration of the same compound in the same species of livestock and poultry meat between different deep-frying times. * indicates that the drug residue concentrations do not meet the requirements of non-detectable (CAP) or lower than MRLs (TAP, FF (sum of FF and FFA)), as stipulated by the Chinese standard GB 31650-2019 and (EU) No 37/2010 after deep-frying.

It is evident from the above that boiling and deep-frying can effectively reduce the concentrations of four amphenicols and metabolites in livestock and poultry meat and that drug residue levels continue to decrease with the prolongation of cooking time. The loss of amphenicols and metabolites during cooking questions their stability when heated. Shakila et al. [15] have reported that CAP is an unstable drug destroyed during cooking and boiling. Tian [20] detected seven degradation products and metabolites of CAP in cooked mussels containing CAP, and structures were proposed for six. Similarly, Franje et al. [11] demonstrated that FF residues in chicken meat degraded to produce TAP in water at 100 °C by identifying the degradation structures of amphenicols after processing. The loss of amphenicols and metabolites observed in the present study after boiling and deep-frying suggests that they might have been destroyed or degraded to other substances. Moreover, it is also possible that the drug migrated from the livestock and poultry meat tissue into the surrounding liquid or meat juices during cooking, resulting in decreased residual concentration.

There was a difference in the effect of microwaving on the concentration of residues of amphenicols and metabolites in livestock and poultry meat over time compared with boiling and deep-frying (Table 7). From 0 to 1.25 min, CAP, TAP, FF and FFA showed

an increasing or first decreasing and then increasing trend in pork, beef, lamb and chicken. At 1.25 min, the concentrations of all four drugs increased in the livestock and poultry meat matrices compared with the control groups. The increase rate was 8.43–43.84% for pork, 23.16–33.27% for beef, 6.50–80.29% for lamb and 26.66–135.92% for chicken. This result is inconsistent with the previous proposal by Nashwa et al. [21] that microwave heating was the most effective method for reducing drug residues in meat. In this experiment, microwaves did not cause a reduction in the levels of residues of amphenicols and metabolites. The reason for this may be that microwave processing caused a large amount of rapid water evaporation from livestock and poultry meat and a serious loss of quality (Figure 2c), which significantly reduced the water content of the meat while the drug abatement was at a low level. Overall, the livestock and poultry meat matrices are equivalent to being concentrated, and, therefore, the concentration of drug residues in the samples was elevated [22].

Table 7. Effect of microwave time on residues of amphenicols and metabolites in livestock and poultry meat.

Compound	Time (min)	Concentration (µg/kg) [Increase Rate (%)]			
		Pork	Beef	Lamb	Chicken
CAP	0	19.80 ± 1.66 [d]	19.51 ± 1.04 [c]	20.16 ± 0.63 [a]	20.37 ± 0.64 [b]
	0.25	20.73 ± 0.82 [d] (4.70)	21.39 ± 1.70 [bc] (9.64)	15.45 ± 1.25 [b] (−23.36)	18.25 ± 0.07 [c] (−10.41)
	0.50	23.07 ± 0.37 [c] (16.52)	22.53 ± 1.72 [bc] (15.48)	13.80 ± 0.28 [b] (−31.55)	18.05 ± 1.46 [c] (−11.39)
	0.75	26.29 ± 0.59 [b] (32.78)	27.73 ± 1.85 [a] (42.13)	15.29 ± 0.17 [b] (−24.16)	20.55 ± 1.18 [b] (0.88)
	1.00	26.57 ± 0.66 [b] (34.19)	24.86 ± 0.89 [ab] (27.42)	21.53 ± 0.93 [a] (6.80)	22.16 ± 0.71 [b] (8.79)
	1.25	28.48 ± 0.26 [a] (43.84) *	24.26 ± 0.87 [abc] (24.35) *	21.47 ± 2.77 [a] (6.50) *	25.80 ± 0.65 [a] (26.66) *
TAP	0	103.33 ± 7.46 [b]	96.56 ± 0.93 [b]	98.71 ± 3.20 [d]	98.65 ± 2.66 [d]
	0.25	99.33 ± 5.92 [b] (−3.87)	93.89 ± 6.13 [b] (−2.77)	128.82 ± 1.41 [cd] (30.50)	134.46 ± 4.19 [c] (36.30)
	0.50	102.42 ± 3.31 [b] (−0.88)	100.22 ± 12.31 [b] (3.79)	120.24 ± 2.39 [cd] (21.81)	145.52 ± 7.46 [c] (47.51)
	0.75	104.36 ± 5.91 [ab] (1.00)	123.88 ± 8.89 [a] (28.29)	141.51 ± 1.64 [bc] (43.36)	179.68 ± 9.72 [b] (82.14)
	1.00	105.41 ± 1.19 [ab] (2.01)	132.29 ± 14.44 [a] (37.00)	170.69 ± 7.32 [ab] (72.92)	179.58 ± 11.25 [b] (82.04)
	1.25	112.04 ± 2.90 [a] (8.43) *	128.69 ± 12.07 [a] (33.27) *	177.96 ± 2.97 [a] (80.29) *	232.74 ± 1.90 [a] (135.92) *
FF	0	286.87 ± 9.50 [b]	198.55 ± 3.08 [b]	200.68 ± 2.11 [bc]	98.10 ± 1.76 [d]
	0.25	303.27 ± 18.35 [b] (5.72)	192.76 ± 7.72 [b] (−2.92)	166.86 ± 14.41 [cd] (−16.85)	128.49 ± 12.96 [c] (30.98)
	0.50	305.81 ± 4.83 [b] (6.60)	190.03 ± 15.32 [b] (−4.29)	159.32 ± 2.47 [d] (−20.61)	145.82 ± 1.76 [c] (48.64)
	0.75	344.22 ± 5.64 [a] (19.99)	239.59 ± 18.25 [a] (20.67)	182.48 ± 12.85 [cd] (−9.07)	175.61 ± 6.35 [b] (79.01)
	1.00	357.21 ± 16.69 [a] (24.52)	264.34 ± 27.65 [a] (33.14)	227.29 ± 9.85 [ab] (13.26)	172.52 ± 11.96 [b] (75.86)
	1.25	334.82 ± 6.43 [a] (16.71) *	263.52 ± 17.13 [a] (32.72) *	237.40 ± 1.34 [a] (18.30) *	210.00 ± 12.32 [a] (114.07) *
FFA	0	300.40 ± 8.32 [bc]	200.78 ± 4.87 [c]	201.72 ± 1.51 [b]	101.03 ± 1.22 [d]
	0.25	290.38 ± 6.00 [b] (−3.34)	187.40 ± 13.56 [cd] (−6.66)	213.94 ± 2.68 [b] (6.06)	146.64 ± 17.16 [c] (45.15)
	0.50	309.49 ± 3.85 [b] (3.03)	175.94 ± 2.90 [d] (−12.37)	216.04 ± 0.03 [b] (7.10)	166.85 ± 27.39 [bc] (65.15)
	0.75	304.38 ± 4.52 [bc] (1.32)	203.23 ± 15.55 [c] (1.22)	270.97 ± 16.91 [a] (34.33)	213.37 ± 14.89 [a] (111.19)
	1.00	344.83 ± 12.91 [a] (14.79)	228.32 ± 0.54 [b] (13.72)	269.04 ± 0.85 [a] (33.37)	192.02 ± 15.40 [ab] (90.06)
	1.25	338.78 ± 6.50 [a] (12.78) *	247.29 ± 2.68 [a] (23.16) *	276.57 ± 6.09 [a] (37.11) *	179.19 ± 5.78 [abc] (77.36) *

Different lowercase letters in the same column indicate significant differences ($p < 0.05$) in the concentration of the same compound in the same species of livestock and poultry meat between different microwave times. * indicates that the drug residue concentrations do not meet the requirements of non-detectable (CAP) or lower than MRLs (TAP, FF (sum of FF and FFA)), as stipulated by the Chinese standard GB 31650-2019 and (EU) No 37/2010 after microwaving.

3.4. Effect of Cooking Methods on Residues of Amphenicols and Metabolites in Livestock and Poultry Meat

In order to compare the effects of different cooking methods on the concentration changes of amphenicols and metabolites in livestock and poultry meat, each cooking endpoint was selected for analysis in this study (Figure 3). Among the three cooking methods, microwaving increased the concentration of the four drug residues in the meat matrices of livestock and poultry, while boiling and deep-frying had the opposite effect, and the removal effects of the two were also different. Figure 3 illustrates that the removal rates of CAP and FF in four types of livestock and poultry meat and of TAP in pork, beef and lamb by boiling were significantly higher than those in deep-frying ($p < 0.05$), but there was no significant difference between the two for TAP in chicken ($p > 0.05$). In terms of FFA, there was no significant difference between boiling and deep-frying in pork, beef

and chicken ($p > 0.05$), while the removal rate of boiling was lower than that of deep-frying in lamb ($p < 0.05$). These results have shown that different cooking methods have different effects on the removal of amphenicols and metabolites from livestock and poultry meat. Boiling showed the highest reduction effect on the drug residues in livestock and poultry meat matrices, followed by deep-frying, while microwaving caused an increase in drug residue concentrations. Based on the previous reports, we speculate that the reduction in drug residue concentrations in the matrices by boiling and deep-frying may be related to moisture loss, drug migration and degradation [11,23,24]. In addition, the overall removal rate of amphenicols and metabolites in livestock and poultry meat observed in this experiment was higher with boiling than with frying. The reason for this may be that, on the one hand, the heating rate of deep-frying is faster than that of boiling, less water is lost in the form of transfer in deep-frying than in boiling for the same degree of mass loss (Figure 2) and less of the drug is lost with it. On the other hand, deep-frying may create a hard crust on the surface of the meat, which, in turn, slows down the rate of drug loss with moisture [25].
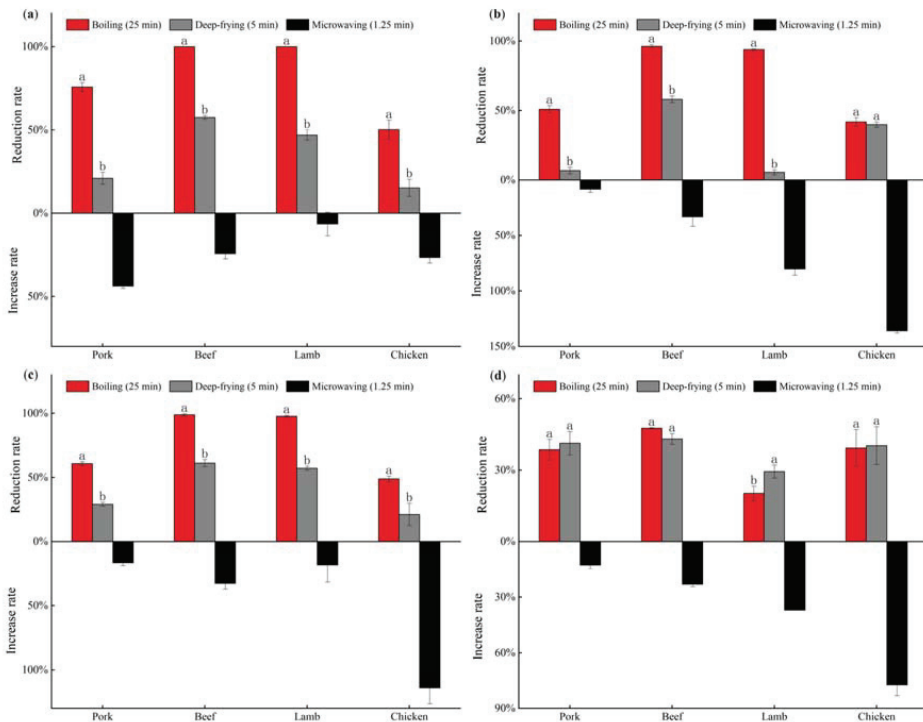
Figure 3. The rate of change in residue concentrations of amphenicols and metabolites in livestock and poultry meat under different cooking methods. (**a**) CAP; (**b**) TAP; (**c**) FF; (**d**) FFA. Different lowercase letters represent significant differences ($p < 0.05$) in the reduction rate of the same drug in the same species of livestock and poultry meat under boiling (25 min) and deep-frying (5 min) treatments. The same lowercase letter indicates no significant difference ($p > 0.05$).

4. Conclusions

According to the Procedural Manual of the Codex Alimentarius Commission (2018), dietary exposure assessments of contaminants in livestock and poultry meat should consider the presence of these contaminants in raw meat as a potential source and account for the effect of food cooking and processing on drug residues. The results of this experiment

indicated that the changes in drug residues in livestock and poultry meat depended on the cooking time, the methods and the type of food matrices. Under both boiling and deep-frying cooking methods, extended heating time effectively reduced the concentration of the four drug residues, thereby reducing the risk of dietary exposure to consumers. However, microwaving led to increased drug residue concentrations. Although boiling and deep-frying cooking are both effective ways to reduce residues of amphenicols and metabolites in meat, there is no guarantee that these residues will always decrease to a safe level in terms of consumer health, especially when drug residue concentrations in raw livestock and poultry meat are higher than the MRLs. In summary, from the safety and toxicological point of view, it is unsafe to rely on cooking to remove residues of amphenicols and metabolites from food. The solution to the food safety problem of veterinary drug residues must start at the source—from the production, operation and use of veterinary drugs—to strengthen supervision in order to establish a regulated veterinary drug market order.

References

1. Pereira, P.; Vicente, A. Meat nutritional composition and nutritive role in the human diet. *Meat Sci.* **2013**, *93*, 586–592. [CrossRef] [PubMed]
2. Mund, M.D.; Khan, U.H.; Tahir, U.; Bahar, E.M.; Fayyaz, A. Antimicrobial drug residues in poultry products and implications on public health: A review. *Int. J. Food Prop.* **2017**, *20*, 1433–1446. [CrossRef]
3. Wang, J.; Cong, M.; Tao, Y.; Huang, L.; Yuan, Z.; Hao, H. Research progress on the elimination rule of antimicrobial drug residues in eggs. *Chin. J. Antibiot.* **2020**, *45*, 1208–1220. [CrossRef]
4. EFSA Panel on Contaminants in the Food Chain. Scientific Opinion on Chloramphenicol in food and feed. *EFSA J.* **2014**, *12*, 3907. [CrossRef]
5. Mbodi, F.E.; Nguku, P.; Okolocha, E.; Kabir, J. Determination of chloramphenicol residues in commercial chicken eggs in the Federal Capital Territory, Abuja, Nigeria. *Food Addit. Contam. Part A Chem. Anal. Control. Expo. Risk Assess.* **2014**, *31*, 1834–1839. [CrossRef]
6. Yang, F.; Yang, F.; Wang, G.Y.; Kong, T.; Wang, H.; Zhang, C.S. Effects of water temperature on tissue depletion of florfenicol and its metabolite florfenicol amine in crucian carp (Carassius auratus gibelio) following multiple oral doses. *Aquaculture* **2020**, *515*, 734542. [CrossRef]
7. Yamamoto, M.; Toda, M.; Sugita, T.; Tanaka, K.; Uneyama, C.; Morikawa, K. Studies on the results of monitoring of veterinary drug residues in food products of animal origin in Japan and other countries. *Kokuritsu Iyakuhin Shokuhin Eisei Kenkyujo Hokoku* **2009**, *127*, 84–92. [CrossRef]
8. Wang, Y.; Zhang, W.; Mhungu, F.; Zhang, Y.; Liu, Y.; Li, Y.; Luo, X.; Pan, X.; Huang, J.; Zhong, X.; et al. Probabilistic Risk Assessment of Dietary Exposure to Chloramphenicol in Guangzhou, China. *Int. J. Environ. Res. Public Health* **2021**, *18*, 8805. [CrossRef]
9. Baynes, R.E.; Dedonder, K.; Kissell, L.; Mzyk, D.; Marmulak, T.; Smith, G.; Tell, L.; Gehring, R.; Davis, J.; Riviere, J.E. Health concerns and management of select veterinary drug residues. *Food Chem. Toxicol.* **2016**, *88*, 112–122. [CrossRef]
10. Filazi, A.; Sireli, U.T.; Dikmen, B.Y.; Aydin, F.G.; Kucukosmanoglu, A.G. The effect of cooking and storage on florfenicol and florfenicol amine residues in eggs. *Ital. J. Food Sci.* **2015**, *27*, 351–356. [CrossRef]

11. Franje, C.A.; Chang, S.K.; Shyu, C.L.; Davis, J.L.; Lee, Y.W.; Lee, R.J.; Chang, C.C.; Chou, C.C. Differential heat stability of amphenicols characterized by structural degradation, mass spectrometry and antimicrobial activity. *J. Pharm. Biomed. Anal.* **2010**, *53*, 869–877. [CrossRef] [PubMed]

12. Foodmate. Available online: http://down.foodmate.net/standard/sort/3/64074.html (accessed on 14 July 2022).

13. Wu, X.; Shen, X.; Cao, X.; Nie, R.; Zhang, H.; Tang, C.; Wang, W. Simultaneous Determination of Amphenicols and Metabolites in Animal-Derived Foods Using Ultrahigh-Performance Liquid Chromatography-Tandem Mass Spectrometry. *Int. J. Anal. Chem.* **2021**, *2021*, 3613670. [CrossRef] [PubMed]

14. Tian, L.; Bayen, S. Thermal degradation of chloramphenicol in model solutions, spiked tissues and incurred samples. *Food Chem.* **2018**, *248*, 230–237. [CrossRef] [PubMed]

15. Shakila, R.J.; Vyla, S.A.P.; Kumar, R.S.; Jeyasekaran, G.; Jasmine, G.I. Stability of chloramphenicol residues in shrimp subjected to heat processing treatments. *Food Microbiol.* **2006**, *23*, 47–51. [CrossRef]

16. Farkas, B.E.; Singh, R.P.; Rumsey, T.R. Modeling heat and mass transfer in immersion frying. II. Model solution and verification. *J. Food Eng.* **1996**, *29*, 227–248. [CrossRef]

17. Zheng, C.; Sun, D.W.; Zheng, L.Y. Correlating colour to moisture content of large cooked beef joints by computer vision. *J. Food Eng.* **2006**, *77*, 858–863. [CrossRef]

18. Zhang, Z.; Fang, H.; Liu, H. Muscle water retention in chilled meat and its influencing factors. *Meat Res.* **2008**, *12*, 15–19. [CrossRef]

19. Clarke, A.D.; Means, W.J.; Schmidt, G.R. Effects of storage time, sodium chloride and sodium tripolyphosphate on yield and microstructure of comminuted beef. *J. Food Sci.* **1987**, *52*, 854–856. [CrossRef]

20. Tian, L. *Thermal Degradation of Antibiotics: Amphenicols as a Case Study*; McGill University: Montreal, QC, Canada, 2016.

21. Nashwa, M.Z.; Arwa, H.N.; Saleh, S.; Nahla, S. Experimental study on the effect of different cooking method of oxytetracycline residues in chicken meat. *Egypt J. Chem Environ. Health* **2016**, *2*, 598–610. [CrossRef]

22. Gajda, A.; Bladek, T.; Gbylik-Sikorska, M.; Posyniak, A. The influence of cooking procedures on doxycycline concentration in contaminated eggs. *Food Chem.* **2017**, *221*, 1666–1670. [CrossRef] [PubMed]

23. Hussein, M.A.; Ahmed, M.M.; Morshedy, A.M. Effect of cooking methods on some antibiotic residues in chicken meat. *Jpn. J. Vet. Res.* **2016**, *64*, S225–S231.

24. Fathy, F.; Ahmed, A.; Moursi, M. Effect of cooking methods on antibiotic residues in broiler chicken meat. In Proceedings of the 2nd International Conference of Food Safety, Suez Canal University Held at Faculty of Veterinary Medicine-Suez Canal University, Ismailia, Egypt, August 2015; pp. 76–81.

25. Zhang, C.; Chen, D. Research progress on the flavor of fried foods. *J. Food Saf. Qual. Test.* **2014**, *5*, 3085–3091. [CrossRef]

Article

Risk Assessment of (Herbal) Teas Containing Pyrrolizidine Alkaloids (PAs) Based on Margin of Exposure Approach and Relative Potency (REP) Factors

Lu Chen [2,†], Qian Zhang [1,†], Ziwei Yi [1], Yu Chen [1], Weihan Xiao [1], Dan Su [3] and Wenbiao Shi [1,*]

[1] Department of Nutrition and Health, Chinese Agriculture University, Beijing 100091, China
[2] Institute of Quality Standards and Testing Technology for Agro-Products, Chinese Academy of Agricultural Sciences, Key Laboratory of Agri-food Quality and Safety, Ministry of Agriculture and Rural Affairs, Beijing 100081, China
[3] Department of Chemistry and Chemical Biology, Cornell University, Ithaca, NY 14850, USA
* Correspondence: wenbiao.shi@cau.edu.cn; Tel.: +86-010-62738589
† These authors contributed equally to this work.

Abstract: Pyrrolizidine alkaloids (PAs) present distinct toxicity potencies depending on their metabolites and in vivo toxicokinetics. To represent the potency differences of various PAs, the interim relative potency (REP) factors have been derived. However, little is known about the risk assessment for (herbal) teas when taking REP factors into account. In this study, a set of 68 individual 1,2-unsaturated PA in 21 types of (herbal) teas was analyzed using LC-MS/MS. The REP factors for these PAs were applied on the PA levels. The margin of exposure (MOE) approach was employed to assess the risks of the exposure to PAs due to consumption of (herbal) teas. The results show that the total PA levels ranged from 13.4 to 286,682.2 µg/kg d.m., which were decreased by REP correction in most of the teas. The MOE values for tephroseris, borage and lemon balm (melissa) tea based on REP-corrected PA levels were below 10,000, assuming daily consumption of one cup of tea during a lifetime, indicating that consuming these teas may raise a concern. Our study also indicates a priority for risk management for tephroseris tea, as having nephrosis tea for more than 11.2 weeks during a 75-year lifetime would result in an MOE of 10,000.

Keywords: herbal tea; pyrrolizidine alkaloids (PAs); margin of exposure (MOE); risk assessment; relative potency (REP)

1. Introduction

Pyrrolizidine alkaloids (PAs) are toxic substances that exist naturally in plants [1]. To date, over 660 types of PAs and PA *N*-oxide have been identified in the estimated six thousand plants [2]. 1,2-unsaturated PAs are particularly of concern as they are hepatotoxicants and genotoxic carcinogens [3]. 1,2-unsaturated PAs can be subdivided by the type of esterification, including monoesters, open chained diesters, and cyclic diesters. In addition, cyclic diester PAs with an azacyclooctanone, instead of a 1,2-dehydropyrrolizidine ring system, represent a special class. The main human exposure route to PAs is consuming plant-derived foods, such as (herbal) teas. PAs can induce hepatotoxicity both in humans and animals [1]. Human poisoning and even deaths from the consumption of PAs have been reported in several countries [4]. Severe outbreaks of the PA contamination once occurred in Afghanistan [5] and central India [6]. In addition, a few cases were reported in Hong Kong [7], Switzerland [8,9], Austria [10] and Tajikistan [11]. As a result, the use of the PA-containing plants as food products or supplements has been restricted in several countries [12]. However, there is still a lack of global consensus in regulatory measures regarding PAs in plant-derived products so far. Possibly, conducting a risk assessment for foodstuff containing PAs may contribute to the development of such a consensus.

(Herbal) teas are a type of PA-containing plant-derived product. The concentration of PAs can vary enormously among (herbal) teas. For instance, the Federal Institute for Risk Assessment (BfR) analyzed 274 types of (herbal) teas and found that the levels of PAs ranged from below the level of detection (LOD) to 5647.2 μg/kg dry material (d.m.) [2]. Later, Mulder et al. (2015) reported that the concentration of PAs could reach up to 4804.5 μg/kg d.m. based on the analyzed 22 types of (herbal) teas [13].

Due to the omnipresence of PAs in (herbal) teas and their detrimental effects, the safety evaluation of PAs associated with the consumption of teas is crucial. Multiple studies have performed risk assessments for PAs in (herbal) teas in the recent years [3,14,15]. Given that 1,2-unsaturated PAs are genotoxic and carcinogens, the risk assessment was conducted based on the margin of exposure (MOE) approach [16]. The MOE is defined as the ratio between the benchmark dose level with a lower confidence limit associated with a 10% extra risk on a cancer incidence above background levels (BMDL$_{10}$) and the estimated daily intake (EDI). To date, the BMDL$_{10}$ values for only two PAs, lasiocarpine and riddelliine, have been derived, whereas the values for the other PAs remained unavailable due to the lack of appropriate animal carcinogenicity studies [17,18]. The European Food Safety Authority (EFSA) used to adopt a BMDL$_{10}$ of 0.07 mg/kg bw/day of lasiocarpine as the point of departure (PoD) for the MOE calculation [19]. A cut-off value of 10,000 for the MOE is usually applied, which incorporates factors including the inter-species and intra-species differences in toxicokinetic and toxicodynamics, the inter-individual human variability in cell cycle control and DNA repair as well as the potential discrepancy between the BMDL$_{10}$ serving as a reference point and a NOAEL (No Observed Adverse Effect Level) [16]. The risk assessment suggested that the long-term consumption of several (herbal) teas may pose a potential health risk in humans, especially when considering a lifetime exposure [3,14,15]. It is worthwhile to mention that the MOE values were calculated based on the mean levels of total PAs in these studies, assuming that the metabolism and toxic potencies of PAs were the same with lasiocarpine. This, however, may result in an overestimation of potential risks from the exposure, since the toxic potencies of individual PAs are distinct and most of them could be lower than lasiocarpine. In addition, the obtained BMDL$_{10}$ value for lasiocarpine (70 μg/kg bw/day) was affected by a high degree of uncertainty [20]. Instead, the EFSA has proposed the BMDL$_{10}$ of riddelliine, which was 237 μg/kg bw/day, for the combined risk assessment of PAs by dose addition. The relative potency factor (REP) correction serves as an approach for the risk assessment for a mixture of chemicals that exhibit a common mode of action. To derive a REP, the potency of each component in a mixture is compared to that of a reference chemical generating a measure of potency for each component with respect to the toxicity of the index chemical [12]. It is more rigorous to perform risk assessments for PA-containing botanicals by determining the REP factor for each PA contained and then adjusting the concentration of each PA in the mixtures for the assessments.

To date, little is known about risk assessments for PAs in botanical samples when taking into account the REP factor of each PA. Additionally, the BMDL$_{10}$ of riddelliine was proposed as the new PoD for the MOE calculation. Considering these facts, the actual exposure and related risk assessment of PAs due to the consumption of (herbal) teas need to be reevaluated. Therefore, the aim of the present study is to determine the PA levels in 21 types of (herbal) teas with and without the correction of REP factors, and to perform risk assessments based on the BMDL$_{10}$ of riddelliine derived MOE approach. To achieve this, in total 68 individual 1,2-unsaturated PAs were analyzed, including cyclic diesters and heliotridine-type (7S) open diesters (e.g., monocrotaline, retrorsine, riddelliine, senecionine, seneciphylliine, senkirkine, heliosupine and lasiocarpine), heliotridine-type (7S) monoesters (e.g., echinatine and heliotrine), retronecine-type (7R) open diesters (e.g., echimidine and symphytine), and retronecine-type (7R) monoesters (e.g., indicine, intermedine and lycopsamine) monoesters, open chained diesters and cyclic diesters. The chemical structure for these PAs and their *N*-oxide form, as well as their corresponding REP factors, has

been previously reported in detail [12]. To clarify the rationale for this study, a graphical workflow is shown as Scheme 1.
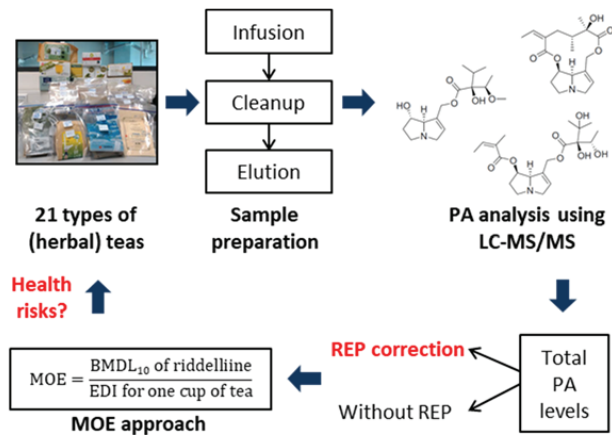
Scheme 1. Graphical workflow for the whole analytical procedure in this study.

2. Materials and Methods

2.1. PA Extraction

Twenty-one types of commercial (herbal) teas were sampled from China and EU countries, including 7 types of teas derived from PA-containing plants and 14 types from non-PA producing plants. Detailed information of the (herbal) teas is listed in Table 1. In total, 147 tea samples, which were present as comminuted leaves, were analyzed. Two grams of (herbal) tea were weighed out and transferred to beaker glasses or brown bottles. Immediately, 150 mL of boiling water was added onto the samples. The infusion was steeped for 10 min, with a gentle stirring for 10 s at 0, 3 and 6 min, respectively. The infusion was allowed to cool down at room temperature, after which it was filtered by passing through a 0.45 μm filter. Fifty milliliters of the infusion were subject to the following cleanup procedure.

Table 1. Ingredients and PA-producing property of the studied (herbal) teas.

Type of (Herbal) Teas	Ingredients	Origin from PA-Producing Plants	Nation of Origin	Year of Sampling
Asteraceae	Asteraceae	Yes	CN	2021
Boraga	Boraga	Yes	ES	2020
Camomile	Chamazulene, bisabolol, apigenin, luteolin	Not	NL	2020
Citroen melisse	Lemon balm (*melissa officinalis*), rooibos, lemon flavouring	Not	NL	2020
Earl grey	Black tea, bergamot and lemon flavouring	Not	NL	2020
Eupatorium	Eupatorium Sp.	Yes	CN	2021
Forest fruit tea	Mint, strawberry, cherry, blueberry, cranberry, guava	Not	NL	2020
Fresh peppermint	Peppermint	Not	NL	2020
Green tea lemon	Green tea, natural flavouring, lemon flavouring (2%)	Not	NL	2020
Gynura segetum	Gynura segetum	Yes	CN	2021
Heliotrope	Heliotrope Sp.	Yes	CN	2021

Table 1. *Cont.*

Type of (Herbal) Teas	Ingredients	Origin from PA-Producing Plants	Nation of Origin	Year of Sampling
Lemon balm & liquorice	Lemon balm leaves (51.5%), rooibos, camomile, liquorice root (6%), strawberry flavouring, orange blossom, sweet blackberry leaves	Not	UK	2020
Lemon balm (melissa)	Rooibos, orange flavouring, lemon balm (*melissa officinalis*)	Not	NL	2020
Lemon verbena	Lemon verbena, lemongrass	Not	NL	2020
Lungwort	Lungwort (*pulmonaria officinalis*)	Yes	NL	2020
Mix herb (1)	Verbena, lemon grass, rosemary, stevia, green tea, jasmine	Not	CN	2021
Mix herb (2)	Lemon balm, hops, lemongrass, raspberry	Not	CN	2021
Mix herb (3)	Mint leaves, lemongrass, lemon balm, flowers, roots	Not	CN	2021
Rooibos	Rooibos	Not	NL	2020
Sage & lemon myrtle	Lemon balm leaves, camomile, nettle, sweet blackberry leaves, sage leaves (6%), lime flavouring, lemon myrtle (2%), angelica root, red clover	Not	UK	2020
Tephroseris	*Tephroseris* sp.	Yes	CN	2021

CN, China; ES, Spain; NL, the Netherlands; UK, United Kingdom.

2.2. Sample Cleanup

The sample cleanup was carried out using reversed phase C18 solid phase extraction (SPE) cartridges (Discovery DSCC18 500 mg/5 mL, Supelco, Bellefonte, PA, USA), as described previously [21]. The SPE cartridges were conditioned using 5 mL of methanol and water, respectively. The cartridges were loaded with 50 mL of the filtered infusion, washed with 6 mL of water and then dried with a vacuum manifold for 10 min. The elution of the PAs for all the tea samples was done by adding 5 mL of methanol. The elution step was repeated. The eluates were combined, dried under a gentle nitrogen stream in a warmed water bath (50 °C, TurboVap, Biotage, Uppsala, Sweden) and reconstituted in 1 mL of methanol/water (5/95, *v/v*). The extracts were transferred into filter columns (Nylon, 0.2 μm, VWR, Darmstadt, Germany) and centrifuged at 13,000× *g* for 2 min at room temperature.

2.3. LC-MS/MS Analysis

The PAs in the samples were measured using a LC-MS/MS system consisting of an UHPLC (Ultimate 3000, Thermo Scientific, San Jose, CA, USA) and a Triple Stage Quadrupole mass spectrometer (TSQ Vantage, Thermo Scientific, San Jose, CA, USA), as described previously with minor modifications [21]. Briefly, chromatographic separation was achieved on 150 × 2.1 mm, 1.9 μm particle sizes, C18 Hypersil Gold column fitted with a guard column (Thermo Scientific, Dreieich, Germany). Eluent A was 100% water with 0.1% formic acid and 5 mM of ammonium formate. Eluent B was 95% methanol and 5% water with 0.1% formic acid and 5 mM of ammonium formate. A stepwise gradient elution was conducted as follows: 0–0.5 min for 95% A/5% B, 7.0 min for 50% A/50% B, 7.5 min for 20% A/80% B, 7.6–9.0 min for 100% B and 9.1–15 min for 95% A/ 5% B. A flow rate of 300 μL/minute was applied and 10 μL of each sample was injected. The column temperature was maintained at 40 °C. Details of the mass parameters are listed in supporting data S1, Table S1.

2.4. Quality Assurance and Quality Control (QA/QC)

Fity-four PA standard compounds were obtained from the following sources: echimidine, indicine, indicine *N*-oxide, intermedine, intermedine *N*-oxide, lycopsamine, lycopsamine *N*-oxide, monocrotaline, monocrotaline *N*-oxide and otosenine from Phytolab (Vestenbergsgreuth, Germany); heliotrine and trichodesmine from Latoxan (Valence, France); usaramine from BOC Sciences (Shirley, Suffolk, NY, USA); florosenine from PRISNA (Leiden, the Netherlands); and Usaramine *N*-oxide and trichodesmine *N*-oxide were in-lab synthesized according to [22] and the rest from Phytoplan (Heidelberg, Germany). An analytical grade of formic acid and ammonium carbonate (Energy Chemical) and a LC-MS grade of acetonitrile and methanol (Sinopharm) were purchased from Shanghai, China.

Quality assurance and quality control (QA/QC) procedures were performed as follows: a procedural blank, a spike blank, a mixed PA sample (1 μg/mL of external standards in methanol, used to spike the (herbal) teas in 25 ng/mL and 100 ng/mL) and a duplicate were run for each batch of 20 samples to check for cross-contamination and instrumental reliability as well as to indicate recoveries. No PAs in the blanks were detected. The standard deviations for standard solution (7-point calibration curves over the range of zero to 250 ng/mL) were controlled within 10%. Recoveries at the level of 100 ng/mL varied from 79 to 110%. The LOD for PAs in the infusion of (herbal) teas was determined as the concentrations of analyses in a sample that showed a peak divided by the signal-to-noise ratio (S/N) of 3. The LOD was estimated at the range of 10 to 20 ng/L and the limit of quantification (LOQ) was obtained at 50 ng/L. For those PAs with no available standard compounds, the corresponding structurally related PA standards were employed for the semi-quantification of those PA levels.

2.5. Estimated Daily Intake (EDI) and MOE Calculation

The EDIs of PAs resulting from the consumption of (herbal) teas was calculated as described before [20], as shown in Equation (1). The interim REP factors for each individual PA, which derived from the data of in vitro cytotoxicity and genotoxicity in *Drosophila* and acute toxicity in rodents (LD50) [12], were used to correct the PA concentrations.

$$\text{EDI} = \frac{\text{Sum of concentration of each PA by or no REP correction} * \text{daily intake of (herbal) tea}}{\text{Body weight}} \quad (1)$$

where the daily intake of (herbal) tea was estimated to be 2 g, which roughly corresponds to one cup of tea; REP factors were 1.0 for cyclic diesters and heliotridine-type (7S) open diesters, 0.3 for heliotridine-type (7S) monoesters, 0.1 for retronecine-type (7R) open diesters and 0.01 for retronecine-type (7R) monoesters (e.g., indicine, intermedine and lycopsamine) (supporting data S1, Table S2). A default adult body weight of 70 kg was used as suggested [23].

The MOE values for the chronic lifetime exposure to (herbal) teas were calculated as follows:

$$\text{MOE} = \frac{\text{BMDL}^{10} \text{of riddelliine}}{\text{EDI}} \quad (2)$$

where the BMDL$_{10}$ of riddelliine is 237 μg/kg bw/day; the MOE values for the short-term exposure were calculated based on Haber's rule and a lifetime expectancy of 75 years, as described previously [21]. The MOE value being below 10,000 suggests a potential health risk related to the exposure that cannot be excluded and high priority might be given for risk management [3].

The maximum number of weeks that could result in an MOE of 10,000 based on the daily consumption of one cup of tea was calculated as Equation (3), according to the previous studies [3,14,15].

$$\text{The maximum number of weeks} = \frac{\text{BMDL10 of riddelliine} * 75 \text{ years} * 52 \text{ weeks}}{\text{EDI} * \text{MOE}} \quad (3)$$

All calculations above were based on an assumption that the concentrations reported are representative for the specific tea and that the exposure to PAs is exclusively due to that tea.

3. Results

3.1. PA Concentrations in (Herbal) Teas

In this study, a total of 68 individual PAs were analyzed, of which 23 PAs were not detected in all the investigated (herbal) teas (supporting data S2). Seventeen PAs were found in lemon balm (melissa) tea, ranked first regardless of the REP correction, followed by tephroseris and lemon balm & liquorice (Table 2). None of the targeted PAs were present in citroen melisse and fresh peppermint tea. Most of the teas (92.5%) were detected with PAs, with the measured total levels varying from 13.4 µg/kg d.m. to 286,682.2 µg/kg d.m. (Table 2). In terms of the total PA content, tephroseris, borage and lungwort were the top three teas, which all originated from PA-producing plants. When taking the REP factors into account, the concentrations of total PAs were ranged from 1.3 µg/kg d.m. to 286,648.3 µg/kg d.m., which were generally lower compared to those measured levels in the (herbal) teas, except for green tea, gynura segetum and rooibos. It is of note that the total PA level for borage tea decreased by about 116.5-fold by the REP correction, amounting to 1440.6 µg/kg d.m. Whereas the PA concentrations in tephroseris were hardly altered by the REP correction, lungwort presented a considerable drop in its total PA level. This drop made the REP-corrected PA level for lungwort even lower than that for some teas from non-PA-generating plants, such as lemon balm, chamomile, rooibos and lemon verbena. Among the teas derived from non-PA-producing plants, lemon balm (melissa) and chamomile ranked first and second with their total PA levels, irrespective of REP correction.

The regulations of Germany and the Netherlands have indicated that the maximum limit for daily intake of 1,2-unsaturated PAs (including *N*-oxides) during a lifetime by a 70 kg person was 0.1 µg/day [24,25]. In this study, we calculated the daily intake of total PAs by consuming one cup of tea with and without REP correction. The results showed that there were nine types of teas resulting in the daily intake of PAs above 0.1 µg/day, regardless of REP correction (Table 2). These teas included tephroseris, borage, lemon balm (melissa), chamomile, eupatorium, rooibos, mix herb (1), lemon verbena and green tea. In addition, the daily intake of PAs due to the consumption of earl grey, lemon balm & liquorice, lungwort and sage & lemon myrtle could exceed the maximum limit when the REP factors were not applied.

According to the top three PAs and their concentrations, senkirkine and its congener neosenkirkine were the dominant PAs in the (herbal) teas from PA-containing plants except for borage and lungwort, while echinatine, retrorsine, integerrimine and senecionine as well as their *N*-ox congeners were frequently occurring in the non-PA-producing teas (Table 2). When taking the REP factors into account, senkirkine, neosenkirkine and petasitenine remained the same levels as their REP factors were derived to be 1 (supporting data S1, Table S2). In contrast, supinine, intermedine and their *N*-oxide congeners plus lycopsamine *N*-oxide correspond with a proposed REP value of 0.01, which could explain for the remarkable decreases in the total PA levels for borage and lungwort due to REP correction. Overall, the types of the top three PAs remained unchanged in most of the studied teas in response to REP correction, with one exception of lemon balm & liquorice, which was due to the REP factors of atropine and scopolamine, set at 0.

Table 2. Total number of detected PAs, total PA levels, daily intake of total PAs when consuming 2 g of tea and the top three PAs and their concentration in 21 types of (herbal) teas with and without REP correction. A complete data overview is shown in supporting data S2.

Type of Tea	Number of PAs above the LOD		Mean (Range) Concentration of Total PAs (µg/kg d.m.)		Daily Intake of Total PAs (µg/Day)		Top Three PAs [a] and Their Concentration (µg/kg d.m.)	
	no REP	REP	no REP	REP	no REP	REP	no REP	REP
Asteraceae	4	4	36.7 (16.5–53.2)	29.6 (14.3–47.1)	0.0734	0.0592	Senkirkine (26.6); lycopsamine N-oxide (4.3); neosenkirkine (3.0)	Senkirkine (26.6); neosenkirkine (2.97); lycopsamine N-oxide (0.04)
Borage	13	13	167,846.6 (68,935.8–465,953.6)	1440.6 (698.4–5782.1)	336	2.88	Supinine N-oxide (65452.4); lycopsamine N-oxide (47295.8); supinine (3174.9)	Supinine N-oxide (654.5); lycopsamine N-oxide (473.0); supinine (31.7)
Chamomile	13	13	772.8 (393.0–1053.2)	703.3 (382.0–997.2)	1.55	1.41	Retrorsine N-oxide (520.6); senecionine N-oxide (74.3); echimidine N-oxide (67.4)	Retrorsine N-oxide (520.6); senecionine N-oxide (74.3); echimidine N-oxide (67.4)
Citroen melisse	0	0	n.d.	n.a.	n.a.	n.a.	n.d.	n.a.
Earl grey	3	3	189.9 (59.7–353.1)	47.0 (17.5–87.2)	0.38	0.094	Echinatine N-oxide (124.9); lycopsamine N-oxide (34.3); echinatine (30.7)	Echinatine N-oxide (37.5); echinatine (9.2); lycopsamine N-oxide (0.3)
Eupatorium	8	7	154.0 (86.9–257.4)	140.7 (80.9–239.5)	0.308	0.281	Senkirkine (109.7); neosenkirkine (25.0); echinatine (6.5)	Senkirkine (109.7); neosenkirkine (25.0); echinatine (2.0)
Forest fruit tea	2	2	21.3 (7.4–35.2)	6.4 (2.1–10.7)	0.0426	0.0128	Echinatine N-oxide (15.3); echinatine (6.0)	Echinatine N-oxide (4.6); echinatine (1.8)
Fresh peppermint	0	0	n.d.	n.a.	n.a.	n.a.	n.d.	n.a.
Green tea	5	5	72.8 (38.2–298.2)	72.8 (38.2–298.2)	0.146	0.146	Integerrimine N-oxide (42.2); integerrimine (35.9); retrorsine N-oxide (18.5)	Integerrimine N-oxide (42.2); integerrimine (35.9); retrorsine N-oxide (18.5)
Gynura segetum	2	2	13.4 (n.d.–26.8)	13.4 (n.d.–26.8)	0.0268	0.0268	Senkirkine (10.2); neosenkirkine (3.2)	Senkirkine (10.2); neosenkirkine (3.2)
Heliotropium	7	7	29.4 (8.5–73.9)	20.4 (7.8–56.2)	0.0588	0.0408	Senkirkine (15.2); lycopsamine N-oxide (4.5); neosenkirkine (3.8)	Senkirkine (15.2); neosenkirkine (3.8); echinatine N-oxide (0.6)
Lemon balm (melissa)	17	17	845.1 (169.5–1258.3)	831.2 (163.5–1216.3)	1.69	1.66	Senecionine N-oxide (539.0); integerrimine N-oxide (107.6); senecionine (85.0)	Senecionine N-oxide (539.0); integerrimine N-oxide (107.6); senecionine (85.0)
Lemon balm & liquorice	15	13	52.0 (17.5–163.2)	16.9 (6.5–54.6)	0.104	0.0338	Atropine (18.8); scopolamine (18.5); europine N-oxide (10.9)	Lasiocarpine N-oxide (4.9); europine N-oxide (3.3); heliotrine N-oxide (3.3)

Table 2. *Cont.*

Type of Tea	Number of PAs above the LOD		Mean (Range) Concentration of Total PAs (µg/kg d.m.)		Daily Intake of Total PAs (µg/Day)		Top Three PAs [a] and Their Concentration (µg/kg d.m.)	
	no REP	REP	no REP	REP	no REP	REP	no REP	REP
Lemon verbena	4	4	647.1 (218.9–987.2)	210.2 (69.3–353.1)	1.29	0.42	Echinatine N-oxide (579.0); echinatine (45.1); heliosupine N-oxide (17.8)	Echinatine N-oxide (173.7); echinatine (13.5); heliosupine N-oxide (17.8)
Lungwort	8	8	1769.7 (996.5–2753.2)	37.8 (18.6–54.8)	3.54	0.0756	Intermedine N-oxide (589.9); lycopsamine N-oxide (421.8); intermedine (300.8)	7-acetyllycopsamine/intermedine N-oxide (12.7); senkirkine (6.2); intermedine N-oxide (5.9)
Mix herb (1)	5	5	84.1 (14.5–253.6)	78.8 (14.5–214.2)	0.168	0.158	Monocrotaline (38.6); senkirkine (23.2); neosenkirkine (10.8)	Monocrotaline (38.6); senkirkine (23.2); neosenkirkine (10.8)
Mix herb (2)	4	3	16.1 (5.4–39.0)	11.4 (5.4–23.0)	0.0322	0.0228	Atropine (76.4); senecionine (9.5); heliotrine N-oxide (3.6)	Senecionine (9.5); heliotrine N-oxide (1.1); heliotrine (1.0)
Mix herb (3)	6	4	15.0 (0.4–63.6)	1.3 (0.4–3.2)	0.03	0.0026	Lycopsamine N-oxide (3.8); intermedine N-oxide (3.5); rinderine N-oxide (2.7)	Rinderine N-oxide (0.8); echinatine N-oxide (0.4); intermedine N-oxide (0.04)
Rooibos	12	12	218.4 (116.8–754.3)	218.4 (116.8–754.3)	0.437	0.437	Senecionine N-oxide (62.3); integerrimine N-oxide (44.6); retrorsine N-oxide (32.2)	Senecionine N-oxide (62.3); integerrimine N-oxide (44.6); retrorsine N-oxide (32.2)
Sage & lemon myrtle	14	12	114.4 (17.6–554.2)	29.2 (4.2–114.8)	0.229	0.0584	Echinatine N-oxide (44.1); echinatine (27.0); intermedine (6.8)	Echinatine N-oxide (13.2); echinatine (8.1); Rinderine (1.6)
Tephroseris	16	14	286,682.2 (185,233.6–366,599.4)	286,648.3 (185,201.6–366,544.4)	573	573	Senkirkine (191241.4); neosenkirkine (50250.6); petasitenine (37318.2)	Senkirkine (191241.4); neosenkirkine (50250.6); petasitenine (37318.2)

n.d. below the LOD; n.a. not applicable. Daily intake of total PAs when consuming 2 g of tea with and without REP correction was calculated and values that exceed the maximum limits for daily intake of PAs during a lifetime (0.1 µg/day) based on the Germany and Dutch regulations are marked in bold [24,25]; according to these values, teas with one value in bold are in Italic while those with both values in bold are underlined. [a] Only two types of PAs were detected out in forest fruit tea and gynura segetum tea.

3.2. Estimated Daily Intake of PAs

Table 3 displays the EDIs for the studied (herbal) teas. With one cup of tea per day, the EDIs calculated based on the quantifiable levels of total PAs were ranged from 3.83×10^{-4} to 8.19 µg/kg bw/day. When using PA levels corrected by REP factors, EDIs were present in the range of 3.71×10^{-5} and 8.19 µg/kg bw/day. It should be noted that tephroseris tea had EDIs of 8.19 µg/kg bw/day, no matter whether REP correction was applied or not. Besides, borage tea exhibited an EDI of 4.80 µg/kg bw/day when REP factors were not considered. These EDI values exceed a "tolerable daily intake" (TDI) of 0.1 µg/kg bw/day for the total PAs in (herbal) preparations or extracts, which was provided by the Dutch national institute for public health and the environment (RIVM) [14]. The TDI was derived based on the NOAEL of 0.01 mg/kg bw/day for non-neoplastic changes due to the chronic exposure of riddelliine in rats and an uncertainty factor of 100, and therefore indicates an exposure level of PAs that may cause non-carcinogenic effects.

Table 3. The EDIs for 21 types of (herbal) teas based on PA levels with or without REP correction.

Type of Tea	EDI (µg/kg bw/day)	
	without REP Correction	Corrected by REP Factors
Asteraceae	1.05×10^{-3}	8.46×10^{-4}
Borage	**4.80**	4.12×10^{-2}
Chamomile	2.21×10^{-2}	2.01×10^{-2}
Citroen melisse	n.a.	n.a.
Earl grey	5.43×10^{-3}	1.34×10^{-3}
Eupatorium	4.40×10^{-3}	4.02×10^{-3}
Forest fruit tea	6.09×10^{-4}	1.83×10^{-4}
Fresh peppermint	n.a.	n.a.
Green tea	2.08×10^{-3}	2.08×10^{-3}
Gynura segetum	3.83×10^{-4}	3.83×10^{-4}
Heliotropium	8.40×10^{-4}	5.83×10^{-4}
Lemon balm (melissa)	2.41×10^{-2}	2.37×10^{-2}
Lemon balm & liquorice	1.49×10^{-3}	4.83×10^{-4}
Lemon verbena	1.85×10^{-2}	6.01×10^{-3}
Lungwort	5.06×10^{-2}	1.08×10^{-3}
Mix herb (1)	2.40×10^{-3}	2.25×10^{-3}
Mix herb (2)	4.60×10^{-4}	3.26×10^{-4}
Mix herb (3)	4.29×10^{-4}	3.71×10^{-5}
Rooibos	6.24×10^{-3}	6.24×10^{-3}
Sage & lemon myrtle	3.27×10^{-3}	8.34×10^{-4}
Tephroseris	**8.19**	**8.19**

n.a. not applicable. The EDIs in bold represent values higher than a TDI of 0.1 µg/kg bw/day for total PAs in (herbal) products, which was calculated by the RIVM [14].

3.3. Risk Assessment for the (Herbal) Teas Based on Lifetime and Shorter Duration Exposure

The MOE values for the 21 types of (herbal) teas were evaluated according to two exposure scenarios, including the consumption of one cup of tea daily throughout the whole lifespan (Figure 1A) and shorter-than-lifetime during two weeks a year for 75 years (Figure 1B). Of the seven PA-producing plants-derived teas, tephroseris, borage and lungwort resulted in the low range of the MOE values between 29 and 4687 upon a lifelong daily consumption without REP correction. The MOE values for tephroseris and borage remained below 10,000 when taking REP factors into account, while that for lungwort was increased by 219,444 (Figure 1A). For tephroseris tea, even short-term consumption of two weeks/year resulted in a low MOE value of 752 regardless of REP correction (Figure 1B), which was well below 10,000, indicating that this tea may pose a potential risk for human health. Having borage tea two weeks per year resulted in an MOE value of 1285, contrasting with an MOE value well above 10,000 due to REP correction. Notably, lemon balm, a tea from non-PA-generating plants, showed MOE values just below 10,000 irrespective

of REP correction when consumed daily for a lifetime. However, in the defined shorter duration exposure scenario, the resulting MOE values for this tea were well above 10,000. Interestingly, since asteraceae, gynura segetum and heliotropium each contained a few PAs at low concentrations, use of these teas resulted in MOE values far above 10,000 regardless of the exposure duration and REP correction, although these teas were obtained from PA-containing plants. Similarly, consumption of citroen melissa, fresh peppermint, mix herb (2), mix herb (3), forest fruit tea and lemon balm & liquorice may not raise health concern as no PAs were found or the resulting MOE values for these teas were multiple orders of magnitude higher than 10,000. In addition, use of earl grey, chamomile, green tea, rooibos, sage & lemon myrtle and eupatorium derived MOE values over 10,000 irrespective of the exposure duration and REP correction, indicating no health concern.
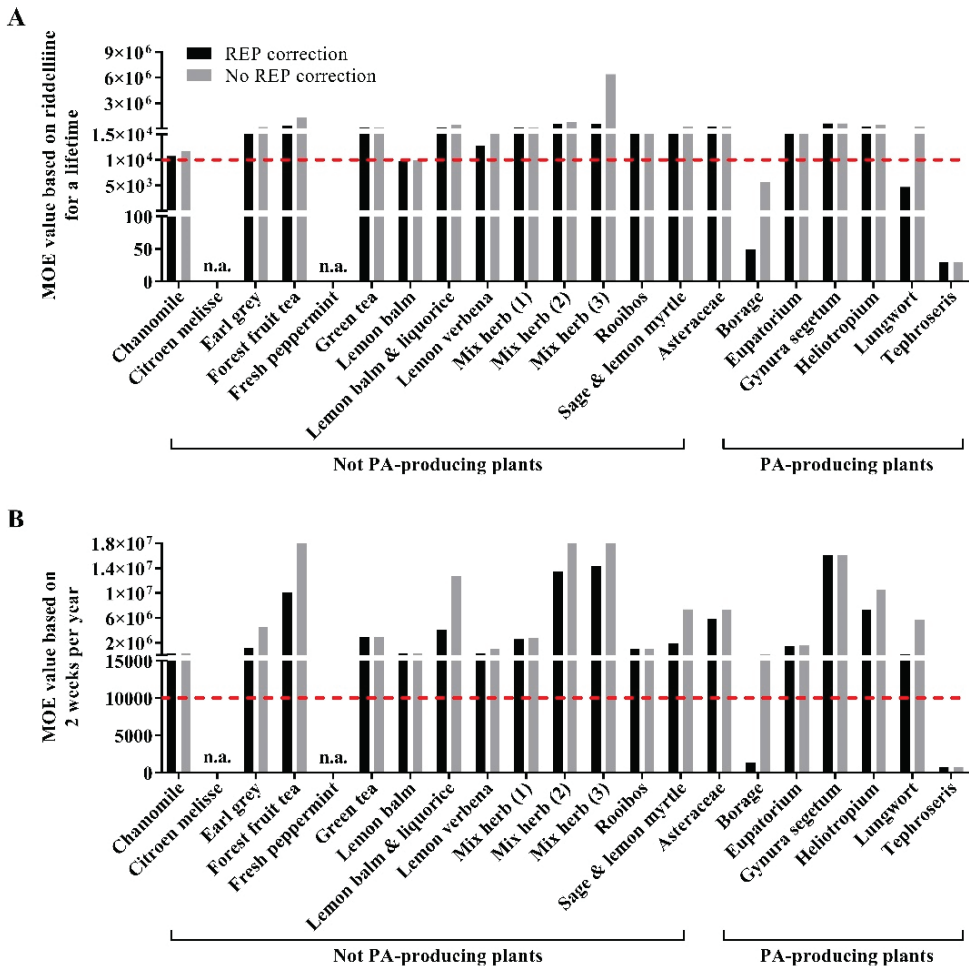
Figure 1. The MOE values calculated based on riddelliine for different types of (herbal) teas with or without REP correction when assuming a daily intake of one cup of tea per day for a lifetime (**A**) and for 2 weeks a year during a lifetime (**B**). Black bars represent the MOE values obtained based on the total PA levels corrected by the corresponding REP factors, while grey bars represent the MOE without REP correction. The red dashed line represents an MOE value of 10,000. n.a. indicates that data are not applicable due to a PA content < LOQ.

3.4. Risk Assessment for the (Herbal) Teas Based on Shorter-Than-Lifetime Consumption

Providing that the number of weeks a year selected for a shorter-than-lifetime exposure has an influence on the MOE values and corresponding conclusion, the number of weeks during a 75-year lifetime that would cause an MOE of 10,000 was calculated in the current study. As shown in Figure 2, consumption of tephroseris tea for more than 11.2 weeks during a lifetime, which is corresponding to 0.1 weeks/year during 75 years, would already raise a concern, no matter whether the REP factors were applied or not. Having borage tea for up to 19.3 weeks during a lifetime (0.3 weeks/year) would be of little concern, whereas the number was increased by REP correction to 2245.6 weeks during a lifetime (29.9 weeks/year). Use of lungwort and lemon balm containing the PA concentrations as measured in this study would result in an acceptable exposure for 1828.0 and 3828.0 weeks during a life time, respectively (equivalent to 24.4 and 51.0 weeks/year, respectively). As the REP factors were applied, the maximal number of weeks for lemon balm tea was 3828.0 weeks, while use of lungwort would raise no concern for the whole lifespan. For the other types of teas, the number of weeks resulting in an MOE of 10,000 exceeded 3900 weeks, suggesting that use of these teas may not pose a health risk.
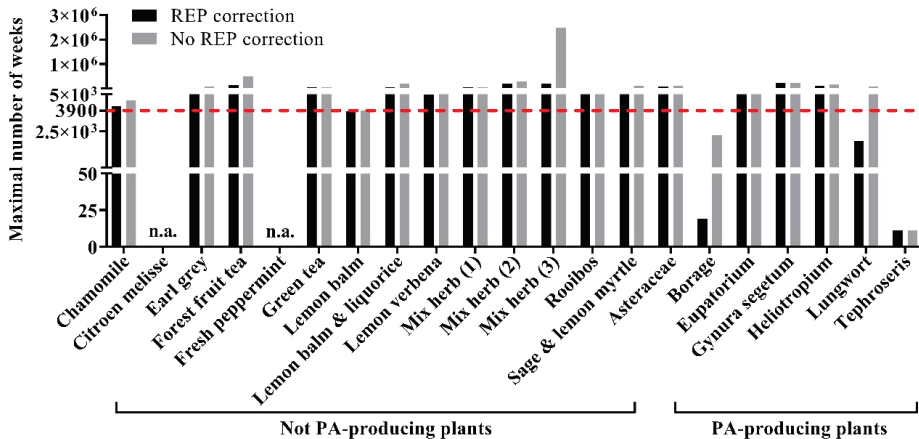
Figure 2. The maximal number of weeks during a 75-year lifetime that a (herbal) tea investigated in this study could be consumed to result in an MOE of 10,000, given that daily intake is one cup of tea. Black bars represent the number of weeks obtained based on the total PA levels corrected by the REP factors, while grey bars represent the values without REP correction. The red dashed line represents a 75-year lifetime (equivalent to 3900 weeks). n.a. indicates that the data are not applicable.

4. Discussion

Here, we investigated the PA levels in 21 types of (herbal) teas that were derived from both PA- and non-PA producing plants, based on which we performed a risk assessment using the MOE approach. In addition, we applied the REP factors for each PA that were analyzed to correct the PA concentrations and further calculated EDI and MOE for the (herbal) teas based on a lifetime and shorter duration exposure. Overall, the PA-containing plants-derived teas present a much wider range of the measured total PA levels from 13.4 to 286,682.2 µg/kg d.m., as compared to the levels ranging from 15.0 to 845.1 µg/kg d.m. for the teas from non-PA producing plants. This is in line with the findings reported by Griffine et al. (2014) [1] and Mulder et al. (2015) [13]. When taking REP factors into consideration, most of the samples showed decreased PA levels and, correspondingly, elevated the EDI and MOE values. Nevertheless, the daily consumption of tephroseris, borage and lemon balm (melissa) tea during a lifetime may pose a potential risk to human health.

One of the advantages in the present study is that a comprehensive set of 68 individual 1,2-unsaturated PAs was included, because we intend to reduce the risk of missing relevant

PAs as much as possible. We found that PAs were occurring in 19 out of 21 types of the (herbal) teas, albeit that 23 PAs were absent from all the tested samples. Multiple studies on risk assessment for (herbal) teas were based on a set of 17–28 PAs [2,3,13]. Several PAs that were enriched in the (herbal) teas analyzed in this study had not been included in those previous studies, such as atropine, petasitenine, neosenkirkine, and integerrimine, supinine, echinatine and *N*-oxide isomers of these three PAs. It is conceivable that due to the omission of the major PAs, the reported total PA levels in the above-mentioned studies would be lower than those measured in the same type of (herbal) teas based on our method. For instance, the total PA level for borage tea has been shown to be 29,694 µg/kg d.m. based on the set of 28 PAs [3], while this amounted to be 167,846.6 µg/kg d.m. when using the set of abundant PAs in this study (Table 2). Of note, our data showed that supinine plus supinine *N*-oxide, which were usually omitted in previous studies, accounted for about 41% of the total PA levels for borage tea. Neosenkirkine was also missing in previous studies but it turned out to be the major PA contributor in five types of teas in the present study. A lower number of analyzed PAs and a lower analytical sensitivity have been implicated with a greater difference in the derived MOE values based on lower bound exposure estimates in the tea samples [3]. Therefore, it may suggest that the set of sufficient types of PAs should be included to improve the accuracy of the evaluation on the total PA levels occurring in (herbal) teas and the associated health risks.

It Is well accepted that the potency to induce toxicity may be different from one type of PA to another due to distinct metabolisms and the toxic effects of PA metabolites. To approach the improved accuracy of the risk assessment due to the exposure, we applied the REP factors for each individual PA that were analyzed and obtained the REP-corrected PA levels. By doing so, we found that the risk assessment for several teas was significantly affected by REP correction. For example, the MOE results indicated that a daily intake of lungwort and the consumption of borage for two weeks a year during a lifetime may pose a health risk, while, by REP correction, the same regime of tea consumption would be of no concern (Figure 1). It should be noticed that the interim REP factors used in this study were derived from the genotoxicity data and did not take some physiological conditions into account, e.g., the tumor formation and in vivo toxicokinetics [12]. This may compromise the accuracy of the risk assessment to some extent when using these REP values. Preferably, the REP factors used for the combined exposure to PAs should be derived from in vivo carcinogenicity potencies, which actually are largely lacking so far. In support of this notion, the Joint FAO/WHO Expert Committee on Food Additives (JECFA) and ESFA considered that the existing data are not sufficient to identify REPs for different PAs [20,26]. Hence, more researches aiming for actual carcinogenicity data that are capable of deriving REP factors for a large set of PAs should be fully encouraged in the future.

To facilitate the risk management for PAs in botanicals and botanical preparations, several organizations have established the regulation to define a maximum daily use and TDI for PA levels. For example, the BfR in Germany and RIVM in the Netherlands proposed a maximum limit for intake of PAs with 0.1 µg/day for a long-term (over six weeks) exposure scenario [24,25]. In the present study, the intake of PAs resulted from the daily consumption of nine types of (herbal) teas that exceeded the maximum limit set by the BfR and RIVM, even after REP correction (Table 2). It should be pointed out that an intake of PAs at 1 µg/day for a lifetime by a 70 kg person would result in an MOE of 16,600, which provides a sufficient safety margin. With respect to the non-cancer effects of PAs, a NOAEL of 0.01 mg/kg bw/day for hepatocyte cytomegaly was derived based on a long-term rat study [18,27]. According to that study and considering the safety factors, the RIVM provided a TDI of 0.1 µg/kg bw/day to indicate an exposure level of PAs that may cause non-carcinogenic effects. From a view of mechanism of action, the occurrence of pyrrole-protein adducts was thought to be the primary cause for PA-induced liver damage, as manifested in both humans and rodents in vivo studies [28–33]. Based on the REP-corrected EDIs calculated in our study, consuming one cup of tephroseris tea daily could be likely to induce non-cancer toxicity to human health. Altogether, our data

suggest that the daily consumption of tephroseris tea may pose both carcinogenic and non-carcinogenic risks to human health, and thus a risk management may be needed.

It should be noted that multiple s"udie' have been done with regards to risk assessment for PAs in (herbal) tea infusions. In 2017, the EFSA Panel on Contaminants in the Food Chain (CONTAM Panel) assessed the risks related to the presence of PAs in tea infusions as well as the other PA-containing foodstuff [20]. To ensure the actuality and robustness of EDI and MOE values for different age groups of the population, the CONTAM Panel employed at least six dietary surveys and over 60 observations per age group, as highly suggested before [34]. With the well-defined consumption survey data, the Panel was able to derive mean and the 95th percentile values of EDI and MOE for different types of teas consumed by the adult (referring to adults, the elderly and very elderly) and young (infants, toddlers and other children) population. For example, based on the chronic mean exposure levels, MOE values were ranged from 4300 to above 1,000,000 and from 1000 to over 1,000,000 for the adult and young population, respectively [20]. In this study, we mainly focused on the individual MOEs for (herbal) teas, assuming that one cup of tea per day is representative of most common behavior and there is no additional exposure to PAs from any other sources. One could argue that our approach may tend to underestimate the intake amounts of PAs and the related risks, since individuals may consume more (herbal) teas and/or add honey, a foodstuff that generally contains abundant PAs [34–36]. Indeed, apart from four teas that may raise a concern, the daily consumption of two cups of chamomile tea and three cups of rooibos tea during a lifetime would result in an MOE value lower than 10,000 based on the measured PA levels in this study (data are not shown). We did not include the young population in the risk assessment for a life-time exposure of PAs from (herbal) tea intake, as we argue that there is an overestimation when considering the fact that their body weights are remarkably increasing before they reach adulthood. It is also worthwhile to mention that we adopted the $BMDL_{10}$ of riddelliine for the MOE calculation, which agrees with the proposal by the CONTAM Panel, resulting in additionally increased MOE values by a factor of 3.4 compared to that that for lasiocarpine of 70 µg/kg bw/day in previous studies [14,15,20,37,38]. Since the MOE approach was proposed by the EFSA in 2005, this approach has been either employed to perform a risk assessment for (herbal) teas or for comparison with the other methods [15,20,39–42].

It is challenging to perform a risk assessment for the combined exposure to PAs due to the intake of different types of (herbal) teas and other PA sources. For instance, a risk assessment report has shown that there are a group of subjects with high PA exposure due to the consumption of PA-containing teas and honey [20]. In addition, herb medicines, which generally contain a large amount of PAs, are used in a group of patients or during a specific period [21,43,44]. The evaluation of more complex scenarios, such as a shorter-than-lifetime exposure, is also a challenging issue in the field of risk assessment. It should be acknowledged that a dedicated survey on the consumption habits of (herbal) teas by the average population and by the 95th percentile population (heavy consumers) should be conducted and will contribute to risk assessment for the exposure to PAs.

5. Conclusions

In the present study, a comprehensive set of PAs in 21 types of (herbal) teas were analyzed using LC-MS/MS and the total PA levels were corrected by the REP factors for each PA. Based on these data, the risk assessment for (herbal) teas was performed using the MOE approach, assuming a daily consumption of one cup of tea. Most of the tea samples (92.5%) were detected with PAs. The measured total PA levels were ranged from 13.4 to 286,682.2 µg/kg d.m., while the levels were decreased by REP correction, ranging from 1.3 to 286,648.3 µg/kg d.m.. Senkirkine plus its isomer neosenkirkine were the dominant PAs in most of the (herbal) teas which were derived from PA-containing plants, while echinatine, retrorsine, integerrimine, senecionine and their *N*-ox isomers were the major PAs detected in the non-PA producing teas. In general, the PA levels in PA-producing plant-derived teas were higher than those from non-PA producing plants. Hence, efforts

should be made to reduce or avoid the use of raw materials from PA-producing plants as tea components in terms of controlling PA intake.

The MOEs for PAs due to the intake of (herbal) teas for a life-time and during a short-term period of two weeks per year were calculated using the $BMDL_{10}$ of riddelliine as the new PoD and 70 kg for the estimated adult body weight, amounting to values ranging from 29 to >1,000,000 and from 725 to >1,000,000, respectively. These values were increased by REP correction in most of the (herbal) teas. Despite this, our data indicate that daily consumption of tephroseris, borage and lemon balm (melissa) tea during a lifetime may raise a concern. In addition, shorter-than-lifetime exposure due to an intake of tephroseris tea would be a health concern and may pose a potential non-carcinogenic risk. Therefore, a priority for a risk management of tephroseris tea should be warranted.

To our best knowledge, this is the first study that applied the REP factors for risk assessment for PA exposure from (herbal) teas. In addition, 68 individual 1,2-unsaturated PAs were included to improve the accuracy of the assessment on associated health risks. The number of the analyzed PAs in our study is higher than the requirement of the ESFA as well as of that in the other studies [2,3,13,42,45,46]. On the other hand, there were some limitations in this study. For example, the lack of sufficient dietary survey data regarding tea consumption for different age population and in different scenarios leads to a compromised evaluation on the actual risks. Additionally, despite that applying Haber's rule may provide a reasonable first approach for an MOE-based risk assessment for a shorter-than-lifetime exposure, this approach awaits to be validated [21]. Nevertheless, the results of the current study present the need for the development of a widely accepted method for assessing the risks of botanicals and botanical preparations containing genotoxic and carcinogenic compounds during a shorter-than-lifetime exposure.

References

1. Griffin, C.T.; Danaher, M.; Elliott, C.T.; Glenn Kennedy, D.; Furey, A. Detection of Pyrrolizidine Alkaloids in Commercial Honey Using Liquid Chromatography-Ion Trap Mass Spectrometry. *Food Chem.* **2013**, *136*, 1577–1583. [CrossRef]
2. Bodi, D.; Ronczka, S.; Gottschalk, C.; Behr, N.; Skibba, A.; Wagner, M.; Lahrssen-Wiederholt, M.; Preiss-Weigert, A.; These, A. Determination of Pyrrolizidine Alkaloids in Tea, Herbal Drugs and Honey. *Food Addit. Contam. Part Chem. Anal. Control Expo. Risk Assess.* **2014**, *31*, 1886–1895. [CrossRef] [PubMed]
3. EFSA, E.F.S. Dietary Exposure Assessment to Pyrrolizidine Alkaloids in the European Population. *EFSA J.* **2016**, *14*, e04572. [CrossRef]
4. Garcia-Alvarez, A.; Egan, B.; de Klein, S.; Dima, L.; Maggi, F.M.; Isoniemi, M.; Ribas-Barba, L.; Raats, M.M.; Meissner, E.M.; Badea, M.; et al. Usage of Plant Food Supplements across Six European Countries: Findings from the PlantLIBRA Consumer Survey. *PLoS ONE* **2014**, *9*, e92265. [CrossRef] [PubMed]
5. Mohabbat, O.; Younos, M.S.; Merzad, A.A.; Srivastava, R.N.; Sediq, G.G.; Aram, G.N. An Outbreak of Hepatic Veno-Occlusive Disease in North-Western Afghanistan. *Lancet Lond. Engl.* **1976**, *2*, 269–271. [CrossRef]
6. Tandon, B.N.; Tandon, H.D.; Tandon, R.K.; Narndranathan, M.; Joshi, Y.K. An Epidemic of Veno-Occlusive Disease of Liver in Central India. *Lancet Lond. Engl.* **1976**, *2*, 271–272. [CrossRef]
7. Kumana, C.R.; Ng, M.; Lin, H.J.; Ko, W.; Wu, P.C.; Todd, D. Herbal Tea Induced Hepatic Veno-Occlusive Disease: Quantification of Toxic Alkaloid Exposure in Adults. *Gut* **1985**, *26*, 101–104. [CrossRef]

8.   Roulet, M.; Laurini, R.; Rivier, L.; Calame, A. Hepatic Veno-Occlusive Disease in Newborn Infant of a Woman Drinking Herbal Tea. *J. Pediatr.* **1988**, *112*, 433–436. [CrossRef]

9.   Prakash, A.S.; Pereira, T.N.; Reilly, P.E.; Seawright, A.A. Pyrrolizidine Alkaloids in Human Diet. *Mutat. Res.* **1999**, *443*, 53–67. [CrossRef]

10.   Sperl, W.; Stuppner, H.; Gassner, I.; Judmaier, W.; Dietze, O.; Vogel, W. Reversible Hepatic Veno-Occlusive Disease in an Infant after Consumption of Pyrrolizidine-Containing Herbal Tea. *Eur. J. Pediatr.* **1995**, *154*, 112–116. [CrossRef]

11.   Schulz, M.; Meins, J.; Diemert, S.; Zagermann-Muncke, P.; Goebel, R.; Schrenk, D.; Schubert-Zsilavecz, M.; Abdel-Tawab, M. Detection of Pyrrolizidine Alkaloids in German Licensed Herbal Medicinal Teas. *Phytomed. Int. J. Phytother. Phytopharm.* **2015**, *22*, 648–656. [CrossRef] [PubMed]

12.   Merz, K.-H.; Schrenk, D. Interim Relative Potency Factors for the Toxicological Risk Assessment of Pyrrolizidine Alkaloids in Food and Herbal Medicines. *Toxicol. Lett.* **2016**, *263*, 44–57. [CrossRef] [PubMed]

13.   Mulder, P.P.J.; Sánchez, P.L.; These, A.; Preiss-Weigert, A.; Castellari, M. Occurrence of Pyrrolizidine Alkaloids in Food. *EFSA Support. Publ.* **2015**, *12*, 859E. [CrossRef]

14.   BfR (Bundesinstitut für Risikobewertung). *Pyrrolizidine Alkaloids in Herbal Teas and Teas*; No. 018/2013; BfR Opinion: Berlin, German, 5 July 2013.

15.   Chen, L.; Mulder, P.P.J.; Louisse, J.; Peijnenburg, A.; Wesseling, S.; Rietjens, I.M.C.M. Risk Assessment for Pyrrolizidine Alkaloids Detected in (Herbal) Teas and Plant Food Supplements. *Regul. Toxicol. Pharmacol. RTP* **2017**, *86*, 292–302. [CrossRef] [PubMed]

16.   EFSA. Opinion of the Scientific Committee on a Request from EFSA Related to A Harmonised Approach for Risk Assessment of Substances Which Are Both Genotoxic and Carcinogenic. *EFSA J.* **2005**, *3*, 282. [CrossRef]

17.   National Toxicology Program. Bioassay of Lasiocarpine for Possible Carcinogenicity. *Natl. Cancer Inst. Carcinog. Techical Rep. Ser.* **1978**, *39*, 1–66.

18.   National Toxicology Program. Toxicology and Carcinogenesis Studies of Riddelliine (CAS No. 23246-96-0) in F344/N Rats and B6C3F1 Mice (Gavage Studies). *Natl. Toxicol. Program Techical Rep. Ser.* **2003**, *508*, 1–280.

19.   EFSA (CONTAM), E.P. on C. in the F. Scientific Opinion on the Risks to Animal and Public Health and the Environment Related to the Presence of Nickel in Feed. *EFSA J.* **2015**, *13*, 4074. [CrossRef]

20.   EFSA Panel on Contaminants in the Food Chain (CONTAM); Knutsen, H.K.; Alexander, J.; Barregård, L.; Bignami, M.; Brüschweiler, B.; Ceccatelli, S.; Cottrill, B.; Dinovi, M.; Edler, L.; et al. Risks for Human Health Related to the Presence of Pyrrolizidine Alkaloids in Honey, Tea, Herbal Infusions and Food Supplements. *EFSA J. Eur. Food Saf. Auth.* **2017**, *15*, e04908. [CrossRef]

21.   Chen, L.; Mulder, P.P.J.; Peijnenburg, A.; Rietjens, I.M.C.M. Risk Assessment of Intake of Pyrrolizidine Alkaloids from Herbal Teas and Medicines Following Realistic Exposure Scenarios. *Food Chem. Toxicol. Int. J. Publ. Br. Ind. Biol. Res. Assoc.* **2019**, *130*, 142–153. [CrossRef]

22.   Chou, M.W.; Wang, Y.-P.; Yan, J.; Yang, Y.-C.; Beger, R.D.; Williams, L.D.; Doerge, D.R.; Fu, P.P. Riddelliine N-Oxide Is a Phytochemical and Mammalian Metabolite with Genotoxic Activity That Is Comparable to the Parent Pyrrolizidine Alkaloid Riddelliine. *Toxicol. Lett.* **2003**, *145*, 239–247. [CrossRef]

23.   EFSA. Guidance on Selected Default Values to Be Used by the EFSA Scientific Committee, Scientific Panels and Units in the Absence of Actual Measured Data. *EFSA J.* **2012**, *10*, 2579. [CrossRef]

24.   Bekanntmachung über die Zulassung und Registrierung von Arzneimitteln. *Transfus. Med. Hemother.* **1987**, *14*, 131–132. [CrossRef]

25.   Beatrix, W. Besluit van 19 januari 2001, houdende vaststelling van het Warenwetbesluit Kruidenpreparaten. *Staatsblad Van Het Koninkr. Der Ned.* **2001**, *56*, 12.

26.   JECFA (World Health Organization: Joint FAO/WHO Expert Committee on Food Additives). *Summary and Conclusions*; Issued 6 July 2015, JECFA/80/SC; JECFA: Geneva, Switzerland, 2015.

27.   COT (Committee on Toxicity of Chemicals in Food, Consumer Products and the Environment). *COT Statement on Pyrrolizidine Alkaloids in Food*; 2008/06; COT: London, UK, 2008.

28.   Chen, T.; Mei, N.; Fu, P.P. Genotoxicity of Pyrrolizidine Alkaloids. *J. Appl. Toxicol. JAT* **2010**, *30*, 183–196. [CrossRef] [PubMed]

29.   Edgar, J.A.; Molyneux, R.J.; Colegate, S.M. Pyrrolizidine Alkaloids: Potential Role in the Etiology of Cancers, Pulmonary Hypertension, Congenital Anomalies, and Liver Disease. *Chem. Res. Toxicol.* **2015**, *28*, 4–20. [CrossRef]

30.   Fu, P.P. Pyrrolizidine Alkaloids: Metabolic Activation Pathways Leading to Liver Tumor Initiation. *Chem. Res. Toxicol.* **2017**, *30*, 81–93. [CrossRef]

31.   Zhu, L.; Xue, J.; Xia, Q.; Fu, P.P.; Lin, G. The Long Persistence of Pyrrolizidine Alkaloid-Derived DNA Adducts in Vivo: Kinetic Study Following Single and Multiple Exposures in Male ICR Mice. *Arch. Toxicol.* **2017**, *91*, 949–965. [CrossRef]

32.   Yang, M.; Ruan, J.; Gao, H.; Li, N.; Ma, J.; Xue, J.; Ye, Y.; Fu, P.P.-C.; Wang, J.; Lin, G. First Evidence of Pyrrolizidine Alkaloid N-Oxide-Induced Hepatic Sinusoidal Obstruction Syndrome in Humans. *Arch. Toxicol.* **2017**, *91*, 3913–3925. [CrossRef]

33.   Yang, X.; Li, W.; Sun, Y.; Guo, X.; Huang, W.; Peng, Y.; Zheng, J. Comparative Study of Hepatotoxicity of Pyrrolizidine Alkaloids Retrorsine and Monocrotaline. *Chem. Res. Toxicol.* **2017**, *30*, 532–539. [CrossRef]

34.   EFSA. Use of the EFSA Comprehensive European Food Consumption Database in Exposure Assessment. *EFSA J.* **2011**, *9*, 2097. [CrossRef]

35.   Kempf, M.; Reinhard, A.; Beuerle, T. Pyrrolizidine Alkaloids (PAs) in Honey and Pollen-Legal Regulation of PA Levels in Food and Animal Feed Required. *Mol. Nutr. Food Res.* **2010**, *54*, 158–168. [CrossRef] [PubMed]

36. Brugnerotto, P.; Seraglio, S.K.T.; Schulz, M.; Gonzaga, L.V.; Fett, R.; Costa, A.C.O. Pyrrolizidine Alkaloids and Beehive Products: A Review. *Food Chem.* **2021**, *342*, 128384. [CrossRef]

37. BfR (Bundesinstitut für Risikobewertung). *Analytik und Toxizität von Pyrrolizidinalkaloiden Sowie Eine Einschätzung des Gesundheitlichen Risikos Durch Deren Vorkommen in Honig*; Stellungnahme Nr. 038/2011 des BfR vom 11; BfR Opinion: Berlin, German, 2011; ergänzt am 21 Januar 2013.

38. BfR (Bundesinstitut für Risikobewertung). *Pyrrolizidinalkaloide Gehalte in Lebensmitteln Sollen Nach Wie vor so Weit Wie Möglich Gesenkt Werden*; Stellungnahme Nr. 030/2016 des BfR vom 28; BfR Opinion: Berlin, German, 2016.

39. Mädge, I.; Cramer, L.; Rahaus, I.; Jerz, G.; Winterhalter, P.; Beuerle, T. Pyrrolizidine Alkaloids in Herbal Teas for Infants, Pregnant or Lactating Women. *Food Chem.* **2015**, *187*, 491–498. [CrossRef] [PubMed]

40. Habs, M.; Binder, K.; Krauss, S.; Müller, K.; Ernst, B.; Valentini, L.; Koller, M. A Balanced Risk-Benefit Analysis to Determine Human Risks Associated with Pyrrolizidine Alkaloids (PA)—The Case of Tea and Herbal Infusions. *Nutrients* **2017**, *9*, 717. [CrossRef] [PubMed]

41. Mulder, P.P.J.; López, P.; Castellari, M.; Bodi, D.; Ronczka, S.; Preiss-Weigert, A.; These, A. Occurrence of Pyrrolizidine Alkaloids in Animal- and Plant-Derived Food: Results of a Survey across Europe. *Food Addit. Contam. Part Chem. Anal. Control Expo. Risk Assess.* **2018**, *35*, 118–133. [CrossRef]

42. Dusemund, B.; Nowak, N.; Sommerfeld, C.; Lindtner, O.; Schäfer, B.; Lampen, A. Risk Assessment of Pyrrolizidine Alkaloids in Food of Plant and Animal Origin. *Food Chem. Toxicol. Int. J. Publ. Br. Ind. Biol. Res. Assoc.* **2018**, *115*, 63–72. [CrossRef]

43. Bunchorntavakul, C.; Reddy, K.R. Review Article: Herbal and Dietary Supplement Hepatotoxicity. *Aliment. Pharmacol. Ther.* **2013**, *37*, 3–17. [CrossRef]

44. Zhu, L.; Zhang, C.-Y.; Li, D.-P.; Chen, H.-B.; Ma, J.; Gao, H.; Ye, Y.; Wang, J.-Y.; Fu, P.P.; Lin, G. Tu-San-Qi (Gynura Japonica): The Culprit behind Pyrrolizidine Alkaloid-Induced Liver Injury in China. *Acta Pharmacol. Sin.* **2021**, *42*, 1212–1222. [CrossRef]

45. Shimshoni, J.A.; Duebecke, A.; Mulder, P.P.J.; Cuneah, O.; Barel, S. Pyrrolizidine and Tropane Alkaloids in Teas and the Herbal Teas Peppermint, Rooibos and Chamomile in the Israeli Market. *Food Addit. Contam. Part Chem. Anal. Control Expo. Risk Assess.* **2015**, *32*, 2058–2067. [CrossRef]

46. Kaltner, F.; Stiglbauer, B.; Rychlik, M.; Gareis, M.; Gottschalk, C. Development of a Sensitive Analytical Method for Determining 44 Pyrrolizidine Alkaloids in Teas and Herbal Teas via LC-ESI-MS/MS. *Anal. Bioanal. Chem.* **2019**, *411*, 7233–7249. [CrossRef] [PubMed]

Effect of Radiant Catalytic Ionization and Ozonation on *Salmonella* spp. on Eggshells

Katarzyna Grudlewska-Buda [1], **Natalia Wiktorczyk-Kapischke** [1], **Ewa Wałecka-Zacharska** [2], **Joanna Kwiecińska-Piróg** [1], **Grzegorz Gryń** [3], **Karolina Jadwiga Skowron** [4], **Jakub Korkus** [2], **Eugenia Gospodarek-Komkowka** [1], **Jarosław Bystroń** [2], **Anna Budzyńska** [1], **Stefan Kruszewski** [5], **Zbigniew Paluszak** [6], **Małgorzata Andrzejewska** [7], **Monika Wilk** [1] and **Krzysztof Skowron** [1,*]

[1] Department of Microbiology, Nicolaus Copernicus University in Toruń, Ludwik Rydygier Collegium Medicum, 85-094 Bydgoszcz, Poland
[2] Department of Food Hygiene and Consumer Health, Wrocław University of Environmental and Life Sciences, 50-375 Wrocław, Poland
[3] Plant Breeding and Acclimatization Institute–National Research Institute, 85-090 Bydgoszcz, Poland
[4] Institute of Telecommunications and Computer Science, Jan and Jędrzej Śniadecki University of Technology in Bydgoszcz, 85-094 Bydgoszcz, Poland
[5] Biophysics Department, Nicolaus Copernicus University in Toruń, Ludwik Rydygier Collegium Medicum, 85-067 Bydgoszcz, Poland
[6] Department of Microbiology and Food Technology, Jan and Jędrzej Śniadecki University of Technology in Bydgoszcz, 85-094 Bydgoszcz, Poland
[7] Department of Hygiene, Epidemiology, Ergonomy and Postgraduate Education, Ludwik Rydygier Collegium Medicum in Bydgoszcz, Nicolaus Copernicus University in Toruń, 95-094 Bydgoszcz, Poland
[*] Correspondence: skowron238@wp.pl

Abstract: Three *Salmonella enterica* strains were used in the study (serovars: *S. enteritidis*, *S. typhimurim* and *S. virchow*). This study evaluated the efficacy of radiant catalytic ionization (RCI) and ozonation against *Salmonella* spp. on eggshell (expressed as log CFU/egg). The egg surface was contaminated three different bacterial suspension (10^3 CFU/mL, 10^5 CFU/mL and 10^8 CFU/mL) with or without poultry manure. Experiments were conducted at 4 °C and 20 °C in three different time period: 30 min, 60 min and 120 min. Treatment with RCI reduced *Salmonella* numbers from 0.26 log CFU/egg in bacterial suspension 10^8 CFU/mL, 4 °C and 20 °C, with manure for 30 min to level decrease in bacteria number below the detection limit (BDL) in bacterial suspension 10^5 CFU/mL, 20 °C, with or without manure for 120 min. The populations of *Salmonella* spp. on eggs treated by ozonizer ranged from 0.20 log CFU/egg in bacteria suspension 10^8 CFU/mL, 20 °C, with manure for 30 min to 2.73 log CFU/egg in bacterial suspension 10^5 CFU/mL, 20 °C, with manure for 120 min. In all treatment conditions contamination with poultry manure decrease effectiveness the RCI and ozonation. In summary, RCI technology shows similar effectiveness to the ozonation, but it is safer for poultry plant workers and consumers.

Keywords: eggs; *Salmonella* spp.; radiant catalytic ionization; ozonation; disinfection

1. Introduction

For many years *Salmonella* spp. has been one of the most important foodborne pathogens. The European Food Safety Agency (EFSA), in 2018, reported 91,857 confirmed cases of salmonellosis in the European Union (EU). The most prevalent serovars were: *S. enteritidis*, *S. typhimurium* and *S.* Infantis [1]. The significant source of human infections are eggs and egg products, which in 2018 accounted for 45.6% of salmonellosis foodborne outbreaks [1]. A multi-country outbreak of *S. enteritidis*, linked to eggs, has been ongoing in the EU for several years. From 1 February 2017 to 14 January 2020, 15 EU countries reported 656 confirmed cases and 202 probable cases [2].

There are two possible routes of bacterial contamination of eggs shell: either vertically or horizontally. Horizontal transmission occurs during the laying of eggs and depending on the eggshell architecture and bacterial serotype. Vertical transmission can originate from the hen reproductive tract. *S. enteritidis* is usually transmitted vertically, while *S.* Infantis contaminates the egg via a horizontal route [3]. Minor flaws of the eggshell favor bacterial colonization and transmission [4]. Bacterial contamination of eggshells depends on various environmental factors such as the presence of food, water, feces, dust, litter, the type of birds' housing system, the laying rate and/or cuticle state [5]. The thickness of particular layers, pore distribution, ultrastructure and transparency affect the eggshell penetration [6]. Furthermore, workers, domestic animals, rodents, contaminated feed, litter and water [7] or food production environment (transfer belt, packaging materials) can be the source of eggs contamination [8].

Cleaning and disinfection are the most common methods used to remove microbiological contamination from the egg surface [9]. Cleaning with chemical agents, e.g., alkaline solutions or sodium hydroxide removes the cuticle layer resulting in a visually clean egg [10]. Cleaning significantly reduced the number of Enterobacterales bacteria [11]. Regularly applied disinfectants include agents based on chlorine, iodine, hydrogen peroxide, ozone and quaternary ammonium compounds [12].

Methods of egg disinfection must limit the growth of microorganisms outside the shell and limit the penetration of microorganisms into the inside of the egg [13]. The ozonation may use for the disinfection of hatcheries, eggs and poultry carcasses. Ozone has a good bactericidal effect and causes a quick inactivation of microorganisms. The effectiveness of ozonation increases with the extension of the exposure time of the eggs. It is related to the increase in ozone concentration over time [14]. The hydrophobic protein layer (cuticle) hinders bacterial penetration. This thin outermost layer desiccates immediately after eggs laying and protects eggs against bacterial invasion and water loss [15].

Researchers are still searching for innovative technologies allowing the eradication of pathogens from the egg surface. Such methods should eliminate microbiological contaminants ensuring egg freshness and consumer safety. New technologies include physical and chemical processes such as high hydrostatic pressure, ionizing radiation, ultrasounds, pulsed electric field, UV radiation and plasma, which inactivate microorganisms at ambient or sublethal temperatures [16]. Additionally, some preparations are applied directly to the eggshell, e.g., colloidal silver, substances of natural origin (propolis) or plant extracts such as thyme and cinnamon, allicin, oregano oil or red grapefruit juice [17]. An innovative solution, successfully applied in the air purification system, is radiant catalytic ionization (RCI) [18]. This technology uses the photocatalysis phenomenon in the presence of UV radiation and photocatalysts, such as TiO_2, which form a hydrophilic coating of the matrix surface in the RCI module [19]. The RCI cell consists of matrices forming a honeycomb structure. The coating of the dies also includes clusters of other elements such as rhodium, silver and copper. On the opposite site a broad-spectrum UV light source of 100 and 367 nm is located [19,20]. Catalytic oxidation, stimulated by UV radiation, at the boundary of heterogeneous phases (gas-solid), leads to reactive oxygen forms generation (ROS): hydroxyl radicals ($OH^\bullet$), hydrogen peroxide (H_2O_2) and superoxide anion (O^{2-}). The total number of generated ions is about 5.0×10^4 ions $\times$ cm^{-3} of air [21]. ROS interact with DNA, lipids and proteins, contributing to the destruction of genetic material, lipid peroxidation and amino acid degradation [22–24].

To date, RCI has been used primarily in the air purification industry. The method successfully eliminated biofilm and planktonic cells from various surfaces, indicating its applicability for disinfecting food processing surfaces and healthcare equipment [21]. Studies by Ortega et al. [23] and Skowron et al. [25] have demonstrated the utility of using RCI against various pathogens, including *Salmonella* spp. from different surfaces. The discussed technology has also proven effective when removing biofilms from abiotic surfaces contaminated with food pulp [21] and from vegetable and fruit surfaces [22], suggesting its possible application in food disinfection.

This study aimed to assess and compare the efficacies of radiant catalytic ionization (RCI) and ozonation against *Salmonella* spp. on the eggshell, with different initial inocula, exposure time and processing temperature.

2. Materials and Methods

2.1. Bacterial Strains

The study was conducted on 3 *Salmonella enterica* strains isolated in 2017 from poultry meat, representing different serovars: *S. enteritidis*, *S. typhimurim* and *S. virchow* (most commonly identified salmonellosis serovars in Poland and Europe). Study strains represented different phage types (DTs) (*S. enteritidis*–DT8 (commonly associated with consumption of eggs), *S. typhimurim*–DT2), for *S.* Virchow phage type could not be determined.

2.2. Eggshells Contamination with Salmonella spp.

Fresh eggs of class M (medium eggs, with weight ranging from 53 to 63 g) were wiped with a fine damp cloth to remove visible soil. Next, eggs were sterilized with a high-energy electron beam (20 kGy) in the Institute of Nuclear Chemistry and Technology in Warsaw, Poland. The efficacy of disinfection was confirmed by taking swabs from the egg surface and plating them onto Columbia Agar with 5% blood sheep (bioMérieux, Marcy-l'Etoile, France) (37 °C, 24 h).

This study used bacterial suspensions of three different densities, 10^8 CFU/mL (ranged from 8.43 log CFU/mL to 8.60 log CFU/mL), 10^5 CFU/mL (ranged from 5.68 log CFU/mL to 5.76 log CFU/mL) and 10^3 CFU/mL (ranged from 2.70 log CFU/mL to 2.83 log CFU/mL), representing heavy, medium and light contamination, respectively. This step was used to establish the initial number of bacteria in prepared suspensions with which the eggs were contaminated, therefore the number is referred to as CFU/mL.

The 0.5 McFarland's bacterial suspension (8.43 log to 8.60 log CFU/mL) was prepared as 10^8 CFU/mL (initial bacterial contamination level). Then, this initial suspension was diluted to obtain the inoculum of 10^3 or 10^5 CFU/mL. Another variant of the experiment was the contamination of the egg with organic pollution. The microbial suspensions were mixed in a volumetric ratio (v/v) 1:1 with fresh poultry manure (from a hen farm in Poland, collected in March 2021). Poultry manure was stored at 4 °C until testing.

Each side of the egg surface was contaminated with hundred drops (5 µL each) of bacterial suspension and dried (20 min in a laminar chamber (1 m³) per one side of the egg). The drops did not flow freely down the egg. Experiments were conducted at 4 °C (fridge, standard size) and 20 °C (hermetic chamber, 1 m³). We used 324 eggs for each strain, including all variants and repetitions.

Figure 1 shows the design of the experiment.

Figure 1. Scheme of experiment variants.

2.3. Exposure of Salmonella spp. Contaminated Eggshells to Radiant Catalytic Ionization and Ozonation

The eggs contaminated with bacterial suspension were placed on a wire stand (which allowed the device to operate evenly on the egg) at a distance of 0.5 m from Induct 750 ActiveTek apparatus (Kielce, Poland) (not generating ozone), Dawid 2 ozonizer (ECS Piotr Paruszewski, Ostrzeszów, Poland) (generating 10 g/h O_3) or the fan (control treatment) and exposed for 30 min, 60 min or 120 min to RCI, ozone or the flowing air, respectively. To determine the number of bacteria reisolated from eggshells, eggs were placed in sterile plastic containers with closures filled with 100 mL of sterile saline (Avantor, Gliwice, Poland). Next, they were sonicated (Ultrasonic DU-4 sonicator, Nickel-Electro, Oldmixon, Great Britain) for 5 min and shaken (400 rpm) for 10 min (benchtop shaker). Three non-treated with RCI or ozone eggs allowed determining the initial number of bacteria reisolated after contamination of eggshells with tested suspensions. After sonication, serial 10-fold dilutions in sterile saline for each bacterial suspension obtained after sonication and shaking were prepared. The enumeration was performed on tryptic soy agar (TSA) (bioMerieux). After 24-h incubation at 37 °C the number of colonies per egg was calculated (log CFU/egg) (Figure 2). The procedure included three repetitions for each tested strain and each variant.
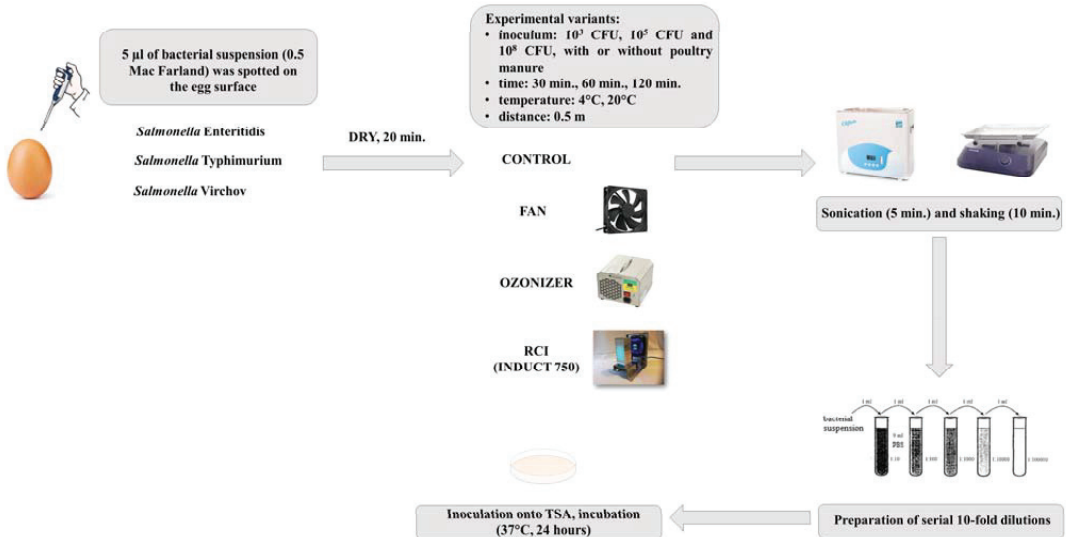
Figure 2. A scheme of experiment procedure.

Decrease in the number of bacteria (DB) (log CFU/egg) after treatment was calculated using the formula: DB = A − B

Where:

A—initial number of bacteria [log CFU/egg];

B—number of bacteria after treatment [log CFU/egg].

2.4. Statistical Analysis

Each experiment was repeated three times. A multivariate ANOVA and the Tukey post-hoc test with Statistica (TIBCO Software Inc., Palo Alto, CA, USA) were performed to determine whether statistical differences existed between different experimental groups. Significance was set at a level of $p \leq 0.05$.

3. Results

In our experiment, differences between strains were not statistically significantly different ($p > 0.05$). Therefore, we decided to average the results for all serovars. Detailed

results regarding the changes of the bacterial number of the tested *Salmonella* spp. serovars in the bacterial suspension of 10^3 CFU/mL, 10^5 CFU/mL and 10^8 CFU/mL were included in the Supplementary Information (Tables S1–S3).

3.1. Effectiveness of Radiant Catalytic Ionization and Ozonation Treatment against Salmonella spp. for Bacterial Suspension of 10^3 CFU/mL

The bacterial number reisolated from the eggshell in the control group (not exposed to any technology) ranged from 1.59 log CFU/egg to 1.67 log CFU/egg, and was not significantly different ($p > 0.05$) (Table 1). After 30 min of exposure, the bacterial number ranged from 0.03 log CFU/egg (RCI, 20 °C, without poultry manure) to 0.69 log CFU/egg (ozonizer, 20 °C, with poultry manure). Statistically significant differences were observed in all bacterial contamination level (4 °C with poultry manure, 20 °C without poultry manure, 20 °C with poultry manure) (Table 1). The 60-min and 120-min application of ozonizer and RCI-emitter decreased the bacteria number to detection limit, which is <100 CFU/egg.

Table 1. The final number of *Salmonella* spp. on eggshells contaminated with bacterial suspension of 10^3 CFU/mL with or without the addition of poultry manure.

Variant		Temperature 4 °C		Temperature 20 °C	
		PM (−)	PM (+)	PM (−)	PM (+)
		Average [log CFU/egg] (±STD) *	Average [log CFU/egg] (±STD)	Average [log CFU/egg] (±STD)	Average [log CFU/egg] (±STD)
Control		1.59 [h] (±0.09)	1.67 [h] (±0.09)	1.59 [h] (±0.09)	1.67 [h] (±0.09)
30 min [†]	Fan	0.58 [e,f] (±0.02)	0.96 [g] (±0.02)	0.57 [d,e,f] (±0.00)	0.98 [g] (±0.02)
	Ozonizer	0.34 [b,c,d,e] (±0.04)	0.61 [e,f] (±0.02)	0.41 [c,d,e,f] (±0.02)	0.69 [f,g] (±0.01)
	RCI	0.09 [a,b] (±0.07)	0.28 [a,b,c,d] (±0.05)	0.03 [a] (±0.09)	0.20 [a,b,c] (±0.06)

*—standard deviation, [†]—time of action; PM (+)—with poultry manure; PM (−)—without poultry manure CFU–colony forming units; [a,b,c,…]—values marked with different letters differ statistically significant, applies to the entire table.

Treatment with RCI reduced bacteria number ranged from 1.39 log CFU/egg (30 min, 4 °C, with poultry manure) to level decrease in bacteria number below the detection limit (BDL) (60 min and 120 min, 4 °C and 20 °C, without and with poultry manure). For ozonizer reduction in the number of bacteria ranged from 0.98 log CFU/egg (30 min, 20 °C, with poultry manure) to BDL (60 min and 120 min, 4 °C and with poultry manure, 20 °C and without poultry manure, 20 °C and with poultry manure) (Table 2).

Table 2. Decrease in the number of bacteria [log CFU/egg] on eggshells after treatment.

Variant			Temperature 4 °C		Temperature 20 °C	
			PM (−)	PM (+)	PM (−)	PM (+)
Bacterial suspension 10^3 CFU	30 min [†]	Fan	1.01 [h,i,j,k,l,ł,m,n]	0.71 [d,e,f,g,h,i]	1.01 [h,i,j,k,l,ł,m,n]	0.69 [c,d,e,f,g,h,i]
		Ozonizer	1.24 [k,l,ł,m,n,o,p]	1.05 [h,i,j,k,l,ł,m,n]	1.17 [i,j,k,l,ł,m,n,o]	0.98 [h,i,j,k,l,ł,m]
		RCI	1.50 [n,o,p,r,s]	1.39 [ł,m,n,o,p,r]	1.56 [o,p,r,s,t]	1.47 [m,n,o,p,r,s]
	60 min	Fan	BDL *	BDL	BDL	BDL
		Ozonizer	BDL	BDL	BDL	BDL
		RCI	BDL	BDL	BDL	BDL
	120 min	Fan	BDL	BDL	BDL	BDL
		Ozonizer	BDL	BDL	BDL	BDL
		RCI	BDL	BDL	BDL	BDL

Table 2. *Cont.*

Variant		Temperature 4 °C		Temperature 20 °C	
		PM (−)	PM (+)	PM (−)	PM (+)
Bacterial suspension 10^5 CFU					
30 min †	Fan	0.38 a,b,c,d,e,f,g	0.13 a,b	0.38 a,b,c,d,e,f,g	0.13 a,b
	Ozonizer	1.12 i,j,k,l,ł,m,n,o	0.28 a,b,c,d,e,f	0.97 a	0.26 a,b,c,d,e
	RCI	1.28 l,ł,m,n,o,p	0.30 a,b,c,d,e,f	1.37 l,m,n,o,p,r	0.32 a,b,c,d,e,f
60 min	Fan	0.76 f,g,h,i,j,k	0.21 a,b,c	0.74 e,f,g,h,i,j	0.21 a,b,c
	Ozonizer	2.00 t,u	0.39 a,b,c,d,e,f,g	1.83 r,s,t,u	1.17 i,j,k,l,ł,m,n,o
	RCI	1.95 s,t,u	0.40 a,b,c,d,e,f,g	2.59 w,x	1.22 j,k,l,ł,m,n,o,p
120 min	Fan	1.70 p,r,s_t,u	0.37 a,b,c,d,e,f,g	1.36 l,m,n,o,p,r	0.36 a,b,c,d,e,f,g
	Ozonizer	2.14 u,w	0.59 b,d,e,f,g,h	2.64 x,y	2.73 y
	RCI	2.15 u,w,x	0.59 b,d,e,f,g,h	BDL	BDL
Bacterial suspension 10^8 CFU					
30 min †	Fan	0.32 a,b,c,d,e,f	0.09 a	0.32 a,b,c,d,e,f	0.09 a
	Ozonizer	0.94 h,i,j,k,l,ł	0.22 a,b,c,d	0.85 g,h,i,j,k,l	0.20 a,b,c
	RCI	0.98 h,i,j,k,l,ł,m	0.26 a,b,c,d,e	1.05 h,i,j,k,l,ł,m,n	0.26 a,b,c,d,e
60 min	Fan	0.60 b,d,e,f,g,h	0.19 a,b,c	0.59 b,d,e,f,g,h	0.19 a,b,c
	Ozonizer	1.34 l,ł,m,n,o,p,r	0.34 a,b,c,d,e,f	1.10 ij,k,l,ł,m,n,o	0.32 a,b,c,d,e,f
	RCI	1.65 o,p,r,s,t,u	0.36 a,b,c,d,e,f,g	2.12 u,w	0.38 a,b,c,d,e,f,g
120 min	Fan	0.98 h,i,j,k,l,ł,m	0.38 a,b,c,d,e,f,g	0.95 h,i,j,k,l,ł	0.39 a,b,c,d,e,f,g
	Ozonizer	1.91 s,t,u,w	0.52 a,b,c,d,e,f,g,h	1.36 l,m,n,o,p,r	0.49 a,b,c,d,e,f,g,h
	RCI	1.87 s,t,u,w	0.51 a,b,c,d,e,f,g,h	3.54 z	0.55 a,b,c,d,e,f,g,h

*—decrease in bacteria number below the detection limit, †—time of action; PM (+)—with poultry manure; PM (−)—without poultry manure CFU–colony forming units; a,b,c,...—values marked with different letters differ statistically significant, applies to the entire table.

The bacterial number after 60 min and 120 min of fan action was 0.00 log CFU/egg. However, a shorter time of exposure (30 min) reduced the number of bacteria from 0.57 log CFU/egg (20 °C and without poultry manure) to 0.98 log CFU/egg (20 °C and with poultry manure). The reduction was significantly different ($p < 0.05$) lower compared to RCI-exposure for the same time in all variants.

3.2. Effectiveness of Radiant Catalytic Ionization and Ozonation Treatment against Salmonella spp. for Bacterial Suspension of 10^5 CFU/mL

The differences in the control group were not statistically significant ($p > 0.05$) (Table 3). The bacterial number reisolated from the eggshell ranged from 2.65 log CFU/egg to 2.75 log CFU/egg. The application of ozonizer and RCI-emitter reduced bacterial number. After 30 min-exposure, the bacterial number ranged from 1.29 log CFU/egg (RCI, 20 °C and without poultry manure) to 2.48 log CFU/egg (ozonizer, 20 °C and with poultry manure). There were no statistically significantly differences between both methods.

After 60 min-exposure, the bacterial number ranged from 0.07 log CFU/egg (RCI, 20 °C and without poultry manure) to 2.36 log CFU/egg (ozonizer, 4 °C and with poultry manure). Statistically significant differences ($p \leq 0.05$) were found between RCI at 20 °C without poultry manure and fan under all conditions, and ozonizer at 4 °C and 20 °C with poultry manure and RCI at 4 °C and 20 °C with poultry manure.

After 120 min. of exposure, the lowest number of *Salmonella* spp. was noted for RCI at 20 °C with or without poultry manure (0.00 log CFU/egg) and for ozonizer at 20 °C with and without poultry manure. These values were statistically different ($p \leq 0.05$) from all methods at 4 °C with poultry manure or fan at 20 °C with poultry manure (Table 3).

For treatment with RCI bacterial number ranged from 0.30 log CFU/egg (30 min, 4 °C, with poultry manure) to BDL (120 min, 20 °C, without and with poultry manure). For ozonizer bacterial reduction ranged from 0.26 log CFU/egg (30 min, 20 °C, with poultry manure) to 2.73 log CFU/egg (120 min, 20 °C, with poultry manure) (Table 2).

Table 3. The final number of *Salmonella* spp. on eggshells contaminated with bacterial suspension of 10^5 CFU/mL with or without the addition of poultry manure.

Variant		Temperature 4 °C		Temperature 20 °C	
		PM (−)	PM (+)	PM (−)	PM (+)
		Average [log CFU/egg] (±STD) *	Average [log CFU/egg] (±STD) *	Average [log CFU/egg] (±STD) *	Average [log CFU/egg] (±STD) *
Control		2.65 [a,b] (±0.21)	2.75 [a] (±0.20)	2.65 [a,b] (±0.21)	2.75 [a] (±0.20)
30 min [†]	Fan	2.27 [a,b,c,d] (±0.17)	2.61 [a,b] (±0.18)	2.28 [a,b,c,d] (±0.17)	2.62 [a,b] (±0.18)
	Ozonizer	1.53 [a,b,c,d,e,f] (±0.10)	2.46 [a,b,c] (±0.17)	1.69 [a,b,c,d,e,f] (±0.11)	2.48 [a,b,c] (±0.17)
	RCI	1.37 [b,c,d,e,f] (±0.08)	2.45 [a,b,c] (±0.17)	1.29 [c,d,e,f,g] (±0.07)	2.43 [a,b,c] (±0.16)
60 min	Fan	1.89 [a,b,c,d,e] (±0.13)	2.54 [a,b,c] (±0.18)	1.91 [a,b,c,d,e] (±0.13)	2.53 [a,b,c] (±0.18)
	Ozonizer	0.66 [e,f,g,h] (±0.01)	2.36 [a,b,c] (±0.16)	0.82 [e,f,g,h] (±0.07)	1.57 [a,b,c,d,e,,f] (±0.16)
	RCI	0.71 [e,f,g,h] (±0.01)	2.35 [a,b,c] (±0.15)	0.07 [g,h] (±0.09)	1.53 [a,b,c,d,e,f] (±0.15)
120 min	Fan	0.96 [d,e,f,g,h] (±0.04)	2.37 [a,b,c] (±0.16)	1.30 [c,d,e,f,g] (±0.07)	2.38 [a,b,c] (±0.16)
	Ozonizer	0.52 [f,g,h] (±0.01)	2.16 [a,b,c,d] (±0.14)	0.01 [g,h] (±0.03)	0.01 [g,h] (±0.05)
	RCI	0.50 [f,g,h] (±0.01)	2.15 [a,b,c,d] (±0.17)	0.00 [h] (±0.00)	0.00 [h] (±0.00)

*—standard deviation, [†]—time of action; PM (+)—with poultry manure; PM (−)—without poultry manure CFU–colony forming units; [a,b,c,...]—values marked with different letters differ statistically significant, applies to the entire table.

The bacterial number after fan action ranged from 0.96 log CFU/egg (120 min, 4 °C, without poultry manure) to 2.62 log CFU/egg (30 min, 20 °C, with poultry manure). Moreover, reduction number of bacteria for the fan were the lowest and ranged from 0.13 log CFU/egg (30 min, 4 °C and 20 °C, with poultry manure) to 1.70 log CFU/egg (120 min, 4 °C, without poultry manure).

3.3. Effectiveness of Radiant Catalytic Ionization and Ozonation Treatment against Salmonella spp. for Bacterial Suspension of 10^8 CFU/mL

The number of reisolated *Salmonella* spp. in the control group ranged from 5.81 log CFU/egg to 5.89 log CFU/egg, but differences were not statistically significant ($p > 0.05$). (Table 4). In all time variants, the number of reisolated bacteria was higher than at the concentration of 10^5 CFU/mL.

Table 4. The final number of *Salmonella* spp. on eggshells contaminated with bacterial suspension of 10^8 CFU/mL with or without the addition of poultry manure.

Variant		Temperature 4 °C		Temperature 20 °C	
		PM (−) Average [log CFU/egg] (±STD) *	PM (+) Average [log CFU/egg] (±STD)	PM (−) Average [log CFU/egg] (±STD)	PM (+) Average [log CFU/egg] (±STD)
Control		5.81 [a,b] (±0.51)	5.89 [a] (±0.50)	5.81 [a,b] (±0.51)	5.89 [a] (±0.50)
30 min [†]	Fan	5.48 [a,b,c,d] (±0.47)	5.80 [a,b] (±0.49)	5.49 [a,b,c,d] (±0.47)	5.79 [a,b] (±0.49)
	Ozonizer	4.86 [f,g,h] (±0.41)	5.67 [a,b,c,d] (±0.48)	4.96 [e,f,g] (±0.42)	5.69 [a,b,c] (±0.48)
	RCI	4.83 [f,g,h] (±0.41)	5.63 [a,b,c,d] (±0.48)	4.75 [f,g,h] (±0.40)	5.63 [a,b,c,d] (±0.48)
60 min	Fan	5.21 [d,e,f] (±0.45)	5.70 [a,b] (±0.48)	5.22 [c,d,e,f] (±0.45)	5.70 [a,b] (±0.48)
	Ozonizer	4.47 [h,i] (±0.37)	5.55 [a,b,c,d] (±0.47)	4.71 [g,h] (±0.40)	5.57 [a,b,c,d] (±0.47)
	RCI	4.16 [i,j] (±0.34)	5.53 [a,b,c,d] (±0.47)	3.69 [j] (±0.29)	5.51 [a,b,c,d] (±0.46)
120 min	Fan	4.83 [f,g,h] (±0.41)	5.51 [a,b,c,d] (±0.46)	4.85 [f,g,h] (±0.41)	5.50 [a,b,c,d] (±0.46)
	Ozonizer	3.90 [j] (±0.32)	5.37 [b,c,d,e] (±0.45)	4.45 [h,i] (±0.37)	5.40 [b,c,d,e] (±0.45)
	RCI	3.93 [j] (±0.32)	5.38 [b,c,d,e] (±0.45)	2.27 [k] (±0.15)	5.34 [b,c,d,e] (±0.45)

*—standard deviation, [†]—time of action; PM (+)—with poultry manure; PM (−)—without poultry manure CFU–colony forming units; [a,b,c,...]—values marked with different letters differ statistically significant, applies to the entire table.

After 30 min of exposure, the bacterial number ranged from 4.83 log CFU/egg (RCI, 4 °C, without poultry manure) to 5.69 log CFU/egg (ozonizer, 20 °C, with poultry manure). After RCI-emitter and ozonizer treatment at both tested temperatures, the number of bacteria was significantly different higher with the poultry manure ($p \leq 0.05$) (Table 4).

After 60 min of exposure, the bacterial number ranged from 3.69 log CFU/egg (RCI, 20 °C, without poultry manure) to 5.57 log CFU/egg (ozonizer, 20 °C, with poultry manure).

After 120 min of exposure, the lowest number of bacteria was found for RCI at 20 °C without poultry manure (2.27 log CFU/egg). The value was significantly different ($p \leq 0.05$) from the value for the ozonizer under the same experimental conditions. The ozonizer treatment at 20 °C with poultry manure caused the lowest reduction (5.40 log CFU/egg). In all time variants, at both temperatures RCI and ozonizer reduced statistically significantly higher the bacterial number in the absence of poultry manure (Table 4).

RCI treatment caused a decline of bacteria ranged from 0.26 log CFU/egg (30 min, 4 °C and 20 °C, with poultry manure) to 3.54 log CFU/egg (120 min, 20 °C, without poultry manure). For ozonizer bacterial reduction ranged from 0.20 log CFU/egg (30 min, 20 °C, with poultry manure) to 1.91 log CFU/egg (120 min, 4 °C, without poultry manure) (Table 2). RCI treatment statistically significantly higher ($p \leq 0.05$) reduce of *Salmonella* spp. number in bacterial contamination level 10^8 CFU/mL in 60 min and 120 min-exposure, 20 °C, without poultry manure than other tested methods.

4. Discussion

Commonly used methods for egg disinfection include chemical agents, but adverse effects of high temperature on, e.g., fatty acids, vitamins or cholesterol, are widely known. However, increased consumers' awareness forced the researchers to search for new methods, effective against microbes and safe for the environment and public health. New technologies such as RCI can reduce the use of disinfectants, but are not intended to completely replace them. The combined use of different physical and chemical methods results in increased microbiological safety of eggs. RCI technology, for maximum effectiveness, requires adequate working time, the right time of contact of active air with egg shells and the appropriate distance [26]. Such devices could be placed directly in laying hen houses or in egg stores or in hatching apparatuses. Then the working time of the technology could be sufficiently long. This technology is safe for humans and animals and is designed for continuous operation. Research conducted on the influence of RCI technology on hatchability of eggs, weight of chicks and occurrence of developmental defects did not show significant differences compared to the control variant without the use of this technology (unpublished data).

In the current study, we determined the effect of RCI and ozonation on the eggshells contaminated with *Salmonella* spp. Both methods significantly reduced the bacterial number of all tested serotypes, but their effectiveness varied depending on the variant used.

The initial bacterial contamination seems to play a crucial role in the efficacy of tested technology. However, our study shows that both methods are efficient even at high bacterial density. In low bacterial contamination level (10^3 CFU log/egg) and shorter time exposure (30 min) RCI-technology was more effective, suggesting its application as the disinfection method in egg processing plants. Soljour et al. [27] indicated that sodium carbonate, sodium hypochlorite and potassium hydroxide applied at the recommended concentrations eliminate *S. enteritidis* from eggshells contaminated with 10^4 or 10^6 CFU/mL of the bacterial suspension.

Moreover, temperature, organic solution and exposure time of RCI or ozone largely affect the decontamination power. Our previous research showed the lowest reduction of bacteria number for surfaces contaminated with meat and fish pulp before the action of RCI (24 h, 0.5 m, 20 °C). The reduction rate was equal to 0.89 log CFU $\times$ cm^{-2} for *Staphylococcus aureus*, 1.17 log CFU $\times$ cm^{-2} for *Listeria monocytogenes*, 1.43 log CFU $\times$ cm^{-2} for *S. enteritidis* and 1.61 log CFU $\times$ cm^{-2} for *Escherichia coli* O157:H7 [26]. The influence of poultry manure on the survival of bacteria was noticeable in these studies. Each time

their addition decreased the effectiveness of the tested methods and increased the survival rate of *Salmonella* spp. Furthermore, Bing et al. [28] showed that feces protect bacteria on eggshells against the bactericidal effects of other methods, e.g., UV-C radiation.

In most cases, the effectiveness of RCI was higher than that of ozonation, but usually, these differences were not statistically significant. Mannozzi et al. [22] indicated the reduction of bacteria (*E. coli*, *S. typhimurium* and *Listeria innocua*) from the surface of apple peel and spinach leaves after 90 min of exposure to RCI. For cantaloupe researchers obtained reductions of 94% and 88% for *E. coli* and *S. typhimurium*, respectively. The effectiveness of the RCI was influenced by the operating time of the device and the type of surface [22].

In our study, the treatment with ozone (10 g/h) reduced bacterial number on the eggshell. This number decreased with the exposure time extension, in both variants of the bacterial suspension density and at both temperatures. On the contrary, Braun et al. [14] have reported complete inactivation of *S. enteritidis* (contamination level of 10^2–10^4 CFU/g) on the eggshell after 120 min treatment with 1% ozone. In turn, Rodriguez-Romo and Yousef [29] applying ozonation for 10 min (15 lb/in2 [103.421 kPa], 4 to 8 °C) reduced up to 5.9 log CFU/g of *S. enteritidis*. The discrepancy between our research and the studies discussed above can result from the different strains, experimental conditions and ozone concentration used. A fundamental aspect of the use of ozone for egg disinfection is its safety. Wlazlo et al. [17] have demonstrated that ozone treatment reduced hatching of eggs and significantly increased egg mortality. This finding may indicate the negative impact of this gas on developing embryos. Some studies indicated that exposure of hen eggs to ozone deteriorated the nutritive characteristics of the eggs (low amount of yolk tocols, carotenoids, cholesterol and lipid oxidative status) and lowered eggshell breaking strength [30,31].

The conducted study has a several limitations that should be supplemented in further studies. In next experiments, it is worth considering other bacteria that may also be present on the shells of hens' eggs (e.g., *E. coli*, *Campylobacter* spp., *Staphylococcus* spp., *Streptococcus* spp., *Yersinia* spp. and *L. monocytogenes*). It is also worth considering shorter exposure times, e.g., a few minutes. If satisfactory efficiency were demonstrated, the technology could be applied at stages other than egg storage. Valuable information would also be provided by the study of hatching eggs, including the impact of RCI technology on their hatchability as well as the health and survival of chicks.

5. Conclusions

In conclusion, a constant urge to meet the consumer expectations of fresh, microbiologically safe food products results in the search for new disinfection methods. The findings of the present study indicate that the most effectiveness treatment was RCI and ozonation at contamination level 10^3 CFU/mL especially with treatment duration of 60 and 120 min. However, at the higher initial contamination levels of 10^5 and 10^8, the effectiveness of RCI and ozonation was also high with longer treatment. The addition of poultry manure reduced the effectiveness of both methods each time. Because of RCI effectively eliminates *Salmonella* spp. on the eggshells this technology may be a good candidate for the enhancement of biosecurity at farms and egg processing plants.

References

1. European Food Safety Authority (EFSA). The European Union One Health 2018 Zoonoses Report. *EFSA J.* **2019**, *15*, 5926.
2. European Centre for Disease Prevention and Control (ECDC). Multi-Country Outbreak of Salmonella Enteritidis Infections Linked to Eggs. Third Update (6 February 2020). 2020. Available online: https://efsa.onlinelibrary.wiley.com/doi/pdfdirect/10.2903/sp.efsa.2020.EN-1799 (accessed on 14 December 2020).
3. Okamura, M.; Kamijima, Y.; Miyamoto, T.; Tani, H.; Sasai, K.; Baba, E. Differences among six *Salmonella* serovars in abilities to colonize reproductive organs and to contaminate eggs in laying hens. *Avian Dis.* **2001**, *45*, 61–69. [CrossRef] [PubMed]
4. De Reu, K.; Grijspeerdt, K.; Messens, W.; Heyndrickx, M.; Uyttendaele, M.; Debevere, J.; Herman, L. Eggshell factors influencing eggshell penetration and whole egg contamination by different bacteria, including *Salmonella* Enteritidis. *Int. J. Food Microbiol.* **2006**, *112*, 253–260. [CrossRef] [PubMed]
5. Trudeau, S.; Thibodeau, A.; Côté, J.-C.; Gaucher, M.-L.; Fravalo, P. Contribution of the Broiler Breeders' Fecal Microbiota to the Establishment of the Eggshell Microbiota. *Front. Microbiol.* **2020**, *11*, 666. [CrossRef]
6. Chousalkar, K.K.; Flynn, P.; Sutherland, M.; Roberts, J.R.; Cheetham, B.F. Recovery of *Salmonella* and *Escherichia coli* from commercial eggshells and effect of translucency on bacterial penetration in eggs. *Int. J. Food Microbiol.* **2010**, *142*, 207–213. [CrossRef]
7. Jones, F.T.; Rives, D.V.; Carey, J.B. *Salmonella* contamination in commercial eggs and an egg production facility. *Poultr. Sci.* **1995**, *74*, 753–757. [CrossRef]
8. Mayes, F.J.; Takeballi, M.A. Microbial contamination of the hen's egg: A review. *J. Food Prot.* **1983**, *46*, 1092–1098. [CrossRef]
9. Park, C.M.; Hung, Y.C.; Lin, C.S.; Brackett, R.E. Efficacy of electrolyzed water in inactivating *Salmonella* Enteritidis and *Listeria monocytogenes* on shell eggs. *J. Food Prot.* **2005**, *68*, 986–990. [CrossRef]
10. Wang, H.; Slavik, M.F. Bacterial penetration into eggs washed with various chemicals and stored at different temperatures and times. *J. Food Prot.* **1998**, *61*, 276–279. [CrossRef]
11. Musgrove, M.T.; Jones, D.; Northcutt, J.K.; Cox, N.A.; Harrison, M.K. Identification of Enterobacteriaceae from washed and unwashed eggs. *J. Food Prot.* **2004**, *67*, 2613–2616. [CrossRef]
12. Upadhyaya, I.; Yin, H.-B.; Surendran Nair, M.; Chen, C.-H.; Lang, R.; Darre, M.J.; Venkitanarayanan, K. Inactivation of *Salmonella enteritidis* on shell eggs by coating with phytochemicals. *Poult. Sci. Assoc.* **2016**, *95*, 2106–2111. [CrossRef] [PubMed]
13. Melo, E.F.; Clímaco, W.L.S.; Triginelli, M.V.; Vaz, D.P.; de Souza, M.R.; Baião, N.C.; Pompeu, M.A.; Lara, L.J.C. An evaluation of alternative methods for sanitizing hatching eggs. *Poult. Sci.* **2019**, *98*, 2466–2473. [CrossRef] [PubMed]
14. Braun, P.G.; Fernandez, N.; Fuhrmann, H. Investigations on the effect of ozone as a disinfectant of egg surfaces. *Ozone Sci. Eng. J. Int. Ozone Assoc.* **2011**, *33*, 374–378. [CrossRef]
15. Fuhrmann, H.; Rupp, N.; Buchner, A.; Braun, P. The effect of gaseous ozone treatment on egg components. *J. Sci. Food Agric.* **2010**, *90*, 593–598. [CrossRef]
16. Fernández, A.; Thompson, A. The inactivation of Salmonella by cold atmospheric plasma treatment. *Food Res. Int.* **2012**, *45*, 678–684. [CrossRef]
17. Wlazlo, L.; Drabik, K.; Al-Shammari, K.I.A.; Batkowska, J.; Nowakowicz-Debek, B.; Gryzińska, M. Use of reactive oxygen species (ozone, hydrogen peroxide) for disinfection of hatching eggs. *Poult. Sci.* **2020**, *99*, 2478–2484. [CrossRef]
18. Space Fundation, Radiant Catalytic Ionization Air & Water Purification. Available online: http://www.spacefoundation.org/programs/space-certification/certified-products/space-technology/radiant-catalytic-ionization-air (accessed on 4 November 2020).
19. Grinshpun, S.A.; Adhikari, A.; Honda, T.; Kim, K.Y.; Toivola, M.; Rao, K.S.R.; Reponen, T. Control of aerosol contaminants in indoor air: Combining the particle concentration reduction with microbial inactivation. *Environ. Sci. Technol.* **2007**, *41*, 606–612. [CrossRef]
20. Małecka, I.; Borowski, G. Dezynfekcja powietrza promieniami UV i promieniową jonizacją katalityczną w instalacjach wentylacyjnych. *Zesz. Nauk.—Inżyniera Lądowa I Wodna W Kształtowaniu Sr.* **2011**, *3*, 25–30.

21. Skowron, K.; Grudlewska, K.; Krawczyk, A.; Gospodarek-Komkowska, E. The effectiveness of radiant catalytic ionization in inactivation of *Listeria monocytogenes* planctonic and biofilm cells from food and food contact surfaces as a method of food preservation. *J. Appl. Microbiol.* **2018**, *124*, 1493–1505. [CrossRef]

22. Mannozzi, J.T.; Filbert, V.J.; Mackay, W.J.; Fulford, D.E.; Steele, C.W. Evaluation of radiant catalytic ionization in reducing *Escherichia coli, Listeria innocua* and *Salmonella* Typhimuriom on representative food contact surfaces. *Tex. J. Sci.* **2018**, *70*, 6.

23. Ortega, M.T.; Franken, L.J.; Hatesohl, P.R.; Marsden, J.L. Efficacy of radiant catalytic ionization cell and ozone at reducing microbial populations on stainless steel surfaces. *J. Rapid Methods Autom. Microbiol.* **2007**, *15*, 359–368. [CrossRef]

24. Pal, A.; Pehkonen, S.O.; Yu, L.E.; Ray, M.B. Photocatalytic inactivation of Gram-positive and Gram-negative bacteria using fluorescent light. *J. Photochem. Photobiol. A Chem.* **2007**, *186*, 335–341. [CrossRef]

25. Skowron, K.; Grudlewska, K.; Kwiecińska-Piróg, J.; Gryń, G.; Śrutek, M.; Gospodarek-Komkowska, E. Efficacy of radiant catalytic ionization to reduce bacterial populations in air and on different surfaces. *Sci. Total Environ.* **2018**, *610–611*, 111–120. [CrossRef] [PubMed]

26. Skowron, K.; Wałecka-Zacharska, E.; Grudlewska, K.; Kwiecińska-Piróg, J.; Wiktorczyk, N.; Kowalska, M.; Paluszak, Z.; Kosek-Paszkowska, K.; Brożek, K.; Korkus, J.; et al. Effect of Selected Environmental Factors on the Microbicidal Effectiveness of Radiant Catalytic Ionization. *Front. Microbiol.* **2020**, *10*, 3057. [CrossRef] [PubMed]

27. Soljour, G.; Assanta, M.A.; Messier, S.; Boulianne, M. Efficacy of egg cleaning compounds on eggshells contaminated with *Salmonella enterica* serovar Enteritidis. *J. Food Prot.* **2004**, *67*, 706–712. [CrossRef] [PubMed]

28. Bing, S.; Zang, Y.T.; Li, Y.J.; Shu, D.Q. The synergistic effects of slightly acidic electrolyzed water and UV-C light on the inactivation of *Salmonella enteritidis* on contaminated eggshells. *Poult. Sci.* **2019**, *98*, 6914–6920. [CrossRef]

29. Rodriguez-Romo, L.A.; Yousef, A.E. Inactivation of *Salmonella enterica* serovar Enteritidis on shell eggs by ozone and UV radiation. *J. Food. Prot.* **2005**, *68*, 711–717. [CrossRef]

30. Mattioli, S.; Ortenzi, R.; Scuota, S.; Cartoni Mancinelli, A.; Dal Bosco, A.; Cotozzolo, E.; Castellini, C. Impact of ozone and UV irradiation sanitation treatments on the survival of *Salmonella* and the physical–chemical characteristics of hen eggs. *J. Appl. Poult. Res.* **2020**, *29*, 409–419. [CrossRef]

31. Yüceer, M.; Caner, C. The effects of ozone, ultrasound and coating with shellac and lysozyme–chitosan on fresh egg during storage at ambient temperature. Part II: Microbialquality, eggshell breaking strength and FT-NIR spectral analysis. *Int. J. Food Sci.* **2020**, *55*, 1629–1636. [CrossRef]

Article

Mitigation of Acrylamide Content in Biscuits through Combined Physical and Chemical Strategies

Emanuela Lo Faro [1], Tommaso Salerno [1], Giuseppe Montevecchi [1,2,*] and Patrizia Fava [1,2]

[1] Department of Life Sciences (Agri-Food Science Area), University of Modena and Reggio Emilia, Via Amendola 2 (Pad. Besta), 42124 Modena, Italy

[2] BIOGEST-SITEIA Interdepartmental Centre, University of Modena and Reggio Emilia, Piazzale Europa 1, 42124 Modena, Italy

* Correspondence: giuseppe.montevecchi@unimore.it; Tel.: +39-0522-523541

Abstract: Acrylamide in biscuits represents a major concern. This research work was aimed at modifying the current formulation of biscuits to reduce the acrylamide content while maintaining the chemical, physical, and sensory characteristics of the original product. A strategy based on the FoodDrinkEurope Acrylamide Toolbox was adopted. The content of the leavening agent ammonium bicarbonate, the baking temperature program, and the time duration of steam released during the baking process were the three factors evaluated through a factorial design of experiment. The partial replacement of ammonium bicarbonate (from 9.0 g to 1.5 g per 500 g of flour) with sodium bicarbonate (from 4.5 g to 12.48 g), lowering of the temperature in the central phase of the baking process (from 170 °C to 150 °C), and the release of steam for 3 min resulted in an 87.2% reduction in acrylamide concentration compared to biscuits of reference. CIELab color indices and a_w were the parameters that showed the most significant correlation with acrylamide concentration in biscuits and could, therefore, become markers to predict the acrylamide content along production lines for an instant evaluation.

Keywords: neo-formed contaminant; steam release; ammonium bicarbonate replacement; QuEChERS; acrylamide Toolbox

1. Introduction

Acrylamide is a neo-formed contaminant (NFC) that has been found in different kinds of foods that contain a high quantity of carbohydrates and are cooked by baking, roasting, or frying at temperatures higher than 100 °C [1]. In 1994, acrylamide was classified by IARC as Group 2A (potential carcinogen and neurotoxic to humans). This contaminant has genotoxic properties and causes carcinogenesis since it bonds strongly with DNA [2]. For these reasons, acrylamide levels in food are strictly controlled by European Food Safety Authority (EFSA) [3].

The highest levels of contamination, among the foods investigated, have been found in french fries, coffee, and biscuits. The European authorities have established benchmark levels for food classes in Regulation (EU) n. 2017/2158 (Attachment IV). The critical acrylamide threshold for biscuits and waffles is 350 μg/kg$_{FW}$, while remarkable attention has been put on infant biscuits, setting a very low threshold of 150 μg/kg$_{FW}$. Because baby foods can pose significantly higher health risks due to the lower body weight of infants, baby food manufacturers have to abide by stringent parameters and undergo careful scrutiny.

Most acrylamide is formed primarily through the Maillard reaction, which specifically involves the amino group of asparagine, the carbonyl group of reducing sugars, and intermediate molecules of the Maillard reaction [4]. Another way acrylamide forms is through a reaction that involves acrolein [5]. Both chemical reactions are strongly dependent

on the time–temperature factor, which means that the final result is similar when high temperatures and a short processing time or the reverse are applied [6].

Currently, there are no technological strategies to completely prevent acrylamide formation, although there are some ways to mitigate its concentration in food [7–10]. The acrylamide Toolbox lists the intervention steps that may be applied to reduce formation of acrylamide in specific manufacturing processes and products. The "ALARA" principle (As Low As Reasonably Achievable), which the Toolbox relies upon, states that the acrylamide presence needs to be reduced to the minimum, taking into account the risk presented, other legitimate considerations, such as potential risks from other contaminants, sensory properties and quality of the final product, and the feasibility and effectiveness of controls [11]. Moreover, the most effective methods applied so far have involved: (i) use of the asparaginase enzyme [12,13], (ii) use of different kinds of flours with low asparagine levels [14], (iii) replacement of ammonium bicarbonate (through the release of NH_3, which supports the presence of Maillard reaction intermediates such as glyoxal and methylglyoxal) with non-ammoniagenic leavening agents [15,16], and (iv) assessment of different methods of baking, such as steaming (40% relative humidity), vacuum baking, and time–temperature optimization [11,17]. In fact, steam application helps to move the water activity (a_w) value from the Maillard reaction's optimum, hence takes place more slowly [11].

While reducing the quantity of acrylamide in biscuits is paramount, keeping the biscuits' sensory characteristics, such as color and size, without losing their nutritional value is also essential. However, asparaginase poses several technological challenges for which the main objective of studies on food technologies aims to find suitable alternative strategies. These challenges include: asparaginase, which is currently and effectively employed as an acrylamide-mitigating agent [13], but makes the confectionery production process less cost-effective; the commercial preparation of the enzyme comes from the microorganism *Aspergillus niger*, a classified self-cloned micro-organism thus considered a genetically modified organism (GMO) and recently banned from the "organic" regime regulations.

Many researchers have focused their attention on the recipe modification, considering the influence of the substitution of inverted sugar with sucrose [18] and the replacement of wheat with other grains [14]. Good results have been obtained with the introduction of legume flours [19,20], even if sometimes the sensory properties are not always accepted by consumers [19]. The effect of cookie ingredients and cookie formulation has also been studied [21]. Of course, processing, i.e., the time–temperature condition of baking, plays an important role in acrylamide formation [8]. Oven-type baking processes affect acrylamide formation [18]. In particular, baking in ventilated mode promotes acrylamide formation, unlike baking in static mode [22]. Conversely, microwave baking has been studied for its capability to reduce thermal processing hazards and, consequently, acrylamide concentrations [23]. Vacuum-combined baking possesses these same capabilities and seems to be able to reduce acrylamide by about 30% in comparison with conventional baking [24].

Despite the possibly infinite combinations of recipes and baking conditions and the feasibility of such solutions in an industrial environment, this work considered only a slight modification of the recipe (i.e., the ratio of two different leavening agents) and the introduction of steam into a phase of the time–temperature program with a fixed total baking time, emulating the industrial conditions. Therefore, the present work aimed to investigate the influence, on the acrylamide amount in biscuits, of four baking conditions that differ in time/temperature cooking programs and use two different times of steam release to prepare biscuits from two recipes in which the ratios of the leavening agents ammonium bicarbonate/sodium bicarbonate were equal to 1:8 and 1:2. To achieve this goal, a factorial design of experiment (FDOE) 2^3 was applied to produce eight batches of experimental biscuits that were compared with reference biscuits obtained from standard recipes and baking conditions. As a secondary goal, size parameters (thickness, length, and width), color coordinates in the CIELab space (L*, a*, and b*), and water activity of the sample biscuits were measured to assess the magnitude of their correlation with the acrylamide content.

2. Materials and Methods

2.1. Biscuit Preparation

The ingredients: soft wheat flour (Italian type "0"), sugar syrup, fats, flavoring agents, and leavening agents (sodium bicarbonate and ammonium bicarbonate) were bought at a local market. The formulation for the biscuits was obtained using the creaming method, which consisted of adding the ingredients into a kneading machine equipped with a leaf-shape beater (PastaMatic Gourmet 1950 Edition, De Longhi Appliances Srl, Campi Bisenzio, Italy), following two steps (Figure 1): (i) mixing the liquid ingredients (i.e., sucrose syrup and butter) for 10 min; and (ii) adding the powders (i.e., soft wheat flour and leavening agents) and thoroughly homogenizing them for 15 min.
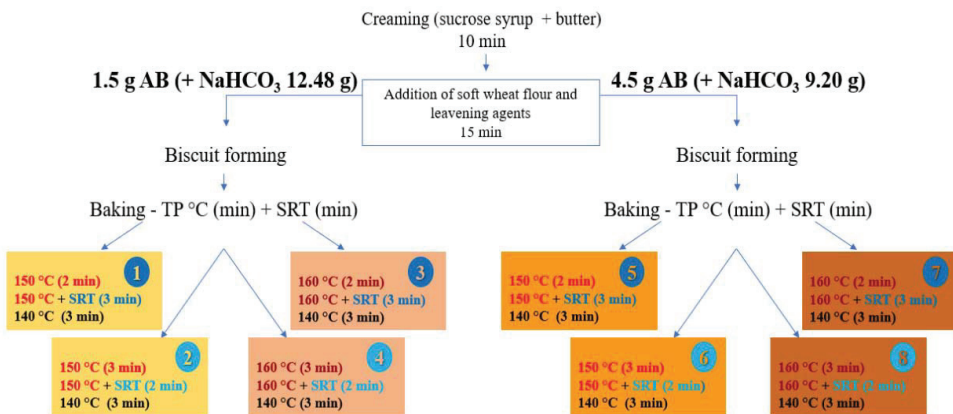
Figure 1. Diagram of the whole process and of the sample set obtained through the FDOE. AB, ammonium bicarbonate; TP, baking temperature program; SRT, steam release time.

Once the doughs were obtained, biscuits were molded using stainless steel cookie cutters according to the following dimensions: thickness 2 mm, width 2.5 mm, and length 6 mm. The samples were baked in an electric oven (EKF 616 E UD, Tecnoeka S.r.l., Borgoricco, Italy) for 8 min. For each batch, 12 biscuit doughs positioned in the same arrangement on a perforated stainless-steel pan were baked. The pan was placed in the oven chamber on the third shelf (out of six) from the top.

Preliminary tests were carried out to optimize the temperature program to emulate as closely as possible the physical and sensory characteristics of a standard industrial biscuit (SIB). A reference biscuit (RIB) was prepared using a standard recipe and without the introduction of steam during baking. Aside from the use as a control sample, one RIB batch per week (for a total of three batches) was prepared to rule out every possible influence coming from changing environmental conditions.

2.2. Factorial Design of Experiment (FDOE)

An FDOE was created to optimize the number of experiments. The choice fell on a 2^3 FDOE to assess the three most critical factors: the steam release time (SRT), the baking temperature program (TP), and the amount of leavening agent (ammonium bicarbonate, AB). For each of the eight experiments, Figure 1 shows the levels of the three factors selected for the FDOE application, which were established after accurate tests on the TP to obtain experimental samples as similar as possible to the SIB. The oven temperature was controlled using the thermocouple system with an indication on the oven display and by introducing a certified thermometric probe with an accuracy of ± 1 °C.

The steam was produced using tap water connected to the oven hose nozzle through a plastic pipeline. The release was regulated to achieve a relative humidity of 40% inside the oven.

Different relative quantities of leavening agents were used. For the preparation of 500 g of dough, the RIB contained ammonium bicarbonate 9.00 g and sodium bicarbonate 4.50 g, whereas the samples called "4.5 g AB" contained ammonium bicarbonate 4.50 g and sodium bicarbonate 9.20 g, and, finally, the samples called "1.5 g AB" contained ammonium bicarbonate 1.50 g and sodium bicarbonate 12.48 g (Figure 1).

The eight batches of biscuits from FDOE were cooked according to a balanced Latin square to compose an arrangement of eight rows and eight columns and considering only the first three columns as replicates (Table 1). The replicates were prepared in 3 days, once a week. The reference biscuits were also cooked on the same day.

Table 1. Latin square design used to randomize the cooking of the eight batches of biscuits, according to the FDOE design.

Batches from FDOE	Rep. 1	Rep. 2	Rep. 3
1	1	2	8
2	2	3	1
3	3	4	2
4	4	5	3
5	5	6	4
6	6	7	5
7	7	8	6
8	8	1	7

After baking, biscuits were left to sit for 60 min until complete cooling was achieved. For each of the eight FDOE points, eight biscuits were wrapped and sealed in oriented polypropylene bags using a FoodSaver sealing bar (IFS001X, JCS Europe Ltd., Cheadle, UK) and kept until analyses that were scheduled 7 days later.

2.3. Chemicals

All solvents and reagents were of analytical grade. Acrylamide, with a purity of 99% to be used as the external standard, acrylamide-2,3,3-d_3 (acrylamide d_3), with a purity of 99% to be used as the internal standard, and acetonitrile (Chromasolv® Plus purity for LC-MS) were obtained from Sigma-Aldrich Merck KGaA (Milan, Italy).

QuEChERS pouches containing $MgSO_4$ 4.0 g + NaCl 0.5 g were purchased from Agilent Technologies Italia S.p.A. (Milan, Italy). Deionized water was obtained through an Elix 3^{UV} purification system (Millipore Merck KgaA, Milan, Italy).

2.4. Biscuit Size

The size parameters (thickness, length, and width) of the biscuits were measured 1 h after baking with the use of a vernier caliper.

2.5. Color Determination

Color was measured using a tristimulus colorimeter (Spectrophotometer CM-700d, Konica Minolta, Milan, Italy) in transmittance mode over the visible spectrum (from 380 to 770 nm), using the illuminant D65 and 10° standard observer [25]. The parameters of the CIELab space L* (brightness), a* (green-red axis), and b* (blue-yellow axis) were measured on all of the baked biscuits (12 per experimental condition).

Color distance (ΔE) was calculated as reported in the literature [26] using the following equation:

$$\Delta E = [(L*_1 - L*_2)^2 + (a*_1 - a*_2)^2 + (b*_1 - b*_2)^2]^{1/2} \tag{1}$$

where 1 e 2 are two different samples.

Hue angle (h°) [22] was also calculated according to the following formula:

$$h° = [\arctan (b*/a*)/2\,\pi] \times 360 \tag{2}$$

2.6. Water Activity (a_w)

The a_w was measured on three biscuits for each sample using an AQUALAB 4TE water activity meter (Decagon Devices Inc., Pullman, WA, USA).

2.7. Extraction Protocol for Acrylamide

For each one of the eight FDOE points, experimental biscuits (around 35 g) were finely ground with a blender. The powder obtained was separated into its particle size classes using decreasing pore size sieves (Giuliani Tecnologie S.r.l., Torino, Italy) with the following meshes: 850 μm, 500 μm, 212 μm, and 63 μm. The powder fraction recovered on the 63 μm sieve (size within 63–212 μm) was used for the extraction.

An aliquot of 2.50 g from each gross sample was transferred into a 50 mL polypropylene flat-top screw cap tube, acrylamide d3 (500 uL; 0.4 mg/kg) was added, and a ceramic homogenizer for QuEChERS was introduced. Afterwards, 7 mL of water and 10 mL of acetonitrile were introduced, and the tube was manually shaken for 1 min following the addition of each solvent. A ready-to-use mixture of QuEChERS pouch composed of $MgSO_4$ 4.0 g + NaCl 0.5 g was added and manually shaken for 1 min and then vortexed for 3 min to facilitate the acrylamide migration into the acetonitrile phase. Each tube was twice centrifuged for 3 min at 3500 rpm to assure the separation of the layers. A portion of the upper layer (measured at exactly 5.0 mL) was withdrawn and evaporated to dryness using a rotational vacuum concentrator (Eppendorf concentrator 5301, Eppendorf, Hamburg, Germany). The sample was re-dissolved in 1 mL of water. Following centrifugation (Mini Spin, Eppendorf Italy, Milan, Italy), the supernatant of each sample was introduced into a 2 mL vial. The same extraction procedure was carried out and analyzed in triplicate using three different aliquots of each ground gross sample.

2.8. LC-ESI-MS/MS Optimized Analytical Conditions

Acrylamide determination was carried out through liquid chromatography coupled with mass spectrometry using an Agilent Technologies RP-LC-ESI-MS/MS triple quad system (Santa Clara, CA, USA), consisting of an HPLC (Agilent Technologies 1200 Series) equipped with a degasser, a binary pump, an autosampler, and a 6410B triple quadrupole mass spectrometer.

The MS/MS parameters (parent ion, product ion, fragmentor, collision energy, and polarity of the ESI ion source) were optimized using standard solutions (0.125 mg/L) of acrylamide and acrylamide d3 through their individual introduction into the MS source. Selected reaction monitoring (SRM) transitions of the most abundant fragments (product ions) were used.

Vials containing the samples were then loaded into an autosampler carousel at a controlled temperature (20 °C), and 5 μL of each sample were injected into a Gemini RP C_{18} column (Phenomenex, Torrance, CA, USA) (25 cm × 2 mm i.d. × 5 μm particle size × 110 Å pore size). The solvent system was composed of water with formic acid 0.1% (solvent A) andacetonitrile with formic acid 0.1% (solvent B). The elution (17 min of run + 10 min of post-run) was carried out according to the following gradient: 0% B (6.5 min), 95% B (7.5 min), 95% B (13.0 min), 0% B (13.1 min), 0% B (17.0 min) with a flow rate of 0.23 mL/min at a controlled temperature of 20 °C (pressure of about 180 bars at run start).

Source parameters were optimized as follows: gas (N_2) temperature, 300 °C; N_2 flow, 3 L/min; nebulizer pressure, 30 psi; capillary, positive 2500 V and negative 1500 V. Peak identification included comparison of peak retention times to those obtained with calibrants and evaluation of the tandem mass spectroscopic experiments. Quantification was performed by external standard calibration in the presence of acrylamide d3 as the internal standard, and the chromatograms were processed using MassHunter Workstation Quantitative Analysis software vB05.00 (Agilent Technologies Inc., Santa Clara, CA, USA).

2.9. Evaluation of Linearity, Limit of Detection and Lower Limit of Quantification (Detectability), Intra-Day and Inter-Day Repeatability (Precision), and Recovery Test (Trueness)

Solutions with increasing concentrations of diluted pure standards were prepared to evaluate the linearity of the instrumental response. The range of concentrations (0.02–1.00 mg/L) was established on the basis of the data already present in the literature and by exploring the chromatographic traces of some real samples. Because biscuits can cause a matrix effect that can affect acrylamide determination, linearity was also evaluated using an analyte-free biscuit matrix in which known concentrations of acrylamide were added.

In the aqueous reference solution, the instrumental limit of detection (LOD) and the lower limit of quantification (LLOQ) were obtained by applying the equation:

$$LOD \text{ or } LLOQ = (K \times sy/x)/b \tag{3}$$

where sy/x and b are the estimated regression standard deviation and the slope of the relevant analytical calibration function, respectively. K = 3 and K = 10 were chosen in order to obtain the LOD and LLOQ, respectively.

Precision was evaluated with an intra-day repeatability test on a sample and a standard solution of acrylamide (0.125 mg/L) each injected five times, and an inter-day repeatability test carried out on a sample injected over the course of five consecutive days in the same conditions. The relative standard deviations were calculated for each substance.

The trueness was evaluated through a recovery test where a known quantity of a standard acrylamide solution (0.25 mg/L) was added in the presence of the internal standard in samples consisting of a biscuit matrix previously deprived of the analyte and applying the extraction and chromatographic determination protocols.

2.10. Statistical Analysis

Employing different aliquots of each sample, three repetitions of each measurement were performed for each kind of analytical determination. Data were expressed as mean values (±standard deviations). FDOE was set using Microsoft Excel 365.

Because parametric ANOVA assumption tests (such as normality, equal variance and equal or near-equal sample size) were not satisfied, we performed the non-parametric Kruskal–Wallis equality-of-population rank test [27] and the non-parametric Wilcoxon rank-sum (Mann–Whitney U test) [28], using the temperature program (TP), the steam release time (SRT), and the ammonium bicarbonate percentage (AB) as statistical factors to observe the differences in median values in the sample set. Nevertheless, the ANOVA was also run, and its results were compared to those of the Kruskal–Wallis test.

An evaluation of the significant correlation among all parameters that showed significant differences in the Wilcoxon rank-sum (Mann–Whitney U test), i.e., thickness, L*, a*, b*, a_w, and acrylamide concentration, was performed using the non-parametric Spearman rank order correlation test to assess correlations among acrylamide and the other variables. All tests were performed using Stata/SE 11.0 for Windows (StataCorp LP, College Station, TX, USA).

3. Results and Discussion

3.1. Optimization of the Reference Industrial Biscuit (RIB)

The use of industrial-scale machinery for the preparation of the SIB implies substantial differences compared with the samples obtained using laboratory-scale equipment. For this reason, preliminary tests were carried out to try to balance the most evident differences and obtain experimental samples with specific physical characteristics, such as thickness, a_w, and color similar to those of the SIB.

The challenge of this research work lay in obtaining good reproducibility of the industrial process conditions in producing the RIB with lab equipment while simultaneously trying to emulate the characteristics of the SIB. Therefore, the first step was to analyze the differences between the two systems in detail to understand the causes of divergence

between the RIB and the SIB. Some technological differences were, however, deemed in-surmountable. One such difference was the ability to develop the same extent of gluten network during the creaming phase owing to the higher quantity of industrial heat that commonly triggers a more relevant leavening effect in the biscuits. Other technological differences, such as molding and the speed of production, were considered less relevant.

The differences between the two baking systems may have a tremendous impact on the experimental biscuits. After several attempts, a temperature program that made RIB almost identical to the SIB was finally found (Figure 2):
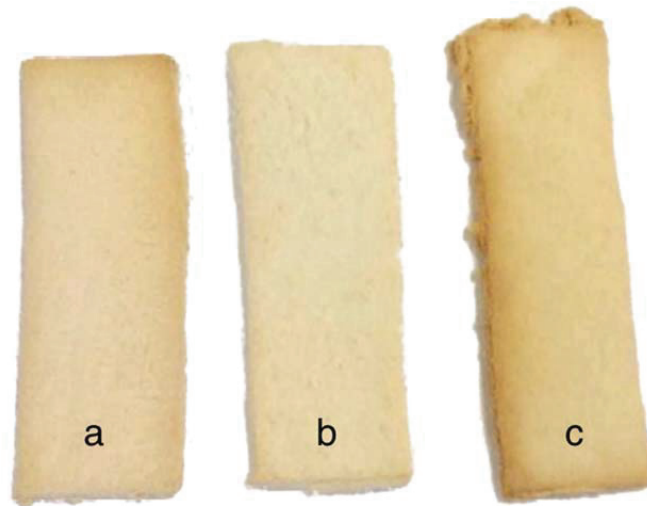
Figure 2. Experimental samples 4 (**a**) and 6 (**b**) and reference biscuit (RIB) (**c**).

160 °C (2 min) − 170 °C (3 min) − 140 °C (3 min).

However, the resulting biscuits had a_w lower than that of the SIB and a slightly lower height, whereas the color was similar. Unfortunately, further variations of the TP led to a further negative impact on one of the measured parameters (a_w), although height and color were very close to the original results. For this reason, it was decided to keep the height and color of the RIB as similar as possible to the SIB, to the detriment of the a_w.

3.2. Steam Release and Temperature Program Assessment

Attempts to include the steam release in the FDOE led to further fine-tuning of the baking TP. Furthermore, the steam released during baking in the FDOE would certainly have increased a_w values of the samples (becoming closer to the SIB value).

Once the optimal 3-phase TP was set up, it was decided that the steam would be released in the middle phase rather than the initial or final phases for two different reasons: First, the initial phase was excluded because the most intense chemical leavening of the product takes place during this phase, and water supply would have considerably altered this phenomenon. Second, it was not sensible to introduce steam in the final phase when the biscuits needed to lose water to reach proper dryness. Had this recommendation been disregarded, a product with a higher a_w would have been obtained, reducing its shelf-life. Additionally, the biscuit would have been sensorially altered, reducing its friability and, therefore, its consumer acceptability.

Following the introduction of steam, four different TP around the optimal one, each consisting of three phases, were included in the FDOE:

150 °C (2 min) − 150 °C (3 min + STR 40% r.h.) − 140 °C (3 min)
150 °C (3 min) − 150 °C (2 min + STR 40% r.h.) − 140 °C (3 min)
160 °C (2 min) − 160 °C (3 min + STR 40% r.h.) − 140 °C (3 min)

160 °C (3 min) − 160 °C (2 min + STR 40% r.h.) − 140 °C (3 min)

3.3. Validation of the MS/MS Parameters

Table 2 shows the optimized parameters (dwell time, fragmentor voltage, and collision energy). Both the coefficients of determination (R^2) of the acrylamide to acrylamide d3 ratio calibration straight lines that were calculated using (1) aqueous acrylamide solutions of known concentration and (2) analyte-free biscuit matrix with additions of known acrylamide concentrations were higher than 0.99 (Table 2). This demonstrated a satisfactory linear correlation between concentration and response, also confirmed by visual inspection [29].

Table 2. List of the main MS parameters optimized and results of the method validation.

Analyte	ESI	MW (g/mol)	Parent Ions (*m/z*)	Product Ions (*m/z*)	Dwell Times (msec)	Fragmentor Voltage (V)	Collision Energy (V)		
Acrylamide	+	71.08	72.1 (M + H)$^+$	55	80	70	8		
Acrylamide d3	+	74.10	75.1 (M + H)$^+$	58	80	70	8		

	Linearity			Detectability		Trueness	Precision		
	Range of concentration (mg/L)	R^2 (aqueous solutions of acrylamide of known concentration)	R^2 (analyte-free biscuit matrix with addition of known acrylamide concentrations)	LOD (mg/L)	LLOQ (mg/L)	% recovery	Intra-day on a biscuit sample (*n* = 5) (RDS %)	Intra-day using a standard solution of acrylamide (*n* = 5) (RDS %)	Inter-day on a biscuit sample (*n* = 5) (RDS %)
Acrylamide	0.02 ÷ 1.00	0.995	0.998	0.03	0.10	98.31	5.57	2.61	6.16

ESI: electrospray ionization; R^2: coefficient if determination; LOD: limit of detection; LLOQ: lower limit of quantification (LLOQ); RSD, relative standard deviation.

Regarding detectability, the LOD and LLOQ values were respectively 0.03 mg/L and 0.10 mg/L, which are far lower than the concentration of acrylamide in the extracts and also lower compared with the values found in previous studies carried out with SPE extraction [30,31]. Precision was well within 10% in all tests performed.

Trueness was assessed in terms of percentage recovery of acrylamide solutions spiked at different concentrations using biscuit matrix previously deprived of the analyte. Results showed an excellent average recovery of 98.31%.

3.4. Comparison between the Acrylamide Concentrations of the Eight FDOE Samples and the Reference Biscuits (RIB)

Table 3 shows the results for the acrylamide concentrations obtained in the FDOE sample set as well as in the RIB samples. All of the samples belonging to the FDOE showed acrylamide concentrations lower than those of the RIB, demonstrating that the combination of using a lower baking temperature with the introduction of steam in the middle step along with decreasing the amount of ammonium bicarbonate in the recipe is a promising strategy to mitigate acrylamide in biscuits. The Kruskal–Wallis equality-of-population rank test was run to highlight any significant difference among the sample medians, in particular those belonging to the FDOE (samples 1 to 8) and the RIB. This non-parametric test showed a moderately significant difference across the samples (p = 0.0530). Although nonapplicable, the one-way ANOVA also showed significant differences ($p \leq 0.001$) among the samples. Among the FDOE samples, a post hoc test showed significant differences only for samples 1 and 8, which exhibited the lowest and the highest acrylamide concentrations, respectively. The comparison of the conditions applied to the preparation of samples 1 and 8 indicated that all experimental factors (SRT, TP, and AB) were substantially different (Figure 1). The former showed an 87.2% reduction in acrylamide in comparison with the RIB, whereas the latter showed a 63.2% reduction.

Table 3. Results of measurements of size, CIELab color parameters, water activity, and acrylamide (expressed as mg/kg$_{FM}$; $_{FM}$: fresh matter) carried out on FDOE samples (samples 1–8) and reference samples (RIB).

Samples	Thickness (mm)	Length (mm)	Width (mm)	L*	a*	b*	a_w	Acrylamide (mg/kg$_{FM}$)	Percentage Reduction Compared with RIB (%)
1	5.7 ± 0.5	80.7 ± 1.4	27.6 ± 2.2	75.41 ± 0.91	6.36 ± 0.62	30.53 ± 0.68	0.325 ± 0.018	0.229 ± 0.010	87.2
2	5.6 ± 0.5	80.4 ± 1.1	26.5 ± 1.6	75.81 ± 0.89	6.25 ± 0.47	30.67 ± 0.60	0.271 ± 0.034	0.363 ± 0.005	79.7
3	5.7 ± 0.6	80.4 ± 1.7	26.6 ± 1.6	74.39 ± 1.17	7.27 ± 0.63	31.35 ± 0.62	0.298 ± 0.026	0.401 ± 0.007	77.6
4	5.6 ± 0.7	80.0 ± 1.2	27.4 ± 1.6	74.61 ± 1.07	7.00 ± 0.69	31.21 ± 0.74	0.244 ± 0.035	0.455 ± 0.003	74.6
5	6.0 ± 0.8	80.6 ± 1.4	27.6 ± 2.0	76.94 ± 1.03	5.76 ± 0.53	27.69 ± 0.85	0.384 ± 0.039	0.372 ± 0.004	79.2
6	5.3 ± 0.4	79.8 ± 1.7	27.2 ± 1.8	77.25 ± 1.00	5.91 ± 0.73	27.91 ± 1.03	0.257 ± 0.036	0.470 ± 0.030	73.7
7	6.1 ± 0.4	79.0 ± 1.3	26.8 ± 1.4	76.62 ± 0.97	6.36 ± 0.64	28.60 ± 0.80	0.337 ± 0.029	0.478 ± 0.010	73.3
8	5.8 ± 0.6	80.0 ± 1.8	26.7 ± 1.6	76.60 ± 0.94	6.65 ± 0.74	29.04 ± 1.09	0.245 ± 0.053	0.658 ± 0.092	63.2
RIB	5.9 ± 0.6	79.1 ± 1.3	27.9 ± 1.6	71.71 ± 2.26	9.64 ± 1.09	33.10 ± 1.11	0.109 ± 0.031	1.788 ± 0.111	

The colors used to indicate the samples and cell backgrounds refer to the colors used in Figure 1.

In sample 1, the TP used and the amount of AB in the recipe were the lowest. At the same time, the amount of steam administered was the maximum in terms of time. As hypothesized, this combination of parameters resulted in the lowest acrylamide value among all of the samples, whereas the diametrically opposite conditions of TP, RST, and AB were applied to sample 8, in which the highest amount of acrylamide was found within the FDOE.

Samples 2 and 5 followed sample 1 in terms of acrylamide content. These samples were obtained with the lowest baking TP and only one of the other two factors most favorable to the mitigation of acrylamide (1.5 g of AB and 3 min of SRT for samples 2 and 5, respectively). Sample 3 also had only one factor out of three that differed from sample 1, namely the highest baking TP. However, TP caused the most intense effect on acrylamide formation, as widely demonstrated [8–10] and recommended [11]. It emerged that sample 3 showed contaminant concentrations higher than those in samples 2 and 5. Finally, samples 4, 6, and 7, all of which had higher acrylamide values than the previous samples, showed only one favorable mitigation factor out of three, i.e., the lowest AB amount, the lowest TP, and the highest SRT, respectively.

The obtained data seemed to demonstrate the formulated hypothesis, according to abundant scientific evidence derived from experimental works on biscuits and concerning the use of steam-cooking [32] or on different starchy matrices, such as bread and potatoes [10,32,33]. As far as the contribution to acrylamide formation by AB is concerned, the present data agree with data from the scientific literature and demonstrate that diminishing this leavening agent is an interesting approach: some authors [21] concluded that ammonium bicarbonate is the most effective ingredient in terms of causing the formation of acrylamide in biscuits and that its complete elimination from the recipe may be a solution. However, the complete replacement of a leavening agent such as AB would require the reformulation of the industrial process to obtain a biscuit appreciated by consumers.

3.5. All Parameters Measured on the Eight FDOE Samples

The application of the Wilcoxon rank-sum (Mann–Whitney U test) made it possible to reach some general considerations on the contributions that the individual three factors made to the formation of acrylamide in the experimental biscuit matrix. For this reason, the RIB was excluded from this test. Table 4 shows that a significant reduction in the acrylamide concentration in the experimental biscuits was obtained by decreasing the amount of AB in the recipe, using 1.5 g instead of 4.5 g, while also reducing the baking TP (150 °C in the initial phase and in the middle phase instead of 160 °C in both of them). However, as for the two SRT (2 and 3 min), no significant effect was shown with respect to acrylamide concentration.

Table 4. Wilcoxon rank-sum (Mann–Whitney U test).

	Thickness (mm)	Length (mm)	Width (mm)	L*	a*	b*	a_w	Acrylamide (mg/kg$_{FM}$)
TP	n.s.	n.s.	n.s.	n.s.	0.0238	n.s.	n.s.	0.0356
SRT	*0.0574*	n.s.	n.s.	n.s.	n.s.	n.s.	**0.0022**	n.s.
AB	n.s.	n.s.	n.s.	**0.0016**	*0.0659*	**<u>0.0008</u>**	n.s.	0.0312

Results of the Wilcoxon rank-sum (Mann–Whitney U test) in the samples set are reported as *p*-value. *p* < 0.001, very strong significant effect (bold and underlined); *p* < 0.01, strong significant effect (bold); *p* < 0.05, moderate significant effect (standard); *p* < 0.1, weak significant effect (italics); *p* > 0.1, n.s.: not significant. SRT: steam release time; TP: temperature program; AB: ammonium bicarbonate percentage.

The concentration of acrylamide increased in parallel with the increase in both the TP and AB due to the crucial role that these two factors play in triggering and quickening the Maillard reaction and the non-enzymic browning in general, while SRT seemed to play a less relevant role.

The statistical analysis was also extended to the other parameters analyzed. In addition to acrylamide concentration in biscuits, Table 3 shows the data concerning the values of the sample sizes, the CIELab color coordinates, and a_w. The Wilcoxon rank-sum (Mann–Whitney U test) was applied to evaluate the influence of TP, SRT, and AB on the studied parameters (Table 4). As for the size parameters, length and width did not show any significant effect, whereas SRT significantly affected thickness (*p* = 0.0574). Indeed, by enhancing the SRT, the biscuit thickness significantly increased.

The small differences deriving from the manual preparation of the forms did not cause any substantial changes in length and width during the baking process. Conversely, the SRT influenced the thickness of the samples. This phenomenon could be explained by making different hypotheses: (i) the steam flow could have reduced the water loss from the biscuit because it decreases the vapor pressure between the surrounding environment and the biscuit surface [33], (ii) when the water evaporates, it stretches the gluten net where it is physically trapped, since, when the water tries to leave the dough, the latter is dragged upwards due to the passage of the water [33].

Contrarily, TP and AB did not have any significant effect on biscuit thickness. Temperature variation did not affect the rate of decomposition of the leavening agents, which occurs at temperatures far lower than 100 °C [34]. Concerning the AB concentration, the results show that the partial replacement of this leavening agent with sodium bicarbonate-cream of tartar was successful, and it did not cause any changes in the structure of the biscuits [15].

Regarding the color parameters, the wide difference in the RIB values compared with the experimental samples of the FDOE was clear. In the RIB samples, the values of redness (a*) and yellowness (b*) increased consistently with the increase in acrylamide concentration, to the detriment of values of brightness (L*), which were at the same time reduced.

Having excluded RIB from the statistical comparison to carry out a finer evaluation of the combination of the FDOE factors, other aspects also emerged. L* was significantly affected (*p* = 0.0016) by AB level, causing higher brightness when AB increased. This influence was also revealed by other authors [23,35], also considering different elaborations of the CIELab color parameters: for example, the E-value [36] and the browning index (BI) [22], both dependent on the L* values. The a* coordinate showed a significant effect for TP (*p* = 0.0238), giving a higher tendency to redness as temperature was increased. A weaker effect was shown by a* due to AB (*p* = 0.0659), while AB heavily affected the b* coordinate (*p* = 0.0008), thus giving a more intense yellowness as higher temperatures and lower AB levels were applied.

The higher concentration of AB significantly increased L* and decreased b* in the FDOE samples. This twofold effect was related to the ammonia release [11]. Contrarily, the lower concentration of AB entailed a higher concentration of sodium ions (from sodium bicarbonate), which yielded a darker biscuit surface color during baking [37,38].

On the other hand, the effect of TP on the behavior of color parameters was more predictable. Higher TP values significantly affected a* and b*, increasing both values. Taking into consideration that a* refers to the value on the green–red axis and b* refers to the value on the blue–yellow axis, it can be assumed that the more intense the thermal damage produced, the more evident the browning phenomenon on the surface.

Another way to compare colors of different samples is the evaluation of the color distance (ΔE). ΔE is a dimensionless parameter that arises from the combination of the L*, a*, and b* values when pairs of samples are considered. ΔE of sample pairs leads to determining whether or not there is a difference in the colors perceived by the human eye according to specific thresholds [39], i.e., ΔE < 0.2 indicates an imperceptible difference between colors; 0.2 < ΔE < 0.5, a very small difference between colors; 0.5 < ΔE < 1.5, a small difference between colors; 2 < ΔE < 3, a barely distinguishable difference between colors; 3 < ΔE < 6, a very distinguishable difference between colors; 6 < ΔE < 12, a large color difference; and ΔE >12, completely different colors.

Table 5 shows the data obtained when applying these thresholds to the ΔE of sample pairs in the present work. This diversity of colors could easily be distinguished by the naked eye for most of the FDOE samples when compared to the RIB, while with regards to samples 5 and 6, the "difference" was even larger. In order to further investigate this point, specific sensory analyses should be run to understand if this discrepancy may lead consumers to reject the product.

Table 5. Color distance (ΔE) calculated for all possible pairs of samples. Samples 1–8 belong to the FDOE; RIB is the reference biscuit.

	1	2	3	4	5	6	7	8	RIB
1									
2	0.43								
3	1.87	1.59							
4	1.51	1.23	0.37						
5	3.23	3.29	4.41	4.71					
6	3.13	3.23	4.36	4.67	0.42				
7	2.23	2.28	3.36	3.66	1.03	1.14			
8	1.86	1.93	2.97	3.25	1.50	1.66	0.53		
RIB	3.82	3.99	3.60	3.62	6.70	6.89	5.46	5.90	

The last parameter considered was a_w. The different levels of TP and AB did not have significant effects on the a_w in biscuits, while this a_w was affected only by SRT (Table 4). Indeed, samples 1, 3, 5, and 7, obtained with a 3 min RST, showed higher a_w values than those obtained with a 2 min application only. For this reason, a careful assessment of shelf-life in combination with the product's sensory properties should be taken into consideration. However, a_w values of the FDOE biscuits were around 0.3, which represents a reference value for this type of food matrix.

3.6. Study of the Correlations among Parameters

At the end of the study, an evaluation of the significant correlations was carried out to establish if one or more of the other parameters could be considered as chemical markers of the quantity of acrylamide present in the samples. This evaluation included all of the biscuits produced, those originating from both the FDOE and the RIB samples. One of the most interesting correlations was found between acrylamide and a_w (r = −0.73; $p \leq 0.001$). It was a negative correlation, meaning the higher the a_w, the lower the acrylamide content. Acrylamide was also positively correlated to the thickness to the a_w ratio (r = 0.66; $p \leq 0.01$).

Furthermore, acrylamide was positively correlated with a* (r = 0.57; $p \leq 0.02$). However, the most relevant correlation was found with a combination of the three CIELab color coordinates, that is, h° (r = −0.84; $p \leq 0.001$); (a*/b*) × L (r = 0.87; $p \leq 0.001$); and a*/b* (r = 0.84; $p \leq 0.001$), as some authors have previously described [22,40]. This would lead to

the prediction of the extent of acrylamide content in samples by comparing the coupling of a_w and CIELab color indices. The lower the a_w and the higher the color indices, the higher the acrylamide concentration in biscuits.

4. Conclusions

The present research study showed that proper modulation of the baking temperature, as well as partial replacement of the ammonium bicarbonate in the recipe with a more suitable leavening agent, are the physical and chemical factors that can be jointly applied to mitigate the formation of acrylamide in biscuits. The steam release during the central baking phase favorably affected the thickness and water content, parameters critically linked to consumers' acceptability of the biscuits.

With the best combination of the factors explored, an 87.2% average reduction in acrylamide content was achieved compared with the reference sample, which was produced in the laboratory to mimic the industrial biscuit.

The significant correlations of the acrylamide content with the a_w and CIELab color indices are compelling, as variables of this type could easily be evaluated by means of an optical sensor placed on the production line to exploit the properties of NIR spectroscopy and determine the color CIELab parameters by reflectance. Furthermore, the possibility of gathering a larger database of data could likely lead to highlighting other relevant relationships between color indices and acrylamide content.

Finally, this work lays the foundations for further in-depth investigations, where different mitigation techniques could be combined with those of the present study with the goal of lowering the acrylamide content in other types of food products.

References

1. Lingnert, H.; Grivas, S.; Jägerstad, M.; Skog, K.; Törnqvist, M.; Åman, P. Acrylamide in food: Mechanisms of formation and influencing factors during heating of foods. *Scand. J. Nutr.* **2002**, *46*, 159–172. [CrossRef]
2. Koszucka, A.; Nowak, A.; Nowak, I.; Motyl, I. Acrylamide in human diet, its metabolism, toxicity, inactivation and the associated European Union legal regulations in food industry. *Crit. Rev. Food Sci. Nutr.* **2020**, *60*, 1677–1692. [CrossRef] [PubMed]
3. European Food Safety Authority. Update on acrylamide levels in food from monitoring years 2007 to 2010. *EFSA J.* **2012**, *10*, 2938. [CrossRef]

4. Skog, K.I.; Murkovic, M.; Mottram, D.; van Boekel, T.; Zondervan, C.; van Klaveren, J.D. *Heat-Generated Food Toxicants, Identification, Characterisation and Risk Minimisation*; Project no. 506820 HEATOX; National Veterinary Institute: Oslo, Norway, 2007; Available online: https://edepot.wur.nl/4663 (accessed on 7 July 2022).

5. Liu, Y.; Wang, P.; Chen, F.; Yuan, Y.; Zhu, Y.; Yan, H.; Hu, X. Role of plant polyphenols in acrylamide formation and elimination. *Food Chem.* **2015**, *186*, 46–53. [CrossRef] [PubMed]

6. De Paola, E.L.; Montevecchi, G.; Masino, F.; Garbini, D.; Barbanera, M.; Antonelli, A. Determination of acrylamide in dried fruits and edible seeds using QuEChERS extraction and LC separation with MS detection. *Food Chem.* **2017**, *217*, 191–195. [CrossRef]

7. Rannou, C.; Laroque, D.; Renault, E.; Prost, C.; Sérot, T. Mitigation strategies of acrylamide, furans, heterocyclic amines and browning during the Maillard reaction in foods. *Food Res. Int.* **2016**, *90*, 154–176. [CrossRef]

8. Mesias, M.; Delgado-Andrade, C.; Morales, F.J. An updated view of acrylamide in cereal products. *Curr. Res. Food Sci.* **2022**, *46*, 100847. [CrossRef]

9. Sarion, C.; Codina, G.G.; Dabija, A. Acrylamide in bakery products: A review on health risks, legal regulations and strategies to reduce its formation. *Int. J. Environ. Res. Public Health* **2021**, *18*, 4332. [CrossRef]

10. Pal Murugan, M.; Agathian, G.; Semwal, A.D.; Sharma, G.K. A review on acrylamide mitigation strategies in various processed foods. *Int. J. Adv. Res.* **2016**, *4*, 1025–1040. [CrossRef]

11. FoodDrinkEurope. Acrylamide Toolbox 2019. Available online: https://www.fooddrinkeurope.eu/wp-content/uploads/2021/05/FoodDrinkEurope_Acrylamide_Toolbox_2019.pdf (accessed on 7 July 2022).

12. Anese, M.; Quarta, B.; Frias, J. Modelling the effect of asparaginase in reducing acrylamide formation in biscuits. *Food Chem.* **2011**, *126*, 435–440. [CrossRef]

13. Anese, M.; Quarta, B.; Peloux, L.; Calligaris, S. Effect of formulation on the capacity of l-asparaginase to minimize acrylamide formation in short dough biscuits. *Food Res. Int.* **2011**, *44*, 2837–2842. [CrossRef]

14. Žilić, S.; Aktağ, I.G.; Dodig, D.; Filipović, M.; Gökmen, V. Acrylamide formation in biscuits made of different wholegrain flours depending on their free asparagine content and baking conditions. *Food Res. Int.* **2020**, *132*, 109109. [CrossRef] [PubMed]

15. Graf, M.; Amrein, T.M.; Graf, S.; Szalay, R.; Escher, F.; Amadò, R. Reducing the acrylamide content of a semi-finished biscuit on industrial scale. *LWT-Food Sci. Technol.* **2006**, *39*, 724–728. [CrossRef]

16. Van Der Fels-Klerx, H.J.; Capuano, E.; Nguyen, H.T.; Ata ç Mogol, B.; Kocadağlı, T.; Göncüoğlu Taş, N.; Hamzalıoğlu, A.; Van Boekel, M.A.J.S.; Gökmen, V. Acrylamide and 5-hydroxymethylfurfural formation during baking of biscuits: NaCl and temperature–time profile effects and kinetics. *Food Res. Int.* **2014**, *57*, 210–217. [CrossRef]

17. Claus, A.; Mongili, M.; Weisz, G.; Schieber, A.; Carle, R. Impact of formulation and technological factors on the acrylamide content of wheat bread and bread rolls. *J. Cereal Sci.* **2008**, *47*, 546–554. [CrossRef]

18. Aarabi, F.; Seyedain Ardebili, M. The effect of sugar type and baking condition on formation of acrylamide in industrial rotary moulded biscuit. *J. Food Meas. Char.* **2020**, *14*, 2230–2239. [CrossRef]

19. Galani, J.H.Y.; Patel, N.J.; Jayant, G.; Talati, J.G. Acrylamide-forming potential of cereals, legumes and roots and tubers analyzed by UPLC-UV. *Food Chem. Toxicol.* **2017**, *108*, 244–248. [CrossRef]

20. Schouten, M.A.; Fryganas, C.; Tappi, S.; Romani, S.; Fogliano, V. The use of kidney bean flour with intact cell walls reduces the formation of acrylamide in biscuits. *Food Control.* **2022**, *140*, 109054. [CrossRef]

21. Sung, W.C.; Chen, C.Y. Influence of cookies formulation on the formation of acrylamide. *J. Food Sci. Nutr. Res.* **2017**, *5*, 370–378. [CrossRef]

22. Schouten, M.A.; Tappi, S.; Glicerina, V.; Rocculi, P.; Angeloni, S.; Cortese, M.; Caprioli, G.; Vittori, S.; Romani, S. Formation of acrylamide in biscuits during baking under different heat transfer conditions. *LWT-Food Sci Technol.* **2022**, *153*, 112541. [CrossRef]

23. Dong, L.; Qiu, C.; Wei, F.; Yu, Z.; Zhang, Y.; Wang, S. The effect of microwave baking conditions on the quality of biscuits and the control of thermal processing hazards in the Maillard Reaction. *Front. Nutr.* **2022**, *9*, 825365. [CrossRef] [PubMed]

24. Yıldız, H.G.; Palazoğlu, T.K.; Miran, W.; Kocadağlı, T.; Gökmen, V. Evolution of surface temperature and its relationship with acrylamide formation during conventional and vacuum-combined baking of cookies. *J. Food Eng.* **2017**, *197*, 17–23. [CrossRef]

25. McLaren, K. XIII—The development of the CIE 1976 (L* a* b*) uniform colour space and colour-difference formula. *J. Soc. Dyers Colour.* **1976**, *92*, 338–341. [CrossRef]

26. Hunt, R.W.G.; Pointer, M.R. *Measuring Colour*, 4th ed.; Wiley & Sons: Chichester, UK, 2011.

27. Kruskal, W.H.; Wallis, W.A. Use of ranks in one-criterion variance analysis. *J. Am. Stat. Assoc.* **1952**, *47*, 583–621. [CrossRef]

28. Wilcoxon, F. Individual comparisons by ranking methods. *Biom. Bull.* **1945**, *1*, 80–83. [CrossRef]

29. Miller, J.; Miller, J.C. *Statistics and Chemometrics for Analytical Chemistry*, 6th ed.; Pearson Education Ltd.: Harlow, UK, 2010.

30. Wenzl, T.; Karasek, L.; Rosen, J.; Hellenaes, K.; Crews, C.; Castle, L.; Anklam, E. Collaborative trial validation study of two methods, one based on high performance liquid chromatography–tandem mass spectrometry and on gas chromatography–mass spectrometry for the determination of acrylamide in bakery and potato products. *J. Chromatogr. A* **2006**, *1132*, 211–218. [CrossRef] [PubMed]

31. Bortolomeazzi, R.; Munari, M.; Anese, M.; Verardo, G. Rapid mixed mode solid phase extraction method for the determination of acrylamide in roasted coffee by HPLC–MS/MS. *Food Chem.* **2012**, *135*, 2687–2693. [CrossRef]

32. Isleroglu, H.; Kemerli, T.; Sakin-Yilmazer, M.; Guven, G.; Ozdestan, O.; Uren, A.; Kaymak-Ertekin, F. Effect of steam baking on acrylamide formation and browning kinetics of cookies. *J. Food Sci.* **2012**, *77*, E257–E263. [CrossRef]

33. Keramat, J.; LeBail, A.; Prost, C.; Jafari, M. Acrylamide in baking products: A review article. *Food Bioproc. Tech.* **2011**, *4*, 530–543. [CrossRef]
34. Arepally, D.; Reddy, R.S.; Goswami, T.K.; Datta, A.K. Biscuit baking: A review. *LWT-Food Sci. Technol.* **2020**, *131*, 109726. [CrossRef]
35. Fernandes, C.L.; Carvalho, D.O.; Guido, L.F. Determination of acrylamide in biscuits by high-resolution Orbitrap Mass Spectometry: A novel application. *Foods* **2019**, *8*, 597. [CrossRef] [PubMed]
36. Arribas-Lorenzo, G.; Fogliano, V.; Morales, F.J. Acrylamide formation in a cookie system as influenced by the oil phenol profile and degree of oxidation. *Eur. Food Res. Technol.* **2009**, *229*, 63–72. [CrossRef]
37. Simsek, S.; Martinez, M.O. Quality of dough and bread prepared with sea salt or sodium chloride. *J. Food Process. Eng.* **2016**, *39*, 44–52. [CrossRef]
38. Sinesio, F.; Raffo, A.; Peparaio, M.; Moneta, E.; Civitelli, E.S.; Narducci, V.; Turfani, V.; Ferrari Nicoli, S.; Carcea, M. Impact of sodium reduction strategies on volatile compounds, sensory properties and consumer perception in commercial wheat bread. *Food Chem.* **2019**, *301*, 125252. [CrossRef]
39. Riva, M. Approfondimenti: Il Colore degli Alimenti e la sua Misurazione 2003. Dipartimento di Scienze e Tecnologie Alimentari e Microbiologiche, University of Milan, Milan. Available online: https://documen.site/download/il-colore-degli-alimenti_pdf (accessed on 7 July 2022).
40. Anese, M.; Valoppi, F.; Calligaris, S.; Lagazio, C.; Suman, M.; Manzocco, L.; Nicoli, M.C. Omega-3 enriched biscuits with low levels of heat-Induced toxicants: Effect of formulation and baking conditions. *Food Bioproc. Tech.* **2016**, *9*, 232–242. [CrossRef]

Single, Subsequent, or Simultaneous Treatments to Mitigate Mycotoxins in Solid Foods and Feeds: A Critical Review

Alaa Abou Dib [1,2], Jean Claude Assaf [1], André El Khoury [1,*], Sami El Khatib [2], Mohamed Koubaa [3] and Nicolas Louka [1]

[1] Centre d'Analyses et de Recherche (CAR), Unité de Recherche Technologies et Valorisation Agro-Alimentaire (UR-TVA), Faculté des Sciences, Campus des Sciences et Technologies, Université Saint-Joseph de Beyrouth, Mar Roukos, Matn 1104-2020, Lebanon

[2] Department of Food Sciences and Technology, Facuty of Arts and Sciences, Bekaa Campus, Lebanese International University, Khiyara, Bekaa 1108, Lebanon

[3] TIMR (Integrated Transformations of Renewable Matter), Centre de Recherche Royallieu, Université de Technologie de Compiègne, ESCOM—CS 60319, CEDEX, 60203 Compiègne, France

[*] Correspondence: andre.khoury@usj.edu.lb; Tel.: +9611421389

Abstract: Mycotoxins in solid foods and feeds jeopardize the public health of humans and animals and cause food security issues. The inefficacy of most preventive measures to control the production of fungi in foods and feeds during the pre-harvest and post-harvest stages incited interest in the mitigation of these mycotoxins that can be conducted by the application of various chemical, physical, and/or biological treatments. These treatments are implemented separately or through a combination of two or more treatments simultaneously or subsequently. The reduction rates of the methods differ greatly, as do their effect on the organoleptic attributes, nutritional quality, and the environment. This critical review aims at summarizing the latest studies related to the mitigation of mycotoxins in solid foods and feeds. It discusses and evaluates the single and combined mycotoxin reduction treatments, compares their efficiency, elaborates on their advantages and disadvantages, and sheds light on the treated foods or feeds, as well as on their environmental impact.

Keywords: mycotoxins; mitigation treatments; decontamination rates; single treatments; combined treatments

1. Introduction

In a world full of economic, health, and environmental crises, food security concerns have become one of the most important dilemmas of our era. Fungal infection and the resulting production of mycotoxins in crops are major problems caused by climate change as a result of global warming [1,2]. Cereals and grains are considered highly susceptible to such types of infection during the pre-harvest and post-harvest stages of their production; their availability has a vital role in preventing hunger and food insecurity [3]. Mycotoxins, the secondary metabolites of fungi, are considered a food safety challenge, threatening the lives of humans and animals due to their immune toxicity, carcinogenicity, hepatotoxicity, nephrotoxicity, mutagenicity, and teratogenicity [4,5]. The pathogenicity and the toxigenic potentials of many fungal species, such as *Aspergillus*, *Claviceps*, *Fusarium*, *Penicillium*, and *Alternaria*, have been reported in various crops [6]. Their occurrence and presence in a specific food product at a specific geographic region depend on extrinsic factors related to environmental conditions fluctuation, such as temperature and relative humidity, which explain the effect of global climate change on the formation of these mycotoxins in agricultural commodities [7–9]. The type and the number of mycotoxins in foods and feeds are directly related to many intrinsic factors, such as the moisture content, the pH, the composition of the food, and many other extrinsic factors, such as the relative humidity and the storage temperature [10]. The most

commonly known mycotoxins to contaminate foods and feeds are aflatoxins AFs (AFB$_1$, AFB$_2$, AFG$_1$, AFG$_2$, AFM$_1$), ochratoxin (OTA), trichothecenes (deoxynivalenol: DON, nivalenol: NIV, T-2 toxin: T-2, HT-2 toxin: HT-2), zearalenone (ZEN), fumonisins B1 (FB1), enniatins (EN) [11–13], moniliformin (MON), beauvericin (BEA), and fusaproliferin (FUS) [14,15].

According to Food and Agriculture Organization (FAO) reports, 25% of the crops in the world are contaminated by mycotoxins [5,16,17]. Eskola et al., found that this percentage is underestimated and that 60 to 80% of crops are contaminated by mycotoxins [18]. In the United States, aflatoxin contamination causes great losses in the corn industry, reaching up to USD 1.68 billion. According to the Rapid Alert System for Food and Feed (RASFF), most rejection notifications at the EU border are due to mycotoxin contamination [19]. Regulations for mycotoxins are not available worldwide, especially in African countries. Mycotoxins in food and feed are extensively regulated in Europe. At the same time, aflatoxins in foods, particularly AFB$_1$, are the most commonly regulated mycotoxins in many countries. Total aflatoxin limits in food were established in 2003 in 48 countries [20,21]. The maximum acceptable levels of the total AFs are 4μ/kg in the European Union and 20 μg/kg in the United States [16]. Globally, the maximum levels for AFs (B$_1$, B$_2$, G$_1$, and G$_2$), AFM$_1$, and OTA in food are regulated by the codex standard CXS 193-1995 and established by the Codex Alimentarius Commission of the Food [18].

"Prevention is better than cure", and this should be the first strategy for reducing mycotoxins in feeds and foods [22]. This preventive strategy aims at controlling the fungal growth and the production of these metabolites in foods and feeds in the pre-harvest and post-harvest stages by applying good agricultural practices and monitoring storage and processing conditions [23,24]. Practically, complete prevention of the formation of mycotoxins in crops is not feasible, which has triggered the need for alternative strategies aiming at decreasing or eliminating the amount of already produced mycotoxins in food and feed materials [25–27].

Chemical, physical, and biological technologies and treatments have been established and studied to mitigate mycotoxins in foods [28,29]. The success and efficiency of the method used to reduce mycotoxins depend on the food or feed characteristics [10]. Many studies have provided insights on a number of techniques designed for the detoxification of mycotoxins in liquid medium [30,31], such as in milk and dairy products using lactic acid bacteria biofilm [32], chitin, and shrimp shells [33] or by chemical treatment, such as ozonation [34] in fruit juices and wine [35,36] and in solid foods and feeds [37,38]. These technologies can be implemented separately, one by one, or combined in order to attain additive or synergistic effects in the reduction of mycotoxins in food or feed.

In this review, we focus on mitigating mycotoxins in solid foods and feeds only. We evaluate the effectiveness of chemical, physical, and biological treatments applied to solid foods and feeds to reduce mycotoxins when implemented separately and/or subsequently or simultaneously combined, as shown in Figure 1. In addition, we evaluate the effect of the different treatment modalities on the quality of the treated food materials providing their advantages and disadvantages.
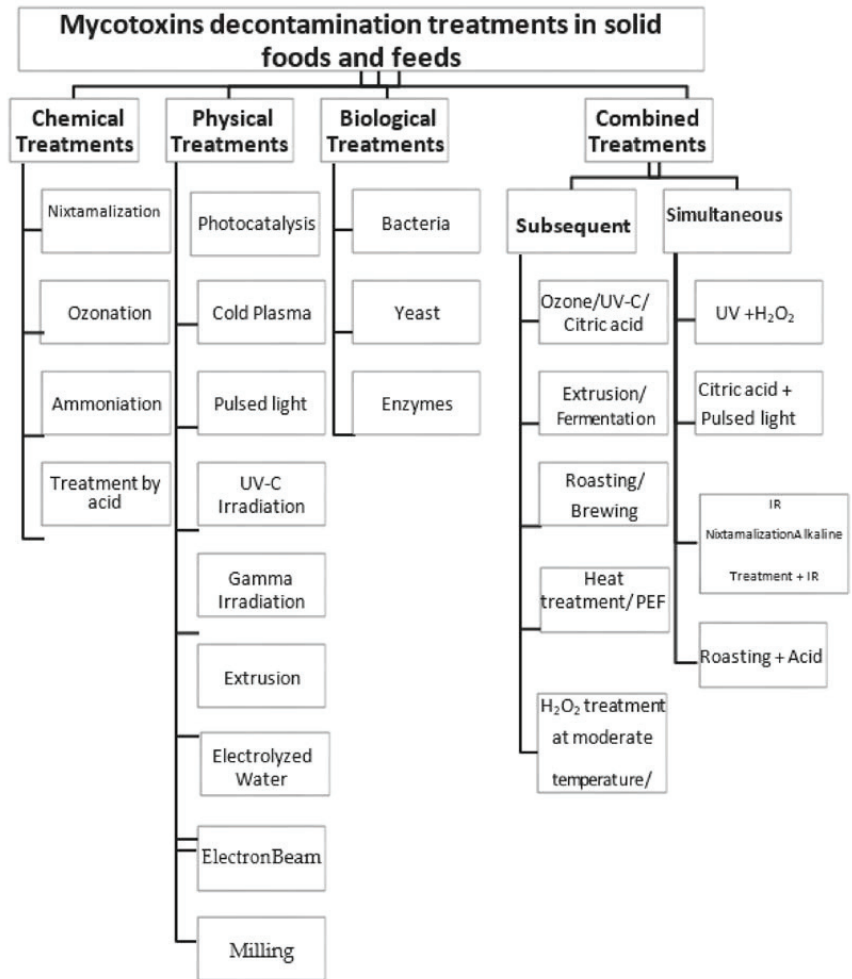
Figure 1. Flow chart of the different mycotoxin decontamination methods discussed in this review.

2. Single Detoxification Treatments Used in Solid Foods and Feeds

In this section, we summarize the chemical, physical, and biological treatments applied separately, their effect on the reduction rates of different mycotoxins, and the quality of the treated materials.

2.1. Chemical Treatments

Chemical decontamination is used in many industries [26]. It can be used for the destruction of mycotoxins or their neutralization [39]. Many chemical agents are used for the decontamination of solid foods and feed, such as limewater [40], organic acids [41], ozone [42], and ammonia [43]. All these treatments are discussed below in this section (Table 1).

Table 1. Chemical treatments for the reduction of mycotoxins in solid foods and feeds.

Technique	Feeds/Foods	Contaminants	Experimental Parameters	Reduction Rate	Advantages/Disadvantages	References
Ozonation	Powdered sun-dried herbs and spices	AFs	Ozone concentration = 3 ppm/time 210 min	Highest level of aflatoxin reduction: 93.75% for licorice 90% for peppermint	Advantages: Fumigation with Ozone: 3 ppm/time: 280 min—Sanitation and reduction of microbial load; Active against a wide range of microorganisms, viruses, Gram-negative and Gram-positive bacteria, spores, and fungi; Instability of Ozone—transformation into O_2-O_3 has a Gras status; The major biologically active constituent attributed to the medical properties of the chamomile flower was increased. Disadvantages: Reduction of chamomile essential oil by 57.14% and peppermint by 26.67%.	[44]
Ozonation	Parboiled Rice	Mycotoxins	Parboiled rice grains treated with ozone	Significant reduction of mycotoxins contamination, regardless of the time and period of application and the mycotoxin evaluated	Advantages: After soaking samples in ozone for 3 and 5 h: Higher head rice yield, luminosity and hardness, decreased cooking time, percentage of defective grains, and soluble protein.	[45]
Ozonation	Aqueous medium	Trichothecene-Mycotoxins (TC)	Saturated aqueous ozone (≈25 ppm)	Degradation of TC mycotoxins to materials that were not detected by UV or MS	Disadvantages: Ozone is a toxic gas, so all preparations were conducted in a fume hood.	[46]
			At lower levels (≈0.25 ppm) of aqueous ozone	Intermediate products were observed		
			Ozonation was sensitive to pH. pH 4 to 6 pH 9	Maximum reduction rates No reaction		

Table 1. *Cont.*

Technique	Feeds/Foods	Contaminants	Experimental Parameters	Reduction Rate	Advantages/Disadvantages	References
Ozonation	Wheat	DON	↓ initial concentrations of DON solution treated with ↑ concentrations of ozone, and ↑ times	↑ DON degradation rates	Advantages: No significant changes in the protein content, sedimentation value, pasting properties, and water absorption; Improvement in the flour quality. Slight ↑ in dough development time and stability time; No decrease in the quality of wheat for end-users; Products produced from ozone-treated wheat flour (noodles) have a longer shelf life, lower darkening rate, and microbial growth; No harmful residues, easy to use, and no waste. Disadvantages: Ozone treatment in solution is faster than gaseous treatment of scabbed wheat.	[47]
			In Solution: Processing time = 30 s; Ozone concentration = 1 mg L^{-1}	Degradation rate of DON = 54.2%		
			In scabbed wheat: Processing time = 12h; Moisture content = 17%; Ozone gas concentration = 60 mg L^{-1}	Degradation rate of DON = 57.3%		
			Gaseous ozone	Effective against DON in scabbed wheat		
			↑ Ozone concentration and ↑ processing time	↑ Degradation rate of DON		
Ozonation	Grains	AFs	Ozone concentration = 47,800 ppm The average retention time = 1.8 min. Screw Conveyor System	Decreased *Aspergillus flavus* counts in a single pass through the screw conveyor: ↓ 96%; Reduction rate of aflatoxin: 20–30%	Advantages: Treatments with humidified and dry ozone: similar effects on fungi and insects; ↑ residence time: ↑ insect mortality and mold reduction. Disadvantages: The total electricity cost for running the equipment at maximum load was USD 3.98/h based on an electricity rate of USD 0.11/kWh; The reduction was not sufficient enough to be of commercial value; Electricity and equipment are needed.	[48]

Table 1. *Cont.*

Technique	Feeds/Foods	Contaminants	Experimental Parameters	Reduction Rate	Advantages/Disadvantages	References
Ozonation	Rice	Filamentous fungi	An application of 0.393 kg O_3 m^{-3} rice	Different concentrations of ozone along the silo: 10^{-1}, 10^{-2}, and 10^{-3} (mol m^{-3}) for the portions IP, CP, and SP, respectively; highest concentration of ozone in the inferior part of the silo at the ozone inlet = Strong fungi reduction	Advantages: No damage to grain quality; No significant alteration of the quality of rice, starch modifications, lipid peroxidation, protein profile, and microstructure alterations.	[49]
Nixtamalization	Maize	AF and Fumonisins	Soaking in a solution of: • 1% slaked lime ((Ca(OH)2) • Or 1% traditional liquid ash	AF: up to 90% Fumonisins: up to 80%	Advantages: • Increased Niacin content; • Peak Viscosity: lime-nixtamalized maize flour < ash-nixtamalized flour < non-nixtamalized maize flour; • Good consumer acceptability after sensorial evaluation of products; • Cost-effective due to better pasting properties; • Wood ash nixtamalization improves safety and quality. Disadvantages: • Washing and drying steps are required at 60 °C for 16 h; • Slight reduction in fat, sugar, protein, and dietary fiber content.	[50]
Nixtamalization	Maize	AF	Traditional Nixtamalization Process-TNP	Not efficient enough to eliminate aflatoxins present in contaminated maize	Disadvantages: • This process generates a large amount of wastewater; • Possible reversibility in an acid medium such as the stomach.	[51]

Table 1. *Cont.*

Technique	Feeds/Foods	Contaminants	Experimental Parameters	Reduction Rate	Advantages/Disadvantages	References
Nixtamalization	Tortilla	AFB$_1$	Alkaline pH of the maize-dough = 10.2, Resting time = 30–40 min of resting at room temperature	AFB1: 100%		[52]
Nixtamalization	Maize and Sorghum	FBs, DON, NIV, and ZEN	The use of 5 cooking ingredients—1 g of cooking ingredient/400 mL of water at 92 °C for 40 min		Advantages: Sodium hydroxide and potassium hydroxide are good alternatives to calcium hydroxide; Sodium hydroxide could be used in the industrial nixtamalization process. Disadvantages: Environmental concerns about using calcium hydroxide; The high pH of the byproducts and wastewater when using calcium hydroxide; Calcium chloride is not effective in reducing mycotoxins.	[53]
			Calcium chloride as a cooking ingredient	The least effect on mycotoxin reduction		
Ammoniation	Groundnut press cake	AFs	Ammoniation at (0.5–2.0%) to feed materials/moisture content: 12–16%, at 45–55 psi, and at 80–100 °C for 20–60 min	Reductions in the levels of aflatoxin of between 96% and 99%	Disadvantages: Insufficient information was available to conclude on the safety and efficacy of the proposed decontamination process; No evidence that the proposed process is sufficient to ensure irreversibility in acid medium (GIT).	[54]
Ammoniation	Wheat kernels	DON	Treatment with Ammonia vapor at 90 °C for 2 h	Degradation of DON >75%	Advantages: In silico evaluation estimated a decrease in toxicity and biological effects.	[37]
			With an initial level of DON up to 2000 µg/kg	Treatment efficacy is not affected		

Table 1. *Cont.*

Technique	Feeds/Foods	Contaminants	Experimental Parameters	Reduction Rate	Advantages/Disadvantages	References
Ammoniation	Corn	AFs	The use of aqua-ammonia	Effective and inexpensive	Advantages: Effective and inexpensive, and it can be applied on the farm at low cost by sealing the grain in plastic. Disadvantages: Corn treated with ammonia turns dark because the sugar (altrose) is caramelized and the grain temperature increases by about 10 °F at the time of treatment; Not an FDA-approved process and treated corn cannot be legally shipped out of state; • Personal safety precautions must be taken as ammonia reacts with copper, and a motor in the air stream could cause an explosion; • Corn treated with aqua ammonia requires drying for storage after treatment.	[55]
Ammoniation	Maize	AFs	The effect of ammonia	More destructive to aflatoxins G_1 and G_2 compared with aflatoxin B_1 and B_2		[56]
			Highest detoxification rate	Aflatoxins G_1 (95%) Aflatoxin G_2 (93%)		
			Lowest degradation rate	Aflatoxin B_1 (85%) Aflatoxin B_2 (83%)		

Table 1. *Cont.*

Technique	Feeds/Foods	Contaminants	Experimental Parameters	Reduction Rate	Advantages/Disadvantages	References
Acid	Selected Nuts	AFs	Moisture Levels: walnut (10 ± 3 and 16 ± 3%); pistachio (10 ± 3%); peanuts (10 ± 3%) Citric, Lactic and propionic acid at 9% Time: 15 min	Reduction rate of aflatoxins: citric acid (99%); lactic acid (99.9%); propionic acid (96.07%)	Advantages: Food-grade organic acids do not affect the nuts' quality.	[57]
			Citric acid	Considerable reduction of the 4 aflatoxins; No formation of hazardous residues		
			Lactic acid	Significant reduction of AFB_1 and Total Afs; Increase in AFB_2 and AFG_2; Lactic acid converts AFB_1 into AFB_2 (less toxic)		
			Propionic acid	More efficient to reduce AFB_1		
Acid	Feeds/Foods	DON	5% solutions of lactic acid and citric acid	Reduction of the concentration of common trichothecene mycotoxins, especially DON and its derivate 15Ac-DON		[58]
			5% solutions of lactic acid and citric acid	No or only small effects on zearalenone, fumonisins, and culmorin		
			Lactic acid treatment	Decreased concentration of nivalenol		

Table 1. *Cont.*

Technique	Feeds/Foods	Contaminants	Experimental Parameters	Reduction Rate	Advantages/Disadvantages	References
Acid	-	AFB_1	1 M citric acid—at Room temperature—Time: 96 h	conversion of AFB_1 to AFB_{2a} >97%	Advantages: Organic acids have few detrimental effects; Under these conditions, > 71% of AFB_1 was hydrated to AFB_{2a} and did not show any reversion to the parent compound after being transferred to a neutral solution; Conversion of AFB_1 to AFB_{2a} in a gastric environment can be enhanced by the addition of citric acid. Disadvantages: Discoloration of various types of meats including beef, pork, and fish along with minor alterations in odor and taste.	[59]
			0.1 and 1 M citric acid—at boiling temperature—Time: 20 min	Conversion of AFB_1 to AFB_{2a} > 98%		

2.1.1. Nixtamalization

Nixtamalization is a traditional process used for maize. It is a chemical treatment based on the alkaline hydrolysis of aflatoxins by the addition of lime and subsequent cooking for a predefined time. This process causes the opening of the lactone ring of aflatoxins leading to their inactivation by the high pH medium and heating process. The efficiency of this process is related to many factors, such as the quantity of the lime used, the temperature of the process, and the contact time between the solution and the grains [60]. The disadvantage of the traditional nixtamalization process (TNP) is the generation of a large quantity of wastewater and a large amount of nejayote (water containing solid fractions of maize tip cap, pericarp, germ, and aflatoxins). Nejayote imposes a safety problem because it is reused in some regions as animal feed, for another nixtamalization process, or to water plants [51].

Inconsistent results have been shown concerning the use of the traditional nixtamalization process to reduce aflatoxins in corn. High reduction rates of aflatoxin B_1 (AFB_1) and aflatoxicol of 96% and 70%, respectively, were achieved by Anguiano–Ruvalcaba et al., supporting the use of TNP to mitigate aflatoxins in corn [61]. Another study was conducted in the Huasteca Potosina region in the central part of Mexico to measure the efficiency of TNP and showed that this process is not efficient enough to mitigate the aflatoxins in maize grains [51].

To determine the optimal pH for the alkaline treatment of maize dough used for tortilla production, an alkaline treatment at pH 10.2 was appropriate to achieve the total elimination of aflatoxin AFB_1 with a resting time of 30–40 min at room temperature. [52].

The cooking ingredients used to perform the nixtamalization may have a critical role in mitigating aflatoxins and decreasing the detrimental effect on food and feed quality, as well as the environment [53]. A study was conducted on maize, and two cooking solutions were used (1% slaked lime or 1% traditional liquid ash). Their efficiencies were similar, and the reduction rates of 90% and 80% of aflatoxins and fumonisins, respectively, were achieved by soaking the maize grains. The flours prepared from the treated grains showed a decreased peak viscosity, as compared with the non-nixtamalized maize flours, associated with a slight reduction in the fat, sugar, protein, and dietary fiber contents. The ash and the niacin content were increased, and the acceptability of the products produced using the treated grains by consumers was high, making this method a cost-effective alternative to fumonisins and aflatoxins detoxification of maize [50].

Another study showed that calcium hydroxide is consistently used for cooking maize grains and for producing nixtamal, but this causes environmental pollution issues due to the high pH of the wastewater and the byproducts ensuing from this process. Alternatively, the authors proposed the use of different cooking solutions, such as sodium and potassium hydroxides, that can be used as an alternative to calcium hydroxide after showing their effective reducing effect on fusarium mycotoxins [53].

2.1.2. Ozonation

Ozone (O_3) is a greenhouse gas made of three oxygen atoms. It is present naturally in the atmosphere (friend O_3) or generated by human beings (foe O_3) [26]. It can be produced by several methods, including UV-irradiation, electrical discharge of oxygen, and electrolysis of water. It is a highly reactive molecule having a high oxidizing effect (redox potential = 2.07 V), and it is used to mitigate many types of contaminants in food [62].

Ozone is used to reduce mycotoxins in food and feed, and it showed sanitation and antimicrobial effectiveness against viruses, bacteria, spores, and fungi [44]. The application of ozone to reduce or eliminate mycotoxins in foods and feeds can be performed by fumigation or in solution; the latter method is faster, as confirmed by a study where ozone solution at a concentration of 10 mg·L^{-1} was used to treat a 1 µg mL^{-1} of deoxynivalenol (DON) solution for 30 s achieving a degradation rate of 54.2%. Meanwhile, the degradation rate was higher in scabbed wheat (moisture content = 17%) reaching 57.3%, when treated for 12 h with ozone gas (Concentration = 60 mg L^{-1}). The high degradation rate of DON

can be established by increasing the concentration of ozone in solution and gas and by prolonging the application time [47].

Ozone fumigation of sun-dried herbs and spices showed that the main factors for achieving high microbial reduction and high aflatoxin degradation are the concentration of ozone and the exposure times. Ozone fumigation at 3 ppm for 210 min showed a considerable decrease in the total aflatoxins concentration by 93.75% in licorice and by 90% in peppermint. The disadvantage of this method is the reduction of the essential oil of chamomile by 57.14% and peppermint by 26.67% [44].

The degradation of trichothecene mycotoxins by aqueous ozone showed a pH sensitivity with maximum effectiveness at acidic pH of 4–6 and no effectiveness at alkaline pH of 9 [46].

Ozone treatment can be implemented during the storage of crops in a silo. In a previous study aiming at the decontamination of filamentous fungi, it was difficult to achieve homogeneity of ozone concentration in the silo during rice treatment following the application of 0.393 kg O_3 m^{-3} rice. The highest concentration of ozone was in the lower part of the silo, at the proximity of the ozone's inlet, suggesting a strong reduction of fungi in this area, while the effect of ozone gradually decreased while moving toward the upper parts of the silo [49].

Ozone is naturally unstable, leaving no residues in foods and feeds after its transformation into oxygen in the treated samples. It has a GRAS status (generally recognized as safe). It causes no waste and does not impose pollution problems [44,47]. At the industrial scale, the cost of ozone must be considered in developing countries [63].

Ozone gas applied to the rice silo did not damage the rice quality. No significant changes were perceived, especially in starch modifications, lipid peroxidation, protein profile, and microstructure alteration [49]. Concurrently, the treatment of parboiled rice during the maceration stage showed many advantages in the quality of the treated rice, such as higher head rice yield, higher luminosity and hardness, decreased cooking time, percentage of defective grains, and the abundance of soluble protein [45].

As shown in Table 1, the ozonation appears to be more effective in reducing the microbial load than in reducing mycotoxins already produced in food or feed. Higher aflatoxin reduction rates are achieved in powdered herbs and spices than in intact grains, wheat, and rice. The organoleptic and nutritional characteristics are affected differently in diverse food matrices. They range from no significant modification, or a slight improvement in quality attributes of wheat and rice, to a detrimental effect on the essential oil of herbs and spices [44,47–49].

2.1.3. Ammoniation

Ammonia (NH_3) is a gas stored in water solution or pressurized bottles. It is used to detoxify mycotoxins in different food matrices. Most studies have focused on aflatoxins [37]. Many studies supported the use of ammonia to detoxify aflatoxins in foods and feeds and proposed it as an effective, economic alternative [55,56]. High reduction rates of aflatoxins have resulted in ammoniation reaching 96 and 99% [54].

Ammonia is more effective against aflatoxins G_1 and G_2 than aflatoxins B_1 and B2. This is confirmed by a study that demonstrated that the degradation rate was 95% for aflatoxin G_1, 93% for aflatoxin G_2, 85% for aflatoxin B_1, and 83% for aflatoxin B_2 in artificially contaminated maize crops [56].

The highest efficiency of ammoniation in aflatoxin detoxification is achieved by the use of 0.5 to 2.0% ammonia at moisture levels between 12 and 16% and under pressure (45–55 psi) at high temperatures reaching 80–100 °C for 20 to 60 min where the recovery of the ammonia is conducted by evaporation at the end of the process [54,64].

The degradation of deoxynivalenol (DON) in contaminated wheat kernels was confirmed, and the achieved degradation rates were 75% or higher. The initial concentrations of DON in the kernels were up to 2000 µg/kg and vapor ammonia was implemented at a high temperature reaching 90 °C for 2 h. The toxicity of the ammoniation products is lower than DON [37].

Aflatoxins-contaminated corn is detoxified by the use of aqua-ammonia (liquid) or anhydrous ammonia (gas). The treatment with aqua-ammonia imposes the drying of the crops before storage. Ammoniation could affect the organoleptic characteristics of the treated corn by causing grain darkness as a result of the caramelization of sugar (altrose) caused by the increase in the temperature during treatment [55].

2.1.4. Acid

Food-grade acids can be used for the degradation of many mycotoxins [62]. These acids affect mycotoxins differently. Ochratoxins are reduced through their conversion to phenylalanine and lactone acid. Aflatoxins could be reduced by an acid-catalyzed addition of water to the vinyl ether double bond of AFB_1 and AFG_1, and they will be converted to their hemiacetal [58].

The high efficiency of food-grade acids in the reduction of aflatoxins is confirmed when used at a concentration of 9% for 15 min at two moisture levels (10 ± 3% and 16 ± 3%), reaching 99% for citric acid, 99.9% for lactic acid, and 96.07% for propionic acid. The most favorable results are obtained following the use of citric acid because of its efficiency in the reduction of the four aflatoxins (AFB_1, AFB_2, AFG_1, AFG_2) without the formation of any hazardous residues or metabolites [57].

The conversion rate of AFB_1 to AFB_{2a} by citric acid solution (1 M) reached more than 97% when implemented at room temperature for 96 h. This rate increased to 98% and the process was accelerated so that it could be accomplished in only 20 min when boiling was used [59].

Another study evaluated the effect of citric acid and lactic acid solution on the reduction of DON and its derivatives. This study showed that the 5% solutions of both acids are effective in reducing the DON and its derivative 15Ac-DON but have no or small effect on zearalenone, fumonisins, and culmorin [58]. The organic acid may affect the quality of some products causing discoloration and slight changes in odor and taste [59]. The high cost of organic acids is a challenge for their use in the detoxification of feeds [62].

The instability of ozone may support its safety in being used for the degradation of mycotoxins in food and feed without leaving harmful residues in the treated materials. The results shown from different studies in Table 1 put forward the efficiency of the ozonation and ammoniation. Ammonia was able to achieve higher reduction rates of AF and DON than ozone in different food materials. It is worth noting that ammoniation has not been approved by the FDA and may cause many sensorial quality problems [55], and its effect on aflatoxins may be reversible in an acid medium such as the gastrointestinal tract [54]. Many studies proved the high efficiency of citric acid solution in the reduction of mycotoxins and, especially, aflatoxins, reaching 99% with few detrimental effects on food quality. The limitation of its scalability and its use at the industrial level is related to the high cost of these acids [58].

Nixtamalization is a processing step of maize that can be used as a means to eliminate or reduce the number of mycotoxins [65]. Contradictory results about the effectiveness of the traditional nixtamalization process (TNP) are presented in Table 1. Maureen et al., proposed the high efficiency of this process to reduce AF (up to 90%) [50], while Rodríguez–Aguilar et al., declared that TNP is not efficient in reducing the AF in maize and confirmed the contribution of this process to environmental pollution through the high amount of wastewater generated during its execution [51,52]. A potential solution to this harmful effect on the environment could be attributed to the change in the cooking ingredient [53]. The absence of the ideal chemical treatment for the mitigation of mycotoxins imposed the necessity to find other alternatives to be discussed in the next section.

2.2. Physical Treatments

Many traditional methods, such as cleaning and sorting, are used. These methods are capable of physical separation by removing the contaminated portions from the crops and preventing the transfer of the pathogens to the non-contaminated portions. These are not able to neutralize or degrade the mycotoxins already produced in the crops; they only isolate the contaminated portions [28,66,67]. Several industrial processes require the use of conventional cooking at temperatures below 100 °C. Most mycotoxins are heat stable, and it is not possible to mitigate them by these conventional heat treatment processes [68].

The physical detoxification methods explained in this section (Table 2) include thermal treatments or invasive methods such as extrusion [68], and non-thermal treatments or non-invasive methods such as photocatalysis [69], cold plasma [70,71], electrolyzed oxidizing water [72], and irradiation [73,74]. These technologies are beneficial since they are safely used for many food matrices without causing negative effects on the nutritional and organoleptic quality of treated food. The limited scalability at the industrial level may be considered a disadvantage of many physical treatments [75].

2.2.1. Photocatalytic Treatment

The use of UV-visible irradiation combined with a semi-conductive photocatalyst showed high efficiency in the reduction of aflatoxins in a liquid medium [62]. DON was degraded in contaminated wheat samples by 72.8% following the use of photocatalyst UCNP@TiO$_2$ (8 mg mL^{-1}) for 90 min with a ratio of wheat to liquid of 1:2 [76].

The photocatalytic efficiency NaYF$_4$:Yb,Tm@TiO$_2$ on the degradation of DON was greater in solution than in wheat. This decrease in efficiency may be caused by the attachment of toxins to starch or proteins in the wheat, or to other wheat components, or even the shielding effect of wheat grains that hinder the light from reaching all contaminated surfaces. A complete degradation was achieved in a solution containing 10 μg mL^{-1} of DON when treated with simulated sunlight using NaYF$_4$:Yb,Tm@TiO$_2$ (6 mg mL^{-1}) at pH 7 for 60 min. This rate was decreased to 69.8% when artificially contaminated wheat was treated with UCNPs aqueous solution (Ratio 1:1) by illuminating the samples with a Xe lamp for 120 min [69].

Table 2. Physical treatments for the reduction of mycotoxins in solid foods and feeds.

Technique	Feeds/Foods	Contaminants	Experimental Parameters	Reduction Rate	Advantages/Disadvantages	References
Photocatalysis	Wheat	DON	In solution: DON concentration = 10 μg/mL, time = 60 min, simulated sunlight: using $NaYF_4$:Yb,Tm@TiO_2 (6 mg/mL), pH = 8.0	Rate of DON degradation ≈ 100%	Disadvantages: Decreased efficiency caused by shielding effect.	[69]
			3 photocatalytic degradation products were identified	$C_{15}H_{20}O_8$, $C_{15}H_{20}O_7$, and $C_{15}H_{20}O_5$		
			In wheat: 1 mL of 50 μg/mL DON standard solution + 5 g wheat-soaked and naturally dried. Toxic grains + UCNPs aqueous solution/ratio 1:1 After 1 h of adsorption equilibrium, the wheat samples were illuminated by Xe lamp (200–2500 nm) for 5, 15, 30, 60, 90, and 120 min, respectively	Degradation rate at 120 min = 69.8%		
Photocatalysis	Wheat	DON	In wheat: The dosage of photocatalyst UCNP@TiO_2 was 8 mg mL^{-1} Time: 90 minRatio of wheat to liquid: 1:2	Degradation rate at 90 min = 72.8%	Advantages: • Little effect on the starch content, protein content, amino acid content, and fatty acid value of wheat. Disadvantages: • The gluten content and pasting properties of wheat flour decreased significantly; • The whiteness of wheat flour decreased, and the yellowness increased; • The surfaces of starch granules were damaged to varying degrees with the prolongation of illumination time; • The fatty acid value and wet gluten content and pasting properties of wheat decreased significantly during photocatalysis; • The composite is easily removed by washing = low exposure dose.	[76]

Table 2. *Cont.*

Technique	Feeds/Foods	Contaminants	Experimental Parameters	Reduction Rate	Advantages/Disadvantages	References
Plasma	Corn	AFB_1	CAP is generated by a Surface Barrier Discharge (SBD) system operating in ambient air, yielding RONS by a generation of non-equilibrium atmospheric pressure plasma in ambient air	Reduction rate of AFB_1 after 60 s: 96%	Advantages: • It requires less time than UV irradiation; • Surface Barrier Discharge (SBD) plasma system was employed due to its practicability and scalability in the agri-food field.	[77]
			Initial concentration of AFB_1 = 35 µg/ml	100% AFB_1 decontamination in less than 120 s of treatment		
Plasma	Oat Flour	T-2 and HT-2	Low-pressure dielectric barrier discharge (DBD) plasma/different gases/time: 10–30 min		Disadvantages: • Time-dependent effect of T-2 toxin treatment for the 4 gases; • This treatment has similar thermal processing on mycotoxins such as cooking, roasting, and extrusion; • Possible explanation-conversion of T-2 into HT-2 toxin and complex degradation pattern.	[78]
			Exposure to nitrogen for 30 min	The maximal reduction of T-2 toxin degradation (43.25%)		
			Exposure to nitrogen for 30 min	The maximal reduction of HT-2 toxin degradation (29.23%)		
			Mean degradation rate of T-2 toxins in all experiments	25.01%		
			Mean degradation rate of HT-2 toxins in all experiments	20.98%		
			Oxygen and air as working gas	No significant reduction of T-2 and HT-2		

Table 2. *Cont.*

Technique	Feeds/Foods	Contaminants	Experimental Parameters	Reduction Rate	Advantages/Disadvantages	References
Plasma	Maize	AFB_1 and FB_1	Pulsed dielectric barrier discharge (DBD) jet: Spiked maize grains are placed at 12 mm beneath plasma jet—Time = 10 min Concentration of AFB_1 = 1.25 ng/g Concentration of FB_1 = 259 ng/g	Degradation rate after 10 min of plasma exposure = 65% Degradation rate after 10 min of plasma exposure = 64%	Advantages: • Minimal impact on the organoleptic characteristics (e.g., firmness, color, pH); • Minimal impact on the nutritional value of the treated foods (ascorbic acid, flavonoids); • The low penetration depth of CAPP treatment is thought to limit degradation to a thin surface layer and so protects the majority of nutrients. Disadvantages: • Its influence was shown to be dependent on the produce exposed, with losses in antioxidants or lipids reported; • An enclosed environment is necessary to improve detoxification rates.	[79]
Plasma	Roasted coffee	OTA	Treatment with cold plasma: Imput power = 30 W/output voltage = 850 V/Helium flow = 1.5 L/min for 30 min Using the brine shrimp (Artemia salina) lethality assay	OTA reduction rate = 50% Untreated roasted coffee = Toxic Treated roasted coffee = Slightly Toxic		[80]

Table 2. *Cont.*

Technique	Feeds/Foods	Contaminants	Experimental Parameters	Reduction Rate	Advantages/Disadvantages	References
Pulsed Light	Red pepper powder	AFB$_1$, Total AF, OTA	The highest fluence applied (9.1 J/cm^2, 61 pulses, 20 s)	2.7, 3.1, and 4.1 log CFU/g reduction of yeasts, molds, and total plate counts (TPC), where initial microbial loads were 4.6, 5.5, and 6.5 log CFU/g, respectively	Advantages: • The significant and apparent increase in total phenols. Disadvantages: • Total color difference = slight difference; • Proportional increase in temperature of the samples, max 59.8 °C.	[81]
			The highest fluence applied (9.1 J/cm^2, 61 pulses, 20 s)	A maximum reduction of 67.2, 50.9, and 36.9% of (AFB$_1$), (AF), and (OTA) was detected, respectively		
Pulsed Light	Solid medium	AFB$_1$ and AFB$_2$	PL at different initial concentrations of AFB$_1$ (229.9, 30.7 and 17.8 µg/kg) and AFB$_2$ (248.2, 32.2 and 19.5 µg/kg) and irradiation intensities (2.86, 1.60 and 0.93 W/cm^2) of PL	The degradation of AFB1 and AFB$_2$ followed the second-order reaction kinetic model well (R2 > 0.97); The degradation rate was proportional to the intensities of PL irradiation and the initial concentrations of aflatoxins		[82]
Pulsed Light	Rice	AFB$_1$ and AFB$_2$	PL treatment of 0.52 J/cm^2/pulse for 80 s to rough rice	AFB$_1$ reduction rate = 75% AFB$_2$ reduction rate = 39.2%	Advantages: • Safer working environment for those involved in post-harvest handling and milling operations.	[83]
			PL treatment of 0.52 J/cm^2/pulse for 15 s to rice bran	AFB$_1$ reduction rate = 90.3%AFB$_2$ reduction rate = 86.7%		

Table 2. *Cont.*

Technique	Feeds/Foods	Contaminants	Experimental Parameters	Reduction Rate	Advantages/Disadvantages	References
UV-C Irradiation	Brown, black, and red rice (Moisture content = 13%)	Aflatoxin (B₁,B₂, G1, and G2), DON, OTA, and ZEN	In black and red rice–the UV-C irradiation treatment (dosage of 2.06 kJ/cm²) for 1 h	Effective in fungal decontamination, photo-degradation of mycotoxins	Advantages: (dosage of 2.06 kJ/cm²) for 1 h: ○ Release of bound phenolics in black and red rice grains; ○ No changes in cooking and color properties. Disadvantages: (dosage of 6.18 kJ/cm²) for 3 h: ○ Reduced the total content of phenolic compounds in black and red rice; ○ Browning grains.	[73]
			In black and red rice—the UV-C irradiation treatment (dosage of 6.18 kJ/cm²) for 3 h	Increased the efficiency of fungal decontamination and reduced mycotoxins		
			In brown rice, the treatment conditions need to be optimized since only the dosage of 6.18 kJ/cm²	Reduction of fungal contamination		
UV-C Irradiation	Maize and peanut	AFB₁	After ten days of incubation and irradiation treatment delivering a dose of 8370 mJ/cm2	The highest reduction of *A. flavus* count was 4.4 log CFU/g in maize and 3.1 log CFU/g in peanut	Advantages: • Only minimal changes in the evaluated sensory and physical characteristics (color and texture).	[84]
			Depending on the treatment	AFB₁ reduction level:In maize ranged from 17 to 43% In peanut ranged from 14 to 51%		

Table 2. *Cont.*

Technique	Feeds/Foods	Contaminants	Experimental Parameters	Reduction Rate	Advantages/Disadvantages	References
UV-C Irradiation	Peanut	AFB$_1$	The darkening of the UV indicator (AgCl)	Linearly proportional to the UV dosage from 0 to 120 mJ/cm² delivered on peanuts	Advantages: • Reducing time-consuming tasks, such as replacing manual color measurement with automatic imaging processing technology, should also be considered. Disadvantages: • For scaling up the process, more parameters, such as the dimensions of peanuts, or the friction between peanuts and the chamber, should be considered; • The increase was not significant and the skins remaining on hollows of peanuts could protect AFB1 from being fully exposed to UV; • The AFB1 spiking process could also contribute to the result.	[85]
			Rotation at 11 rpm in the cylindrical chamber	Significant improvement in UV uniformity		
			UV irradiation: 2.3 mW/cm² UV-C for 2 h with rotation at 11 rpm	Reduction percentage by 23.4% (from 14.3 ± 3.4% to 17.7 ± 4.5%)		
			UV irradiation: 2.3 mW/cm² UV-C for 2 h with rotation at 11 rpm	Increased AFB$_1$ degradation rate from 60.8 ± 15.3 pmol g^{-1}h^{-1} to 75.0 ± 10.9 pmol g^{-1}h^{-1}		
Gamma Irradiation	Maize	AF and OTA	Gamma irradiation dose of 6.0 kGy	Completely inhibited the growth of the two molds		[86]
			Gamma irradiation dose of 4.5 kGy	Reduced the production of their mycotoxins		
			Gamma irradiation dose of 20 kGy	Maximum reduction rate is as follows: • AFB1: 40.1% • AFB2: 33.3% • OTA: 61.1%		

Table 2. *Cont.*

Technique	Feeds/Foods	Contaminants	Experimental Parameters	Reduction Rate	Advantages/Disadvantages	References
Gamma Irradiation	Wheat flourgrape juiceandwine	OTA	In wheat flour, a radiation dose of 30.5 kGy	OTA reduction rate = 24%	Advantages: • OTA was easily degraded by gamma irradiation when dissolved in water. Disadvantages: • OTA is very sensitive to irradiation in water solutions but resistant in its dry form and in food matrices; • Dry OTA was extremely resistant to gamma radiation.	[87]
			In grape juice, a radiation dose of 30.5 kGy	OTA reduction rate = 12%		
			In wine, a radiation dose of 30.5 kGy	OTA reduction rate = 23%		
Gamma Irradiation	Sorghum	OTA and AFB$_1$	Gamma irradiation dose of 3 kGy	Sufficient to eliminate 90% of the natural fungal load of sorghum		[88]
			At a radiation dose of 10 kGy	The maximum reduction rate of AFB$_1$ = 59%		
			At a radiation dose of 10 kGy	The maximum reduction rate of OTA = 32%		
Extrusion	Whole grain triticale flour	DON, 3- and 15-AcDON, HT-2, TEN, AME	Optimal parameters of co-rotating twin-screw extruder for lowering the concentration of each investigated mycotoxins in naturally contaminated flour were: SS = 650 rpm, FR = 30 kg/h, MC = 20 g/100 g	Reduction rate of mycotoxins: DON: 9.5%; 3-AcDON: 27.8%; 15-AcDON: 28.4%; HT-2: 60.5%; TEN: 12.3%; AME: 85.7%		[89]

Table 2. *Cont.*

Technique	Feeds/Foods	Contaminants	Experimental Parameters	Reduction Rate	Advantages/Disadvantages	References

Extrusion	Cornmeal	AF: B_1, B_2, G_1, G_2	Extrusion in the absence of high-amylose cornstarch	A reduction in aflatoxins level: (B_1: 83.7%, B_2: 80.5%, G_1: 74.7%, and G_2: 87.1%)	Disadvantages:
					• The bioaccessibility indicates that:
					  ○ Part of aflatoxins reduction observed after the extrusion may be caused by their interactions with food matrix macromolecules;
					  ○ Once the digestion is completed, part of these toxins becomes available for absorption in the small intestine.
						[90]

			Extrusion in the presence of high-amylose cornstarch	Higher aflatoxins reductions were observed: (B_1-89.9%, B_2-88.6%, G_1-75.0%, and G_2-89.9%)		
Electrolyzed Water	Wheat grains	DON	For AcidEW pH 5.5 pH 2.5 For AlkEW pH 9.5 pH from 8.5 to 12.5	Optimal pH for DON elimination Optimal pH for fungal reduction Optimal pH for DON elimination Strong elimination activity on fungi	Advantages: • Both pH 5.5 AcidEW and pH 9.5 AlkEW did not change the basic properties of wheat, including whiteness, moisture content, crude protein content, and wet gluten content; • No remarkable change in isolated starch morphology; • AcidEW can improve the farinograph property of wheat flours with higher stability time and FQN and a lower degree of softening; • AcidEW is a promising way for large-scale wheat milling operations to eliminate DON and mycological contaminations in wheat grains.	[91]

Table 2. *Cont.*

Technique	Feeds/Foods	Contaminants	Experimental Parameters	Reduction Rate	Advantages/Disadvantages	References
Electron Beam	Red pepper powder	OTA	Treatment at 6 kGy	Reduction of yeast count by 3 log CFU/g. Reduction of mold count by 4.4 log CFU/g	Advantages: • Retention of more than 85% of total phenols, carotenoids, and antioxidants activity; • No detrimental effect on the physicochemical quantities of the red pepper powder. Disadvantages: • Slight color differences.	[92]
			Treatment at 10 kGy for 23 s	Reduction of total plate counts by 4.5 log CFU/g		
			Treatment at 30 kGy	Reduction rate of OTA: 25%		
Milling	Maize	Mycotoxins	Grain cleaning	Reduction of fungal metabolites by 1.2–2 times	Advantages: • Flaking grits is the healthier milling product of maize with the lowest mycotoxins content. Disadvantages: • Highest mycotoxins content in animal feed products threatening animal health; • Redistribution of mycotoxins in maize fractions after milling; • Most mycotoxins are concentrated in the germ.	[93]

Table 2. *Cont.*

Technique	Feeds/Foods	Contaminants	Experimental Parameters	Reduction Rate	Advantages/Disadvantages	References
Milling	Maize	B-series fumonisins (FBs)	Grain cleaning	• Reduction rates of FBs: 42%	**Advantages:** • Higher reduction rates of FBs are achieved by tempering degermination; • The separation of horny endosperm from the fine fractions is better in the tempering process; • Higher reduction rates are achieved in the highest-sized flaking grits. **Disadvantages:** • The germ and animal feed flours contain a higher amount of FBs than other milling products.	[94]
			Dry-degermination process of uncleaned kernels	Reduction rates: • Maize flour: 50% • Break meal: 83% • Pearl meal: 87%		
			Tempering degermination Process of uncleaned kernels	Reduction rates: • Small grits: 78% • Medium grits: 88% • Flaking grits: 94%		

Many factors make the use of these techniques more advantageous. They are completely inorganic and do not result in the formation of secondary metabolites, causing pollution. They are cost-effective and easy to apply, requiring mild conditions [95]. Photocatalysis did not cause significant changes in the starch, the protein contents, or the amino acid value in wheat. However, there are also many disadvantages, such as the increased yellowness and decreased whiteness of the wheat flour, the damaged surfaces of starch granules when a prolonged illumination time is applied, and decreased fatty acid value, wet gluten content, and pasting properties of wheat [76].

2.2.2. Cold Plasma

The common states of matter are solid, liquid, and gas; plasma, the fourth, uncommon state, is formed by supplying enough energy to substances to assure the transition from the solid to the ionized state [96].

Cold atmospheric plasma (CAP) is a non-thermal technology that has shown its efficiency in reducing fungal pathogens and their toxins [64]. This technology is a successful alternative to the traditional treatments (heat treatment, wet chemistry, or UV-irradiation) usually implemented. These treatments proved their inefficiency in mitigating AF without affecting the food and feed quality [77].

Complete degradation of aflatoxin B1 is achieved by the effect of CAP-RONS (Reactive Oxygen Plasma and Nitrogen Species), which have a high oxidative potential and high affinity to react with the vinyl bonds in organic molecules. These RONS are yielded by the generation of non-equilibrium atmospheric in ambient air. The same degradation rate is achieved by applying the same CAP system to contaminated corn kernels. CAP treatment is faster than UV-C treatment and is significantly more efficient in AFB_1 reduction than UV-C treatment [77].

A different study explored the effect of low-pressure dielectric barrier discharge (DBD) plasma on the degradation of T-2 and HT-2 toxins in oat flour by using different working gases. Only partial degradation of T-2 and HT-2 toxins was achieved by applying this technology, and all the experiments yielded similar results to those obtained by the thermal treatments usually applied during food processing, such as cooking, extrusion, or roasting. None of the used gases in this study could completely detoxify the oat flour samples. The highest degradation rate of T-2 and HT-2 toxins reached 43.25% and 29.23%, respectively, after treating the samples with nitrogen for 30 min. CAP treatments using molecular oxygen and air as working gases did not affect these toxins [78].

Another study confirmed the results of the previous one that DBD plasma is not capable of achieving complete detoxification of AFB_1 and FB1 in food matrices. In this study, spiked maize kernels were exposed to a pulsed dielectric barrier discharge (DBD) plasma jet for 10 min. The detoxification rate was 65% for maize grains spiked with AFB_1 with an initial concentration of 1.25 ng/g and 64% for maize grains spiked with FB1 with an initial concentration of 259 ng/g [79].

Roasted coffee beans artificially contaminated with ochratoxin A (OTA) were treated with cold plasma for 30 min, and the degradation rate reached 50%. This result was satisfactory as per the EU standards. The brine shrimp lethality assay was used to evaluate toxicity, and the result was "Toxic" for the untreated beans and "Slightly Toxic" for the treated ones [80].

CAP has a low detrimental effect on the organoleptic and nutritional quality of foods and feeds. This treatment could explain this treatment's low penetration depth, so the degradation may affect only the superficial layers and protect all internal components. The generated RONS may affect the antioxidants and lipids present in the product [79]. SBD plasma has been shown to be more efficient than DBD plasma in the reduction of aflatoxins and other mycotoxins (Table 2), which seems to be more practical and scalable at the agri-food industrial level [77].

2.2.3. Pulsed Light

Pulsed light is a non-thermal treatment used to improve food safety and maintain the quality of food products by preventing the effect of heat treatment adopted in other techniques. It is generated by the flash repetition of non-coherent, broad-spectrum, high-intensity light [97]. It includes infrared, ultraviolet, and visible rays. It has been FDA approved since 1996 to be used for the superficial decontamination of food products (maximum fluence 12 J cm^{-2}) [62,98].

This technology achieved higher reduction rates of AFB$_1$ and AFB$_2$ in rice bran than in rough rice because of its high efficiency on the surface and external parts [83]. Another study showed a positive relationship between the aflatoxins degradation rate and the initial concentrations in solid medium and the intensity of pulsed light treatment [82].

The effect of pulsed light on red pepper powder to mitigate microorganisms and mycotoxins such as total AF, AFB$_1$, and OTA was investigated. The application of 61 pulses at high fluence (9.1 J/cm^2) for 20 s effectively reduced the yeast and molds and the total plate count in red pepper powder. The same treatment parameters were applied to cause the reduction of total aflatoxins by 50.9%, aflatoxin B$_1$ by 67.2%, and ochratoxin A by 36.9%. Total phenols increased apparently and significantly, while the total color was slightly changed [81].

2.2.4. UV-C Irradiation

UV light is another non-thermal treatment used as an alternative to thermal and chemical treatments to reduce the negative effects on the quality of treated foods and prevent the formation of residues and byproducts. UV light is classified into different bands according to the wavelength used. UV-C, which ranges from 200 to 280 nm, is commonly used because of its high efficiency against microorganisms, specifically at 250 and 260 nm [99].

The effect of UV-C irradiation on different types of rice was studied using UV irradiation at 254 nm for 1 and 3 h (moisture content of rice = 13%). The one-hour treatment was able to achieve a dose of 2.06 KJ cm^{-2}, causing fungal decontamination and mycotoxin reduction in black and red rice without affecting the cooking and color characteristics. In contrast, the three-hour treatment increased the dose to 6.18 KJ/cm^2 and increased the efficiency with a reduction of the total phenolic compounds. In brown rice, only the high dose achieved by the three-hour treatment was effective in reducing the fungal decontamination while causing undesirable browning of grains [73].

Low penetrability and the shadowing effect are two hurdles to the success of UV-C irradiation [100]. To overcome these problems and to increase the efficiency of UV irradiation, a customized rotational cylindrical chamber was established by Shen and Singh. In this study, the authors used a UV indicator applied to peanut kernels and treated with UV-C irradiation at 2.3 mW cm^{-2} for 2 h with a continuous rotational movement at 11 rpm. The uniformity of the UV-C treatment was significantly improved when the reduction percentage of AFB$_1$ was increased by 23.4% [85].

In another study, innovative vibrational decontamination equipment was designed for the decontamination of maize and peanut to increase the efficiency of this technology. UV-C irradiation was applied at a range of 1080 to 8370 mJ cm^{-2}. After incubation for 10 days, the samples irradiated with 8370 mJ cm^{-2} showed the lowest count of *A. flavus* in peanuts and maize. AFB$_1$ reduction rates reached 43% and 51% for maize and peanut, respectively [84].

2.2.5. Gamma Irradiation

Gamma irradiation is a treatment that can be used to disinfect crops by reducing the number of fungi or by mitigating mycotoxins already produced by the fungi in these crops [64]. A gamma source, such as cobalt-60, must be used to generate very high-energy photons. These photons are capable of killing spoilage and pathogenic microorganisms by causing damage to their DNA. The free radicals and ions that occur after the interaction of

the energy with water molecules present naturally in food products or crops will attack microbial DNA [101,102].

The important role of water in the successful use of gamma irradiation was supported by a study that investigated the degradation rate of OTA in aqueous solution and different food products (wine, grape juice, and wheat flour). The sensitivity of OTA irradiated at 30.5 kGy reached the maximum in water solutions. It was also demonstrated that OTA is highly resistant to the same irradiation dose in solid matrices or dry foods [87].

Another study confirmed the use of gamma irradiation to inhibit *A. flavus* and *A. ochraceus* and reduce AF and OTA in maize. In this study, low doses of 6 kGy lead to the inhibition of mold growth. The reduction of the formed AFB_1 by 40.1%, AFB_2 by 33.3%, and OTA by 61.1% in maize required higher doses (20 kGy) [86]. A different gamma irradiation study was performed on sorghum and showed that the reduction of natural fungi in sorghum reached 90% at 3 kGy with maximum reduction rates of 59% for AFB_1 and 32% for OTA realized at 10 kGy [88].

2.2.6. Extrusion

Mycotoxin reduction could result from food processing operations, such as extrusion, which can simultaneously improve product quality and increase food safety levels by reducing toxins [103]. Conventional cooking treatments (conducted at temperatures below 100 °C) cannot participate in the mitigation of mycotoxins in food products because most of these toxins are heat stable. Alternative cooking treatments, such as extrusion, are performed at higher temperatures and show efficiency in reducing mycotoxin contamination [68].

A study conducted by Massarolo et al. used a single-screw extruder at 50 ng g^{-1} to reduce aflatoxins on spiked cornmeal samples. The reduction rates of all aflatoxins were higher in the samples after the addition of high amylose corn starch, reaching 89.9% for AFB_1 and AFG_2, 88.6% for AFB_2, and 75% for AFG_1. Extrusion may cause possible interactions of the toxins with food components, decreasing their bio-accessibility. Their availability in the small intestine increased significantly after digestion [90]. Another study was conducted by Janić Hajnal et al., and focused on the effect of co-rotating twin-screw extruder on other mycotoxins (DON, 3- and 15-AcDON, HT-2, TEN, and AME) in whole grain triticale flour. The optimal reduction rate of all studied mycotoxins was achieved at a screw speed of 650 rpm with a feed rate of 30 kg/h and moisture content of 20 g/100 g. A higher reduction rate was found in AME, while the lowest rate was detected for DON [89].

2.2.7. Electrolyzed Oxidizing Water

EOW is prepared by introducing tap water and salt into an electrolysis chamber. It is considered a sanitizer or disinfectant because of its bactericidal and fungicidal effects. It is characterized by its specific pH value, its oxidation-reduction potential, ORP, and the available chlorine concentration, ACC [104]. The physicochemical properties of EOW used to treat foods are ACC from 10 to 100 ppm and ORP from −800 mV to higher than 1000 mV. The pH depends on the type of water used in the research, acid, slightly acid, neutral, or alkaline electrolyzed water [104,105]. Research was conducted to study the effect of different pH values of EOW on fungal elimination and DON reduction in wheat grains. This study showed that for acid-electrolyzed water, the optimal pH for reducing fungi was 2.5 and 5.5 to eliminate DON. For alkaline electrolyzed water, the optimal pH value to eliminate DON was 9.5, while pH values between 8.5 and 12.5 were effective for eliminating fungi also. The optimal pH values of the alkaline EOW (pH 9.5) and the acid EOW (pH 5.5) did not affect the wheat characteristics such as color, moisture content, and protein and gluten contents. The starch morphology also did not change significantly. A beneficial effect was caused by the acid-electrolyzed water on wheat flour, causing higher stability, increased farinograph quality numbers, and lowered softening degree [91].

2.2.8. Electron Beam Irradiation

The electron beam is a type of ionizing irradiation [99]. It is generated by the use of a safe dose of an electric accelerator [63]. It is a non-invasive, non-thermal, and eco-friendly detoxification method used for cereal-based products in order to reduce microbial and mycotoxin contamination [106,107]. This irradiation treatment was used to decontaminate naturally contaminated red pepper powder. Low doses of 6 and 10 kGy reduced the yeasts and mold count and the total plate counts by 3, 4.4, and 4.5 log CFU/g, respectively. A higher dose of 30 kGy achieved a 25% reduction in OTA. Electron beam irradiation is more effective in the reduction of microorganisms than mycotoxins. It is worth noting that this treatment had low detrimental effects on the quality of the treated pepper powder, causing a slight change in color and less than 15% reduction of total phenols, carotenoids, and antioxidant activity [92]. Another study conducted by *Kim et al.* used irradiation as a non-thermal decontamination method for an uncooked Korean cereal product called Saengshik. Electron beam irradiation was conducted at 10 kGy and showed an increase in the total phenolics and a decrease in the total carotenoids and chlorophylls with preservation of antioxidant capacity when the irradiation was conducted at doses lower than 10 kGy [108].

2.2.9. Milling

The milling process is effective in reducing mycotoxins in feeds and foods [68,109]. The weakness of this method lies in the redistribution of mycotoxins in the resulting fractions of milling and their concentration in the products intended for animal feed [67].

Scarpino et al., showed that cleaning maize grains may cause a reduction in the fungal metabolites by 1.2 to 2 times. In this study, the milling process of maize kernel caused an unequal redistribution of the mycotoxins in the different maize fractions and concentrated most mycotoxins in the germ. The highest mycotoxin contents were found in animal feed products, and the healthier products are large flaking grits [93]. A study was conducted using this principle by implementing dry and wet de-germination to maize and showed that the latter was more efficient for decreasing fumonisins in the milled products. Cleaning the kernels reduced FBs by 42%. Furthermore, the tempering degermination process of the uncleaned kernels achieved high reduction rates as compared to the dry degermination, reaching 94% for the largest-sized flaking grits. This process was able to facilitate the separation of the horny endosperm from the fine milling fractions. [94].

By evaluating the results of the different chemical treatments in Table 1 and the results of the different physical treatments in Table 2, we can conclude that chemical treatments are able to achieve the highest degradation rates of different mycotoxins in solid foods and feeds. In contrast, the physical treatments achieve lower degradation rates, but their effects on the quality of treated materials are smaller.

The shadowing or shielding effect is the principal limitation related to the use of photocatalysis and UV-C irradiation in the reduction protocols of mycotoxins in solid food materials. Many studies (Table 2) tried to overcome this limitation by rotating the irradiated peanuts to ensure UV uniformity, but no significant increase in the reduction rates occurred. Photocatalysis achieved higher reduction rates of DON, reaching a total elimination of DON in wheat [76]. CAP is a superficial treatment with low penetration depth. It showed good efficiency in reducing AFT and AFB_1 without deterioration in the quality of the treated product. Furthermore, SBD plasma was more effective than DBD plasma since it achieved the complete elimination of AFB_1 [77,79]. As working gas, nitrogen achieved the highest reduction rates as compared to oxygen and air when using the DBD system [78]. The pulsed light effectiveness was superficial and showed greater AF reduction rates when applied to rice bran than to rough rice. The AFB reduction rates are defined by the PL intensity and the initial concentration of mycotoxins in the food to be treated [83]. Gamma irradiation showed good effectiveness in reducing mycotoxins in food containing a high amount of water and reducing the fungal load in solid food. Low gamma irradiation doses were able to eliminate fungi and reduce mycotoxin formation in maize, but higher doses were required to reduce the already produced OTA in this material. Mycotoxins were not

completely eliminated in any of the mentioned studies (Table 2) [86–88]. The electron beam showed its efficiency as a disinfectant by the reduction of different microorganisms such as bacteria, yeasts, and molds, but it was not effective in the reduction of OTA in red pepper powder [92]. The milling process resulted in the reduction of mycotoxins in many edible fractions of maize but caused the concentration of these fungal metabolites in the germ, especially in the fractions used as animal feeds [93].

2.3. Biological Treatments

Biocontrol showed high efficiency in the prevention of AFs formation in the pre-harvest stage when non-aflatoxigenic biological control strains are inoculated in the fields and competed with aflatoxinenic strains of *Aspergillus* for nutrients and place and causing their exclusion [110,111]. The studies discussed in this section aimed to mitigate the already formed mycotoxins in feeds and foods by biological treatments and not to prevent their formation in crops (Table 3).

Most studies about the mitigation of mycotoxins by biological means focused on the treatment of liquid food or milk [32,33,112], assessing the effect of yeast, bacteria, or their enzymes on the mycotoxins in buffers or solutions [30,113,114]. Biological detoxification could be the result of binding the targets by adsorption mechanisms or by degradation. This detoxification of mycotoxins can be conducted using microorganisms (bacteria, biofilm, or yeast) or their metabolites and enzymes [115]. In this section, we screen various studies using biological control strategies to mitigate the mycotoxins in solid food and feeds (Table 3).

ZEN-detoxifying *bacillus* strains were used to detoxify highly contaminated maize with an initial concentration of 5 mg kg^{-1} of ZEN. The degradation of ZEN is related directly to the esterase activity, which has been found in all tested strains, with the maximum activity in B1 and B2 strains. The highest ZEN degradation rate was attained in B2 strains, reaching 56%. B2 strains showed their efficiency in the detoxification of other mycotoxins with different rates—AFB$_1$: 3.8%, DON: 25%, FB1: 39.5%, T2 toxin: 9.5%. The presence of ZEN enhanced the fermentation process of the contaminated maize compared to the non-contaminated grains [116].

CotA laccase is found in the endospore coat of *Bacillus*. It protects spores from UV light and hydrogen peroxide and has an oxidizing capacity. CotA laccase was immobilized onto chitosan microspheres and used to degrade ZEN in artificially contaminated cornmeal samples. The free CotA laccase form achieved a degradation rate of 70%, while the immobilized form was faster and more effective, achieving a higher degradation rate reaching 90%. The most important advantage is the reuse of the immobilized enzyme. Guo et al., showed that the degradation rate decreased to 54% following multiple uses of the immobilized CotA laccase in the third cycle, reaching only 21% in the fifth one [117]. Lactic acid bacteria (LAB) were used to mitigate mycotoxins in wheat-based products. The *Pediococcus acidilactici* LUHS29 strain achieved the highest reduction rates of mycotoxins when used alone in sourdough fermentation for 48 h. It removed 15-AcDON, AOH, D3G, toxins H-2 and HT-2, completely removed ENNB1, and reduced the DON by 44–69%. The combined fermentation using this LAB with *Lactobacillus Plantarum* LUHS135 strain showed great efficiency and increased the reduction rate of DON to 79–100% [118]. In a study conducted by Alberts et al., enzymatic detoxification was examined using Fumonisin Esterase FumD to degrade FB in maize. This enzyme can hydrolyze and remove the tricarballylic acid groups when added to maize during the conditioning step (for 250 min) during the dry milling process. The use of 40 U/kg of FumD in maize resulted in a 99% degradation of FBT in total hominy feed but did not accomplish any degradation of FBT in super maize meal [119].

The fungal growth and/or the mycotoxin production was controlled in bread using specific yeast strains and achieving reduction rates varying between 16.4 and 33.4% for DON, 18.5 and 36.2% for NIV, and 14.3 and 35.4% for ZEA [120]. The heat treatment of peanut samples at 100 °C for 15 min before solid-state fermentation by *Zygosaccharomyces rouxii* showed great efficiency in the mitigation of AFB$_1$, and the reduction rate reached 97.52% [121].

Table 3. Microbial and enzymatic treatments for the reduction of mycotoxins in solid foods and feeds.

Treatment	Feeds/Foods	Contaminants	Experimental Parameters	Reduction Rates	Advantages	References
Bacteria: ZEN-detoxifying *Bacillus* (ZDB) strains	Maize	ZEN	The highest level of ZEN degradation	B2 strain-reduction rate = 56%	• Esterase activity is demonstrated in all strains; • The stronger esterase activity: B1 and B2 strains;	[116]
			B2 strain detoxifies other mycotoxins	Reduction rates: AFB₁: 3.8%; DON: 25%; FB1: 39.5%; T2 toxin: 9.5%	• Fermentation of ZEN-contaminated maize by B2 strain compared to ZEN-free maize: Better fermentation characteristics: (lactic acid > 110 mmol·L−1; acetic acid < 20 mmol·L−1; pH < 4.5).	
Bacteria: *Bacillus lichenformis* spore CotA laccaseapplication of immobilized laccase in contaminated corn meal	Corn meal	ZEN	Treatment with immobilized CotA laccase onto chitosan microspheres for 12-h	Degradation rate: 90%	• Immobilized CotA laccase is much faster and more effective than free CotA laccase in degrading ZEN;	[117]
			Treatment with free CotA laccase for 12-h	Degradation rate: 70%	• Immobilization has higher thermal stability over free CotA laccase, maintaining about 87% of its initial activity after heat treatment at 80 °C for 30 min;	
			Reuse of immobilized enzymes for 5 cycles	Decreased degradation rate on each after each cycle: Cycle 1: 90%; Cycle 2: 77%; Cycle 3: 54%; Cycle 4: 30%; Cycle 5: 21%	• Reusability: Immobilized CotA laccase could be recovered from corn meal solution and repeatedly used.	
Bacteria—Fermentation: Lactic acid bacteria	Wheat-based products	DON 15 -AcDON AOH D3G, toxins H-2 and HT-2: Enniatin ENNB1	*Pediococcus acidilactici* LUHS29 strain	The strongest mycotoxins decontamination effect		[118]
			Prolonged fermentation at 35 °C for 48 h with *Pediococcus acidilactici* LUHS29 strain	DON: 44–69% 15-AcDON, AOH, D3G, toxins H-2 and HT-2: Removal Enniatin: 5–70% ENNB1: complete removal	*Pediococcus acidilactici* LUHS29 strain has the strongest mycotoxins decontamination effect;	
			Combined fermentation (Lactic acid bacteria 7 (JCM 1149) and Pediococcus acidilactici LUHS29 (DSM 20284))	Complete elimination or effective reduction of DON: 79–100%	• Combined fermentation showed more efficiency and complete elimination of DON.	

Table 3. *Cont.*

Treatment	Feeds/Foods	Contaminants	Experimental Parameters	Reduction Rates	Advantages	References
Enzyme	Maize	FB	FB degradation during dry milling of maize		• Highest enzyme concentration: 32 U/100 g maize: Complete conversion into HFB1; • Cost-effectiveness of upscaling the FumD FB dry milling method to an industrial level requiring up to 40,000 U FumD/ton maize, will depend on the safety benefits of consuming the milling products as well as the commercial value of the total hominy feed lacking FBT.	[119]
Fumonisin esterase FumD			Enzyme concentration: 40 U/kg	Reduction rates FBT: • 99% in total hominy feed; • 48% in semolina; • 7% in special maize meal • No reduction in super maize meal.		
Yeast	Wheat grains and bread	Fusarium Mycotoxins: DON, NIV ZEN	Bread prepared by baking with the addition of an inoculum of the test yeast	Reduction rates: DON: 16.4% to 33.4%; NIV:18.5% to 36.2%; ZEA: 14.3% to 35.4%	• The biocontrol yeasts strains may arrest fungal growth, reduce mycotoxin production, or both.	[120]
Yeast	Peanut meal	AFB_1	Peanut samples are heated at 40, 60, 80, 100, or 110 °C for 10 min			
			The residual rates after heat treatment at the following temperature for 10 min: (T:% of residual AFB_1)	80 °C: 61.08%; 100 °C: 63.46%; 110 °C: 49.63%		
			The residual rates after fermentation by *Z. rouxii*: (Temperature: % of residual AFB_1)	(40 °C:32.73%)-(60 °C:20.85%)-(80 °C:16.18%)-(100 °C:5.13%)-(110 °C:5.10%)		
			100 °C	The optimal temperature achieved the highest reduction rate		
			Peanut samples are heated at 100 °C for 5, 10, 15, or 20 min			
			The residual rates after heating at 100 °C for different times: (time: % of residual AFB_1)	(5 min: 21.06%)-(10 min: 5.13%)-(15 min: 2.48%)-(20 min: 2.44%)		
			15 min	The optimal time		
			Optimal treatment (100 °C -15 min):	Residual % of AFB_1,: 2.48%		

3. Subsequent Detoxification Treatments Used in Solid Foods and Feeds

The efficiency of the above-mentioned techniques on mycotoxin reduction showed great variability when implemented singly [122]. The additive or synergistic effect of using many combined treatments subsequently are summarized in Table 4 and evaluated below.

3.1. O_3, UV-C, and Citric Acid

Ozone and acid treatment, when implemented individually, can reduce AFB_1 and AFG_1 more than AFB_2 and AFG_2. In contrast to O_3 and acid treatment, UV-C by itself has great efficiency in the degradation of AFB_2 and AFG_2. This difference made the combination of the three treatments a great opportunity to increase the degradation rates of aflatoxins in contaminated pistachio samples. The subsequent treatments of the contaminated pistachio with 3N citric acid, followed by O_3 exposure for half an hour, and UV-C irradiation for 36 h, achieved high reduction rates of more than 90% for AFB_1 and AFB_2 and more than 99% for AFG_1 and AFG_2. This combination did not cause significant changes in the organoleptic and nutritional quality of the pistachio compared to non-treated pistachio samples [123].

3.2. Extrusion and Fermentation

Extrusion is a type of high-temperature treatment, and as discussed previously, it can decrease the number of mycotoxins in cereals [68]. Contradictory results were indicated by Zokaityte et al. They found that extrusion may affect the mycotoxin levels differently by increasing, decreasing, or not changing their concentrations in the samples. The combination of extrusion at different temperatures (115 and 130 °C), over different screw speeds (16, 20, and 25 rpm), with fermentation for 24 h at 30 °C by using 2 strains of LAB (*Lactobacillus casei* and *Lactobacillus paracasei*) and their effects have also been studied. This combination increased the amount of lactic acid and decreased bacterial contamination as a result of pH reduction. The effect of extrusion on different mycotoxins contradicted the results obtained in other studies. The 15-DON concentration increased in all extruded samples, and the fermentation of the samples decreased them to acceptable levels. The capacity of fermentation to decrease mycotoxin levels in the food or feed samples may be caused by the binding capacity of LAB. Mycotoxin types and their initial concentrations in the food matrix, the physicochemical characteristics of this matrix, and the fermentation variables, such as temperature and duration, play a major role in determining the binding percentages [124].

3.3. Roasting and Brewing

The combination of roasting and brewing of naturally contaminated coffee beans by using the traditional Qatari method was studied to show its effect on the reduction of AF and OTA. The roasting temperature is the main factor affecting the reduction rates of AF and OTA in the coffee beans. The reduction rates were proportional to the roasting temperature. The maximum reduction rates achieved with the high roasting scheme were 61.52% and 57.43% for AFs and OTA, respectively. Brewing alone was effective in reducing OTA more than AF. Brewing showed high efficiency in the reduction of both mycotoxins in roasted coffee beans by a low roast scheme. The best combination was defined at a high roast scheme with traditional brewing, and the cumulative reduction rates were 62.38% for AFs and 64.7% for OTA. It is worth noting that roasting temperatures applied to coffee beans in Arab countries are lower than those applied in other countries to preserve the traditional organoleptic characteristics such as color and flavor [125].

3.4. PEF and Thermal Treatment

The effect of the thermal process, the pulsed electric field, and the combination of both treatments on the reduction of AFT and AFB_1 were studied. Following the optimization of both treatment modalities, mycotoxins were affected by the thermal process time at alkaline pH, the thermal process temperature at neutral, and acid pH values when this process was implemented individually. The highest reduction rates were obtained after treatment at 110.36 °C for 15 min at pH 10, reaching 96.696% and 95.473% for AFB_1 and AFT, respectively. On the other hand, PEF treatment was also optimized, and the highest reduction rates were achieved at a pulse width of 65 μs and output voltage of 26%. It seems that the combination of both treatments did not achieve a great improvement in the reduction rates of AFT and AFB_1. As compared with the optimal thermal treatment implemented alone, this combination increased the reduction rates by 0.185% for AFB_1 and 0.248% for AFT [126].

3.5. H_2O_2 Treatment at Moderate Temperature after Roasting

The effect of H_2O_2 on aflatoxins reduction in peanuts was investigated and showed higher efficiency following its application at 50 °C instead of room temperature (20 °C), while the reduction rate increased from 30% to 73%. The same H_2O_2 treatment (30 g/hg H_2O_2 at 50 °C) was implemented on unroasted peanuts for 8 h, achieving a higher AF reduction rate of 86%. The combination of this treatment with pre-roasting the peanuts at 140 °C for 10 min caused the inactivation of catalase and increased the reduction rate slightly to reach 90%. The constructive points of this combination were the preservation of the oil quality of the treated peanuts, the absence of significant weight loss, and the conservation of the peanut's form since the temperature did not reach that of starch gelatinization. Moreover, the combination is eco-friendly, leaving no H_2O_2 residues after air drying the treated peanuts at 35 °C for 12 h [127].

Table 4. Subsequent techniques to mitigate mycotoxins in solid foods and feeds.

Combination	Feeds /Foods	Contaminant	Experimental Parameters	Reduction Rate	Advantages/Disadvantages	References
Ozone/UV-C/Citric acid	Pistachio nuts	Aflatoxins	Combination of the immersion of the samples in 3 N CA, 30 min exposure to O3, and 36 h exposed to UV-C radiation	AFB_1 and $AFB_2 > 90\%$ AFG_1 and $AFG_2 > 99\%$	Advantages: • No significant changes were observed in total fat content, protein content, acid and peroxide content, total phenolic compounds, soluble and insoluble carbohydrates of pistachios; • No significant changes between sweetness, acidity, flavor, color, and overall quality of treated and non-treated samples; • The combination of O_3, UV-C, and CA was much more effective than the effect of each of them alone.	[123]
			The UV-C	More effect on AFB_2 and AFG_2		
			The O_3 treatment	Degradation of AFB_1 and AFG_1, more than AFB_2 and AFG_2		
			Acid treatment	More effect on AFB_1 and AFG1, against AFB_2 and AFG_2		
Extrusion/Fe	Wheat bran	Mycotoxins	Extrusion at 130 °C—Screw speed: 20 rpm + fermentation with *L. casei* and *L paracasei* strains at 30 ± 2 °C for 24 h.	The lowest overall concentration of the tested mycotoxins.	Advantages: • Appropriate extrusion parameters and LAB strain selection lead to the higher formation of L-(+)-lactic acid and lower WPBP microbial contamination (except for the M/Y count); • Extrusion, as well as extrusion in combination with fermentation, reduces the total biogenic amines content (by 2 times on average).	[124]
			Extrusion at 130 °C—Screw speed: 25 rpm + fermentation with *L. casei* and *L paracasei* strains at 30 ± 2 °C for 24 h.			

Table 4. *Cont.*

Combination	Feeds/Foods	Contaminant	Experimental Parameters	Reduction Rate	Advantages/Disadvantages	References
Roasting/Brewing	Coffee	AF and OTA	**Treatment** After roasting After reduction after brewing After roasting and brewing **Treatment** After roasting After brewing After roasting and brewing	**OTA reduction** Low roasting: 15.17% / Medium roasting: 46.78% / High roasting: 57.43% Low roasting: 43.57% / Medium roasting: 4.11% / High roasting: 7.28% Low roasting: 58.74% / Medium roasting: 60.88% / High roasting: 64.7% **AF reduction** Low roasting: 31.98% / Medium roasting: 46.36% / High roasting: 61.52% Low roasting: 10.19% / Medium roasting: 1.50% / High roasting: 0.86% Low roasting: 40.18% / Medium roasting: 47.86% / High roasting: 62.38%	Advantages: • Roasting is performed at a suitable low temperature to preserve the traditional color and flavor.	[125]
Heat treatment/PEF	Artificially spiked potato dextrose agar (PDA)	AFT—AFB$_1$	**Thermal process:** At pH 10 At pH 4 and 7 **PEF:** Fixed parameters: pulse frequency (50 Hz), burst (10), energy (1 KJ) Time: 10 s Variables: pulse width (ms) and output voltage (%), and pH of the PDA/different combination. (20 µs 10%; 51 µs 26% and 65 µs 26% for pH 4, 7, and 10 respectively) **Combined effect of Thermal process + PEF:** Thermal process: T = 110 °C +t = 15 min + PEF (65 µs 26%, pH 10)	The effect of process time was observed to affect both AFB1 and AFT content more significantly than the temperature. The effect of temperature on toxin reduction was more evident. Reduction rates of AFB$_1$: 79–96% The maximum degradation: AFB1 = 96.881%; AFT = 95.721%	Disadvantages: • The rate of degradation of aflatoxin increases with an increase in the moisture content of heated food, the potato dextrose agar used as a model system for the study was of high moisture content; • When the optimized parameters were adapted to the real food matrix, the degradation percentage of the toxin may vary with its moisture content.	[126]

Table 4. *Cont.*

Combination	Feeds /Foods	Contaminant	Experimental Parameters	Reduction Rate	Advantages/Disadvantages	References
High Conc. H_2O_2 at Moderate temperature/roasting	Peanuts	AF	30 g/hg H_2O_2 at 20 °C	AF reduction rate = 30%	• The oil quality was not seriously affected by the treatment; • The weight loss and oil quality change of the treated peanuts were negligible; • Peanuts were able to keep intact after the treatment because the temperature of the treatment was lower than that of the starch gelatinization; Eco-friendly process; • Most H_2O_2 was removed by drying H_2O_2-treated peanuts at 35 °C for 12 h.	[127]
			30 g/hg H_2O_2 at 50 °C	AF reduction rate = 73%		
			30 g/hg H_2O_2 at 50 °C for 8 h —unroasted peanuts	AF reduction rate = 86%		
			Combined effect: 30 g/hg H_2O_2 at 50 °C for 8 h + roasted peanuts at 140 °C for 10 min	AF reduction rate = 90%		

4. Simultaneous Detoxification Treatments Used in Solid Foods and Feeds

In this section, we discuss many combined treatments applied simultaneously to food or feed matrices, and these combinations are represented in Table 5.

4.1. UV with H_2O_2

UV-C is used in combination with H_2O_2 to degrade aflatoxins in peanuts. It represents an eco-friendly technique leaving no toxic or harmful byproducts, with unique residual compounds limited to water and oxygen. The simultaneous application of these two treatments for 1 h (UV-C: 2.76 mW/cm^2—H_2O_2: 1 g/hg) accelerated the degradation rates of AF in both whole peanut kernels and milled kernels to 30% and 60%, respectively. The advanced oxidative processes (UV and H_2O_2) affected the quality of the oil in milled kernels and caused the darkening of the whole kernels [128].

4.2. Pulsed Light with Citric Acid

The combination of pulsed light with citric acid showed great efficiency on AFT, AFB$_1$, and AFB$_2$ in peanuts, with reduction rates reaching about 98.2%, 98.9%, and 98.1%, respectively. The chemical quality did not show significant changes as a result of this combined effect, but a significant change in the color of peanuts occurred [129]. In previously discussed studies about pulsed light treatments, the reduction rates of AFT, AFB$_1$, and AFB$_2$ were in the range of 39.2 to 90.2% in red pepper powder and rice with different fluence ranges applied [81,83]. Therefore, combining an acid with pulsed light can be considered a beneficial combination, demonstrating higher efficiency in mitigating aflatoxins than each treatment alone.

4.3. Infrared with Alkaline Treatment

There are contradictory results concerning the nixtamalization efficiency in reducing aflatoxins in maize by using the traditional process. Rodríguez–Aguilar et al., proposed the non-efficiency of the traditional nixtamalization process (TNP) in the elimination of aflatoxins from contaminated maize [51]. Meanwhile, Zavala–Franco et al., found that TNP can degrade aflatoxins in maize by 98.35%. The same study proposed using infrared as an alternative to heat treatment in the nixtamalization process. The applied protocol satisfactorily achieved a degradation rate of 93.82%. No formation of AFB$_1$-Lys occurred with the infrared nixtamalization process. This combination of alkaline treatment with infrared seems to be promising for mitigating mycotoxins while generating fewer toxic materials than the traditional process [130].

4.4. Roasting with Acid

Aflatoxin levels can be reduced by using high-temperature treatment, such as roasting. Degradation rates in the range of 50 to 70% in peanuts and the range of 40 to 80% in maize were achieved [68]. Roasting pistachio nuts at 120 °C for 1 h is optimized when used in combination with the addition of citric acid and lemon juice. The high amount of used acids increased the AFB$_1$ degradation rate to reach 93.1%, which negatively affected the physical quality of the pistachio. Decreasing the acid amount by half decreased the degradation rate to 49.2% but maintained the desired appearance of the treated pistachio [131].

Table 5. Simultaneous techniques to mitigate mycotoxins in solid foods and feeds.

Combination	Feeds/Foods	Mycotoxins	Experimental Parameters	Reduction Rate	Advantages/Disadvantages	References
UV + H_2O_2	Peanuts	AFs	Advanced Oxidation Processes by UV and H_2O_2		Advantages: • The AOP treatment can be considered environmentally friendly; • No waste—the degradation compounds are only water and oxygen; • This combination accelerates the degradation rate of AF; • Drying peanuts at 35 °C for 12h: complete removal of residual H_2O_2. Disadvantages: • The oil quality was slightly affected by the AOP treatment in whole kernels, but a more severe influence on oil quality was observed in the milled kernels; • The color of whole kernels slightly darkened but not considerably affect its appearance.	[128]
			1 h AOP (2.76 mW/cm² UV-C, 1 g/hg H_2O_2) of whole peanut kernels	Degradation rate of AF = 33%		
			1 h AOP (2.76 mW/cm² UV-C, 1 g/hg H_2O_2) of milled kernels	Degradation rate of AF = 60%		
Citric acid + Pulsed light	Peanuts	AFB	PL + CA treatment	AFT ≈ 98.2% AFB_1 ≈ 98.9% AFB_2 ≈ 98.1%	Advantages: • No significant changes in chemical quality. Disadvantages: • Significant changes in color.	[129]
IR Nixtamalization (alkaline treatment + IR)	Maize tortillas	AFs	The infrared nixtamalization process (IRNP)—Cooking in a cooker that generates infrared radiation (14.2 A, 1704 W)	The degradation rate of AF: 93.82%	Advantages: • They did not show adduct AFB1-Lys formation; • An effective method for aflatoxin detoxification in maize tortillas, as it generates degradation products less toxic than those used in traditional nixtamalization.	[130]
			Traditional nixtamalization process (TNP)	The degradation rate of AF: 98.35%		

Table 5. *Cont.*

Combination	Feeds/Foods	Mycotoxins	Experimental Parameters	Reduction Rate	Advantages/Disadvantages	References
Roasting + acid	Pistachio nuts	AFB$_1$	Treatment 1: 50 g Pistachio—addition of 30 mL water + 30 mL lemon juice + 6 g of citric acid—roasting at 120 °C for 1 h	AFB$_1$ = 93.1 ± 8.2%	Advantages: • Useful and safe degradation method of AFB1 in naturally contaminated pistachio nuts; • Treatment 2 caused no noticeable change in the desired appearance of pistachios. Disadvantages: • Treatment 1 altered the desired physical properties.	[131]
			Treatment 2: 50 g Pistachio—addition of 30 mL water + 15 mL lemon juice + 2.25 g of citric acid—Roasting at 120 °C for 1 h	AFB$_1$ = 49.2 ± 3.5%		

5. Comparison between the Different Mycotoxin Decontamination Treatments

In general, chemical treatments achieved higher reduction rates of mycotoxins than physical treatments in solid foods and feeds. This effectiveness is accompanied by many side effects, such as the detrimental impacts on the quality of the treated food materials (ammoniation) and the formation of unavoidable chemical residues causing an environmental problem (nixtamalization). All the chemical treatments presented in this review showed possible scalability, except the acid treatment, due to the high cost of using organic acids. The physical treatments showed lower degradation rates. This can be seen in the shielding effect in the case of irradiation or the presence of the skin on some foods, such as peanuts. It is worth noting that these physical treatments usually have low penetrability where the effect remains superficial, treating a thin layer. The biological treatments of solid foods or feeds were commonly less available than other treatments. They showed good results and achieved high reduction rates with a beneficial effect of LAB on fermentation by increasing lactic acid production in maize. Combined fermentation using two LAB strains achieved higher reduction rates than those using each strain individually. The results obtained using the biological decontamination treatments prove its suitability to be considered an alternative to physical and chemical treatments by providing a safe, eco-friendly, and cost-effective method with a minimal negative effect on the quality of treated materials.

Concerning the combined treatment and by comparing the subsequent treatments in Table 4 and the simultaneous treatments in Table 5, we can spotlight many successful combinations, such as the subsequent application of O_3/UV-C/citric acid and high concentration H_2O_2 treatment at moderate temperature/roasting, which achieved a reduction of AFs in pistachio and peanuts, respectively. The reduction of AFs by PEF/heat treatment attained high reduction rates in agar, but it was decreased when implemented in dry food, hypothesizing that the presence of water contributes to its success in AF elimination. Roasting/brewing was able to reduce mycotoxins without reaching the complete elimination of AFs and OTA from coffee beans. All the simultaneous treatments mentioned in this review showed their success in reducing or eliminating AFs; reduction rates exceeding 93% were accomplished by implementing citric acid with pulsed light to peanuts, IR nixtamalization to maize, and roasting with acid to pistachio.

6. Conclusions

In this review, we screened, evaluated, and discussed different chemical, physical, biological, and combined techniques to mitigate mycotoxins in solid foods and feeds. Many chemical treatments showed their effectiveness by achieving approximately a total elimination of AFs under certain conditions, such as optimized nixtamalization, ammoniation, and acid. Physical treatments such as photocatalysis and cold plasma were able to achieve the complete elimination of DON and AFB_1, respectively. Chemical treatments showed higher reduction rates of mycotoxins than physical treatments, but the latter treatments were favorable from a quality perspective. Their effect was superficial, causing minimal changes in the quality of treated materials. Biological treatments are considered safe, eco-friendly, and cost-effective methods for mitigating mycotoxins. *Zygosaccharomyces rouxii* or a combination of LAB strains attained high reduction rates. Two or more treatments were used subsequently or simultaneously in order to find a synergistic effect of the combination to achieve high reduction rates in solid food materials without inducing any extreme impacts in each one. Nine combinations are presented in the last two tables, showing the higher reduction rates of aflatoxins (>90%) achieved by the following two combinations when implemented subsequently: O_3/UV-C/citric acid and high H_2O_2 concentration treatment at moderate temperature/roasting. Other combinations were applied simultaneously, also showing their efficiency in the reduction of aflatoxins (>93%), such as citric acid with pulsed light and roasting with acid. These combinations affected the physical characteristics of the treated nuts. Future research should focus on the optimization of physical treatments to increase their mycotoxin reduction efficiency and on the elaboration of more combination possibilities to find the best synergistic effect to protect the product quality and the envi-

ronment. It is highly important to focus more on implementing detoxification techniques on naturally contaminated materials than spiked or artificially contaminated materials. Natural contamination may be caused by several mycotoxins and may occur differently. Furthermore, these studies should examine the effectiveness of these techniques at the industrial scale more than at the laboratory scale.

Data Availability Statement: Data is contained within the article.

Conflicts of Interest: The authors declare no conflict of interest.

References

1. Medina, A.; Akbar, A.; Baazeem, A.; Rodriguez, A.; Magan, N. Climate Change, Food Security and Mycotoxins: Do We Know Enough? *Fungal Biol. Rev.* **2017**, *31*, 143–154. [CrossRef]
2. Gomez, K.S.; Castañeda Roldán, E.; Ávila Sosa, R.; Munguía-Pérez, R. Mycotoxins and Climate Change. In *The Impact of Climate Change on Fungal Diseases*; Frías-De-León, M.G., Brunner-Mendoza, C., del Rocío Reyes-Montes, M., Duarte-Escalante, E., Eds.; Fungal Biology Book Series; Springer International Publishing: Cham, Switzerland, 2022; pp. 239–256. ISBN 978-3-030-89664-5.
3. Matumba, L.; Namaumbo, S.; Ngoma, T.; Meleke, N.; De Boevre, M.; Logrieco, A.F.; De Saeger, S. Five Keys to Prevention and Control of Mycotoxins in Grains: A Proposal. *Glob. Food Secur.* **2021**, *30*, 100562. [CrossRef]
4. Puri, S.; Shingh, S.; Tiwari, P. Mycotoxins: A Threat to Food Security and Health. *Int. J. Appl. Sci. Biotechnol.* **2019**, *7*, 298. [CrossRef]
5. Marc, R.A. *Implications of Mycotoxins in Food Safety*; IntechOpen: Cluj-Napoca, Romania, 2022; ISBN ISBN 978-1-83962-904-4.
6. Hassan, H.F.; Koaik, L.; Khoury, A.E.; Atoui, A.; El Obeid, T.; Karam, L. Dietary Exposure and Risk Assessment of Mycotoxins in Thyme and Thyme-Based Products Marketed in Lebanon. *Toxins* **2022**, *14*, 331. [CrossRef] [PubMed]
7. Chilaka, C.A.; Obidiegwu, J.E.; Chilaka, A.C.; Atanda, O.O.; Mally, A. Mycotoxin Regulatory Status in Africa: A Decade of Weak Institutional Efforts. *Toxins* **2022**, *14*, 442. [CrossRef] [PubMed]
8. El-Sayed, R.A.; Jebur, A.B.; Kang, W.; El-Demerdash, F.M. An Overview on the Major Mycotoxins in Food Products: Characteristics, Toxicity, and Analysis. *J. Future Foods* **2022**, *2*, 91–102. [CrossRef]
9. Mycotoxins in Lebanese Food Basket—Final.Pdf. 2022. Available online: https://www.usj.edu.lb/intranet/actu/pdf/11610_19 52.pdf (accessed on 10 August 2022).
10. Pleadin, J.; Frece, J.; Markov, K. Chapter Eight—Mycotoxins in Food and Feed. In *Advances in Food and Nutrition Research*; Toldrá, F., Ed.; Academic Press: Cambridge, MA, USA, 2019; Volume 89, pp. 297–345.
11. Xu, R.; Kiarie, E.G.; Yiannikouris, A.; Sun, L.; Karrow, N.A. Nutritional Impact of Mycotoxins in Food Animal Production and Strategies for Mitigation. *J. Anim. Sci. Biotechnol.* **2022**, *13*, 69. [CrossRef]
12. Smith, M.-C.; Madec, S.; Coton, E.; Hymery, N. Natural Co-Occurrence of Mycotoxins in Foods and Feeds and Their in Vitro Combined Toxicological Effects. *Toxins* **2016**, *8*, 94. [CrossRef]
13. Cinar, A.; Onbaşı, E. Mycotoxins: The Hidden Danger in Foods. In *Mycotoxins and Food Safety*; IntechOpen: London, UK, 2019; ISBN 978-1-78984-874-8.
14. Jajić, I.; Dudaš, T.; Krstović, S.; Krska, R.; Sulyok, M.; Bagi, F.; Savić, Z.; Guljaš, D.; Stankov, A. Emerging Fusarium Mycotoxins Fusaproliferin, Beauvericin, Enniatins, and Moniliformin in Serbian Maize. *Toxins* **2019**, *11*, 357. [CrossRef]
15. Fapohunda, S.O.; Anjorin, T.S.; Sulyok, M.; Krska, R. Profile of Major and Emerging Mycotoxins in Sesame and Soybean Grains in the Federal Capital Territory, Abuja, Nigeria. *Eur. J. Biol. Res.* **2018**, *8*, 121–130.
16. Mahato, D.K.; Lee, K.E.; Kamle, M.; Devi, S.; Dewangan, K.N.; Kumar, P.; Kang, S.G. Aflatoxins in Food and Feed: An Overview on Prevalence, Detection and Control Strategies. *Front. Microbiol.* **2019**, *10*, 2266. [CrossRef]
17. Yang, Y.; Li, G.; Wu, D.; Liu, J.; Li, X.; Luo, P.; Hu, N.; Wang, H.; Wu, Y. Recent Advances on Toxicity and Determination Methods of Mycotoxins in Foodstuffs. *Trends Food Sci. Technol.* **2020**, *96*, 233–252. [CrossRef]
18. Eskola, M.; Kos, G.; Elliott, C.T.; Hajšlová, J.; Mayar, S.; Krska, R. Worldwide Contamination of Food-Crops with Mycotoxins: Validity of the Widely Cited 'FAO Estimate' of 25%. *Crit. Rev. Food Sci. Nutr.* **2020**, *60*, 2773–2789. [CrossRef]
19. Alshannaq, A.; Yu, J.-H. Occurrence, Toxicity, and Analysis of Major Mycotoxins in Food. *Int. J. Environ. Res. Public. Health* **2017**, *14*, 632. [CrossRef]
20. Altomare, C.; Logrieco, A.F.; Gallo, A. Mycotoxins and Mycotoxigenic Fungi: Risk and Management. A Challenge for Future Global Food Safety and Security. In *Encyclopedia of Mycology*; Zaragoza, Ó., Casadevall, A., Eds.; Elsevier: Oxford, UK, 2021; pp. 64–93. ISBN 978-0-323-85180-0.
21. Luo, S.; Du, H.; Kebede, H.; Liu, Y.; Xing, F. Contamination Status of Major Mycotoxins in Agricultural Product and Food Stuff in Europe. *Food Control* **2021**, *127*, 108120. [CrossRef]
22. Stroka, J.; Gonçalves, C. Mycotoxins in Food and Feed: An Overview. In *Encyclopedia of Food Chemistry*; Elsevier: Amsterdam, The Netherlands, 2019; pp. 401–419. ISBN 978-0-12-814045-1.

23. Awuchi, C.G.; Ondari, E.N.; Ogbonna, C.U.; Upadhyay, A.K.; Baran, K.; Okpala, C.O.R.; Korzeniowska, M.; Guiné, R.P.F. Mycotoxins Affecting Animals, Foods, Humans, and Plants: Types, Occurrence, Toxicities, Action Mechanisms, Prevention, and Detoxification Strategies—A Revisit. *Foods* **2021**, *10*, 1279. [CrossRef]

24. Cheli, F.; Pinotti, L.; Novacco, M.; Ottoboni, M.; Tretola, M.; Dell'Orto, V. Mycotoxins in Wheat and Mitigation Measures. In *Wheat Improvement, Management and Utilization*; Wanyera, R., Owuoche, J., Eds.; InTech: Milan, Italy, 2017; ISBN 978-953-51-3151-9.

25. Wan, J.; Chen, B.; Rao, J. Occurrence and Preventive Strategies to Control Mycotoxins in Cereal-based Food. *Compr. Rev. Food Sci. Food Saf.* **2020**, *19*, 928–953. [CrossRef]

26. Conte, G.; Fontanelli, M.; Galli, F.; Cotrozzi, L.; Pagni, L.; Pellegrini, E. Mycotoxins in Feed and Food and the Role of Ozone in Their Detoxification and Degradation: An Update. *Toxins* **2020**, *12*, 486. [CrossRef]

27. Piotrowska, M. Microbiological Decontamination of Mycotoxins: Opportunities and Limitations. *Toxins* **2021**, *13*, 819. [CrossRef]

28. Liu, M.; Zhao, L.; Gong, G.; Zhang, L.; Shi, L.; Dai, J.; Han, Y.; Wu, Y.; Khalil, M.M.; Sun, L. Invited Review: Remediation Strategies for Mycotoxin Control in Feed. *J. Anim. Sci. Biotechnol.* **2022**, *13*, 19. [CrossRef]

29. Gonçalves, B.L.; Uliana, R.D.; Coppa, C.F.S.C.; Lee, S.H.I.; Kamimura, E.S.; Oliveira, C.A.F.; Corassin, C.H. Aflatoxin M1: Biological Decontamination Methods in Milk and Cheese. *Food Sci. Technol.* **2022**, *42*, e22920. [CrossRef]

30. Assaf, J.C.; Atoui, A.; Khoury, A.E.; Chokr, A.; Louka, N. A Comparative Study of Procedures for Binding of Aflatoxin M1 to Lactobacillus Rhamnosus GG. *Braz. J. Microbiol. Publ. Braz. Soc. Microbiol.* **2018**, *49*, 120–127. [CrossRef]

31. Ragoubi, C.; Quintieri, L.; Greco, D.; Mehrez, A.; Maatouk, I.; D'Ascanio, V.; Landoulsi, A.; Avantaggiato, G. Mycotoxin Removal by Lactobacillus Spp. and Their Application in Animal Liquid Feed. *Toxins* **2021**, *13*, 185. [CrossRef] [PubMed]

32. Assaf, J.C.; Khoury, A.E.; Chokr, A.; Louka, N.; Atoui, A. A Novel Method for Elimination of Aflatoxin M1 in Milk Using Lactobacillus Rhamnosus GG Biofilm. *Int. J. Dairy Technol.* **2019**, *72*, 248–256. [CrossRef]

33. Assaf, J.C.; El Khoury, A.; Atoui, A.; Louka, N.; Chokr, A. A Novel Technique for Aflatoxin M1 Detoxification Using Chitin or Treated Shrimp Shells: In Vitro Effect of Physical and Kinetic Parameters on the Binding Stability. *Appl. Microbiol. Biotechnol.* **2018**, *102*, 6687–6697. [CrossRef] [PubMed]

34. Assaf, J.C.; Nahle, S.; Chokr, A.; Louka, N.; Atoui, A.; El Khoury, A. Assorted Methods for Decontamination of Aflatoxin M1 in Milk Using Microbial Adsorbents. *Toxins* **2019**, *11*, 304. [CrossRef] [PubMed]

35. Pallarés, N.; Berrada, H.; Tolosa, J.; Ferrer, E. Effect of High Hydrostatic Pressure (HPP) and Pulsed Electric Field (PEF) Technologies on Reduction of Aflatoxins in Fruit Juices. *LWT* **2021**, *142*, 111000. [CrossRef]

36. Nan, M.-N.; Bi, Y.; Qiang, Y.; Xue, H.-L.; Yang, L.; Feng, L.-D.; Pu, L.-M.; Long, H.-T.; Prusky, D. Electrostatic Adsorption and Removal Mechanism of Ochratoxin A in Wine via a Positively Charged Nano-MgO Microporous Ceramic Membrane. *Food Chem.* **2022**, *371*, 131157. [CrossRef]

37. Borràs-Vallverdú, B.; Ramos, A.J.; Marín, S.; Sanchis, V.; Rodríguez-Bencomo, J.J. Deoxynivalenol Degradation in Wheat Kernels by Exposition to Ammonia Vapours: A Tentative Strategy for Detoxification. *Food Control* **2020**, *118*, 107444. [CrossRef]

38. Abdel-Aal, E.-S.M.; Miah, K. Kinetics of Deoxynivalenol Flux in Wheat Kernels Steeped in Different Solutions for Improved Food Safety. *Food Control* **2022**, *133*, 108606. [CrossRef]

39. Wu, N.; Ou, W.; Zhang, Z.; Wang, Y.; Xu, Q.; Huang, H. Recent advances in detoxification strategies for zearalenone contamination in food and feed. *Chin. J. Chem. Eng.* **2021**, *29*, 168–177. [CrossRef]

40. Gilbert Sandoval, I.; Wesseling, S.; Rietjens, I.M.C.M. Aflatoxin B1 in Nixtamalized Maize in Mexico; Occurrence and Accompanying Risk Assessment. *Toxicol. Rep.* **2019**, *6*, 1135–1142. [CrossRef]

41. Méndez-Albores, A.; Arámbula-Villa, G.; Loarca-Piña, M.G.F.; Castaño-Tostado, E.; Moreno-Martínez, E. Safety and Efficacy Evaluation of Aqueous Citric Acid to Degrade B-Aflatoxins in Maize. *Food Chem. Toxicol.* **2005**, *43*, 233–238. [CrossRef]

42. Mallakian, S.; Rezanezhad, R.; Jalali, M.; Ghobadi, F. The Effect of Ozone Gas on Destruction and Detoxification of Aflatoxin. *Bull. Société R. Sci. Liège* **2017**, *86*, 1–6. [CrossRef]

43. Park, D.; Price, W. Reduction of Aflatoxin Hazards Using Ammoniation. *Rev. Environ. Contam. Toxicol.* **2001**, *171*, 139–175. [CrossRef]

44. Ouf, S.A.; Ali, E.M. Does the Treatment of Dried Herbs with Ozone as a Fungal Decontaminating Agent Affect the Active Constituents? *Pollut.* **2021**, *277*, 116715. [CrossRef]

45. Da Luz, S.R.; Almeida Villanova, F.; Tuchtenhagen Rockembach, C.; Dietrich Ferreira, C.; José Dallagnol, L.; Luis Fernandes Monks, J.; de Oliveira, M. Reduced of Mycotoxin Levels in Parboiled Rice by Using Ozone and Its Effects on Technological and Chemical Properties. *Food Chem.* **2022**, *372*, 131174. [CrossRef]

46. Young, J.C.; Zhu, H.; Zhou, T. Degradation of Trichothecene Mycotoxins by Aqueous Ozone. *Food Chem. Toxicol.* **2006**, *44*, 417–424. [CrossRef]

47. Li, M.M.; Guan, E.Q.; Bian, K. Effect of Ozone Treatment on Deoxynivalenol and Quality Evaluation of Ozonised Wheat. *Food Addit. Contam. Part A* **2015**, *32*, 544–553. [CrossRef]

48. McDonough, M.X.; Campabadal, C.A.; Mason, L.J.; Maier, D.E.; Denvir, A.; Woloshuk, C. Ozone Application in a Modified Screw Conveyor to Treat Grain for Insect Pests, Fungal Contaminants, and Mycotoxins. *J. Stored Prod. Res.* **2011**, *47*, 249–254. [CrossRef]

49. Savi, G.D.; Gomes, T.; Canever, S.B.; Feltrin, A.C.; Piacentini, K.C.; Scussel, R.; Oliveira, D.; Machado-de-Ávila, R.A.; Cargnin, M.; Angioletto, E. Application of Ozone on Rice Storage: A Mathematical Modeling of the Ozone Spread, Effects in the Decontamination of Filamentous Fungi and Quality Attributes. *J. Stored Prod. Res.* **2020**, *87*, 101605. [CrossRef]

50.   Maureen, N.; Kaaya, A.N.; Kauffman, J.; Narrod, C.; Atukwase, A. Enhancing Nutritional Benefits and Reducing Mycotoxin Contamination of Maize through Nixtamalization. *J. Biol. Sci.* **2020**, *20*, 153–162. [CrossRef]
51.   Rodríguez-Aguilar, M.; Solís-Mercado, J.; Flores-Ramírez, R.; Díaz-Barriga, F.; Zuki-Orozco, A.; Cilia-López, V.G. Aflatoxins and the Traditional Process of Nixtamalisation in Indigenous Communities from the Huasteca Potosina Region. *World Mycotoxin J.* **2020**, *13*, 391–399. [CrossRef]
52.   Moreno-Pedraza, A.; Valdés-Santiago, L.; Hernández-Valadez, L.J.; Rodríguez-Sixtos Higuera, A.; Winkler, R.; Guzmán-de Peña, D.L. Reduction of Aflatoxin B1 during Tortilla Production and Identification of Degradation By-Products by Direct-Injection Electrospray Mass Spectrometry (DIESI-MS). *Salud Publica Mex.* **2015**, *57*, 50–57. [CrossRef] [PubMed]
53.   Odukoya, J.O.; De Saeger, S.; De Boevre, M.; Adegoke, G.O.; Audenaert, K.; Croubels, S.; Antonissen, G.; Vermeulen, K.; Gbashi, S.; Njobeh, P.B. Effect of Selected Cooking Ingredients for Nixtamalization on the Reduction of Fusarium Mycotoxins in Maize and Sorghum. *Toxins* **2021**, *13*, 27. [CrossRef] [PubMed]
54.   EFSA Panel on Contaminants in the Food Chain (CONTAM); Schrenk, D.; Bignami, M.; Bodin, L.; Chipman, J.K.; del Mazo, J.; Grasl-Kraupp, B.; Hoogenboom, L.; Leblanc, J.; Nebbia, C.S.; et al. Assessment of an Application on a Detoxification Process of Groundnut Press Cake for Aflatoxins by Ammoniation. *EFSA J.* **2021**, *19*, e07035. [CrossRef] [PubMed]
55.   Sumner, P.; Hammond, C. *Treating Aflatoxin-Contaminated Corn with Ammonia*; University of Georgia: Athens, GA, USA, 2009.
56.   Nyandieka, H.S.; Maina, J.O.; Nyamwange, C. Detoxification of Aflatoxin in Artificially Contaminated Maize Crop by Ammonia-tion Procedures. *Discov. Innov.* **2009**, *21*, 77. [CrossRef]
57.   Jubeen, F.; Sher, F.; Hazafa, A.; Zafar, F.; Ameen, M.; Rasheed, T. Evaluation and Detoxification of Aflatoxins in Ground and Tree Nuts Using Food Grade Organic Acids. *Biocatal. Agric. Biotechnol.* **2020**, *29*, 101749. [CrossRef]
58.   Humer, E.; Lucke, A.; Harder, H.; Metzler-Zebeli, B.; Böhm, J.; Zebeli, Q. Effects of Citric and Lactic Acid on the Reduction of Deoxynivalenol and Its Derivatives in Feeds. *Toxins* **2016**, *8*, 285. [CrossRef]
59.   Rushing, B.R.; Selim, M.I. Effect of Dietary Acids on the Formation of Aflatoxin B$_{2a}$ as a Means to Detoxify Aflatoxin B$_1$. *Food Addit. Contam. Part A* **2016**, *33*, 1456–1467. [CrossRef]
60.   Schaarschmidt, S.; Fauhl-Hassek, C. Mycotoxins during the Processes of Nixtamalization and Tortilla Production. *Toxins* **2019**, *11*, 227. [CrossRef]
61.   Anguiano-Ruvalcaba, G.L.; Vargas-Cortina, A.V.y.; Peña, D.G.-D. Inactivation of aflatoxin B1 and aflatoxicol through traditional "nixtamalización" of corn and their regeneration by acidification of corn dough. *Salud Pública México* **2005**, *47*, 369–375. [CrossRef]
62.   Guo, Y.; Zhao, L.; Ma, Q.; Ji, C. Novel Strategies for Degradation of Aflatoxins in Food and Feed: A Review. *Food Res. Int.* **2021**, *140*, 109878. [CrossRef]
63.   Nunes, V.M.; Moosavi, M.; Mousavi Khaneghah, A.; Oliveira, C.A. Innovative Modifications in Food Processing to Reduce the Levels of Mycotoxins. *Curr. Opin. Food Sci.* **2021**, *38*, 155–161. [CrossRef]
64.   Sipos, P.; Peles, F.; Brassó, D.L.; Béri, B.; Pusztahelyi, T.; Pócsi, I.; Győri, Z. Physical and Chemical Methods for Reduction in Aflatoxin Content of Feed and Food. *Toxins* **2021**, *13*, 204. [CrossRef]
65.   Cabrera-Meraz, J.; Maldonado, L.; Bianchini, A.; Espinal, R. Incidence of Aflatoxins and Fumonisins in Grain, Masa and Corn Tortillas in Four Municipalities in the Department of Lempira, Honduras. *Heliyon* **2021**, *7*, e08506. [CrossRef]
66.   Murugesan, P.; Brunda, D.K.; Moses, J.A.; Anandharamakrishnan, C. Photolytic and Photocatalytic Detoxification of Mycotoxins in Foods. *Food Control* **2021**, *123*, 107748. [CrossRef]
67.   Hoffmans, Y.; Schaarschmidt, S.; Fauhl-Hassek, C.; Van der Fels-Klerx, H. (Ine) Factors during Production of Cereal-Derived Feed That Influence Mycotoxin Contents. *Toxins* **2022**, *14*, 301. [CrossRef]
68.   Karlovsky, P.; Suman, M.; Berthiller, F.; De Meester, J.; Eisenbrand, G.; Perrin, I.; Oswald, I.P.; Speijers, G.; Chiodini, A.; Recker, T.; et al. Impact of Food Processing and Detoxification Treatments on Mycotoxin Contamination. *Mycotoxin Res.* **2016**, *32*, 179–205. [CrossRef]
69.   Wu, S.; Wang, F.; Li, Q.; Wang, J.; Zhou, Y.; Duan, N.; Niazi, S.; Wang, Z. Photocatalysis and Degradation Products Identification of Deoxynivalenol in Wheat Using Upconversion Nanoparticles@TiO2 Composite. *Food Chem.* **2020**, *323*, 126823. [CrossRef]
70.   Ott, L.C.; Appleton, H.J.; Shi, H.; Keener, K.; Mellata, M. High Voltage Atmospheric Cold Plasma Treatment Inactivates Aspergillus Flavus Spores and Deoxynivalenol Toxin. *Food Microbiol.* **2021**, *95*, 103669. [CrossRef]
71.   Marshall, H.; Meneely, J.P.; Quinn, B.; Zhao, Y.; Bourke, P.; Gilmore, B.F.; Zhang, G.; Elliott, C.T. Novel Decontamination Approaches and Their Potential Application for Post-Harvest Aflatoxin Control. *Trends Food Sci. Technol.* **2020**, *106*, 489–496. [CrossRef]
72.   Gonçalves Lemos, J.; Stefanello, A.; Olivier Bernardi, A.; Valle Garcia, M.; Nicoloso Magrini, L.; Cichoski, A.J.; Wagner, R.; Venturini Copetti, M. Antifungal Efficacy of Sanitizers and Electrolyzed Waters against Toxigenic Aspergillus. *Food Res. Int.* **2020**, *137*, 109451. [CrossRef] [PubMed]
73.   Ferreira, C.D.; Lang, G.H.; da SIlva Lindemann, I.; da Silva, N.T.; Hoffmann, J.F.; Ziegler, V.; de Oliveira, M. Postharvest UV-C Irradiation for Fungal Control and Reduction of Mycotoxins in Brown, Black, and Red Rice during Long-Term Storage. *Food Chem.* **2021**, *339*, 127810. [CrossRef] [PubMed]
74.   Pérez-Santaescolástica, C.; Fraeye, I.; Barba, F.J.; Gómez, B.; Tomasevic, I.; Romero, A.; Moreno, A.; Toldrá, F.; Lorenzo, J.M. Application of Non-Invasive Technologies in Dry-Cured Ham: An Overview. *Trends Food Sci. Technol.* **2019**, *86*, 360–374. [CrossRef]

75. Liu, Y.; Joseph Hubert, G.; Gong, Y.Y.; Orfila, C. A Review of Post-Harvest Approaches to Reduce Fungal and Mycotoxin Contamination of Foods. *Compr. Rev. Food Sci. Food Saf.* **2020**, *19*, 1521–1560. [CrossRef] [PubMed]
76. Wu, S.; Wang, F.; Li, Q.; Zhou, Y.; He, C.; Duan, N. Detoxification of DON by Photocatalytic Degradation and Quality Evaluation of Wheat. *RSC Adv.* **2019**, *9*, 34351–34358. [CrossRef]
77. Hojnik, N.; Modic, M.; Walsh, J.L.; Žigon, D.; Javornik, U.; Plavec, J.; Žegura, B.; Filipič, M.; Cvelbar, U. Unravelling the Pathways of Air Plasma Induced Aflatoxin B1 Degradation and Detoxification. *J. Hazard. Mater.* **2021**, *403*, 123593. [CrossRef]
78. Kiš, M.; Milošević, S.; Vulić, A.; Herceg, Z.; Vukušić, T.; Pleadin, J. Efficacy of Low Pressure DBD Plasma in the Reduction of T-2 and HT-2 Toxin in Oat Flour. *Food Chem.* **2020**, *316*, 126372. [CrossRef]
79. Wielogorska, E.; Ahmed, Y.; Meneely, J.; Graham, W.G.; Elliott, C.T.; Gilmore, B.F. A Holistic Study to Understand the Detoxification of Mycotoxins in Maize and Impact on Its Molecular Integrity Using Cold Atmospheric Plasma Treatment. *Food Chem.* **2019**, *301*, 125281. [CrossRef]
80. Casas-Junco, P.P.; Solís-Pacheco, J.R.; Ragazzo-Sánchez, J.A.; Aguilar-Uscanga, B.R.; Bautista-Rosales, P.U.; Calderón-Santoyo, M. Cold Plasma Treatment as an Alternative for Ochratoxin A Detoxification and Inhibition of Mycotoxigenic Fungi in Roasted Coffee. *Toxins* **2019**, *11*, 337. [CrossRef]
81. Woldemariam, H.W.; Harmeling, H.; Emire, S.; Teshome, P.G.; Toepfl, S.; Aganovic, K. Pulsed Light Treatment Reduces Microorganisms and Mycotoxins Naturally Present in Red Pepper (*Capsicum annuum* L.) Powder. *J. Food Process Eng.* **2021**, *45*, e13948. [CrossRef]
82. Wang, B.; Mahoney, N.E.; Khir, R.; Wu, B.; Zhou, C.; Pan, Z.; Ma, H. Degradation Kinetics of Aflatoxin B$_1$ and B$_2$ in Solid Medium by Using Pulsed Light Irradiation: Degradation Kinetics of Aflatoxins in Solid Medium Using Pulsed Light Irradiation. *J. Sci. Food Agric.* **2018**, *98*, 5220–5224. [CrossRef]
83. Wang, B.; Mahoney, N.E.; Pan, Z.; Khir, R.; Wu, B.; Ma, H.; Zhao, L. Effectiveness of Pulsed Light Treatment for Degradation and Detoxification of Aflatoxin B1 and B2 in Rough Rice and Rice Bran. *Food Control* **2016**, *59*, 461–467. [CrossRef]
84. Udovicki, B.; Stankovic, S.; Tomic, N.; Djekic, I.; Smigic, N.; Trifunovic, B.S.; Milicevic, D.; Rajkovic, A. Evaluation of Ultraviolet Irradiation Effects on Aspergillus Flavus and Aflatoxin B1 in Maize and Peanut Using Innovative Vibrating Decontamination Equipment. *Food Control* **2022**, *134*, 108691. [CrossRef]
85. Shen, M.-H.; Singh, R.K. Effect of Rotating Peanuts on Aflatoxin Detoxification by Ultraviolet C Light and Irradiation Uniformity Evaluated by AgCl-Based Dosimeter. *Food Control* **2021**, *120*, 107533. [CrossRef]
86. Khalil, O.A.A.; Hammad, A.A.; Sebaei, A.S. Aspergillus Flavus and Aspergillus Ochraceus Inhibition and Reduction of Aflatoxins and Ochratoxin A in Maize by Irradiation. *Toxicon* **2021**, *198*, 111–120. [CrossRef]
87. Calado, T.; Fernández-Cruz, M.L.; Cabo Verde, S.; Venâncio, A.; Abrunhosa, L. Gamma Irradiation Effects on Ochratoxin A: Degradation, Cytotoxicity and Application in Food. *Food Chem.* **2018**, *240*, 463–471. [CrossRef]
88. Ben Amara, A.; Mehrez, A.; Ragoubi, C.; Romero-González, R.; Garrido Frenich, A.; Landoulsi, A.; Maatouk, I. Fungal Mycotoxins Reduction by Gamma Irradiation in Naturally Contaminated Sorghum. *J. Food Process. Preserv.* **2022**, *46*, e16345. [CrossRef]
89. Janić Hajnal, E.; Babic, J.; Pezo, L.; Banjac, V.; Colovic, R.; Kos, J.; Krulj, J.; Vrtač, K.; Jakovac-Strajn, B. Effects of Extrusion Process on Fusarium and Alternaria Mycotoxins in Whole Grain Triticale Flour. *LWT* **2021**, *155*, 112926. [CrossRef]
90. Massarolo, K.C.; Mendoza, J.R.; Verma, T.; Kupski, L.; Badiale-Furlong, E.; Bianchini, A. Fate of Aflatoxins in Cornmeal during Single-Screw Extrusion: A Bioaccessibility Approach. *LWT* **2021**, *138*, 110734. [CrossRef]
91. Lyu, F.; Gao, F.; Zhou, X.; Zhang, J.; Ding, Y. Using Acid and Alkaline Electrolyzed Water to Reduce Deoxynivalenol and Mycological Contaminations in Wheat Grains. *Food Control* **2018**, *88*, 98–104. [CrossRef]
92. Woldemariam, H.W.; Kießling, M.; Emire, S.A.; Teshome, P.G.; Töpfl, S.; Aganovic, K. Influence of Electron Beam Treatment on Naturally Contaminated Red Pepper (*Capsicum annuum* L.) Powder: Kinetics of Microbial Inactivation and Physicochemical Quality Changes. *Innov. Food Sci. Emerg. Technol.* **2021**, *67*, 102588. [CrossRef]
93. Scarpino, V.; Vanara, F.; Sulyok, M.; Krska, R.; Blandino, M. Fate of Regulated, Masked, Emerging Mycotoxins and Secondary Fungal Metabolites during Different Large-Scale Maize Dry-Milling Processes. *Food Res. Int.* **2021**, *140*, 109861. [CrossRef]
94. Vanara, F.; Scarpino, V.; Blandino, M. Fumonisin Distribution in Maize Dry-Milling Products and By-Products: Impact of Two Industrial Degermination Systems. *Toxins* **2018**, *10*, 357. [CrossRef]
95. Sun, S.; Zhao, R.; Xie, Y.; Liu, Y. Photocatalytic Degradation of Aflatoxin B1 by Activated Carbon Supported TiO$_2$ Catalyst. *Food Control* **2019**, *100*, 183–188. [CrossRef]
96. Wu, Y.; Cheng, J.-H.; Sun, D.-W. Blocking and Degradation of Aflatoxins by Cold Plasma Treatments: Applications and Mechanisms. *Trends Food Sci. Technol.* **2021**, *109*, 647–661. [CrossRef]
97. Gómez-López, V.; Noguera-Artiaga, L.; Figueroa, F.; Girón, F.; Carbonell-Barrachina, A.; Gabaldon, J.; Perez-Lopez, A. Effect of Pulsed Light on Quality of Shelled Walnuts. *Foods* **2022**, *11*, 1186. [CrossRef]
98. Bhavya, M.L.; Umesh Hebbar, H. Pulsed Light Processing of Foods for Microbial Safety. *Food Qual. Saf.* **2017**, *1*, 187–202. [CrossRef]
99. Deng, L.-Z.; Tao, Y.; Mujumdar, A.S.; Pan, Z.; Chen, C.; Yang, X.-H.; Liu, Z.-L.; Wang, H.; Xiao, H.-W. Recent Advances in Non-Thermal Decontamination Technologies for Microorganisms and Mycotoxins in Low-Moisture Foods. *Trends Food Sci. Technol.* **2020**, *106*, 104–112. [CrossRef]
100. Shen, M.; Singh, R. Detoxification of Aflatoxins in Foods by Ultraviolet Irradiation, Hydrogen Peroxide, and Their Combination—A Review. *LWT* **2021**, *142*, 110986. [CrossRef]

101. Udomkun, P.; Wiredu, A.N.; Nagle, M.; Müller, J.; Vanlauwe, B.; Bandyopadhyay, R. Innovative Technologies to Manage Aflatoxins in Foods and Feeds and the Profitability of Application—A Review. *Food Control* **2017**, *76*, 127–138. [CrossRef] [PubMed]

102. Balakrishnan, N.; Yusop, S.M.; Rahman, I.A.; Dauqan, E.; Abdullah, A. Efficacy of Gamma Irradiation in Improving the Microbial and Physical Quality Properties of Dried Chillies (*Capsicum Annuum* L.): A Review. *Foods* **2022**, *11*, 97. [CrossRef]

103. Awuchi, C.; Nyakundi Ondari, E.; Ofoedu, C.; Chacha, J.; Rasaq, W.; Morya, S.; Okpala, C. Grain Processing Methods' Effectiveness to Eliminate Mycotoxins: An Overview. *Asian J. Chem.* **2021**, *33*, 2267–2275. [CrossRef]

104. Villarreal-Barajas, T.; Vázquez-Durán, A.; Méndez-Albores, A. Effectiveness of Electrolyzed Oxidizing Water on Fungi and Mycotoxins in Food. *Food Control* **2022**, *131*, 108454. [CrossRef]

105. Rebezov, M.; Saeed, K.; Khaliq, A.; Rahman, S.J.U.; Sameed, N.; Semenova, A.; Khayrullin, M.; Dydykin, A.; Abramov, Y.; Thiruvengadam, M.; et al. Application of Electrolyzed Water in the Food Industry: A Review. *Appl. Sci.* **2022**, *12*, 6639. [CrossRef]

106. Mousavi Khaneghah, A.; Hashemi Moosavi, M.; Oliveira, C.A.F.; Vanin, F.; Sant'Ana, A.S. Electron Beam Irradiation to Reduce the Mycotoxin and Microbial Contaminations of Cereal-Based Products: An Overview. *Food Chem. Toxicol.* **2020**, *143*, 111557. [CrossRef]

107. Mohammadi, X.; Matinfar, G.; Khaneghah, A.M.; Singh, A.; Pratap-Singh, A. Emergence of Cold Plasma and Electron Beam Irradiation as Novel Technologies to Counter Mycotoxins in Food Products. *World Mycotoxin J.* **2021**, *14*, 75–83. [CrossRef]

108. Kim, G.-R.; Ramakrishnan, S.R.; Ameer, K.; Chung, N.; Kim, Y.-R.; Kwon, J.-H. Irradiation Effects on Chemical and Functional Qualities of Ready-to-Eat Saengshik, a Cereal Health Food. *Radiat. Phys. Chem.* **2020**, *171*, 108692. [CrossRef]

109. Milani, J.; Maleki, G. Effects of Processing on Mycotoxin Stability in Cereals. *J. Sci. Food Agric.* **2014**, *94*, 2372–2375. [CrossRef]

110. Reis, T.A.; Oliveira, T.D.; Zorzete, P.; Faria, P.; Corrêa, B. A Non-Toxigenic Aspergillus Flavus Strain Prevents the Spreading of Fusarium Verticillioides and Fumonisins in Maize. *Toxicon* **2020**, *181*, 6–8. [CrossRef]

111. Molo, M.S.; Heiniger, R.W.; Boerema, L.; Carbone, I. Trial Summary on the Comparison of Various Non-Aflatoxigenic Strains of Aspergillus Flavus on Mycotoxin Levels and Yield in Maize. *Agron. J.* **2019**, *111*, 942–946. [CrossRef]

112. Du, G.; Liu, L.; Guo, Q.; Cui, Y.; Chen, H.; Yuan, Y.; Wang, Z.; Gao, Z.; Sheng, Q.; Yue, T. Microbial Community Diversity Associated with Tibetan Kefir Grains and Its Detoxification of Ochratoxin A during Fermentation. *Food Microbiol.* **2021**, *99*, 103803. [CrossRef]

113. Ul Hassan, Z.; Al Thani, R.; Atia, F.A.; Alsafran, M.; Migheli, Q.; Jaoua, S. Application of Yeasts and Yeast Derivatives for the Biological Control of Toxigenic Fungi and Their Toxic Metabolites. *Environ. Technol. Innov.* **2021**, *22*, 101447. [CrossRef]

114. Li, X.; Tang, H.; Yang, C.; Meng, X.; Liu, B. Detoxification of Mycotoxin Patulin by the Yeast Rhodotorula Mucilaginosa. *Food Control* **2019**, *96*, 47–52. [CrossRef]

115. Nahle, S.; El Khoury, A.; Savvaidis, I.; Chokr, A.; Louka, N.; Atoui, A. Detoxification Approaches of Mycotoxins: By Microorganisms, Biofilms and Enzymes. *Int. J. Food Contam.* **2022**, *9*, 3. [CrossRef]

116. Chen, S.-W.; Wang, H.-T.; Shih, W.-Y.; Ciou, Y.-A.; Chang, Y.-Y.; Ananda, L.; Wang, S.-Y.; Hsu, J.-T. Application of Zearalenone (ZEN)-Detoxifying Bacillus in Animal Feed Decontamination through Fermentation. *Toxins* **2019**, *11*, 330. [CrossRef]

117. Guo, Y.; Wang, Y.; Liu, Y.; Ma, Q.; Ji, C.; Zhao, L. Detoxification of the Mycoestrogen Zearalenone by Bacillus Licheniformis Spore CotA Laccase and Application of Immobilized Laccase in Contaminated Corn Meal. *LWT* **2022**, *163*, 113548. [CrossRef]

118. Zadeike, D.; Vaitkeviciene, R.; Bartkevics, V.; Bogdanova, E.; Bartkiene, E.; Lele, V.; Juodeikiene, G.; Cernauskas, D.; Valatkeviciene, Z. The Expedient Application of Microbial Fermentation after Whole-Wheat Milling and Fractionation to Mitigate Mycotoxins in Wheat-Based Products. *LWT* **2021**, *137*, 110440. [CrossRef]

119. Alberts, J.F.; Davids, I.; Moll, W.-D.; Schatzmayr, G.; Burger, H.-M.; Shephard, G.S.; Gelderblom, W.C.A. Enzymatic Detoxification of the Fumonisin Mycotoxins during Dry Milling of Maize. *Food Control* **2021**, *123*, 107726. [CrossRef]

120. Podgórska-Kryszczuk, I.; Solarska, E.; Kordowska-Wiater, M. Reduction of the Fusarium Mycotoxins: Deoxynivalenol, Nivalenol and Zearalenone by Selected Non-Conventional Yeast Strains in Wheat Grains and Bread. *Molecules* **2022**, *27*, 1578. [CrossRef] [PubMed]

121. Zhou, G.; Chen, Y.; Kong, Q.; Ma, Y.; Liu, Y. Detoxification of Aflatoxin B1 by Zygosaccharomyces Rouxii with Solid State Fermentation in Peanut Meal. *Toxins* **2017**, *9*, 42. [CrossRef] [PubMed]

122. Gavahian, M.; Mathad, G.N.; Oliveira, C.A.F.; Mousavi Khaneghah, A. Combinations of Emerging Technologies with Fermentation: Interaction Effects for Detoxification of Mycotoxins? *Food Res. Int.* **2021**, *141*, 110104. [CrossRef] [PubMed]

123. Babaee, R.; Karami-Osboo, R.; Mirabolfathy, M. Evaluation of the Use of Ozone, UV-C and Citric Acid in Reducing Aflatoxins in Pistachio Nut. *J. Food Compos. Anal.* **2022**, *106*, 104276. [CrossRef]

124. Zokaityte, E.; Lele, V.; Starkute, V.; Zavistanaviciute, P.; Klupsaite, D.; Bartkevics, V.; Pugajeva, I.; Bērziņa, Z.; Gruzauskas, R.; Sidlauskiene, S.; et al. The Influence of Combined Extrusion and Fermentation Processes on the Chemical and Biosafety Parameters of Wheat Bran. *LWT* **2021**, *146*, 111498. [CrossRef]

125. Al Attiya, W.; Hassan, Z.U.; Al-Thani, R.; Jaoua, S. Prevalence of Toxigenic Fungi and Mycotoxins in Arabic Coffee (Coffea Arabica): Protective Role of Traditional Coffee Roasting, Brewing and Bacterial Volatiles. *PLoS ONE* **2021**, *16*, e0259302. [CrossRef]

126. Subramanian, V.; Shanmugam, N.; Ranganathan, K.; Kumar, S.; Reddy, R. Effect of Combination Processing on Aflatoxin Reduction: Process Optimization by Response Surface Methodology. *J. Food Process. Preserv.* **2017**, *41*, e13230. [CrossRef]

127. Shen, M.-H.; Singh, R.K. Detoxifying Aflatoxin Contaminated Peanuts by High Concentration of H2O2 at Moderate Temperature and Catalase Inactivation. *Food Control* **2022**, *142*, 109218. [CrossRef]

128. Shen, M.-H.; Singh, R.K. Decomposing Aflatoxins in Peanuts Using Advanced Oxidation Processes by UV and H2O2. *Food Bioprocess Technol.* **2022**, *15*, 1647–1657. [CrossRef]

129. Abuagela, M.; Marshall, M.; Yagiz, Y.; Mostafa, H.; Iqdiam, B. Combined Effects of Citric Acid and Pulsed Light Treatments to Degrade B-Aflatoxins in Peanut. *Food Bioprod. Process.* **2019**, *117*, 396–403. [CrossRef]

130. Zavala-Franco, A.; Arámbula-Villa, G.; Ramírez-Noguera, P.; Salazar, A.M.; Sordo, M.; Marroquín-Cardona, A.; de Dios Figueroa-Cárdenas, J.; Méndez-Albores, A. Aflatoxin Detoxification in Tortillas Using an Infrared Radiation Thermo-Alkaline Process: Cytotoxic and Genotoxic Evaluation. *Food Control* **2020**, *112*, 107084. [CrossRef]

131. Rastegar, H.; Shoeibi, S.; Yazdanpanah, H.; Amirahmadi, M.; Khaneghah, A.M.; Campagnollo, F.B.; Anderson, S.S. Removal of Aflatoxin B1 by Roasting with Lemon Juice and/or Citric Acid in Contaminated Pistachio Nuts. *Food Control* **2017**, *71*, 279–284. [CrossRef]

Application of Nanomaterial Modified Aptamer-Based Electrochemical Sensor in Detection of Heavy Metal Ions

Zanlin Chen [1], Miaojia Xie [1], Fengguang Zhao [2] and Shuangyan Han [1,*]

[1] Guangdong Key Laboratory of Fermentation and Enzyme Engineering, School of Biology and Biological Engineering, South China University of Technology, Guangzhou 510006, China; 202121050086@mail.scut.edu.cn (Z.C.); 201921046785@mail.scut.edu.cn (M.X.)

[2] School of Light Industry and Engineering, South China University of Technology, Guangzhou 510006, China; fgzhao@scut.edu.cn

* Correspondence: syhan@scut.edu.cn; Tel./Fax: +86-020-3938-0618

Abstract: Heavy metal pollution resulting from significant heavy metal waste discharge is increasingly serious. Traditional methods for the detection of heavy metal ions have high requirements on external conditions, so developing a sensitive, simple, and reproducible detection method is becoming an urgent need. The aptamer, as a new kind of artificial probe, has received more attention in recent years for its high sensitivity, easy acquisition, wide target range, and wide use in the detection of various harmful substances. The detection platform that an aptamer-based electrochemical biosensor (E-apt sensor) provides is a new approach for the detection of heavy metal ions. Nanomaterials are particularly important in the construction of E-apt sensors, as they can be used as aptamer carriers or sensitizers to stimulate or inhibit electrochemical signals, thus significantly improving the detection sensitivity. This review summarizes the application of different types of nanomaterials in E-apt sensors. The construction methods and research progress of the E-apt sensor based on different working principles are systematically introduced. Moreover, the advantages and challenges of the E-apt sensor in heavy metal ion detection are summarized.

Keywords: heavy metal ions; aptamer; electrochemical biosensor; nanomaterials

1. Introduction

With the rapid development of industry and the improvement of urbanization, more and more chemical substances are used in daily life and agricultural production. Increasingly frequent industrial activities such as mining, metallurgy, and oil extraction produces many toxic and harmful substances. These toxic and harmful substances, even after purification treatment, will still leave some residues in the natural water system, including heavy metals, inorganic salts, and agricultural veterinary drugs, which cause pollution and damage the water environment [1–3]. Unlike organic pollutants, heavy metals cannot be biodegraded under natural conditions [4] and will be passively ingested by plants through drinking and irrigation, and eventually, will enter the human body through continuous accumulation in the food chain. Mercury, cadmium, lead, Chromium, Thallium, Antimony, and arsenic are the most common heavy metal pollutants. According to WHO standards, they usually do not exceed 2 ppb. The heavy metals ingested into the human body are likely to form complexes with biological substances such as proteins, enzymes, and nucleic acids. The formation of such complexes alters the molecular composition and mechanism of biological matter, causing it to fail to perform its original physiological function or causing distortion [5]. The accumulation of these elements can cause serious damage to the gut, bones, central nervous system, liver, kidneys, and reproductive system. Since these elements cannot be removed by normal removal methods, even trace amounts of heavy metals can pose a serious threat to living things [6].

In these cases, detection of heavy metal ions in environmental and water systems to prevent heavy metal pollution from the source of the food chain is a vital need. In recent years, many detection methods for heavy metal ions have been developed. Traditional detection methods mainly calculate the concentration of an atom based on its characteristic spectral intensity, including atomic absorption spectroscopy (AAS), inductively coupled plasma mass spectroscopy (ICP-MS), X-ray fluorescence spectrometry (XRF), neutron activation analysis (NAA), and inductively coupled plasma-atomic emission spectrometry (ICP-AES) [7]. These methods can perform accurate qualitative and quantitative analyses of heavy metal ions with high sensitivity, but they are also expensive and require laborious pre-processing [8]. Therefore, a cost-effective, fast, and efficient detection method for heavy metal ions needs to be developed.

Biosensors play an indispensable role in the development of biotechnology and are a fast analytical tool for detection at the molecular level. Usually, the recognition factor used in this technology is an antibody, but the emergence of the aptamer brings new prospects and possibilities to the field of biosensor analysis [9]. An aptamer is an artificial, single-stranded oligomer probe of DNA and RNA consisting of 10–100 bases, obtained by the SELEX index enrichment method. In Figure 1 the general process of SELEX is shown in detail. The initial ssDNA library was exposed in a container filled with target molecules, and the sequences with specific binding ability to the target were separated from the library. Then, a PCR reaction was used for bulk amplification and the next round of screening was carried out until ssDNA with the highest affinity to the target was obtained. Aptamers can fold into complex structures, selectively binding to the target with high affinity and specificity, known as artificial antibodies [10–13]. Compared with antibodies, aptamers have obvious advantages such as high chemical stability, low cost, easy operation, and they are easy to obtain [14]. Aptamers have a wide range of recognition targets, such as proteins, small molecules, agricultural veterinary drugs, bacteria, and heavy metal ions [15–19], which have broad application prospects in the field of food detection. A variety of biosensors using aptamers as recognition factors have been developed and applied to the detection of heavy metal ions, providing a new, efficient, and fast platform for the detection of heavy metal ions.
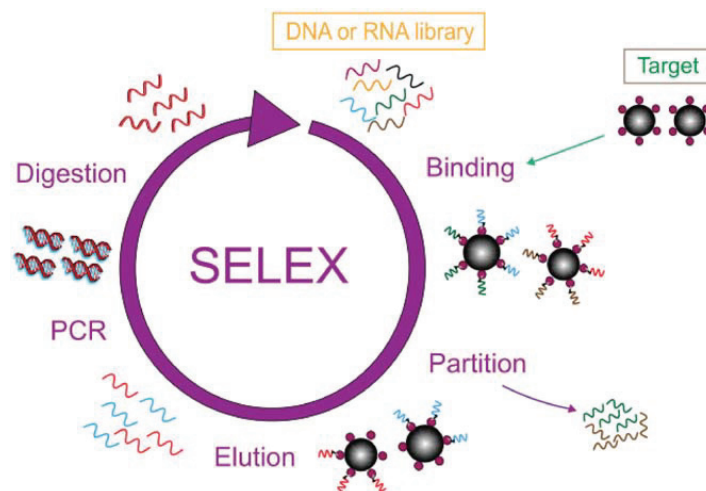

Figure 1. SELEX flowchart.

The electrochemical aptamer sensor (E-apt sensor), which is composed of biometric elements and signal sensors, has attracted more and more attention for this purpose. The signal sensor usually consists of an electrode substrate, modified layer, and electrochemical signal detection system. The most widely used electrode substrates include a gold electrode

(AuE), glassy carbon electrode (GCE), indium tin oxide electrode (ITO), reduced graphene electrode (ERGO), and screen-printed electrode (SPE). Different electrode materials can have different degrees of signal enhancement after being modified by an appropriately modified layer and a variety of nanomaterials can be selected for the modified layer. The aptamer is fixed on the surface of the electrode by intermolecular force with the modified layer. This operation will change the impedance of the electrode and cause a current change. Therefore, nanomaterial modification in electrodes becomes an important part of electrochemical sensor construction. The electrochemical signal detection system includes a signal amplifier, a processor, and a display screen. The electrochemical sensor has been widely used in recent years because of its advantages of simplicity, high efficiency, strong specificity, and high sensitivity. As shown in Figure 2, the number of papers and patents published with the keywords "Electrochemical" and "Aptamer" has increased year by year since 2012 (data for 2022 is up to March).
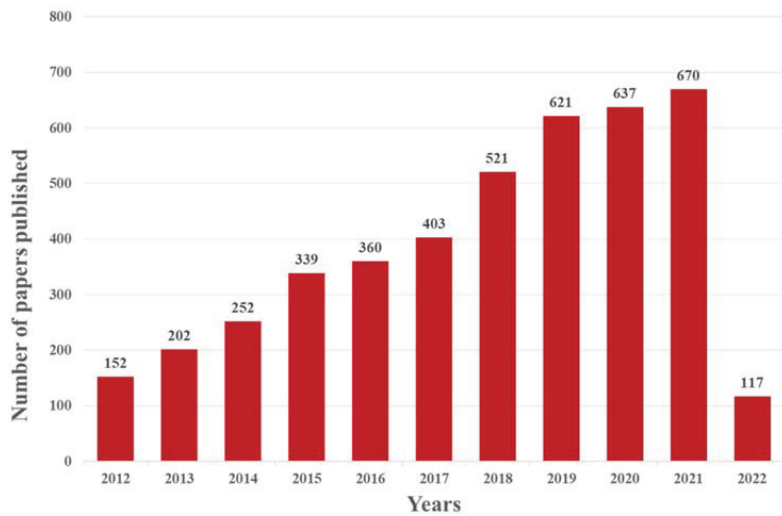
Figure 2. Web of Science report for the number of indexed papers and patents about the application of the E-apt sensor (keyword: "Electrochemical" and "Aptamer" accessed on 27 March 2022).

This paper reviews the application of the E-apt sensor for the detection of heavy metal ions in recent years and systematically introduces the working principles of electrochemical sensors with different configurations of various nanomaterials. A Schematic diagram of nanomaterial modified aptamer-based electrochemical sensor are briefly illustrated in Figure 3. The strengths and limitations of this technology are summarized and its future challenges and application trends are envisioned.
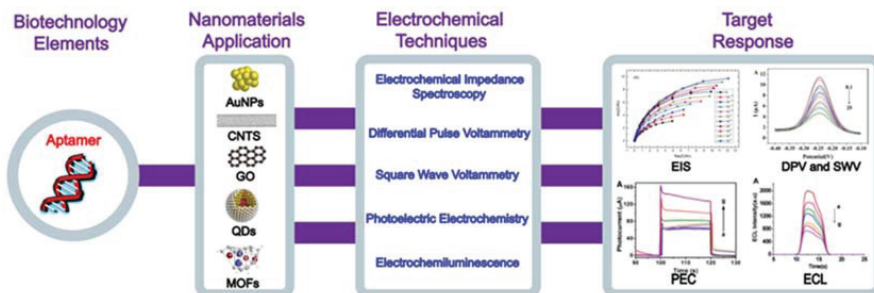
Figure 3. Schematic diagram of nanomaterial modified aptamer-based electrochemical sensor.

2. Application of Nanomaterials in Aptamer-Based Electrochemical Sensors

In recent years, the successful synthesis of various nanomaterials has attracted significant attention. Their unique physical and chemical properties, including high surface area/volume ratio, high reactivity, size dependence, and high functionalization, make them widely used in chemical analysis, therapy, diagnosis, and food safety [20–24]. In addition to the binding activity of the aptamer, the reason why the electrochemical aptamer sensors can detect heavy metal ions as low as fM is largely attributed to the rational use of nanomaterials. Sensing platforms are formed by immobilizing aptamers on nanomaterial surfaces through intermolecular forces or catalyzing chemical reactions in sensors as sensitizers to enhance electrical signals and improve the specificity and sensitivity of sensors [25]. Due to their recognized properties, the coupling of aptamers on nanomaterials has great potential to form biosensor platforms.

Gold nanoparticles, carbon nanotubes, graphene, quantum dots, and metal-organic frameworks are common and basic nanomaterials used in E-apt sensors. These materials can be mixed or coupled with other substances to create new composite materials. They have shown many advantages such as high specific surface area, good biocompatibility, high electrical conductivity, high magnetic properties, and unique electro-optic and physicochemical properties [26–28]. In addition to being used as sensitizers, most nanomaterials in E-apt sensors are used to fix aptamers to form couplings with a better capture effect. Researchers often use couplings as probes to obtain better detection results. Figure 4 indicates how popular nanomaterials (shown as their microscopic morphology) are coupled with aptamers.
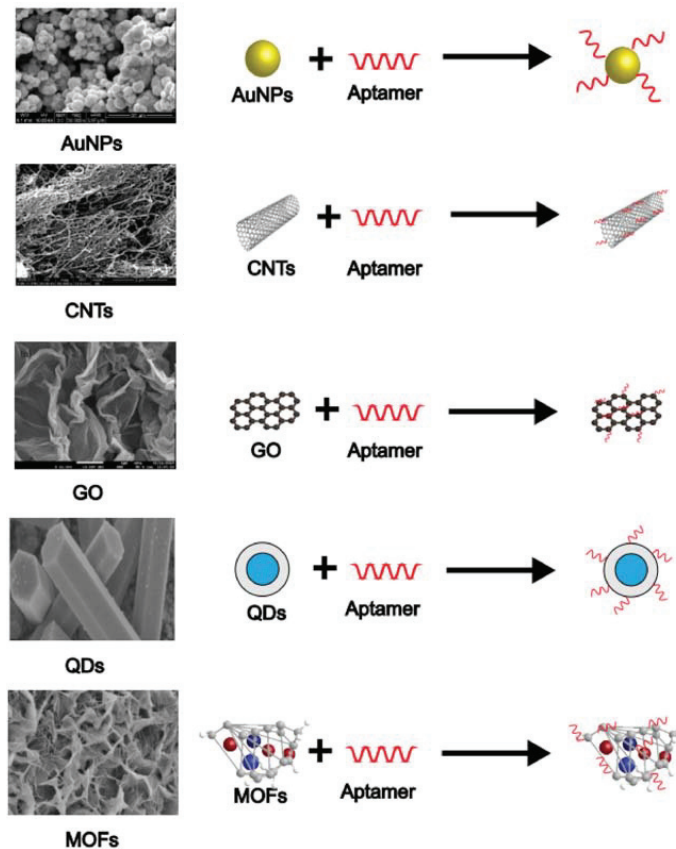

Figure 4. SEM images and combination modes of various nanomaterials.

2.1. Gold Nanoparticles

Among the aptamer-based sensors developed, metal nanoparticles such as gold nanoparticles (AuNPs) are the most common advanced materials. They have high stability and oxidation resistance and can be prepared through various physical and chemical methods, among which the most classical preparation method was proposed by Turkevich et al. in 1951 [29]. The high surface-volume ratio and excellent optical properties of AuNPs contribute to the high sensitivity and selectivity of the target detection. The optical properties of AuNPs are largely dependent on the size, shape, and aggregation state of nanoparticles. Colloidal AuNPs are usually red or pink and turn purplish-blue when aggregated, forming the basis of colorimetric detection [30]. AuNPs are also conductive and fluorescent and, thus, have the ability to respond to external electrochemical and optical stimulation.

One of the most common approaches to using AuNPs in electrochemical sensors is to anchor aptamers. The aptamer is usually fixed by the force of the Au-S bond; Yuan et al. [31] used this method to develop a sensor for detecting Pb^{2+} and Cd^{2+} at the same time. Due to the specific binding of aptamers to metal ions, methylene blue or ferrocene labeled aptamers were competitively separated from the gold electrode, resulting in a weaker electrochemical signal. The detection limits of Cd^{2+} and Pb^{2+} were 89.31 and 16.44 pM. Deng et al. [32] deposited L-cysteine and AuNPs layers on the electrode surface successively providing a large surface area to anchor many sulfur-capped auxiliary probes through the mercaptan-gold interaction. Additionally, to fix the aptamer, Liu et al. used chitosan to attach AuNPs to the electrode to enhance electron transfer, thus improving the sensitivity of the sensor [33].

In addition to being used alone, AuNPs are also used as composite materials coupled with other metal ions. The composite materials tend to enhance the electrochemical signal so that even subtle changes can be detected. Silver and gold alloy nanoparticles (Ag-Au alloy NPs) promise to create inexpensive and stable electrochemical sensors [34]. This is because silver-gold alloy nanoparticles have a large specific surface area and good electrical conductivity which can act as a conductive center and promote electron transfer, thus trapping more heavy metal ions on the electrode. Zhao et al. [35] used DNA enzyme functionalized (Ag-Au alloy) NPs to form core-shell nanoparticles, which can be used as signal tags. Because the core-shell structure increases the specific surface area and catalyzes the reaction, the electrochemical signal can be enhanced. Ag-Au Alloy NPs were also used to modify GCE and the resulting sensor had higher sensitivity and reproducibility. Miao et al. [36] used Fe_3O_4@AuNPs to carry a DNA probe, and the other two were labeled with independent electrochemical substances which can detect both Hg^{2+} and Ag^{2+}. Due to their excellent signal amplification, AuNPs have been one of the most used transduction materials to construct E-apt sensors for the analysis of food and water contaminants.

2.2. Carbon Nanotubes

Carbon nanotubes (CNTs) are a kind of carbon nanomaterial with unique electrical transmission properties and a large specific surface area, with excellent chemical, mechanical, and thermal stability, and direct binding with other molecules. Therefore, they have received great attention in biosensor design [37,38]. They can be thought of as cylindrical tubes made of one or more sheets of graphene rolled and folded. Nanotubes formed from a single sheet of graphene are called single-walled nanotubes (SWNT), with diameters between 0.4~2 nm, and multi-walled carbon nanotubes(MWCNTs) are 2~10 times larger [39]. Graphene contains SP^2 hybrid carbon atoms, and nucleic acids can easily be attached to the surface of the nanotubes through π-π bonds, so CNTs are often used to carry ssDNA or RNA. In 2005, So et al. [40] constructed a biosensor using single-walled CNTs by using aptamer as a molecular recognition element for the first time. Since then, the potential of CNTs in sensing platforms has been gradually explored.

It is more common to modify electrodes with MWCNTs and then fix aptamers on the surface of MWCNTs. Zhu et al. [41] used carboxylic acid group functionalized MWCNTs to fix aptamers. Because the material has a large surface area and good charge transferability,

the DNA attachment amount and sensor performance could be significantly improved. The sensor could detect Pb^{2+} in the range of 5.0×10^{-11}~1.0×10^{-14} M. Additionally, Zou et al. [42] covalently immobilized aptamers on carboxylic functionalized MWCNTs by EDC/NHS chemistry. CNTs can not only carry aptamers in sensors but also provide binding sites for the reactions between aptamers and other nanomaterials. Rabai et al. [43] modified the electrode surface with CNTs, then deposited AuNPs on the composite electrode. Finally, with the aptamer fixed, the sensor had a detection limit of 0.02 pM for Cd^{2+}. He et al. [44] developed an electrochemical sensor with a $Zn_3(PO_4)_2$ modified aptamer and found that the sensor with MWCNTs had higher sensitivity.

2.3. Graphene

Graphene is a two-dimensional carbon nanomaterial with SP^2 hybrid connected carbon atoms tightly packed into a single layer honeycomb lattice structure. Due to its excellent electrical properties, graphene has attracted great interest in recent years. Graphene has a unique type of structure that also gives it features not found in many other nanomaterials; its large specific surface area makes it an ideal candidate for immobilizing large numbers of functionalized metal oxides and noble metal nanoparticles [45]. Exceptional carrier mobility offers great prospects for nanoscale applications, such as electronic devices and chemical/biological sensors. In addition, its high electron transfer efficiency and wide electrochemical window make graphene an ideal material for constructing a highly sensitive E-apt sensor [46]. In recent years, graphene as a REDOX molecule in electrochemical sensors has attracted great attention.

The most common use of graphene in sensors is to modify electrodes. Zhang et al. [47] developed an Hg^{2+} detector for a graphene-fixed aptamer probe with a detection limit of 5 pM. Using graphene-modified electrodes, the modified electrode surface can be reused. Similar to AuNPs, it is more likely that graphene will be coupled with other nanomaterials to form new composite materials for better modification. Hai et al. [48] modified the electrode with AuNPs coupled with graphene. The aptamer was self-assembled on the electrode, and the detection limit of Pb^{2+} was as low as 3.8 pM. Jiang et al. [49] designed a new nanometer composite material consisting of TiO_2, AuNPs, and nitrogen-doped graphene. The composite exhibits excellent optical properties, increasing the exciton lifetime and improving the charge transfer photocurrent intensity to 18.2 times higher than that of original TiO_2. Wang et al. [50] synthesized another new material modified electrode by using CS instead of AuNPs for the detection of Pb^{2+}. The modified electrode showed good repeatability, stability, and specificity to other interfering metal ions. Li et al. [51] prepared a sensor for mercury ions based on a perylene-3, 4, 9, 10-tetracarboxylic acid/graphene oxide (PTCA/GO) and quercetin-copper(II) complex. They efficiently promoted the separation of photoexcited carriers and enhanced the photocurrent.

2.4. Quantum Dots

Quantum dots (QDs), also known as semiconductor nanocrystals, are mixtures of cadmium and selenium or tellurium with nanoscale clusters with diameters of 1–20 nm [52]. Due to their unique properties, such as high quantum yield, excitation-dependent emission, surface modification versatility, and long-term photostability [53,54], QDs have been used in many research fields, especially in nanoelectronics, optoelectronics, and biological analysis [55]. The physical size of the nanocrystals determines the wavelength of the emitted fluorescence, so multiple analyses can be performed using a single excitation source. With the rapid development of nanotechnology, such nanomaterials have been widely used to improve the sensitivity of sensors. When they are incorporated into the design of biosensors, they can be used as tags, as part of a signal sensor [56].

QDs are mainly used in electrochemical luminescence sensors and photoelectric electrochemistry sensors. When the aptamer reacts with the corresponding target, the brightness of the QDs will also change due to the resonance energy transfer, thus improving the sensitivity of the sensor. CdTe QDs are most frequently used in sensors; Shi et al. [57]

developed a new method for the detection of Pb^{2+} based on the sensitization effect of CdTe QDs. When the target is present, the labeled QDs close to the electrode surface produce a sensitization effect and the photocurrent intensity is enhanced. Feng et al. [58] modified CdTe QDs with MIL-53 and determined Hg^{2+} and Pb^{2+} simultaneously by the ECL method with good recovery. Except for CdTe QDs, there are many other types of QDs, such as CdS and nitrogen-doped graphene (NG) [59,60], and their principle of action is roughly the same. When the conformation of the aptamer changes, the distance between the QDs and the electrode alters, and the electrical signal is either enhanced or weakened. This property makes QDs widely used to design E-apt sensors for food and water analysis.

2.5. Metal-Organic Frameworks

In recent years, more and more metal-organic frameworks (MOFs) have been found to effectively coordinate polymer nanomaterials and have received extensive attention as effective quenching materials. MOFs are a kind of crystalline nanomaterial composed of metal ions and organic ligands. Due to their water dispersibility, adjustability, biocompatibility, low cost, controllable shape, ultra-high porosity, and high specific surface area [61], MOFs have been increasingly used in biosensors, electrocatalysis, energy storage, and conversion. The large specific surface area and ultra-high porosity of MOFs provide more reaction sites for aptamers and targets. Organic ligands with rich functional groups make MOFs easy to be functionalized with various molecules and materials [62]. In addition, MOF compositions take a variety of forms (e.g., nanosheets, cages, tubes, rods, cubes, etc.) and can be easily adjusted according to the selection of various organic connectives and metal ions [63].

Aptamers are securely fixed in the MOFs by encapsulation. The main framework of MOFs can facilitate various interactions with analytes through functional groups in organic ligands, thus achieving high sensitivity and high selectivity recognition. Therefore, MOFs can be used as signal probes for different detection methods. Zhang et al. [64] used a Zr-based MOF embedded with three kinds of aptamer. Ling et al. [65] prepared streptavidin functionalized zirconium porphyrin MOF (PCN-222@SA) using a covalent method as a signal nanoprobe. Introducing this signal nanoprobe into the sensor surface significantly amplified the electrocatalytic current. Zhang et al. [66] synthesized a core-shell nanostructured composite material composed of Fe (III)-based MOF (Fe-MOF) and mesoporous $Fe_3O_4@C$ nanocapsules (Fe-MOF@mFe_3O_4 @MC) that exhibited excellent electrochemical activity, water stability, and high specific surface area, resulting in strong biological binding to heavy metal ion targeting aptamer chains.

3. Electrochemical Techniques

E-apt sensors have proven to be effective tools for detecting heavy metal ions. They are cheap, portable, and easy to operate, making them popular with researchers. The concentration of the target is detected by collecting the changes in voltage, current, conductivity, impedance, and other electrochemical signals [67,68]. Table 1 summarizes the application of the E-apt sensor in the detection of heavy metal ions in recent years. According to different electrochemical principles, electrochemical characterization and detection methods can be divided into cyclic electrochemical impedance spectroscopy (EIS), differential pulse voltammetry (DPV), square wave voltammetry (SWV), photoelectric electrochemistry (PEC), electrochemical luminescence (ECL), and other methods [69]. When the analyte is around, the target-induced signal is generated and recorded as the corresponding electrochemical signal, which can be detected in a few minutes with relatively high sensitivity. Sensors with different principles use different nanomaterials and sensitizers, as well as different construction methods. Various electrode structures, construction methods, and responses to inspection objects are summarized in Figure 5.
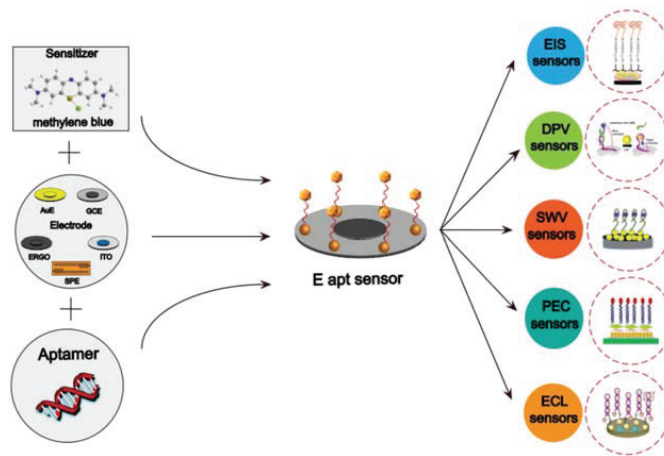
Figure 5. Electrochemical sensor technology is based on aptamers and different electrodes.

3.1. Electrochemical Impedance Spectroscopy

EIS is an effective technique for detecting complex formations on the electrode surface by detecting interface phenomena [70,71].

It measures the resistive and capacitive properties of the electrode upon perturbation with a small amplitude AC excitation. The frequency is varied over a wide range to generate the impedance spectrum, and the steady-state electrical impedance of the electrode/electrolyte interface is measured over an appropriate frequency range by applying a small sinusoidal voltage [72]. Impedance can be understood as the ratio of the voltage phasor to the current phasor of the system. When the impedance changes, it indicates that the detection target has been combined with the biometric element fixed on the electrode surface. EIS is usually able to distinguish between two or more electrochemical reactions occurring at the same time, identify diffusion-limiting reactions, mathematically evaluate experimental results using equivalent circuits (EEC), and reliably provide quantitative electrochemical data.

AuNPs are mainly used as electrodes and modification materials in EIS sensors [73–76]. When gold is used as the electrode, the aptamer is usually fixed on the surface of the gold electrode to generate a huge charge transfer resistance (Rct). When the corresponding target substance is added, the aptamer falls off from the surface of the gold electrode and combines with the target to produce an electrical signal transformation. Gu et al. developed an ultra-sensitive As^{3+} biosensor based on the hybridization chain reaction and RecJf exonuclease catalyzed reaction. In the presence of As^{3+}, the aptamer specifically binds to As^{3+}, resulting in DNA dissociation. The release of the hybrid chain reaction (HCR) product significantly reduced the Rct, and the detection limit was 0.26 nM. Moreover, the sensor has good selectivity. Even though the concentration of potential interfering ions is ten times higher than that of As^{3+}, the change in Rct is negligible and only sensitive to As^{3+} [77]. Rabai et al. modified the surface of the gold electrode by a diazonium salt (CMA) electrochemical reduction method for the fixation of the aptamer. When Cd^{2+} was present, the aptamer changed from a random coil structure to a complex. This interaction blocks electron transfer, increasing the surface resistance, which is proportional to the concentration of Cd^{2+} in the sample [78]. In addition to traditional gold electrodes, the use of inkjet-printed gold electrodes as a reliable method for the detection of trace Hg^{2+} in water and organic solvents was first proposed in 2019. They applied water droplets of gold ink to a substrate and sintered it under the right conditions to produce printed gold electrodes. The aptamer was fixed to the electrode by the force of disulfide bonds, and then the interface was assembled layer by layer using impedance spectroscopy (PEIS) via RCT under optimal manufacturing conditions. With the increase in layers, RCT increases

gradually. The interfacial resistance increases from an average of 20.6 U to 144.5 U when the aptamer is fixed on the surface. With the addition of Hg^{2+}, the ssDNA aptamer will change its secondary conformation by folding into a hairpin structure, establishing a bridge between the two thymidine residues, and forming a base pair, with a significantly reduced RCT. Figure 6a shows evidence of a directly proportional relationship between the response variable (RCT) and the target concentrations under optimal conditions. The working principle, signal strength, and linearity are also shown in Figure 6. The sensor has good stability and significant repeatability under harsh conditions and can detect Hg^{2+} at 0.005 ppM in organic solvents. Even when compared with high concentrations of cadmium, lead, and arsenic (50 ppM), it still has good selectivity [79].
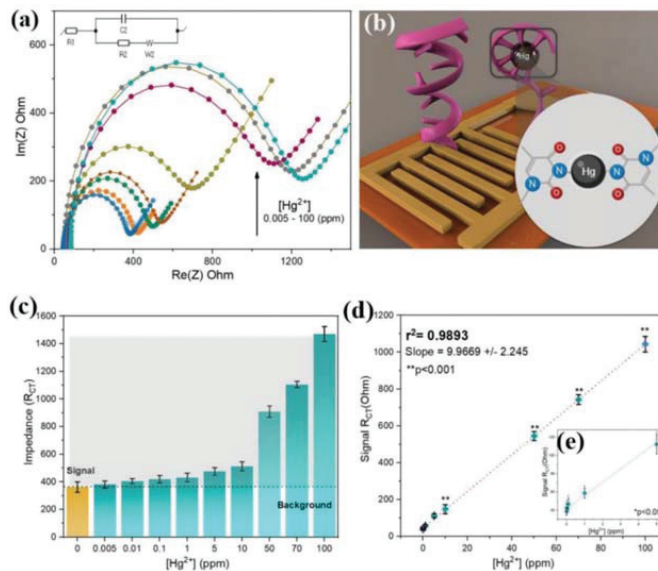

Figure 6. Inkjet−printed electrochemical apt sensor performance analysis; (**a**) Analytical Faradaic impedance response under optimal fabrication conditions; (**b**) Working electrode diagram; (**c**) The bar chart represents the overall reaction, and the shaded area represents the signal strength after subtracting the background; (**d**) Linear correlation between signal and target concentration; and (**e**) All the results correspond to the mean value from 5 independent replicates and the error bars represent 1 SD from the mean. Reprinted with permission from ref. [79]. Copyright 2019 Elsevier.

AuNPs are commonly used to modify various carbon-based materials such as graphene oxide (GO), CNTs, etc. The high porosity of GO provides a large number of reaction sites for the bonding of AuNPs with aptamers. Wang et al. [80] used gold to modify porous GO (Au@p-rGO) and used it to fix substrate aptamers. Gold-modified GO (AuNPs@GO) was attached to the complementary chain as a signal probe; the current signal was obtained by recording the electrocatalytic conditions of H_2O_2. With the increase in Pb^{2+} concentration, the current response showed signal attenuation, and the lower limit of detection was 1.67 pmol/L. Rabai et al. [43] first dispersed CNTs in chitosan (CS) to modify a glassy carbon electrode (GCE). Chitosan improves its solubility and biocompatibility, and AuNPs are then electrically grafted onto the CNT-Cs/GCE. The synergistic effect of the two will make electron transfer easier, have good electrical conductivity, high surface electrical activity, and a detection limit as low as 0.02 ppm. Because the aptamer does not react with other heavy metal ions and the two-dimensional structure does not change, the sensor also has good selectivity. Yadav et al. [81] used silver (Ag)-Gold (Au) alloy nanoparticles (NP)-aptamer on a modified glassy carbon electrode (GCE) to detect Pb^{2+}. Ag-Au bimetallic nanoparticles have electronic polarity which attracts the charged adsorption and promotes

the attachment of adsorption to the loading platform on the surface of GCE. A large number of binding sites can improve the sensitivity and stability of the electrode and reduce its detection limit.

3.2. Differential Pulse Voltammetry

The working principle of DPV is the constant voltage pulse amplitude overlayed on the step potential; immediately before each potential change measuring the electric current. The implementation response is the pulse strength at the beginning of the two currents between the resulting peak response; the difference between the two currents minimizes the amount of capacitance current, generating a higher signal-to-noise ratio of voltammograms [82]. DPV is a universal technique that can be used for both quantitative chemical analysis and the study of the mechanism, kinetics, and thermodynamics of chemical reactions. DPV is very sensitive and can routinely detect analytes at a part per billion level with a resolution higher than that achieved by cyclic voltammetry (CV), therefore, DPV is superior to CV when higher selectivity is required.

Reduced graphene (rGO) is commonly used in DPV sensors. It can be coupled with other nanomaterials as signal amplifiers or directly used as electrodes, which can significantly change the electrochemical properties. Luo et al. [83] used Fe_3O_4/rGO nanocomposite as a signal amplifier and many directional platinum nanotube arrays (PtNAs) crystallized in situ on flexible electrodes as sensing interfaces; a Hg^{2+} sensor was prepared. The schematic illustration of the assembly process and the detection strategy is shown in Figure 7. Due to its large surface area, it facilitates electrochemical performance and fixation of captured DNA (cDNA) and reporter DNA (rDNA). In the presence of Hg^{2+}, part of the junction DNA binds closely to cDNAs through a thymine nucleotide pair (T-Hg^{2+}-T). The Fe_3O_4/rGO nanoprobes attached to rDNAs were then fixed to the electrode by matching the remaining linker DNA with the rDNAs. Under optimal conditions, the Hg^{2+} aptamer sensor showed synergistic amplification performance with a linear range from 0.1 nM to 100 nM and a detection lower limit of 30 pM. When the heavy metal ions were not mercury ions, the aptamers could not undergo conformational changes through thymine nucleotides so this sensor had good selectivity. In addition, the E-apt sensor also showed reliable performance in the detection of real lake water samples.
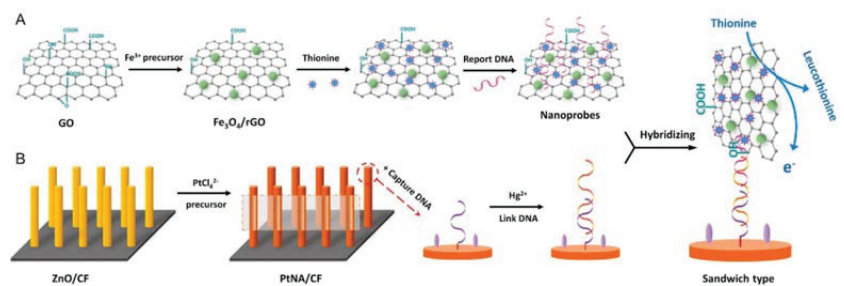
Figure 7. Schematic illustration of the assembly process and the detection strategy; (**A**) Preparation of nano-probe; (**B**) Modification of flexible electrode. Reprinted with permission from ref. [83]. Copyright 2018 Elsevier.

When used as an electrode, aptamers can be fixed on rGO electrodes (ERGO) by π-π interaction. The ERGO electrode modified by aptamers can improve the value of Rct. Lee et al. [84] fixed the aptamer probe (Apt) labeled with methylene blue (MB) and part of its complementary DNA (cDNA) on the ERGO electrode to form the aptamer double-stranded structure, which blocked the effective electron transfer of MB to the electrode. After adding Cd^{2+}, the aptamer unlocked the link and released the cDNA. This can quantitatively promote the electron transfer efficiency of MB, leading to the enhancement of electrochemical signals. Su et al. [85] also used this strategy to detect ultra-

trace Pb^{2+}, as the existence of Pb^{2+} could make Apt fold into a G-quadruplex structure. The formation of the G-quadruplex leads to the separation of Apt from ERGO/GCE, which changes the REDOX current of MB labels with a detection limit of 0.51 fM. The sensor was tested in the presence of various metal ions (Cd^{2+}, Co^{2+}, Ag^+, Cu^{2+}, Mg^{2+}, Ni^{2+}, Zn^{2+}, and Fe^{2+}), but only Pb^{2+} resulted in a significant change in voltammetry response and had good repeatability. In addition to MB, toluidine blue (TB) molecules are also commonly used for electron migration in sensors, and the peak current of TB interacting with double-stranded DNA (dsDNA) is higher than that of single-stranded DNA (ssDNA). Ding et al. [86] used the composites of Au nanoparticles and a Polypyrene (Au@Py) modified screen printing electrode to amplify the current signal, fix the complementary chain on the electrode, and combined it with the aptamer to form a double chain structure. When Pb^{2+} was combined with an aptamer, the double chain structure was destroyed, and the peak current decreased continuously. Ma et al. [87] developed a sensor for Hg^{2+} ultra-sensitive determination, also using TB to characterize electron migration, using mesoporous silica nanocontainers (MSNs) as containers. MSNs have a rich porous structure that can trap TB molecules using AuNPs to link specific ssDNA. Hg^{2+} induces ssDNA to form a hairpin structure and the stored tuberculous molecules are released from MSNs. The electron transfer signal of TB was stably detected by micro DPV, which was correlated with the concentration of Hg^{2+}, with a low detection limit of 2.9 pM. Jin et al. [88] developed an electrochemical adaptive sensor for Pb^{2+} detection using porous carbon (PCs) loaded platinum nanoparticles (PtNPs) to catalyze the hydroquinone-H_2O_2 system in the form of simulated enzymes. PtNPs@PCs were fixed on the electrode surface by the specific binding of streptavidin and biotin and catalyzed the oxidation of hydroquinone in the presence of Pb^{2+} and H_2O_2. The resulting electrochemical signal was dependent on the concentration of Pb^{2+}.

3.3. Square Wave Voltammetry

SWV is a pulsed method in which the waveform is defined by step potential, amplitude, and period. The excitation signal used consists of a symmetrical square wave pulse superimposed on the stepped waveform, where the forward pulse of the waveform corresponds to the step to form a rectangular wave [89]. The current intensity is obtained at the end of each applied pulse during the potential sweep cycle. The difference between positive and negative pulse currents is recorded at the pulse time, and the difference between the forward and reverse currents over the same period is called the net current. The advantages of SWV are improved speed, background discrimination and sensitivity, and good discrimination of non-Faraday or charging currents.

In recent years, screen-printed electrodes (SPE) have been widely used in the design of biosensors. Their diverse functions, low cost, and easy use have attracted great interest. Moreover, the SPE can be modified with nanomaterials to enhance its electrochemical performance. Fakude et al. [90] first proposed an E-apt sensor for Cd^{2+} detection based on flexible polyester SPE. A Cd^{2+} join makes the fit body configuration change; an iron/ferrocyanide REDOX probe can then go more easily through the electrode surface, and the carbon nanofibers (CNF) can promote a simple electron transfer reaction. CNF after acid treatment on the polyester SPE is increased by the electrical activity of the electrode surface area and catalytic REDOX process of the iron/ferrocyanide, which enhances electron flow. Fakude [91] also modified the SPE with carbon black nanoparticles and AuNPs. The strategy is to deposit AuNPs by CV after modifying the electrode with carbon nanoparticles, so the Faraday current can increase up to 80% with a detection limit of 0.14 ppb. This strategy has also been used to detect As^{3+} in water [92], but the electrode used in this sensor is a glassy carbon electrode (GCE). The interface properties of the electrode are characterized by charge transfer resistance and double layer capacitance. The presence of nanoparticles on the detection limit GCE shows a significant decrease in the Rct value. The detection limit was 0.092 ppb and the specificity was well.

Si et al. [93] proposed an electrochemical biosensor based on aptamer-terminal deoxynucleotidyl transferase (TdT), which catalyzed the continuous polymerization of ade-

nine bases, resulting in the formation of long polyA which enabled Si-DNA to be anchored on the electrode surface and enhanced electrical signals. The introduction of Hg^{2+} leads to the formation of the T-Hg^{2+}-T complex, which prevents TdT from forming polyA, resulting in the absence of Si-DNA on the electrode surface and the decrease in the electrochemical signal.

3.4. Photoelectric Electrochemistry

PEC is a kind of photoelectric analysis technology developed gradually based on electrochemistry in recent years. It is a highly sensitive and fast analysis method. PEC converts chemical energy into electrical energy by using light as the excitation source, and the photocurrent generated is used as the detection signal. It has the advantages of low background noise and high sensitivity and has been widely used in chemical synthesis, catalysis, and biological analysis [94].

In the process of PEC sensor construction, photoactive materials play an indispensable role, and their properties directly determine the performance of the sensor [95]. Various materials such as TiO_2, ZnO, CdSe, and CdS are used to manufacture PEC sensors. ZnO nanomaterials are a kind of N-type semiconductor and have attracted extensive attention due to their advantages of low cost, good chemical stability, and excellent electrical and optical properties. Cao et al. [55] modified ZnO nanosheets on an ITO electrode, and then modified CdS nanoparticles on the surface of ZnO nanosheets to form a CdS/ZnO-sensitized structure through continuous ion layer adsorption and the reaction of Cd^{2+} and S^{2-}. Then, CdSe QDs were introduced into the sensing system through a hybridization reaction, forming a double co-sensitization structure, realizing high selectivity, high sensitivity, and high stability detection of Pb^{2+}. Niu et al. [96] designed a ZnO and Reduced graphene oxide (ZnO-RGO) nanocomposite as a photoactive material, adding AuNPs to further enhance the electrical conductivity. Moreover, AuNPs can anchor the aptamer and its complementary chain to form a double chain structure in which MB can amplify the current response. When the sensor captures Cd^{2+}, the aptamer and its complementary chain break, and MB is separated from the electrode surface, reducing the photocurrent response, resulting in a detection limit of 1.8×10^{-12} mol/L. Niu also designed ZnO-TiO_2 nanocomposites as photoactive substrates and covered them with gold nanochains. One part of the aptamer was connected to the gold nanochain, and the other part was coupled to graphite-like Carbon Nitride (G-C_3N_4). When Cd^{2+} was detected by the aptamer sensor, the aptamer formed a stable hairpin structure, and the signal sensitizer G-C_3N_4 was closer to the electrode, making the changes in the photocurrent signal more sensitive. The detection limit was 1.1×10^{-11} mol/L, slightly lower than that of the first method. Both sensors have significant specificity because the aptamer usually reacts only after contact with its corresponding target, resulting in changes in secondary structure. Niu [97] developed a PEC sensor for Pb^{2+}, again using AuNPs as a fixed aptamer, and CdS-TiO_2 as a photoactive material, The difference is quercetin-copper(II) complex as intercalator and electron donor. The detection limit was 1.6×10^{-12} mol/L, which was satisfactory.

3.5. Electrochemiluminescence

Electrochemiluminescence (ECL) has received considerable interest in the development of an ultrasensitive detection technique in recent years. It works by bringing the system or component of the electric biomass into an excited state through electron transfer and then returning it from the excited state to the ground state to produce a chemiluminescence phenomenon. It combines the advantages of both electrochemical and chemiluminescent biosensors, with relatively low cost, simplicity, rapidity, and high selectivity [98,99].

Ruthenium (II) tris (bipyridine) ($Ru(bpy)_3^{2+}$) and its derivatives remain the most popular ECL reagents due to their recyclability, high quantum yields, and suitability in different pH levels, It interacts with the electrode surface to produce a strong ECL signal, usually by using hairpin DNA to interact with $Ru(bpy)_3^{2+}$ away from the electrode surface, thereby reducing the ECL signal [100]. According to this principle, Strand Displacement Amplifica-

tion (SDA) is also widely used in the construction of ECL sensors. SDA was proposed and improved in 1992, relying on the combination of the strand-displacing polymerase and the nicking endonuclease to generate an exponential accumulation of single-stranded DNA (ssDNA) [101]. Zhu et al. [102] prepared a sensor for As^{3+} based on SDA technology. By using polydopamine nanospheres (PDANS) as inhibitors, hairpin DNA was constrained by PDANS and the SDA process was inhibited. $Ru(bpy)_3^{2+}$ as an ECL probe could diffuse the ITO electrode surface and generate a strong ECL response. However, the presence of As^{3+} makes hairpin DNA no longer constrained and triggers the SDA process with the help of polymerase and incisor endonuclease to generate dsDNA, which interacts with $Ru(bpy)_3^{2+}$ to form the dsDNA- $Ru(bpy)_3^{2+}$ complex. Due to electrostatic repulsion, it is difficult for the complex to approach the ITO electrode surface, resulting in a low ECL response, the detection limit is 1.2×10^{-3} ppb. This strategy has also been applied to the detection of Cd^{2+} [103]. The difference is that Xu et al. used magnetic Fe_3O_4-GO nanosheets to constrain hairpin DNA, and the detection limit was 1.1×10^{-4} ppb. Ma et al. [104] did not use an SDA reaction for DNA amplification but hybridized a ruthenium complex with an aptamer and its complementary chain. The combination of Hg^{2+} and T-T mismatch induced adaptive folding and compression of the aptamer, keeping the Ruthenium complex away from the electrode and weakening the ECL signal. Li et al. [59] functionalized $Ru(bpy)_3^{2+}$ with 3-aminopropyltriethoxysilane and mixed it with silica nanoparticles and graphene quantum dots to form an ECL composite material for mercury ion detection, which has good detection performance.

In addition to $Ru(bpy)_3^{2+}$, the ECL resonance energy transfer (RET) of QDs and precious metal nanoparticles (such as AuNPs) is also considered to be a sensitive and reliable analysis technique, but their ECL intensity is usually lower than $Ru(bpy)_3^{2+}$. Wang et al. [105] synthesized cadmium sulfide QDs doped with lanthanum ions and designed an ECL sensor based on the QDs and AuNPs. The surface plasmon resonance of AuNPs enhanced the strength of ECL. Secondly, in the presence of Hg^{2+}, oligo-base pairs change from linear chains to hairpins. The realized ECL quenched, and finally, after incubation with TB, produced a strong and stable transfer, which resulted in the eventual recovery of the ECL signal. The detailed process is shown in Figure 8.
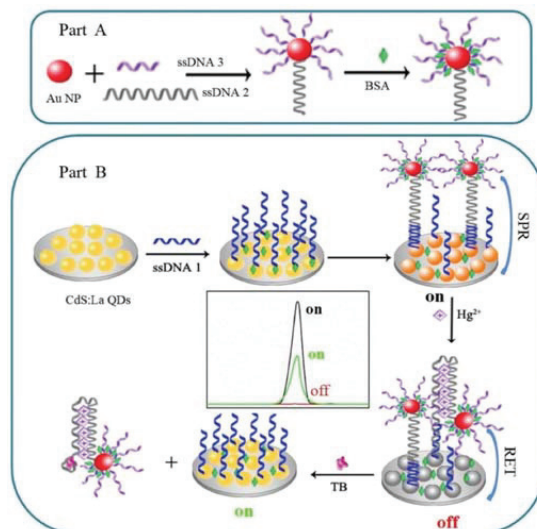

Figure 8. Fabrication of the ECL-RET aptasensor for Hg^{2+} and TB, respectively based on the resonance energy transfer between CdS:La QDs film and AuNPs; (**A**) Preparation of aptamer probe; (**B**) Electrode surface modification and sensor reaction principle. Reprinted with permission from ref. [105]. Copyright 2019 Elsevier.

Table 1. Application of the electrochemical sensor in the detection of heavy metal ions.

Method	Target	LOD (nM)	Linear Range (nM)	Aptamer Sequence	Sample	Reference
EIS	Hg^{2+}	0.071	0.1~50	5'-CCCCCCCCCCCCTTCTTTCTTCCCCTTGTTTGTT-3'	Tap water	[44]
	Hg^{2+}	25	25~500	5'-TTTCTTCTTTCTTCCCCCCTTGTTTGTTT-3'	Water	[79]
	Cd^{2+}	0.275	1~1×10⁶	5'-ACCGACCGTGCTGGACTCTGGACTGTTGTGGTATTATTTTTGGTTG TGCAGTATGAGCGAGCGTTGCG-3'	River water	[78]
	Pb^{2+}	1.67×10^{-3}	5×10^{-3}~1	5'-HS-TTTTTTCGATAACTCACTATAGGAAGAGATG-3'	Serum Water	[80]
	As^{3+}	0.26	1.3~6.5	5'-TGATGTTTGTTTACGCATGTGTGAGGAGGCTGGGGTGATGAATCCAATCCC-3'	Tap water	[77]
	Pb^{2+} As^{3+}	2.27×10^{-3} 6.73×10^{-3}	0.01~10.0	5'-CAACGGTGGGTGTGGTTGG-3' 5'-GGTAATACGACTCACTATAGGGAGATACCA GCTTATTCAATTTTACAGAA CAACCAACGTGCGTCCGGGTACTTCTTCATCGAGATAGTAAGTGCAATCT-3'	River water	[66]
DPV	Hg^{2+}	0.03	0.01~100	5'-SH-(CH₂)₆-AAAAATTTCCTTTGCTTT-3'	Lake water	[35]
	Hg^{2+}	5×10^{-3}	$0.025~1 \times 10^{-6}$	5'-(NH₂C₆)-CTT GCT TTC TGT-3'	Lake water	[47]
	Hg^{2+}	0.03	0.1~100	5'-SH-(CH₂)₆-ACCGTGTTTGCCTTTGAC CTC-3'	Lake water	[83]
	Hg^{2+}	2.9×10^{-3}	$0.01~1 \times 10^{5}$	5'-COOH-CTTCTTCCCCCCCTTCTTC-SH-3'	River water	[87]
	Hg^{2+}	5×10^{-3}	0.01~500	5'-SH-(CH₂)₆-TCATGTTTGTTTGTGGCCCCCCCTTCTTTCTTA-Fe-3'	Tap water	[106]
	Hg^{2+}	0.33	1~200	5'-Bio-TCTTTCTTCCCTTGTTTGT-3'	Tap water	[107]
	Cd^{2+}	5×10^{-5}	1×10^{-3}~100	5'-ACCGACCGTGCTGGACTCTGGACTGTTGTGGGTATTATTTTTGGTTGTGCAGT ATGAGCGAGCGTTGCG-3'	Tap water	[33]
	Cd^{2+}	6.5×10^{-7}	1×10^{-6}~1	5'-GGGGGGGGACTGTTGTGGTATTATTTTTGGTTGTGCAGT-MB-3'	Valley water	[84]
	Pb^{2+}	4.3×10^{-9}	$1.0 \times 10^{-8}~5.0 \times 10^{-5}$	5'-GGGTGGGTGGGTGGGT-3'	Springwater	[41]
	Pb^{2+}	1.6×10^{-3}	4.8×10^{-3}~4.8	5'-GGTTGGGCGGGATGGGTG-3'	Tea and Rice	[50]
	Pb^{2+}	5.1×10^{-7}	1×10^{-6}~1	5'-MB-GGTGGTGGTTGGTTGGTGGTGGTGG-3'	Tap water	[85]
	Pb^{2+}	2.88	2.4~120	5'-GGGTGGGTGGGTGGGT-3'	Soil	[86]
	Pb^{2+}	0.018	$0.05~1 \times 10^{3}$	5'-GGGTGGGTGGGTGGGTAT-3'	Tap water	[88]
	Pb^{2+}	0.312	0.5~50	5'-GGGTGGGTGGGTGGGT-3'	Serum	[108]
	As^{3+}	4×10^{-5}	0.13~130	5'-HS-GGTAATACGACTCATAAGGGAGAGATGCTTATTCAATTTTACA GAACACCAAGTCGCTTACTTCTTCATCGAGATAGTAAGTGCAATCT-3'	River water	[34]

Table 1. *Cont.*

Method	Target	LOD (nM)	Linear Range (nM)	Aptamer Sequence	Sample	Reference
SWV	Hg^{2+}	1.79	10~100	5'-MB-CGCTTTAGATG-3'	Juice	[36]
	Hg^{2+}	1×10^{-4}	2×10^{-3}~20	5'-SH-AATTCTCTCTTCGACGTTGTGTGTT-3'	Tap water	[93]
	Hg^{2+}	0.094	1~5×10^3	5'-SH-$(CH_2)_6$-CTGTTTTCTTTCGGACGA CCCCCCTCGTCCGTTTGTTTTCAG-MB^+-3'	River water	[109]
	Cd^{2+} Pb^{2+}	0.089 0.016	0.1~1000	5'-CTCAGGACGACGGGTTCACAGTCCGTTGTC-Fc-3' 5'-GGT TGG TGT GGT TGG-MB-3'	Lettuce Orange	[31]
	Cd^{2+}	0.014	0.1~5	5'-HS$(CH_2)_6$GGACTGTTGTGGTATTATTTTGGTTGTGCAGTATG-3'	Tap water	[91]
	As^{3+}	0.7	3.83~766	5'-HS-GGTAATACGACTCATTAGGGAGAATCAGCTTATTCAATTTTACAGAACA ACCAACGTCGCTCCGGTACTTCTTCATCGAGATAGTAAGTGCAATCT-3'	None	[92]
PEC	Hg^{2+}	3.33×10^{-6}	1×10^{-5}–1×10^{-3}	5'-NH_2-$(CH_2)_6$-TTTTTTTTTTTTTTTTTT-3'	Tap water	[51]
	Cd^{2+}	1.8×10^{-3}	5×10^{-3}~29	5'-GGACTGTTGTGGTATTATTTTTGGTTGTGCAGTATG-3'	Lake water	[96]
	Cd^{2+}	0.011	0.03~40	5'-SH-GGACTGTTGTGGTATTATTTTTGGTTGTGCAGTATG-NH_2-3'	Lake water	[110]
	Pb^{2+}	3×10^{-4}	1×10^{-3}~5	5'-TTGGGTGGGTGGGTGGGT-3'	Tap water	[49]
	Pb^{2+}	1.67×10^{-5}	5×10^{-5}~1×10^3	5'-NH_2-$(CH_2)_6$-TTGGGTGGGTGGGTGGGT-P-3'	Reservoir water	[57]
	Pb^{2+}	0.05	0.1~50	5'-NH_2-$(CH_2)_6$-TTGGGTGGGTGGGTGGGT-3'	Tap water	[60]
	Pb^{2+}	1.6×10^{-3}	5×10^{-3}~10	5'-SH-GGGTGGGTGGGTGGGT-3'	Soil	[97]
	Pb^{2+}	0.34	1~1×10^4	5'-NH_2-$(CH_2)_6$-TTGGGTGGGTGGGTGGGT-3'	River water	[55]
ECL	Hg^{2+}	0.01	0.05~1×10^3	5'-NH2-TTGTTTGTCCCCTCTTTCTTA-(CH2)3-SH-3'	Tap water	[59]
	Hg^{2+}	4×10^{-5}	1×10^{-4}~0.01	5'-amino-(CH2)6-O-TCTCCAGCGTCGTTTGTTTGCGGGAGCTTTCTTAAAT CTCGAGCTAAA-3'	Water	[104]
	Hg^{2+}	3×10^{-4}	1×10^{-3}~1×10^4	5'-GGTTGGTGTGGTTGGTCTTTCTTCCCTGTTTGTT(CH2)6-SH-3'	None	[105]
	Hg^{2+} Pb^{2+}	4.1×10^{-6} 2.4×10^{-5}	1.0×10^{-5}~0.01 1.0×10^{-4}~10	5'-TTTTTTAAAATTTTTT-SH-3' 5'-COOH-$(CH_2)_{10}$-AAAAAAAAAGGGG-SH-3'	Shrimp	[58]
	Cd^{2+}	9.7×10^{-4}	0.26~2.6×10^6	5'-ACCGACCGTCGCTGCCGACTCGGCTGTGTGTGTATTATTTTGGTTGTGCA GTATGAGCGAGCGTTGCG-3'	Extracting solution of sophora	[103]
	Pb^{2+}	4×10^{-8}	1.0×10^{-7}~0.1	5'-GGTTGGTGTGGTTGG-3'	Soil	[32]

Table 1. *Cont.*

Method	Target	LOD (nM)	Linear Range (nM)	Aptamer Sequence	Sample	Reference
	Pb^{2+}	3.82×10^{-6}	$1.0 \times 10^{-5} \sim 1.0 \times 10^{-2}$	5′-SH- $(CH_2)_6$-TTTTTACCCAGGGTGGGTGGG-TGGGT-$(CH_2)_6$-NH_2-3′	River water	[48]
	As^{3+}	9.2×10^{-3}	$15.3 \sim 1.53 \times 10^4$	5′-GGTAATACGACTCACTATAGGGAGATACCAGCTTATTCAATTTTACAGAA CAACCAACGTCGCTCCGGGTACTTCTTCATCGAGATAGTAAGTGCAATCT-3′	Extracting solution of sophora	[102]

4. Prospects and Challenges

This review provides an overview of the recently developed E-apt sensors and the use of different nanomaterials in sensors. These sensors can be applied to the analysis of various food and water contaminants. By using aptamers with high affinity and specificity for the target and one or more effective signal amplification steps, most sensors exhibit good sensor behavior, including high sensitivity and selectivity.

However, the practical application of electrochemical sensors is still in the preliminary stage, and most heavy metal detection is carried out under laboratory conditions. Results obtained in the laboratory are difficult to verify with results from real samples; there is still a long way to make developments in the practical identification of heavy metal ions. Therefore, further research perspectives that must be taken into account in this area are as follows. The efficiency of the sensor largely depends on the affinity of aptamers, so screening new aptamers with high affinity is the first prerequisite to constructing excellent sensors. In addition, adaptation is also highly dependent on nanomaterials. The design of highly active nanomaterials with long-term stability and reproducibility is the main goal of future efforts. Future research can be carried out towards the advancement of E-apt sensors based on advanced technologies for the multi-residue determination of heavy metal ions in various environments.

Electrochemical sensors have bright application prospects, but there are still some problems that need to be solved Firstly, the binding efficiency of the aptamer and heavy metal ions should be considered. The detection ability of the aptamer sensor depends largely on whether the aptamer can detect the existence of the target sensitively. If the aptamer and the target are combined inefficiently, it is difficult to achieve the ideal detection effect. Secondly, the efficiency of the SELEX method and the specificity of the selected aptamer still need to be improved. Because the aptamer selection method is time-consuming, low cost, and with low efficiency, there are not many aptamers on the market for the detection of heavy metal ions which greatly hinders the development of aptamer-based sensors. Third, because E-apt sensors usually need to use nanomaterials to improve their sensitivity, the cost of nanomaterials is affected by the price of nanomaterials. The development of low-cost nanomaterials with significant effects is also crucial to the construction of sensors. Finally, the survey found that most of the aptamer-based sensors are often only for single heavy metal ion detection and usually, more than in the sample, there are multiple kinds of heavy metal ion pollution. The development of multiple target detection sensors then has important practical significance and broad application prospects.

In conclusion, an aptamer-based biosensor design provides a promising method for the fast and on-site monitoring of heavy metal ions in food safety, but further research and development are still needed.

References

1. Sall, M.L.; Diaw, A.K.D.; Gningue-Sall, D.; Efremova Aaron, S.; Aaron, J.-J. Toxic Heavy Metals: Impact on the Environment and Human Health, and Treatment with Conducting Organic Polymers, a Review. *Environ. Sci. Pollut. Res.* **2020**, *27*, 29927–29942. [CrossRef] [PubMed]
2. Karaouzas, I.; Kapetanaki, N.; Mentzafou, A.; Kanellopoulos, T.D.; Skoulikidis, N. Heavy Metal Contamination Status in Greek Surface Waters: A Review with Application and Evaluation of Pollution Indices. *Chemosphere* **2021**, *263*, 128192. [CrossRef] [PubMed]
3. Saravanan, A.; Senthil Kumar, P.; Jeevanantham, S.; Karishma, S.; Tajsabreen, B.; Yaashikaa, P.R.; Reshma, B. Effective Water/Wastewater Treatment Methodologies for Toxic Pollutants Removal: Processes and Applications towards Sustainable Development. *Chemosphere* **2021**, *280*, 130595. [CrossRef]
4. Fakhri, Y.; Saha, N.; Miri, A.; Baghaei, M.; Roomiani, L.; Ghaderpoori, M.; Taghavi, M.; Keramati, H.; Bahmani, Z.; Moradi, B.; et al. Metal Concentrations in Fillet and Gill of Parrotfish (Scarus Ghobban) from the Persian Gulf and Implications for Human Health. *Food Chem. Toxicol.* **2018**, *118*, 348–354. [CrossRef] [PubMed]
5. Aragay, G.; Pons, J.; Merkoçi, A. Recent Trends in Macro-, Micro-, and Nanomaterial-Based Tools and Strategies for Heavy-Metal Detection. *Chem. Rev.* **2011**, *111*, 3433–3458. [CrossRef] [PubMed]
6. Al Hamouz, O.C.S.; Akintola, O.S. Removal of Lead and Arsenic Ions by a New Series of Aniline Based Polyamines. *Process Saf. Environ. Prot.* **2017**, *106*, 180–190. [CrossRef]
7. Malik, L.A.; Bashir, A.; Qureashi, A.; Pandith, A.H. Detection and Removal of Heavy Metal Ions: A Review. *Environ. Chem. Lett.* **2019**, *17*, 1495–1521. [CrossRef]
8. Harrington, C.F.; Clough, R.; Drennan-Harris, L.R.; Hill, S.J.; Tyson, J.F. Atomic Spectrometry Update. Elemental Speciation. *J. Anal. At. Spectrom.* **2011**, *26*, 1561. [CrossRef]
9. Xie, M.; Zhao, F.; Zhang, Y.; Xiong, Y.; Han, S. Recent Advances in Aptamer-Based Optical and Electrochemical Biosensors for Detection of Pesticides and Veterinary Drugs. *Food Control* **2022**, *131*, 108399. [CrossRef]
10. Li, F.; Yu, Z.; Han, X.; Lai, R.Y. Electrochemical Aptamer-Based Sensors for Food and Water Analysis: A Review. *Anal. Chim. Acta* **2019**, *1051*, 1–23. [CrossRef]
11. Wang, T.; Chen, C.; Larcher, L.M.; Barrero, R.A.; Veedu, R.N. Three Decades of Nucleic Acid Aptamer Technologies: Lessons Learned, Progress and Opportunities on Aptamer Development. *Biotechnol. Adv.* **2019**, *37*, 28–50. [CrossRef] [PubMed]
12. Zhu, G.; Chen, X. Aptamer-Based Targeted Therapy. *Adv. Drug Deliv. Rev.* **2018**, *134*, 65–78. [CrossRef] [PubMed]
13. Ni, S.; Zhuo, Z.; Pan, Y.; Yu, Y.; Li, F.; Liu, J.; Wang, L.; Wu, X.; Li, D.; Wan, Y.; et al. Recent Progress in Aptamer Discoveries and Modifications for Therapeutic Applications. *ACS Appl. Mater. Interfaces* **2021**, *13*, 9500–9519. [CrossRef] [PubMed]
14. Wang, T.; Chen, L.; Chikkanna, A.; Chen, S.; Brusius, I.; Sbuh, N.; Veedu, R.N. Development of Nucleic Acid Aptamer-Based Lateral Flow Assays: A Robust Platform for Cost-Effective Point-of-Care Diagnosis. *Theranostics* **2021**, *11*, 5174–5196. [CrossRef]
15. Wu, S.; Zhang, H.; Shi, Z.; Duan, N.; Fang, C.; Dai, S.; Wang, Z. Aptamer-Based Fluorescence Biosensor for Chloramphenicol Determination Using Upconversion Nanoparticles. *Food Control* **2015**, *50*, 597–604. [CrossRef]
16. Emrani, A.S.; Danesh, N.M.; Lavaee, P.; Ramezani, M.; Abnous, K.; Taghdisi, S.M. Colorimetric and Fluorescence Quenching Aptasensors for Detection of Streptomycin in Blood Serum and Milk Based on Double-Stranded DNA and Gold Nanoparticles. *Food Chem.* **2016**, *190*, 115–121. [CrossRef]
17. Ouyang, Q.; Wang, L.; Ahmad, W.; Rong, Y.; Li, H.; Hu, Y.; Chen, Q. A Highly Sensitive Detection of Carbendazim Pesticide in Food Based on the Upconversion-MnO$_2$ Luminescent Resonance Energy Transfer Biosensor. *Food Chem.* **2021**, *349*, 129157. [CrossRef]
18. You, H.; Bai, L.; Yuan, Y.; Zhou, J.; Bai, Y.; Mu, Z. An Amperometric Aptasensor for Ultrasensitive Detection of Sulfadimethoxine Based on Exonuclease-Assisted Target Recycling and New Signal Tracer for Amplification. *Biosens. Bioelectron.* **2018**, *117*, 706–712. [CrossRef]
19. Zhou, C.; Zou, H.; Sun, C.; Ren, D.; Xiong, W.; Li, Y. Fluorescent Aptasensor for Detection of Four Tetracycline Veterinary Drugs in Milk Based on Catalytic Hairpin Assembly Reaction and Displacement of G-Quadruplex. *Anal. Bioanal. Chem.* **2018**, *410*, 2981–2989. [CrossRef]
20. Chen, Q.; Sheng, R.; Wang, P.; Ouyang, Q.; Wang, A.; Ali, S.; Zareef, M.; Hassan, M.M. Ultra-Sensitive Detection of Malathion Residues Using FRET-Based Upconversion Fluorescence Sensor in Food. *Spectrochim. Acta Part A Mol. Biomol. Spectrosc.* **2020**, *241*, 118654. [CrossRef]
21. Dolati, S.; Ramezani, M.; Nabavinia, M.S.; Soheili, V.; Abnous, K.; Taghdisi, S.M. Selection of Specific Aptamer against Enrofloxacin and Fabrication of Graphene Oxide Based Label-Free Fluorescent Assay. *Anal. Biochem.* **2018**, *549*, 124–129. [CrossRef] [PubMed]
22. Zhang, S.; Geryak, R.; Geldmeier, J.; Kim, S.; Tsukruk, V.V. Synthesis, Assembly, and Applications of Hybrid Nanostructures for Biosensing. *Chem. Rev.* **2017**, *117*, 12942–13038. [CrossRef] [PubMed]
23. Yao, S.; Swetha, P.; Zhu, Y. Nanomaterial-Enabled Wearable Sensors for Healthcare. *Adv. Healthc. Mater.* **2018**, *7*, 1700889. [CrossRef] [PubMed]
24. Baig, N.; Sajid, M.; Saleh, T.A. Recent Trends in Nanomaterial-Modified Electrodes for Electroanalytical Applications. *TrAC Trends Anal. Chem.* **2019**, *111*, 47–61. [CrossRef]
25. Cheng, N.; Song, Y.; Fu, Q.; Du, D.; Luo, Y.; Wang, Y.; Xu, W.; Lin, Y. Aptasensor Based on Fluorophore-Quencher Nano-Pair and Smartphone Spectrum Reader for on-Site Quantification of Multi-Pesticides. *Biosens. Bioelectron.* **2018**, *117*, 75–83. [CrossRef]

26. Roushani, M.; Rahmati, Z.; Hoseini, S.J.; Hashemi Fath, R. Impedimetric Ultrasensitive Detection of Chloramphenicol Based on Aptamer MIP Using a Glassy Carbon Electrode Modified by 3-Ampy-RGO and Silver Nanoparticle. *Colloids Surf. B Biointerfaces* **2019**, *183*, 110451. [CrossRef]

27. Charbgoo, F.; Soltani, F.; Taghdisi, S.M.; Abnous, K.; Ramezani, M. Nanoparticles Application in High Sensitive Aptasensor Design. *TrAC Trends Anal. Chem.* **2016**, *85*, 85–97. [CrossRef]

28. Fernandes, P.M.V.; Campiña, J.M.; Silva, A.F. A Layered Nanocomposite of Laccase, Chitosan, and Fe$_3$O$_4$ Nanoparticles-Reduced Graphene Oxide for the Nanomolar Electrochemical Detection of Bisphenol A. *Microchim. Acta* **2020**, *187*, 262. [CrossRef]

29. Turkevich, J.; Stevenson, P.C.; Hillier, J. A Study of the Nucleation and Growth Processes in the Synthesis of Colloidal Gold. *Discuss. Faraday Soc.* **1951**, *11*, 55. [CrossRef]

30. Priyadarshini, E.; Pradhan, N. Gold Nanoparticles as Efficient Sensors in Colorimetric Detection of Toxic Metal Ions: A Review. *Sens. Actuators B Chem.* **2017**, *238*, 888–902. [CrossRef]

31. Yuan, M.; Qian, S.; Cao, H.; Yu, J.; Ye, T.; Wu, X.; Chen, L.; Xu, F. An Ultra-Sensitive Electrochemical Aptasensor for Simultaneous Quantitative Detection of Pb2+ and Cd2+ in Fruit and Vegetable. *Food Chem.* **2022**, *382*, 132173. [CrossRef] [PubMed]

32. Deng, W.; Hong, L.-R.; Zhao, M.; Zhuo, Y.; Gao, M. Electrochemiluminescence-Based Detection Method of Lead(II) Ion via Dual Enhancement of Intermolecular and Intramolecular Co-Reaction. *Analyst* **2015**, *140*, 4206–4211. [CrossRef] [PubMed]

33. Liu, Y.; Lai, Y.; Yang, G.; Tang, C.; Deng, Y.; Li, S.; Wang, Z. Cd-Aptamer Electrochemical Biosensor Based on AuNPs/CS Modified Glass Carbon Electrode. *J. Biomed. Nanotechnol.* **2017**, *13*, 1253–1259. [CrossRef]

34. Yadav, R.; Kushwah, V.; Gaur, M.S.; Bhadauria, S.; Berlina, A.N.; Zherdev, A.V.; Dzantiev, B.B. Electrochemical Aptamer Biosensor for As $^{3+}$ Based on Apta Deep Trapped Ag-Au Alloy Nanoparticles-Impregnated Glassy Carbon Electrode. *Int. J. Environ. Anal. Chem.* **2020**, *100*, 623–634. [CrossRef]

35. Zhao, Y.; Xie, X. A Novel Electrochemical Aptamer Biosensor Based on DNAzyme Decorated Au@Ag Core-Shell Nanoparticles for Hg2+ Determination. *J. Braz. Chem. Soc.* **2018**, *29*, 232–239. [CrossRef]

36. Miao, P.; Tang, Y.; Wang, L. DNA Modified Fe$_3$O$_4$ @Au Magnetic Nanoparticles as Selective Probes for Simultaneous Detection of Heavy Metal Ions. *ACS Appl. Mater. Interfaces* **2017**, *9*, 3940–3947. [CrossRef]

37. Ajayan, P.M. Nanotubes from Carbon. *Chem. Rev.* **1999**, *99*, 1787–1800. [CrossRef]

38. Charbgoo, F.; Behmanesh, M.; Nikkhah, M. Enhanced Reduction of Single-Wall Carbon Nanotube Cytotoxicity *in Vitro*: Applying a Novel Method of Arginine Functionalization. *Biotechnol. Appl. Biochem.* **2015**, *62*, 598–605. [CrossRef]

39. Wilder, J.W.G.; Venema, L.C.; Rinzler, A.G.; Smalley, R.E.; Dekker, C. Electronic Structure of Atomically Resolved Carbon Nanotubes. *Nature* **1998**, *391*, 59–62. [CrossRef]

40. So, H.-M.; Won, K.; Kim, Y.H.; Kim, B.-K.; Ryu, B.H.; Na, P.S.; Kim, H.; Lee, J.-O. Single-Walled Carbon Nanotube Biosensors Using Aptamers as Molecular Recognition Elements. *J. Am. Chem. Soc.* **2005**, *127*, 11906–11907. [CrossRef]

41. Zhu, Y.; Zeng, G.; Zhang, Y.; Tang, L.; Chen, J.; Cheng, M.; Zhang, L.; He, L.; Guo, Y.; He, X.; et al. Highly Sensitive Electrochemical Sensor Using a MWCNTs/GNPs-Modified Electrode for Lead (II) Detection Based on Pb $^{2+}$ -Induced G-Rich DNA Conformation. *Analyst* **2014**, *139*, 5014. [CrossRef] [PubMed]

42. Wongkaew, N.; Simsek, M.; Griesche, C.; Baeumner, A.J. Functional Nanomaterials and Nanostructures Enhancing Electro-chemical Biosensors and Lab-on-a-Chip Performances: Recent Progress, Applications, and Future Perspective. *Chem. Rev.* **2019**, *119*, 120–194. [CrossRef] [PubMed]

43. Rabai, S.; Teniou, A.; Catanante, G.; Benounis, M.; Marty, J.-L.; Rhouati, A. Fabrication of AuNPs/MWCNTS/Chitosan Nanocom-posite for the Electrochemical Aptasensing of Cadmium in Water. *Sensors* **2021**, *22*, 105. [CrossRef] [PubMed]

44. He, L.; Zhang, S.; Wang, M.; Peng, D.; Yan, F.; Zhang, Z.; Zhou, L. Facile Fabrication of Zinc Phosphate-Based Nanocomposites for High-Performance Electrochemical Sensing of Hg(II). *Sens. Actuators B Chem.* **2016**, *228*, 500–508. [CrossRef]

45. Tao, Z.; Zhou, Y.; Duan, N.; Wang, Z. A Colorimetric Aptamer Sensor Based on the Enhanced Peroxidase Activity of Functionalized Graphene/Fe$_3$O$_4$-AuNPs for Detection of Lead (II) Ions. *Catalysts* **2020**, *10*, 600. [CrossRef]

46. Biswas, C.; Lee, Y.H. Graphene Versus Carbon Nanotubes in Electronic Devices. *Adv. Funct. Mater.* **2011**, *21*, 3806–3826. [CrossRef]

47. Zhang, Y.; Xie, J.; Liu, Y.; Pang, P.; Feng, L.; Wang, H.; Wu, Z.; Yang, W. Simple and Signal-off Electrochemical Biosensor for Mercury(II) Based on Thymine-Mercury-Thymine Hybridization Directly on Graphene. *Electrochim. Acta* **2015**, *170*, 210–217. [CrossRef]

48. Hai, H.; Yang, F.; Li, J. Highly Sensitive Electrochemiluminescence "Turn-on" Aptamer Sensor for Lead(II) Ion Based on the Formation of a G-Quadruplex on a Graphene and Gold Nanoparticles Modified Electrode. *Microchim. Acta* **2014**, *181*, 893–901. [CrossRef]

49. Jiang, D.; Du, X.; Chen, D.; Zhou, L.; Chen, W.; Li, Y.; Hao, N.; Qian, J.; Liu, Q.; Wang, K. One-Pot Hydrothermal Route to Fabricate Nitrogen Doped Graphene/Ag-TiO$_2$: Efficient Charge Separation, and High-Performance "on-off-on" Switch System Based Photoelectrochemical Biosensing. *Biosens. Bioelectron.* **2016**, *83*, 149–155. [CrossRef]

50. Wang, L.; Peng, X.; Fu, H. An Electrochemical Aptasensor for the Sensitive Detection of Pb^{2+} Based on a Chitosan/Reduced Graphene Oxide/Titanium Dioxide. *Microchem. J.* **2022**, *174*, 106977. [CrossRef]

51. Li, H.; Xue, Y.; Wang, W. Femtomole Level Photoelectrochemical Aptasensing for Mercury Ions Using Quercetin–Copper(II) Complex as the DNA Intercalator. *Biosens. Bioelectron.* **2014**, *54*, 317–322. [CrossRef] [PubMed]

52. Esteve-Turrillas, F.A.; Abad-Fuentes, A. Applications of Quantum Dots as Probes in Immunosensing of Small-Sized Analytes. *Biosens. Bioelectron.* **2013**, *41*, 12–29. [CrossRef] [PubMed]

53. Shahdost-fard, F.; Roushani, M. Designing an Ultra-Sensitive Aptasensor Based on an AgNPs/Thiol-GQD Nanocomposite for TNT Detection at Femtomolar Levels Using the Electrochemical Oxidation of Rutin as a Redox Probe. *Biosens. Bioelectron.* **2017**, *87*, 724–731. [CrossRef] [PubMed]

54. Khonsari, Y.N.; Sun, S. A Novel Label Free Electrochemiluminescent Aptasensor for the Detection of Lysozyme. *Mater. Sci. Eng. C* **2019**, *96*, 146–152. [CrossRef]

55. Cao, J.-T.; Liao, X.-J.; Wang, Y.-L.; Liu, Y.-M. A Novel Photoelectrochemical Strategy for Lead Ion Detection Based on CdSe Quantum Dots Co-Sensitized ZnO-CdS Nanostructure. *J. Electroanal. Chem.* **2021**, *880*, 114828. [CrossRef]

56. Adegoke, O.; Daeid, N.N. Alloyed AuFeZnSe Quantum Dots@gold Nanorod Nanocomposite as an Ultrasensitive and Selective Plasmon-Amplified Fluorescence OFF-ON Aptasensor for Arsenic (III). *J. Photochem. Photobiol. A Chem.* **2022**, *426*, 113755. [CrossRef]

57. Shi, J.-J.; Zhu, J.-C.; Zhao, M.; Wang, Y.; Yang, P.; He, J. Ultrasensitive Photoelectrochemical Aptasensor for Lead Ion Detection Based on Sensitization Effect of CdTe QDs on MoS2-CdS:Mn Nanocomposites by the Formation of G-Quadruplex Structure. *Talanta* **2018**, *183*, 237–244. [CrossRef]

58. Feng, D.; Li, P.; Tan, X.; Wu, Y.; Wei, F.; Du, F.; Ai, C.; Luo, Y.; Chen, Q.; Han, H. Electrochemiluminescence Aptasensor for Multiple Determination of Hg2+ and Pb2+ Ions by Using the MIL-53(Al)@CdTe-PEI Modified Electrode. *Anal. Chim. Acta* **2020**, *1100*, 232–239. [CrossRef]

59. Li, L.; Chen, B.; Luo, L.; Liu, X.; Bi, X.; You, T. Sensitive and Selective Detection of Hg2+ in Tap and Canal Water via Self-Enhanced ECL Aptasensor Based on NH2–Ru@SiO2-NGQDs. *Talanta* **2021**, *222*, 121579. [CrossRef]

60. Zang, Y.; Lei, J.; Hao, Q.; Ju, H. "Signal-On" Photoelectrochemical Sensing Strategy Based on Target-Dependent Aptamer Conformational Conversion for Selective Detection of Lead(II) Ion. *ACS Appl. Mater. Interfaces* **2014**, *6*, 15991–15997. [CrossRef]

61. Yi, H.; Qin, R.; Ding, S.; Wang, Y.; Li, S.; Zhao, Q.; Pan, F. Structure and Properties of Prussian Blue Analogues in Energy Storage and Conversion Applications. *Adv. Funct. Mater.* **2021**, *31*, 2006970. [CrossRef]

62. Lv, M.; Zhou, W.; Tavakoli, H.; Bautista, C.; Xia, J.; Wang, Z.; Li, X. Aptamer-Functionalized Metal-Organic Frameworks (MOFs) for Biosensing. *Biosens. Bioelectron.* **2021**, *176*, 112947. [CrossRef] [PubMed]

63. Pavadai, R.; Amalraj, A.; Subramanian, S.; Perumal, P. High Catalytic Activity of Fluorophore-Labeled Y-Shaped DNAzyme/3D MOF-MoS 2 NBs as a Versatile Biosensing Platform for the Simultaneous Detection of Hg 2+, Ni 2+, and Ag + Ions. *ACS Appl. Mater. Interfaces* **2021**, *13*, 31710–31724. [CrossRef] [PubMed]

64. Zhang, Z.-H.; Duan, F.-H.; Tian, J.-Y.; He, J.-Y.; Yang, L.-Y.; Zhao, H.; Zhang, S.; Liu, C.-S.; He, L.-H.; Chen, M.; et al. Aptamer-Embedded Zirconium-Based Metal–Organic Framework Composites Prepared by De Novo Bio-Inspired Approach with Enhanced Biosensing for Detecting Trace Analytes. *ACS Sens.* **2017**, *2*, 982–989. [CrossRef] [PubMed]

65. Ling, P.; Lei, J.; Ju, H. Porphyrinic Metal-Organic Framework as Electrochemical Probe for DNA Sensing via Triple-Helix Molecular Switch. *Biosens. Bioelectron.* **2015**, *71*, 373–379. [CrossRef]

66. Zhang, Z.; Ji, H.; Song, Y.; Zhang, S.; Wang, M.; Jia, C.; Tian, J.-Y.; He, L.; Zhang, X.; Liu, C.-S. Fe(III)-Based Metal–Organic Framework-Derived Core–Shell Nanostructure: Sensitive Electrochemical Platform for High Trace Determination of Heavy Metal Ions. *Biosens. Bioelectron.* **2017**, *94*, 358–364. [CrossRef] [PubMed]

67. Wei, M.; Yue, S.; Liu, Y. An Amplified Electrochemical Aptasensor for Ochratoxin A Based on DNAzyme-Mediated DNA Walker. *J. Electroanal. Chem.* **2021**, *891*, 115269. [CrossRef]

68. Li, Y.; Liu, D.; Zhu, C.; Wang, M.; Liu, Y.; You, T. A Ratiometry-Induced Successive Reusable Electrochemical Aptasensing Platform: Efficient Monitoring of Aflatoxin B1 in Peanut. *Sens. Actuators B Chem.* **2021**, *336*, 129021. [CrossRef]

69. El-Moghazy, A.Y.; Amaly, N.; Istamboulie, G.; Nitin, N.; Sun, G. A Signal-on Electrochemical Aptasensor Based on Silanized Cellulose Nanofibers for Rapid Point-of-Use Detection of Ochratoxin A. *Microchim. Acta* **2020**, *187*, 535. [CrossRef]

70. Yola, M.L.; Atar, N.; Özcan, N. A Novel Electrochemical Lung Cancer Biomarker Cytokeratin 19 Fragment Antigen 21-1 Immunosensor Based on Si3N4/MoS2 Incorporated MWCNTs and Core–Shell Type Magnetic Nanoparticles. *Nanoscale* **2021**, *13*, 4660–4669. [CrossRef]

71. Vu, Q.K.; Tran, Q.H.; Vu, N.P.; Anh, T.-L.; Dang, T.T.L.; Matteo, T.; Nguyen, T.H.H. A Label-Free Electrochemical Biosensor Based on Screen-Printed Electrodes Modified with Gold Nanoparticles for Quick Detection of Bacterial Pathogens. *Mater. Today Commun.* **2021**, *26*, 101726. [CrossRef]

72. Jin, W.; Maduraiveeran, G. Nanomaterial-Based Environmental Sensing Platforms Using State-of-the-Art Electroanalytical Strategies. *J. Anal. Sci. Technol.* **2018**, *9*, 18. [CrossRef]

73. Yola, M.L. Sensitive Sandwich-Type Voltammetric Immunosensor for Breast Cancer Biomarker HER2 Detection Based on Gold Nanoparticles Decorated Cu-MOF and Cu2ZnSnS4 NPs/Pt/g-C3N4 Composite. *Microchim. Acta* **2021**, *188*, 78. [CrossRef] [PubMed]

74. Mayorga-Martinez, C.C.; Chamorro-Garcia, A.; Merkoçi, A. Electrochemical Impedance Spectroscopy (Bio)Sensing through Hydrogen Evolution Reaction Induced by Gold Nanoparticles. *Biosens. Bioelectron.* **2015**, *67*, 53–58. [CrossRef]

75. Mahmoud, A.M.; Alkahtani, S.A.; Alyami, B.A.; El-Wekil, M.M. Dual-Recognition Molecularly Imprinted Aptasensor Based on Gold Nanoparticles Decorated Carboxylated Carbon Nanotubes for Highly Selective and Sensitive Determination of Histamine in Different Matrices. *Anal. Chim. Acta* **2020**, *1133*, 58–65. [CrossRef]

76. Sun, K.; Xia, N.; Zhao, L.; Liu, K.; Hou, W.; Liu, L. Aptasensors for the Selective Detection of Alpha-Synuclein Oligomer by Colorimetry, Surface Plasmon Resonance and Electrochemical Impedance Spectroscopy. *Sens. Actuators B Chem.* **2017**, *245*, 87–94. [CrossRef]

77. Gu, H.; Yang, Y.; Chen, F.; Liu, T.; Jin, J.; Pan, Y.; Miao, P. Electrochemical Detection of Arsenic Contamination Based on Hybridization Chain Reaction and RecJf Exonuclease-Mediated Amplification. *Chem. Eng. J.* **2018**, *353*, 305–310. [CrossRef]

78. Rabai, S.; Benounis, M.; Catanante, G.; Baraket, A.; Errachid, A.; Jaffrezic Renault, N.; Marty, J.-L.; Rhouati, A. Development of a Label-Free Electrochemical Aptasensor Based on Diazonium Electrodeposition: Application to Cadmium Detection in Water. *Anal. Biochem.* **2021**, *612*, 113956. [CrossRef]

79. Diaz-Amaya, S.; Lin, L.-K.; DiNino, R.E.; Ostos, C.; Stanciu, L.A. Inkjet Printed Electrochemical Aptasensor for Detection of Hg2+ in Organic Solvents. *Electrochim. Acta* **2019**, *316*, 33–42. [CrossRef]

80. Wang, Y.; Zhao, G.; Zhang, Q.; Wang, H.; Zhang, Y.; Cao, W.; Zhang, N.; Du, B.; Wei, Q. Electrochemical Aptasensor Based on Gold Modified Graphene Nanocomposite with Different Morphologies for Ultrasensitive Detection of Pb2+. *Sens. Actuators B Chem.* **2019**, *288*, 325–331. [CrossRef]

81. Yadav, R.; Berlina, A.N.; Zherdev, A.V.; Gaur, M.S.; Dzantiev, B.B. Rapid and Selective Electrochemical Detection of Pb2+ Ions Using Aptamer-Conjugated Alloy Nanoparticles. *SN Appl. Sci.* **2020**, *2*, 2077. [CrossRef]

82. Du, H.; Xie, Y.; Wang, J. Nanomaterial-Sensors for Herbicides Detection Using Electrochemical Techniques and Prospect Applications. *TrAC Trends Anal. Chem.* **2021**, *135*, 116178. [CrossRef]

83. Luo, J.; Jiang, D.; Liu, T.; Peng, J.; Chu, Z.; Jin, W. High-Performance Electrochemical Mercury Aptasensor Based on Synergistic Amplification of Pt Nanotube Arrays and Fe$_3$O$_4$/RGO Nanoprobes. *Biosens. Bioelectron.* **2018**, *104*, 1–7. [CrossRef] [PubMed]

84. Lee, C.-S.; Yu, S.H.; Kim, T.H. A "Turn-on" Electrochemical Aptasensor for Ultrasensitive Detection of Cd2+ Using Duplexed Aptamer Switch on Electrochemically Reduced Graphene Oxide Electrode. *Microchem. J.* **2020**, *159*, 105372. [CrossRef]

85. Yu, S.H.; Lee, C.-S.; Kim, T.H. Electrochemical Detection of Ultratrace Lead Ion through Attaching and Detaching DNA Aptamer from Electrochemically Reduced Graphene Oxide Electrode. *Nanomaterials* **2019**, *9*, 817. [CrossRef] [PubMed]

86. Ding, J.; Zhang, D.; Liu, Y.; Yu, M.; Zhan, X.; Zhang, D.; Zhou, P. An Electrochemical Aptasensor for Detection of Lead Ions Using a Screen-Printed Carbon Electrode Modified with Au/Polypyrrole Composites and Toluidine Blue. *Anal. Methods* **2019**, *11*, 4274–4279. [CrossRef]

87. Ma, N.; Ren, X.; Wang, H.; Kuang, X.; Fan, D.; Wu, D.; Wei, Q. Ultrasensitive Controlled Release Aptasensor Using Thymine–Hg^{2+}–Thymine Mismatch as a Molecular Switch for Hg^{2+} Detection. *Anal. Chem.* **2020**, *92*, 14069–14075. [CrossRef]

88. Jin, H.; Zhang, D.; Liu, Y.; Wei, M. An Electrochemical Aptasensor for Lead Ion Detection Based on Catalytic Hairpin Assembly and Porous Carbon Supported Platinum as Signal Amplification. *RSC Adv.* **2020**, *10*, 6647–6653. [CrossRef]

89. Williams, T.; Shum, R.; Rappleye, D. Review—Concentration Measurements In Molten Chloride Salts Using Electrochemical Methods. *J. Electrochem. Soc.* **2021**, *168*, 123510. [CrossRef]

90. Fakude, C.T.; Arotiba, O.A.; Arduini, F.; Mabuba, N. Flexible Polyester Screen-printed Electrode Modified with Carbon Nanofibers for the Electrochemical Aptasensing of Cadmium (II). *Electroanalysis* **2020**, *32*, 2650–2658. [CrossRef]

91. Fakude, C.T.; Arotiba, O.A.; Mabuba, N. Electrochemical Aptasensing of Cadmium (II) on a Carbon Black-Gold Nano-Platform. *J. Electroanal. Chem.* **2020**, *858*, 113796. [CrossRef]

92. Mushiana, T.; Mabuba, N.; Idris, A.O.; Peleyeju, G.M.; Orimolade, B.O.; Nkosi, D.; Ajayi, R.F.; Arotiba, O.A. An Aptasensor for Arsenic on a Carbon-gold Bi-Nanoparticle Platform. *Sens. Bio-Sens. Res.* **2019**, *24*, 100280. [CrossRef]

93. Si, X.; Tang, S.; Wang, K.; Zhou, G.; Xia, J.; Zhao, Y.; Zhao, H.; Shen, Q.; Liu, Z. Electrochemical Amplification for Hg(II) Quantification by Anchoring an Enzymatically Extended Aptamer. *Anal. Lett.* **2019**, *52*, 2883–2895. [CrossRef]

94. Wen, J.; Zeng, G. Chemical and Biological Assessment of Cd-Polluted Sediment for Land Use: The Effect of Stabilization Using Chitosan-Coated Zeolite. *J. Environ. Manag.* **2018**, *212*, 46–53. [CrossRef] [PubMed]

95. Kong, W.; Qu, F.; Lu, L. A Photoelectrochemical Aptasensor Based on P-n Heterojunction CdS-Cu2O Nanorod Arrays with Enhanced Photocurrent for the Detection of Prostate-Specific Antigen. *Anal. Bioanal. Chem.* **2020**, *412*, 841–848. [CrossRef] [PubMed]

96. Niu, Y.; Xie, H.; Luo, G.; Zhuang, Y.; Wu, X.; Li, G.; Sun, W. ZnO-Reduced Graphene Oxide Composite Based Photoelectrochemical Aptasensor for Sensitive Cd(II) Detection with Methylene Blue as Sensitizer. *Anal. Chim. Acta* **2020**, *1118*, 1–8. [CrossRef] [PubMed]

97. Niu, Y.; Luo, G.; Xie, H.; Zhuang, Y.; Wu, X.; Li, G.; Sun, W. Photoelectrochemical Aptasensor for Lead(II) by Exploiting the CdS Nanoparticle-Assisted Photoactivity of TiO2 Nanoparticles and by Using the Quercetin-Copper(II) Complex as the DNA Intercalator. *Microchim. Acta* **2019**, *186*, 826. [CrossRef]

98. Yuan, Y.; Li, X.; Chen, A.-Y.; Wang, H.-J.; Chai, Y.-Q.; Yuan, R. Highly-Efficient Luminol Immobilization Approach and Exponential Strand Displacement Reaction Based Electrochemiluminescent Strategy for Monitoring MicroRNA Expression in Cell. *Biosens. Bioelectron.* **2019**, *132*, 62–67. [CrossRef] [PubMed]

99. Tang, H.; Chen, W.; Li, D.; Duan, X.; Ding, S.; Zhao, M.; Zhang, J. Luminol-Based Ternary Electrochemiluminescence Nanospheres as Signal Tags and Target-Triggered Strand Displacement Reaction as Signal Amplification for Highly Sensitive Detection of Helicobacter Pylori DNA. *Sens. Actuators B Chem.* **2019**, *293*, 304–311. [CrossRef]

100. Xie, X.; Wang, H.; Zhang, L.; Liu, Y.; Chai, Y.; Yuan, Y.; Yuan, R. A Novel Electrochemiluminescence Immunosensor Based on Functional β-Cyclodextrin-Ferrocene Host-Guest Complex with Multiple Signal Amplification. *Sens. Actuators B Chem.* **2018**, *258*, 1146–1151. [CrossRef]

101. Walker, G.T.; Fraiser, M.S.; Schram, J.L.; Little, M.C.; Nadeau, J.G.; Malinowski, D.P. Strand Displacement Amplification—an Isothermal, *in Vitro* DNA Amplification Technique. *Nucleic Acids Res.* **1992**, *20*, 1691–1696. [CrossRef] [PubMed]
102. Zhu, X.; Zhang, S.; Li, W.; Zhan, Y.; Yu, L.; Wu, X.; Li, J.; Xu, H.; Yang, G. Label-Free and Immobilization-Free Electrochemiluminescent Sensing Platform for Highly Sensitive Detection of As(III) by Combining Target-Induced Strand Displacement Amplification with Polydopamine Nanospheres. *Sens. Actuators B Chem.* **2020**, *311*, 127818. [CrossRef]
103. Xu, H.; Zhang, S.; Zhang, T.; Huang, W.; Dai, Y.; Zheng, R.; Wu, G. An Electrochemiluminescence Biosensor for Cadmium Ion Based on Target-Induced Strand Displacement Amplification and Magnetic Fe_3O_4-GO Nanosheets. *Talanta* **2022**, *237*, 122967. [CrossRef]
104. Ma, F.; Chen, Y.; Zhu, Y.; Liu, J. Electrogenerated Chemiluminescence Biosensor for Detection of Mercury (II) Ion via Target-Triggered Manipulation of DNA Three-Way Junctions. *Talanta* **2019**, *194*, 114–118. [CrossRef] [PubMed]
105. Wang, C.; Chen, M.; Wu, J.; Mo, F.; Fu, Y. Multi-Functional Electrochemiluminescence Aptasensor Based on Resonance Energy Transfer between Au Nanoparticles and Lanthanum Ion-Doped Cadmium Sulfide Quantum Dots. *Anal. Chim. Acta* **2019**, *1086*, 66–74. [CrossRef] [PubMed]
106. Liu, Y.; Deng, Y.; Li, T.; Chen, Z.; Chen, H.; Li, S.; Liu, H. Aptamer-Based Electrochemical Biosensor for Mercury Ions Detection Using AuNPs-Modified Glass Carbon Electrode. *J. Biomed. Nanotechnol.* **2018**, *14*, 2156–2161. [CrossRef]
107. Wu, D.; Wang, Y.; Zhang, Y.; Ma, H.; Pang, X.; Hu, L.; Du, B.; Wei, Q. Facile Fabrication of an Electrochemical Aptasensor Based on Magnetic Electrode by Using Streptavidin Modified Magnetic Beads for Sensitive and Specific Detection of Hg 2+. *Biosens. Bioelectron.* **2016**, *82*, 9–13. [CrossRef]
108. Taghdisi, S.M.; Danesh, N.M.; Lavaee, P.; Ramezani, M.; Abnous, K. An Electrochemical Aptasensor Based on Gold Nanoparticles, Thionine and Hairpin Structure of Complementary Strand of Aptamer for Ultrasensitive Detection of Lead. *Sens. Actuators B Chem.* **2016**, *234*, 462–469. [CrossRef]
109. Jia, J.; Chen, H.G.; Feng, J.; Lei, J.L.; Luo, H.Q.; Li, N.B. A Regenerative Ratiometric Electrochemical Biosensor for Selective Detecting Hg^{2+} Based on Y-Shaped/Hairpin DNA Transformation. *Anal. Chim. Acta* **2016**, *908*, 95–101. [CrossRef]
110. Niu, Y.; Chen, Y.; Zhang, X.; Xie, H.; Luo, G.; Sun, W. Target-Enhanced Photoelectrochemical Aptasensor for Cd(II) Detection Using Graphite-like Carbon Nitride as Sensitizer with High Sensitivity. *Microchem. J.* **2021**, *168*, 106394. [CrossRef]

MDPI